A Genome-wide Screen for Starvation-induced Autophagy Identifies New Modulators of Autophagy

Nicole Carla McKnight

University College London

and

Cancer Research UK London Research Institute

PhD Supervisor: Sharon A. Tooze

A thesis submitted for the degree of

Doctor of Philosophy

University College London

January 2011

Declaration

I, Nicole C. McKnight confirm that the work presented in this thesis is my own. Where information has been derived from other sources, I confirm that this has been indicated in the thesis.

Abstract

Autophagy is a catabolic mechanism by which cytoplasmic components are sequestered and transported by a double-membrane vesicle called an autophagosome to the lysosome for degradation. This recycling of organelles and macromolecules provides the cell with amino acids in times of nutrient deprivation though we do not fully know how the process is triggered or controlled. It is a highly regulated process in mammalian cells and its deregulation has been shown to contribute to multiple diseases.

In order to find new regulators of mammalian autophagy, I performed a genome-wide screen using the Dharmacon human siRNA library in a stable human cell line expressing GFP-LC3, a specific marker for autophagosomal membranes. First I incubated the cells with the siRNA pools then I starved the cells of amino acids. This initiated the formation of GFP-LC3-labelled autophagosomes that I quantified using the Cellomics VTiScan microscope and accompanying software. I measured the effect of specific siRNA-mediated knock-down on multiple parameters including spot count. Accounting for cell death and normalising the data, I generated a Z-score for each siRNA pool and retested the best 500 autophagy-increasing and 500 autophagy-decreasing siRNAs as above. The 190 strongest siRNA pools were deconvoluted leaving 20 hits that reproduced the phenotype with three or four out of four duplexes. These 20 hits were then assayed for endogenous LC3 lipidation in a different cell line and the ability of their siRNA to reduce mRNA levels was determined.

Four increasers of GFP-LC3 spots increased endogenous LC3 lipidation, suggesting that these proteins are either negative regulators of autophagy or inhibit the maturation or degradation of autophagosomes. Five decreasers of GFP-LC3 spots also inhibited endogenous LC3 lipidation and I have characterised two of these proteins required for autophagy. SCOC colocalises with early autophagy markers and may be providing a scaffold for autophagy machinery. WAC, through its reported binding partners, may be playing a role in both the autophagic and ubiquitin/proteasome pathways.

Acknowledgements

I would like to acknowledge the following people for all the assistance and support they have given me:

First, I would like to thank my examiners Nick Ktistakis and Kevin Ryan for reading my thesis and travelling to London for what I hope will be an interesting seminar and viva examination.

My thesis committee of Julian Downward and Nic Tapon has provided important guidance for my project over the last four years. Sally Leevers and the supporters of the London Research Institute PhD student program have also been a great help. I would like to acknowledge UCL and thank them for generously providing me with an Overseas Research Scholarship. The most monetary support however, has come from Cancer Research UK. Thank-you to all of the generous supporters for funding my studentship and this expensive project.

Within the LRI there are multiple people to acknowledge. Thanks to all of the employees of the cell services and the lab aides, especially Nicky who helped me gather many of the tissue culture reagents for the screen. Also, the people of the equipment park do a great job. Richard Mitter of the BABS lab provided important bioinformatics and advice. Most vital to the success of this screen was the HTS lab. Ming Jiang, Rachael Instrell, Becky Saunders and especially Mike Howell were indispensable and I have enjoyed working with you (I could not have done this without you guys).

My fellow PhD students (especially intake group 2006) have made the last four years more fun than expected and I wish you all great success and look forward to meeting up with you as we spread across the globe.

The SPW lab, past and present, has been the centre of my life at the LRI and I thank you for all of the encouragement and fun times (as well as serious science stuff). Special thanks go out to Ed Chan for making such a good stable cell line and a solid diving board for this project. Thank-you Sharon for trusting me with such an ambitious project and giving me the freedom and support to follow my hits.

Thanks to all my friends and family in the US and the UK, especially you Luke for all of your love and support.

Table of Contents

Table of figures

List of tables

Abbreviations

3-MA	3-methyladenine
A	Adenine
AD	Alzheimer’s disease
ALS	Amyotrophic lateral sclerosis
AV	autophagic vesicle
C	Cytosine
°C	degrees Celcius
CC	coiled-coil domain
CCVs	clathrin coated vesicles
CHC	clathrin heavy chain
CMA	chaperone-mediated autophagy
COG	conserved oligomeric Golgi
Co-IP	co-immunoprecipitation
CVT	cytoplasm-to-vacuole pathway
DAPI	4',6-diamidino-2-phenylindole
EBSS	Earle’s buffered salt solution
EM	Electron microscopy
ER	endoplasmic reticulum
FBS	foetal bovine serum

G	Guanine
GEF	guanine nucleotide exchange factor
GO	Gene Ontology
GRIP	golgin-97, RanBP2alpha, Imh1p and p230/golgin-245 domain
GTP	guanosine triphosphate
HCS	high-content screening
HD	Huntinton's disease
HPRD	Human Protein Reference Database
HRP	horseradish peroxidase
HTS	high-throughput screening
htt	huntingtin
IBD	inflammatory bowel disease
IF	immuno-fluorescence
IM	isolation membrane
LC3	MAPLC3B or Microtubule associated protein light chain 3, isoform b
LiCl	lithium chloride
LIR	LC3-interacting region
MAD	median absolute deviation
MEFs	Mouse embryonic fibroblasts

mL	millilitre
MVB	multivesicular body
mTOR	mammalian target of rapamycin or mechanistic target of rapamycin
ng	nanogram
nM	nanomolar
NRK	normal rat kidney cells
OC	object count (number of valid nuclei)
ORF	open reading frame
PAS	pre-autophagosomal structure or phagophore assembly site
PBS	phosphate-buffered saline
PD	Parkinson's disease
PE	phosphatidylethanolamine
PIs	phosphoinositides
PI3-K	phosphatidylinositol 3-kinase
PI(3)P	phosphatidylinositol 3-phosphate
PI3KC3	class III PI3-kinase
PIK3R4	phosphoinositide-3-kinase, regulatory subunit 4 (p150)
PM	plasma membrane
PML	promyelocytic leukaemia

PS	phosphatidylserine
PtdIns	phosphatidylinositol
RA	Ras association domain
RISC	RNA-induced silencing complex
RNAi	RNA interference
ROS	reactive oxygen species
SCOC	short coiled-coil protein
SCPO	spot count per object
siRNA	short interfering RNA
SNP	single nucleotide polymorhism
STAPO	spot total area per object
STIPO	spot total intensity per object
T	Thymine
TBS	TRIS-buffered saline
TGN	Trans-Golgi network
TGN	*trans*-Golgi network
TRAPP	transport protein particle
Ub	ubiquitin
UBA	ubiquitin association domain

UBL	ubiquitin-like
UBQ	ubiquitin homologue domain
µg	microgram
µL	microlitre
ULK	unc-51-like kinase
µM	micromolar
UPS	ubiquitin-proteasome system
Vps	vacuolar protein sorting
WAC	WW domain containing adaptor with coiled-coil
WD	WD40 repeat domain
WW	WW domain

Chapter 1. Introduction

1.1 Degradative pathways

There are two major degradative pathways in mammalian cells: macroautophagy and the ubiquitin-proteasome pathway. Macroautophagy is a catabolic, mostly unselective pathway that channels bulk portions of the cytoplasm to the lysosome to generate amino acids and macromolecules and is generally responsible for degrading long-lived proteins and large cellular structures. A selective version of autophagy, chaperone-mediated autophagy, also uses the lysosome for degradation and responds to prolonged nutrient deprivation by recycling a subset of cytosolic proteins. The ubiquitin-proteasome system is responsible for degrading damaged proteins in the proteasome and is specific in its selection of proteins and protein aggregates. By balancing these degradative pathways with new protein synthesis, cells are able to survive development, grow and maintain equilibrium.

1.1.1 Macroautophagy

Macroautophagy, hereafter referred to as autophagy, is a term generated from the Greek words, 'phagy,' meaning to eat and 'auto,' for self. It is a highly conserved intracellular membrane trafficking pathway that is exhibited in all eukaryotes from yeast to humans. It responds to nutrient deprivation as its most evolutionarily conserved function but is also triggered by cellular stress and the accumulation of protein aggregates and damaged organelles, especially in higher organisms. Autophagy generates the means for survival by degrading cytosolic proteins and whole organelles and recycling these back to the cytosol as amino acids and macromolecules. As a result, autophagy maintains cellular homeostasis by clearing the cell of misfolded or long-lived proteins and damaged parts and has also developed to rid the cell of invading microorganisms.

Autophagy is characterised by the formation of double-membrane vesicles, called autophagosomes that travel to the lysosome where they fuse and the contents of which are degraded by hydrolases. The autophagosome was originally observed using microscopy in the late 1950s and was first characterised by de Duve in 1966 when he described degradative vesicles that were seen to contain both cytoplasmic components and mitochondria (De Duve and Wattiaux, 1966). He saw the vesicles merge with

lysosomes and called the process of 'nonspecific bulk segregation and digestion' autophagy. Since a massive resurgence of research into the process of autophagy beginning in the early 1990s, cell biologists have dissected the progression of the autophagosome from its formation or nucleation, its expansion, its maturation including fusion with components of the endocytic pathway and its eventual degradation by the lysosome. Also, great strides have been made to determine how the process is triggered and how the autophagy machinery is initiated. Many autophagy-specific proteins, called Atg proteins, have been discovered in yeast through to humans and we know that the process requires these components as well as other cytosolic proteins and intracellular organelles such as the endoplasmic reticulum (ER) and Golgi apparatus, in addition to the endosome-lysosome system.

During autophagy, cytoplasmic components are sequestered in a growing phagophore or isolation membrane (IM) in mammals, called the pre-autophagosomal structure, or PAS in yeast (Figure 1.1). This double-membrane structure expands around portions of the cytoplasm containing proteins, aggregated proteins and organelles and then closes, forming the autophagic vesicle (AV) or autophagosome. Most mature autophagosomes are approximately 0.5 to 1μm in diameter; they can fuse with endocytic pathway vesicles including early endosomes, multivesicular bodies (MVBs), and late endosomes thus forming amphisomes. Eventually, the AV fuses with the lysosome, becoming an autolysosome, and the acidic hydrolases within break down the captured components to macromolecules and amino acids that are released back to the cytosol by transporters and permeases delivered with the lysosomal membrane. After degradation by autophagy, the recycled products can be used to maintain the cell processes whose compromising initiated the entire pathway (Xie and Klionsky, 2007).

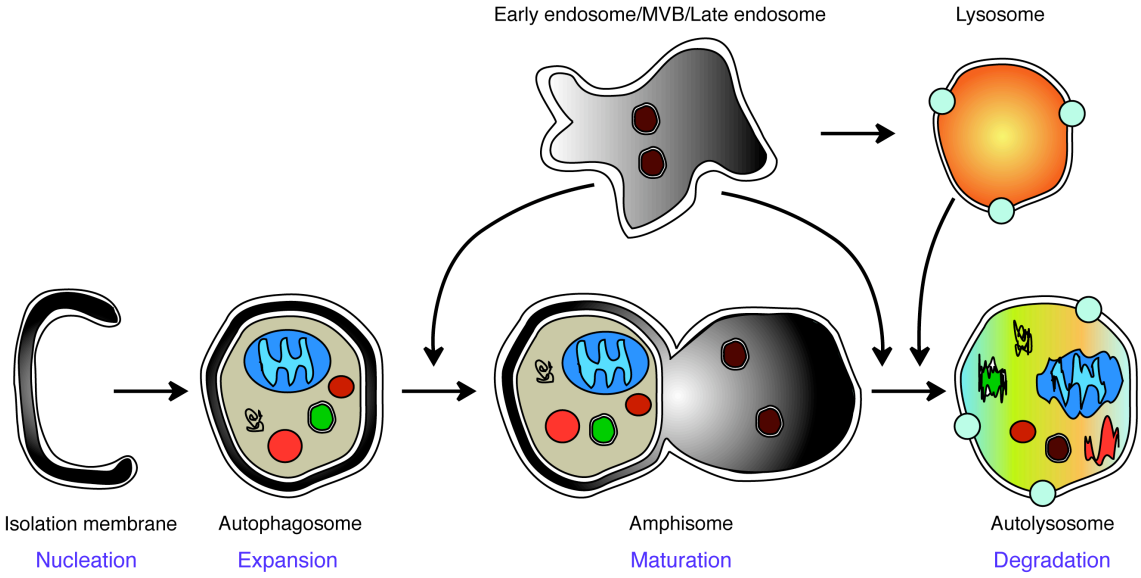

Figure 1.1 Mammalian autophagy
During mammalian autophagy, first an isolation membrane (IM), also known as a phagophore is formed or nucleated. The IM engulfs portions of the cytoplasm and can take up mitochondria (blue), misfolded proteins and various vesicles in a step called expansion. During maturation, the autophagosome can fuse with endocytic vesicles to become an amphisome. The mature autophagosome or amphisome fuses with the lysosome and becomes degradative. Adapted from Simonsen and Tooze, (Simonsen and Tooze, 2009).

Autophagy is responsible for clearing the cell of large structures such as organelles and protein aggregates and in this way functions as a sort-of cellular garbage disposal. In yeast, the cytoplasm-to-vacuole (CVT) pathway, which shares many of the core components with autophagy, and both pexophagy and mitophagy (the specific autophagic degradation of peroxisomes and mitochondria respectively) are considered selective forms of yeast autophagy. Until quite recently mammalian autophagy was believed to be an unspecific process, capturing random parts of the cell, but now it is believed to also specifically engulf protein aggregates, organelles and bacteria as cargo as these have been seen to selectively and exclusively incorporate into autophagosomes. The organelle-specific pathways of pexophagy, mitophagy and even ER-phagy have been observed in human cells though how these organelles are recognised and targeted by the autophagosome is unknown. In addition, the source of the membrane is a subject of intense research and great debate. In most cases, autophagy allows for cellular survival in times of stress such as hypoxia, infection, and starvation though much of the pre-nucleation process and the steps leading to its initiation remain to be elucidated. Autophagy in mammals is highly evolved and has become a tightly regulated process. In turn, its misregulation is associated with many diseases.

1.1.2 Chaperone-mediated autophagy

Chaperone-mediated autophagy (CMA), like macroautophagy, uses the lysosome for degradation of cytosolic proteins, but is induced after prolonged nutrient deprivation or oxidative stress (Dice, 2007). CMA is stimulated by molecular chaperones such as hsc70 and hsp90 that not only activate the pathway by recognising a consensus motif on the proteins that are targeted for degradation, but also unfold the substrates. Then, by directly associating with the lysosomal membrane through lysosome-associated membrane protein type 2A (LAMP-2A), proteins are translocated into the degradative vesicle. Levels of LAMP-2A control CMA activity and in turn, CMA activity has been suggested to be a factor of ageing. Like macroautophagy, when CMA is compromised it can contribute to disease. Recently discovered regulators of CMA, GFAP and EF1α respond to GTP and explain how CMA is regulated by energy levels (Bandyopadhyay et al., 2010), implicating GTP levels as a potential switch between CMA and macroautophagy.

1.1.3 Ubiquitin-proteasome system

Cellular stress leads to damaged proteins and these accumulate; in order that these do not become toxic to the cell, the proteins are unfolded, ubiquitinated and taken to the proteasome for degradation. The ubiquitin-proteasome system (UPS) is a selective mechanism that works on abnormal short-lived proteins and sometimes organelles and, unlike autophagy, degrades nuclear proteins and misfolded ER proteins. Though the previous view was that the UPS and autophagy act in a mutually exclusive way, recent work has shown that the two pathways are linked through their common modulator, p62/SQSTM1 (Korolchuk et al., 2009).

1.2 Autophagy core machinery

The molecular machinery responsible for autophagy initiation and autophagosome nucleation and expansion was discovered first in *S. cerevisiae* through genetic screens that identified essential autophagy proteins that respond to amino acid starvation (Takeshige et al., 1992), (Tsukada and Ohsumi, 1993). Currently, there are 34 known Atg proteins involved in both autophagy and the CVT pathway in yeast and most, if not all, human counterparts of the autophagy-specific proteins have been discovered (Klionsky et al., 2003). In mammals, there are twenty core autophagy proteins (sixteen

if one does not consider family members) and multiple auxiliary proteins that contribute to and control autophagy. The human Atg proteins can be divided into four groups listed in the order that they are thought to act: the ULK1 kinase complex, the Vps34/class III PI3-kinase complexes, the ubiquitin-like proteins Atg12 and Atg8/LC3 and their conjugation systems, and the Atg9 cycling complex, including WIPI2. Also, a set of proteins is responsible for transferring degraded material back into the cytoplasm. The four protein groups act early on in the autophagy pathway and are recruited to the isolation membrane and the recent explosion of autophagy research has lead to a somewhat comprehensive idea of how they operate to form the autophagosome.

1.2.1 ULK1 (and ULK2) kinase complex

The first-identified yeast autophagy gene was ATG1 (Matsuura et al., 1997). It transcribes a serine/threonine kinase that was shown to initiate autophagy directly downstream of the amino-acid sensor and the negative regulator of autophagy, TOR kinase. Atg1 initiates both starvation-induced autophagy and the CVT pathway in yeast and does so through interactions with at least seven other Atg proteins. Autophagy is initiated through the starvation-dependent dephosphorylation of the interacting partner Atg13 that causes it and the third member of the complex, Atg17, to bind Atg1 tightly, activating its kinase activity (Kabeya et al., 2005). This occurs directly as a result of the inhibition of TOR either by amino-acid deprivation or treatment with the TOR inhibitor rapamycin. But it is Atg17, not Atg1 or Atg13 that is at the top of the hierarchy of Atg proteins, as determined by systematic analysis of yeast mutants (Suzuki et al., 2007). Atg1 also seems to play a kinase-independent, structural role in autophagy in that it provides a scaffold for and recruits other proteins to the PAS to aid nucleation (for review see (Chan and Tooze, 2009)).

Atg1 in *Drosophila* and *C. elegans* (in which it is called UNC-51) together with Atg13 and Atg17 are also critical in these organisms' control of autophagy but Atg1 is also involved in apoptosis and development through multiple non-Atg binding partners (Chan and Tooze, 2009). In addition, Atg1/UNC-51 is required for neuronal vesicular trafficking and development possibly through its indirect interaction with microtubule motors (Toda et al., 2008). As in yeast, *Drosophila* Atg13 binds more strongly to Atg1 during autophagy but opposite to yeast, induction of autophagy upon nutrient deprivation in flies is characterised by increased phosphorylation of Atg13 and a loss of

phosphorylation of Atg1 by TOR (Chang and Neufeld, 2009). Also, TOR remains complexed with Atg1 in both nutrient-rich and starvation conditions.

Two of the mammalian homologues of Atg1, called unc-51-like kinase 1 and 2 (ULK1 and 2) were first discovered to be involved in autophagy by our laboratory in 2007 (Chan et al., 2007). The discovery of the Atg17 orthologue came shortly after and though it shares little sequence homology to the yeast protein, FIP200, also known as RB1CC1 for RB-1inducible coiled-coil 1, shares a functional role as an autophagy scaffolding protein (Hara et al., 2008). FIP200 has been shown to bind ULK1 in both nutrient-rich and amino acid-free conditions (Ganley et al., 2009), but ULK1 phosphorylates FIP200 in starvation (Figure 1.2) and they then travel together to the site of autophagosome formation (Jung et al., 2009). Our lab also uncovered the Atg13 homologue through sequence analysis and showed that it not only binds both ULK1 and ULK2 but is also a substrate for both kinases (Chan et al., 2009). Atg13 itself binds FIP200 (Hosokawa et al., 2009) (Jung et al., 2009) and it is proposed that Atg13 serves to stabilise the interaction of ULK1 and FIP200. Again, ULK1 kinase activity is highest when it is complexed together with Atg13 (or FIP200) and Atg13 is seen to go to the IM upon starvation (Chan et al., 2009), (Ganley et al., 2009), (Hosokawa et al., 2009).

Exciting new research has shown that the mammalian TOR kinase complex, mTORC1 directly binds to the ULK1-Atg13-FIP200 complex and that Raptor and ULK1 bind in nutrient-rich conditions but dissociate upon starvation (Hosokawa et al., 2009). In addition, multiple groups have shown that mTOR directly phosphorylates ULK1/2 and also Atg13 (Ganley et al., 2009), (Hosokawa et al., 2009), (Jung et al., 2009). Atg101, a fourth Atg13-binding protein that is not conserved in yeast was seen to interact with the Atg13-ULK1-FIP200 complex in an Atg13-dependent manner and is required for and possibly promotes autophagy by stabilising Atg13 (Mercer et al., 2009). Corroborating evidence of the importance of ULK1 and its interactions with its adaptor proteins and mTOR itself for the initiation of autophagy, a recent study of the hierarchy of mammalian autophagy proteins places ULK1 and FIP200 as the most upstream at the site of autophagosome formation (Itakura and Mizushima, 2010).

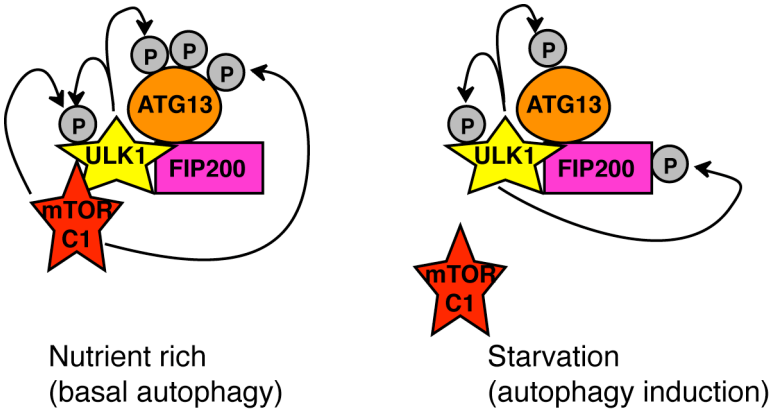

Figure 1.2 ULK1 kinase complex
In nutrient-rich conditions ULK1 binds to partners Atg13 and FIP200 and also raptor of the mTORC1 kinase complex. ULK1 autophosphorylates and phosphorylates Atg13. mTORC1 phosphorylates ULK1 and Atg13. In amino-acid starvation conditions, mTORC1 dissociates from the ULK1 kinase complex and no longer phosphorylates ULK1 or Atg13. ULK1 still autophosphorylates but phosphorylates Atg13 less. ULK1 also now phosphorylates FIP200. Modified from Chan and Tooze (Chan and Tooze, 2009).

There are five potential paralogues in the ULK family, ULK1, ULK2, ULK3, ULK4 and STK36 also known as Fused (Chan and Tooze, 2009). ULK1 and ULK2 show the most homology to Atg1 of other species and thus to each other. ULK3, ULK4, and Fused exhibit homology to Atg1 only in their kinase domains. Being most similar, ULK1 and ULK2 share functionality during development in mammals and though ULK1 and ULK2 are very similar it is only ULK1 knock-down that inhibits starvation-induced autophagy in HEK293 cells; ULK2 is not required (Chan et al., 2007). It has been shown that ULK2 binds Atg13 and FIP200 with different efficiency to ULK1 (Jung et al., 2009) suggesting that ULK2 cannot be exchanged for ULK1 in the model above (Figure 1.2). We have shown that though overexpression of kinase-dead versions of both ULK1 and ULK2 blocks autophagy, acting as dominant-negatives, overexpression of wild-type ULK1 and ULK2 has differential effects (Chan et al., 2009). Confounding, mice with a targeted deletion of ULK1 develop normally and exhibit generally functional autophagy, though they do show defects in autophagic mitochondrial clearance (Kundu et al., 2008). The most likely theory to explain the discrepancy between the actions of ULK1 and ULK2 is that ULK2 compensates for ULK1 during long-term deletion experiments but not short-term siRNA-based knock-downs. Recently, a role for ULK3 in autophagy-mediated oncogene induced senescence has been described suggesting this paralogue has specific non-starvation-induced functions (Young et al., 2009).

1.2.2 PI3-kinase complexes

The action of the autophagy-regulating class III PI3-kinase complex, like the ULK1 complex, acts early in the process and is required for nucleation of the isolation membrane. It was discovered very early on that treatment with 3-methyladenine (3-MA), an inhibitor of the PI3-kinases, inhibits autophagy (Seglen and Gordon, 1982). Since then, it has emerged that the production of Phosphatidylinositol(3)P, also known as PtdIns(3)P or PI(3)P, is essential for the formation of the autophagosome and it is the class III phosphatidylinositol (PI) 3-kinase Vps34 that is responsible through its phosphorylation of phosphoinositides (PIs) at position 3 on their inositol ring to produce PI(3)P (Simonsen and Tooze, 2009). 3-MA also inhibits the class I PI3-kinase that produces PI(3,4,5)P3 that in turn activates mTOR by way of Akt/PKB, thereby signalling to inhibit autophagy. However, the effect of inhibition of Vps34 wins out over the Akt pathway as the class III PI3-kinase, also known as PI3KC3, and production of PI(3)P are both essential requirements for autophagy.

The lipid kinase vacuolar protein sorting (Vps) 34 and its complex, including the Vps15 regulatory subunit and the accessory autophagy proteins Atg14 and Atg6 were first described as requirements for autophagy in yeast (Kihara et al., 2001b). The mammalian homologue of Vps15 is p150 and is also called PIK3R4 for phosphoinositied-3-kinase, regulatory subunit 4; this protein anchors the Vps34 complex to membranes (Figure 1.3). The mammalian homologue of Atg6 is Beclin 1 or BECN, a coiled-coil protein, and together with the newly identified human orthologue of Atg14, they form the mammalian PI3K Complex 1 (Figure 1.3).

Human Atg14 was only recently identified and was also called BARKOR, standing for beclin 1-associated autophagy-related key regulator (Itakura et al., 2008), (Sun et al., 2008). Atg14 has since been shown to be required for autophagosome formation and more specifically for the recruitment of Atg16 and LC3, essential proteins of the isolation membrane to be discussed below, to the site of autophagosome formation (Itakura et al., 2008), (Zhong et al., 2009), (Matsunaga et al., 2009). Unique as a member of the PI3-K complex, Atg14 interacts with both Beclin 1 and Vps34 and its coiled-coil domain is key for its binding. Atg14 itself is recruited to Atg16-positive and LC3-positive IM structures but Atg14 is found on these structures without Beclin 1 and Vps34 and the kinase activity of Vps34 is not required, suggesting it is Atg14 that

dictates when and where autophagosome nucleation occurs possibly by recruiting Vps34 to this site and even stimulating its activity (Matsunaga et al., 2009). Overexpression of Atg14 increases autophagosome formation and it is required for the autophagy-mediated elimination of salmonella (Sun et al., 2008).

Another coiled-coil protein UVRAG (UV radiation resistance associated gene) binds to Beclin 1 (Liang et al., 2006) and UVRAG does not associate directly with Vps34 Complex 1 but actually forms a distinct complex containing p150, Vps34 and Beclin 1, but not Atg14 (Itakura et al., 2008), (Figure 1.3). Though Itakura *et al* claim it is not required for autophagy, Liang *et al* show that UVRAG directly associates with Beclin 1 and is in turn required for autophagy (Liang et al., 2008). UVRAG seems to compete with Atg14 for Beclin 1 binding leading to two mutually exclusive complexes (Sun et al., 2008), though the role of the UVRAG complex in autophagy is still unknown. The protein Bif-1, also called SH3GLB1 or SH3-domain GRB2-like endophilin B1 may provide some insight; Bif-1 is required for autophagy (Takahashi et al., 2007). Like many others, it has a coiled-coil domain and interacts with Beclin 1 through a direct interaction with UVRAG. Bif-1 has other roles in membrane traffic and is required for fission of Golgi carriers; it is suggested that Bif-1 may be required for autophagosome membrane expansion and curvature through its N-BAR membrane curvature domain and its binding to the tethering factor ARF-GAP (Simonsen and Tooze, 2009). Following on, recently Bif-1 was shown not to act on autophagy initiation but to regulate degradative endocytic traffic and in turn, autophagosome maturation (Thoresen et al., 2010).

Among the recent eruption of research surrounding the Vps34 kinase complex is data describing yet-another Beclin 1-binding protein, RUBICON (an acronym for run domain Beclin-1 interacting and cysteine-rich containing protein, still annotated as KIAA0226) (Matsunaga et al., 2009), (Zhong et al., 2009). Rubicon resides in a separate complex to UVRAG and binds Atg14, complexing with Beclin 1 and Vps34 to form the Rubicon complex (Figure 1.3). Opposite to Atg14, RUBICON knock-down increases autophagy by inhibiting fusion of the autophagosome with the lysosome and also the maturation of endosomal vesicles to lysosomes (Matsunaga et al., 2009). GFP-tagged RUBICON is found on endosomes and lysosomes and over-expression of RUBICON inhibits autophagosome turnover confirming its role as a negative regulator

of fusion. Zhong *et al* also show that over-expression of the protein causes aberrant expansion of late endosomes and lysosomes (Zhong et al., 2009).

A sixth Beclin 1-binding protein, Ambra1 also contributes to a distinct Vps34 complex (Fimia et al., 2007), (Figure 1.3). The WD-repeat-containing protein is not only a positive regulator of Beclin 1 but is also required for starvation-induced autophagy. The role of the Ambra1 complex in autophagy initiation is not known.

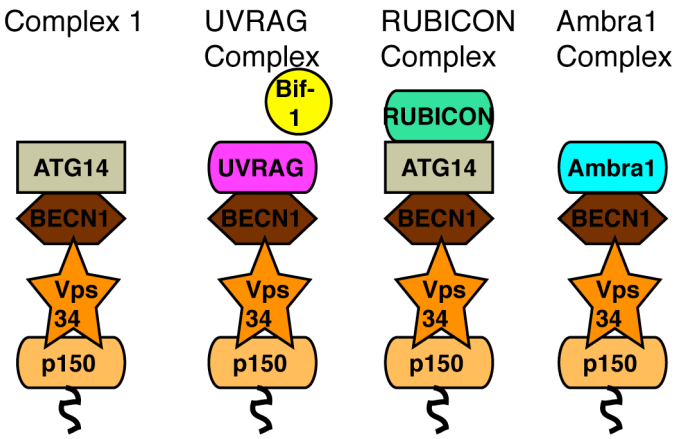

Figure 1.3 PI3-kinase complexes that control autophagy
Four distinct PI3-Kinase complexes, Complex 1, the UVRAG Complex including UVRAG-binding protein Bif-1, the Rubicon Complex and the Ambra1 complex are shown. The complexes all share the components p150, Vps34, and Beclin 1 (BECN). Complex 1 and the Ambra1 complex are positive regulators of autophagy while the Rubicon complex is a negative regulator. Contrasting roles of the UVRAG complex are reported. Adapted from Simonsen and Tooze (Simonsen and Tooze, 2009).

Though p150 is a shared regulatory component of the complex and Vps34 is the essential kinase, Beclin 1 is the protein that mediates the interactions of the auxiliary proteins that distinguish the four known complexes. Through its differential binding, Beclin 1 may act as a switch between the complexes in order to coordinate the regulation of autophagy in highly evolved species. As a master regulator, Beclin 1 may balance autophagosome nucleation and maturation by toggling between Complex1 and the UVRAG complex and also the RUBICON complex. Beclin 1 also plays a role in apoptosis through its binding to the anti-apoptotic protein Bcl-2 (Pattingre et al., 2005). Bcl-2 negatively regulates Beclin 1 by keeping it away from its PI3-kinase complex partners and thereby preventing autophagy. Beclin 1 may not only be important for the balance of autophagosome formation and maturation but sits between autophagy and apoptosis, making it an important modulator of cell death versus survival.

1.2.3 Ubiquitin-like conjugation systems

Two ubiquitin-like conjugation reactions produce the Atg5-Atg12-Atg16 complex and lipidated Atg8 and are essential for the formation and elongation of the autophagosome. Many detailed studies have resulted in a thorough understanding of how these critical autophagy proteins contribute to the expansion of the double-membrane vesicle (Klionsky, 2005).

1.2.3.1 Atg12 conjugation reaction

In mammalian cells, Atg12, a ubiquitin-like (UBL) protein is conjugated to Atg5 through a multi-step conjugation reaction that requires the enzymatic activities of E1-like and E2-like proteins. First Atg12 is activated by the E1-like enzyme Atg7 and then transferred to the E2-like enzyme Atg10 which then catalyses the conjugation of Atg5 to Atg12 (Mizushima et al., 1998b), (Figure 1.4). Subsequently, the Atg5-Atg12 complex is covalently bound to Atg16 and this trimeric complex homodimerises to become a large, 800 kDa complex (Mizushima et al., 2003). Mammalian Atg5 is an important marker for early autophagosome formation and GFP-tagged Atg5 localises to the isolation membrane (Mizushima et al., 2001). Atg5 is an essential gene and is required for survival in the post-natal starvation period (Kuma et al., 2004). Mammalian Atg16 differs from yeast in that it contains a C-terminal WD40 repeat domain for multi-protein complex assembly and, as mentioned above, is recruited to the isolation membrane, most likely by Atg14.

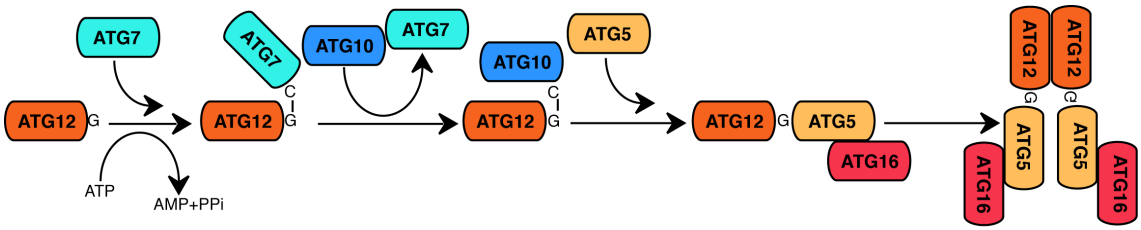

Figure 1.4 Atg5-Atg12 conjugation system
Atg5 is conjugated to a C-terminal glycine on the UBL Atg12 through the actions of the E1-like Atg7 and E2-like Atg10. Atg16 is added to the complex which then homodimerises.

1.2.3.2 Atg8/LC3 conjugation reaction

Atg8, the yeast UBL protein that is lipidated and integrated into the autophagosomal membrane has multiple homologues in mammals grouped into LC3-like and GABARAP-like subgroups. LC3, short for microtubule-associated protein 1 light chain 3 beta, is the best characterised Atg8 homologue and was the first to be shown to localise to the autophagosome with electron microscopy (EM) (Kabeya et al., 2000). To begin the LC3 lipidation reaction, LC3 is primed by the cysteine endopeptidase Atg4, exposing a C-terminal glycine (Hemelaar et al., 2003), referred to as the LC3I form. Next, Atg7, which serves as the E1-like enzyme for both conjugation reactions, activates LC3 and then the E2-like enzyme Atg3 facilitates the conjugation of phosphatidylethanolamine (PE) to LC3 (Tanida et al., 2002), (Figure 1.5). In the same way, GABARAP and GABARAPL2 (also known as GATE16) can be post-translationally processed and bound to PE (Kabeya et al., 2004). It has been demonstrated that phosphatidylserine (PS) can also be conjugated to LC3 *in vitro* (Sou et al., 2006) but it has been shown that factors such as the pH of the cytosol *in vivo* dictate the preferential lipidation of LC3 with PE (Oh-oka et al., 2008). Once LC3 is lipidated and becomes part of the autophagosome, it remains membrane-bound and can be followed from isolation membrane expansion until fusion with and degradation by the lysosome. As a result, LC3 and GFP-tagged LC3 are bone fide markers of the AV (Rubinsztein et al., 2009), and we can measure LC3's flux through the pathway visually or by western blot analysis in order to monitor autophagy (Klionsky et al., 2008).

After closure of the autophagosome, Atg4 cleaves LC3 from PE thereby removing LC3 from the mature autophagosome (Tanida et al., 2004), a step that is critical for its fusion with endosomes and lysosomes. Experiments with an Atg4 mutant have shown that priming LC3 is critical for the early Atg7-mediated step of the conjugation pathway but the Atg4 mutant also led to defects in the closure of the expanded autophagosome, suggesting that the lipidated, or LC3II form of the protein is needed for the membrane curvature required to close the vesicle (Fujita et al., 2008).

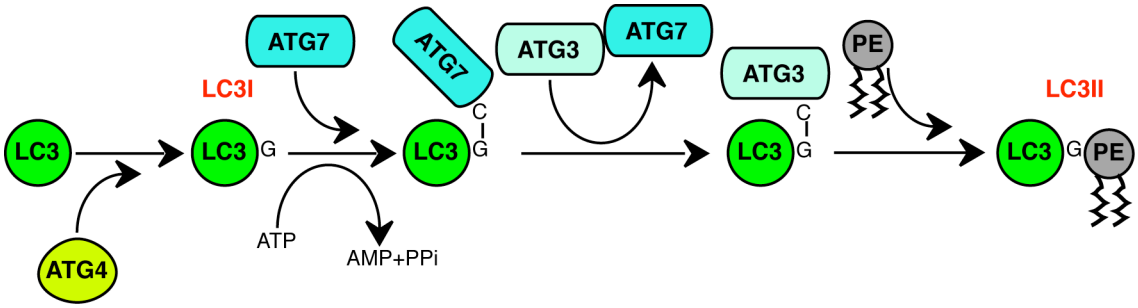

Figure 1.5 LC3 is conjugated to PE
Atg4 cleaves a C-terminal cysteine on LC3, exposing a glycine to which Atg7 is added then replaced by Atg3, which catalyses the conjugation of the phospholipid, phosphatidylethanolamine (PE) to LC3. The unlipidated form of LC3 is referred to as LC3I and the lipidated as LC3II. Adapted from Sou *et al*, (Sou et al., 2006).

1.2.3.3 Cross-talk between the two ubiquitin-like pathways

Current evidence points to an interplay between the ubiquitin-like conjugation pathways, beyond sharing their E1-like enzyme Atg7. It is generally believed that the Atg5-Atg12 reaction occurs upstream of the LC3 lipidation pathway and a recent paper solidifies the notion that the Atg5-Atg12-Atg16 complex lies before LC3 lipidation in that the trimeric complex is required for the recruitment of LC3II to the site of autophagosome formation (Fujita et al., 2008). The authors, by artificially forcing Atg16 to the plasma membrane, captured lipidated LC3 on the PM where it is normally not seen. Because LC3 has no localisation signal of any kind, they suggest that Atg16 defines the site of vesicle formation. In addition, exciting evidence shows, at least *in vitro*, that the Atg5-Atg12 complex acts as an E3-like enzyme, conferring specificity to the conjugation of LC3 to PE (Hanada et al., 2007). Conversely, overexpressed Atg3 enhances Atg5-Atg12 conjugation (Tanida et al., 2002) and it has been shown that LC3 conjugation is important for the formation of the Atg5-Atg12 complex using Atg3 negative mouse embryonic fibroblasts (MEFs), which are impaired for Atg5-Atg12 conjugation (Sou et al., 2008). Supporting the role for lipidated LC3 in membrane fusion or closure, these Atg3 negative cells also show a distinct reduction of autolysosomes. Solidifying the evidence for cross-talk between the two pathways, Atg3, the E2-like enzyme for LC3 lipidation is also a substrate for Atg12 conjugation (Radoshevich et al., 2010). Though this novel Atg3-Atg12 conjugate is not required for starvation-induced autophagy it does seem to regulate mitochondrial homeostasis

because without it, mitochondria were seen to swell and mitochondrial-mediated cell death was compromised.

1.2.4 Atg9 recycling complex and WIPI2

The only membrane-spanning autophagy core complex protein is Atg9. It has six trans-membrane spanning domains and its association with membrane and extrapolation from yeast studies suggests that mammalian Atg9 (mAtg9) may deliver membrane to forming autophagosomes; but as of now, there is no known function designated to Atg9. In yeast, Atg9 is seen to cycle between the PAS and a peripheral pool that has recently been shown to comprise of clusters of vesicles and tubules often found close to mitochondria (Mari et al., 2010). Atg1 is required for this cycling but Atg9's movement is not dependent on Atg1 kinase activity (Reggiori et al., 2004). The localisation of Atg9 to the PAS depends on a small set of proteins: Atg2, Atg8, Atg14, and Atg18 (Suzuki et al., 2007), and retrieval from the PAS, which occurs prior to autophagosome formation requires Atg1, Atg2, Atg18, which localises Atg2 and PI3-kinase (Reggiori et al., 2004). The mammalian homologue of Atg2 has been annotated but to this date, has not been characterised.

Mammalian Atg9 is required for autophagy and is an essential gene for survival; Atg9 knock-out mice cannot survive past P0 much like Atg3, Atg5 and Atg7 knock-out mice (Saitoh et al., 2009). Similar to yeast Atg9, mAtg9 cycles between two pools, residing in a juxta-nuclear Golgi pool in full medium but dispersing to a peripheral, perhaps endosomal, pool upon amino-acid withdrawal (Young et al., 2006). As in yeast, this translocation requires ULK1 and we recently showed that it also requires Atg13 (Chan et al., 2009). Regulation of autophagy was recently linked to the p38 MAP kinase pathway through Atg9, for it was demonstrated that the cycling of Atg9 requires the Atg9- and p38-interacting protein p38IP and through these interactions, p38α acts as a negative regulator of autophagy (Webber and Tooze, 2010).

Atg18 interacts with Atg9 in yeast and recently the mammalian homologues of Atg18, WIPI (WD-repeat protein Interacting with PhosphoInosides) family proteins, have been characterised (Proikas-Cezanne et al., 2004), (Polson et al., 2010). WIPI2 is contains a non-canonical PI(3)P binding region and WIPI2, as well as being required for autophagy, forms puncta upon starvation that partially localise with Atg16, GFP-LC3

and ULK1, placing it very early in the hierarchy of autophagy proteins. As it is not seen to bind endosomes, WIPI2 is thought to be a specific effector of the autophagy-specific cellular pool of PI(3)P.

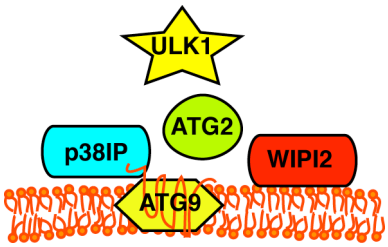

Figure 1.6 Putative mammalian Atg9 recycling complex
Mammalian Atg9, with its six transmembrane-spanning regions, is shown. Atg9-interacting protein p38IP and putative interacting partners Atg2 and WIPI2, the mammalian homologue of Atg18, are shown. ULK1 is required for the relocalising of Atg9 from the Trans-Golgi network (TGN) to a peripheral pool.

1.2.5 Summary of mammalian and yeast Atg proteins

Mammalian name	Mammalian reference	Function	Yeast name	Yeast reference
ULK1	(Chan et al., 2007)	Serine/threonine kinase	ATG1	(Matsuura et al., 1997)
ULK2	(Chan et al., 2007)	Serine/threonine kinase	N/A	N/A
ULK3	(Young et al., 2009)	Serine/threonine kinase	N/A	N/A
ATG2	x	Interacts with ATG18	ATG2	(Reggiori et al., 2004)
ATG3	(Tanida et al., 2002)	E2-like enzyme for LC3 lipidation	ATG3	(Schlumpberger et al., 1997)
ATG4	(Hemelaar et al., 2003)	Cysteine protease primes Atg8/LC3	ATG4	(Lang et al., 1998)
ATG5	(Mizushima et al., 2001)	Conjugated to Atg12	ATG5	(Mizushima et al., 1998a)
BECN1	(Liang et al., 1999)	Core component of the Vps34 PI3-kinase complex	ATG6/VPS30	(Kihara et al., 2001b)
ATG7	(Tanida et al., 2002)	E1-like enzyme	ATG7	(Tanida et al., 1999)
MAP1LC3B	(Kabeya et al., 2000)	UBL conjugated to PE; incorporated into AV membrane	ATG8	(Lang et al., 1998)
GABARAP	(Kabeya et al., 2004)	UBL conjugated to PE	N/A	N/A
GABARAPL2	(Kabeya et al., 2004)	UBL conjugated to PE	N/A	N/A

ATG9	(Young et al., 2006)	Integral membrane protein	ATG9	(Noda et al., 2000)
ATG10	(Mizushima et al., 1998b)	E2-like enzyme for Atg5-Atg12 conjugation	ATG10	(Mizushima et al., 1998a)
ATG12	(Mizushima et al., 1998b)	Ubiquitin-like protein conjugated to Atg5	ATG12	(Mizushima et al., 1998a)
ATG13	(Chan et al., 2009)	Phosphoprotein; part of ULK1 kinase complex	ATG13	(Funakoshi et al., 1997)
ATG14	(Itakura et al., 2008), (Sun et al., 2008)	Protein binder; accessory to the Vps34 PI3-kinase complex	ATG14	(Kihara et al., 2001b)
ATG16	(Mizushima et al., 2003)	Atg5-Atg12 super complex component	ATG16	(Mizushima et al., 1999)
FIP200	(Hara et al., 2008)	Scaffolding protein	ATG17	(Kamada et al., 2000)
WIPI2	(Polson et al., 2010)	Mammals: PI(3)P-binding protein. Yeast: membrane protein that localises Atg2	ATG18	(Barth et al., 2001)

Table 1.1 Summary of the mammalian autophagy genes
The mammalian name, yeast name and function and corresponding references for 20 autophagy genes are listed. Adapted from Klionsky *et al* (Klionsky et al., 2003).

1.3 Autophagy signalling/regulation of autophagy

In yeast, autophagy is directly activated by the loss of negative regulation by TOR through amino acid starvation or TOR inhibition with rapamycin (Noda and Ohsumi, 1998). In mammalian cells, the mTOR kinase complex mTORC1 also acts as the key negative regulator of autophagy as well a positive regulator of cell growth and autophagy is activated by inhibition of TOR with drugs such as rapamycin (Figure 1.7). Amino acids stimulate TOR and promote the phosphorylation of ribosomal S6 protein (RS6) by p70S6 kinase and a decrease in phosphorylated RS6 reflects an induction of autophagy by starvation or rapamycin (Blommaart et al., 1995). Recently, Rag GTPases and three proteins in a complex called the 'Ragulator' have been shown to signal mTOR in response to amino acid starvation and also translocate mTOR to the lysosome membrane (Sancak et al., 2010). mTOR loss stimulates autophagy by directly affecting ULK1, but adding complexity, ULK1 and ULK2 have been shown to feedback to the mTOR-p70S6 kinase pathway (for review, see (Chan and Tooze, 2009)). In fact, in *Drosophila* autophagy inhibits cell growth and Atg1 itself can directly inhibit Tor signalling suggesting positive feedback (Neufeld, 2007).

Nutrients like amino acids can directly signal mTOR through the Rag-Ragulator complex but a lack of amino acids can also activate autophagy independently from mTOR. For instance, amino acids inhibit the Raf-1-MEK1/2-ERK1/2 signalling cascade that in turn inhibits autophagy (Ogier-Denis et al., 2000). Other TOR-independent autophagy activation pathways have been reported including that induced by lithium chloride, which appears to act through modulation of myo-inositol-1,4,5 triphosphate (IP_3) levels (Sarkar et al., 2005). Although conflicting data does exist, one group reports that resveratrol also drives autophagy independent of TOR by activating sirtuins that deacetylate autophagy proteins which activates autophagy (Morselli et al., 2010).

As previously discussed, 3-MA and also wortmannin inhibit autophagy through the inhibition of the class III PI3-K product PI(3)P; but 3-MA also inhibits class I PI3-K which is a negative regulator of autophagy through the Akt-TSC1/2-Rheb-mTOR signalling pathway (Petiot et al., 2000). Growth factor (insulin) signalling inhibits autophagy through stimulation of IRS1 and IRS2, which activate the class I PI3-kinase. Alternately, overexpression of PTEN stimulates autophagy by inhibiting the inhibitory Akt pathway (Arico et al., 2001). The anti-apoptotic protein Bcl-2 inhibits autophagy by sequestering Beclin 1 away from Vps34 and it was recently demonstrated that starvation removes Bcl-2, through direct phosphorylation by JNK1, from the class III PI3-kinase complex 1 (Wei et al., 2008). In addition, energy inhibits LKB1, a positive regulator of autophagy that activates AMPK (which also senses reduced ATP levels itself), and this pathway is activated in stress conditions (Liang et al., 2007). Autophagy is also influenced by p53, a master regulator of cell cycle progression and apoptosis, in opposing ways. Basal levels of the cytoplasmic form of the protein inhibit autophagy and its degradation leads to the induction of autophagy (Tasdemir et al., 2008a) but in times of cellular stress, p53 can activate both autophagy and apoptosis (Vousden and Ryan, 2009).

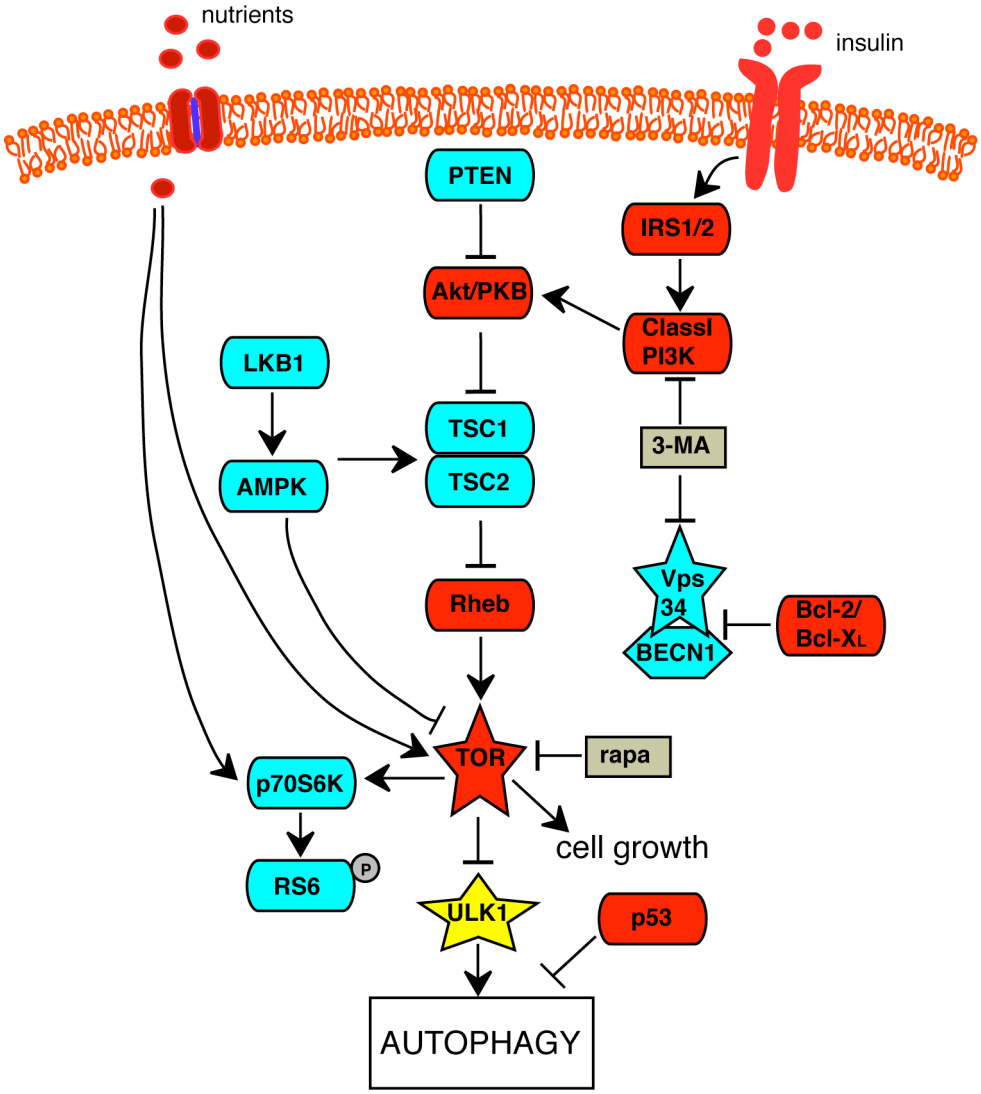

Figure 1.7 Mammalian autophagy signalling
Inhibitory (red) and activating (blue) autophagy signalling proteins. Nutrients (amino acids, glucose) and insulin and other growth factors inhibit autophagy through multiple pathways. 3-MA is 3-methyladenine, rapa is rapamycin. Adapted from Yang and Klionsky (Yang and Klionsky, 2010).

1.4 Source of the autophagosome membrane

Though many of the essential proteins and machinery required for autophagosome nucleation and expansion are known (as discussed above), the source of the membrane and the mechanism for IM formation are mostly unknown. The origin of the membrane has been in question since the discovery of the double membraned vesicle and is recently the subject of intense debate and concentrated research. Autophagy scientists strive to determine whether the membrane forms de novo from localised lipid synthesis or is derived from a pre-existing organelle or organelles. In yeast it is perhaps more

simple, as autophagosomes always form at the PAS and next to the vacuole. But in mammalian cells, autophagosomes seem to be able to form anywhere in the cytoplasm and a distinct place of origin, like the PAS, does not exist. Isolation membranes may form from a PAS-like structure or the IM itself could be the mammalian equivalent of the PAS, but this is not known. Perhaps the difficulty arises from a lack of protein markers, both for the autophagosome and of other membrane sources found in the autophagosomal membrane (Overbye et al., 2007). Using current methods, it is difficult to differentiate between the autophagosome membrane and the membrane of the organelles it engulfs and our two primary marker proteins, Atg5 and LC3 associate with the isolation membrane only after it begins to form so earlier markers and non-transient markers are needed (Tooze and Yoshimori, 2010). Multiple recent studies have increased our knowledge of the origin of the autophagosome and point to the ER, mitochondria and even the plasma membrane as possible sources of the membrane (Hayashi-Nishino et al., 2009), (Yla-Anttila et al., 2009), (Hailey et al., 2010), (Ravikumar et al., 2010).

1.4.1 De novo formation of autophagosomes

The autophagosome membrane is unique in many ways. Containing two lipid bilayers, the organelle requires a large amount of membrane, but a distinct lack of organelle markers obtained from purified fractions of the mammalian autophagosomes is remarkable (Stromhaug et al., 1998). In addition, the autophagosome membrane is for the most part devoid of transmembrane proteins and, in general, the membrane is relatively protein-poor (Fengsrud et al., 2000). These findings suggest that autophagosomes are distinct from other membrane-bound vesicles, supporting a de novo mechanism of lipid synthesis and construction in unspecified locations throughout the cell. To this date, however, no lipid synthesising enzymes have been found at the phagophore assembly site.

1.4.2 Golgi apparatus as a source of the autophagosomes

In yeast, the Golgi apparatus is the only organelle with evidence to support its donation to the autophagosome membrane. The essential membrane-bound protein Atg9, as discussed previously, cycles between the Golgi and various cytoplasmic punctate structures and is hypothesised to be involved in supplying membrane to the

PAS. Upon starvation, Atg9 disperses and the peripheral Atg9-containing structures are essential for the generation of the PAS and have been shown to be derived from the Golgi (van der Vaart and Reggiori, 2010). Recently, multiple Golgi proteins have been shown to play a role in autophagy in yeast. Golgi-localising Sec7 and guanine nucleotide exchange factors (GEFs) Gea1 and Gea2 control autophagy by activating GTPases Arf1 and Arf2 (van der Vaart et al., 2010). The GEFs normally control exit from the Golgi but their function is also required for autophagy; interestingly, they seem to be required not for PAS localisation but for expansion of the phagophore. Independently, Dan Klionsky's group have shown that the post-Golgi proteins Sec2 (a GEF) and downstream GTPase Sec4 are also required for autophagy perhaps by diverting membrane to the Golgi to expand the autophagosome (Geng et al., 2010). Last, the TRAPP complex 3, which serves as a Golgi tethering factor has been shown to localise to the PAS (Yen et al., 2010). The subunits of the conserved oligomeric Golgi (COG) are involved in autophagosome formation and are speculated to fuse together Golgi-derived membranes and the PAS. Perhaps Atg9 is also acting as a Golgi-derived regulator of this process, helping to tether together the Golgi and the PAS because Atg9 directly interacts with the COG subunits and Sec7 mutants show a blockage of transport of Atg9 membranes to the PAS, thereby inhibiting autophagosome formation (van der Vaart et al., 2010).

Extrapolating to mammalian cells, Atg9 could also shuttle membrane to the growing phagophore and Atg9 is recruited to the forming autophagosome from the TGN where it localises in nutrient-rich conditions. Although more evidence for the role of Atg9 in vesicle expansion is needed, its subcellular localisations support a role for both the juxta nuclear Golgi region and endosomal compartments. Like Atg9, Beclin 1 localises to the TGN in full growth conditions (Kihara et al., 2001a) and is essential for IM nucleation. Bif-1 is another Golgi-resident protein (it is also associated with mitochondria) and it activates class III PI3-kinase to induce autophagy (Takahashi et al., 2007) and more recently is linked to autophagosome expansion and maturation (discussed above). Together, these proteins support a role for a post-ER Golgi compartment in the formation of the autophagosome.

1.4.3 Endoplasmic reticulum (ER) as a source for the autophagosome

Original observations of mammalian autophagosome lead De Duve to believe that the autophagic vesicles' membrane came from pre-existing membrane like the ER (De Duve and Wattiaux, 1966), though it has been difficult to distinguish between the autophagic degradation of the ER (ER-phagy), a process that was discovered early on in autophagy research (Bolender and Weibel, 1973), and the use of the ER membrane for the formation of the autophagosome.

Recent exciting data illustrates how the endoplasmic reticulum forms a platform for autophagosome formation. The discovery of the ER protein DFCP-1 links the ER to autophagosome formation (Axe et al., 2008). Through its double FYVE-domain, DFCP-1 binds the autophagic pool of PI(3)P and translocates from the Golgi to sites close to ER membrane where it congregates in response to amino acid starvation. These sites, called omegasomes, are rich in PI(3)P and autophagosomes are seen to emerge from the omegasome. Though knock-down of DFCP-1 does not inhibit starvation-induced autophagy, the recruitment of ULK1, Atg14 and also the PI(3)P effector protein WIPI2 to the omegasome is essential (Axe et al., 2008), (Polson et al., 2010). The ER membrane is not rich in PI(3)P and so it is critical that the PI(3)P-binding protein WIPI2 translocates to omegasomes in order bring the phospholipid so that omegasomes progress to autophagosomes. DFCP-1-containing omegasomes serve as ER platforms for the recruitment of the Atg5 and then LC3 and in turn, autophagosome formation, though the physical properties that anchor the omegasome to the ER and then allow the autophagosomes to bud off from the omegasome remain to be discovered.

Two complementary tomography studies have demonstrated physical interactions between the isolation membrane and the ER (Hayashi-Nishino et al., 2009), (Yla-Anttila et al., 2009). Tomatsu Yoshimori's group show in NIH3T3 cells and MEFs, that the IM and the ER are interconnected. They demonstrate isolation membranes sandwiched between two ER membranes, labelled with DFCP-1; the ER-juxtaposed phagophores suggest a "cradle" model where enwrapped isolation membranes grow out of omegasomes. Eeva-Liisa Eskelinen's tomography work on normal rat kidney cells also reveals connections between the ER and phagophore and they show enriched ER membranes within the budding autophagosomes.

As mentioned, the ER is not an ample source of PI(3)P and thus this lipid must be recruited to omegasomes in order for autophagy to proceed. Most recently, it was uncovered that Atg14 targets the PI3-kinase complex to the ER leading to the production of PI(3)P and the recruitment of autophagy proteins (Matsunaga et al., 2010). Knock-down of Atg14 abolishes the omegasome, suggesting that Atg14 anchors to the ER and recruits DFCP-1 and the ER localisation of Atg14 is critical for autophagosome formation. Atg14 localises to the ER in nutrient-rich conditions, contains an ER-targeting domain and is enriched in the organelle upon starvation, a process that requires ULK1.

1.4.4 Mitochondria as a source for the autophagosome

One artificial marker of the mitochondrial outer membrane has lately been shown to also colocalise with the autophagy proteins Atg5 and LC3 (Hailey et al., 2010). Experiments suggest that the colocalisation of tagged LC3 and an outer leaflet-anchored protein is not due to selective autophagic degradation of the mitochondria (mitophagy) and the authors believe that this phenomenon has been underreported because people ascribe similar findings to mitophagy. Using high-resolution imaging, the group shows that autophagosomes colocalise with mitochondria but also establish that mitochondrial membrane proteins are sterically excluded from the forming autophagosomes. A protein that connects the ER to the mitochondria, mitofusin2, is critical for autophagy induction suggesting that interplay between the two organelles is important. Also, the ER and the mitochondria have recently been shown to connect through the ERMES protein complex (Kornmann, 2010). Mitochondria are more enriched for PE than the ER and could supply newly synthesised lipid for forming autophagosomes.

1.4.5 Plasma membrane as a source for the autophagosome

LC3 can also be recruited to plasma membrane (PM)-derived membranes (Sanjuan et al., 2007) and recent evidence suggests that endocytic clathrin coated vesicles (CCVs) derived from the PM contribute to the formation of isolation membranes (Ravikumar et al., 2010). David Rubinsztein's group discovered that Atg16 interacts with clathrin heavy chain (CHC) and AP2 which are required for vesicle budding from the PM and sorting endosomes and cargo recruitment to CCVs onto the

PM and early endosomes respectively. Knock-down of CHC and AP2 significantly decreased basal autophagy and blocking clathrin-dependent endocytosis inhibited the number of newly formed autophagosomes, though marginally, suggesting that the PM is not the only source of the membrane. Atg16 was found on IM precursor structures close to the plasma membrane and marking these membranes with cholera toxin lead to the incorporation of the toxin in the autophagosomal membrane. The plasma membrane is highly dynamic and contains a large amount of lipid bilayer that may be utilised when a drastic increase in the number of autophagosomes is required, like during amino-acid starvation.

Taken together, these results suggest that the Golgi, ER and mitochondria are important for autophagosome formation. In addition, it has been demonstrated that endosomes are required for autophagy (for review, see (Longatti and Tooze, 2009)). Together with the plasma membrane, all of these could be sources of lipid for the autophagosomes. The origin of the isolation membrane is difficult to determine because it seems that ER or mitochondrial membrane proteins are excluded from newly formed autophagosomes. It is conceivable that there are multiple sources of the AV membrane and that different inductions of autophagy exploit different membranes, especially basal versus starvation-inducing conditions, and even different cargos may dictate membrane recruitment. In addition, supply of the membrane could depend on the organism or cell or tissue type. Overall, the diverse nature of the formation of the autophagosome supports the notion that autophagy is critical but adaptable.

1.5 Role of p62 in autophagy

Autophagy is responsible for the degradation of long-lived proteins but also degrades damaged or unfolded proteins. These short-lived proteins become polyubiquitinated and are targeted to the UPS but can also be sent to the autophagy pathway. p62, also known as sequestosome 1 (SQSTM1) is responsible for directing these proteins to the autophagosome; it is a multi-functional adaptor protein that binds polyubiquitinated proteins and aggregates by oligomerisation (Wooten et al., 2008). Though p62 is not required for starvation-induced autophagy, it is a specific substrate for the process and its autophagy-induced degradation can be used as a read-out for autophagy function (Pankiv et al., 2007). In addition to binding ubiquitin (Ub), it also

binds to LC3 thereby recruiting the ubiquitinated proteins to the autophagosome (Shvets et al., 2008b), (Ichimura et al., 2008). Even large p62-positive inclusions can be degraded by basal constitutive autophagy making it an important neuroprotective process and the p62-dependent formation and degradation of polyubiquitin-containing bodies by autophagy maintains cell health. Together with LC3, p62 forms a casing around aggregates of mutant huntingtin thereby protecting the cell against Huntingtin-induced cell death (Bjorkoy et al., 2005). p62 has recently been demonstrated to translocate into the nucleus where it colocalises with promyelocytic leukaemia (PML) bodies and the nucleoplasm to cytoplasm shuffling of p62, which is possibly controlled by phosphorylation events, may serve as a regulatory mechanism for its role in autophagy (Pankiv et al., 2010).

Another LC3- and Ub-binding protein, neighbour of BRCA1 gene 1 (NBR1), also serves as autophagic receptor for ubiquitinated targets (Kirkin et al., 2009). Like p62, NBR1 contains an LC3-interacting region (LIR) and this motif is required for NBR1's degradation by autophagy, though p62 is not required. It seems that NBR1 cooperates with p62 to direct autophagic degradation of ubiquitinated targets and both can serve as markers of pathological inclusions. The clearance of these inclusions is an important homeostatic function that autophagy has gained in higher organisms, although the exact mechanism of how autophagy selectively degrades these substrates is not known.

1.6 Autophagy in Disease

Autophagy serves a critical purpose by regenerating macromolecules and amino acids to be used for the maintenance of vital cellular functions after conditions of cellular stress such as hypoxia, starvation and infection. Autophagy is also required during poor growth conditions directly after birth when nutrient supply from the placenta is disrupted. These are all normal situations cells or organisms will face and autophagy has adapted to maintain cellular house-keeping and protects against pathogens and aggregate-prone proteins; but when autophagy is disrupted multiple diseases can occur (Mizushima et al., 2008). In addition, the cell may use autophagy to fight xenobiotic invasion and other diseases. Thus, efficient autophagy is essential for cell heath and contributes to normal ageing and immunity as well as disease and cell death.

1.6.1 Crohn's Disease

A direct link between autophagy and inflammatory bowel disease was found as mutations in two autophagy genes are associated with increased Crohn's disease risk. A single Thymine to Adenine mutation of ATG16 confers increased risk and highlights the importance of autophagy in intestinal homeostasis and also immunity, both of which are involved in Crohn's disease (Hampe et al., 2007), (Rioux et al., 2007). It was shown that ATG16 is broadly expressed in the intestinal system as well as in immune cells. The T300A mutation is in the C-terminal WD repeat of the protein, a region not conserved in yeast, and neither the WD domain nor the mutated Thymine are required for canonical autophagy (Fujita et al., 2009). Instead, this region may be important for the stability of the Atg16 protein as the level of Atg16 is important for autophagy and Fujita *et al* suggest the levels are tightly maintained by the UPS. A mutation in the immunity-related GTPase family, M (IRGM) gene is also implicated in Crohn disease risk (Parkes et al., 2007). IRGM activates autophagy and clears intracellular mycobacteria through the induction of large autolysosomes (Singh et al., 2006). Together with other studies on the role of autophagy in both innate and adaptive immune responses (reviewed in (Levine and Deretic, 2007)), (Munz, 2010), these findings show that autophagy can capture and eliminate intracellular bacteria, process antigens for presentation, enhance innate immune responses and even control epithelial and immune cell fate thereby playing a critical role in cellular defence against pathogens.

1.6.2 Cancer

The cytoprotective functions of autophagy including the removal of damaged proteins and organelles and its response to cellular stress to mitigate damage caused by genotoxic stress not only restore balance but also protect the cell from cancer. In turn, multiple autophagy proteins are known tumour suppressors. Beclin 1 is a haploinsufficient tumour suppressor and the deletion of one Beclin 1 allele occurs in 40-75% of human breast, prostate, and ovarian cancer (Liang et al., 1999), (Aita et al., 1999). Beclin $1^{+/-}$ mice develop spontaneous tumours (Yue et al., 2003) and, as discussed above, Beclin 1 not only plays a critical role in autophagy but is also involved in apoptosis with Beclin 1 and the Bcl-2 antiapoptotic proteins controlling the balance between the two systems. UVRAG is also a tumour suppressor and overexpression of

the gene in a colon cancer cell line with a UVRAG mutation rescued autophagy (Liang et al., 2006). Mice lacking Atg4C show increased tumourigenesis due to impaired autophagy (Marino et al., 2007) and hypermethylation of Atg16 is associated with poorer prognosis in response to anti-cancer treatments (Dunwell et al., 2010) and as in Crohn's disease, the levels of Atg16 protein may dictate autophagy function. Also, the loss of PTEN function in cancer cells inhibits autophagy suggesting that autophagy contributes to the important tumour suppressor properties of PTEN (Arico et al., 2001). The role of the classic tumour suppressor p53 in autophagy is more complicated most likely due to the diverse cellular functions it controls including apoptosis, senescence, DNA repair and even metabolism (Vousden and Ryan, 2009). As mentioned above, basal cytoplasmic p53 inhibits autophagy and it does so in a cell-cycle-dependent fashion and deletion or inhibition of p53 induces autophagy (Tasdemir et al., 2008c), (Tasdemir et al., 2008b). But activation of p53 by DNA damage and cellular stress causes p53 to translocate into the nucleus and stimulate autophagy-inducing genes, thus acting as a tumour suppressor; one of these p53 target genes, DRAM, is a lysosomal protein with roles in both autophagy and apoptosis (Crighton et al., 2006). Autophagy protects the cell from and DNA damage (Mathew et al., 2007) and ROS, which have been shown to directly activate autophagy by oxidation of Atg4 (Scherz-Shouval et al., 2007). A mechanism for how autophagy suppresses tumourigenesis has recently been described: metabolic stress induces p62 to accumulate thus activating the DNA damage response (Mathew et al., 2009).

During cancer, autophagy can also protect through its function as a non-apoptotic, or type II cell death pathway. When apoptosis is not functioning, cells trigger autophagic cell death and thereby do not undergo necrosis that can result in local inflammation, which can promote tumour growth (Degenhardt et al., 2006). But autophagy in cancer is often referred to as a double-edged sword, as young, nutrient-hungry tumours can hijack the autophagy pathway in order to sustain rapid growth before they can recruit sustenance-supplying blood vessels through angiogenesis. In this way, autophagy acts as a cancer cell survival pathway (Mizushima et al., 2008). mTOR inhibitors are used to treat many cancers as they inhibit cell growth but mTOR inhibition also activates metabolism and autophagy, promoting tumour survival. Eileen White has shown promising new data suggesting that the combination of an mTOR

inhibitor with an autophagy inhibitor may shrink tumour xenographs in mice (White et al., 2010).

1.6.3 Neurodegeneration

Neurons are especially sensitive to the accumulation of damaged or aggregated cytosolic proteins or membranes and constitutive basal autophagy protects cells from this damage thereby preventing neurodegeneration (Tooze and Schiavo, 2008). Suppression of basal autophagy through the loss of the autophagy genes Atg5 or Atg7 causes neurodegeneration in mice (Komatsu et al., 2006), (Hara et al., 2006) and Atg7 is essential for the maintenance of axonal homeostasis; without it, intracellular proteins accumulate to toxic levels and axons degenerate (Komatsu et al., 2007). As discussed before, autophagy as well as the proteasome degrade misfolded proteins but p62 seems to distinguish when to direct these aggregates to the lysosome thereby preventing cell death (Bjorkoy et al., 2005).

Alterations of autophagy have been observed in many protein conformation diseases and one neurodegenerative disease with which it is associated is Huntington's disease (HD), caused by a polyglutamine expansion mutation in the huntingtin protein (htt) that confers a toxic gain-of-function. Autophagy degrades aggregate-prone mutant huntingtin (Ravikumar et al., 2002) and this is mTOR dependent (Ravikumar et al., 2004). In turn, the promotion of autophagy by rapamycin decreases these aggregates and it is proposed that combining rapamycin with another autophagy-inducing drug, lithium provides synergistic protection against neurodegeneration in HD animal models (Sarkar et al., 2008). A new small molecule was shown to upregulate neuronal autophagy in an mTOR-independent way (Tsvetkov et al., 2010); it is an exciting potential treatment against protein folding disease without the known side-effects of mTOR-inhibiting drugs. Giving further evidence for the role of autophagy in HD, recently it was found that an Atg7 polymorphism influences the age of onset and those with the mutation showed symptoms earlier (Metzger et al., 2010).

Alzheimer's disease (AD) and Parkinson's disease (PD) are protein folding diseases associated with protein aggregates called inclusions in the brain. The toxic proteolytic product β-ameloid accumulates in AD brains causing dystrophic neurites and the aggregates are not fully degraded when autophagy is impaired perhaps leading

to further propagation (Yu et al., 2005). Most recently it was revealed that the AD-related transmembrane protein presenilin-1 is itself required for acidification of lysosomes and thus autophagy (Lee et al., 2010). This may provide a mechanism for the early-onset form of AD that is linked to mutations in the presenilin-1 gene. Both autophagy and CMA contribute to the degradation of α-synuclein-inclusions associated with Parkinson's disease but the inability of CMA to specifically degrade mutant α-synuclein contributes to its pathogenesis (Cuervo et al., 2004). Lysosome impairment has also been recently linked to PD and explains why an increased number of autophagosomes is seen in the brains of PD patients (Dehay et al., 2010). Other neurodegenerative diseases such as Amyotrophic lateral sclerosis (ALS), which is characterised by the presence of intracellular aggregates within motor neurons, and even prion disease are associated with impaired autophagy.

Despite the recent surge of publications delving into the molecular mechanisms of autophagic function, there are many remaining questions. Of critical importance is to determine how and where the isolation membrane forms in mammalian cells and what other proteins are required to act at this site. Perhaps this would get us closer to understanding the origin of the autophagosome membrane. What confers specificity to cargo and how p62 and other Ub- and LC3-interacting proteins differentially send protein aggregates to the lysosome or proteasome are also interesting subjects. Autophagy is critical for maintaining proper cell wellbeing and is involved in multiple diseases. Striving to uncover the mysteries of the process, autophagy scientists will find new drug targets that may provide the framework for therapies for multiple conditions and diseases, including ageing, cancer and neurodegeneration. During my PhD studentship, I performed a genome-wide siRNA-based screen in order to find new modulators of mammalian autophagy that may possibly shed light on some of the questions put forth in this summary of autophagy.

Chapter 2. Materials and Methods

2.1 Cell culture

HEK293A cells were obtained from Cell Services, Clare Hall, LRI. HeLa cells were obtained from Eeva-Liisa Eskelinen University of Helsinki, Helsinki, Finland. GFP-LC3-HEK cells were made and characterised by Edmond Chan (Chan et al., 2007).

All cells were cultured at 37º Celsius, with 10% CO_2.

Full medium is: Dulbecco's Modified Eagle Medium 1x (DMEM) (GIBCO, 2169), 9% Foetal Bovine Serum (FBS) (SIGMA, F7524), 1.5% L-glutamine, Pen./Strep. Starvation (amino-acid free) medium is Earle's Buffered Salt Solution (EBSS): NaCl (0.2grams/litre), $NaHCO_3$ (1.1gram/litre), KCl, $CaCl_2$, $MgSO_4$, NaH_2PO_4, D-Glucose (1gram/litre), 1% Phenol red, Pen./Strep.

EBSS, L-glutamine, PBS, Trypsin, Versene, Pen/strep were supplied by LRI laboratory services.

2.2 Intein reporter assay experiments

2.2.1 Cloning intein constructs

I received intein constructs (containing *Ssp. Staphylococcus* inteins) from Kanno *et al*: pX8luc, pcmLV, pDcV, and pmLDn (in pcDNA3.1(-)), (Kanno et al., 2006). Received human ATG3, ATG7, ATG7CS, LC3 and LC3ΔG from Isei Tanida (National Institute of Infectious Diseases, Tokyo, Japan): Tag2B-LC3 wt, Tag2B-LC3ΔG, Tag2B-hAtg3, Tag2B-hAtg3CS, 3xMyc-hAtg7 WT, 3xMyc-hAtg7 CS. Received RasV12 and Raf from Julian Downward (LRI): mRaf pEFH PLINK (a pEF PLINK2 derivative with an H6 and myc tag at N-terminus) and V12H-Ras (cloned into pcDNA3). The following primers were used to clone the intein constructs:

Construct	Restriction enzymes (N-terminal, C-terminal)	Forward primer sequence (5'-3')	Reverse primer sequence (5'-3')
Atg3 pDcV	XhoI, XbaI	ctcgaggccaccatgcagaatgtgattaat	atctagacccattgtgaagtgtcttgt
Atg7 pDcV	NotI, XbaI	taggcggccgcgccaccatggcggcagcta cgggg	atctagaccgatggtctcatcgtcgct

Atg7CS pDcV	NotI, XbaI	taggcggccgcgccaccatggcggcagctacgggg	atctagaccgatggtctcatcgtcgct
LC3 pDcV	XhoI, XbaI	ctcgaggccaccatgccgtcggagaagacc	atctagacccactgacaatttcatccc
LC3ΔG pDcV	XhoI, XbaI	ctcgaggccaccatgccgtcggagaagacc	atctagacccactgacaatttcatgaa
pmLDn Atg3	BamHI, EcoRI	tagggatcccagaatgtgattaatact	aatgaattcttacattgtgaagtgtct
pmLDn Atg7	EcoRI, NotI	taggaattcagcggcagctacgggggat	aatgcggccgctcagatggtctcatcgtc
pmLDn LC3	BamHI, EcoRI	tagggatccccgtcggagaagaccttc	aatgaattcttacactgacaatttcat
pmLDn LC3ΔG	BamHI, EcoRI	tagggatccccgtcggagaagaccttc	aatgaattcttacactgacaatttcat
Raf pDcV	XhoI, XbaI	ctcgaggccaccatggagcacatacaggga	atctagaccgaagacaggcagcctcgg
pmLDnRasV12	BamHI, EcoRI	tagggatccaccgaatacaagcttgtt	aatgaattctcaggaaagcacacactt

Table 2.1 Intein construct cloning enzymes and primers
Intein construct name, N-terminal and C-terminal restriction enzymes, N-terminal and C-terminal primer sequences (both shown 5' to 3') are shown.

Accuprime Pfx DNA polymerase is from Invitrogen. T4 DNA ligase (reactions done at 16ºC overnight, typical 1:3 plasmid:insert), XhoI, XbaI, NotI, BamHI, EcoRI, and restriction enzyme buffers are from New England Biolabs.

Plasmids were transformed into DH5α chemical competent bacteria (Invitrogen), grown in Luria broth (LB) medium (2% Tryptone, 0.5% Yeast extract, 10mM NaCl)(LRI laboratory services).

PCR Purification Kit, QIAquick Gel Extraction Kit, Miniprep Kit, DyeEx 2.0 Spin Kit, Endo-free Plasmid DNA Maxiprep Kit all from Qiagen. DNA sequencing was preformed using BigDye terminator (BDT) on the ABI Prism 377 DNA sequencer (Applied Biosystems) by the LRI sequencing service.

2.2.2 Overexpression of intein-containing constructs

For the luciferase assay, HEK or HeLa cells were plated typically at 1250 cells/well in 96-well Plates, Polystyrene, White, Tissue Culture Treated (Matrix, 4934) in 100μL full medium without antibiotics and grown overnight. On day 2 a conventional transfection was performed: typically, 0.1μg pX8luc, 0.1μg pGL4.74 luciferase (Promega, E6921), 0.25μg pDcV construct and 0.25μg pmLDn construct (or 0.25μg pcmLV and 0.25μg pcDNA3.1) were mixed in 10μL OPTI-MEM I (GIBCO, 31958); 0.4μL Lipofectamine2000 (Invitrogen) were mixed in 10μL OPTI-MEM. The DNA-containing and transfection reagent-containing liquids were mixed for 20 minutes

following manufacturer's recommendations (Invitrogen). 20µL of medium was removed from each well and 20µL of transfection mix is added to each well and cells were incubated overnight. On day 3, cells are treated and luciferase activity was measured.

For measuring expression, HEK or HeLa cells were plated typically at 2500 cells/well in 24-well clear, tissue culture treated plates. On day 2, 1µg DNA was transfected with 2µL Lipofectamine2000 as described above. On day 3, expression is measured by western blot.

2.2.3 Luciferase Assay

Transfected cells were dosed with 0.2µM rapamycin (Calbiochem) or 10mM lithium chloride (Sigma) for 24 hours or 11.0µM rapamycin for 2 hours. An equal volume to medium (75µL) of Dual-Glo Luciferase Reagent (Dual-Glo Luciferase Assay System, Promega E2920) was added, incubated for 10 minutes, and firefly luminescence was read on the EnVision 2102 Multilabel Reader (Perkin Elmer). 75µL of Dual-Glo Stop&Glo Reagent was added, incubated for 10 minutes, and renilla luminescence was read. Luciferase firefly luminescence values were corrected for renilla luminescence values, triplicate corrected values were averaged and sometimes further corrected by dividing by the corresponding values for full medium.

2.2.4 Western blotting

2.2.4.1 Checking expression

Cells were washed with PBS and lysed in 100µL NP40 buffer (50mM TRIS, 150mM NaCl, 1.0% NP-40, pH 8.0) plus Complete, EDTA-free protease inhibitors (Roche, 11873580001). A Bradford Assay was performed to determine protein concentration compared to IgG standards (Protein Assay, BIO-RAD 500-0006).

Samples were mixed with NuPAGE Sample buffer (Invitrogen) and run on SDS-PAGE NuPAGE Novex 4-12% Bis-Tris gels (Invitrogen) and transferred onto Immobilon PVDF Transfer Membrane (Millipore) (PVDF was activated with methanol) using a semi-dry transfer cell (BIO-RAD). Membranes were stained with PonceauS and probed with anti-myc 9B11 (Cell Signaling, 2276) or anti-LexA (Invitrogen, R990-25) primary antibodies. Blots were washed in TBS with 0.05% Tween and probed with

ECL anti-mouse IgG, HRP-linked whole antibody (from sheep) (GE Healthcare, NA931V) or ECL Anti-rabbit IgG, HRP-linked whole antibody (from donkey) (GE Healthcare, NA934V). Membranes were incubated with ECL (GE Healthcare, RPN2106VI) and exposed onto film.

2.2.4.2 Endogenous LC3 lipidation assay

Cells were transfected in a 24-well plate as described above. Autophagy is induced with lithium chloride or rapamycin as described above. Cells were washed with PBS, lysed in 50µL cold TNTE (20mM Tris-HCl, 150mM NaCl, 0.3% TX-100, 5mM EDTA, pH 7.5) plus protease inhibitors on ice and spun for 5 minutes at 11,000 rpm at 4ºC. Supernatant was added to 5x SDS Laemmli sample buffer (15%SDS (w/v), 312.5mM Tris-HCl (v/v) pH 6.8, 50% glycerol (w/v), 16% β-mercaptoethanol, bromophenol blue; all Sigma), incubated for 10 minutes at 65ºC and loaded onto a hand-poured 12% gel (4% stack). The gel was transferred onto PVDF as above and blotted with anti-LC3 5F10 monoclonal (Nanotools, 0231-100/LC3-5F10) or anti-β -tubulin polyclonal (Cell Signaling).

2.2.5 Co-immunoprecipitation

Cells were transfected for 24 hours as above (scaled-up as appropriate) in 6cm or 10cm dishes so that cells were grown to 80%-90% confluency at the time of transfection. Cells were washed in cold PBS, lysed in cold TNTE supplemented with protease inhibitors and PhosSTOP phosphatase inhibitors (Roche 04906837001) and spun for 5 minutes at 4ºC at 12000rpm. 40µL Protein A bead slurry (Protein A sepharose in PBS, Sigma) or Protein G bead slurry (Protein G sepharose in PBS, Sigma) were washed 2 times with cold TNTE and once with cold TNTE plus protease inhibitors. Anti-myc 9E10 antibody (LRI Cell services) was added to the beads (or not for 'no antibody' control). 50µL of supernatant (input) was held from each lysate. Lysate is added to each tube (or not for 'no lysate' control). IPs were incubated overnight at 4ºC. 50µL of supernatant (unbound supernatant) was held from each IP. Beads were washed three times with TNTE plus protease and eluted in 25-50µL 3x sample buffer and heated to 95ºC for 5 minutes. Samples were run on SDS-PAGE NuPAGE Novex 4-12% Bis-Tris gels, transferred onto PVDF, stained with PonceauS and probed with anti-LexA antibody.

2.2.6 Making stable cell lines

Low-passage HeLa cells were transfected with pX8luc and selected with 1ug/mL G418. Clones were picked and measured for luciferase activity as above after transfection with pcmLV control.

2.3 Image-based screen optimisation and primary, secondary and deconvolution screen

GFP-LC3-HEK cells were generated by Edmond Chan with an eGFP-LC3 construct obtained from Y. Kabeya. Rat LC3 was cloned into pEGFP-CI (Clontech) using BamHI and EcoRI.

2.3.1 Imaging GFP-LC3-HEK cells

GFP-LC3-HEK cells were plated on the following: Microtest 96-well Assay Plate, Optilux, Black/Clear Bottom, TC Surface Sterile, With lid (BD Falcon, REF 353948) or Imaging plate, Flat bottom (BD Falcon, REF 353219). Plates were coated with Poly-D-lysine hydrobromide (Sigma, P0899). Of note, if the Poly-D-lysine was not adequately washed off the plates before the cells were added and subsequently transfected using lipid transfection reagents such as Lipofectamine2000 then the cells would suffer from toxicity (data not shown). Thus, the plates needed to be washed well after treatment with Poly-D-Lysine or alternatively a lower concentration or a higher quality of reagent was also used.

During optimisation, autophagy was induced in GFP-LC3-HEK cells using the following conditions or chemicals: 50μM vinblastine (Sigma Aldrich V1377) 2 hours, 2 hour incubation in EBSS, 2 hour incubation in EBSS plus 0.25mg/mL leupeptin (Roche, 1529048) or 11μM rapamycin for 2 hours. The GFP-LC3-HEK cell line was derived from HEK293A cells, where the 'A' stands for adherent. The HEK293A cells, despite their name, do not stick as well as other adherent cells such as HeLa cells and tend to become detached from the plate when manipulated. This posed a challenge for me because, in order to induce autophagy by culturing the cells in EBSS, all the full medium needed to be washed off. For cells in 96-well plates this required washing two to three times with EBSS or PBS before the addition of fresh EBSS or EBSS with leupeptin and this had to be done slowly and carefully when attempting to do so by hand. I minimised cell loss by gently pipetting with a multi-channel pipette.

After induction of autophagy, cells were washed 1x in room temperature PBS, fixed with 3% para-formaldehyde (Pfa) for 20 minutes, washed 1x in PBS, incubated in 5μg/mL Hoechst B226 in PBS (1:200 from 1mg/mL stock, Sigma, 33258), incubated for 20 minutes, washed 1x in PBS and changed into 100uL fresh PBS. The plate is sealed and kept at 4ºC.

Plates were processed in the Cellomics ArrayScan VTI HCS Reader (Thermo Scientific) using a 20X 0.45NA lens (of note, capturing at 20x is about 196 fields per well; 40x is about 400 fields per well). Images were analysed on-the-fly using the Cellomics SpotDetector V3 Bioapplication. The GFP channel (GFP-LC3 spots) was used to set the focus with fixed illumination time and spots were defined as having the following broad characteristics: SpotArea 1.75-18, SpotShapeBFR 0.33-1.4, SpotShapeBAR 1-3, SpotAvgInten 44-888, SpotTotalInten 250-13000, in an area 22 microns surrounding and external to the nuclear region as defined by the DAPI stain (i.e. excluding any contribution from nuclear spots) thereby restricting the analysis to perinuclear and cytoplasmic GFP-LC3 spots. Several parameters were recorded including the number of nuclei (object count; OC) from the DAPI channel, the number of GFP-LC3 spots per cell (spot count per object; SCPO), the total intensity of GFP-LC3 spots per cell (spot total intensity per object; STIPO), and the total area covered by GFP-LC3 spots per cell (spot total area per object; STAPO).

2.3.2 Reverse transfection for siRNA knock-down

2.3.2.1 Transfection reagents tested

The 20 cationic lipid transfection reagents tested are as follows:(1) siPORT NeoFX Transfection Agent, (2) siPORT Amine Transfection Agent (Ambion); (3) Metafectene (Bionex); (4) Dharmafect 1 (Dharmacon), (5) GeneSilencer (GTS); (6) Lipofect RNAiMax, (7) Oligofectamine, (8) Lipofectamine2000, (9) Lipofectamine (Invitrogen); (10) TransIT-siQuest, (11) TransIT-TKO (Mirus); (12) TransPassR1 (New England Biolabs); (13) DreamfectGold, (14) Lullaby (OZ Bioscience); (15) HiPerFect (Qiagen); (16) Interferin (PolyPlus); (17) CodeBreaker (Promega); (18) siRNA transfection reagent (Santa Cruz); (19) NTER nanoparticles (Sigma); (20) siIMPORTER (Upstate).

The eight transfection reagents tested with a more-specified range of concentrations (shown in μL per well) are as follows: (1) siPORT NeoFX Transfection Agent (Ambion) 0.4, 0.5, 0.6; (2) siPORT Amine Transfection Agent (Ambion) 0.3, 0.4, 0.5; (3) Metafectene (Biomex) 0.25, 0.3, 0.35; (5) GeneSilencer (GTS) 0.15, 0.2, 0.25; (6) Lipofect RNAiMax (Invitrogen), 0.3, 0.5, 0.7; (8) Lipofectamine2000 (Invitrogen) 0.3, 0.45, 0.6; (13) DreamfectGold (OZ Bioscience), 0.1, 0.2, 0.3; (15) HiPerFect (Qiagen) 0.1, 0.25, 0.4.

Western blot analysis with three transfection reagents was done using reverse transfection (see below) with 0.4μL transfection reagent and 50nM siRNA. siRNA used was: COPB1 siGenome duplex-03 siRNA (Dharmacon, D-017940-03) and western blots were probed with an anti-COPB1 serum produced in rabbits immunised with COPB1 peptide.

2.3.2.2 Optimised reverse transfection protocol

Optilux 96-well plates were coated with poly-D-lysine and washed with water three times. 0.4μL Lipofectamine2000 was added to 10μL OPTI-MEM; 37.5nM siRNA was added to 10μL OPTI-MEM; these two were mixed together by inverting five times and then incubated for 20 minutes. GFP-LC3-HEK cells were trypsinised, brought up in 10mL full medium (with antibiotics), and counted. 4000 cells were resuspended in 80μL of full medium (with antibiotics). 20μL of transfection mix was added to each well and 4000 cells in 80μL full medium was added to each well. Cells were incubated for 48 hours. On day 3, the medium was replaced with fresh full medium. On day 4, autophagy was induced and the cells were fixed or lysed as appropriate.

2.3.3 The primary screen

2.3.3.1 Materials

I sent the GFP-LC3-HEK cells away to our cell services facility where they underwent testing for mycoplasm infection, the result of which was negative. I also created a stock of frozen cells in case something went wrong with the cells that were expanded for the screen and a large amount were needed quickly. I expanded a large amount of cells and froze down 50 vials of cells at passage 12.

The following materials were used during the primary screen after their batches/lots had been tested: Lipofectamine2000 (Invitrogen, 11668019, 1.5mL, Lot 394876) (note: I needed 23 1.5mL vials and negotiated a discounted price ultimately receiving £204 off of each); Leupeptin (Roche, 1529048, batch no. 70122530 and 70138029) (note: I also negotiated a discounted price for the 1.4 grams required), Poly-D-lysine hydrobromide suitable for cell culture (Sigma, P6407), OPTI-MEM, and HBSS (GIBCO, 14170).

I obtained siRNA for the negative and positive controls to fill the two empty columns on each plate. These were tested to ensure that the siRNA Smartpools were performing as before. The siRNA negative and positive controls were as follows:

RISCfree: siControl RISC-free siRNA #1, D-001220-01-05

siControl: siCONTROL Non-targeting siRNA pool #1, D-001206-13-05

siULK1: siGENOME Smartpool, M-005049-00

siATG7: siGENOME Smartpool, M-020112-01

siATG13: KIAA0652 siGENOME Smartpool, M-020765-01

siNRBP2: LOC340371 siGENOME duplex-01, D-005340-01 (GGAGAUGGCUGUACUGGAAUU)

I prepared a large amount of medium for the screen. I ordered 20 litres of full growth medium to which I added FBS, penicillin and streptomycin and supplemental L-glutamine, assuring that the FBS that I added was the same batch that I had been using during optimisation. I ordered 10 litres of EBSS for the starvation incubation and tested this batch to assure that autophagy induction was achieved.

I prepared the plates for the screen. A small number of plates were coated with Poly-D-lysine and tested. These plates were sufficient as the GFP-LC3-HEK cells remained attached during washing and no Poly-D-lysine seemed to remain, causing toxicity. The remaining plates were then coated with Poly-D-lysine and washed and barcodes were added (1.4 to 267.6). The siRNA library was aliquoted onto the coated plates (at 375nM in 10 µL HBSS), resealed, and kept at -20ºC until day 1 of the screen.

I prepared the cells for the screen. The GFP-LC3-HEK cells to be used in the screen were thawed from their lowest passage available (from their original freeze after stable GFP-LC3 expression was obtained) and these cells, at passage seven, were tested for their ability to be induced for autophagy. I then tested that the cells survived

transfection as described above and measured the effect of positive and negative control siRNA on these cells, now at passage 9. These cells responded as before and were expanded in order to have enough cells for the screen. The cells used in the primary screen were at passage 11.

The Dharmacon siGenome library consists of four sub-libraries: Plates 1-10, Protein Kinase (Cat No: G-003500); Plates 11-17, G Protein-Coupled Receptors (Cat No: G-003600); Plates 18-93, Human Druggable Set (Cat No: G-004600) Plates 94-267, Human Genome Set (Cat No: G-005000).

The screen was performed in four batches of 200 cells. These batches by bar codes are as follows: Batch 1, 2.4-66.6; Batch 2, 67.4-132.6; Batch 3, 133-198.6; Batch 4, 199.4-267.6.

The following robots were used during the screen: Matrix WellMate 8-channel Microplate Dispenser (Thermo Scientific) and ELx405 Microplate Washer (BioTek).

2.3.3.2 Primary screen protocol

Day 1:

First I prepared the positive and negative siRNA controls for the sixteen empty wells on each plate. The siRNA was resuspended in HBSS to achieve a concentration of 375nM 10µL so that the final concentration would be 37.5nM in 100µL total volume of each well. This was done only once in the morning before the screen began. The plates containing 10µL of siGENOME siRNA in HBSS in each well were thawed and spun. The foil was removed and the control siRNA was added by hand. I prepared the cells to be added; I trypsinised twelve 175cm flasks, counted the cells with a Haemocytometer, and resuspended the cells so that there would be 4000 cells in 80µL of full growth medium. Meanwhile, 0.4µL of Lipofectamine2000 diluted in 10µL Opti-MEM medium was added to each well of each plate using one of two Thermo Scientific Matrix WellMate 8-channel Microplate Dispensers in two tissue culture hoods. The 20µL siRNA/transfection reagent was left to mix on the plate for 20 minutes and then 80µL of cells in full growth medium was added. The plates were stacked and placed in one of three incubators and left for 48 hours. This process was then repeated three times over the course of the day.

Day 2.

A selection of wells from a selection of plates from each of the three incubators were examined to check the density and viability of the cells.

Day 3.

The transfection medium was removed using a BioTek Microplate Washer and 100µL fresh full medium was added using the Matrix WellMate Microplate Dispenser at slow speeds in order to cause as little disruption to the cells as possible. This was done in sterile conditions.

Day 4.

The plates were again processed in four batches of 200 plates and the induction step again required the efforts of four people. The full growth medium was removed and the plates were washed by dunking the plates, two at a time, in a large tub filled with PBS and then excess PBS was removed. 60µL of EBSS with 0.25mg/mL leupeptin was immediately added to each well using a WellMate Microplate Dispenser and the plates were placed back into the incubator for two hours. The cells were then fixed by the addition of 60µL 8% formaldehyde and incubated in this 4% formaldehyde solution for at least 20 minutes at room temperature, sealed and kept over-night at 4°C. On day 5, the plates were de-sealed, 100µL of PBS was added and plates were kept at 4°C.

Dapi staining.

Batches of plates to be read were stained with DAPI the day of image acquisition. Fixed cells were treated with 1µg/mL DAPI (Sigma) for 20 minutes, the stain was removed, 100µL of PBS was added and plates were sealed.

Image acquisition.

The 16 wells containing positive and negative control siRNA were compared to a plate that was treated with full medium, not EBSS with leupeptin in order to optimise the Cellomics SpotDetector parameters for the screen. Of note, the parameters that gave the most accurate spot calling and best fold induction between the uninduced plate and the RISCfree negative control wells on the induced plates were set so that the least number of spots were counted on the uninduced plate. We set the thresholds for spots were set quite high and only big, bright spots of GFP-LC3 intensity were counted as ‘spots.’

2.3.3.3 Data normalisation

Further details of the B-score and Z-score normalisation can be found in the Appendix section 9.1.

2.3.4 The secondary screen

The cells, siRNA controls and all other reagents were re-tested before the secondary screen. The secondary screen was performed as the primary screen.

2.3.5 The deconvolution screen

A custom order of 190 deconvoluted siGenome Smartpools was made to Dharmacon. I arranged the sets of 4 siRNA duplexes on 10 plates, leaving the first two columns free for siRNA controls as before using Dharmacon's custom order template. The cells, siRNA controls and all other reagents were re-tested before the deconvolution screen. The deconvolution screen was performed as the primary screen.

2.4 Gene annotation

Candidate genes were annotated using the following databases:

Entrez Gene: http://www.ncbi.nlm.nih.gov/entrez/query.fcgi?db=gene

Human Protein Reference Database (HPRD): http://www.hprd.org/query

Online Mendelian Inheritance in Man (OMIM): http://www.ncbi.nlm.nih.gov/sites/entrez?db=omim

UniProtKB: http://www.uniprot.org

The 51 'validated-by-deconvolution' hits were analysed for GO term annotations using the Generic GO term Mapper and generic GO slim terms (http://go.princeton.edu/), (http://go.princeton.edu/GOTermMapper/goSlimFiles/goslim_generic.obo) and analysed using Panther annotation for protein class (http://www.pantherdb.org).

2.5 Further validation

2.5.1 siRNA duplexes

The two best siRNA duplexes for the 20 'three-out-of-four' hits were chosen from the deconvolution screen. 2.0 nmol was ordered for each of the following:

Gene symbol	siGENOME siRNA number	Target sequence duplex A	Target sequence duplex B
CDH19	D-013105-02,-03	GAUAAUGGUACAAUCACUA	GCUGAGGAGUAGUACCAUA
SUPT5H	D-016234-01,-04	CGGAAGGGCUUUCUGUUCA	GCGAGUAUUACAUGAAGAA
C1orf198	D-015001-02,-03	GCGCUUCACUUACUUCUCG	GGUCUUGCCUCCCUGCUAC
GHSR	D-005513-01,-03	GGGUGAAGCUGGUCAUCUU	GGACCAGAACCACAAGCAA
LARP1	D-027187-01,-04	GCACCGAGCUUUACAGUGU	UGAACAACAUCACCUACUA
NAA25	D-014530-01,-02	GACCGGAGUUAGUUACAAA	CCAAUGUUGUGGAUCAUAU
SCOC	D-014916-02,-03	CAGAUGACAUAGACCAUUC	GAACUCCAACACACACUUG
PAFAH1B2	D-008797-03,-04	GUGAGAAACCCAAUCCUUU	GAUCGAGGCCAUUGUACAA
WAC	D-013325-03,-04	GAGACAAACCCGUAUCACA	CGAUCCACGUGUUCAUUAA
TLK2	D-005389-03,-04	CCAAAGAUCUCAAAUAAAG	GCAUGGAGCUAACAUCACA
RBM12	D-010094-03,-04	GGAAUGGAUUGGUUAAGUU	CCACCUAGCUCAGGAAUGA
CNOT1	D-015369-02,-04	CAAGUUAGCACUAUGGUAA	GCAAUAUAAUCGUGCAGUU
FBXL14	D-015718-01,-04	GCCAGAAGCUCACAGAUCU	GCUCAACAUUGGACAGUGU
KIF25	D-010082-01,-03	GGAAGAGGAGGCCGGAUUG	CCUACUCACUUCUCUCUUG
STAT2	D-012064-01,-04	GGACUGAGUUGCCUGGUUA	CUGCUAGGCCGAUUAACUA
ADHFE1	D-008453-03,-04	GAGCAGCAGUUACAAAGGA	GAAGCAAGGUCUCAUAUGC
RASIP1	D-020794-03,-04	GGACUUCGAUCAGUUGACU	CGACAUUGCCACUGAGUUC
WDR6	D-013085-02,-03	CAAGGAACGUUGUCGGUAC	GCAGGAUUCUGGGCGGAUU
RASGRF2	D-024516-04,-06	GAAGGAACACCAAACUUUA	GCACAGUACUUGCUUGACA
SNX20	D-016514-01,-03	GCACUUAGACACACACAGU	GCACGUCAAACUGCUCUUU

Table 2.2 siRNA duplexes acquired for each of the 20 validated-by-deconvolution hits
The gene symbol, siGENOME siRNA order numbers and sequences for the two duplexes are shown.

2.5.2 Induction screen

The induction screen was performed on the following plates:

Plates 1, 2, 3: full medium + 0.25mg/mL leupeptin 24 hours

Plates 4, 5, 6: full medium + 10mM LiCl 24 hours

Plates 7, 8, 9: full medium + 0.25mg/mL leupeptin 2 hours

Plates 10, 11, 12: EBSS 2 hours

Plates 13, 14, 15: EBSS + 0.25mg/mL leupeptin 2 hours

Plates 16, 17, 18: full medium + 250nM Torin + 0.25mg/mL leupeptin 2 hours

Plates 19, 20, 21: full medium + 128μM Resveratrol + 0.25mg/mL leupeptin 2 hours

Plate 22: NO siRNA, just Lipofectamine 2000, fresh full medium 2 hours

Torin is from D.M. Sabatini, (MIT, Boston, USA); Resveratrol is from Sigma.

2.5.3 24 well knock-down of GFP-LC3-HEK cells

The 96-well reverse transfection was scaled up to a 24-well format: 24-well plates were coated with poly-D-lysine and washed well. 37.5nM siRNA in 50µL OPTI-MEM was mixed with 1.25µL Lipofectamine 2000 in 50µL OPTIMEM and incubated for 20 minutes. 100µL of transfection mix was added to plates. 7 x 10^4 GFP-LC3-HEK cells in 400µL in full growth medium were added to each well, incubated for 48 hours; the media was changed to 500µL full growth medium; incubate for 24 hours (total: 72 hours). Autophagy was induced (after washing 3 times) with EBSS plus 0.25mg/mL leupeptin for hours.

2.5.3.1 Confocal images

Glass coverslips were placed in 24-well plates, coated with poly-D-lysine, washed and transfection mix then GFP-LC3-HEK cells were added on top of the coverslips and the reverse transfection procedure was followed, as above. Negative control siRNA was RISCfree control siRNA, and single duplexes were used for siULK1 and siNRBP2: siGenome ULK1 siRNA duplex-04 (Dharmacon, D-005049-04, UGUAGGUGUUUAAGAAUUGUU); siGenome LOC340371 siRNA duplex-01 (Dharmacon, D-005340-01, GGAGAUGGCUGUACUGGAAUU). RISCfree cells were treated with either full medium or EBSS plus 0.25mg/mL leupeptin for two hours and siULK1, siNRBP2, and all test siRNA duplexes were treated with EBSS plus 0.25mg/mL leupeptin for two hours. Cells were fixed with 3% PFA (Sigma) for 20 minutes, quenched with 50nM NH_4Cl/PBS for 10 minutes, washed in PBS, incubated in Hoechst in PBS for 20 minutes, washed and mounted with moviol onto glass slides. Cells were imaged with an LSM 510 laser scanning confocal microscope at 63x with a 1.4NA, Plan Apochromat oil-immersion objective (Carl Zeiss MicroImaging, Inc.). Laser and all intensity settings were identical when capturing every image. Images were processed using LSM 510 software.

2.5.3.2 Measuring mRNA levels by qRTPCR

Side-by-side to the knock-downs performed on coverslips, two wells of a 24-well plate were transfected with each siRNA duplex above. On day 4, GFP-LC3-HEK

cells were not induced for autophagy. Instead, total RNA was isolated from cells in two wells using the RNeasy mini kit (Qiagen). The RNA was eluted in 30µL RNAase-free water and the RNA concentration was measured using a NanoDrop spectrophotometer (Thermo Scientific). All RNA was stored at -80ºC.

cDNA was reverse transcribed from the 1.0µg RNA using Superscript RTII and oligo dT (Invitrogen). mRNA levels were determined by quantive real-time polymerase chain reaction (qRTPCR) using SYBRGreen PCR Master Mix (Applied Biosystems 4309155) in a 20µL reaction (2.5µL of cDNA (in 50µL RNAse-free water), 5.5µL water, 10µL SYBRGreen and 2µL QuantiTect Primer). Cycles were performed on a 7900HT Fast Real-Time PCR System (Applied Biosystems) and data was normalised to β-actin control (Qiagen, ACTB QT00095431). Qiagen QuantiTect Primer Assays ("containing a mix of lyophilized forward and reverse primers for a specific target") were used for the 20 candidate hits:

Gene symbol	**Gene ID**	**Accession number**	**Qiagen QuantiTect primer number**
CDH19	28513	NM_021153	QT00009359
SUPT5H	6829	NM_003169	QT00059423
C1orf198	84886	NM_032800	QT00090293
GHSR	2693	NM_004122	QT01666217
LARP1	23367	NM_015315	QT00043701
C12orf30/NAA25	80018	NM_024953	QT00099834
SCOC	60592	NM_032547	QT00069846
PAFAH1B2	5049	NM_002572	QT01845550
WAC	51322	NM_016628	QT00060480
TLK2	11011	NM_006852	QT01666518
RBM12	10137	NM_006047	QT00214004
CNOT1	23019	NM_016284	QT00080136
FBXL14	144699	NM_152441	QT01031184
KIF25	3834	NM_005355	QT00024934
STAT2	6773	NM_005419	QT00095704
ADHFE1	137872	NM_144650	QT00040999
RASIP1	54922	NM_017805	QT00035637
WDR6	11180	NM_018031	QT01841056

RASGRF2	5924	NM_006909	QT00028462
SNX20	124460	NM_153337	QT01671334

Table 2.3 qRTPCR primers for the 20 validated-by-deconvolution hits
Gene symbol, GeneID, Accession number and Qiagen QuantiTect primer assay catalogue number for each of the 20 hits.

2.5.4 LC3 lipidation assay in HeLa cells with Licor

The 24-well reverse transfection protocol was performed as described for monitoring GFP-LC3 spot formation in GFP-LC3-HEK cells (section 1.5.3.1 above) except that HeLa cells were plated at a higher concentration of 1.5 x 10^5 cells per well. On day 4, duplicate test wells were transferred to fresh full medium, EBSS, or EBSS plus 0.25mg/mL leupeptin for two hours (as before, the cells were washed three times before the addition of starvation medium).

Cells that received full medium were washed with cold PBS and all cells were lysed with 50µL cold TNTE supplemented with protease inhibitors. Cells were then spun at 12,000 for five mintes at at 4°C. 20µL of lysate was transferred to a fresh tube and 5µL of 5x Laemmli sample buffer was added. Tubes were heated at 65°C for 10 minutes and loaded onto NuPAGE Novex 4-12% Bis-Tris Midi Gels (20 well) (Invitrogen, WG1403) and run in MES running buffer. The gels were transferred onto (methanol-activated) Immobilon-FL PVDF Transfer Membrane (Millipore, IPFL0010, pore size 0.45µm) using a semi-dry transfer cell. After transfer, membranes were stained with PonceauS and blocked with a 50% solution of Licor Blocking Buffer (Odyssey, 927-40000) in PBS for one hour. Membranes were probed with anti-Actin AC40 monoclonal (Sigma) at 1:1000 in PBS or anti-LC3 5F10 monoclonal (Nanotools) at 1:250 in PBS overnight at 4°C. Membranes were washed with PBS plus 0.05% Tween (5 x 12minutes). The secondary antibody was Alexa Fluor 680 goat anti-mouse IgG (H+L) (Invitrogen, A21058) and membranes were again washed with PBS-Tween and scanned on the LI-COR Odyssey Infrared Imager. Protein band strength was quantified using Metamorph software by drawing narrow boxes around the band thereby recording average pixel intensity and then background intensity was subtracted.

2.6 SCOC experiments

2.6.1 SCOC annotation

SCOC homologues were determined using tBLASTn (performed by Richard Mitter, LRI): (http://blast.ncbi.nlm.nih.gov/Blast.cgi?PROGRAM=tblastn&BLAST_PROGRAMS=tblastn&PAGE_TYPE=BlastSearch&SHOW_DEFAULTS=on&LINK_LOC=blasthome) and BLASTp (performed by me): (http://blast.ncbi.nlm.nih.gov/Blast.cgi?PROGRAM=blastp&BLAST_PROGRAMS=blastp&PAGE_TYPE=BlastSearch&SHOW_DEFAULTS=on&LINK_LOC=blasthome). The isoform schematic was built using UniProt: (UniProtKB: http://www.uniprot.org). Molecular weights were predicted using ExPASy compute pI/Mw tool (*expasy.org/tools/pi_tool.html)*.

2.6.2 SCOC immunoprecipitation

SCOC-myc and the affinity purified anti-SCOC rabbit polyclonal antibody were obtained from Richard Kahn (Emory University). Cloning and generation of the antibody are described in Van Valkenburgh *et al* (Van Valkenburgh et al., 2001).

To perform the endogenous immunoprecipitation, HEK cells were plated on a 6cm dish and the next day were washed in cold PBS and lysed in 750 µL TNTE plus protease inhibitors plus phosphatase inhibitors. 40µL of protein A bead slurry was washed three times in TNTE plus protease inhibitors. 1µL of anti-SCOC was added to the beads and then lysate was added. The tubes were rotated on a spinning wheel overnight at 4°C. The tubes were spun slowly at 3000 rpm at 4°C and lysate was to load as unbound supernatant. Beads were washed 3 times in TNTE plus protease inhibitors and beads were boiled for 10 minutes at 95°C. 1.3% input and unbound post-IP supernatant were loaded as well as bead eluate. The gel was transferred to PVDF as above and probed with anti-SCOC antibody at 1:400 and anti-rabbit HRP secondary at 1:1000. The film was developed using ECL reagents as described above and exposed over the weekend.

2.6.3 GFP-LC3 confocal images, pRTPCR and LC3 lipidation

GFP-LC3-HEK cell confocal imaging and qRTPCR were performed as described above (1.5.3). LC3 lipidation was performed as described above (1.5.4). Additional siRNA duplexes used are as follows:

siRNA duplex	siRNA number	Target sequence
SCOC-01	Dharmacon D-014916-01	CAUGUCAGCUUCUAGUGUU
SCOC-41	Ambion s34141 (cat no 4427037)	AGAUCUCUCUGCAAGAGUAtt
SCOC-42	Ambion s34142	CCAAAAGUUUGUUACCCAAtt
SCOC-43	Ambion s34143	ACAUUUCUCUUGCAGAUGAtt
Amb siC#1	Silencer® Select Negative Control #1 Cat#: 4390843	
Amb siC#2	Silencer® Select Negative Control #2 Cat#: 4390846	

Table 2.4 Additional siRNA duplexes for SCOC and Ambion siRNA controls
One Dharmacon siRNA duplex and three Ambion siRNA duplexes targeting SCOC additionally ordered are described above. Also, Ambion siRNA controls are shown

2.6.4 p62 degradation assay

The p62 degradation assay was performed with GFP-LC3-HEK cells. $8x10^4$ cells were knocked down using siSCOC-01,-02,-03, siULK-04 or RISCfree control using the 24-well reverse transfection protocol described above. On day 4, cells were starved in EBSS for four hours without leupeptin. Cells were lysed in 50µL TNTE plus protease inhibitors, spun for 5 minutes at 10,000 rpm, and run on NuPAGE 4-12% Bis-Tris gels, transferred to PVDF-FL and blotted following the Licor protocol described above. The membranes were probed with anti-p62 monoclonal antibody at 1:500 (SQSTM, BD Translabs) and anti-actin AC40 monoclonal antibody. Gels were scanned using the Licor imager and quantified using metamorph as described above. Cells for qRTPCR were knocked down side-by-side with the cells used for p62 blotting and SCOC mRNA levels were determined as described above.

2.6.5 Cloning SCOC-GFP and GFP-SCOC

SCOC isoform Q9UIL1-3 was cloned into pEGFP-N1 (Clontech) to create N1-SCOC-GFP (aka SCOC-GFP) and into pEGFP-C1 (Clontech) to create C1-GFP-SCOC

(aka GFP-SCOC). The open reading frame of SCOC isoform PCR'ed from the IMAGE clone BC062684 using Sal1 and BamHI the following primers:

N1 Sal1 forward	5' ATATGTCGACGGACGGGTCCAGGAAAGAG
N1 BamHI reverse	5' TATAGGATCCTTACTTTCTTTTGCTTTTTGT
C1 Sal1 forward	5' ATATGTCGACGACGGGTCCAGGAAAGAG
C1 BamHI reverse	5' TATAGGATCCTTACTTTCTTTTGCTTTTTGT

2.6.6 Knock-down then overexpression of SCOC

HEK cells were knocked down with the seven SCOC siRNA duplexes as above (24-well plate, 37.5nM siRNA, 1.25µL Lipofectamine 2000, $8x10^5$ cells). On day 3, cells were washed with full medium minus Pen./Strep. and transfected for overexpression. 3.2µL Lipofectamine/mL and 0.8µg of DNA (N1, SCOC-GFP or SCOC-myc) were combined in 300µL OPTI-MEM, incubated for 20minutes and added to the cells. The cells were incubated in this 300µL for 3 to 6 hours and then the medium was changed to full medium minus Pen./Strep. Membranes were probed with anti-Actin AC40 (Sigma), anti-GFP 3E10 monoclonal (LRI Cell Services), or anti-myc 9E10 monoclonal (LRI Cell Services) and scanned using Licor or probed with anti-SCOC polyclonal and developed using ECL as described above.

For rescue experiments the protocol above was followed but $1.5x10^5$ HeLa cells per well were plated. Endogenous LC3 lipidation was assessed as above using the Licor protocol and SCOC-myc expression was assessed using anti-myc 9E10.

2.6.7 SCOC immunofluorescence

Endogenous SCOC staining was performed with the anti-SCOC polyclonal antibody using the following protocol adapted from Van Valkenberg *et al* (Van Valkenburgh et al., 2001): HEK cells, GFP-LC3-HEK cells or GFP-DFCP1-HEK cells (obtained from Nicolas Ktistakis (Babraham Institute, Cambridge, UK)) were fixed in 3% paraformaldehyde for 20 minutes, quenched with 50nM NH_4Cl/PBS for 10 minutes, permeabilised in 0.2% saponin for 3 minutes, and blocked with 10% goat serum in PBS. All antibody incubations were done in 10% goat serum and coverslips were washed with 5% goat serum then PBS and finally mounted using moviol onto glass slides. Overexpressed SCOC (SCOC-myc or GFP-SCOC) immunofluorescence was performed

using the following protocol: HEK cells were fixed in 3% paraformaldehyde for 20 minutes, quenched with 50nM NH_4Cl/PBS for 10 minutes, permeabilised in 0.2% Triton for 3 minutes, and blocked with 0.2% gelatin in PBS. All antibody incubations were done in 0.2% gelatin in PBS and coverslips were washed with 0.2% gelatin in PBS then PBS and finally mounted using moviol onto glass slides.

The following antibodies were used for immunofluorescence:

Antibody	**Antigen**	**Species**	**Dilution**	**Supplier**
anti-SCOC	SCOC	Rabbit	1:200	R. Kahn
anti-mAtg9	mAtg9	Armenian hamster	1:1000	LRI
anti-TGN46	TGN46	Sheep	1:500	AbD Serotec
anti-GM130	GM130	Mouse	1:500	BD Transduction
anti-Atg12	Atg12	Mouse	1:100	Abgent (AM1816)
anti-LC3	LC3B	Mouse	1:200	MBL
anti-9E10	myc	Mouse	1:500	Sigma
anti-ULK1	ULK1	Rabbit	1:250	Santa Cruz
anti-Atg16	Atg16	Rabbit	1:400	Cosmo Bio
STO 285*	Atg16	Rabbit	1:200	LRI (affinity purified by S.Tooze)
anti-HA.11	HA-tag	Mouse	1:1000	Covance
Alexa Fluor 488, 555	anti-rabbit 2º	Goat	1:1000	Molecular Probes (Invitrogen)
Alexa Fluor 488, 555	anti-mouse 2º	Goat	1:1000	Molecular Probes (Invitrogen)
Cy3	anti-armenian hamster 2º	Goat	1:1000	Jackson Immunoresearch
Alexa Fluor 555	anti-sheep 2º	Donkey	1:1000	Molecular Probes (Invitrogen)

Table 2.5 Antibodies used for SCOC immunofluorescence
Antigen, organism in which the antigen was produced, concentration used and the supplier of the antibodies used during SCOC immunofluoresence experiments are shown.

*This anti-Atg16 antibody was made against a peptide in Atg16 and affinity purified by Sharon Tooze (N-term peptide SSGLRAADFDRWKRHISEQ(c)). Knock-down of Atg16 with the ON-TARGET plus siRNA Smartpool (Dharmacon, L-021033-

01) decreases Atg16 levels as detected by IF and westernblot (Figure2.1). Knock-down of Atg16 also inhibits GFP-LC3 spots and LC3 lipidation (Figure 2.1).

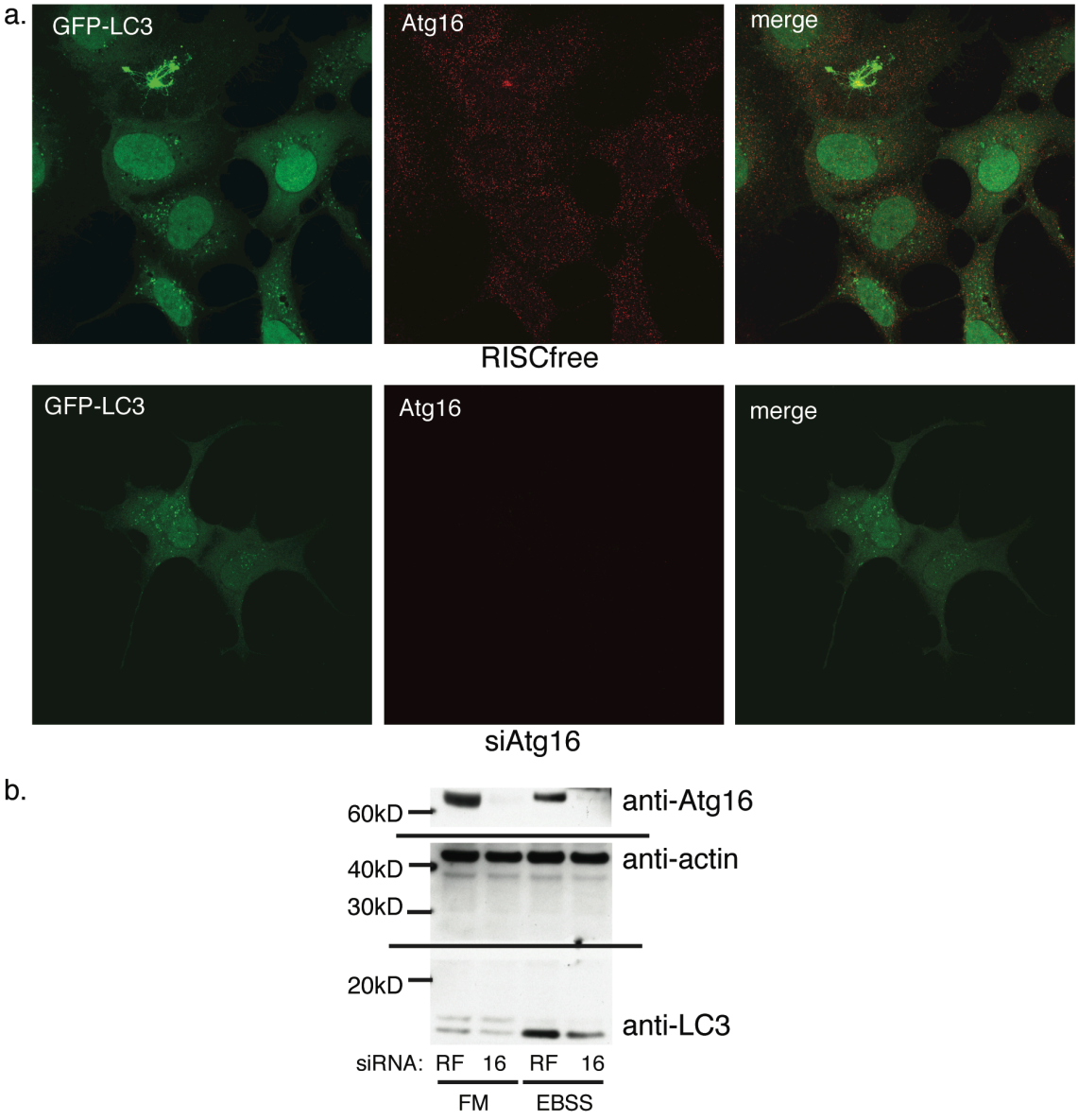

Figure 2.1 Atg16 affinity purified rabbit antibody
a. GFP-LC3-HEK cells were transfected with RISCfree control or siAtg16 siRNA, starved for 2 hours in EBSS, fixed and stained with anti-STO285 antibody. b. Anti-STO285, -actin, and –LC3 blots after indicated siRNA treatment (RF is RISCfree, 16 is siATG16) and mediua conditions in GFP-LC3-HEK cells.

2.6.8 Co-immunoprecipitations

GFP-FEZ1 was provided by Caroline Whitehouse (King's College London, UK). HEK cells were grown on 6cm dishes and transfected with 1µg SCOC-myc and 1µg GFP-FEZ1, incubated in full medium or EBSS for two hours. Cells were lysed and

incubated with protein G beads and 1.5µL anti-GFP 4E12 as described above (1.6.2). Blots were probed with anti-SCOC polyclonal and anti-FEZ1 goat polyclonal (Abcam, ab53562) primary antibodies and anti-rabbit and anti-Goat (Dako, P0449) secondary antibodies. Note that the anti-FEZ1 Abcam goat polyclonal antibody shows a nonspecific band that is not reduced by siRNA against FEZ1 (Figure 2.2). Endogenous FEZ1 is not detected but overexpressed GFP-FEZ1 is detected by this antibody.

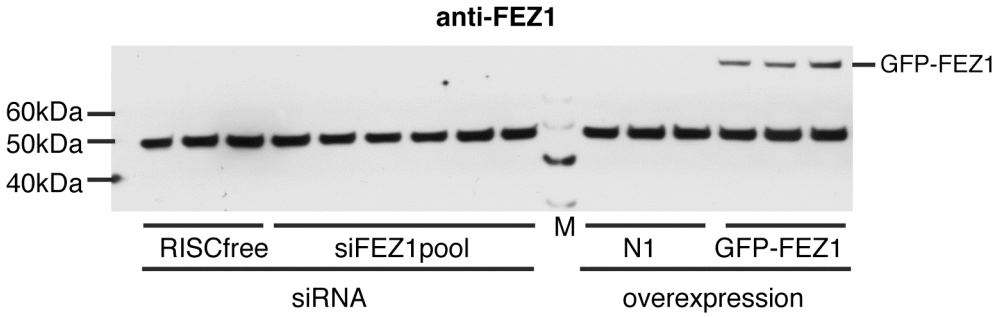

Figure 2.2 Anti-FEZ1 detects overexpressed GFP-FEZ1 but not endogenous FEZ1
Anti-FEZ1 blot (using Abcam anti-FEZ1 goat polyclonal). HEK cells were transfected with indicated siRNA or overxpressed with indicated construct.

HA-TLK2 was provided by Tamara Gruener and Richard Treisman (LRI). HEK cells were grown on 6cm dishes and transfected with 1µg SCOC-myc and 1µg HA-TLK2 and incubated with protein G beads and 2.0µL anti-HA.11 monoclonal (as described above (1.6.2)). Blots were probed with anti-SCOC polyclonal antibody and anti-HA polyconal (1:1000).

2.6.9 FEZ1 and ARL1 experiments

The siRNA pool against FEZ1 was generated by combining the siGenome siRNA duplexes-01, -02, and -04. mRNA levels were determined using a QuantiTect primer (Qiagen, QT00034447).

The siRNA pool against ARL1 was generated by combineing the siGenome siRNA duplexes -01 (gcaauggaaugguuaguug), -03 (uagagacggugacguacaa), -04 (gaacucgggaaaugagaau) (Dharmacon, D-019265). mRNA levels were determined using a QuantiTect primer (Qiagen, QT00044303).

2.7 WAC experiments

2.7.1 WAC annotation

WAC disease associations were determined by Richard Mitter using EMBL-EBI ATLAS (E-GEOD-1751: (Borovecki et al., 2005)); (E-GEOD-3790: (Hodges et al., 2006)). WAC and SCOC disease associations were also determinted using Ingenuity curated findings. WAC conservation was determined using Homologene (NCBI). WAC isoforms were determined using UniProt. The NLS of WAC was determined using ExPaSy tools: http://expasy.org/tools/. The predicted WAC phosphorylation sites were obtained from HPRD (HPRD:18291).

2.7.2 Assesing the effect of WAC knock-down

The following additional siRNA duplexes targeting WAC were obtained:

siRNA duplex	siRNA number	Target sequence
WAC-01	Dharmacon D-013325-01	CAACAUAACGUCUCUGAUU
WAC-02	Dharmacon D-013325-02	UAAGCACACCUCAAACUAA
WAC-53	Ambion s27953	GCACUUAAGUAUUCAUCGAtt
WAC-54	Ambion s27954	CAGUAGCGGUGAUCACAGAtt
WAC-55	Ambion s27955	GUACUCCAGUAGUUAAGCAtt

Table 2.6 Additional WAC duplexes used
Two Dharmacon siRNA duplexes and three Ambion siRNA duplexes targeting WAC additionally ordered are described above.

All GFP-LC3-HEK cell knock-downs for qRTPCR and confocal analysis and all HeLa LC3 lipidation experiments were performed as SCOC experiments as explained above (1.6.3). The WAC p62 degradation experiemnts were performed as above (1.6.4). p62 mRNA levels were determined using a QuantiTect primer assay for p62 (Qiagen).

2.7.3 WAC cloning

WAC cloning was performed using an IMAGE clone obtained for the WAC isoform NM_016628. (NBRC, AK290174). This ORF was subcloned into

pcDNA3.1(-) adding a myc tag to either the N- and C-terminals or a FLAG tag to the C-terminal of the WAC ORF using the following primers:

WAC NT myc:

EcoRVNtermMycWAC 5’
TAGAGATATCACCACCATGGAGCAAAAGCTCATTTCTGAGGAAGATCTCAA
TGGTGTAATGTATGCGAGGAAA

WAC BamHI rev: 5’ TCTAGGATCCTCACACCATGAAGGAATT

WAC CT myc:

EcoRV WAC for: 5’ TAGAGATATCACCACCATGGTAATGTATGCGAGG

WAC Cterm myc BamHI rev: 5’
TCTAGGATCCCTAACCATTGAGATCTTCCTCAGAAATGAGCTTTTGCTCCAC
CATGAAGGAATTCTG

WAC CT Flag:

EcoRV WAC for: 5’ TAGAGATATCACCACCATGGTAATGTATGCGAGG

Wac Cterm flag BamHI rev: 5’
TCTAGGATCCCTACTTGTCATCGTCATCCTTGTAGTCCACCATGAAGGAATT
CTG

2.7.4 WAC antibody

Rabbit polyclonal antibodies were generated using peptides listed below. The serum from Bleed 4 of rabbit STO296 was affinity purified by Sharon Tooze.

STO 293/294 WAC NT1 MVMYARKQQELSDG(C)

STO 295/296 WAC NT2 SKSHPSSGDHRHEKMRDAG(C)

STO 297/298 WAC CT (C)LRQQIKELEKLKNQNSFMV

2.7.5 WAC immunofluorescence

WAC immunofluorescence was performed as follows: HEK cells were fixed in 3% paraformaldehyde for 20 minutes, quenched with 50nM NH_4Cl/PBS for 10 minutes, permeabilised in 0.2% Triton for 3 minutes, and blocked with 0.2% gelatin in PBS. All antibody incubations were done in 0.2% gelatin in PBS and coverslips were washed with 0.2% gelatin in PBS then PBS and finally mounted using moviol onto glass slides.

Antibody	Antigen	Species	Dilution	Supplier
anti-WAC (STO296)	WAC	Rabbit	1:200	LRI
Anti-p62	P62	Mouse	1:250	BD
anti-GABARAP	GABARAP	Sheep* use with donkey 2º	1:100	Abcam (AP1821)
anti-Atg12	Atg12	Mouse	1:100	Abgent (AM1816)
Anti-A1Up	UBQLN4	Mouse	1:50	Santa Cruz
Alexa Fluor 488, 555	anti-rabbit 2º	Goat	1:1000	Molecular Probes (Invitrogen)
Alexa Fluor 488, 555	anti-mouse 2º	Goat	1:1000	Molecular Probes (Invitrogen)
Alexa Fluor 555	anti-sheep 2º	Donkey	1:1000	Molecular Probes (Invitrogen)

Table 2.7 Additional Antibodies
Antibodies used during WAC immunofluorescence experiements are described.

pEGFP-Htt-Q80 was received from Elizabeth Sztul (Tower et al., 2010).

2.7.6 WAC and ULK1 western blotting

Western blotting for ULK1 and WAC was done using the ECL proceedure above. Affinity purified WAC antibody was used at 1:1000 and anti-ULK1 (Santa Cruz) was used at 1:250, both in 5% milk/TBS.

2.7.7 WAC UPS reporter assays

The UbG76V-GFP HeLa cells were obtained from Florian Salomons at the KI (Karolinska Institute, Stockholm, Sweeden), (Dantuma et al., 2000), and the MelJuso UbG76V-YFP cells were received from Nico Dantuma (Karolinska Institute, Stockholm, Sweeden), (Menendez-Benito et al., 2005). MG132 was obtained from Sigma and used at at concentration of 10μM MG132 treatment. Anti-GFP, -p62 and -actin blots were produced using the Licor protocol above.

Chapter 3. Screen Optimisation

3.1 High content siRNA screening

In order to discover new modulators of mammalian autophagy, I performed a genome-wide siRNA-based screen. RNA interference (RNAi) is a powerful tool that allows researchers to pinpoint the function of a single gene in the context of a living cell. By promoting the specific degradation of a target gene's mRNA, small interfering RNA (siRNA) oligonucleotide duplexes inhibit that gene's protein production (Hannon, 2002). If this induces a loss-of-function or a gain-of-function in terms of a certain biological process (in this case, autophagy) then one can hypothesise that the target gene is a modulator of this process. Commercially available libraries consisting of pools of siRNA duplexes targeting the approximately 21,000 currently annotated human genes can be combined with high-throughput screening (HTS) assays in order to probe the human genome with a given question. Recently, developments in microscopy have made it a robust platform for high-content screening (HCS) and large-scale image acquisition can be combined with on-the-fly quantification to generate large amounts of data (Krausz, 2007). Measuring the physiology of intact cells allows researchers to determine the effect of an siRNA pool on a whole cell and not just a single gene, a caveat of reporter gene assays. In addition, it potentially allows the researcher to control for the biological heterogeneity within cell populations and eliminate outliers.

Many HCS projects have increased our knowledge of multiple cellular processes. An image-based siRNA screen of the human kinome for both clathrin- and raft-mediated endocytosis has greatly expanded the knowledge of the signalling pathways and mechanisms involved in this key cellular process (Pelkmans et al., 2005). More recently, a genome-wide siRNA screen of macrophages infected with virulent *Mycobacterium tuberculosis* implicated a large number of required host factors many of which are involved in the regulation of autophagy (Kumar et al., 2010). siRNA screens are made even more powerful when combined with gene array and proteomics data in order to determine expression patterns of target genes. Recently a combined gene array and siRNA-based screen identified the insulin-signalling pathway as a modulator of autophagy-mediated clearance of huntingtin aggregates (Yamamoto et al., 2006). An

image-based screen of a small compound library (480 compounds) illustrated that GFP-tagged LC3 can be visually analysed as a marker for autophagosome formation and provides proof-of-principle for my genome-wide siRNA screen for starvation-induced autophagy (Zhang et al., 2007b).

3.2 Intein-Mediated Luciferase Assay as a basis for the screen

3.2.1 Intein-Mediated Luciferase Reporter Gene Assay

When I began my PhD studentship, the London Research Institute (LRI) did not possess a microscopy system capable of such high-content screening. In order to perform a genome-wide siRNA-based screen to find novel regulators of autophagy, I attempted to create a new assay for autophagy that would utilise the protein-protein interactions that are required for autophagy induction. In early 2006, Kanno *et al* described a novel luciferase-based assay that can monitor cytosolic protein-protein interactions in living mammalian cells. The assay exploits the ability of inteins, or protein "introns," to create a fusion protein that can in turn drive luciferase activity (Kanno et al., 2006). One interacting protein is fused to DnaEn, the N-terminal half of a bacterial DnaE intein, and modified LexA (mLexA) (pmLDn) and the other interacting protein is fused to a DnaEc, the C-terminal half of the protein splicing element and the transcriptional activation domain of VP16 (VP16AD) (pDcV). mLexA is a DNA binding protein modified in order to keep the mLexA/DnaEn fusion protein out of the nucleus constitutively by deletion of its intrinsic NLS. VP16AD is the transcriptional activation domain from a herpes simplex virus and it activates transcription of a reporter gene whenVP16AD and mLexA are spliced together. The reporter assay was based on the ability of inteins, or protein "introns" to post-translationally catalyze, excise and ligate proteins through their autocatalytic endonuclease activity (Chong et al., 1996) so that when the two over-expressed fusion proteins come together in the cell the inteins are in close enough proximity to fold and induce protein splicing, creating a new fusion product of the mLexA and VP16AD (Figure 3.1). The intein-mediated splicing reaction creates a stable peptide bond between the DNA binding protein and the transcriptional-activating protein and this fusion protein diffuses into the nucleus where mLexA binds to a LexA operon upstream of the firefly luciferase reporter gene and the VP16AD

drives transcription of luciferase. In turn, the interaction of the proteins of interest can be quantified by measuring luciferase activity.

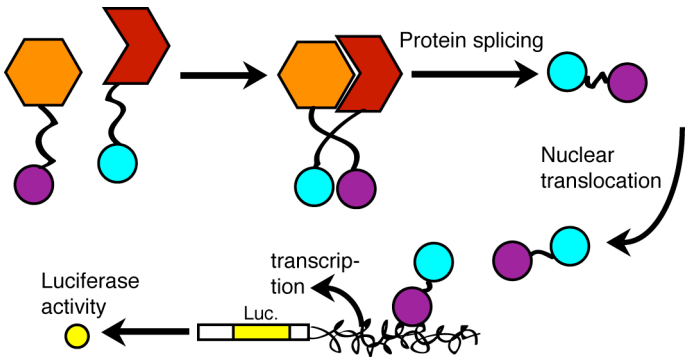

Figure 3.1 Schematic of the principles of the intein-mediated luciferase reporter assay
Schematic displaying how protein-protein interactions lead to intein splicing and luciferase transcription. Plum ball mLexA Blue ball VP16AD, Orange is Protein X and Red is Protein Y. Luc. Represents the luciferase reporter. Adapted from Kanno *et al*, 2006.

The pX8luc reporter gene, the pDcV and pmLDn constructs, and a pcmLV positive control that contains the mLexA and a VP16AD permanently fused together with a short linker between them were obtained from Kanno *et al*. The backbone of these constructs is pcDNA3.1(+) with a two-amino-acid substitution to delete the nuclear localisation signal. A renilla luciferase pGL4.74 reporter gene was used as a control for transfection efficiency of the constructs and in addition, the luciferase activity observed can be normalised to this renilla luciferase activity. This luciferase assay also had the potential to be multiplexed with other assays such as those that measure cell viability. For example, CellTiter-Blue reagent can be combined with luciferin reagents providing a fluorescence read-out of metabolic activity.

3.2.2 Utilising the Intein Luciferase assay to monitor autophagy

Conjugation of LC3 to PE occurs upon induction of autophagy and is the result of the interaction of LC3 with the E1-like enzyme Atg7 and with the E2-like enzyme Atg3 (See introduction, Figure 1.5). If these protein-protein interactions increase as a result of autophagy induction then the induction could be measured using luciferase activity produced by the intein-mediate reporter gene assay. In turn, I could measure the effect of siRNA-mediated gene knock-down on the induction of autophagy by

measuring luciferase activity. To these ends, I cloned LC3, Atg7 and Atg3 into both pDcV and pmLDn (Figure 3.2).

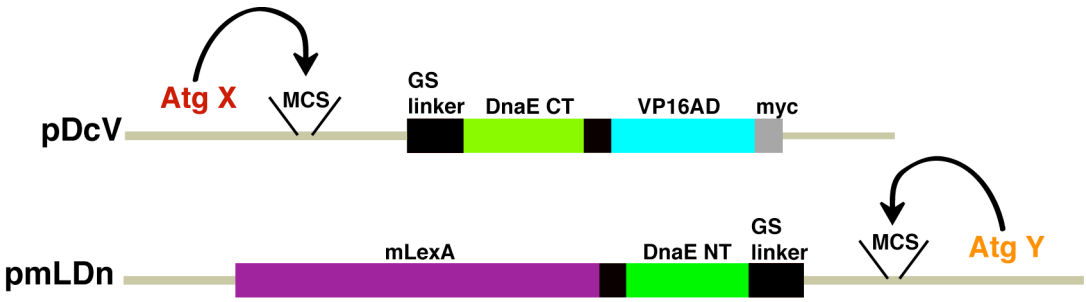

Figure 3.2 Intein construct cloning strategy
Schematic of cloning strategy for the addition of genes-of-interest to pmLDn and pDcV constructs.

I created the following constructs using pDcV (20 kDa) as a backbone: Atg3 pDcV (58 kDa), Atg7 pDcV (98 kDa), and LC3 pDcV (36 kDa) and the following constructs using pmLDn (47 kDa) as a backbone: pmLDn Atg3 (82 kDa), pmLDn Atg7 (120 kDa), pmLDn LC3 (62 kDa). All constructs express at similar levels and at the sizes expected for the fusion proteins (Figure 3.3). In addition to cloning the wild-type LC3 into each backbone, I cloned LC3 missing the C-terminal glycine (LC3ΔG), which is the amino-acid that is exposed by Atg4, where Atg7 and Atg3 bind during conjugation and onto which PE is added into pDcV and pmLDn. The LC3 pDcV constructs allowed me to assess the extent to which LC3 exists in its primed or G-exposed form. When Atg4 cleaves the LC3 wild-type pDcV a smaller protein containing the DnaEc, VP16AD and myc remains but when the G is missing as in the LC3ΔG pDcV this cleavage does not occur and the full fusion protein is expressed (Figure 3.3). It appears that all of the LC3 pDcV exists in its cleaved state suggesting that Atg4 constitutively primes LC3 in HEK cells.

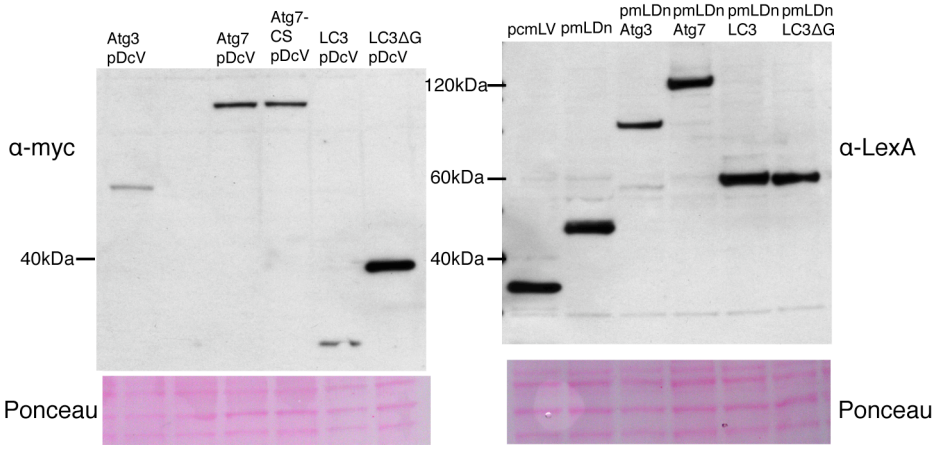

Figure 3.3 Expression of Atg-Intein constructs
Intein-containing fusion proteins are expressed in HeLa cells. Lysates are probed with anti-myc anti-bodies to detect pDcV-containing proteins and with anti-LexA anti-bodies to detect pmLDn-containing proteins.

I transfected Atg-containing intein pairs, the pX8luc reporter gene, and pGL4.74 renilla luciferase control reporter gene into either HEK or HeLa cells plated in 96-well white plates, induced autophagy with Rapamycin and measured firefly luminescence and renilla luciferase activity using Promega's Dual-Luciferase Reporter (DLR) Assay System. I also transfected pcmLV as a positive control and the empty pDcV and pmLDn together as a negative control. All values for luciferase luminescence were normalised to the corresponding renilla luminescence values for that given well. Each test was done in triplicates at least, and often with many more replicates; these replicates were averaged. The values for the positive control, pcmLV, in full medium were set equal to 1 and data for the test pairs was plotted accordingly (Figure 3.4). Corrected luciferase values for the pcmLV were consistently higher, usually at least five-fold higher than any transfected intein pair. Similar activity is seen when the two empty intein constructs are transfected as to when two Atg-containing intein constructs are transfected. I analysed the interaction of the Atg7 pDcV and Atg3 pmLDn intein constructs because I saw a trend that their activity increased with the addition of Rapamycin. This was perhaps a good pair to analyse because they had been shown to co-immunoprecipitate (co-IP) in mammalian cells (Tanida et al., 2002) and Atg3 and Atg7 form an E1-E2 complex as in yeast that is required for autophagosome expansion. Although this complex was shown to occur in non-starvation conditions, after ten experiments I did see a small but consistent increase upon the addition of Rapamycin

with this pair but it was not statistically significant (Figure 3.4). Discouragingly, I did not see a similar increase when Atg3 and Atg7 were cloned into the opposite intein constructs (pDcV and pmLDn accordingly).

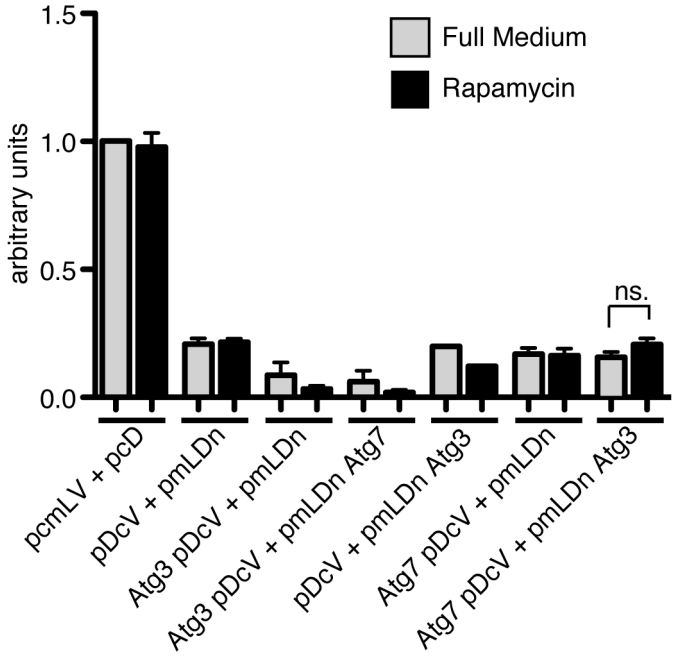

Figure 3.4 Intein luciferase assay analysing Atg7 and Atg3 interaction
HEK or HeLa cells were transfected with reporter genes and shown intein pairs and incubated in full medium or full medium plus 11μM Rapamycin for 4 hours. Corrected luciferase values shown after normalisation to pcmLV+pcDNA3.1 (pcD). pcmLV + pcD (n=10); pDcV + pmLDn (n=8); Atg3 pDcV + pmLDn (n=2); Atg3 pDcV + pmLDn Atg7 (n=2); pDcV + pmLDn Atg3 (n=1); Atg7 pDcV + pmLDn (n=6); Atg7 pDcV + pmLDn Atg3 (n=10). Atg7 pDcV + pmLDn Atg3 p-value = 0.0857.

In order to potentially increase the luciferase activity from intein pairs that included Atg7, I cloned an Atg7 mutant, Atg7CS into the pDcV backbone (Figure 3.3). The Atg7CS mutation should improve the binding of Atg7 to LC3 as it changes the thiol-ester bond between Atg7 and LC3 to an irreversible covalent bond (Tanida et al., 2006). In turn, if this bond it non-reversible I might be able to increase the number of instances where Atg7 and LC3 are bound together, thereby increasing luciferase activity. This, however, was not the case in my intein-mediated luciferase assay (Figure 3.5). Though there was a very small increase in activity in the Atg7CS-LC3 pairing compared to the Atg7 wild-type-LC3 pairing this increase was not significant. As well, the Atg7CS pDcV construct did not improve the activity compared to Atg7 pDcV when binding to pmLDn Atg3 or pmLDn Atg7. If anything, the luciferase activity decreases

after the addition of Rapamycin for these two pairings, though these decreases are not statistically significant (Figure 3.5).

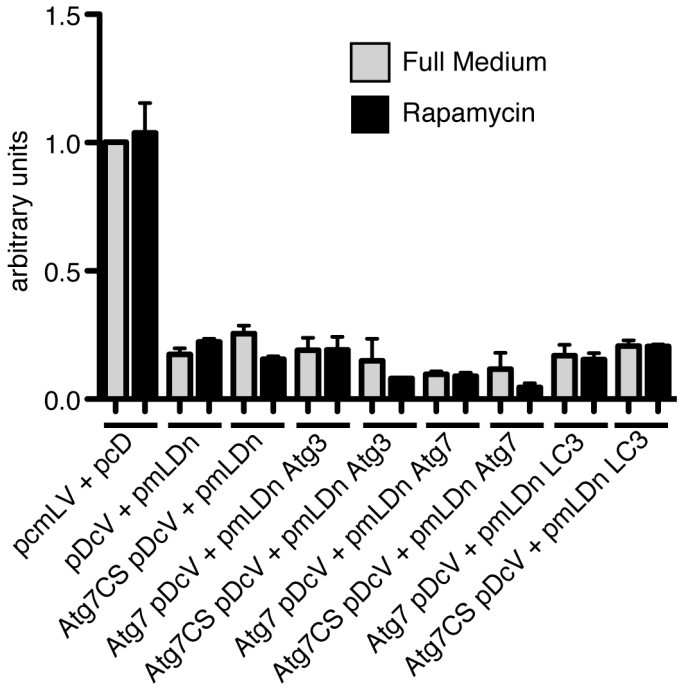

Figure 3.5 Intein luciferase assay with Atg7CS construct
HEK or HeLa cells were transfected with reporter genes and shown intein pairs and incubated in full medium or full medium plus 11μM Rapamycin for 4 hours. Corrected luciferase values shown after normalisation to pcmLV+pcDNA3.1 (pcD). pcmLV+ pcD (n=4); pDcV + pmLDn (n=4); Atg7CS pDcV + pmLDn (n=2); Atg7 pDcV + pmLDn Atg3 (n=4); Atg7CS pDcV + pmLDn Atg3 (n=2); Atg7 pDcV + pmLDn Atg7 (n=4); Atg7CS pDcV + pmLDn Atg7 (n=2); Atg7 pDcV + pmLDn LC3 (n=4); Atg7CS pDcV + pmLDn LC3 (n=4).

Atg3 has been shown to co-IP with Atg7 and the intein-mediated luciferase assay results suggest that binding of Atg7 pDcV to pmLDn Atg3 possibly increases after induction of autophagy by Rapamycin, though not significantly. I attempted to confirm this binding through co-IP experiments and overexpressed Atg7 pDcV and pmLDn Atg3 in HEK cells, incubated lysates with anti-myc antibody (for the pDcV constructs contain a myc-tag), and blotted for LexA, contained in the pmLDn construct. I could confirm pull-down of pmLDn Atg3 with Atg7 pDcV, although the amount of pmLDn Atg3 is not decreased in the unbound supernatant when compared to an equal amount of input lysate taken before co-IP (Figure 3.6, part a). The amount of pmLDn Atg3 pulled down by the co-IP does not increase with the addition of Rapamycin to the cells. Interestingly, Atg7 pDcV appears to be covalently bound to pmLDn Atg3 after co-IP for I observe a band corresponding to the size of Atg7 pDcV in the IP lane that, as

seen in the anti-myc blot, does appear to be reduced after co-IP incubation. In addition, I appear to be co-immunoprecipitating a band of approximately 39 kilo Daltons that may correspond to the fusion protein containing mLexA, VP16AD, myc and linker that is created as a result of the intein-mediated protein splicing event. I also tested the Atg7-containing intein constructs together as Atg7 is reported to homodimerise (Komatsu et al., 2001), though I do not see an increase in luciferase activity over controls for the Atg7 pDcV plus pmLDn Atg7 pairing (Figure 3.5). When I overexpress Atg7 pDcV and pmLDn Atg7 and co-IP as above I see almost identical results as the Atg7 pDcV-pmLDn Atg3 binding. Namely, pmLDn Atg7 is detected after anti-myc immunoprecipitation, a band corresponding to Atg7 pDcV is seen to be bound to this complex, and a band of 39 kDa is seen in the eluate as well (Figure 3.6, part b). Interestingly, a band of over 200 kDa is observed in the anti-myc blot, which may correspond to a pDcV Atg7-pmLDn Atg7 dimer.

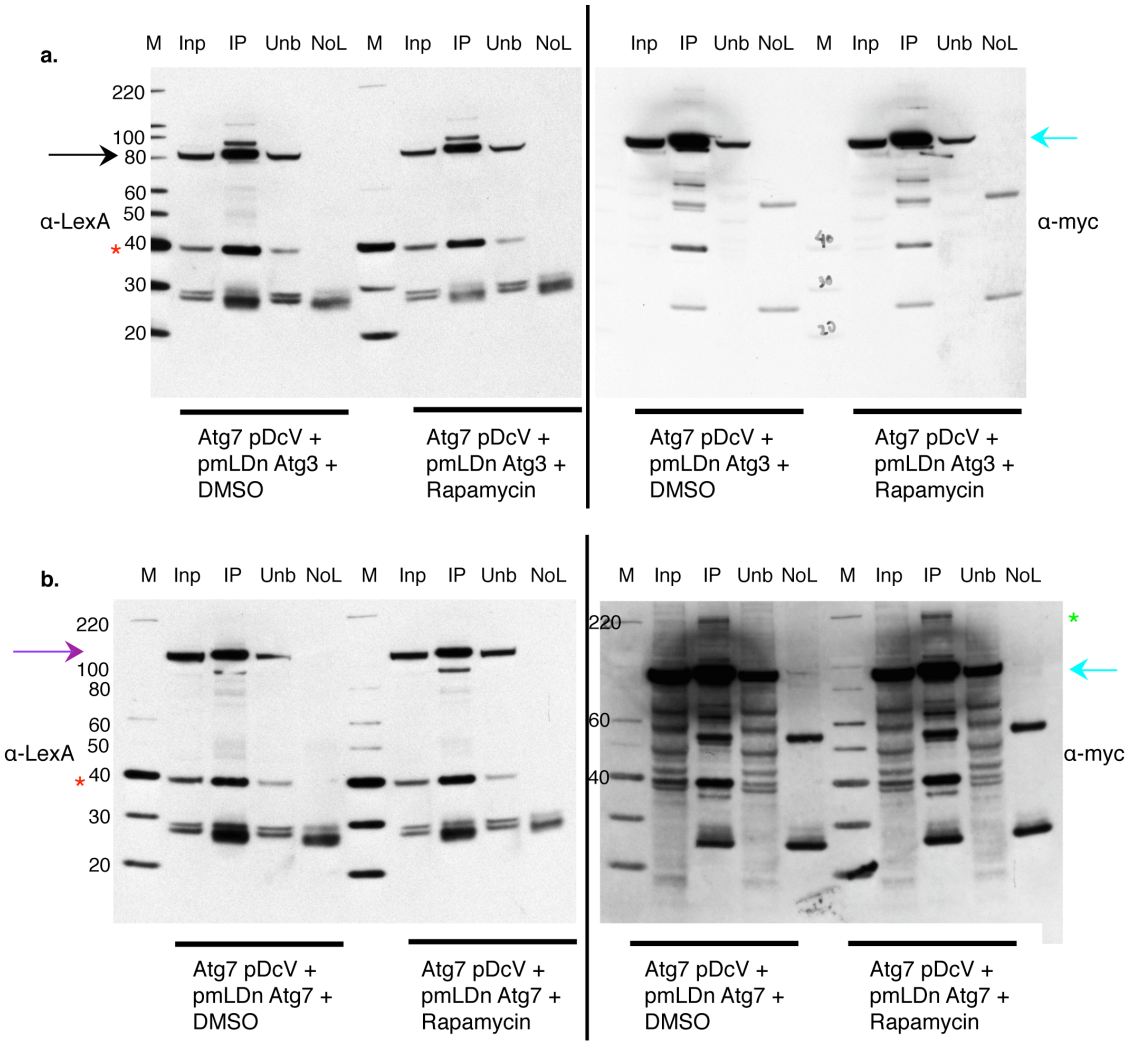

Figure 3.6 Co-Immunoprecipitations of Atg7 and Atg3 intein-containing constructs and Atg7 and Atg7 intein-containing constructs
a. Atg7 pDcV co-IPs pmLDn Atg3. Constructs are overexpressed in HEK cells, incubated with protein G beads and α-myc antibody, blotted for LexA, and stripped and blotted for myc. M is marker; Inp is 5% input or lysate; IP is beads, antibody and lysate; Unb is unbound supernatant after IP; NoL is beads and antibody with no lysate. Black arrow indicates pmLDn Atg3; blue arrow indicates Atg7 pDcV; red asterix indicates possible mLexA-VP16AD splicing product **b.** Atg7 pDcV co-IPs pmLDn Atg7. Constructs are overexpressed in HEK cells, incubated with protein G beads and α-myc antibody, blotted for LexA, and stripped and blotted for myc. Plum arrow indicates pmLDn Atg7; green asterix indicates possible Atg7 pDcV-pmLDn Atg7 dimer.

The intein-mediated luciferase assay at this point did not seem capable of reflecting an induction of autophagy upon Rapamycin treatment using Atg proteins known to bind to each-other as components. In order to test the intein assay in my cell line and transfection conditions I attempted to use the Raf-1 and Ras intein constructs that served as proof-of-principle for Kanno *et al*. I was unable to obtain the Raf-1

pDcV and pmLDn Ras DNA constructs so I cloned Raf-1 and RasV12 into pDcV and pmLDn accordingly using constructs containing Raf and RasV12 (J. Downward, LRI). I chose to use RasV12 because this constitutively active mutant of Ras interacts with Raf-1 without EGF stimulation (Sun et al., 2000). I overexpressed Raf pDcV and pmLDn RasV12 in the luciferase reporter gene assay as above, measured luciferase activity and did not see an increase above the empty intein constructs alone (Figure 3.7). In fact, if anything, the signal was decrease with the Raf-RasV12 pair.

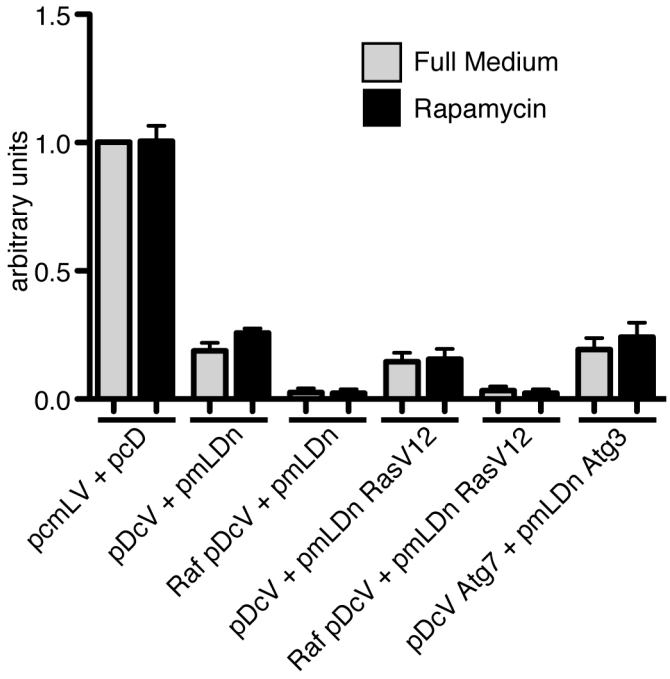

Figure 3.7 Raf and RasV12 intein constructs do not bind as exhibited by the intein luciferase assay

HEK or HeLa cells were transfected with reporter genes and shown intein pairs and incubated in full medium or full medium plus 11μM Rapamycin for 4 hours. Corrected luciferase values shown after normalisation to pcmLV+pcDNA3.1 (pcD). pcmLV+ pcD (n=3); pDcV + pmLDn (n=3); Raf pDcV + pmLDn (n=3); pDcV + pmLDn RasV12 (n=3); Raf pDcV + pmLDn RasV12 (n=3); Atg7 pDcV + pmLDn Atg3 (n=3).

Raf-1 and RasV12 are expected to interact and this interaction has been demonstrated using the intein-mediated luciferase assay, though I could not replicate this data. I attempted to confirm the interaction of Raf pDcV and pmLDn RasV12 by co-IP as before and do see binding of the two constructs (Figure 3.8). In contrast to the Atg7 pDcV co-IPs with pmLDn Atg3 and pmLDn Atg7, when I co-IP Raf and RasV12 intein constructs I do not see bands of approximately 39 kDa potentially corresponding to the mLexA-VP16AD-myc intein-splicing product. This may explain why the

luciferase levels I observe for Raf pDcV plus pmLDn RasV12 are so much lower than pDcV plus pmLDn alone (Figure 3.7); it appears that the presence of the Raf pDcV construct inhibits intein-mediated splicing. I asked whether the addition of pDcV to Raf was preventing the Raf1-RasV12 interaction and attempted to co-IP myc-tagged Raf with pmLDn RasV12. Opposite to this hypothesis, only a very weak band of pmLDn RasV12 is seen to co-IP with myc-tagged Raf (Figure 3.8).

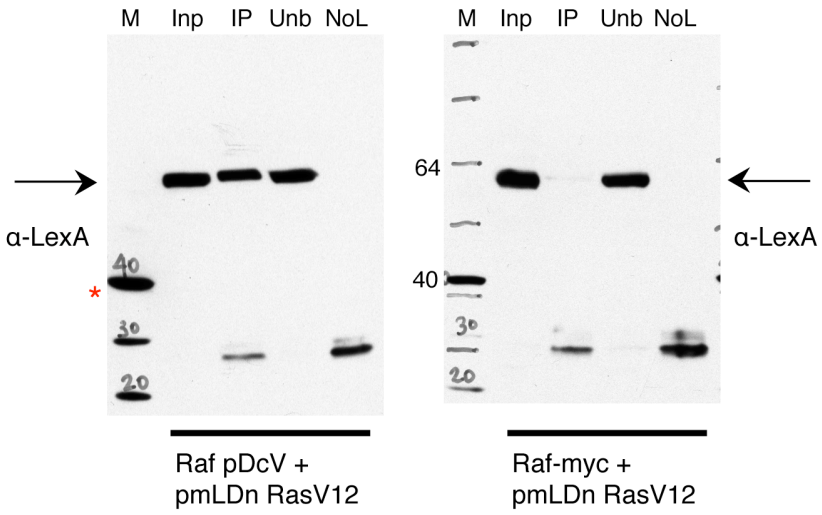

Figure 3.8 Raf pDcV and pmLDn RasV12 co-IP but Raf-myc does not co-IP pmLDn RasV12
Constructs are overexpressed in HEK cells, incubated with protein G beads and α-myc antibody, blotted for LexA. Black arrow indicates pmLDn RasV12. Red asterix indicates 39 kDa band seen after previous intein construct co-IPs. Blots were stripped and blotted for myc and Raf pDcV and Raf-myc were observed in the input and unbound supernatant lanes (data not shown).

I asked whether induction of autophagy with a longer time frame (i.e. longer than two hours of starvation or Rapamycin treatment, as above) would be better suited to my reporter gene system. It may take a significantly longer amount of time after the induction of autophagy for the proteins of the LC3-conjugation system to come together, intein splicing to occur, the mLexA-VP16AD fusion protein to diffuse into the nucleus, and luciferase transcription and translation to occur as compared to observing the formation of GFP-LC3 spots after autophagy induction, for example, which can be visualised after as little as ten minutes (Kochl et al., 2006). I chose to induce autophagy with lithium chloride, whose induction of autophagy had been observed after 48 hours

treatment (Sarkar et al., 2005). Treating the cells with lithium chloride, like Rapamycin, eliminates the handling and cell loss experienced with washing and starvation, but its long incubation time may allow for a higher efficiency of the intein-mediated reporter assay. I transfected HEK cells with luciferase reporter genes and intein-containing constructs as above and then incubated cells in low-dose Rapamycin or lithium chloride for 48 hours and measured luciferase activity. I normalised for renilla as usual but due to a large increase in activity after lithium chloride treatment compared to full medium or Rapamycin, I set the full medium values equal to 1 and plotted the corrected values for Rapamycin and lithium chloride (Figure 3.9, part a). As seen previously, Rapamycin does not induce luciferase activity above 1 but increased activity compared to the pcmLV plus pcDNA3.1 control for three intein pairs: Atg7 pDcV plus pmLDn Atg3, Atg7 pDcV plus pmLDn LC3, and Atg3 pDcV plus pmLDn LC3.

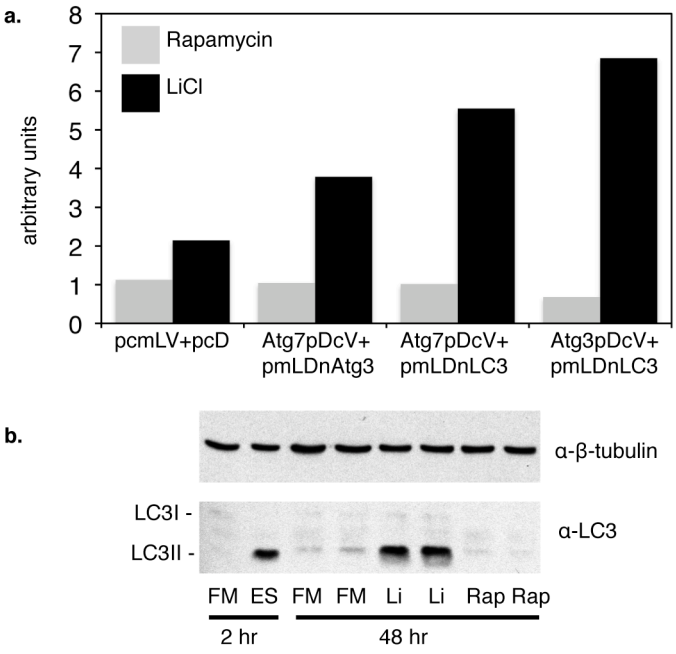

Figure 3.9 LiCl induces intein-mediated luciferase activity and LC3 lipidation
a. HEK cells were transfected with reporter genes and shown intein pairs and dosed with 0.2μM rapamycin or 10mM lithium chloride (LiCl) for 48 hours. Corrected luciferase values were normalised to full medium values. **b.** Western blots against β-tubulin and LC3 after 2 hours incubation in full medium (FM) or Earle's Buffered Saline Solution (ES) or 48 hours incubation in FM, 10mM lithium chloride (Li), or 0.2μM Rapamycin (Rap).

In order to measure the extent of autophagy induction after 48 hours of Rapamycin or lithium chloride exposure, I observed LC3 lipidation by western blot.

After two hours of starvation, the LC3II form is in much higher abundance than the LC3I form in HEK cells (Figure 3.9, part b). After 48 hours of LiCl treatment a large accumulation of LC3II is seen, an amount that is perhaps greater than that after two hours starvation. This confirms that autophagy is induced after 48 hours of lithium chloride treatment. Though these results reflect an ability to quantify autophagy induction with the intein-mediated reporter assay, induction of autophagy with lithium chloride is non-canonical in that it is suggested to be mTOR-independent (Sarkar et al., 2005) and therefore not a good inducer for my genome-wide screen for autophagy.

Another possible reason why the intein-mediated reporter assay was not reflecting autophagy induction is that I was overloading the cells with multiple constructs thereby inhibiting the reporter assay itself and over-taxing the cells. In order to decrease the expression-load of the cells, I created a HeLa cell line stably expressing pX8luc, the reporter gene for the assay. In addition to not having to overexpress pX8luc in the cells, I would also theoretically be able to leave out the renilla luciferase control reporter gene because the cell line would show homogenous pX8luc expression. When these cells are transfected with only intein-containing construct pairs, luciferase activity is observed (Figure 3.10). As before, the greatest amount of activity is seen with the positive control pcmLV and similar activity is seem for the empty intein constructs as well as the Atg-containing intein pairs. Also as before, a slight increase of activity is seen upon Rapamycin treatment with the Atg7 pDcV plus pmLDn Atg3 pair.

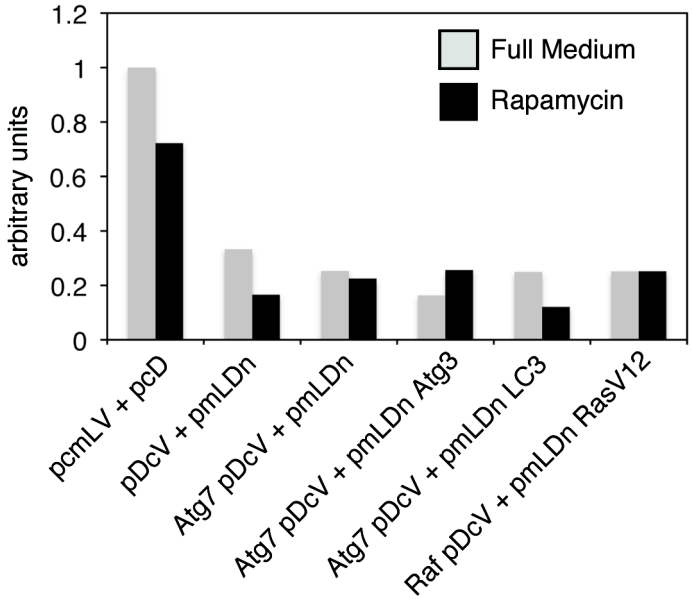

Figure 3.10 Intein-mediated luciferase assay is not improved by measuring interactions in a stable cell line
HeLa cells stably expressing pX8luc were transfected with shown intein pairs and incubated in full medium or full medium plus 11μM Rapamycin for 4 hours. Luciferase values were normalised to pcmLV + pcDNA3.1 (pcD) in full medium.

Taken together, the results of the multiple attempts to use the intein-mediated luciferase reporter gene assay to quantify the interactions of the proteins involved in the LC3-PE conjugation reaction indicate that the assay is not sufficient to monitor autophagy induction. The induction seen with the Atg7-Atg3 intein pair after Rapamycin treatment was not statistically significant, let alone strong enough on which to base a genome-wide screen. In addition, I was unable to observe modulation of this read-out after knock-down of autophagy genes such as ULK1 (data not shown).

3.2.3 Theories as to why the intein-mediated reporter gene assay cannot be used to monitor autophagy

Overall, the intein-mediated reporter gene assay did not show significant-enough fold increase after autophagy induction. One reason for this is that the background signal, that of pDcV and pmLDn alone was disturbingly high. I used co-IP to determine whether these fusion proteins were interacting in the cell. I overexpressed both fusion proteins in HEK cells, immunoprecipitated with anti-myc antibodies and blotted for LexA and could detect pmLDn bound to pDcV (Figure 3.11). Interestingly, I also observed, as before, the 39 kDa band that possibly reflects the mLexA VP16AD protein that here results from a basal interaction between pDcV and pmLDn and this is reflected in the basal luciferase activity seen in the reporter assay. Kanno *et al* refer to the dynamic range of the assay in their report claiming that the increase of activity caused by the Ras and Raf1 interaction is only four fold at most in that the background gives a signal of approximately 10 and maximum is signal of forty (Kanno et al., 2006).

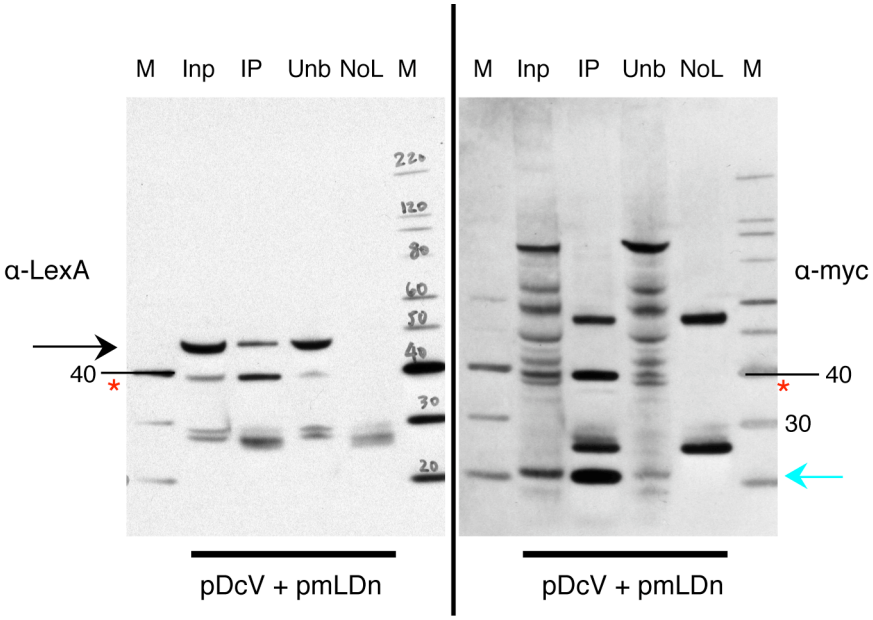

Figure 3.11 Intein-containing backbone constructs pDcV and pmLDn co-IP
pDcV and pmLDn are expressed in HEK cells, incubated with anti-myc antibody and blotted for LexA. Black arrow indicated pmLDn; blue arrow indicates pDcV; red asterix indicates possible mLexA-VP16AD splicing product.

Perhaps the fusion of the autophagy proteins LC3, Atg3, and Atg7 to inteins and either mLexA or VP16AD no longer allows these proteins to perform their normal function. Specifically, Atg7, the largest of the three proteins, is perhaps no longer able to interact with LC3 or Atg3 in order to perform its E1-like enzymatic activity. In addition, Atg7 has been reported to homodimerise yet the intein-mediated luciferase activity of the two Atg7-containing intein constructs is no higher that the empty intein controls. Perhaps adding the bulky inteins and DNA binding proteins to Atg7 sterically hinders this known protein-protein interaction. Similarly, Raf-1 is known to bind to RasV12 yet I do not see increased luciferase activity with their corresponding intein-containing constructs. As shown by co-IP, I do not see binding of myc-tagged Raf-1 with RasV12 when it is expressed in the pmLDn. Confusingly, Raf-1 expressed in the pDcV backbone even inhibits luciferase activity far below that seen with empty intein controls suggesting that the conformation of Raf pDcV is inhibiting the interaction of the intein constructs that is observed at a basal level in the reporter assay, as seen in Figure 3.11.

Overexpression of the three autophagy proteins might drive or even inhibit autophagy. For example, it has been shown that Atg3, though ubiquitously expressed in all human tissue, when overexpressed facilitates the formation of the Atg12-Atg5 conjugate perhaps above its basal levels (Tanida et al., 2002). This might drive autophagy for it has been shown that the Atg12-Atg5 conjugate provides E3-like activity for LC3 conjugation (Hanada et al., 2007) and induction of autophagy with Rapamycin, for instance might not cause a detectable increase above this increased basal autophagy. Conversely, overexpression of Atg7 and Atg3, which I have shown interact if overexpressed in intein-containing constructs and which are known to bind in normal growth conditions, could inhibit autophagy. For these two overexpressed proteins may prefer to exist bound together, and may even bind endogenous Atg7 and Atg3 leaving less protein available to perform their E1- and E2-like activities.

An inherent disadvantage to the intein-mediated reporter assay is that it requires the overexpression multiple proteins, thus multiple DNA transfections. In order to perform the siRNA-based screen I will also have to knock down individual genes by transfecting said siRNA thereby increasing the load to the cells even further. I attempted to reconcile this by creating a stable cell line containing the pX8luc reporter gene. If the assay proved successful, however, I would have had to consider creating a cell line that not only overexpressed the reporter gene but also the chosen intein-containing binding pairs as well.

Another caveat is that the intein-mediated reporter assay may only work in the cell line in which is was first described, CHO cells. Perhaps the assay needs to be optimised and modified for use in HEK or HeLa cells in that different cell types may have differential self-catabolising intein capabilities. It was critical to me that I use human cells for my genome-wide screen, for I would be knocking out human genes with siRNA so an assay that only works in Chinese hamster ovary cells is of little use. Similarly, perhaps the assay only works well to monitor the Ras and Raf-1 interaction. Unfortunately I could not see an increase in activity with RasV12 and Raf-1-containing constructs that I cloned. However, Kanno *et al* went on to utilise the intein-mediated reporter assay to monitor MAPK function by monitoring the Ras-Raf-1 interactions (Kanno et al., 2009). No other publications to date describe successful use of the intein-mediated reporter gene assay to detect other protein-protein interactions or assess

modulations of interactions. Perhaps the assay only works for interactions close to the plasma membrane. Initially Kanno et al state that the assay can be used to detect cytosolic protein-protein interactions but later clarify that the luminescence signals are "sufficient for evaluation of interactions close to cell membranes" or as they later called them "juxtamembrane protein-protein interactions"(Kanno et al., 2006). The conjugation of LC3 occurs throughout the cytoplasm and is not reported to preferentially occur close to the plasma membrane, so perhaps the intein-mediated reporter assay is for this reason, not suited to monitor the protein-protein interactions required for LC3 lipidation.

3.3 Optimisation of Imaged-based screen

As the LRI did not have a suitable microscope and quantitative software to capture GFP-LC3-labelled autophagosomes on a large scale, I attempted, as described above, to create non-image-based but high-throughput assay for autophagy. However, by 2007 the LRI had purchased a fluorescence microscope and accompanying image processing platform, the Thermo Scientific Cellomics ArrayScan VTI High Content Screening (HCS) reader. In 2007, the High-Throughput Screening (HTS) lab was established within the LRI and I worked with members of the HTS lab to set up an image-based screen for autophagy.

GFP-LC3 is incorporated specifically into the autophagosome membrane so that GFP-LC3 is a bona fide marker of autophagosomes and in stable cell lines over-expressing the marker, each GFP-LC3 spot represents an autophagosome and can be quantified (Rubinsztein et al., 2009), (Klionsky et al., 2008). The formation of GFP-LC3-labelled autophagosomes, or 'spots' to which I hereafter refer, can be seen as quickly as ten minutes after induction of autophagy (Kochl et al., 2006). A HEK293A cell line stably expressing eGFP fused to rat LC3, hereafter referred to as HEK-GFP-LC3 cells had been established in the lab (Chan et al., 2007) and was successfully used as the basis of an siRNA-based kinome screen. In this smaller-scale screen, Chan *et al* measured the lipidation of eGFP-LC3 after siRNA knock-down and discovered that ULK1, and not ULK2 was required for the formation of autophagosomes. Furthermore, in 2007 a group published a screen based on a human glioblastoma H4 cell line stably

expressing LC3-GFP (Zhang et al., 2007b) and used the cell line to assay a library consisting of 480 known bioactive compounds and quantified spots using a Cellomics ArrayScan VTI in order to identify those compounds that increased spots, or inducers of autophagy. I set out to utilise the Dharmacon siGenome library comprised of 21,127 siRNA Smartpools, our documented GFP-LC3-HEK cell line, the Cellomics ArrayScan VTI and the HTS lab in order to find novel regulators of autophagy.

3.3.1 Measuring the appearance of GFP-LC3 spots after induction of autophagy

I first established I could both visualise the formation of GFP-LC3 spots but also quantify this induction of autophagy using the Cellomics ArrayScan fluorescence microscope and accompanying quantitative software that simultaneously converts these images into data. GFP-LC3-HEK cells were plated onto clear-bottomed, black, 96-well tissue culture-treated plates, allowed to adhere to the plate and grown in normal nutrient conditions for 24 hours. I induced autophagy either with the addition of Rapamycin as above or by starvation (Figure 3.12). Starvation-induced autophagy was achieved by culturing cells in medium devoid of amino acids (Earle's Buffered Salt Solution, EBSS) or EBSS plus leupeptin, a lysosomal protease inhibitor that partially prevents the degradation, allowing the assessment of the total number of autophagosomes formed during the incubation period. After two hours of Rapamycin treatment or starvation, cells were fixed with Paraformaldehyde and their nuclei stained with Hoechst. In full medium GFP-LC3 displays diffuse cytoplasmic staining and though LC3 is not a nuclear protein, GFP-LC3 that has diffused into the nucleus is also seen (Figure 3.12, panel a). The diffuse cytoplasmic staining represents the unlipidated or GFP-LC3I form of the protein. Upon induction of autophagy, GFP-LC3 is lipidated and this GFP-LC3II is incorporated into the autophagosome membrane, and these appear as spots.

Images were collected using a 20X 0.45NA lens and analysed upon acquisition using the Cellomics SpotDetector V3 Bioapplication beginning in the middle of the plate, in both the DAPI/Hoechst and GFP channels (Channel 1 and Channel 2 respectively). Several parameters were recorded including the number of nuclei (object count; OC) from the Channel 1, and from Channel 2: the number of GFP-LC3 spots per cell (spot count per object; SCPO), the total intensity of GFP-LC3 spots per cell (spot total intensity per object; STIPO), and the total area covered by GFP-LC3 spots per cell

(spot total area per object; STAPO). Induction of autophagy with Rapamycin, EBSS or EBSS plus leupeptin increases SCPO, STIPO and STAPO compared to full medium (Figure 3.12, panel b) and incubation in EBSS plus leupeptin provoked the most robust increase in all three parameters. This data was generated from at least 250 objects and since these were healthy, untransfected cells that were quite confluent this only required acquisition of images from two to three fields.

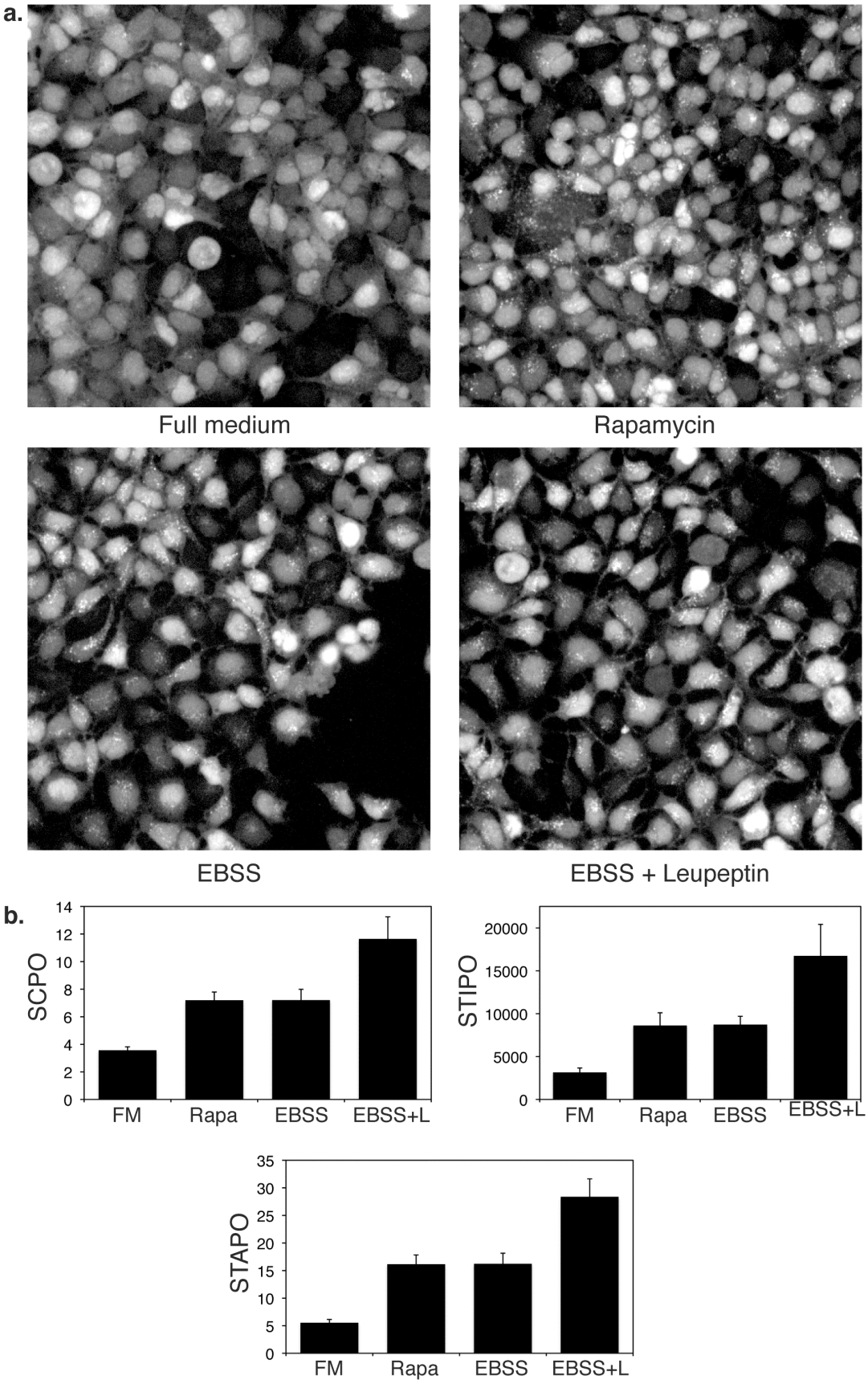
a.
Full medium
Rapamycin
EBSS
EBSS + Leupeptin
b.
SCPO
0
2
4
6
8
10
12
14
FM
Rapa
EBSS
EBSS+L
STIPO
0
5000
10000
15000
20000
FM
Rapa
EBSS
EBSS+L
STAPO
0
5
10
15
20
25
30
35
FM
Rapa
EBSS
EBSS+L

Figure 3.12 Induction of autophagy seen in Cellomics Images
a. Cellomics ArrayScan images of GFP-LC3 spots captured on Channel 2 at 20X after 11μM Rapamycin treatment, EBSS or EBSS with 0.25mg/mL leupeptin for two hours. b. Quantification of SCPO (Spot count per object), STIPO (Spot total intensity per object), and STAPO (Spot total area per object). FM is full medium, Rapa is Rapamycin, and EBSS+L is EBSS plus leupeptin. Error bars represent standard deviation from 4 wells.

As the GFP-LC3-HEK cells do not adhere to tissue-culture-treated plates as well as other adherent cells such as HeLa cells and tend to become detached from the plate when manipulated, I minimised cell loss by gently pipetting with a multi-channel pipette but also coated the plates with Poly-D-Lysine before plating the cells to help them adhere better. We adjusted parameters in the Cellomics SpotDetector V3 Bioapplication in order to accurately determine the number of nuclei which in turn establishes the number of validated objects, or object count (OC). This object count is important for it is used to determine spot count, spot total intensity, and spot area per object. GFP-LC3-HEK cells were plated on 96-well plates, fixed, and stained with Hoechst as above. Images were collected at 20X on Channel l, the DAPI/Hoechst channel, and the SpotDetector program drew a mask, designated with a blue line, around the nuclear staining (Figure 3.13). Staining that did not meet certain criteria set for parameters such as size or shape were not designated as objects and these can be seen as small yellow rings. Some GFP-LC3-HEK cells are multinuclear and also depending on parameters set, these can be included or not. Here, a large multinucleated cell or a clump of cells is called as an object (lower right-hand corner). Objects that lie too close to the edge of the field are not considered in calculations for SCPO, STIPO, or STAPO because parts of their corresponding cytoplasm lie outside the field and spots in those areas will not be counted, thus skewing the data for SCPO, STIPO, and STAPO. These uncounted nuclei are also designated with yellow masks below.

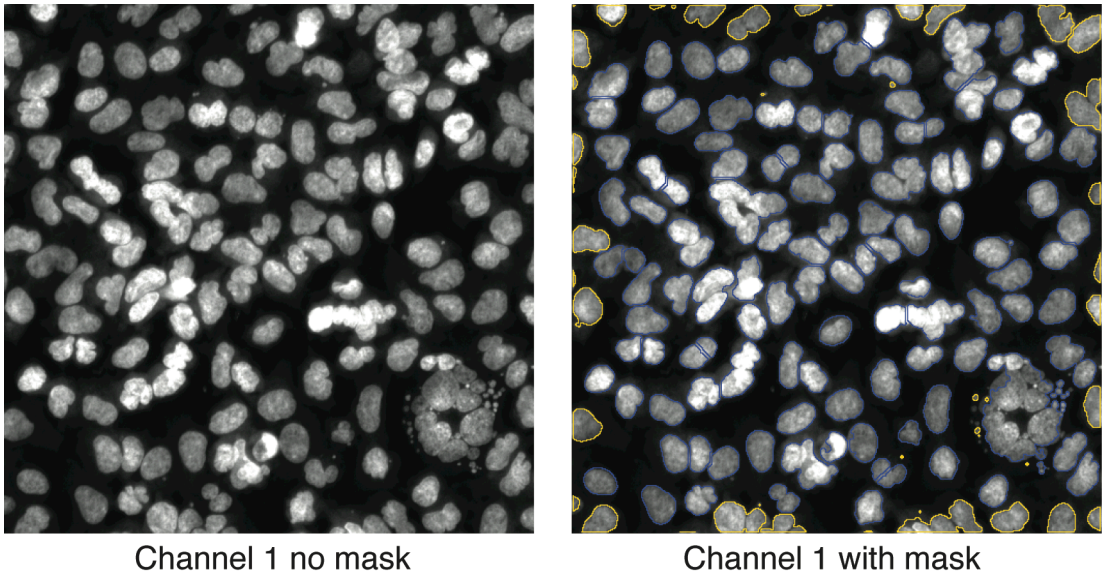

Figure 3.13 Cellomics images depicting nuclear staining and determination of valid object count (OC)
Images of GFP-LC3-HEK cells in Channel 1 (DAPI/Hoechst channel) shown without or with SpotDetector nuclei masks. Nuclei with blue masks contribute to the OC while those with yellow masks do not.

The Cellomics SpotDetector V3 Bioapplication was best suited for counting spots and we confirmed that it was the most capable program to accurately assess changes in GFP-LC3 spots in our stable cell line. GFP-LC3-HEK cells were plated on 96-well plates, allowed to grow for 24 hours and then treated with Vinblastine in order to image the accumulation of autophagosomes (Arstila et al., 1974). The cells were then fixed, stained with Hoechst, and images were captured at 20X in Channel 1 and Channel 2 (Figure 3.14) using the GFP channel (Channel 2) to set the focus with fixed illumination time. In a similar way that a mask is drawn around nuclear staining as shown above, a mask is placed on GFP-LC3 spots in Channel 2 (the GFP channel) in order to designate them as countable spots. First, a line is drawn around the nuclear staining determined by Channel 1 as described above (blue line). Cells on the edge of the field are not counted and receive no blue ring. Then a ring 22 microns from the edge of the nucleus is drawn (green line). Last, GFP-LC3-labelled autophagosomes are defined by adjusting parameters including spot area, shape, and average intensity and marked with magenta spots if they meet said criteria. After each optimisation experiment plates were scanned and adjustments to the SpotDetector parameters were made. This was required because cell density as well as the strength of the induction of

autophagy differed between experiments. We compared uninduced cells with a small number of basal GFP-LC3 autophagosomes per field to induced cells with multiple spots per cell and adjusted the parameters in an attempt to minimise the number of GFP-LC3 spots that were incorrectly not called and minimise the amount of cellular debris or other non-spots that were miscalled. As described above, spots in cells close to the edge of the field are not marked with magenta and do not count towards quantification of SCPO or STIPO as shown (Figure 3.14, panel b). Also we excluded any contribution from nuclear spots or areas of increased GFP intensity in the nucleus or cytoplasmic GFP-LC3 spots that lie above the nucleus thereby restricting the analysis to perinuclear and cytoplasmic GFP-LC3 spots.

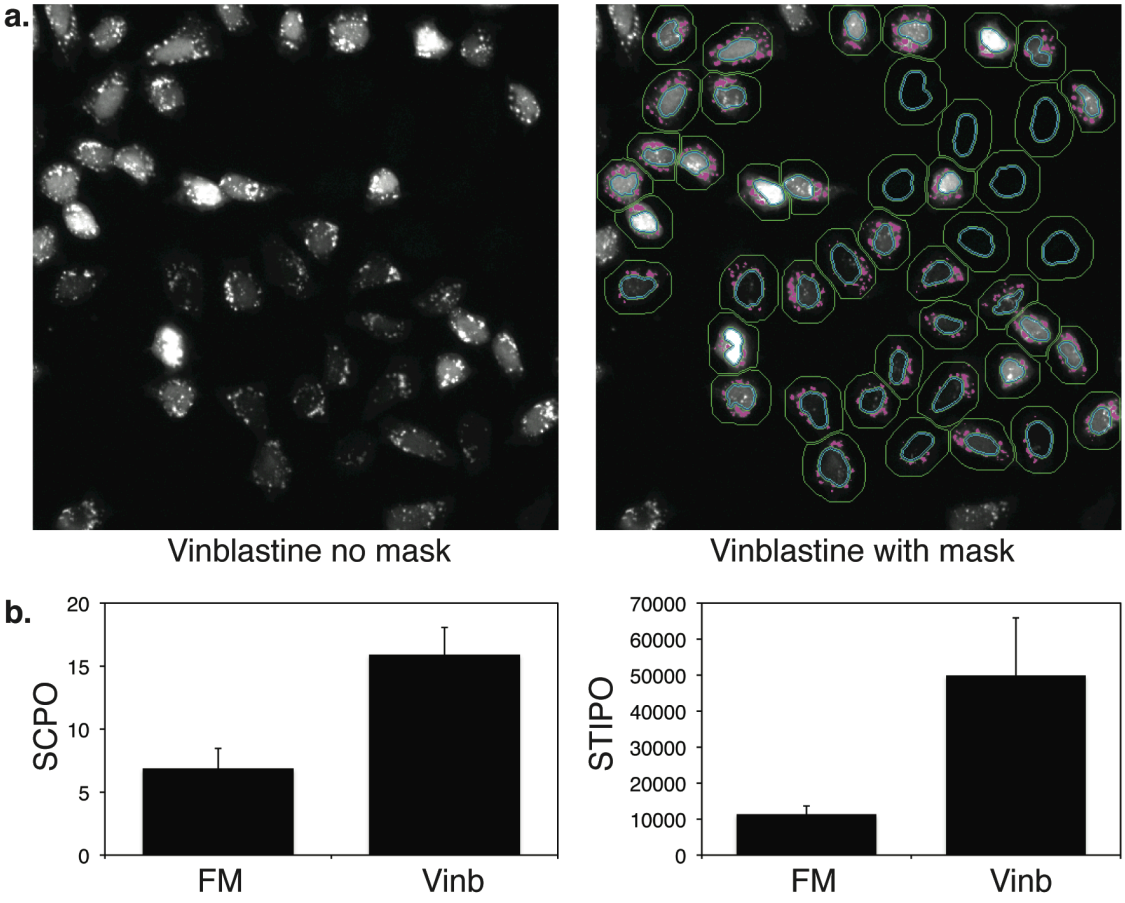

Figure 3.14 Counting GFP-LC3 spots with Cellomics SpotDetector
a. Images of GFP-LC3-HEK cells in Channel 2 (GFP) after 50μM vinblastine treatment for two hours shown without or with SpotDetector nuclear, ring and spot masks. The blue ring designates the nucleus, the green designates the ring within which spots are counted and the magenta designates spots.

In an attempt to determine whether using a different type of plate could lead to a more accurate quantification of GFP-LC3-labled autophagosomes as well as better

resolution in order that we might classify the GFP-LC3 spots in terms of different morphology (Zhang et al., 2007b), I plated GFP-LC3-HEK cells on plates with extra-thin plastic bottoms (Imaging Plates, BD Falcon) and captured images at 20x magnification. The data produced did not reflect the induction of autophagy better and in fact, were troublesome to the Cellomics ArrayScan. The bottoms of the wells were quite fragile and easily damaged and thus, the ArrayScan had trouble focusing on the GFP-LC3 spots and data acquisition was not optimal. Glass-bottomed plates were also tested and had similar problems as the Imaging Plates without significantly improved resolution or spot-calling. We determined that we could capture images of GFP-LC3 spots at 20x magnification (650nm/pixel) and quantification of these spots reflected induction of autophagy but we wanted to ask if the increased resolution resulting from capturing images at 40x would lead to more robust data. The spots were slightly better resolved at higher magnification but the signal to noise ratio was not significantly resolved and the fold induction between uninduced and induced was not significantly greater. In addition, the time needed to process plates from a genome-wide screen captured at 40x would at least double and in the interest of saving processing time, we determined it would not be feasible to capture imaging at 40x. To conclude, I determined that induction could be quantified in terms of GFP-LC3 SCPO, STIPO, and STAPO using a Cellomics ArrayScan and that the best induction of autophagy was seen with EBSS plus leupeptin.

3.3.2 Optimising siRNA transfection

It had been shown that siRNA targeting Atg7 and ULK1 inhibited autophagy in the GFP-LC3-HEK cell line (Chan et al., 2007). In fact, HEK cells are an established system for they are known to be relatively easy to transfect. As a starting point to optimise of siRNA knock-down in GFP-LC3-HEK cells I copied the format of the kinome screen and used 96-well plates and 72 hours total incubation including a 24 hour recovery, with induction of autophagy on day four. Because of the experimental manipulations antibiotics (Penicillin and Streptomycin) were added throughout the screen. It is established that antibiotics often hinder lipid-based transfections so I had to find a transfection method that was effective in the presence of antibiotics.

The kinome screen was done using a conventional transfection protocol in which cells are plated onto the 96-well plates, left to adhere and grow for 24 hours, then

siRNA is incubated with Oligofectamine lipid transfection reagent (Invitrogen) for a short period of time (20 minutes), added to the cells, left for 48 hours, and the cells are finally put to recover in normal full growth medium for 24 hours. Instead, I tested a 'reverse' or 'wet' procedure where the siRNA and transfection reagent are incubated directly on the plate for 20 minutes and the cells are resuspended in 80% of the final volume and added to this mixture; this transfection method was suggested by Dharmacon to provide a more efficient siRNA knock-down ("Rapid Screening for Target Identification," DHARMACON RNA Technologies). For large scale siRNA screens there are several parameters that needed to be addressed. First, on day one of the screen the siRNA will already have been aliquoted onto the plates because it can take up to a day for the robots to aliquot the siRNA library onto the plates due to the large size of the genome library. Second, the number of times the siRNA of the siGenome library is frozen and thawed is limited. I compared the conventional and reverse transfection using Oligofectamine and the cells knocked down by reverse transfection actually survived better (as measured by OC) and looked healthier than those knocked down by conventional transfection. I believe that this is influenced by cell density during transfection: the cells need to be confluent enough to survive the toxicity of the lipid transfection reagent but sparse enough so that there are enough siRNA/lipid transfection reagent molecules for each cell. In addition, the image-based quantification of GFP-LC3 adds another demand on density in that if the cells are too close together at the time of image acquisition and the cytoplasm is not spread out, GFP-LC3 spots appear to be bunched together and are not accurately called. Also, if the cytoplasm is pushed up over the nuclei of the cells the cytoplasmic GFP-LC3 spots are excluded from the SpotDetector analysis, as described above. Last, we have observed in the lab that if cells are too close in proximity to each other (too dense) then they do not starve as well by culturing them in EBSS.

Therefore, I set up experiments to identify the best siRNA transfection reagent for a 72 hour reverse transfection in the presence of antibiotics at a optimal cell density for GFP-LC3-HEK cells. I had observed that knock-down of ULK1 strongly inhibited GFP-LC3 spot formation and that the 72 hour transfection was extremely efficient for ULK1 siRNA. Atg7 siRNA was used to find the best transfection reagent for my assay from a panel of 20 reagents acquired by the HTS lab because I observed that Atg7

knock-down was more variable and often its effect on spot parameters was more subtle. I tested the 20 reagents at three different final concentrations per well combined with or without Atg7 siRNA using reverse transfection. The siRNA was mixed with the different amounts of reagent for 20 minutes, 4000 GFP-LC3-HEK cells in full medium supplemented with antibiotics were added per well, cells were incubated for 48 hours followed by a change to fresh full medium and a 24 hour incubation. Finally, autophagy was induced by incubation in EBSS plus leupeptin for two hours, and the effect on GFP-LC3 spots was measured. The 20 reagents, listed in Materials and Methods (2.3.2.1), had various effects on cell viability and the number of GFP-LC3 spots per cell after Atg7 knock-down (Figure 3.15). Six transfection reagents were toxic to the cells, reducing OC and often skewing SCPO; these reagents included numbers 2, 4, 9, 12, 14, 20. Reagent number 8, Lipofectamine2000 (Invitrogen) was the best, achieving the strongest effect on SCPO at 0.33µL. Although cell viability was not as good, Ambion's siPORT Amine transfection reagent (2) had a dose-responsive effect on SCPO, though data is missing for the high dose of reagent without Atg7 siRNA. Oligofectamine (7, Invitrogen), the reagent used in the kinome screen, does not appear to be very effective in this assay.

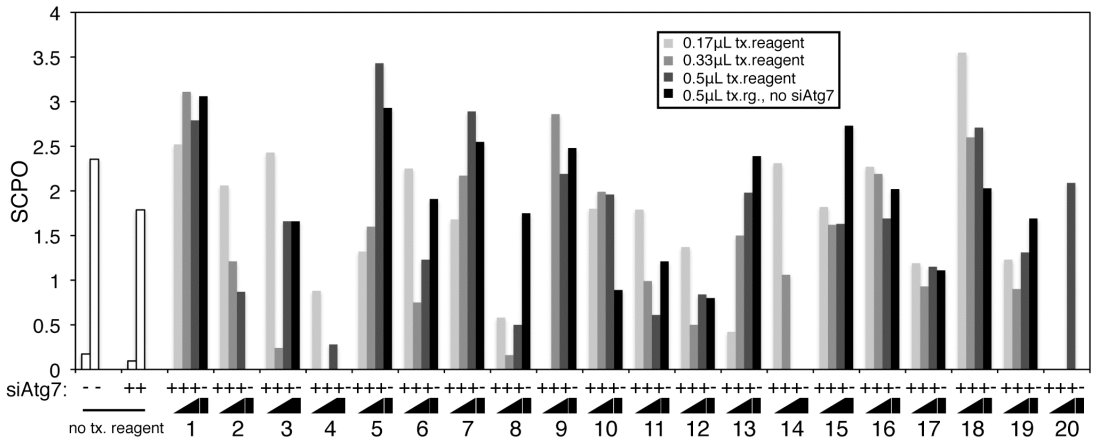

Figure 3.15 20 transfection reagents used to knock-down Atg7 have varying effects on GFP-LC3 spot formation

SCPO after EBSS plus 0.25mg/mL leupeptin for 20 transfection reagents at three doses with or without Atg7 Smartpool siRNA as indicated. Controls (white bars) show effect with no transfection reagent, in full medium or EBSS plus 0.25mg/mL leupeptin, minus or plus Atg7 siRNA and were created from data from four wells. Data for all others come from single wells. 2 is Ambion siPORT Amine; 7 is Invitrogen Oligofectamine; 8 is Invitrogen Lipofectamine 2000.

I retested the best eight reagents in the same assay (Figure 3.16). I adjusted the low, medium and high dose of reagent based on manufacturers' recommendations. Lipofectamine2000 (8) again seems to be the best at decreasing SCPO compared to reagent with no siAtg7 at all three doses (0.3, 0.45, 0.6). Reagent 1, siPORT NeoFX Transfection Agent (Ambion) is working at highest concentration 0.6µL per well, but not at lower concentrations. Similarly, reagent 13, DreamfectGold (OZ Bioscience) is only working at the highest dose, 0.3µL. Again, reagent 2, Ambion's siPORT Amine Transfection Agent is somewhat toxic to the cells and in this experiment I obtained data for the reagent alone (black bar) and can see that SCPO is decreased even without siAtg7, most likely due to toxicity. Reagents 3, 5, 6, and 15, when combined with Atg7 siRNA do not lead to a decrease in GFP-LC3 spot number.

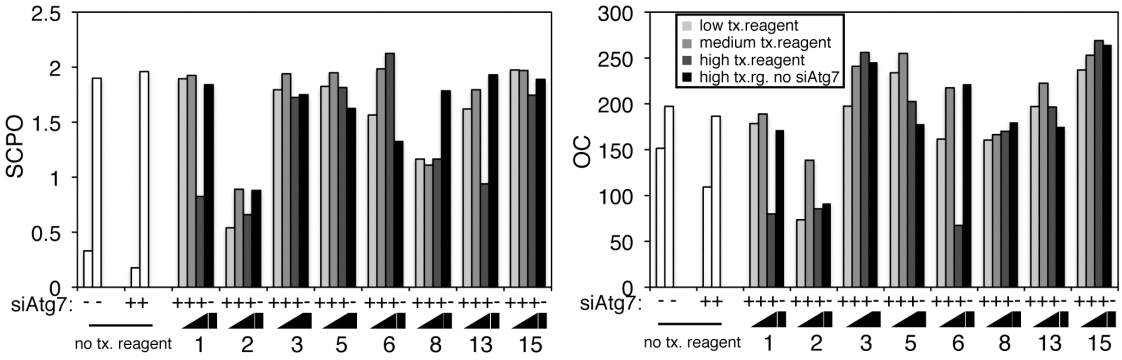

Figure 3.16 Eight transfection reagents used to knock-down Atg7 have varying effects on GFP-LC3 spot formation and object count
SCPO after EBSS plus 0.25mg/mL leupeptin for 8 transfection reagents at three different doses with or without Atg7 siRNA as indicated. Controls (white bars) show effect with no transfection reagent in full medium or EBSS plus 0.25mg/mL leupeptin, minus or plus Atg7 siRNA and were created from data from four wells. Data for all others come from duplicate wells. Ambion siPORT Amine is reagent number 2; Lipofectamine 2000 is reagent number 8.

I next retested the most promising reagent, Lipofectamine2000, the reagent that is best at reducing SCPO when combined with Atg7 siRNA, Ambion's siPORT Amine Transfection Agent, and the reagent used in the kinome screen, Oligofectamine. I tested two doses, 0.3µL and 0.5µL, and measured SCPO and OC when treated with siControl siRNA pool versus siAtg7, in full medium or EBSS plus Leupeptin (Figure 3.17, part a). siPORT reduces SCPO at the higher dose of 0.5µL when comparing siControl to siAtg7 addition but this high dose is compromising cell viability as seen by low OC numbers. Knock-down of Atg7 with Lipofectamine2000 led to the greatest decrease of SCPO without compromising cell viability. Again, we see that knocking down Atg7

with Oligofectamine is not effective at decreasing GFP-LC3 spot formation. In order to assess the efficiency of protein depletion by the three transfection reagents I knocked down COPB1 in GFP-LC3-HEK cells and measured the amount of COPB1 protein remaining and can see the Lipofectamine2000 is best at decreasing proteins levels, siPORT does reduce protein levels, and Oligofectamine is not effective.

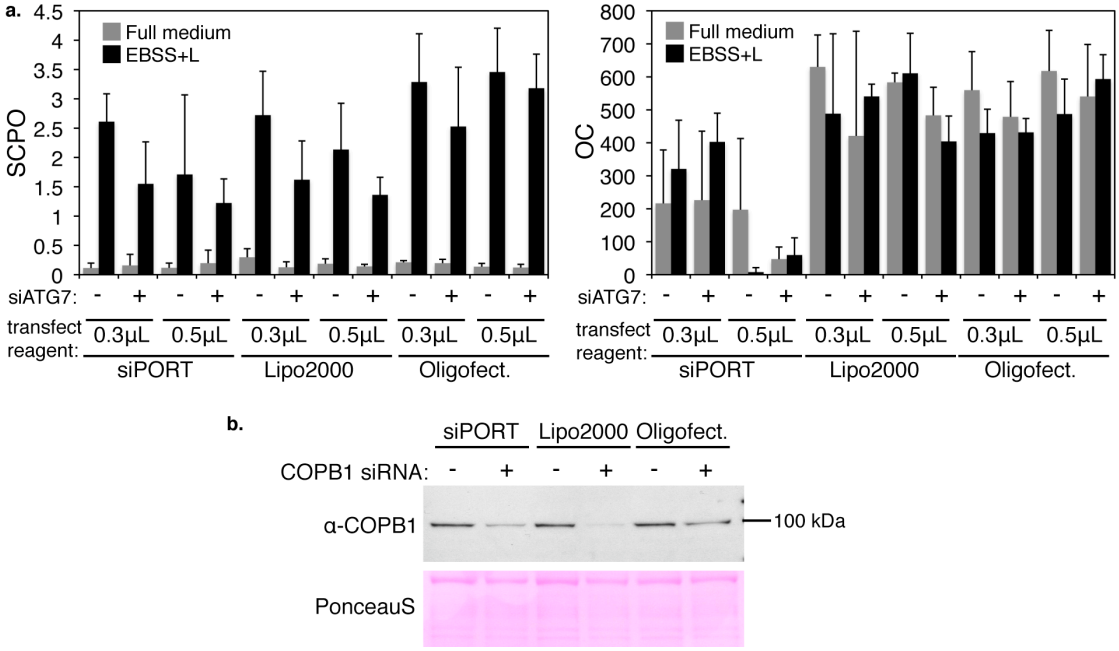

Figure 3.17 Testing the efficacy of three transfection reagents
a. SCPO after full medium or EBSS plus 0.25mg/mL leupeptin (EBSS+L) for 3 transfection reagents at two doses with 50nM siControl siRNA or 50nM Atg7 siRNA as indicated. Error bars represent standard deviation from four wells. b. Western blot showing COPB1 protein after treatment with 0.4uL reagent and 50nM siControl or 50nM siCOPB1 siRNA. PonseauS shows equal loading between samples.

These experiments show that Lipofectamine2000 is the best transfection reagent for GFP-LC3-HEK cells under my screen assay conditions and did not threaten cell viability. I confirmed that 4000 cells per well is the optimal density for efficiency of knock-down and final density of cells for optimal data acquisition in subsequent experiments. Similarly I determined that 0.4µL, not 0.3µL or 0.35µL of Lipofectamine2000 achieved the most significant decrease of GFP-LC3 spot parameter with knock-down of ULK1 and Atg7.

The next parameter to optimise was the concentration of siRNA for the screen. Using the optimal conditions of 0.4µL Lipofectamine2000 and plating 4000 cells per

well I tested siControl, siULK1, siAtg7 and siAtg13 at three siRNA concentrations, 25nM, 37.5nM and 50nM. I measured SCPO after treatment with EBSS plus leupeptin and saw that the concentration of siRNA did not have a drastic effect on GFP-LC3 spot parameters though 37.5nM and 50nM of siRNA against ULK1 and Atg7 seemed slightly better than 25nM at inhibiting SCPO (Figure 3.18). Also, a slightly greater fold induction of autophagy was seen with the siControl siRNA at 37.5nM compared to 50nM. The siGenome library was aliquoted to be used at a concentration of 37.5nM and prepared to be further aliquoted for this final siRNA concentration on the screen plates.

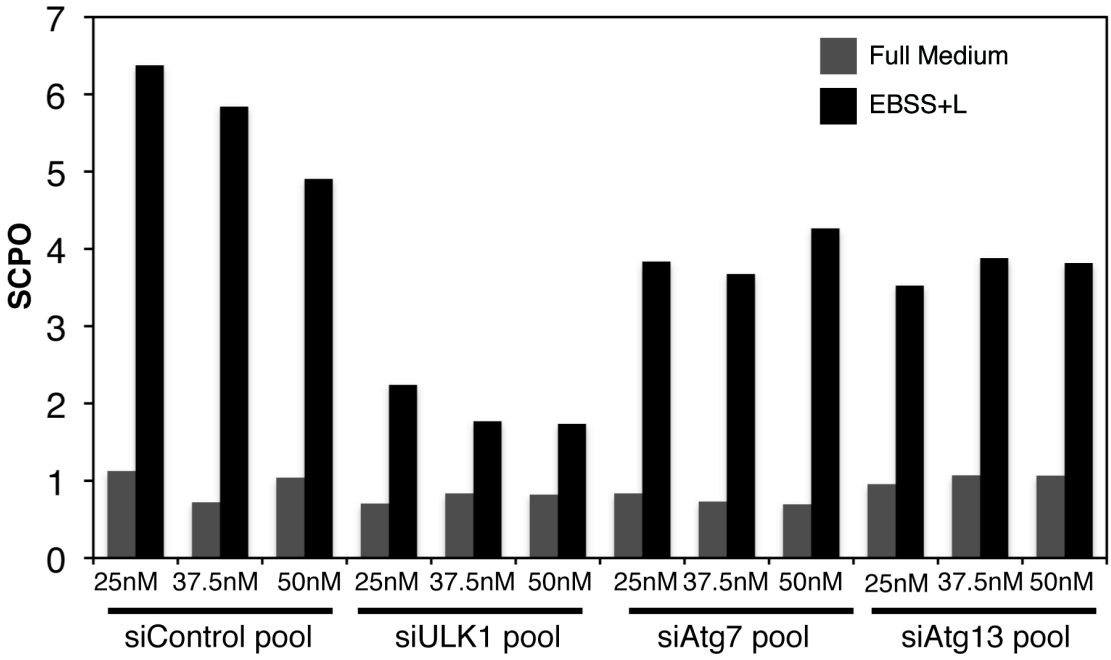

Figure 3.18 Testing to find the optimal siRNA concentration
GFP-LC3-HEK cells were treated with three concentrations of siRNA and incubated in full medium or EBSS plus 0.25mg/mL leupeptin (EBSS+L). Spot Count Per Object (SCPO) was determined. Data represents averaged SCPO from two wells.

Last, using the optimal conditions for reverse transfection I identified the best siRNA controls to use in the screen. The siGenome library was to be aliquoted onto 80 wells of 96-well plates leaving the first two columns of the plate for 16 positive and negative controls. To find negative controls, I tested Dharmacon's siControl non-targeting pool 1 and siControl RISC-free siRNA and found RISCfree did not affect GFP-LC3 spot number, size and intensity as much as the siControl pool. The RNA-

induced silencing complex (RISC) is an effector nuclease that carries siRNA to the nucleus and without it, RNAi does not occur (Hannon, 2002). The siControl pool contains four siRNA duplexes that are not predicted to target any known genes; in GFP-LC3-HEK cells, however, it seems to stress the cells (perhaps by inadvertently target a gene that is required for normal cell maintenance) thereby slightly elevating levels of autophagy. I showed that knock-down of ULK1, Atg7, and Atg13 decreases SCPO, STIPO, and STAPO, though siULK1 was the most efficient positive control for decreasers of spots. The siRNA kinome screen identified an siRNA pool called siLOC340371 that increased GFP-LC3 lipidation (Chan et al., 2007). This protein, now known as NRBP2 or nuclear receptor binding protein 2 is uncharacterised though it has been shown to be induced by differentiation of neural stem/progenitor cells (Larsson et al., 2008). Interestingly, the Drosophila NRBP homologue, CG1098 was found in a RNAi screen to be involved in HRP secretion and Golgi organisation and was shown to localise to cytoplasm and Golgi membranes (Bard et al., 2006). Mammalian NRBP1 has been shown to interact with the small GTPase Rac3, and when overexpressed, perturbs early Golgi membranes in mammalian (De Langhe et al., 2002). Also, NRBP1 is recruited to Golgi membranes upon viral infection (Chua et al., 2004). I found that knock-down of LOC340371 decreases the mRNA levels of NRBP2 and increases SCPO and STIPO above control and thus provides me with a positive control for increasers of GFP-LC3 spots (Figure 3.19, part a, b). Thus I have established parameters that allow quantification of GFP-LC3 spots after autophagy induction when cells are treated with RISC-free siRNA (spots are represented by magenta dots in the Cellomics SpotDetector program and are quantified for count and total intensity (Figure 3.19, part a, b). The number and total intensity of these spots is decreased after ULK1 knock-down and conversely increased after NRBP2 knock-down.

Object calling was further optimised using the nuclear staining, eliminating small nuclei and clumped or multinucleated cells (see yellow ring, Figure 3.19, panel a). Similarly, we further optimised spot calling in Channel 2: cells plated at 4000/cells per well are evenly spread throughout the well at a proper density for autophagy induction and spot calling, examples of which are displayed here. When cells are plated at this density, accurate information is gathered after imaging ten fields, leading to an object count in this experiment in the range of 152 to 537 with an average OC of 366. In

parallel, I knocked down ULK1 using these conditions in GFP-LC3-HEK cells, lysed the cells and probed for ULK1 in order to determine protein levels remaining after ULK1 siRNA treatment (Figure 19, panel c). ULK1 protein levels are significantly reduced by siULK1. As expected, ULK1 protein levels are reduced by Atg13 knock-down, as it has been shown that Atg13 is required for ULK1 stabilisation (Chan et al., 2009), (Ganley et al., 2009).

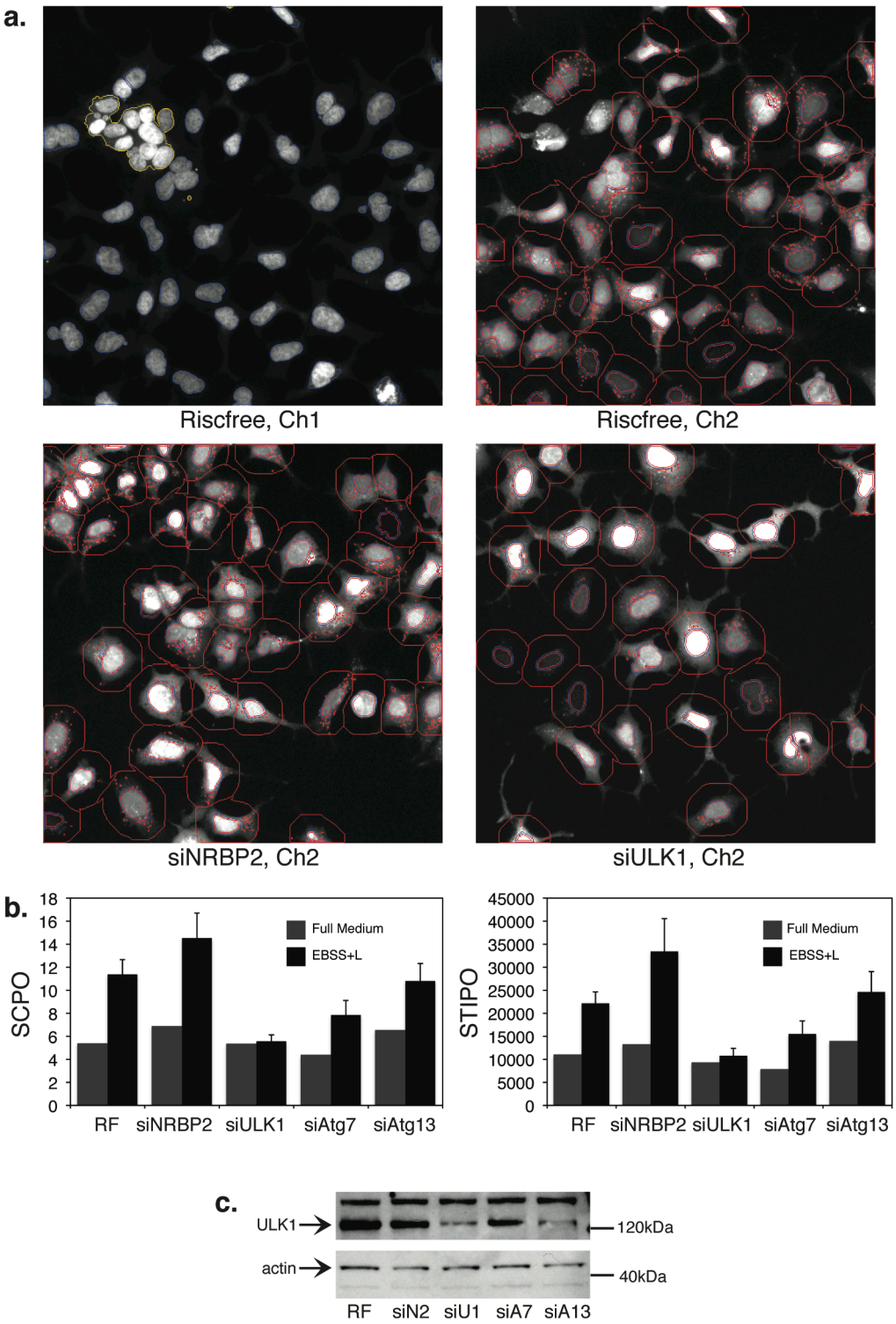

Figure 3.19 Quantification by Cellomics of the effect of control siRNA Smartpools on GFP-LC3 spot formation

a. Cellomics images with masks after indicated siRNA treatment and incubation with EBSS plus 0.25mg/mL leupeptin. The blue line indicates a ring around nuclear staining, the red line is the ring within which spots are counted, and the magenta designates GFP-LC3 spots. b. SCPO, STIPO for indicated siRNA knock-down. RF is RISCfree. Full medium values are generated from averaging duplicates, error bars represent standard deviation of triplicates. c. Western blot after indicated knock-

down in HEK-GFP-LC3 cells. The blot was probed for ULK1 and actin. RF is RISCfree, siN2 is siNRBP2, siU1 is siULK1, siA7 is siAtg7, and siA13 is siAtg13.

An interesting phenomenon that I observed during experiments to optimise the image-based assay for autophagy was the reproducible increase in object count after ULK1 knock-down. When compared to siControl, knock-down of ULK1 increased cell number, represented by the number of nuclei or objects in the Cellomics SpotDetector programme (Figure 3.20). Autophagy inhibits cell growth so conversely it is conceivable that inhibition of proteins required for autophagy might increase cell growth. This is perhaps the reason for the small increase in OC observed with siAtg7 and siAtg13 but this increase is less than that seen with siULK1. The increase of cell growth after ULK1 inhibition is contrary to some data from *D. melanogaster* where it has been shown that ULK1 can directly inhibit TOR leading to cell growth in an autophagy-independent way (Scott et al., 2007). In should be noted that, as discussed in the introduction, Atg1 and TOR in *D. melanogaster* display some different characteristics to ULK1 and mTOR in mammalian cells (Chan and Tooze, 2009). Bearing this in mind, high levels of Atg1 overexpression in Drosophila triggered downstream pathways and stimulated autophagy, reducing cell size and leading to apoptotic cell death (Scott et al., 2007), so perhaps in the opposite way, ULK1 knock-down could increase cell growth. A different study in Drosophila demonstrated that Atg1 inhibits cell growth by positively regulating p70S6 kinase (Lee et al., 2007). In mammalian cells, it has also been shown that both ULK1 and ULK2 can provide feedback regulation upstream to the mTOR-p70S6 kinase pathway, and in this way, ULK1 knock-down could increase cell proliferation.

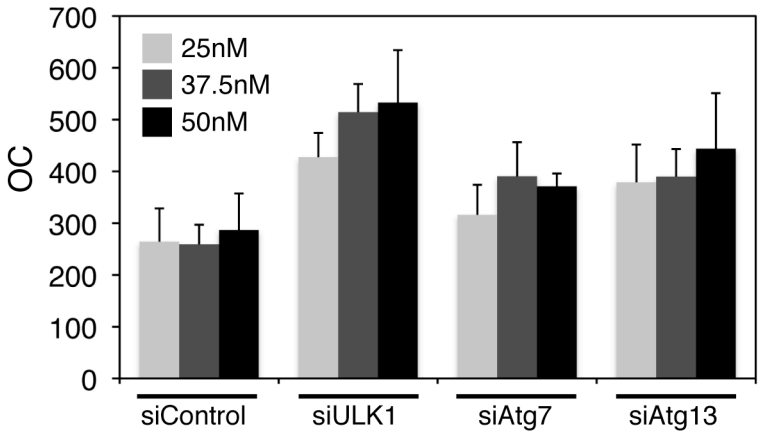

Figure 3.20 Knock-down of ULK1 increases cell number
Valid object count (OC) after knock-down with three doses of indicated siRNA.

3.3.3 Optimising the induction of autophagy

I have previously observed that after a certain number of passages in tissue culture, GFP-LC3-HEK cells begin to loose their GFP-LC3 expression. This can be observed in Figure 3.14 where seven cells, from a culture passaged 17 times, appear as objects based on nuclear staining (indicated by the blue ring) but display no nuclear or cytoplasmic GFP-LC3 (indicated by magenta spots). These cells are counted as objects but do not contribute to spot counting in the GFP channel therefore decreasing the values for spot count, intensity and area per object. I tested the effect of passage number on autophagy induction as measured by SCPO, STIPO and STAPO, comparing GFP-LC3-HEK cells at passage number eight to those at passage number 18. I saw a 24.8% reduction in SCPO when cells at P18 were induced with EBSS plus leupeptin (data not shown). It follows that in order to achieve the best fold induction of GFP-LC3 spots during the screen I must insure that the GFP-LC3-HEK cells are at a low passage number.

I saw that values for SCPO, STIPO and STAPO are greater after induction of autophagy with EBSS plus leupeptin compared with EBSS alone, thus I determined the best concentration of leupeptin in order to obtain the best induction for the screen. The use of leupeptin in the screen also had cost implications. I tested three concentrations of leupeptin, 0.25mg/mL, 0.125mg/mL and 0.083mg/mL and confirmed previous findings that the best induction was seen with the highest dose, 0.25mg/mL of leupeptin. We decided that the greatest possible fold induction of autophagy was needed in order to

capture modulations in the three spot parameters during the screen, despite the high cost of leupeptin.

Last, the optimisation experiments were done using a multi-well pipette to add reagent, wash, induce autophagy, fix and stain. It was important to be gentle while washing the plates and adding EBSS with leupeptin in order to avoid cell loss but equally important for the induction step that all full growth medium was washed away from the cells before the addition of EBSS with leupeptin. It was not, however, possible to manually was the plates of a genome-wide screen in this way. After testing multiple liquid-handling robots and manual washing techniques we determined that washing the plates by inverting them into large vats of PBS then adding the induction medium with a Thermo Scientific Matrix WellMate microplate dispenser at its slowest and gentlest speed was not only gentle enough to maintain cell numbers but efficient in inducing autophagy. We also determined that adding 8 per cent formaldehyde at equal volume directly to the plates after induction using the WellMate would adequately fix the cells at 4 per cent final concentration again without significantly disturbing the cells.

3.3.4 Summary of optimisation conditions

After optimising the image-based assay to measure modulation of starvation-induced autophagy by siRNA knock-down of GFP-LC3-HEK cells the following protocol was established: a reverse knock-down for 72 hours would be used with 0.4μL Lipofectamine2000, 37.5nM siRNA with 4000 cells per well. Formation of GFP-LC3 spots would be induced by incubation in EBSS plus 0.25mg/mL leupeptin for two hours and SCPO, STIPO and STAPO measured using the SpotDetector program that had been optimised for best object and spot calling. I determined the range of the assay under these conditions by combining data from experiments that followed the protocol just described (Figure 3.21). A greater-than-two-fold increase is seen for spot count, intensity and area when cells are treated with RISCfree control siRNA and induced with starvation medium. This induction is significantly decreased by treatment with positive control siRNAs ULK1 and Atg7 and significantly increased by treatment with the positive control NRBP2 siRNA.

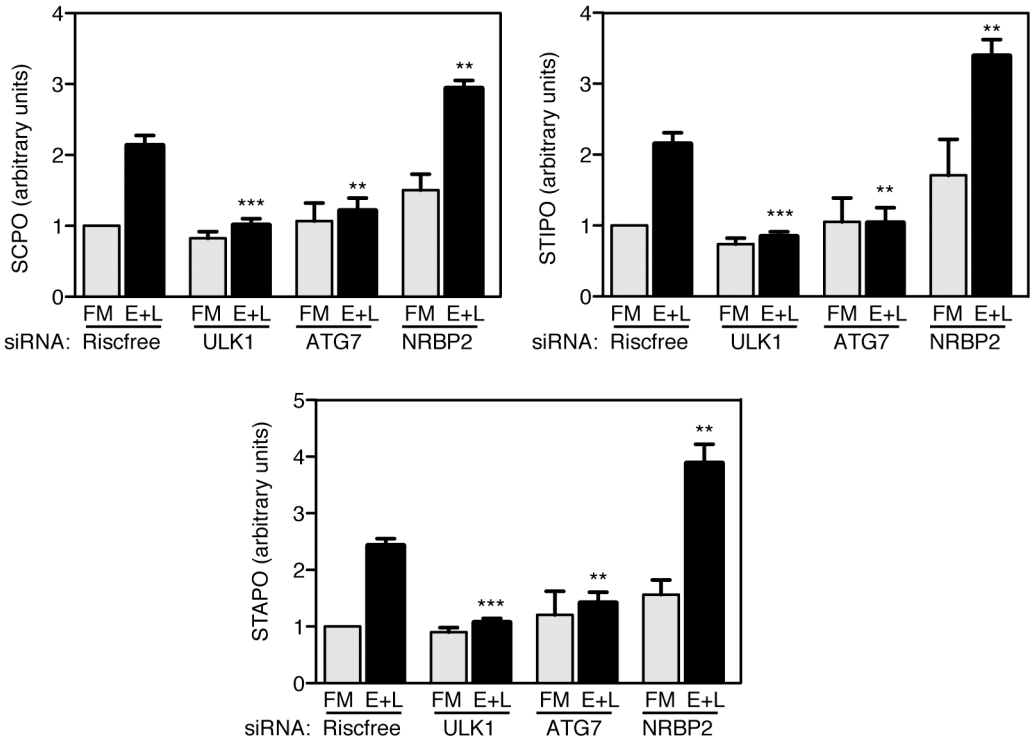

Figure 3.21 The effect of various siRNA treatments on SCPO, STIPO and STAPO
SCPO, STIPO, STAPO after siRNA treatment in GFP-LC3-HEK cells. FM is full medium, E+L is EBSS plus 0.25mg/mL leupeptin. Error bars represent standard error of the mean. Each experiment consists of at least duplicate values. SCPO siULK1 p=0.0002; siAtg7 p=0.0078; siNRBP2 p=0.0088. STIPO siULK1 p<0.0001; siAtg7 p=0.0060; siNRBP2 p=0.0041. STAPO siULK1 p<0.0001; siAtg7 p=0.0037; siNRBP2 p=0.0028. RISCfree (n=5), siULK1 (n=5), siAtg7 (n=3), siNRBP2 (n=3).

3.3.5 Pilot Screens

Before screening the entire genome I had to prove that the assay I developed would provide an accurate read-out for siRNA-based modulations in autophagy, I undertook two small pilot screens. First I assayed plate number ten of the kinome library used previously in the lab following the protocol above on duplicate plates containing negative and positive control siRNAs; this is also plate 10 of the siGenome library. Plate number ten was chosen because it contained ULK1 and ULK2 siRNA and indeed I saw a strong inhibition of GFP-LC3 spot formation by siRNA against ULK1 but not against ULK2. I saw a significant increase of SCPO with siRNA against my positive control NRBP2 and also siRNA against TLK2 (NM_006852).

I also tested a plate that was generated to hold a small library of siRNA against genes that code for nuclear membrane receptor proteins. Duplicate plates were processed and I obtained raw data for SCPO as before and then normalised the data as

might be done in the large-scale screen of the genome. First, I divided the raw data by the individual plate median absolute deviation, creating a Z-score or value indicating standard deviations away from the median. Then I determined the median of the duplicate Z-scores for each well. These median Z-scores range between -2.88 (a strong decreaser of spots) and +4.62 (a strong increaser of spots) (Figure 3.22, part a, b). The two wells that received siULK1 showed strong negative Z-scores and the two wells that received siNRBP2 showed strong positive Z-scores though one of the duplicates wells mistakenly received less transfection reagent and therefore showed a more subtle increase in GFP-LC3 spots. Though the range of the assay is relatively small (approximately two-fold; Figure 3.21), the results are reproducible and the data generates significant Z-scores. Thus, it was determined that the image-based assay was capable of producing robust data in a high-content screen for starvation-induced autophagy.

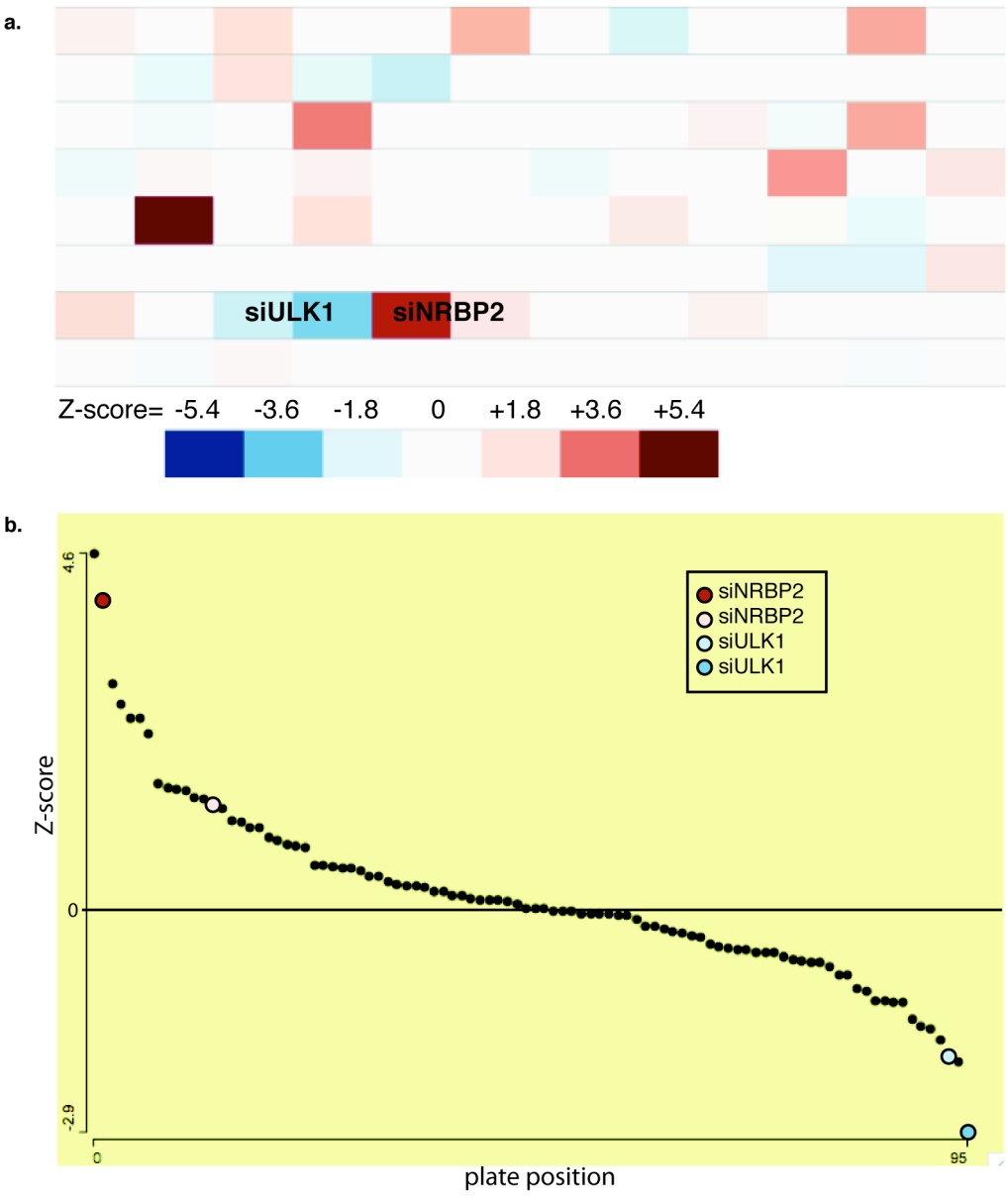

Figure 3.22 Pilot screen of Nuclear Membrane Receptor Protein Plate
a. Heat map of the 96-well plate assayed depicting the strength of median Z-score from duplicate plates. Wells that received siULK1 and siNRBP2 are indicated. b. Scatter plot displaying plate position versus median Z-score for duplicate plates. Two wells with siNRBP2 knock-down and two wells with siULK1 are shown.

Chapter 4. Primary, Repeat and Deconvolution Screens

4.1 Overview of the screening strategy

A genome-wide screen for starvation-induced autophagy in GFP-LC3-HEK cells was preformed on the 21,121 genes targeted by the Dharmacon siGenome library (Appendix Table 9.1, 9.2). The 1000 genes whose knock-down led to the strongest increase or decrease of GFP-LC3 spot count, total area, and total intensity were taken forward and the primary screen assay was repeated (Appendix Table 9.3, 9.4). Images from the secondary screen were visually inspected for 371 of the gene knock-downs and those that were mis-called or that caused cell death were eliminated from the hit list. 200 genes were taken forward to the deconvolution screen during which individual siRNA duplexes that comprise the Dharmacon siGenome Smartpools were individually assayed (Appendix Table 9.5). Of these, 51 genes had at least two out of four siRNA duplexes that repeated the primary and secondary screen spot phenotype. 20 of these had three of four siRNA duplexes that validated and are expected to be expressed in HEK cells. These nine 'decreasers' and 11 'increasers' were taken forward for further validation. This process is summarised in Figure 4.1 and I will now describe the primary screen, secondary/repeat screen and deconvolution screen in greater detail.

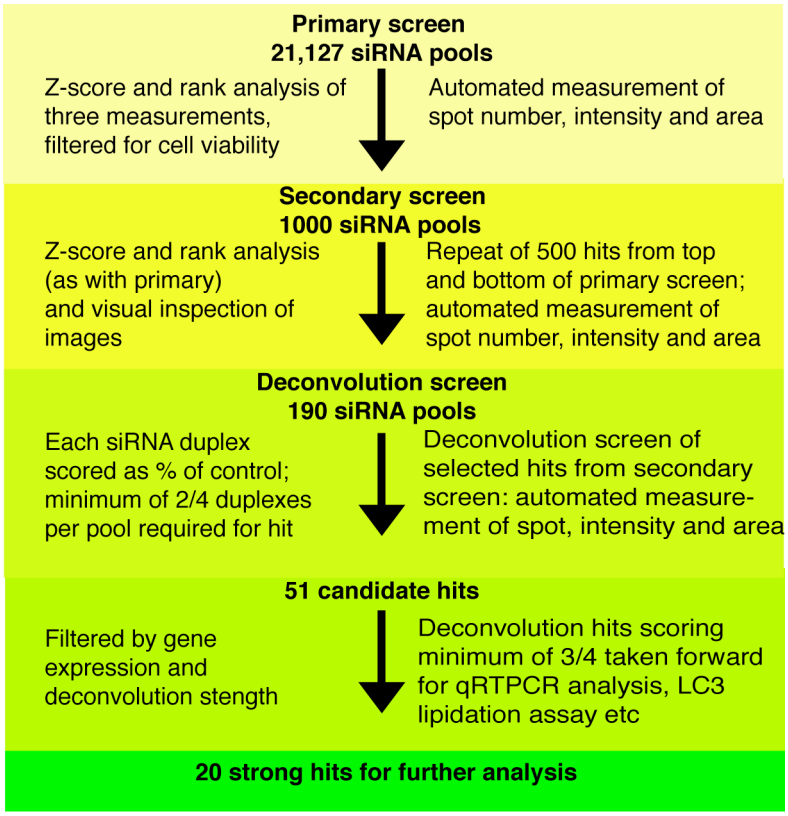

Figure 4.1 Strategy for the genome-wide screen for starvation-induced autophagy
Summary of the primary screen, secondary or repeat screen, deconvolution screen and their results.

4.2 Primary Screen: The autophagy screen of 21,121 genes

4.2.1 Preparing for the primary screen

There were many reagents to purchase and prepare in a large scale before undertaking the primary screen. As I determined that Lipofectamine2000 was the best transfection reagent for my assay, I performed a test screen on a batch and confirmed it gave a robust effect. This batch was purchased and used for the primary, repeat and deconvolution screens as well as the further analysis of the 20 strongest hits, described in chapter 5. As I had determined that a final concentration of 0.25mg/mL of leupeptin in starvation medium was required for the best induction, I similarly tested two lots of the chemical and determined that the effect of these were comparable to that seen during the screen optimisation and obtained the required 1.4 grams. Finally, I ordered and tested all batches of reagents (siRNA controls, Poly-D-lysine, growth medium, EBSS etc.) in test screens before performing the large-scale screen.

The required 801 Falcon Microtest 96-well Optilux Assay Plates were coated with Poly-D-lysine and barcodes were added to the plates. The Dharmacon Human siGENOME siRNA library (including the Protein Kinase and G Protein-Coupled Receptors libraries, and the Human Druggable Set and Human Genome Set) was then aliquoted in onto triplicate plates so that there was 375nM Smartpool siRNA in 10µL Hank's Buffered Salt Solution (HBSS) in each well. The plates were kept at -20°C until day one of the screen.

The GFP-LC3-HEK cells were prepared so that they would be at their optimal health and responsiveness during the screen. Cells were thawed from their lowest passage available (from their original freeze after stable GFP-LC3 expression was obtained) and tested for their ability to be induced for autophagy and affected by siRNA knock-down; the screen was performed with cells at passage number 11. I estimated that I needed 50 175cm flasks and split the cells to a density that was below confluency and optimal for counting on day 1 of the screen.

4.2.2 Performing the primary screen

The primary screen was performed over a four day period. The 801 plates, 267 plates in triplicate, contained the 21,121 genes in the siGENOME library and 16 empty wells for controls per plate and were processed together. We divided the plates into four batches of 200 plates for easier handing on the most labour-intensive of the screening days, day 1 and 4. Using the recommended 20 minute incubation period for siRNA and Lipofectamine mixing we determined that four people were needed to process each of the 200-plate batches in two hours on day 1. In turn, our experimental plan was mostly dictated by the speed at which the WellMate robots could add transfection reagent and cells to the plate (approximately 30 seconds a plate for each addition) (Figure 4.2). I was responsible for preparing the positive and negative siRNA controls and preparing the cells by counting and resuspending them in medium. A detailed protocol of the reverse transfection performed on the 801 plates is contained in the Materials and Methods section.

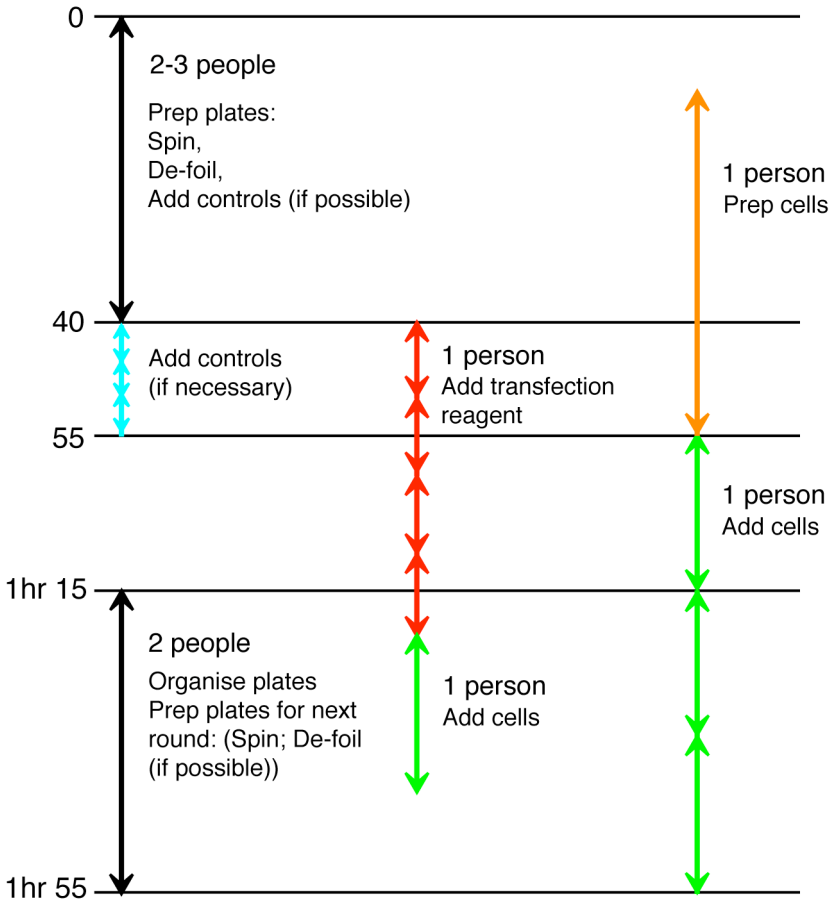

Figure 4.2 Time plan to process 200 plates on Day 1: transfection and plating cells
It required four people to process 200 plates in two hours. Two WellMate liquid handling robots in two tissue culture hoods. Following the reverse transfection protocol previously described, transfection reagent is added to the siRNA on the plate. See Materials and Methods for further details.

The plates were kept at 37°C in three incubators and cells on several plates were checked on day 2 and appeared to be growing well and at an expected density. On day 3 the transfection medium was removed from the plates and fresh full grown medium was added. On day 4 autophagy was induced for two hours in EBSS plus 0.25mg/mL leupeptin and the cells were then fixed with 4% formaldehyde and sealed. On day 5, the plates were de-sealed, the fixation medium was replaced with 100µL PBS, re-sealed and stored at 4°C. Plates were stained with 1µg/mL DAPI for 20 minutes immediately before data acquisition and images were obtained and data simultaneously generated on the Cellomics ArrayScan usually in batches of 20 overnight. As a control for basal GFP-LC3 spot number, a plate of cells that received transfection medium but no siRNA was incubated on day 4 in full medium, not starvation medium, for two hours and fixed. This plate as well as control wells on the screen plates were used to set the spot

thresholds in the Cellomics SpotDetector program and these parameters were used to analyse all plates. The Cellomics machine captured at least 250 cells per well (determined to be valid objects based on nuclei of normal area, shape and intensity, as described above); on average it took approximately 50 minutes to read each plate. In turn, it took approximately two months to image and collect data from the 801 plates.

4.2.3 Normalisation and analysis of data from the primary screen

Data was collected from all sets of triplicate plates except for plate 10 (the last plate of the series of the protein kinase sub-set of the siGenome library), which is the plate that contains the siRNA Smartpool against ULK1. This set of triplicate plates had very few cells remaining after the screen and we determined that this loss was most likely due to these plates being left out of Poly-D-lysine coating or washing. The assay was repeated in triplicate on this plate as in the primary screen at a later date and the data was normalised as below in the exact same way as the screen plates.

Upon examining the 801 screen plates after fixation, I noticed that the density of the cells in each well was not optimal in that the cells were more sparse than previously seen. In turn, this made finding 250 cells per well and reading each plate a longer process than expected. Because the cells seemed to be growing normally and at an expected density up until day 4, I concluded that the cell loss must have occurred on day 4 during the induction of autophagy. The plates were outside of the incubator for longer than when I was working with just one or two plates and therefore not at optimal temperature (37°C) and CO_2 (10%). In addition, because we were taking and putting plates out of and into the incubators often, the incubators themselves did not maintain the desired temperature and percentage CO_2. We believe that this increased the amount of cells lost during washing, incubation in starvation medium and fixation.

It was observed across the entire set of plates that some wells had particularly low cell counts possibly due the siRNA being toxic or manipulation of those cells was especially harsh. We did not want to incorporate results from the wells with low cell counts as these data were possibly skewed because there is a possibility that the remaining cells were not representative. We set a cell number cut-off to 50 cells per well and applied this filter to the raw data such that any wells with a valid object count less than 50 were flagged and not used in any calculation and therefore did not

contribute to the analysis for that siRNA Smartpool. Triplicate wells with more than one replicate flagged as below this 50-cell threshold were not considered in any evaluation and this siRNA Smartpool was not evaluated.

All data was processed with the Cell HTS Normalisation programme (Boutros et al., 2006) by Rebecca Saunders of the HTS lab, LRI. First, raw data for the three individual parameters, Spot Count per Object (SCPO), Spot Total Intensity per Object (STIPO), and Spot Total Area per Object (STAPO) were normalised using the B-score method to correct for plate row and column effects. To determine a B-score, the plate median and estimated well and column effects are subtracted from each well's raw value to account for differences within an individual plate. This first round of normalisation is effective in minimising measurement bias due to so-called edge-effects (defined as the advantages or disadvantages in condition to which an individual well is subjected due to its position on the plate) (see Appendix 9.1.1 for further explanation on B-score normalisation).

Next, this B-score is centred around zero by dividing each well value by the plate median absolute deviation (MAD), thus creating a Z-score (Malo et al., 2006) (see Appendix 9.1.2 for further explanation on Z-score normalisation). The Z-score gives a value for the distance, or units of standard deviation, above or below the plate median and allows us to compare the data across the entire screen. Then triplicate values were summarised by taking the median Z-score for each siRNA Smartpool. These two rounds of normalisation (B-score then Z-score) were essential because we observed a 'bounciness' of the raw data or differences between groups of plates (Figure 4.3, panel a). Once the raw values for SCPO, STAPO, and STIPO were normalised twice as described the range of the median Z-score data across the 267 triplicate plates appears similar (Figure 4.3, panel b.). The differences between plates may have been due to dividing the plating of the cells into four batches on day 1, differences in incubation conditions during the screen, differences in DAPI staining between different batches or even differences between when plates were scanned over the course of the two-month data acquisition period.

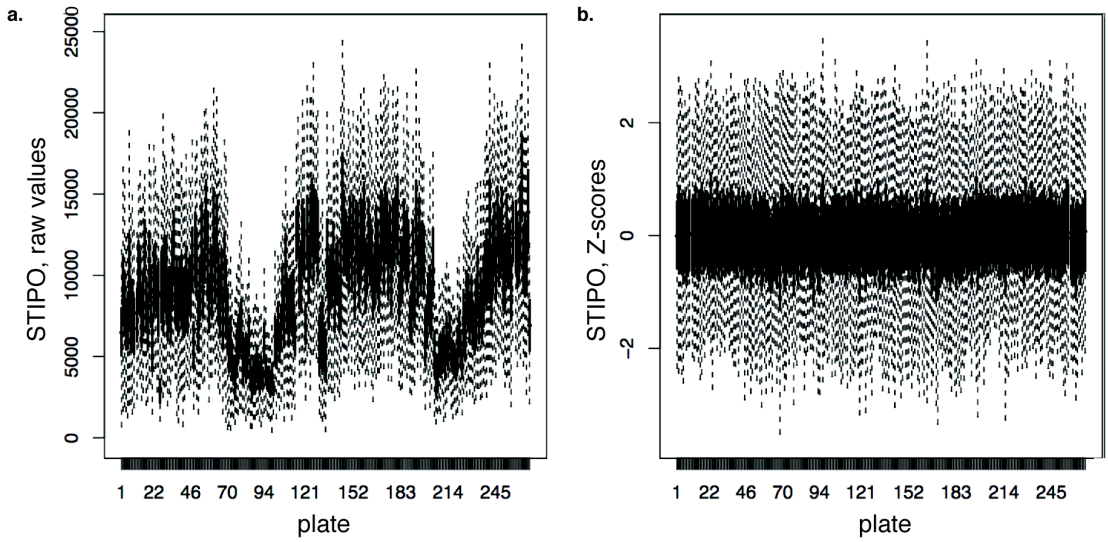

Figure 4.3 STIPO raw values and normalised Z-scores for the Primary screen.
a. Median raw values for STIPO for the 267 triplicate screen plates. b. Z-scores or standard deviations above and below the mean for STIPO for the 267 screen plates.

As mentioned, the SCPO, STAPO, and STIPO Z-score for each siRNA Smartpool was determined by taking the median Z-score for each triplicate. The siRNA Smartpools were then ranked according to their Z-score for each of the three parameters and these were then combined to create a rank product (RP) and a new ranked list was created. In order to assess the overlap between the three spot parameters, I compared the approximate 500 best increasers of SCPO, determined by their SCPO Z-score rank, to the approximate 500 best increasers of STIPO and also to the approximate 500 best increasers of STAPO (Figure 4.4). The knock-down of 212 genes led to an increase of SCPO, STIPO and STAPO that ranked in the approximate top 500 for each parameter. 90 siRNA Smartpools lead to an increase of GFP-LC3 spot number that ranked in the top 480 for SCPO only, 195 siRNA Smartpools lead to an increase of GFP-LC3 total intensity that ranked in the top 498 for STIPO only, and 127 siRNA Smartpools led to an increase in GFP-LC3 spot area that ranked in the top 488 for STAPO only. The knock-down of different genes may affect the three spot parameters differently or the data generated from only one or two of the parameters may reflect the knock-down's affect on autophagy less accurately. It was therefore important to incorporate the data obtained from the analysis of all three spot parameters because the combined data was

more informative than data obtained from the analysis of just one of the spot parameters.

Figure 4.4 Venn Diagram of the overlap of the best increasers of the three parameters
833 total gene knock-downs leading to an increase of SCPO, STIPO or STAPO are shown. Overlap represents siRNA Smartpools whose effect caused them to rank in the top 500 increasers for more than one spot parameter.

I analysed the SCPO Z-scores for all siRNA Smartpools including those from the control wells and plotted these ranked Z-scores (Figure 4.5). The range of SCPO Z-scores is +4.7 for the strongest increaser and -4.1 for the strongest decreaser. Indicated in red are the 267 median SCPO Z-scores for well C01, which held the positive control siRNA Smartpool targeting ULK1. These values are all negative indicating that these knock-downs lead to a decrease in GFP-LC3 spot count per object and most Z-score values are less than -2 indicating a strong effect or greater than 2 standard-deviations distance away from the screen mean. This scatter plot also displays the 1242 wells

whose siRNA treatment lead to fewer than 50 cells per well for at least two out of three of the replicates and therefore whose Z-scores were not generated.

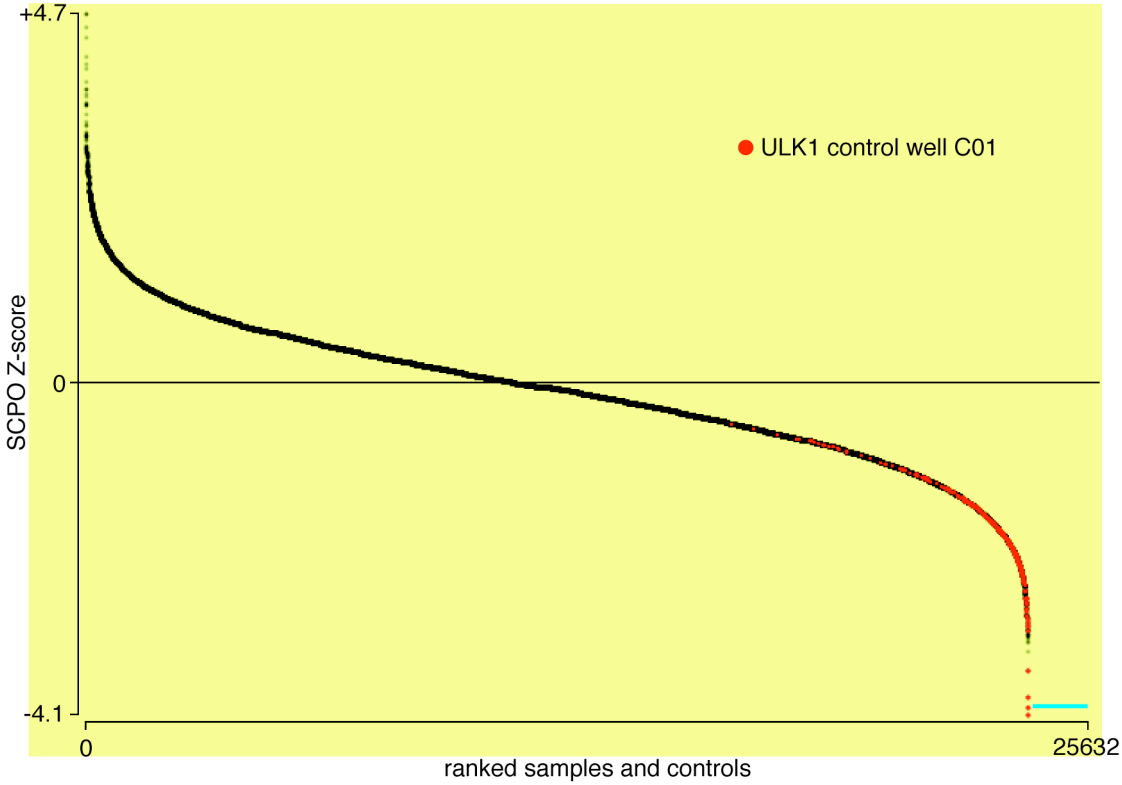

Figure 4.5 Scatter plot of median SCPO Z-scores against rank for all siRNA Smartpools
All tested siRNA Smartpools were ranked in terms of SCPO Z-scores and plotted. The red dots represent median values from well C01, which contained ULK1 siRNA. The blue bar represents siRNA knock-downs that led to less than 50 cells per well in at least two out of three replicates and so Z-scores for these Smartpools were not generated.

All 21,121 siRNA Smartpools were ranked by rank product (RP) as increasers and conversely as decreasers and roughly the top and bottom 500 are shown (Appendix, Table 9.1 and 9.2). These were chosen to be taken forward and the assay was repeated with these 1000 siRNA Smartpools (see section 4.3). Values for SCPO, STAPO and STIPO for the three replicates, corresponding ranks, rank product (RP) and object count (OC) for the three replicates were recorded. When object counts were less than 50 cells, corresponding data was not determined for that replicate designated by a 'ND.' Data for siRNA Smartpools contained on plate 10 are shown at the bottom of each list and genes of interest discussed below are also highlighted.

4.2.4 Results of the primary screen

A number of autophagy-related (Atg) genes previously shown to be required for starvation-induced autophagy were identified as being required for autophagy in the primary screen (Figure 4.6), (Appendix, Table 9.2). siRNA Smartpools targeting two members of the ULK1 kinase complex showed a significant effect: knock-down of ULK1 in the primary screen significantly decreased GFP-LC3 spots confirming previous findings that it is required for autophagy (Chan et al., 2007) and supporting our use of the siRNA again ULK1 as a positive control in the screen. The mammalian orthologue of Atg17 FIP200, when knocked down, also led to a decrease of SCPO, STIPO, and STAPO and ranked 731st among decreasers when ranked by rank product of the three parameters (seen also in Figure 4.7).

Multiple proteins that are included in the four Vps34/PI3-kinase complexes scored significantly in the screen and are discussed below. Atg14, also known as BARKOR, interacts with Beclin1 and positively regulates autophagy (Zhong et al., 2009), (Matsunaga et al., 2009); knock-down of the gene showed strong inhibition of GFP-LC3 spots. siRNA against ATG14 has been shown to inhibit long-lived protein degradation and LC3 lipidation after starvation. These results highlight the importance of Atg14 in autophagosome formation and regulation of autophagy by the PI3-kinase complex 1.

Multiple components of the Atg5-12 conjugation reaction and the LC3 lipidation complexes were also highlighted in the primary screen. Knock-down of ATG4C had the strongest effect on GFP-LC3 spot formation of all the proteins involved in the two conjugation reaction complexes; it ranked 46th out of all genes when listed by rank product (RP) which was 64.5. ATG4C is one of three human ATG4 genes that cleave LC3, priming it for PE conjugation. Interestingly, ATG4C is the only form that has been shown to be required for starvation-induced autophagy, not basal autophagy (Marino et al., 2007): Atg4C knock-out mice are normal and are capable of inducing autophagy during development but show decreased autophagy during starvation. This has not been reported for Atg4A or Atg4B, and interestingly, knock-down of ATG4A and ATG4B did not robustly affect GFP-LC3 spots (Figure 4.6). Atg7 is required for both conjugation reactions and had an average Z-score across the three parameters of -1.0 in the primary screen but did not make the 500 decreaser cut-off. Atg10, the E2-like

enzyme required for Atg5-Atg12 conjugation reaction was seen in the primary screen to increase GFP-LC3 spots when knocked down ranking 19482nd as a decreaser of spots (conversely 639th as an increaser of spots). This result is the opposite of what one would expect as Atg5-Atg12 conjugation is an important requirement for autophagosome membrane elongation. Interestingly, it was recently shown that knock-down of ATG16L2, another essential component of the Atg5-Atg12 complex, increased basal autophagy flux in neuroblastoma H4 cells (Lipinski et al., 2010) and ATG16 knock-down in the primary screen also slightly elevated GFP-LC3 spot parameters.

Last, knock-down of ATG9A with Dharmacon's siRNA Smartpool significantly inhibited GFP-LC3 spots (Figure 4.6, Figure 4.7). It ranked close to FIP200 and ATG7 as Atg9, like these two critical autophagy proteins, has been shown to be required for autophagy (Saitoh et al., 2009).

Accession no	Gene ID	Gene Symbol	Dharmacon name	Dharmacon cat no	Median SCPO	Rank by SCPO	Median STIPO	Rank by STIPO	Median STAPO	Rank by STAPO	Rank product (RP) as decreasers
NM_032852	84938	**ATG4C**	APG4C	M-005788-00	-2.199	115	-2.073	73	-2.451	32	64.5
NM_003565	8408	**ULK1**	ULK1	M-005049-00	-2.012	192	-2.207	40	-1.969	164	108.0
XM_375080	22863	**ATG14/Barkor**	KIAA0831	M-020438-00	-1.558	666	-1.686	295	-1.051	1906	720.8
NM_024085	79065	**ATG9A**	FLJ22169	M-014294-00	-1.536	699	-1.401	731	-1.38	883	767.0
NM_014781	9821	**FIP200**	RB1CC1	M-021117-00	-1.538	695	-1.225	1209	-1.573	562	778.7
NM_006395	10533	**ATG7**	APG7L	M-020112-00	-1.006	2218	-1.026	1850	-0.992	2129	2059.5
NM_022818	81631	**MAP1LC3B**	MAP1LC3B	M-012846-00	-0.884	2881	-1.328	886	-0.674	4041	2176.8
NM_022488	64422	**ATG3**	APG3	M-015375-00	-0.73	3707	-0.954	2246	-1.204	1365	2248.3
NM_004707	9140	**ATG12**	APG12L	M-010212-01	-0.765	3494	-0.697	3739	-0.845	2876	3349.3
NM_003766	8678	**BECN1**	BECN1	M-010552-00	-0.506	5370	-0.593	4694	-0.634	4403	4805.7
NM_014683	9706	**ULK2**	ULK2	M-005396-01	-0.355	6601	-0.375	6297	-0.287	7065	6646.9
NM_014741	9776	**ATG13**	KIAA0652	M-020765-00	0.253	12362	-0.219	7715	-0.361	6466	8511.8
NM_013325	23192	**ATG4B**	APG4B	M-005786-00	-0.131	8581	-0.063	9215	-0.09	8998	8927.4
NM_052936	115201	**ATG4A**	APG4A	M-005789-00	0.004	9965	-0.011	9703	0.038	10548	10065.9
XM_290517	23130	**ATG2A**	KIAA0404	M-026591-00	-0.037	9416	0.024	10158	0.0865	10912	10143.6
NM_173681	285973	**ATG9B**	NOS3AS	M-018082-00	0.152	11510	-0.009	9668	0.303	12988	11306.2
NM_015610	26100	**WIPI2**	DKFZP434J154	M-020521-00	0.27	12546	0.03	10322	0.282	12713	11807.9
NM_004849	9474	**ATG5**	APG5L	M-004374-02	0.415	13888	0.293	12610	0.266	12656	13038.2
NM_017974	55054	**ATG16L1**	APG16L	M-021033-00	0.486	14485	0.633	15301	0.122	11281	13572.6
NM_031482	83734	**ATG10**	APG10L	M-019426-00	1.347	19048	2.111	19814	1.364	19034	19295.3

Figure 4.6 Identification of known Atg genes in Primary Screen
20 Autophagy-related genes identified in the primary screen are listed by increasing Rank Products (RP) expressed as decreasers. Accession number, Gene ID, current Gene Symbol, Dharmacon name (when the siGenome library was purchased); Dharmacon siGenome Smartpool catalogue number, median SCPO, rank determined by SCPO, median STIPO, rank determined by STIPO, median STAPO, rank determined by STAPO and Rank Product of SCPO, STIPO and STAPO ranks are shown.

Other genes whose knock-down was previously shown to affect starvation-induced autophagy but are not classified as Atg proteins were uncovered during the primary screen and some of their Z-scores for SCPO are shown in Figure 4.7. Several

of these proteins are components of the four PI3-kinase complexes (Figure 1.3). Ambra1, named FLJ20294 in the screen, has been shown to be required for starvation-induced autophagy (Fimia et al., 2007) and its knock-down in the primary screen significantly inhibits GFP-LC3 spots, ranking 27th as a decreaser (Appendix Table 9.2). Ambra1 was originally characterised as a Beclin 1 interacting partner and knockdown AMBRA1 with siRNA resulted in less LC3-punctated cells and less LC3 lipidation. Conversely, RUBICON/KIAA0226, a component of the PI3-kinase RUBICON complex has been shown to be a negative regulator of autophagy (Zhong et al., 2009) and consequently it was found among the genes whose knock-down increased GFP-LC3, ranked 1049th. RUBICON is expected to be an increaser when knocked down because it inhibits autophagosome maturation through its inhibition of Vps34 kinase activity. Last, Bif-1 or SH3GLB1 ranked 139th of increasers in the original screen (Appendix Table 9.1). Initially described as a BAX interactor, it is an SH3-domain-containing protein that has recently characterised as a member of the PI3-kinase UVRAG sub-complex that contains p150, VPS34, Beclin1, and UVRAG (Figure 1.3). Bif-1 was shown to regulate not autophagy initiation but degradative endocytic traffic and in turn, autophagosome maturation (Thoresen et al., 2010). Thus knock-down of Bif-1 may inhibit autophagosome maturation and lead to the accumulation of GFP-LC3 spots.

Another gene that is involved in endosome maturation that led to an increase in GFP-LC3 spots is VPS16 (Appendix Table 9.1). Vps16 is a core component of all four of the class C Vps complexes (the three other core components are Vps11, Vps18, and Vps33) (Liang et al., 2008). The class C Vps complexes exist in two main configurations and are responsible for different functions; the CORVET complex (including also Vps3 and Vps8) acts as a vacuole/endosome tethering factor and functions at the endosome. It was shown by Liang *et al* that UVRAG binds the CORVET complex through direct interaction with Vps16 and together they assist in the fusion of the autophagosome to the lysosome in the maturation of endosomes and autophagosomes. Very recently it was shown that a new Drosophila endosomal membrane protein called ema is required for endosomal maturation and binds to the class C Vps complex also through direct binding with Vps16 (Kim et al., 2010). Of note, the human homologue of ema, Clec16A, ranked 2030th as an increaser in the

primary screen. The importance of endosome/lysosome maturation for efficient autophagic flux is highlighted by these results.

Knock-down of ROBLD3 increased GFP-LC3 spots in the primary screen and ranked 709th as an increaser (Figure 4.7). ROBLD3, or p14, is a component of the 'Ragulator,' a necessary regulator of TORC1 activation by amino acids (Sancak et al., 2010). My screen recapitulated the finding that the size and number of GFP-LC3 spots were increased in p14 null cells as expected from the release of suppression of mTORC1 after p14 knock-down.

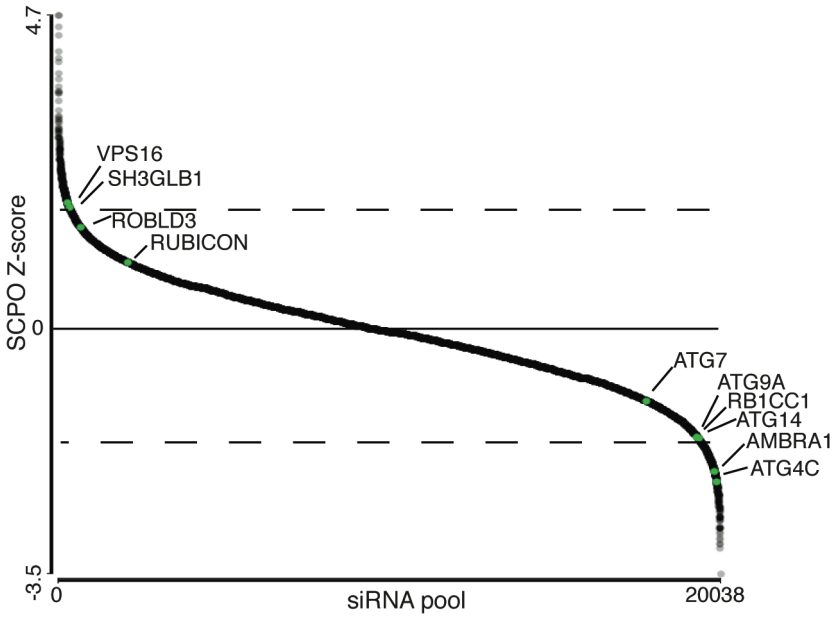

Figure 4.7 Scatter plot of median SCPO Z-scores against rank for siRNA Smartpools assayed in the Primary Screen; some Atg genes and other known autophagy regulators are shown

siRNA Smartpools in the siGenome library were ranked in terms of SCPO Z-scores and plotted. The green dots represent median values for some genes shown to be involved in autophagy. The dashed lines represent the approximate SCPO cut-off corresponding to the 500 cut-off determined by RP. The siRNA Smartpools that lead to less than 50 cells per well in at least two out of three replicates are left out of this plot.

4.3 Secondary Screen: Repeat the autophagy screen with the 1000 best hits

4.3.1 Preparing for the repeat screen

It was decided that a numerical cut-off would be made based on strength of phenotype and the number of siRNA Smartpools I wanted to handle in the second screen. The assay was repeated with the Smartpools that led to the best 500 decreases and best 500 increases of GFP-LC3 spots in the primary screen as determined by the rank product of the three spot parameters. The median Z-score cut-off point for SCPO, STAPO and STIPO was approximately +1.7 for the increasers (those above +1.7 were taken forward) and -1.6 for the decreasers (those below -1.6 were taken forward). This secondary or repeat screen was done in order to improve our confidence in and test the reproducibility of the hits and so that I could make further cut-offs with assurance. We were able to use the siGENOME Smartpool siRNA that was left over after the aliquoting of the library to re-test these 1000 best hits. I 'cherry-picked' the 1000 siRNA Smartpools from the 267 plates containing the left-over reagent placing it into 13 intermediate holder plates. Plates for the repeat screen were coated with Poly-D-lysine, washed and tested as above and the picked siRNA was dispensed from the holder plates in triplicate onto 39 plates (3x13 plates).

A low passage aliquot of GFP-LC3-HEK cells was tested to ensure that the cells responded to the induction of autophagy and that knock-downs of siRNA controls that affected the number of GFP-LC3 spots after induction were working as before. The same lots of control siRNA, Lipofectamine2000 and leupeptin were used as in the primary screen.

4.3.2 Performing the repeat screen

The repeat screen was preformed exactly as the primary screen: on day 1, the reverse knock-down was performed once with one batch of cells. On day 3 the transfection medium was exchanged for fresh, full medium and on day 4 the plates were washed and starvation medium was added as before. Images of 14 fields per well were captured for each well of the 39 plates. At a later point, images of 14 different fields were also captured for each well by beginning image acquisition in a different area of the well. The Cellomics SpotDetector programme was run simultaneously to acquire

images as before and spots were called based on similar settings to the primary screen but optimised for the repeat screen plates as new thresholds were set by maximizing fold induction determined by visual analysis of images from control siRNA treatments (Figure 4.8). The images and data generated from the repeat screen were stored with the primary screen images and data on the High-Throughput Screening Lab's server and, of note, occupied approximately 0.5 terabytes (500 GB) of space.

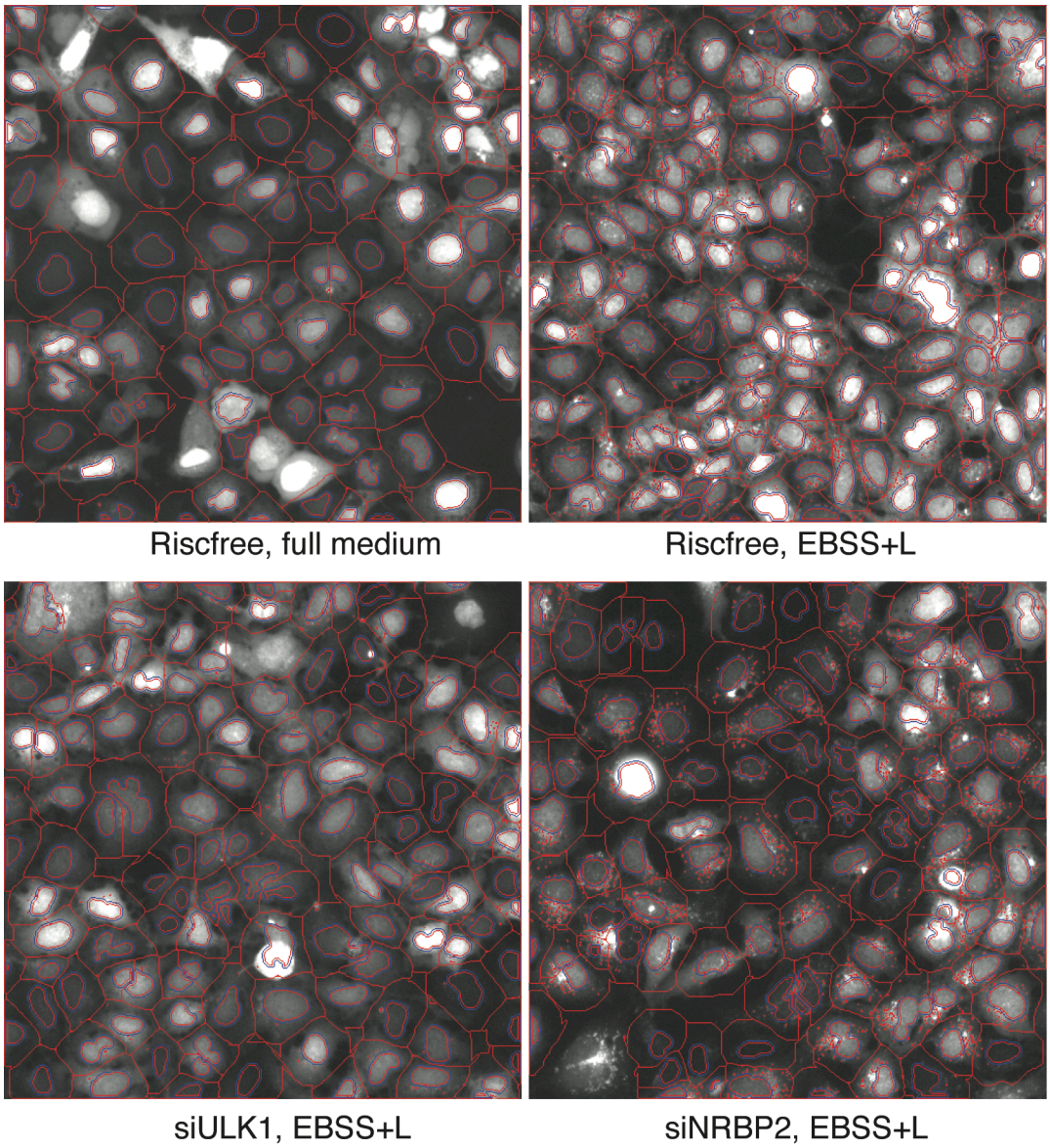

Figure 4.8 Cellomics images of controls from repeat screen
Cellomics images (at 20x) of one field of cells after indicated siRNA treatment and incubation conditions (EBSS+L represents EBSS plus 0.25mg/ml Leupeptin). Masks designate nuclei (objects), rings within which spots are counted and spots. After induction cells are treated with RISCfree control siRNA exhibit multiple many GFP-LC3 spots (shown in red). These spots are diminished after treatment with siRNA

against ULK1 and increased after treatment with siRNA against NRBP2 (see Chapter 3.3.2 and Figure 3.19 for an explanation of the controls chosen for the screen).

4.3.3 Analysis of the repeat screen

4.3.3.1 Normalisation and analysis of data from the repeat screen

Normalisation of the data from the repeat screen was performed as in the primary screen. A threshold of 50 cells per well was required for the replicate to be considered in calculations. As above, raw data for SCPO, STAPO and STIPO were normalised first to adjust for the well's position on the plate by creating a B-score. Then the data was normalised to the plate median, creating a Z-score. The Z-scores for each of the three replicate plates show a linear distribution with a slope close to one, indicating that the Z-scores for the replicates show high correlation and therefore reproducibility (Figure 4.9). The Z-scores for the three control wells that received siRNA against ULK1 are negative and cluster together in the lower left-hand corner of the plot. The median Z-score for the three replicates was determined and the siRNA Smartpools were ranked based on the rank product of the three spot parameters (Appendix Table 9.3 and 9.4). This process was repeated for the second set of images acquired (referred to as "new images"). Finally, the rank product of the primary screen was combined with the rank product generated of the data from the first set of images of the repeat screen to create a combined rank product for the two screens. The 500 increaser and 500 decreaser hits were listed according to this combined rank product and those Smartpools with the best combined rank products (as well as some interesting genes) are listed in Appendix Table 9.3 and 9.4.

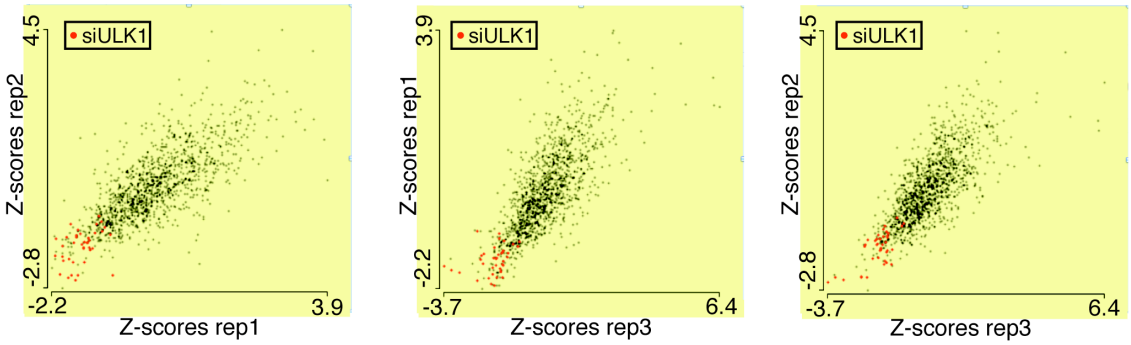

Figure 4.9 Scatter plots comparing replicate plates
Z-scores for three replicate plates are compared for the 1000 siRNA Smartpools plus negative and positive controls tested in the repeat screen. Values for three siULK1 controls wells are shown in red.

As the scale of the repeat screen was much smaller than the primary screen (39 versus 801), the cell density and overall cell heath at the time of fixation was much better than that of the primary screen. The 39 plates were processed much more quickly on day 1 and day 4 and spent less time outside of the incubators, especially during the induction process on day 4, than during the primary screen. On day 4, after addition of the induction medium, plates were transferred to an unoccupied incubator that maintained the desired temperature and CO_2 concentration for the two hour incubation. The result of this more-attentive handling was that the cells, once fixed, were at a more-desired density for imaging (Figure 4.8). In turn, we generated a large number of images (two sets of 14 fields for each replicate) and thus had more confidence in the repeat screen data as the data set (number of valid objects) was much greater.

4.3.3.2 Visual inspection of the repeat screen images

The repeat screen provided me with a large number of images for each siRNA knock-down that I visually inspected. This resource allowed me to eliminate the siRNA Smartpools that had a toxic effect on the GFP-LC3-HEK cells. siRNA that was toxic often caused cells to shrink and round up, leaving little cytoplasm. These were often mis-called as decreaser hits because GFP-LC3 spots were no longer visible or counted in this small cytoplasm. By visually inspecting the wells, I was also able to eliminate the false-positives that may have been classed as decreasers because the Cellomics microscope was out-of-focus when the image was acquired. If multiple fields were captured out-of-focus, spots were under-called skewing the data towards a negative Z-score for all three spot parameters.

I visually examined images from 198 decreaser hits and 173 increaser hits in order to create a new hit list comprising of 100 increasers and 100 decreasers that would be taken forward to the next stage, deconvolution (Appendix Table 9.3, 9.4). I noted for each well GFP-LC3 spottiness or lack of spottiness (namely, if it was a true increaser or decreaser, respectively) and toxicity when observed. Overall, more increaser hits seemed to repeat compared to decreaser hits for two reasons, 1) any toxicity that caused cells to round up leading to reduced cytoplasmic area or unfocused images would both lead to gene knock-downs being incorrectly designated as decreasers of spots and 2) siRNA Smartpools that increase spots because loss of the target genes could increase autophagy through several mechanisms. Loss of these genes could provoke a stress

response that activates autophagy, could lead to an inhibition of the degradation of autophagosomes or if the gene is a negative regulator, its loss could initiate autophagy. Of note, all of these scenarios are of interest for this screen for novel mammalian autophagy regulators. Decreaser hits, however, are most likely only those genes that are required for autophagy and is presumably a smaller set of genes.

As a result of the visual inspection, I came across some interesting GFP-LC3 spot phenotypes in both the spot increaser and decreaser hits that differed from the spot phenotype of cells treated with RISCfree control, ULK1 or NRBP2 siRNA (see Figure 4.8 for typical images of cells after treatment with these controls). For example, after treatment with siRNA for CNOT1 a significant increase in SCPO, STAPO and STIPO was recorded. I visually observed a large number of GFP-LC3 spots but these spots were smaller than normal (Figure 4.10). Also the cells appeared somewhat swollen and the nuclear staining of GFP was not as strong as normally seen. Conversely, knock-down of RPL22 lead to the accumulation of larger-than-normal GFP-LC3 spots that seemed to cluster in a juxta-nuclear region. ZFX also ranked high as an increaser in the primary screen but not in the repeat screen. Upon inspection of the images, I noticed that the GFP-LC3 in the cells was very bright but there did not seem to be many spots perhaps because knock-down of this gene increases the production or turnover of GFP-LC3 protein but does not affect autophagy and in light of the abnormal phenotype, this siRNA Smartpool was not taken forward as a hit. RAB28 was taken forward as a decreaser hit despite the odd spot phenotype that resulted from its siRNA, as the small GTPase proteins are important regulators of membrane trafficking processes and it is thus conceivable that Rab28 plays a potential role in autophagy. A decrease of SCPO, STIPO, and STAPO resulted from RAB28 knock-down (Appendix Table 9.4) but I observed large aggregates of GFP-LC3 in some of the cells and the area of these spots was perhaps above the threshold set and were not recorded as spots. It is conceivable that knock-down of RAB28 causes a type of maturation phenotype where the GFP-LC3-tagged autophagosomes are not degraded by the lysosomes and aggregate in the cytoplasm, and this is of potential interest as we seek to identify proteins involved in autophagosome maturation.

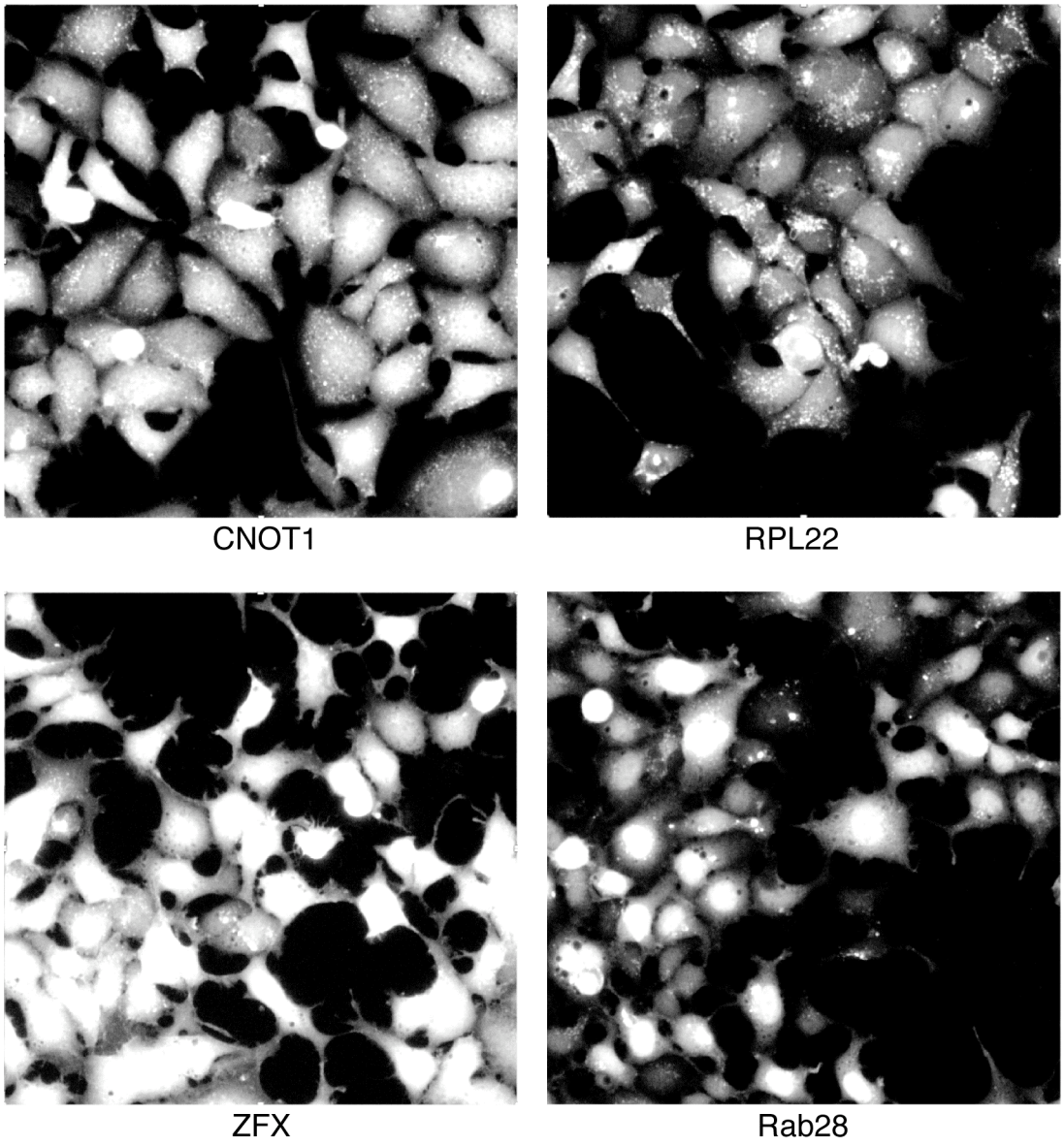

Figure 4.10 Cellomics Images of unusual spot phenotypes
Cellomics images (20x) of GFP-LC3 signal after indicated gene knock-down and induction of autophagy.

4.3.4 Results of the repeat screen

In general, an siRNA Smartpool for a given gene had a similar effect in the primary screen and the repeat screen. The range of Z-scores for SCPO was -2.3 to +3.0. Of the 500 best decreasers from the primary screen 81% had a SCPO Z-score less than 0 in the repeat screen. 59% had a Z-score less than -0.5 and 42% had a Z-score less than -0.75. Of the 500 best increasers from the primary screen 85% had a SCPO Z-

score greater than 0. 58% had a Z-score greater than +0.5 and 48% had a Z-score greater than +0.75.

Of the known autophagy proteins and regulators (discussed above) that made the 500 increaser or decreaser cut-off, ATG4C, AMBRA1, and VPS16 repeated their primary screen phenotype (Appendix Table 9.3 and 9.4). ULK1 was not repeated because it was on plate 10, which was lost in the primary screen and assayed for the first time in the repeat screen. The siRNA against Bif-1 (SH3GLB1), however, did not recapitulate the primary screen results of increasing GFP-LC3 spots, as the Smartpool had no effect in the repeat screen (Appendix Table 9.3). Differences between the primary and repeat screen could be due to a diminished quality of siRNA in the repeat screen as a result of being subjected to at least one but most likely at least two more freeze/thaw cycles compared to the siRNA from the primary screen. Also, the difference in density between the two screens (the cells from primary screen were more sparse at the time of imaging than the cells from repeat screen) could account for differences in results. The density of the cells from both screens appeared to be relatively comparable on day 4 but the cells of the repeat screen survived the washing, induction and fixation to a much greater extent and data from more cells was gathered as a result; it is a possibility that the data from the primary screen was skewed due to a smaller number of cells from which it was generated. Also, the cells of the repeat screen were slightly more dense during the two day incubation with siRNA, which may have altered the effectiveness of a given siRNA Smartpool. There were also instances when the results from the two screens were highly discordant for GFP-LC3 spot parameter data and sometimes even object count. This could perhaps be due to an error made during the picking of the siRNA from the left-over siRNA plate. Perhaps the mostly likely explanation for differences between the primary and secondary screen is the biological variation that occurs when siRNA is used in two separate experiments (to be discussed in greater detail in section 4.5).

As a result of the repeat screen, I gained confidence in the Smartpools that repeated the original screen phenotype. If a given knock-down lead to a robust effect (as measured by a large positive or negative Z-score) in two independent experiments with slightly different densities and conditions then I could be more sure that that Smartpool modulates GFP-LC3 spot formation than if I had only performed the primary

screen. The visual inspection of the images generated from the repeat screen also allowed me to eliminate mis-called hits and the siRNA Smartpools that caused toxicity. Eliminating toxic siRNA Smartpools was not only important because severe toxicity can lead to cells rounding up, making cytoplasmic spots difficult to count but also siRNA that is somewhat toxic may stress the cell triggering autophagy thus an increaser may be mis-designated as a hit not because of a direct effect on autophagy but because it evokes a stress response.

4.3.5 Choosing 190 genes to take forward

Of the siRNA Smartpools that repeated, some were eliminated because it is likely that their knock-downs affected processes unrelated to autophagy. For instance, knock-down of two genes that are subunits of the polymerase (RNA) II complex, POLR2B and POLR2C, lead to a decrease in GFP-LC3 spots presumably because the expression of GFP-LC3 was inhibited. Knock-down of PSMD8, a component of the 26S proteasome caused a large quantity of diffuse cytoplasmic GFP-LC3 perhaps because it could not be degraded by the proteasome causing this gene to be mis-called as an increaser hit. ATG4C and AMBRA1 were taken off the hit list because it was known that they are required for autophagy. Finally, there were 13 genes whose Smartpools caused an increase or decrease but whose deconvoluted sets of siRNA duplexes were not available for purchase from Dharmacon usually because they are designated as pseudogenes or their record has been discontinued or withdrawn as a gene (indicated in Appendix Table 9.3 and 9.4). There is, however, evidence that pseudogenes have a function and the PTEN pseudogene, PTENP1 has recently been shown to be biologically active and contribute to the tumour suppressor functions of PTEN (Poliseno et al., 2010). This study suggests that pseudogenes can not only regulate coding gene expression but also affect non-coding messenger RNA and perhaps the pseudogene Smartpools that had a robust affect on GFP-LC3 spots could be revisited in the future when more is known about the non-coding regions of the human genome.

The ultimate goal of the repeat screen and consequent visual inspection of the images was to create a list of approximately 100 increasers and 100 decreasers to take forward to the next step of validation, deconvolution of the siRNA Smartpools or analysis of the individual siRNA duplexes for each hit. It was determined that we had

only enough funds to buy 190 sets of siRNA for the deconvolution screen. Last, deconvolution of 190 sets of siRNA duplexes when done in triplicate would yield a screen of 30 plates, which was determined by the repeat screen to be a manageable size. Going forward, I felt confident that the chosen 190 Smartpools had a strong and reproducible effect of GFP-LC3 spot phenotype and their targeted genes were potential novel regulators of starvation-induced autophagy. The list of 190 sets of individual siRNA duplexes is contained in Appendix Table 9.5.

4.4 Deconvolution Screen: Increased confidence in 51 hits

In order to determine that the effect of the 190 Smartpools is due to the siRNA-mediated effect on its suggested target gene, I performed a deconvolution screen. It is generally agreed that if two or more individual siRNA duplexes of a so-called deconvoluted set of siRNA duplexes for a given gene induce the same phenotype as their pool then there is increased likelihood that it is knock-down of that specific gene that causes the phenotype (Mike Howell (LRI, HTS lab), personal communication; (Krausz, 2007)). In turn, that hit proceeds closer to becoming validated. Another way to increase confidence that a candidate Smartpool is targeting a gene involved in autophagy is to test an siRNA pool generated by a different vendor that uses alternate algorithms to generate siRNA sequences. Since the GFP-LC3-HEK cell knock-down protocol with Lipofectamine2000 was optimised for Dharmacon siRNA controls, I worried that switching siRNA source would require further optimisation. Thus, I chose to perform a deconvolution screen, testing the four individual siRNA duplexes for each Dharmacon Smartpool using the same image-based assay for starvation-induced autophagy in GFP-LC3-HEK cells.

4.4.1 Performing the screen and normalisation and analysis of the data

Sets of four siGENOME duplexes targeting the chosen 190 hits were ordered from Dharmacon. These siRNA reagents were resuspended and aliquoted onto triplicate plates for the deconvolution screen, again leaving two columns free for control siRNA. The plates, cells and induction conditions were tested to assure that all the materials for the screen were behaving as normal. The deconvolution screen was preformed on 30 plates following the same protocol as the primary and repeat screens described above. Images for 16 fields per well were collected and values for SCPO,

STIPO and STAPO were analysed. The results for each parameter were expressed as the median percent of control with respect to RISCfree control (Appendix Table 9.5). Individual siRNA duplexes were designated a hit if they caused more than a 20% increase or decrease in spot parameters and scored as positive or negative respectively for each parameter.

To increase our confidence in the data and the correct selection of hits to carry forward we repeated the deconvolution screen with sixty sets of four individual siRNA duplexes using several criteria. First, if they had three out of four siRNA duplexes that copied the original screen phenotype, they were potential validated-by-deconvolution hits. Second, I chose to re-test those for which two out of four of the siRNA duplexes showed the desired effect on spots and through two iterations of protein-protein interactions analysis (using the program Cytoscape to analyse network data), it was noted that these proteins interact with the potential three-out-of-four hits through one or two binding partners. These genes are GAB1, MRPS7, CDH18, FOXO4, KIF5B, and TRAM2. The data generated by this repeat deconvolution screen was similar to that of the first deconvolution screen; most importantly, the siRNA duplexes of the potential three-out-of-four hits had the same effects in the repeat deconvolution screen. I therefore based my decisions about each gene's deconvolution success on the first deconvolution screen data only.

In order to classify the genes as having two out of four repeating duplexes or three out of four decreasing duplexes I devised a set of rules. If three out of four of the individual siRNA duplexes repeated the original screen phenotype of increaser or decreaser for any of the three spot phenotypes that gene was designated as a three-out-of-four hit. The designation of two-out-of-four hits was more complex because often at least one of the duplexes did not repeat the primary screen phenotype, having the opposite effect on spots. We did not consider a gene a hit that had two siRNA duplexes that scored as positive and two siRNA duplexes that scored as negative. Two examples of this are SLC27A1 and GAB1. Their siRNA Smartpools decreased GFP-LC3 spots in the primary and repeat screen, but after deconvolution two siRNA duplexes gave positive scores for all three parameters and two siRNA duplexes gave negative scores for all three parameters in the deconvolution screen. However, when two siRNA duplexes for a given gene repeated the primary screen phenotype but one siRNA had

the opposite effect the gene was classed as a two-out-of-four hit. Some examples of this are MLLT7/FOXO4 and SEL1L. Whether a gene was decided to be a two-out-of-four hit or a three-out-of-four hit based on these criteria are indicated in Appendix Table 9.5.

Nine genes had three siRNA duplexes that decreased GFP-LC3 spot parameters and 15 genes had three siRNA duplexes that increased GFP-LC3 spot parameters; these are listed in Table 4.1. 27 genes were two-out-of-four hits for their original screen phenotype. In total, the effects on autophagy for 51 genes were confirmed by deconvolution of siRNA Smartpools.

Gene symbol	Entrez gene ID	Gene symbol	Entrez gene ID
Gene knock-downs that decrease GFP-LC3 spots			
C1orf198 (3/4)	84886	LARP1 (3/4)	23367
C1orf25	81627	MRPS7	51081
C9orf85	138241	NAA25 (3/4)	80018
CDH19 (3/4)	28513	PAFAH1B2 *	5049
CSTB	1476	PLXNA4	91584
FABP4	2167	SCOC (3/4)	60592
FOXO4	4303	SEL1L	6400
GHSR (3/4)	2693	SOX14	8403
GLB1L2	89944	SUPT5H (3/4)	6829
HERC4	26091	WAC (3/4)	51322
HS3ST4	9951		
Gene knock-downs that increase GFP-LC3 spots			
AATK	9625	MFAP5	8076
ADHFE1 (3/4)	137872	MYBPC3 §	4607
ARPP21	10777	NUP160	23279
ASPHD2	57168	RASGRF2 (3/4)	5924
C10orf116 §	10974	RASIP1 (3/4)	54922
C7orf58	79974	RBM12 *	10137
C8orf33	65265	SLC35C1	55343
CNOT1 (3/4)	23019	SNX20 (3/4)	124460
DNAJA3	9093	STAT2 (3/4)	6773
FBXL14 *	144699	TCL1B §	9623
HOXB3	3213	TLK2 (3/4)	11011
KIF25 (3/4)	3834	TRAM2	9697
KLK12	43849	UNC80	285175
KLRG1 §	10219	WDR6 (3/4)	11180
LRRN4	164312	ZSWIM6	57688

Table 4.1 51 gene knock-downs whose effects on autophagy in GFP-LC3-HEK cells were confirmed by deconvolution of siRNA Smartpools
Current gene symbols for genes whose knock-down decrease and increaser GFP-LC3 spots are shown. (3/4) indicates if three out of four siRNA duplexes repeated the spot phenotype. (*) indicates genes that

are three-out-of-fours if alternate normalisation is used. (§) indicates genes that have a tissue-specific distribution (to be discussed later in section 4.4.3).

4.4.2 Annotation of the validated-by-deconvolution hits

Deconvolution of 51 genes was deemed successful in that at least two out of four of the individual siRNA duplex validated the effect on GFP-LC3 spots in the primary and repeat screen. I manually annotated this list of genes using data available in the public domain using several different resources. Using NCBI/PubMed and the Human Protein Reference Database (HPRD), I discovered that these 51 genes are mostly uncharacterised and they do not map to known signalling networks such as the mTOR pathway. Of note, the genes on the list of 190 hits created after the repeat screen were also not enriched for any known signalling pathways. The 51 hits were analysed using Panther annotation for protein class and the hits were classified in terms of molecular function and biological processes. Again, the hits did not form large networks or group together based on these classifications. The 51 hits were then analysed for using GENE ONTOLOGY (GO) tools available in order to discover more about their biological process, molecular function and cellular component. I probed this database to find generic GO slim terms based on their proposed biological process and molecular function and then used the Generic GO Term Mapper to group the 51 genes into broad categories based on these GO slim terms (see Materials and Methods for an HTML table of results). Again, these 51 genes did not group together based on their slim terms.

Last, I determined the cellular localisations of the proteins on the list of 51 validated-by-deconvolution hits, using a GO tool and found that their distribution differs from the proteins of the human genome (Figure 4.11). The proteins on my hit-list are slightly enriched in the Golgi apparatus, endoplasmic reticulum, cytosol, and cytoplasm. This distribution is expected of genes involved in autophagy, a process that takes place in cytoplasm and because proteins of the Golgi apparatus and the ER have been shown to contribute to the formation of autophagosomes (van der Vaart and Reggiori, 2010), (Hayashi-Nishino et al., 2009). Perhaps the most striking difference is seen in the plasma membrane: significantly less plasma membrane proteins are contained in the hit list compared to the genome frequency. Until recent work by the

Rubinsztein lab, few if any plasma membrane-bound proteins had been shown to be involved in autophagy (Ravikumar et al., 2010).

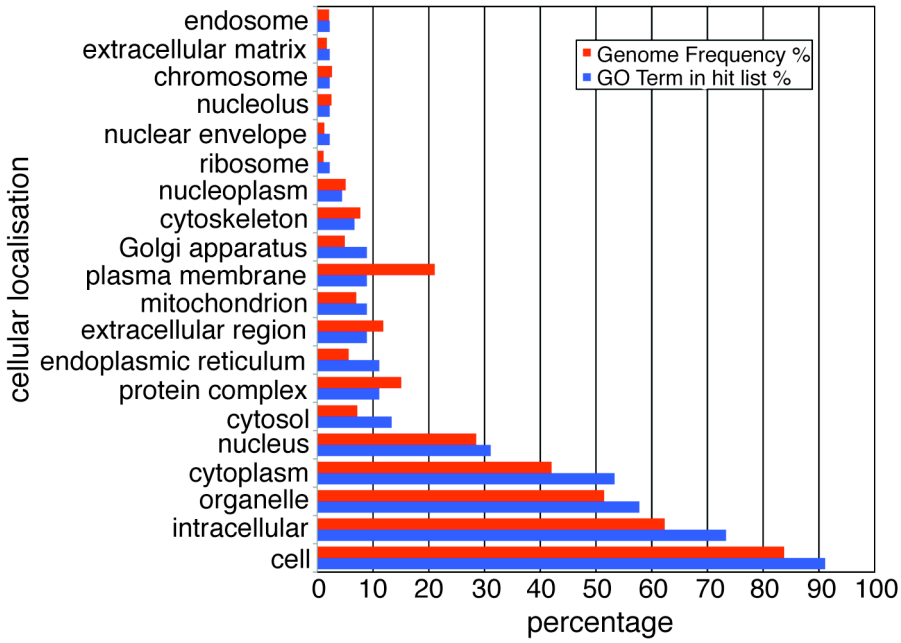

Figure 4.11 Differential frequency of distribution of the list of 51 and the genome
Frequency of cellular localisation of genes in the human genome (red bars) compared to the genes on the list of 51 validated-by-deconvolution hits (blue bars).

Of interest, the following validated-by-deconvolution decreasers are contained in the 'Druggable' gene set of the Dharmacon siGenome library: CDH19, CSTB, FABP4, HERC4, SEL1L, and SUPT5H. Of the validated increasers HOXB3, KIF25, KLRG1, MFAP5, MYBPC3, STAT2, and WDR6 are contained on the 'Druggable' plates. TLK2, the only kinase in the list of 51, could be a potential drug target because of its enzymatic properties. Though I did not confirm that these genes are recorded as drug targets in the literature, it is promising that drugs that target the six decreasers could be more-specific inhibitors of starvation-induced autophagy than the inhibitors currently available, such as 3-MA.

4.4.3 Selection of hits for further validation

Due to a limited amount of time available for me to further validate that these 51 genes are true regulators of autophagy and wanting to have high confidence in the hits, I took the opportunity to be very stringent when determining the cut-off after deconvolution. I decided that I would take forward only those hits that had three out of four individual siRNA duplexes that repeated the primary and repeat screen phenotypes.

Three genes, PAFAH1B2, FBXL14, and RBM12 are designated as having two duplexes that validated by deconvolution (Appendix Table 9.5, Table 4.1) but were taken forward because using an alternate normalisation (values were divided by the screen RISCfree mean instead of the median because plate 13 contained mostly non-knocked-down wells) they achieved a three out of four rank. I did not take forward four genes that had three validated siRNA duplexes but whose expression patterns are limited to a certain cell or tissue type. C10orf116 is expressed in adipose tissue, KLRG1 is expressed in NK cells, MYBPC3 is reported to be expressed only in heart muscle, and TCL1B only in lymph tissue. Of note, knock-down of all four of these genes caused an increase in GFP-LC3 spots and perhaps these siRNA duplexes target different (off-target) genes expressed in HEK cells eliciting a stress response that increases autophagy. Making the decision to exclude these genes I was, however, relying on experimental data in the public domain, the quality of which I could not determine. It is possible that these genes are indeed expressed in GFP-LC3-HEK cells and other tissues and their knock-down may increase autophagy. In turn, their expression levels in tissues could be re-tested the role of these genes in autophagy could be explored.

Thus, nine genes for which three individual siRNA duplexes decreased GFP-LC3 spot parameters were taken forward: C1orf198, CDH19, GHSR, LARP1, NAA25, PAFAH1B2, SCOC, SUPT5H and WAC. Eleven genes for which three individual siRNA duplexes increased GFP-LC3 spot parameters were taken forward: ADHFE1, CNOT1, FBXL14, KIF25, RASGRF2, RASIP1, RBM12, SNX20, STAT2, TLK2, and WDR6.

4.5 Discussion of image-based screens and results

4.5.1 Considerations for the image-based siRNA screens

The image-based high-content screens allowed me to determine the effect of 21,121 siRNA Smartpools on GFP-LC3 spot count, area and intensity after induction of autophagy with starvation. In addition to analysing these multiple parameters, I was able to visually inspect the images and draw conclusions about the effect of the siRNA Smartpools on cell heath and even GFP-LC3 levels in the stable cells. One of the benefits of the Cellomics system is that the stored images can be reanalysed using different thresholds or different programs and thus, the primary data can be analysed to

generate additional information. One possible extension of this could be to classify the GFP-LC3 spot increasers in terms of the distribution or phenotype of GFP-LC3 spots they induce. For instance, these Smartpools could lead to more spots spread throughout the cell or conversely clustered in regions within the cell. Also, the data itself could be revisited and cut-offs could be altered to allow for the analysis of more candidates. After the primary screen, 500 increasers and 500 decreasers were taken forward but there were multiple autophagy genes (ATG9, FIP200, ATG14) whose knock-downs lead to a significant inhibition of GFP-LC3 spots but did not meet the cut-off of 500 (Figure 4.7). If I expanded the cut-off to 1000 increasers and 1000 decreasers these three genes and thus many other potential regulators of autophagy would be included. Also, the data could be normalised differently producing a different data set.

By analysing multiple parameters of GFP-LC3 spots and also cell viability using minimum valid object counts and visually inspecting the cells in addition to eliminating data that was mis-called by the Cellomics HCS reader due to focusing and other issues, I attempted to limit false-positive and false-negative results. Doing the primary, repeat and deconvolution screens in triplicate also improved the results. However, it is thought that image-based cellular assays have more intrinsic variability compared to biochemical assays or reporter gene-based assays, mainly due to the relatively small number of cells analysed (Krausz, 2007). In addition, the screens relied on the even distribution of cells across the area of analysis, which was critical for the microscope to sample enough cells during the automated image acquisition. These are reasons why the repeat screen was so important; because the cells were at optimal density at the time of imaging, a large amount of cells were analysed (usually approaching 1000 cells per replicate, Appendix table 9.3, 9.4). In contrast, the imaged cells of the primary screen were at a less-optimal density due to the problems generated when handling a large number of plates. Improvements for the future could be made by using more incubators or improved incubators that maintain a more constant temperature and CO_2 concentration despite unusual amounts of opening. Because of the density of the cells and the amount of data captured, the repeat screen generated more trust-worthy results.

I found there were differences in the results between the primary screen and the repeat screen that I attribute to biological variability due to slight technical variations (i.e. density during transfection) and the differential ability of siRNA to knock-down a

given gene on a given plate on a given day. The data for the screen is widely distributed, with a majority of the negative controls clustering in the middle and the positive controls clustering at the ends. But there is variation even when examining one control well, as seen with the ULK1 siRNA in well C01 in the primary screen (Figure 4.5). Though every SCPO median Z-score is negative, there is a range of Z-scores and some of these wells are not in the best 500 decreasers and therefore would not make the strict cut-off that was set. In this way, a gene that scored significantly in the primary screen, achieving the 500 marked cut-off but might not have achieved a strong enough effect when assayed again to make the repeat screen's cut-off. In addition, I introduced the variable of human error when creating the siRNA library for the repeat screen because I manually cherry-picked the siRNA Smartpools from plates holding the siGenome library.

Perhaps instead of repeating the image-based GFP-LC3 spot counting screen I could have used a different assay to improve my confidence in the hits. Using a different assay could have provided a different read-out for starvation-induced autophagy. Assays such as LC3-lipidation with and without lysosomal protease inhibitors monitored by western blot and long-lived protein degradation could have provided me with additional information about how the gene knock-downs were affecting the autophagy pathway (Klionsky et al., 2008). These assays, however, are difficult and too time-consuming to do in a large scale, which is why I originally tried the intein-based luciferase assay. Alternatives could have been a flow cytometry-based assay that uses the amount of total GFP-LC3 remaining after autophagy induction to measure modulation in the pathway (Shvets et al., 2008a) or a luciferase-based assay that measures the kinetics of autophagic flux (Farkas et al., 2009). I however, chose to delay the use of alternate assays until I had a small set of candidate hits for which I had high confidence.

The caveats of RNA interference screens are that a given siRNA may not work in a specific assay because of time frame, or the siRNA duplexes themselves may fail. It is thought that the transient and specific silencing of a particular gene using siRNA typically reaches its peak after 24 hours and then declines but then recovers by about 96 hours after transfection and so the window of time between 48 hours to 96 hours is generally optimal (Hannon, 2002). But this depends on the targeted gene and proteins

with a longer half-life may fail to give a phenotype within that time frame. Thus, there were genes that were not optimally targeted by the 72-hour-long transfection period of my screens. In addition, the siRNA duplexes contained within the Dharmacon Smartpools are not guaranteed to target only their intended gene. Though algorithms are constantly improved and non-targeted siRNAs substituted for new ones, the siGenome library is not perfect.

In turn, there is a risk of false positives due to off-target effects; the duplexes contained within a Smartpool may knock-down unknown genes that are themselves causing the autophagy-related phenotype. I tackled this problem by testing the four siRNA duplexes that make up the Dharmacon siGenome Smartpools individually for their effects on autophagy. It is generally thought that if two out of four duplexes phenocopy the Smartpool then one can have confidence in the result. As mentioned above, I could have alternatively used siRNA from a different company that employs different algorithms. The only way to assure that a siRNA is affecting its target is to test the ability of that siRNA to reduce the gene's mRNA levels or protein expression. However, like using an alternate assay for autophagy, measuring knock-down efficiency was only possible to do in a small scale.

4.5.2 Other genome-wide screens for autophagy

Recently, a genome-wide screen for non-induced, basal autophagy was described (Lipinski et al., 2010). Lipinski *et al* also used the Dharmacon siGenome library and the Cellomics HCS platform to quantify GFP-LC3 spot formation in a neuroblastoma cell line. Overall, there is very little overlap between my hits and their hits suggesting the regulation and mechanisms of basal autophagy are highly different to those of starvation-induced autophagy. In the case of one gene, GHSR, their results are opposite to mine. They show that knock-down of GHSR increased basal GFP-LC3 spots but I found that three out of four siRNA duplexes for GHSR in fact inhibited spot parameters (GHSR is further analysed in Chapter section 5.4.1). One Smartpool that we both identified to decrease spot formation was GAB1. In my deconvolution screen, two siRNA duplexes for GAB1 decreased GFP-LC3 spot parameters and two increased and for this reason, we chose not to carry GAB1 forward though it is an interesting gene with many known interacting partners and is involved in insulin receptor signalling, which has been linked to autophagy (Yamamoto et al., 2006).

Another screen was also done to identify regulators of basal autophagy; it utilised proteomics to identify protein interaction subnetworks built upon known autophagy genes (Behrends et al., 2010). There was no overlap between their high-confidence hits (meeting strength, reproducibility and peptide number cut-offs) and my hits but there was some overlap between my hits and their full data set (Table 4.2). In fact, nine of the validated-by-deconvolution hits were found to bind to autophagy interacting proteins, placing them within the autophagy interaction network (AIN).

siRNA screen hit	Bait*	p_value*	WD_Score*	Z_Score
WAC **	BECN1	0.28773972	236.17	12.88
SCOC **	UVRAG	0.28773972	118.09	9.11
SCOC **	NRBF2	0.28773972	118.09	9.11
DNAJA3	WIPI2		18.89	5.86
DNAJA3	UVRAG		4.48	1.97
DNAJA3	SQSTM1		9.45	1.19
DNAJA3	RABGAP1		2.58	0.41
DNAJA3	PRKAB2		11.57	1.97
DNAJA3	ATG2A		18.89	5.86
DNAJA3	GBAS		3.66	1.19
DNAJA3	CLN3		5.78	3.52
DNAJA3	CAMKK2		5.17	2.75
DNAJA3	BECN1		3.66	1.19
DNAJA3	ATG5		2.58	0.41
DNAJA3	ATG4C		3.66	1.19
NUP160	WIPI2		7.46	4.15
NUP160	GBAS		26.24	2.69
NUP160	C12orf44		6.09	2.69
C1orf25	ULK1		2.53	0.9
C1orf25	PRKAA1		14.36	6.1
C1orf25	CLN3		3.58	2.2
C8orf33	ULK1		3.05	1.41
C8orf33	PRKAA1		4.31	3.14
C8orf33	PDPK1		3.05	1.41
C8orf33	KBTBD7		3.05	1.41
CSTB	WIPI2		2.15	0.67
CSTB	ULK2		2.15	0.67
CSTB	TRAF2		3.05	1.83
CSTB	STK4		2.15	0.67
CSTB	SQSTM1		9.28	4.15
CSTB	PRKAB1		3.73	2.99
CSTB	PRKAA2		2.15	0.67
CSTB	PRKAA1		2.15	0.67
CSTB	PIK3C3		9.28	4.15
CSTB	PDPK1		2.15	0.67
CSTB	NEK9		3.73	2.99
CSTB	MAP1LC3A		3.05	1.83
CSTB	KIAA0265		3.05	1.83
CSTB	HIF1A		3.73	2.99
CSTB	GOSR1		2.15	0.67
CSTB	GABARAPL1		6.56	1.83
CSTB	FYCO1		6.56	1.83
CSTB	TECPR1		6.56	1.83
CSTB	ATG10		9.28	4.15
CSTB	ATG4C		2.15	0.67
CSTB	ATG4B		6.56	1.83
LARP1**	WDR45		3.44	-0.04
LARP1**	ULK2		4.22	0.42
LARP1**	ULK1		1.86	-0.49
LARP1**	RASSF5		3.44	-0.04
LARP1**	RABGAP1		4.87	0.87
LARP1**	PRKAB2		1.86	-0.49
LARP1**	PRKAA1		5.96	1.77
LARP1**	NSMAF		3.44	-0.04
LARP1**	NSF		2.27	-0.26
LARP1**	KIAA0831		2.62	-0.04
LARP1**	KIAA0265		4.87	0.87
LARP1**	TECPR1		1.31	-0.71
SUPT5H **	FYCO1		10.01	5.23

Table 4.2 Validated-by-deconvolution hits found in the autophagy interaction network (AIN)
Nine of the 51 hits were found to interact with autophagy proteins or autophagy protein-interacting proteins in a proteomic screen (Behrends et al., 2010). Shown are the gene symbols, baits with which they were pulled down, the p_value, WD_score, and Z-score from the screen. **Denotes hits that passed further validation steps in my screen (described in Chapter 5).

4.5.3 Other interesting hits not taken forward

There were multiple other interesting genes linked in the literature to autophagy in the top 1000 of the screen whose knock-down either decreased GFP-LC3 spots or increased. Due to issues described above, these results were not reproduced in the repeat screen but I think it is of interest to discuss PINK1, RAB7, RILP and PRKAR1A below (these are highlighted in blue in Appendix Table 9.1 and 9.2). In the primary screen, PTEN induced putative kinase 1 or PINK1, ranked 289th as a decreaser required for autophagy. Mutations in the kinase domain of this gene have been shown to cause early-onset Parkinson's disease through increased susceptibility to cellular stress (Valente et al., 2004). More recently, PINK1 has been shown to be recruited to damaged mitochondria and associate with LC3, triggering autophagy (Narendra et al., 2010). It is suggested that the degradation of damaged mitochondria by autophagy (mitophagy) is triggered by PINK1 and Parkin together coordinating the accumulation of damaged mitochondria in a perinuclear aggregates (Kawajiri et al., 2010).

As discussed above, an increase in GFP-LC3 spots could result from a loss of negative regulation of the initiation of autophagy or inhibition of the maturation of autophagosomes. Rab7 is a GTPase that is known to control late endocytic trafficking, a process that is also required for autophagosome maturation (Gutierrez et al., 2004), (Jager et al., 2004). In turn, one would expect that when Rab7 is knocked known in GFP-LC3-HEK cells an accumulation spots would be seen, but in fact RAB7A knock-down in the primary screen led to a somewhat significant decrease in GFP-LC3 spots (ranking 1362nd of decreasers; RP was 1457) suggesting Rab7 is potentially involved in the initiation of autophagy. Conversely, knock-down of Rab interacting lysosomal protein, RILP increased GFP-LC3 spot formation or led to a significant accumulation of GFP-LC3 spots (ranked 451st of increasers; RP was 517). This is perhaps expected as RILP is a downstream effector of Rab7 and has been shown to coordinate with Rab7 to control endosomal maturation and fusion of autophagosomes with lysosomes (Liang et

al., 2008). Most recently, however, it was also shown that the Rab7/RILP interaction can be stimulated by IGF-1 in neurons and that their interaction increased autophagy (Bains et al., 2010); this interaction could perhaps provide a mechanism for the positive regulation of autophagy by Rab7. In my primary screen, PRKAR1A, the regulatory subunit of protein kinase A, increased GFP-LC3 spot formation (ranked 96th of increasers; RP was 127). The protein has been shown to interact with mTOR kinase and affect its activity during starvation thus acting upstream of mTOR as a regulator of autophagy (Mavrakis et al., 2007). Seemingly opposite to my results, Mavrakis *et al* showed that PRKAR1A knock-down activates mTOR, decreasing autophagy efficiency and PRKAR1A knock-down also decreased GFP-LC3 lipidation in the kinome screen performed in our lab (Chan et al., 2007). Perhaps knock-down of PRKAR1A inhibits both autophagosome formation, through mTOR but also autophagosome maturation. Interestingly PRKAR1A has been shown to colocalise with Rab7- and LC3-positive vesicles (Bains et al., 2010) perhaps linking the mTOR complex to autophagosome maturation. Conversely, linking Rab7 to mTOR through Rab7's interaction with PRKAR1A may explain how knock-down of RAB7A inhibited autophagosome formation in the primary screen.

An interesting gene for which only one out of four of the siRNA duplexes reproduced the primary and repeat screen phenotype has also been previously linked to autophagy: SAV1 (salvador homologue 1) knock-down inhibited GFP-LC3 spot parameters. This scaffold protein critical for the Warts (Wts) tumour suppressor pathway (also known as the Hippo pathway) has also been shown, along with other members of the pathway, to be required for autophagy in Drosophila (Dutta and Baehrecke, 2008). The Hippo pathway is regulated by the class I PI3-kinase pathway and is a negative regulator of cell growth (Tapon et al., 2002). Though only one duplex met the threshold of 20% inhibition and thus scored as negative in the deconvolution screen, two other duplexes decreased STIPO and the remaining duplex did not have a significant effect on the spot parameters (Appendix Table 9.5). I have confirmed that this one duplex inhibits LC3 lipidation and if I could rescue the knock-down with expression of an siRNA resistant clone and show that this duplex was also the most effective in reducing SAV1 mRNA or protein levels then salvador homologue 1 could

be a positive regulator of autophagy and potentially link the Hippo and class I PI3-kinase pathways to autophagy.

In conclusion, in order to identify novel autophagy regulators by a genome-wide siRNA screen I relied on a cell model system that provided a robust read-out for autophagy in the form of the quantifiable starvation-dependent formation of GFP-LC3-labelled autophagosomes. The hit-selection strategy to identify both negative and positive regulators of starvation-induced autophagy was based on multiple rounds of screening (primary, secondary, and deconvolution) coupled with the elimination of candidates that did not satisfy strict criteria. Using this approach, I have identified 20 potential negative and positive regulators of starvation-induced autophagy, the further investigation of which is described below. It is likely that relaxation of some of the thresholds in the deconvolution screen or further study of the hits with two out of four or even one out of four deconvoluted siRNA duplexes will reveal more candidate genes in the data set.

Chapter 5. Further Validation of the 'Three-out-of-Four' Hits

Nine genes, when knocked down by three individual siRNA duplexes, cause a decrease in GFP-LC3 spot number, area and/or intensity and were selected to take forward for further confirmation and investigation of their role in autophagy. These 'decreasers' are: C1orf198, CDH19, GHSR, LARP1, NAA25, PAFAH1B2, SCOC, SUPT5H, and WAC. Conversely, eleven gene knock-downs lead to an increase of GFP-LC3 spots. These 'increasers' are: ADHFE1, CNOT1, FBXL14, KIF25, RASGRF2, RASIP1, RBM12, SNX20, STAT2, TLK2, and WDR6. From the data produced in deconvolution screen, I determined which were the two most potent siRNA duplexes in terms of their effects on spots from for each of the genes and also were not toxic to the cells. I used these siRNA duplexes to further validate the involvement of their target genes in autophagy, testing their effects on autophagy after induction in alternate conditions, measuring their ability to knock-down the mRNA levels of their intended target, and measuring their effect with an alternate autophagy assay, a process that I called 'supervalidation.'

5.1 Induction Screen of the 20 validated hits

As a result of the primary, repeat and deconvolution screens I demonstrated that twenty genes were potential modulators of starvation-induced autophagy. I next asked whether these genes were similarly required for GFP-LC3 spots using different inducers of autophagy. Perhaps the most important question I asked was whether the involvement of these hits in autophagy was mTOR-dependent or mTOR-independent. Because the signalling between amino acid sensing and mTOR inactivation that leads to autophagy has not been fully elucidated it is conceivable that a lack of nutrients can directly activate the autophagic machinery, bypassing mTOR. Thus, I asked whether knock-down of my hits would have the same effects with initiation of spot formation with drugs that are reported to induce autophagy in an mTOR-dependent, mTOR-independent, and also Beclin-independent manner. In turn, if the decrease or increase of GFP-LC3 spots after knock-down is repeated in conditions of autophagy activation through the direct inhibition of mTOR but also though mTOR-independent pathways then I can tentatively conclude that my hit is functioning downstream of these signalling

pathways perhaps modulating autophagosome formation or maturation. Conversely, if differential effects were seen as a result of the various induction methods then I could perhaps group the hits into different autophagy induction signalling pathways based on the proposed mechanism of action of the inducers. I also asked whether knock-down of the hits affected autophagic flux during a two-hour period by culturing the cells in starvation medium alone without leupeptin. Of great interest was to discover whether the 20 hits increased or decreased basal autophagy, or autophagy that occurs in full growth medium. The kinome screen of GFP-LC3-HEK cells (Chan et al., 2007) uncovered a that loss of subunits of the COP1 coat complex leads to increased autophagy in full medium conditions because they are required for the fusion of autophagosomes with early endosomes; their loss increases autophagosome accumulation without increasing autophagic flux (Razi et al., 2009).

To determine whether my hits were influencing GFP-LC3 spot parameters through the activity of the negative regulator mTOR, I induced autophagy by treating cells with an inhibitor of mTOR. Tor was originally discovered as the main regulator of autophagy in yeast and it was shown that rapamycin, an inhibitor of TOR, induced autophagosome formation (Noda and Ohsumi, 1998) and rapamycin has been shown to similarly induce autophagy in mammalian cells. Recently Torin, a potent inhibitor of mTOR kinase activity has been shown to be a stronger activator of autophagy compared to rapamycin perhaps by inhibiting mTOR's rapamycin-resistant phosphorylation of the translation initiating factor binding protein 4E-BP1 (Thoreen et al., 2009).

To assess the effect on autophagy that is induced by mechanisms reported to act independently of mTOR, I treated cells with lithium chloride. I have previously shown that treatment with lithium chloride for 48 hours induced LC3 lipidation in HEK cells (Figure 3.9). It is proposed that lithium induces autophagy by inhibiting inositol monophosphatase (IMPase) levels, which decreases free inositol and decreases myo-inositol-1,4,5 triphosphate (IP_3) levels, eventually altering membrane availability (Sarkar et al., 2005). Sarkar *et al* suggest that this process is mTOR independent because rapamycin does not affect IP_3 levels and alternately IP_3 itself does not affect rapamycin efficacy. In addition, lithium and rapamycin work synergistically to clear aggregate-prone mutant proteins (Sarkar et al., 2008).

Resveratrol has been shown to induce autophagy in DLD1 cancer cells and MCF7 breast cancer cells (Trincheri et al., 2008), (Scarlatti et al., 2008). Scarlatti *et al* have shown that this induction in MCF7 cells is insensitive to PI3K inhibitors and have therefore classed resveratrol as a non-canonical, beclin 1/vps34-independent activator of autophagy. Of note, they show that the response is TOR dependent. Another target of resveratrol is the NAD+-dependent deacetylase Sirtuin-1. It has recently been shown that activation of sirtuin-1 induces autophagy and that sirtuin-1 is required for the starvation-induced autophagy response (Morselli et al., 2010). Contrary to Scarlatti *et al* who show that the response to resveratrol is TOR dependent, Morselli *et al* suggest that this sirtuin-1-mediated autophagy response does not involve the inhibition of mTOR or the negative regulator p53. Instead, they suggest that resveratrol activates sirtuins, which in turn deacetylate the autophagy proteins involved in the Atg5/Atg12 complex thereby directly activating autophagy.

I performed the induction screen following the procedure used for the primary and deconvolution screens in 21 96-well plates. On each plate, the two siRNA duplexes for each of the twenty hits and both negative and positive control siRNA duplexes were added. Triplicate plates were incubated in the following treatments: full medium plus leupeptin or lithium chloride for 24 hours, full medium plus leupeptin for 2 hours, EBSS or EBSS plus leupeptin for 2 hours, Torin plus leupeptin for 2 hours, and resveratrol plus leupeptin for two hours. The GFP-LC3 spots were analysed using the Cellomics SpotDetector program and triplicate values for each siRNA treatment were averaged (Figure 5.1). Values for control knock-down with RISCfree or siControl show that there is an increase in GFP-LC3 spots after starvation medium incubations or treatment with Torin or resveratrol. More spots were seen in EBSS supplemented with leupeptin compared to EBSS alone, as seen before. Lithium chloride only leads to a subtle increase of STIPO and STAPO; this treatment caused a morphological change in the cells, suggesting a toxic effect of the drug, and the GFP-LC3 spots were larger and aggregated which presumably led to spot under-calling. The effects of positive control siRNA knock-downs on STAPO and STIPO are more pronounced than on SCPO but are consistent. Knock-down of ULK1 and ATG4C inhibited GFP-LC3 spot parameters for all conditions including basal autophagy. Knock-down of NRBP2 led to an increase after EBSS, EBSS plus leupeptin, Torin and resveratrol but not after lithium chloride or

incubation in full medium suggesting that NRBP2's effects on autophagy are dependent on the activation of mTOR.

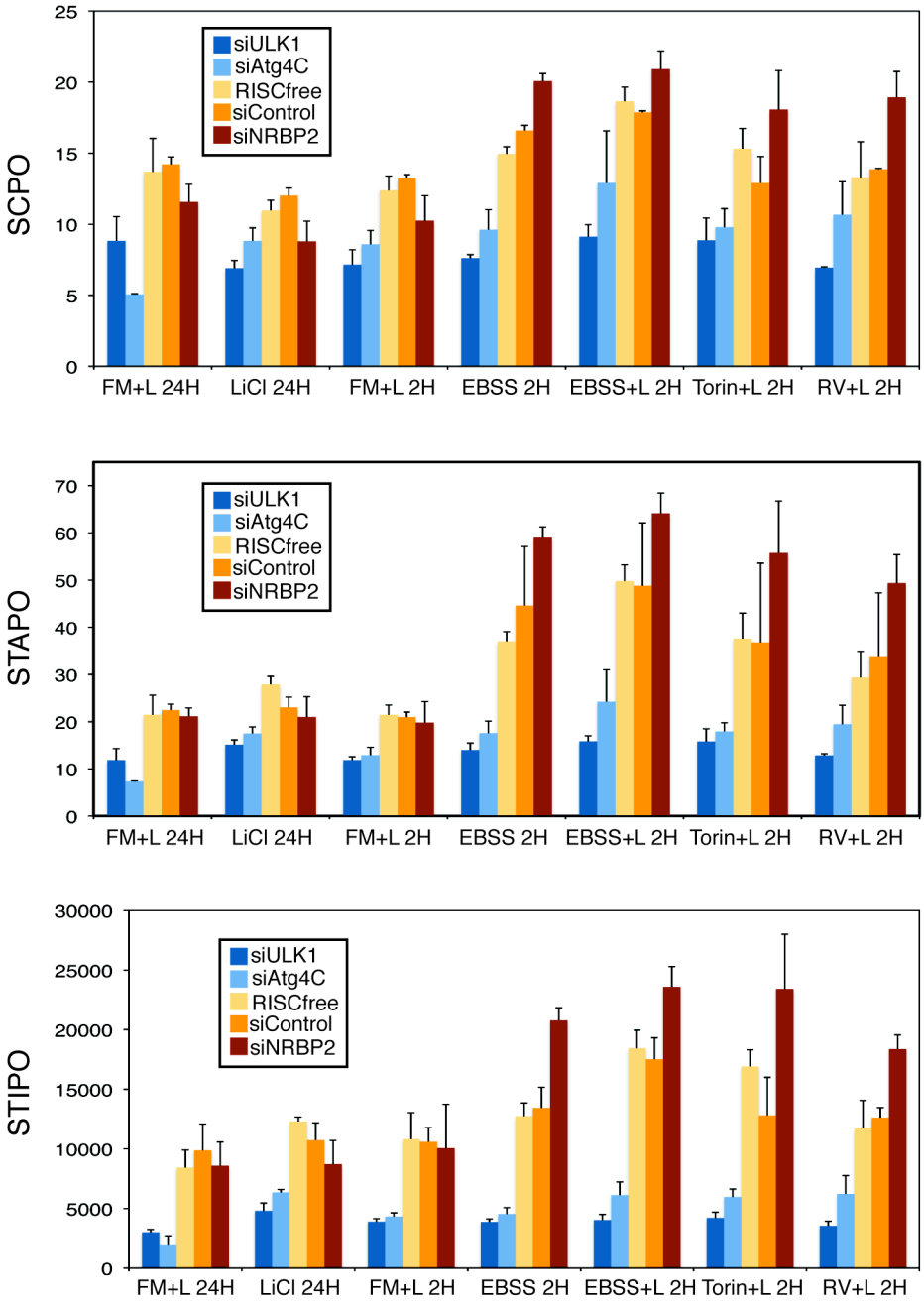

Figure 5.1 GFP-LC3 spot parameters are altered by positive control siRNA in the induction screen

Values for SCPO, STAPO and STIPO after indicated siRNA knock-down and medium conditions in GFP-LC3-HEK cells. 24H is 24 hours treatment, 2H is 2 hours treatment, FM is full medium, LiCl is 10mM lithium chloride, EBSS+L is EBSS plus 0.25mg/mL leupeptin, Torin is 250nM Torin, and RV is 128µM resveratrol. Bars represent averaged triplicate values from three plates that were then pooled and averaged again based on the number of wells occupied by that siRNA (n). Error bars represent standard deviation from averaged pooled triplicate values (RF n=5, siAtg4C n=2, siNRBP2 n=4, siControl n=2, siULK1 n=3).

The results of the induction screen for nine of the hits will be discussed below. To summarise the results from the eleven not discussed below: both siRNA duplexes for C1orf198, CDH19, and NAA25 decreased GFP-LC3 spots in all basal and induced autophagy conditions in the induction screen. Knock-down with duplexes against GHSR lead to a decrease in basal and starvation-induced autophagy but not after induction with Torin or resveratrol. Of the increasers, ADHFE1 and CNOT1 duplexes increased GFP-LC3 spots in all conditions and the ADHFE1 knock-downs greatly increased basal GFP-LC3 spots. The two duplexes against FBXL14, RBM12 and SNX20 had differential effects in the induction screen in that one duplex led to an increase and the other resembled the response with negative control siRNA. Knock-down of STAT2 increased SCPO and STAPO but not STIPO. Knock-down of RASGRF2 increased spots after all inductions but lead to a greater increased after resveratrol treatment. Overall, knock-down of most of the hits caused similar effects on GFP-LC3 parameters in all induction conditions to those seen in the primary and deconvolution screen with EBSS plus leupeptin.

5.2 High-resolution imaging of GFP-LC3-HEK cells and measurement of the efficiency of siRNA knock-down for the 20 validated hits

5.2.1 Analysis and quantification of GFP-LC3 spots by confocal microscopy

In order to obtain high-quality, high-resolution and higher magnification images of GFP-LC3-HEK cells after knock-down with the 20 validated-by-deconvolution hits I plated the cells on glass coverslips and captured images of the cells using confocal microscopy. The use of coverslips required that the experiment be done in a larger-sized well and I scaled-up the screen reverse transfection protocol from a 96-well format to a 24-well format. Two siRNA duplexes for each of the 20 hits were used to knock down cells on coverslips, autophagy was induced by incubation in EBSS plus leupeptin, and the cells were fixed and nuclei were stained with Hoechst dye. The cells were analysed by indirect immunofluorescence microscopy and images were generated from the Hoechst labelling and GFP-LC3 fluorescence at 63X magnification and

identical laser settings. Images of cells treated with negative control RISCfree siRNA and siRNA against ULK1 and NRBP2 were also generated (Figure 5.2, part a). The confocal images mimic the images generated from the epifluorescence Cellomics ArrayScan microscope. GFP-LC3-containing autophagosomes are seen after induction of autophagy, and the number of GFP-LC3 spots is reduced after ULK1 knock-down and increase after NRBP2 knock-down confirming that a scaled-up reverse knock-down in a 24-well format mimics that in a 96-well format.

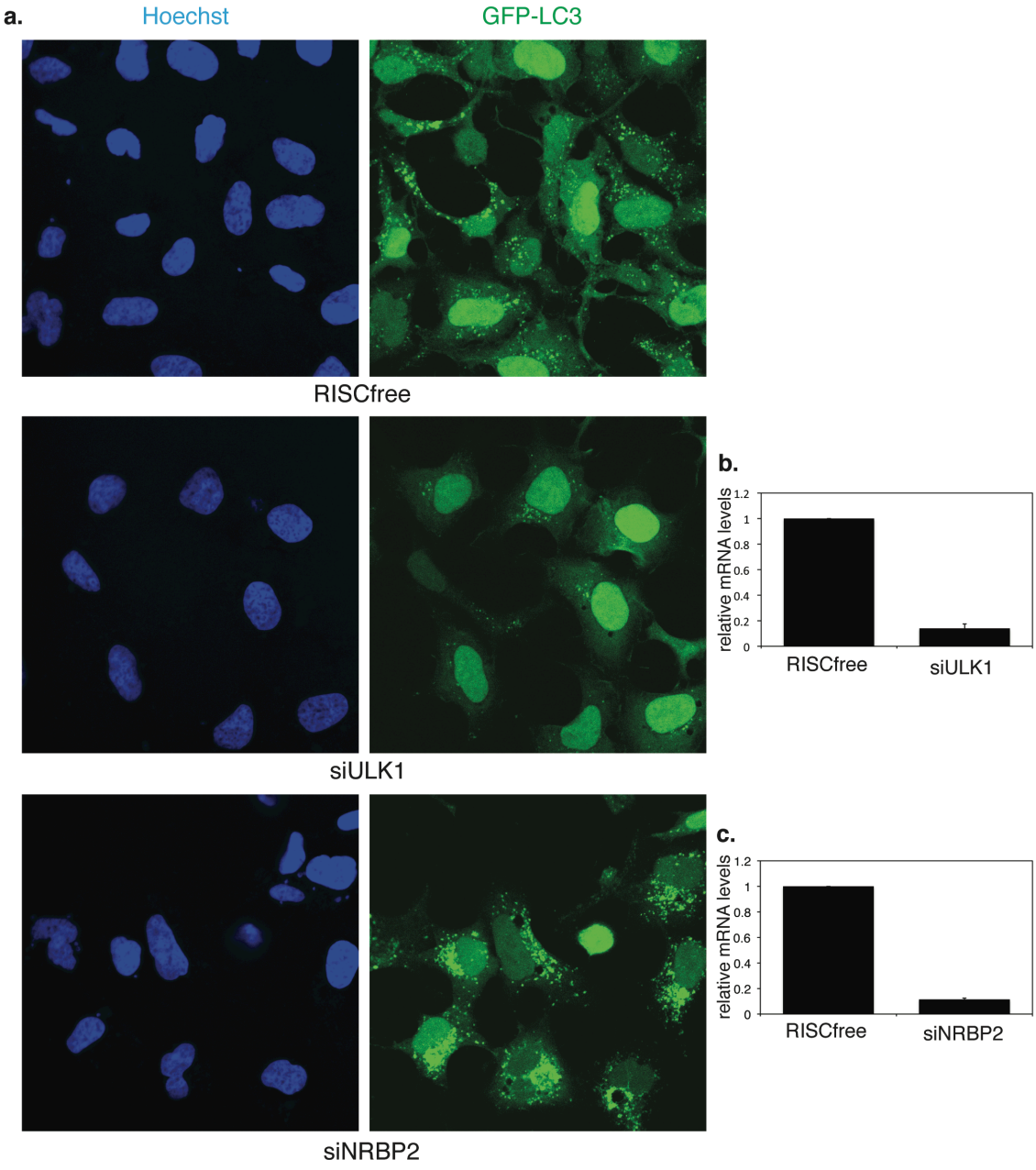

Figure 5.2 Confocal immuno-fluorescence microscopy images of GFP-LC3-HEK cells mimic Cellomics images
a. Confocal images at 63X of GFP-LC3-HEK cells after knock-down with indicated siRNA and incubation in EBSS plus 0.25mg/mL leupeptin. Hoechst labelling (blue) and GFP-LC3 (green) are shown. **b**. Relative ULK1 mRNA levels after treatment with RISCfree or ULK1 siRNA determined by qRTPCR. **c.** Relative NRBP2 mRNA levels after treatment with RISCfree or NRBP2 siRNA determined by qRTPCR from 24-well samples done in parallel with IF.

I quantified the number of GFP-LC3 spots after knock-down with the individual duplexes for the 20 hits. I captured Hoechst and GFP-LC3 confocal images from approximately ten fields (with representative density but chosen randomly) for each siRNA duplex knock-down and converted these images to black and white. Then these images were imported into the Cellomics ArrayScan and analysed using the SpotDetector program as before. Values for object count (OC) were generated from the images of Hoechst labelling and values for SCPO, STAPO and STIPO were generated based on the GFP-LC3 signal. Knock-down with each siRNA duplex for all nine decreaser hits reduced GFP-LC3 spot number, total area and total intensity (Figure 5.3, panel a). The reduction of SCPO for most siRNA duplexes was similar to that seen with ULK1 knock-down though individual duplexes against CDH19, NAA25 and WAC reduced SCPO to a greater extent than the ULK1 siRNA duplex. Quantification of the increase in SCPO, STAPO and STIPO for the confocal images of the increasers of spots was not as successful (Figure 5.3, panel b). Though most siRNA duplexes lead to an increase of STIPO above that of RISCfree control, the STIPO for some was comparable to the negative control, which contrasts with the deconvolution screen data. Visual inspection of the confocal images indicated that the increaser duplexes did in fact increase the number, area and intensity of the GFP-LC3 spots. Perhaps the GFP-LC3 signal was too saturated for the Cellomics machine or the spot-parameters that we set within the Cellomics SpotDetector were not accurate to capture bigger, brighter spots seen with the confocal images at the higher magnification (63x as opposed to 20x). Thus, I concluded that quantifying GFP-LC3 spot parameters using the Cellomics SpotDetector program and confocal images is sufficient to measure a decrease in GFP-LC3 spots but was not fully capable of accurately reflecting increases in GFP-LC3 spots. Overall, as a result of performing reverse knock-down on coverslips and analysing the cells with confocal microscopy, I generated high quality images for the two best duplexes for each hit.

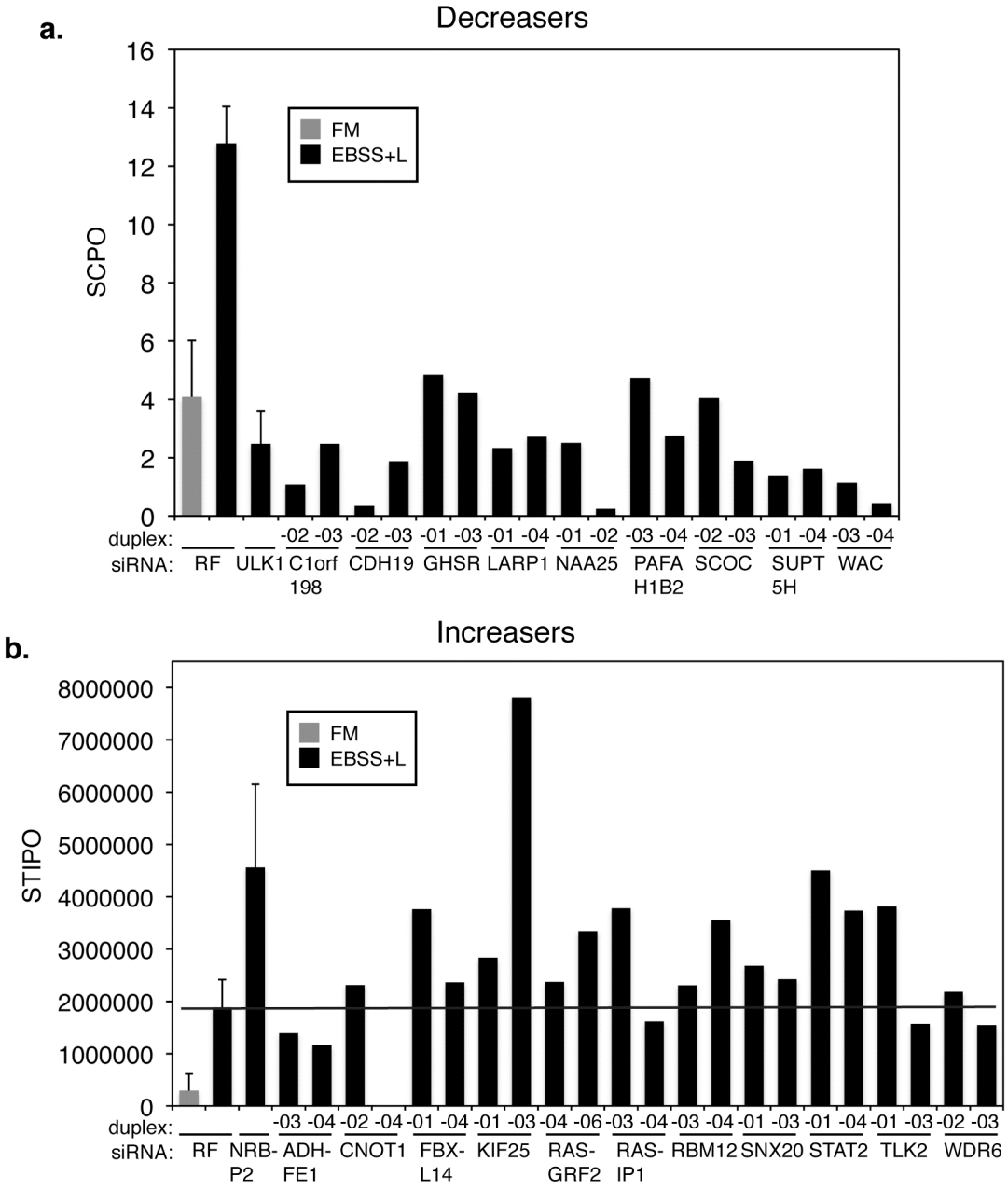

Figure 5.3 Quantification of GFP-LC3 confocal images using Cellomics image processing software

a. SCPO quantified from black-and-white versions of confocal images of GFP-LC3-HEK cells after knock-down with indicated siRNA duplex and incubation in full growth medium (FM) or EBSS with 0.25mg/mL leupeptin (EBSS+L). Sets of approximate 10 images from each coverslip were analysed. Error bars represent standard deviation from the following: 4 RISCfree (RF) coverslips in FM, 2 RF coverslips in EBSS+L, and 3 siULK1 coverslips in EBSS+L were quantified. **b.** STIPO quantified from black-and-white versions of confocal images of GFP-LC3-HEK cells after knock-down with indicated siRNA duplex and incubation in full growth medium (FM) or EBSS with 0.25mg/mL leupeptin (EBSS+L). Error bars represent standard deviation from the following: 4 RISCfree (RF) coverslips in FM, 3 RF coverslips in EBSS+L, and 2 siNRBP2 coverslips in EBSS+L were quantified. The grey line indicates average STIPO for RISCfree control in EBSS+L.

5.2.2 Quantification of the siRNA knock-down efficiency by qRTPCR

I have shown that the treatment of GFP-LC3-HEK cells with siRNA duplexes against the 9 decreaser hits decreased GFP-LC3 spots in a 24-well format as they did in a 96-well format (Figure 5.3, part a). Similarly, I observed that knock-down with siRNA duplexes for the 11 increaser hits increased GFP-LC3 spot formation in a 24-well format (Figure 5.3, part b). I next asked if the individual siRNA duplexes target the gene and decreased the corresponding mRNA levels (shown for siULK1 and siNRBP2 in Figure 5.2). Using Qiagen QuantiTect primers targeting each of the 20 genes and quantitative reverse transcriptase PCR (qRTPCR), I measured relative mRNA levels of the target gene after knock-down with the individual siRNA duplexes compared to levels after RISCfree knock-down .

For 16 of the 20 hits, at least one of the siRNA duplexes significantly decreased relative mRNA levels (nine of these are shown in Figure 5.8 to 5.16). Neither of the two siRNA duplexes against decreaser hits CDH19 and GHSR and against increaser hits ADHFE1 and SNX20 significantly reduced mRNA levels of their target genes (Figure 5.4).

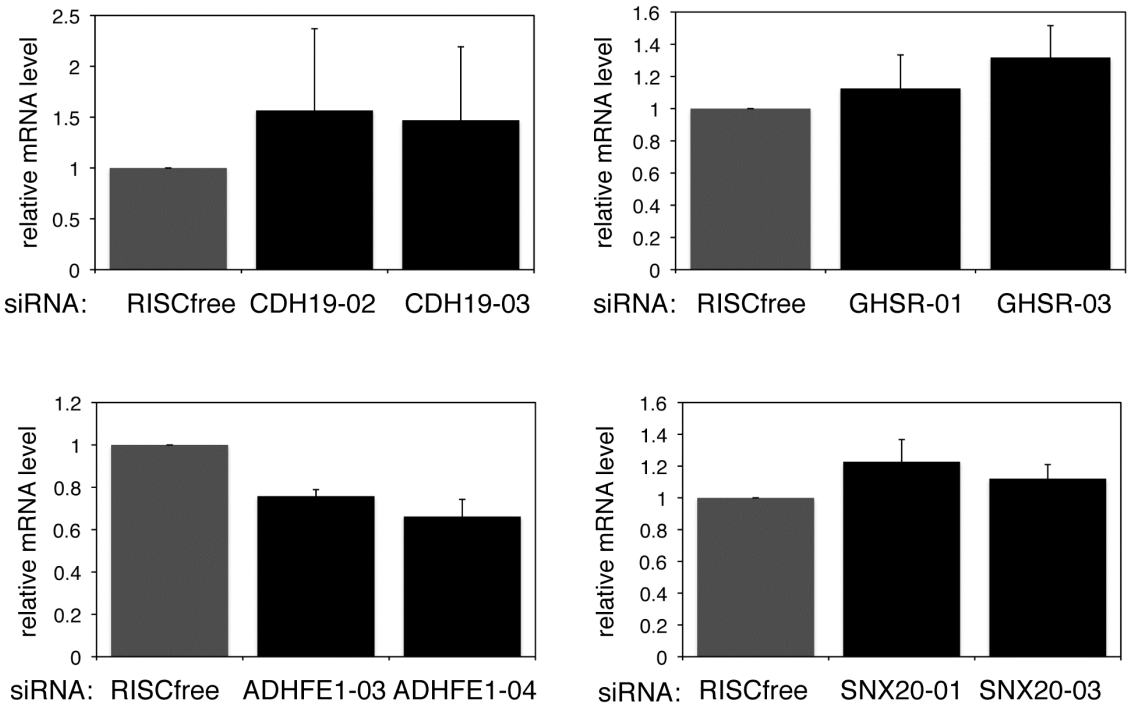

Figure 5.4 siRNA duplexes against four validated-by-deconvolution hits do not reduce corresponding mRNA levels

Abilities of two duplexes against CDH19, GHSR, ADHFE1 and SNX20 to reduce mRNA levels are quantified by qRTPCR. Error bars represent the standard deviation derived from triplicate wells.

5.3 Endogenous LC3 lipidation in HeLa cells

In order to further validate the effects of the siRNA duplexes on autophagy I assayed the extent of endogenous LC3 lipidation after incubation in starvation medium plus leupeptin. In addition, I assayed LC3 lipidation in full growth medium and starvation medium alone. These additional incubation conditions allowed me to distinguish the effects on autophagy initiation versus autophagosomal maturation, which can be affected by perturbation of endocytic pathways. In addition to measuring modulations of autophagy using this better read-out, I used an alternate human cell line, HeLa, to assess endogenous LC3 lipidation. As expected, RISCfree negative control siRNA and ULK1 and NRBP2 positive control siRNA behave identically in HeLa cells as they do in GFP-LC3-HEK cells in which ULK1 and NRBP2 were found to decrease and increase GFP-LC3 lipidation respectively (Chan et al., 2007). When HeLa cells are exposed to RISCfree negative control siRNA, and incubated in full medium, both the unlipidated LC3I form and lipidated LC3II form are observed (Figure 5.5, panel a,e). When autophagy is induced, LC3I is converted to LC3II and a loss of LC3I, an increase in LC3II, and an increase of the ratio of LC3II/LC3I is seen (Figure 5.5, panel a,b,e,f). Decrease in ULK1 protein levels using a single siRNA duplex for ULK1 leads to an inhibition of LC3 lipidation in full medium, starvation medium and starvation medium supplemented with leupeptin in HeLa cells (Figure 5.5 panel a,b). Conversely, knock-down of NRBP2 leads to an increase of endogenous LC3 lipidation in full medium starvation medium and starvation medium with leupeptin (Figure 5.5 panel e,f).

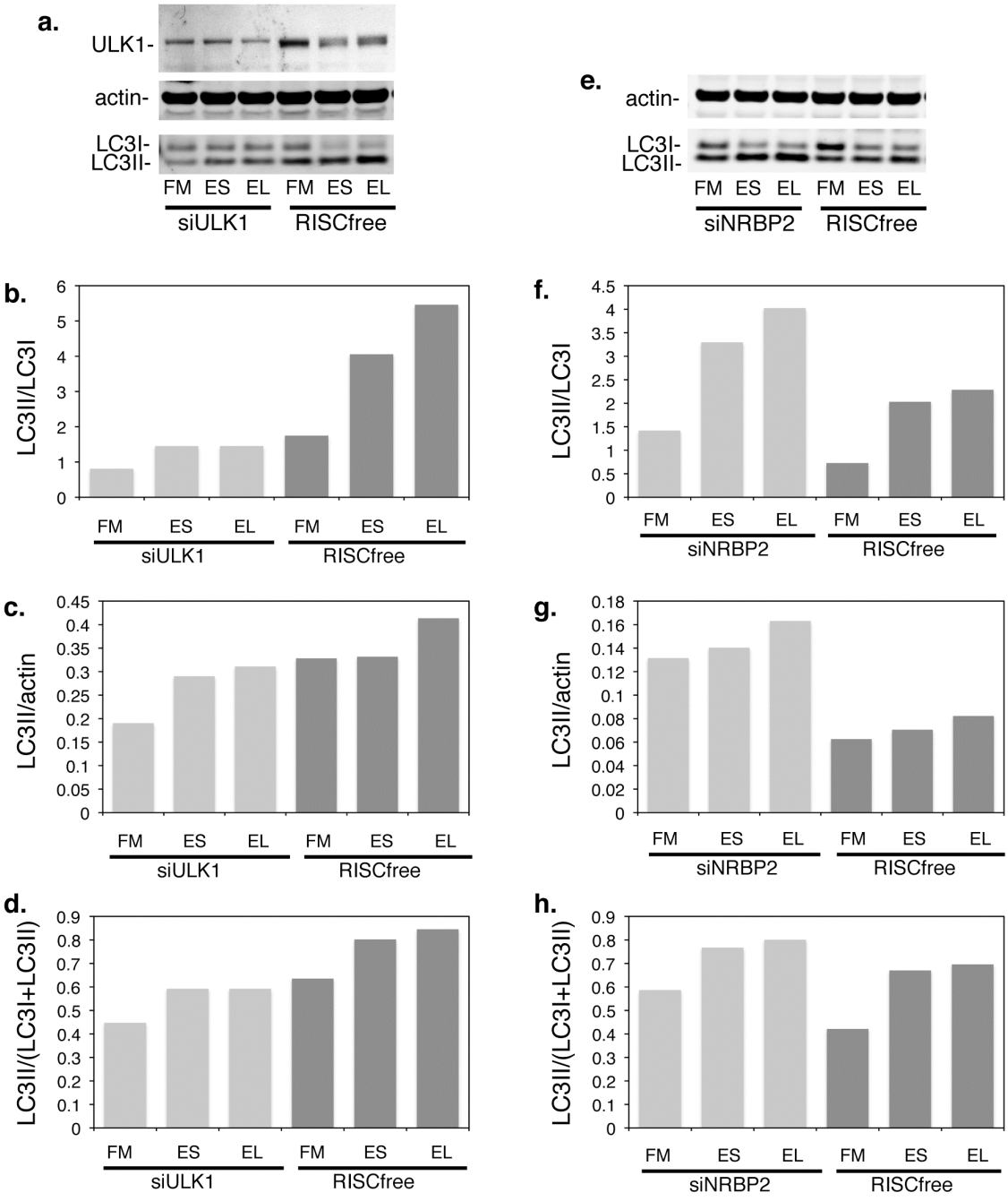

Figure 5.5 Knock-down of ULK1 decreases endogenous LC3 lipidation and knock-down of NRBP2 increases endogenous LC3 lipidation in HeLa cells
a. Anti-ULK1, -Actin, and -LC3 blots after indicated siRNA treatment in HeLa cells and incubation in full medium (FM), EBSS (ES) or EBSS plus 0.25mg/mL leupeptin (EL). **b.,f.** Quantification of LC3II/LC3I after indicated siRNA and incubation conditions. **c.,g.** Quantification of LC3II/actin after indicated siRNA and incubation conditions. **d.,h.** Quantification of LC3II/(LC3I+LC3II) after indicated siRNA and incubation conditions. **e.** Anti-Actin and -LC3 blot after indicated siRNA treatment in HeLa cells and incubation in full medium (FM), EBSS (ES) or EBSS plus 0.25mg/mL leupeptin (EL).

The greatest fold induction of autophagy in HeLa cells after RISCfree control siRNA knock-down is seen when the ratio of LC3II/LC3I is quantified. Induction of

autophagy in HeLa cells appears less dramatic when LC3II levels over actin or LC3II over total LC3 levels are quantified. In addition, the effect of ULK1 or NRBP2 knock-down is most remarkable when the LC3II to LC3I ratios are compared. A higher amount of LC3II is usually observed in HeLa cells in full medium compared to HEK cells possibly reflecting a higher amount of basal autophagy. However, the levels of LC3I and LC3II in full medium in HeLa cells can be dramatically dissimilar in different experiments (Figure 5.5, panel a,e). As a result, I chose to use the ratio of LC3II levels to LC3I levels when assessing the effect of knock-down by the siRNA duplexes of the 20 validated-by-deconvolution hits.

Knock-down with two siRNA duplexes each for C1orf198 and NAA25 caused a decrease in GFP-LC3 spot number (Figure 5.3, panel a) and were effective in reducing the mRNA levels in GFP-LC3-HEK cells but the siRNA for these two hits did not decrease LC3 lipidation in HeLa cells. One possible reason for this is that C1orf198 and NAA25 are required for the transcription or translation of GFP-LC3 and knock-down of these genes leads to a decrease in GFP-LC3 protein levels and in turn, decreases in GFP-LC3 SCPO, STAPO, and STIPO. C1orf198 is an uncharacterised gene but NAA25, also known as MDM20, is a component of the NatB N-acetyltransferase complex and is reported to co-sediment with ribosomal components and is involved in protein translation (Starheim et al., 2008).

I have shown above that knock-down of ADHFE1 or alcohol dehydrogenase, iron containing 1, in GFP-LC3-HEK cells causes a partial reduction of mRNA levels (about 25-35%) (Figure 5.4). These two duplexes caused a significant increase of SCPO, STIPO and STAPO in the deconvolution screen (Appendix Table 9.5) and as previously mentioned, increased GFP-LC3 spots in the induction screen after all induction conditions and notably in basal conditions. Of note, these results were not recapitulated when confocal images of ADHFE1 knock-down cells were quantified for GFP-LC3 STIPO using Cellomics (Figure 5.3, panel b). These two duplexes also led to an increase of LC3 lipidation in basal and starvation conditions in HeLa cells (data not shown). Perhaps only a small decrease of ADHFE1 mRNA is enough to cause a significant decrease of ADHFe1 protein levels and in turn, an increase of autophagy. Or perhaps the ADHFE1 knock-down in GFP-LC3-HEK cells in a 96-well screen

format and in HeLa cells is more effective than in GFP-LC3-HEK cells in a 24-well format. Nonetheless, ADHFE1 was not taken forward as a validated hit from this point.

siRNA duplexes against RASGRF2 and STAT2 decreased their target gene mRNA levels and increased GFP-LC3 spot total intensity (Figure 5.3, panel b) but these siRNA duplexes did not increase LC3 lipidation in HeLa cells. In the induction screen RASGRF2 knock-down increased GFP-LC3 spots in starvation, Torin-treated and Resveratrol-treated conditions and STAT2 knock-down led to the accumulation of very large, bright spots after starvation with leupeptin, as observed by confocal microscopy. However, knock-down of RASGRF2 and STAT2 did not increase GFP-LC3 spots in basal conditions in the induction screen and thus, I do not predict that these genes are required for the fusion of autophagosomes to endosomes or the lysosome or required for the degradative activity of the lysosome. One explanation for these results could be that knock-down of these genes could lead to an increase in the overexpression of GFP-LC3 in GFP-LC3-HEK cells; it would be interesting to test whether knock-down of RASGRF2 or STAT2 increased autophagosome numbers measured with endogenous LC3 in non-overexpressed conditions. The increasers RASGRF2 and STAT2 did not validate as autophagy regulators after testing their effect on endogenous LC3 lipidation in HeLa cells.

Knock-down of FBXL14 with siRNA duplex-01 decreased its target mRNA pool and increased GFP-LC3 spot intensity as measured by confocal microscopy (Figure 5.6, panel c), (Figure 5.3, panel b) and significantly increased GFP-LC3 spot parameters in all basal and induced conditions in the induction screen (Figure 5.6, panel a) (note, FBXL14 duplex-04 does not decrease FBXL14 mRNA levels). When attempting to measure the effect of FBXL14 knock-down on endogenous LC3 lipidation, I came across an unusual phenomenon: knock-down of FBXL14 led to the almost complete reduction of the levels of both LC3I and LC3II (Figure 5.6, panel b). Though the actin levels are slightly reduced after FBXL14 knock-down, this does not account for the great loss of total LC3. One explanation could be that knockdown of FBXL14 increases the rate of autophagy so much that all the LC3 in the cells is used to make autophagosomes and is thus depleted, although if this was the case then the LC3 levels should be rescued in the presence of leupeptin.

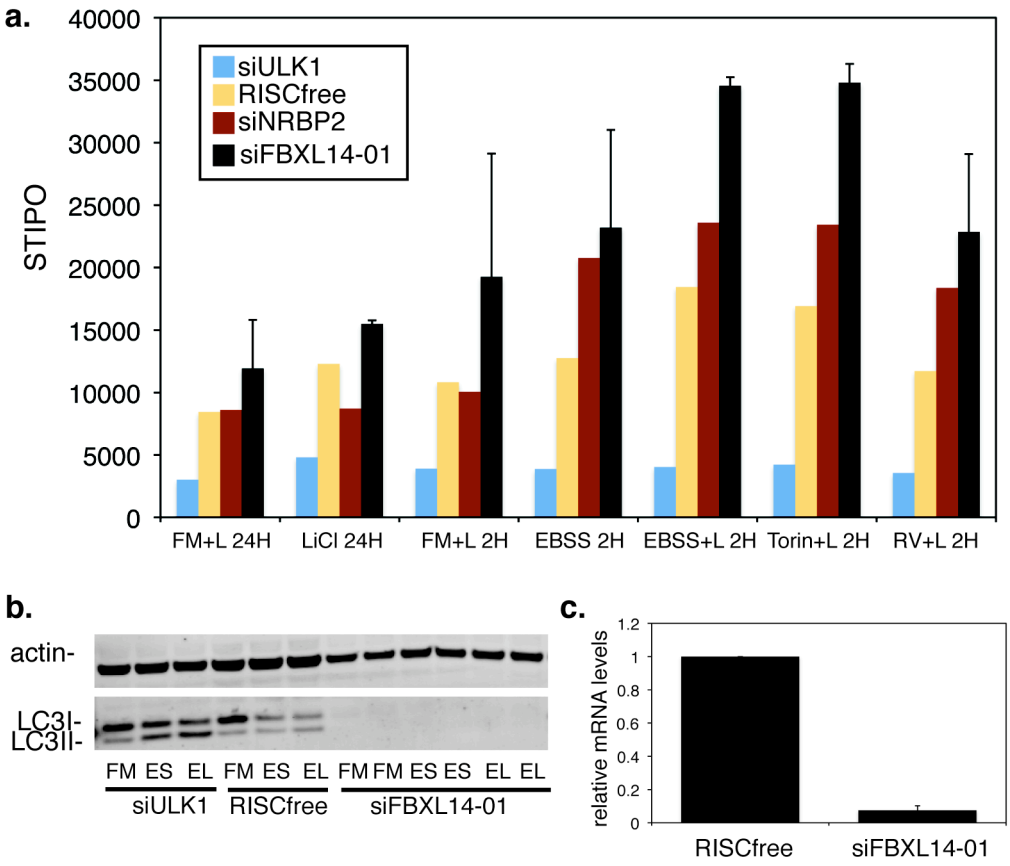

Figure 5.6 Knock-down of FBXL14 increases GFP-LC3 spots but decreases total LC3 levels

a. Quantification of STIPO after indicated siRNA knock-down and inductions in GFP-LC3-HEK cells. 24H is 24 hours treatment, 2H is 2 hours treatment, FM is full medium, LiCl is 10mM lithium chloride, EBSS+L is EBSS plus 0.25mg/mL leupeptin, Torin is 250nM Torin, and RV is 128µM resveratrol. Error bars represent the standard deviation of triplicate well values (from three plates). **b**. Anti-Actin and -LC3 blot after indicated siRNA treatment in HeLa cells and incubation in full medium (FM), EBSS (ES) or EBSS plus 0.25mg/mL leupeptin (EL). This experiment was done once. **c**. Quantification of FBXL14 mRNA levels in GFP-LC3-HEK cells as determined by qRTPCR. Error bars represent the standard deviation derived from triplicate wells.

Knock-down of RBM12, or RNA binding motif protein 12, with both of its duplexes increased GFP-LC3 spots (Figure 5.3, panel b, Appendix Table 8.5) and caused a large (approximately 75%) reduction of RBM12 mRNA levels. However, after knock-down in HeLa cells, an increase of LC3II/LC3I was not observed suggesting that RBM12 does not act as negative regulator of autophagy or induce a stress response that triggers autophagy (Figure 5.7). Instead, knock-down of RBM12 appeared to block maturation of autophagosomes, as the amount of LC3 lipidation in starvation medium without leupeptin was the same compared to starvation medium with leupeptin. In conclusion, FBXL14 knock-down causes a non-canonical effect on

autophagy, increasing GFP-LC3 spot formation and decreasing LC3II levels and RBM12 is perhaps a regulator of autophagosome maturation.

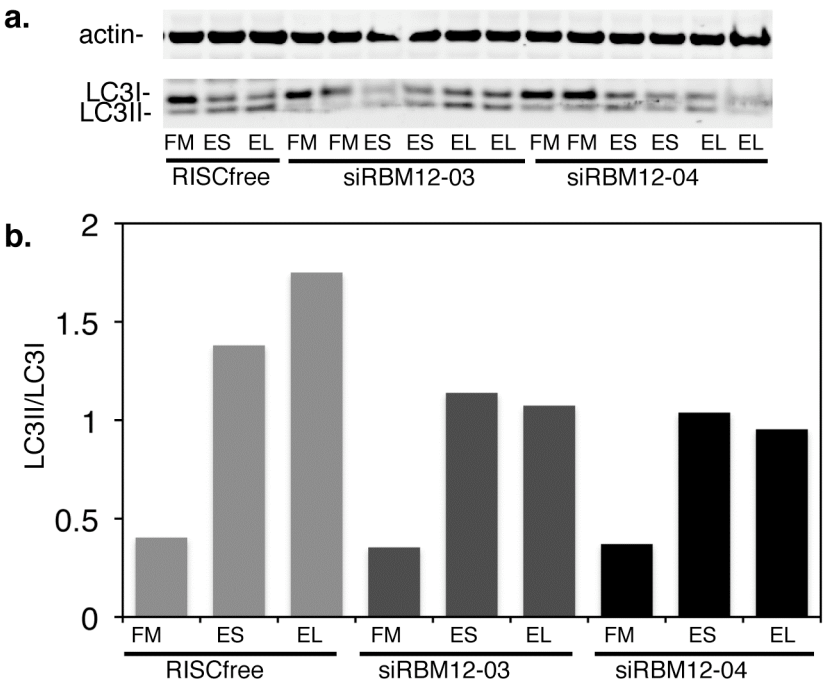

Figure 5.7 RBM12 knock-down possibly inhibits autophagosome maturation
a. Anti-Actin and -LC3 blot after indicated siRNA treatment in HeLa cells and incubation in full medium (FM), EBSS (ES) or EBSS plus 0.25mg/mL leupeptin (EL). b. Quantification of LC3II/LC3I after indicated siRNA and incubation conditions. Values for siRBM12-03 and siRBM12-04 are the averages of duplicates; the experiment was done once.

5.4 The nine that passed further validation

5.4.1 Five 'decreasers'

Using two of the best siRNA duplexes from the deconvolution screen, I could confirm that knock-down of five genes caused a decrease in GFP-LC3 spots, a reduction of mRNA levels with at least one duplex after knock-down in GFP-LC3-HEK cells, and a decrease in endogenous LC3 lipidation in HeLa cells. These further validated knock-down mediated decreasers of autophagy are LARP1, PAFAH1B2, SCOC, SUPT5H and WAC. These results indicate that these genes are required for autophagy and are thus bone fide positive regulators.

LARP1 or La ribonucleoprotein domain family, member 1, like RBM12, is an RNA-binding protein. The LARP family of proteins is characterised by a common N-terminal RNA-binding La domain. This family of proteins is able to traffic into the

nucleus due to a nuclear localisation signal. In Drosophila, larp mutant embryos display impaired mitotic phenotypes and defects in cytokinesis suggesting that larp1 is involved in spermatogenesis, embryogenesis and cell-cycle progression (Blagden et al., 2009). Another member of the La domain-containing family, LARP5 (KIAA0217) was identified as decreaser by the primary and secondary screens but did not pass the deconvolution screen (Appendix Tables 8.5).

Two of the best siRNA duplexes against LARP1, duplex-01 and -04, led to a decrease in of STIPO in GFP-LC3-HEK cells in all basal autophagy and induced conditions similar to ULK1 knock-down (Figure 5.8, panel a). LARP1 mRNA levels were reduced by these two duplexes in GFP-LC3-HEK cells (Figure 5.8, panel b) and the confocal images of these cells after induction of autophagy in EBSS plus leupeptin convey the decrease in GFP-LC3 spots (Figure 5.8, panel c). LARP1 siRNA duplex-01 also inhibits endogenous LC3 lipidation in HeLa cells (Figure 5.8, panel d,e). Confusingly, duplex-04 leads to an increase of LC3 lipidation though this may be caused by a toxicity stress response as the actin and LC3 levels are drastically reduced by this duplex (Figure 5.8, panel d). This quantification, however, may be inaccurate due to low protein levels and different results may be obtained if equal amounts of lysate were loaded.

More recently, LARP1 in human cells has been found at the leading edge of migrating cells and has also been shown to exist in a complex with poly A binding protein and eukaryotic translation initiation factor 4E (EIF4E) and separately with ribosomal subunits consequentially controlling global protein synthesis rates (Burrows et al., 2010). Burrows *et al* show that siRNA-mediated decrease of LARP1 inhibits protein synthesis and perhaps here, knock-down of LARP1 leads to an decrease of autophagy protein expression thereby inhibiting the autophagy machinery.

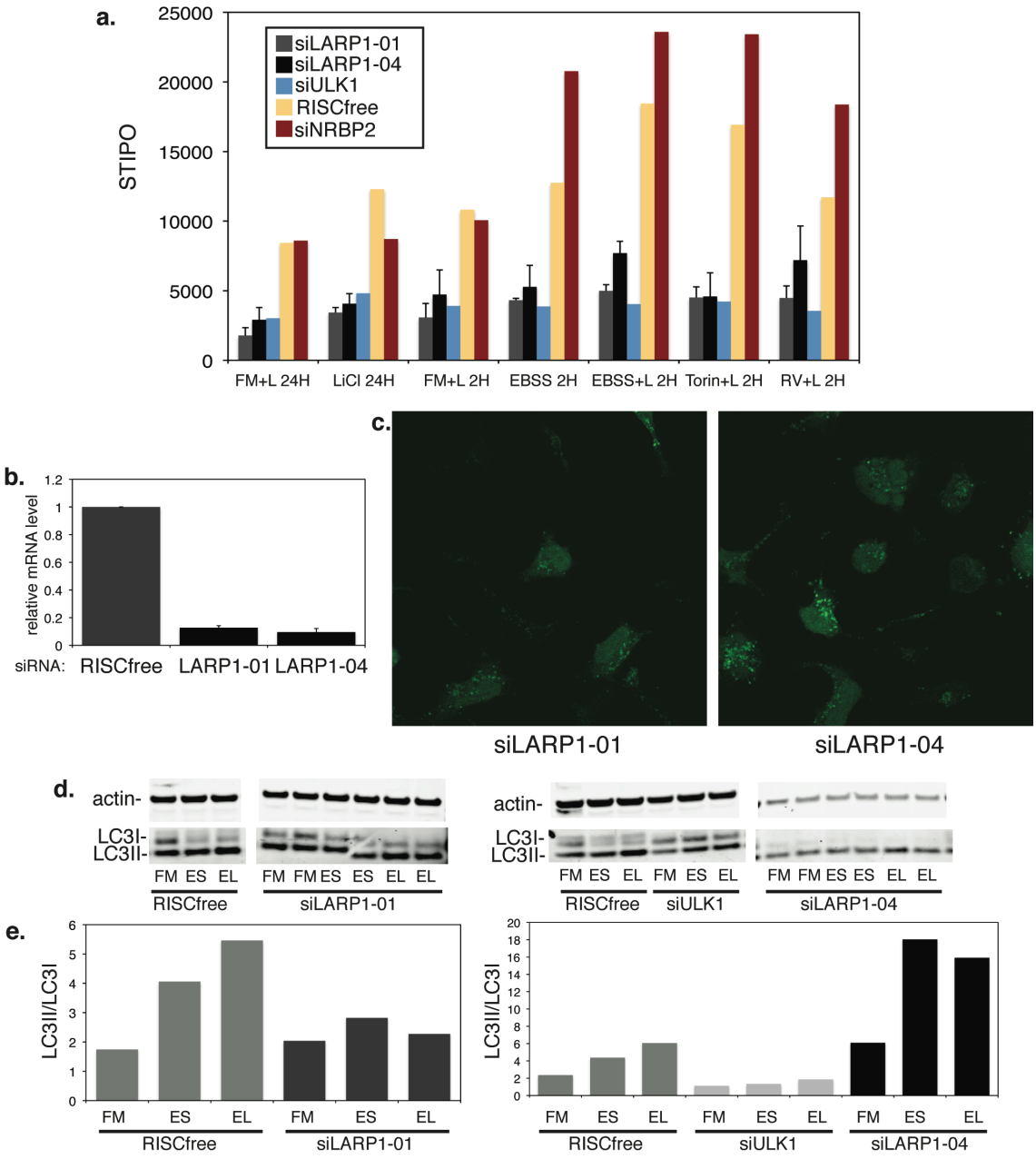

Figure 5.8 Knock-down of LARP1 inhibits autophagy

a. Quantification of STIPO after indicated siRNA knock-down and inductions in GFP-LC3-HEK cells. 24H is 24 hours treatment, 2H is 2 hours treatment, FM is full medium, LiCl is 10mM lithium chloride, EBSS+L is EBSS plus 0.25mg/mL leupeptin, Torin is 250nM Torin, and RV is 128μM resveratrol. Error bars represent the standard deviation of triplicate well values (from three plates). **b.** Quantification of LARP1 mRNA levels in GFP-LC3-HEK cells as determined by qRTPCR. Error bars represent the standard deviation derived from triplicate wells. **c.** GFP-LC3 confocal images at 63X after knock-down with indicated siRNA duplex and induction of autophagy by incubation in EBSS plus 0.25mg/mL leupeptin. Taken with the exact same magnification and settings as images in Figure 5.2 and can be compared to RISCfree control. **d**. Anti-Actin and -LC3 blot after indicated siRNA treatment in HeLa cells and incubation in full medium (FM), EBSS (ES) or EBSS plus 0.25mg/mL leupeptin (EL). **e.** Quantification of LC3II/LC3I after indicated siRNA and incubation conditions. LC3II/LC3I values for siLARP1-01 and siLARP1-04 are the averages of duplicates; the experiment was done once.

PAFAH1B2 or platelet-activating factor acetylhydrolase 1b, catalytic subunit 2 (30kDa) is ubiquitously expressed and is involved in lipid metabolism; it is part of a complex that hydrolyses platelet-activating factor which is a phospholipid reported to play a role in multiple biological processes including spermatogenesis and brain development (Zhang et al., 2007a). siRNA duplex-03 and -04 were the best decreasers of spots in the deconvolution screen and both decreased STIPO in the induction screen, though to a lesser extent than siULK1 control (Figure 5.9, panel a). The siRNA duplexes robustly reduce PAFAH1B2 mRNA level (Figure 5.9, panel b). Some GFP-LC3 spots remain after knock-down (Figure 5.9, panel c) and again the PAFAH1B2 knock-down does not seem as efficient as ULK1 knock-down at reducing spots (Figure 5.9, panel a). Though knock-down with duplex-03 is not sufficient to decrease endogenous LC3 lipidation in HeLa cells, knock-down with duplex-04 does decrease LC3II/LC3I compared to RISCfree controls in starvation conditions. Duplex-04 may have a stronger effect on LC3 lipidation due to its greater ability to decrease PAFAH1B2 mRNA levels.

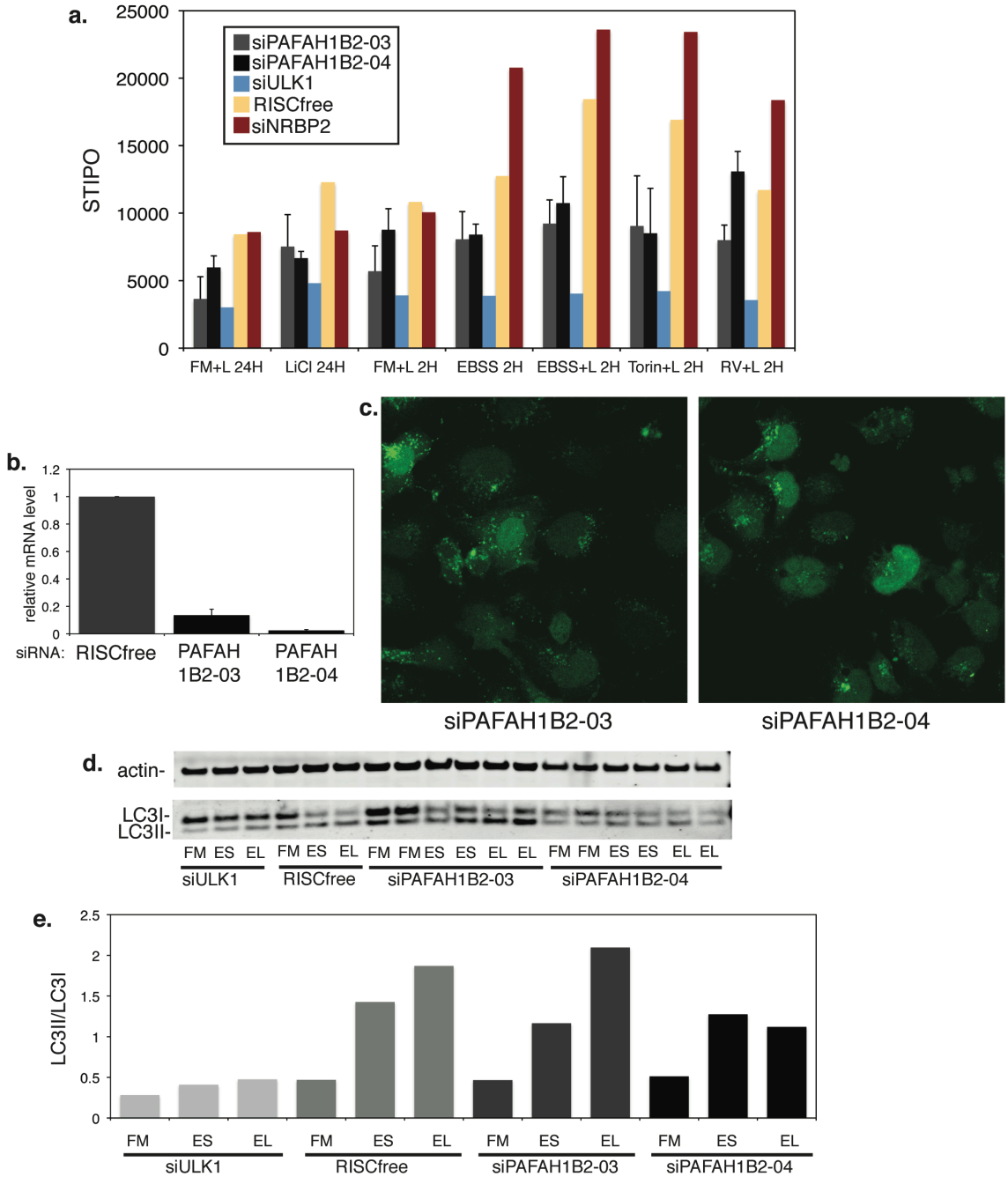

Figure 5.9 Knock-down of PAFAH1B2 inhibits autophagy
a. Quantification of STIPO after indicated siRNA knock-down and inductions in GFP-LC3-HEK cells. 24H is 24 hours treatment, 2H is 2 hours treatment, FM is full medium, LiCl is 10mM lithium chloride, EBSS+L is EBSS plus 0.25mg/mL leupeptin, Torin is 250nM Torin, and RV is 128μM resveratrol. Error bars represent the standard deviation of triplicate well values (from three plates). **b.** Quantification of PAFAH1B2 mRNA levels in GFP-LC3-HEK cells as determined by qRTPCR. Error bars represent the standard deviation derived from triplicate wells. **c.** GFP-LC3 confocal images at 63X after knock-down with indicated siRNA duplex and induction of autophagy by incubation in EBSS plus 0.25mg/mL leupeptin. Taken with the exact same magnification and settings as images in Figure 5.2 and can be compared to RISCfree control. **d.** Anti-Actin and -LC3 blot after indicated siRNA treatment in HeLa cells and incubation in full medium (FM), EBSS (ES) or EBSS plus 0.25mg/mL leupeptin (EL). **e.**

Quantification of LC3II/LC3I after indicated siRNA and incubation conditions. LC3II/LC3I values for siPAFAH1B2-03 and siPAFAH1B2-04 are the averages of duplicates; the experiment was done once.

The gene SCOC encodes a Golgi-resident protein called short coiled-coil protein (Van Valkenburgh et al., 2001). Knock-down of SCOC with the two strongest decreaser duplexes from the deconvolution screen causes a decrease of STAPO after autophagy induction in all conditions in the induction screen and after starvation plus leupeptin in GFP-LC3-HEK cells to a similar extent as ULK1 knock-down (Figure 5.10, panel a,c). Duplex-03 sufficiently reduced SCOC mRNA levels but duplex-02 does not appear to target SCOC (Figure 5.10, panel b). However, knock-down with both duplexes leads to a reduction of LC3 lipidation in HeLa cells (Figure 5.10, panel d,e). Duplex-02 could be decreasing the levels of a different gene that is required for autophagy, having a so-called 'off-target' effect. I further characterised the role of SCOC in autophagy and this is discussed in Chapter 6.

SUPT5H or suppressor of Ty 5 homolog (S. cerevisiae) is a transcription elongation factor that binds enzymes and has been shown to be both a positive and negative regulator of transcription and involved in chromosome activity (Yamada et al., 2006). Also known as SPT5, it has many interactors including cyclin dependent kinases and HIV proteins. It is suggested that SUPT5H suppresses senescence and apoptosis and is phosphorylated during mitosis (Komori et al., 2009). It is related to the zebrafish protein foggy, which is a regulator of transcription elongation and controls neuronal development (Guo et al., 2000). Remarkably, all four siRNA duplexes for SUPT5H decreased GFP-LC3 STIPO to below 80% of control in the deconvolution screen. In the induction screen, both chosen SUPT5H duplexes decreased GFP-LC3 spot intensity in all conditions though duplex-01 was better than duplex-04 (Figure 5.11, panel a). These siRNA duplexes reduced SUPT5H mRNA levels, GFP-LC3 spots as seen by confocal microscopy, and endogenous LC3 lipidation after starvation in HeLa cells (Figure 5.11, panel b,c,d,e). Both duplexes also seem to slightly decrease LC3 lipidation in full medium conditions, though the statistical significance of this has not been determined. Of note, knock-down with duplex-01 increased the levels of both the unlipidated and lipidated forms of LC3 (Figure 5.11, panel d).

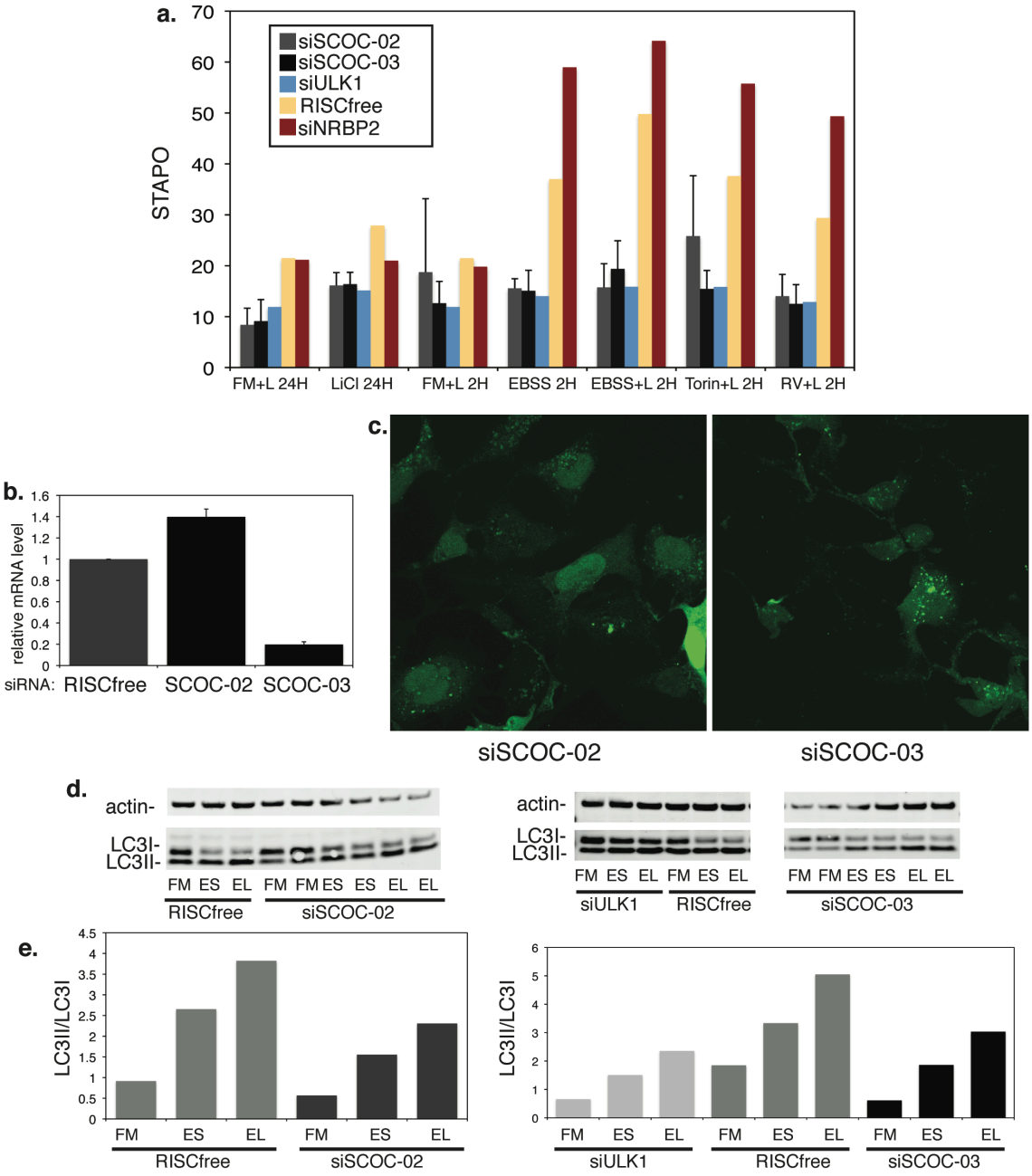

Figure 5.10 Knock-down of SCOC inhibits autophagy

a. Quantification of STAPO after indicated siRNA knock-down and inductions in GFP-LC3-HEK cells. 24H is 24 hours treatment, 2H is 2 hours treatment, FM is full medium, LiCl is 10mM lithium chloride, EBSS+L is EBSS plus 0.25mg/mL leupeptin, Torin is 250nM Torin, and RV is 128μM resveratrol. Error bars represent the standard deviation of triplicate well values (from three plates). **b.** Quantification of SCOC mRNA levels in GFP-LC3-HEK cells as determined by qRTPCR. Error bars represent the standard deviation derived from triplicate wells. **c.** GFP-LC3 confocal images at 63X after knock-down with indicated siRNA duplex and induction of autophagy by incubation in EBSS plus 0.25mg/mL leupeptin. Taken with the exact same magnification and settings as images in Figure 5.2 and can be compared to RISCfree control. **d.** Anti-Actin and -LC3 blot after indicated siRNA treatment in HeLa cells and incubation in full medium (FM), EBSS (ES) or EBSS plus 0.25mg/mL leupeptin (EL). **e.** Quantification of LC3II/LC3I after indicated siRNA and incubation conditions. LC3II/LC3I values for siSCOC-02 and siSCOC-03 are the averages of duplicates. The experiment was done four times; representative blots are shown.

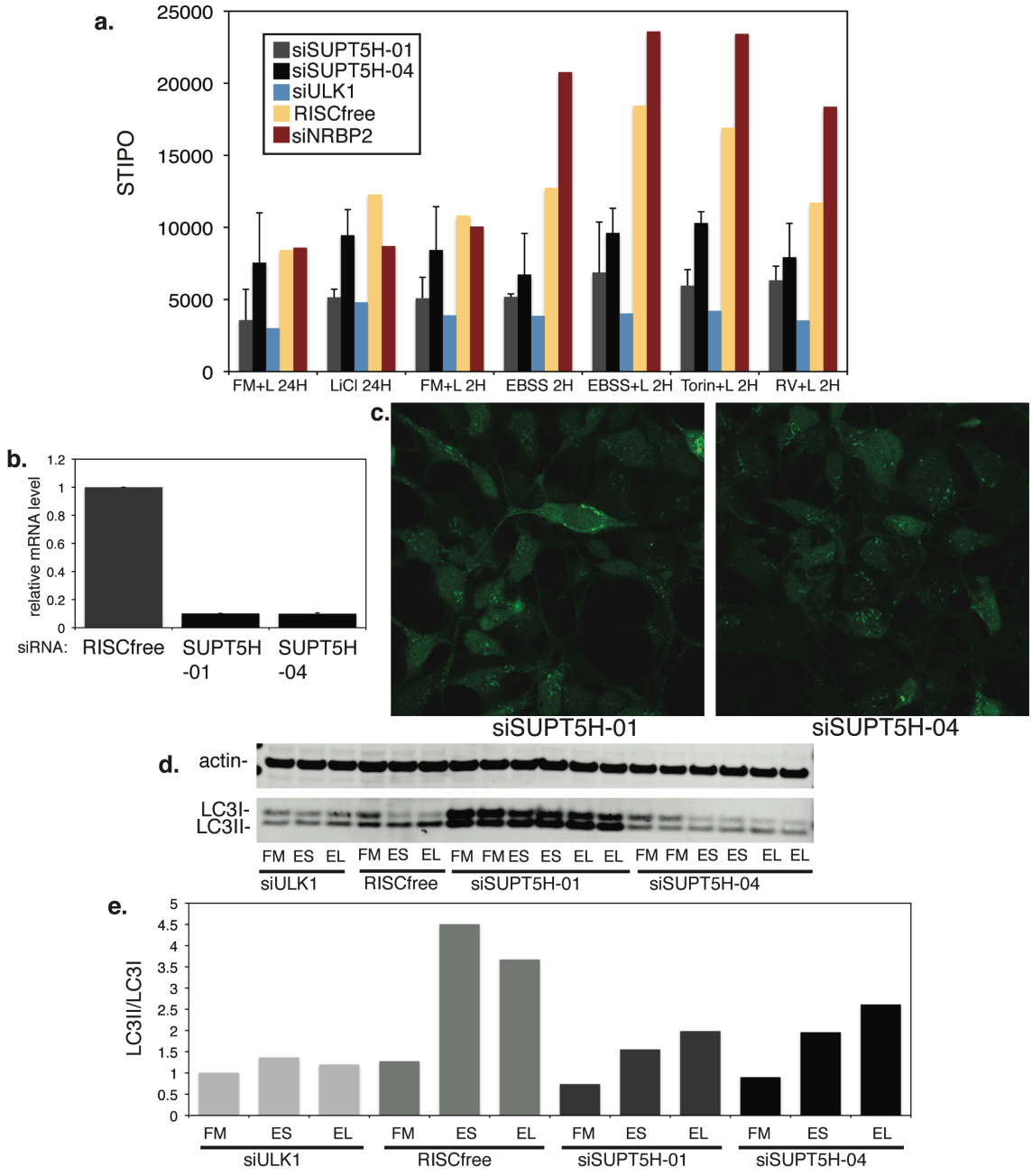

Figure 5.11 Knock-down of SUPT5H inhibits autophagy

a. Quantification of STIPO after indicated siRNA knock-down and inductions in GFP-LC3-HEK cells. 24H is 24 hours treatment, 2H is 2 hours treatment, FM is full medium, LiCl is 10mM lithium chloride, EBSS+L is EBSS plus 0.25mg/mL leupeptin, Torin is 250nM Torin, and RV is 128μM resveratrol. Error bars represent the standard deviation of triplicate well values (from three plates). **b.** Quantification of SUPT5H mRNA levels in GFP-LC3-HEK cells as determined by qRTPCR. Error bars represent the standard deviation derived from triplicate wells. **c.** GFP-LC3 confocal images at 63X after knock-down with indicated siRNA duplex and induction of autophagy by incubation in EBSS plus 0.25mg/mL leupeptin. Taken with the exact same magnification and settings as images in Figure 5.2 and can be compared to RISCfree control. **d.** Anti-Actin and -LC3 blot after indicated siRNA treatment in HeLa cells and incubation in full medium (FM), EBSS (ES) or EBSS plus 0.25mg/mL leupeptin (EL). **e.** Quantification of LC3II/LC3I after indicated siRNA and incubation conditions. LC3II/LC3I values for

siSUPT5H-01 and siSUPT5H-04 are the averages of duplicates. The experiment was done twice; a representative blot is shown.

Knock-down of WW domain containing adaptor with coiled-coil (WAC) decreases autophagy. An extensive inhibition of GFP-LC3 spots was observed after knock-down of WAC with duplexes -03 and -04 (Figure 5.12, panel c) and reduction of STIPO was to the same or even greater extent as ULK1 knock-down in all induction conditions (Figure 5.12, panel a). Both duplexes were effective in reducing WAC mRNA levels to less than 15% of levels in control-treated cells (Figure 5.12, panel b). In addition to the reduction of GFP-LC3 spot count, an overall reduction of GFP-LC3 levels is seen (Figure 5.12, panel c). When used to knock-down WAC in HeLa cells, both duplexes decreased endogenous LC3 lipidation. Like SCOC, I wanted to further characterise WAC and its involvement in autophagy, the results of which are contained later in this thesis in Chapter 7.

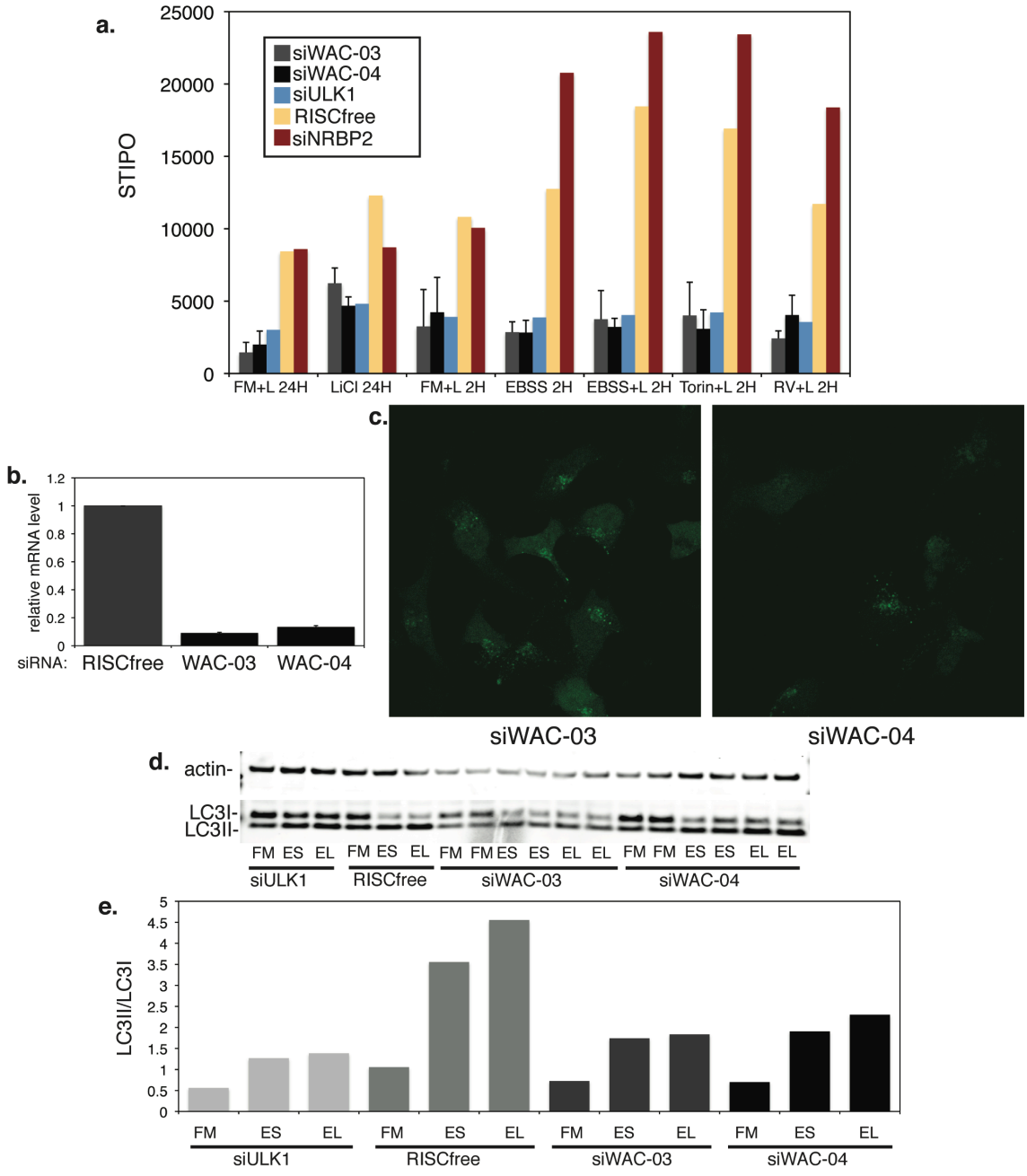

Figure 5.12 Knock-down of WAC inhibits autophagy

a. Quantification of STAPO after indicated siRNA knock-down and inductions in GFP-LC3-HEK cells. 24H is 24 hours treatment, 2H is 2 hours treatment, FM is full medium, LiCl is 10mM lithium chloride, EBSS+L is EBSS plus 0.25mg/mL leupeptin, Torin is 250nM Torin, and RV is 128μM resveratrol. Error bars represent the standard deviation of triplicate well values (from three plates). **b.** Quantification of WAC mRNA levels in GFP-LC3-HEK cells as determined by qRTPCR. Error bars represent the standard deviation derived from triplicate wells. **c.** GFP-LC3 confocal images at 63X after knock-down with indicated siRNA duplex and induction of autophagy by incubation in EBSS plus 0.25mg/mL leupeptin. Taken with the exact same magnification and settings as images in Figure 5.2 and can be compared to RISCfree control. **d.** Anti-Actin and -LC3 blot after indicated siRNA treatment in HeLa cells and incubation in full medium (FM), EBSS (ES) or EBSS plus 0.25mg/mL leupeptin (EL). **e.** Quantification of LC3II/LC3I after indicated siRNA and incubation conditions. LC3II/LC3I values for siWAC-03 and

siWAC-04 are the averages of duplicates. The experiment was done four times; a representative blot is shown.

5.4.2 Four 'increasers'

By measuring the ability of siRNA duplexes to decrease their intended transcription levels and corresponding increase in GFP-LC3 spot formation, and their ability to increase LC3 lipidation in HeLa cells, I confirmed that four hits are validated 'increasers' of autophagy. These potential negative regulators of autophagy are KIF25, RASIP1, TLK2 and WDR6.

Kinesin family member 25 (KIF25), also named kinesin-like 3 (KNSL3) has kinesin motor catalytic domain that is shared among the kinesin family and is responsible for their ATP-binding and microtubule-dependent molecular motor function (Verhey and Hammond, 2009). Kinesins transport organelles throughout the cell and aid cell division by moving chromosomes on microtubules. KIF25 is an uncharacterised member of the kinesin family and its function is not determined. It was cloned using RTPCR and was found to be ubiquitously expressed (Okamoto et al., 1998). Two translated isoforms (called isoform 1 and isoform 2) with differential tissue expression patterns were noted and KNSL3 shares 31% sequence identity with KIF5B, though its C-terminal appeared to be unique among other kinesins. KIF25 is contained in Dharmacon's Druggable library.

Knock-down of KIF25 caused an increase of GFP-LC3 spot parameters after all conditions though only duplex-03 increased GFP-LC3 STAPO in basal conditions (full medium plus leupeptin for 24 hours) (Figure 5.13, panel a). Both siRNA duplexes reduce KIF25 mRNA levels (Figure 5.13, panel b). Both duplexes appear to greatly increase GFP-LC3 spot number and intensity compared to RISCfree control (Figure 5.13, panel c) and when these images were quantified using the Cellomics quantitative software, duplex-03 exhibited the largest increase of all the siRNA duplexes, causing an almost four-fold increase in STIPO over the RISCfree control (Figure 5.3, panel b). I observed an interesting phenotype in the cells that received KIF25 siRNA duplex-03 in that the GFP-LC3 appeared to accumulate in long strings stretched within the cell. Endogenous LC3 lipidation was increased after KIF25 knock-down and duplex-03 increased basal LC3 lipidation. Overall, duplex-03 led to a greater increase of GFP-LC3 spots and LC3 lipidation.

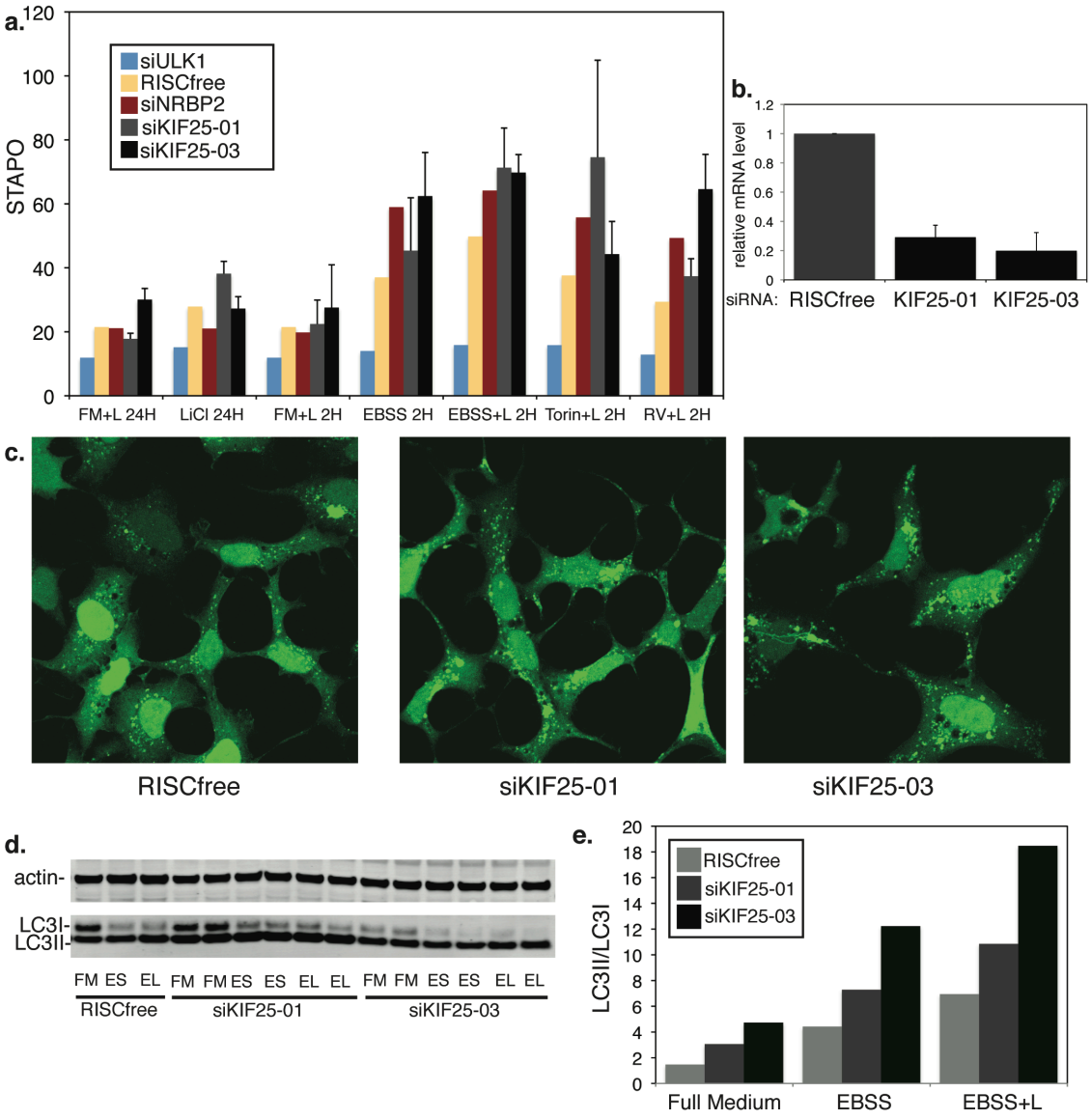

Figure 5.13 Knock-down of KIF25 increases autophagy
a. Quantification of STAPO after indicated siRNA knock-down and inductions in GFP-LC3-HEK cells. 24H is 24 hours treatment, 2H is 2 hours treatment, FM is full medium, LiCl is 10mM lithium chloride, EBSS+L is EBSS plus 0.25mg/mL leupeptin, Torin is 250nM Torin, and RV is 128μM resveratrol. Error bars represent the standard deviation of triplicate well values (from three plates). **b.** Quantification of KIF25 mRNA levels in GFP-LC3-HEK cells as determined by qRTPCR. Error bars represent the standard deviation derived from triplicate wells. **c.** GFP-LC3 confocal images at 63x after knock-down with indicated siRNA duplex and induction of autophagy by incubation in EBSS plus 0.25mg/mL leupeptin. **d.** Anti-Actin and -LC3 blot after indicated siRNA treatment in HeLa cells and incubation in full medium (FM), EBSS (ES) or EBSS plus 0.25mg/mL leupeptin (EL). **e.** Quantification of LC3II/LC3I after indicated siRNA and incubation conditions. LC3II/LC3I values for siKIF25-01 and siKIF25-03 are the averages of duplicates. The experiment was done three times; a representative blot is shown.

Ras interacting protein 1 (RASIP1) was discovered in a yeast-two-hybrid assay searching for hRAS interactors (Mitin et al., 2004). RAIN, as they called it, contains a Ras association (RA) domain and was shown to interact with Ras in a GTP-dependent

manner in that it had a higher affinity for Ras-GTP than Ras-GDP. This interaction required an intact Ras core effector-binding domain and thus they conclude that RASIP1 is a Ras effector. Ras, a small GTPase, is a hub for many cellular functions including growth and differentiation and acts by receiving extracellular signals and then interacting with multiple effectors that then activate multiple signalling cascades. Mitin *et al* discovered that RASIP1 is not a plasma membrane Ras effector but a Golgi Ras effector as it is recruited by activated Ras to the Golgi and localises to perinuclear juxta-Golgi vesicles. RASIP1 has more recently been shown to be required for vessel formation and is strongly expressed in vascular endothelial cells during development in mice and frogs (Xu et al., 2009). Xu *et al* also show that siRNA knock-down of RASIP1 in human endothelial cells impairs angiogenesis (as measured by endothelial tube formation) and cell motility (as shown by 'wound-healing' assays) though it is unclear whether RASIP1 links Ras to vascular development or exerts these effects by impacting other signalling pathways.

When RASIP1 is knocked down by two siRNA duplexes, GFP-LC3 STIPO is increased in all conditions including full medium and lithium treatment (Figure 5.14, panel a). RASIP1 is knocked down by duplex-03 well but not fully by duplex-04. Knock-down with duplex-03 leads to the increased formation of large, bright GFP-LC3 spots scattered throughout the cell with duplex-03 (Figure 5.14, panel b,c). The effect of duplex-04 appears to be different, causing an overall increase of GFP-LC3 and spots but also leading to some cell toxicity. Both duplexes increase endogenous LC3 lipidation in HeLa cells in basal and starvation conditions mimicking the increase in basal GFP-LC3 spots and duplex-03 causes a very large increase in basal lipidation (Figure 5.14, panel d,e). Duplex-04 seems to have a different effect on autophagy, displaying more of a maturation phenotype as the addition of leupeptin to EBSS does not increase LC3 lipidation compared to EBSS alone. Perhaps duplex-04 is targeting a different gene that is involved in autophagosome maturation. Nonetheless, the effects of siRNA duplex-03 show that knock-down of RASIP1 increases basal and nutrient dependent autophagy.

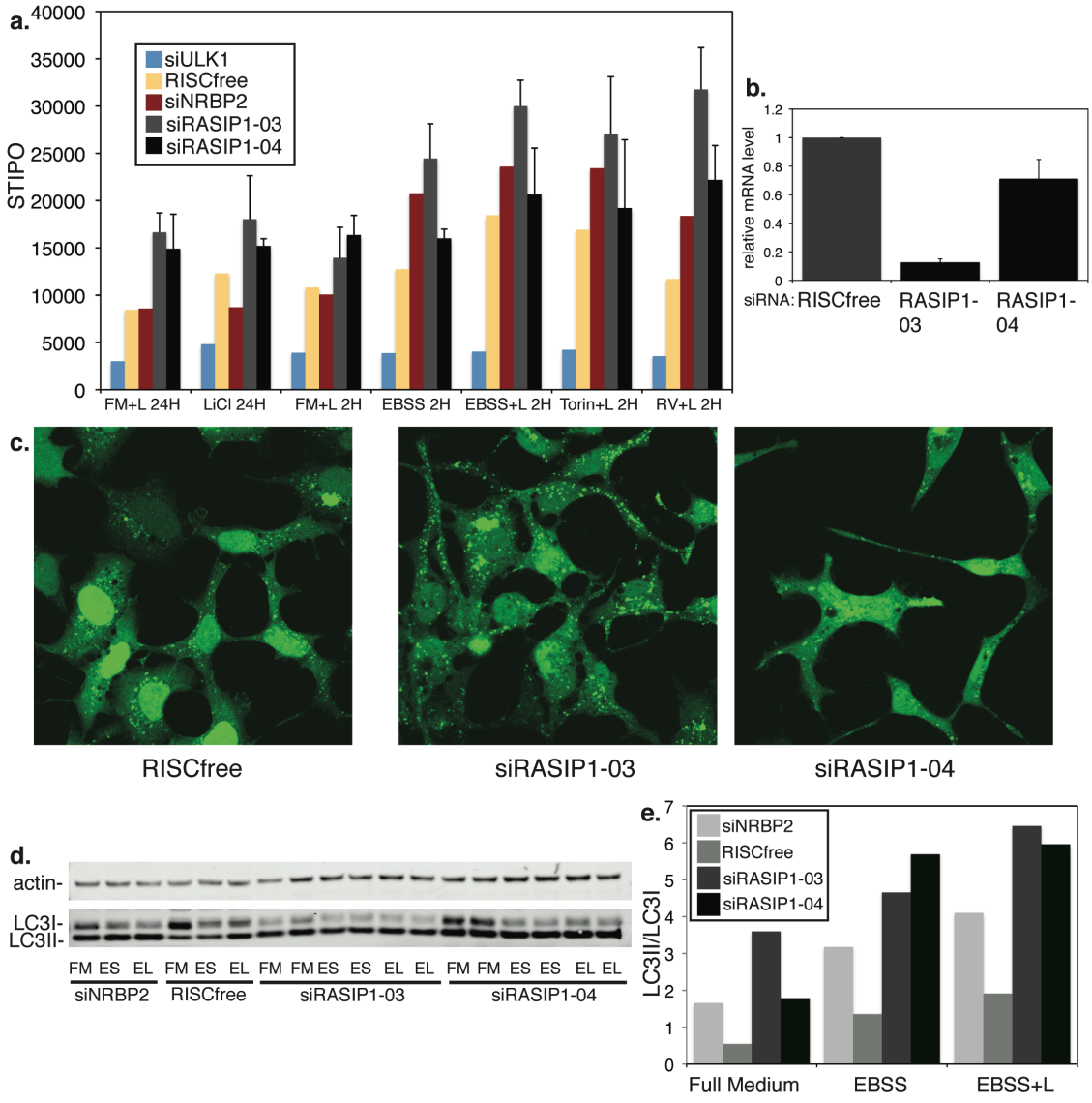

Figure 5.14 Knock-down of RASIP1 increases autophagy
a. Quantification of STIPO after indicated siRNA knock-down and inductions in GFP-LC3-HEK cells. 24H is 24 hours treatment, 2H is 2 hours treatment, FM is full medium, LiCl is 10mM lithium chloride, EBSS+L is EBSS plus 0.25mg/mL leupeptin, Torin is 250nM Torin, and RV is 128μM resveratrol. Error bars represent the standard deviation of triplicate well values (from three plates). **b.** Quantification of RASIP1 mRNA levels in GFP-LC3-HEK cells as determined by qRTPCR. Error bars represent the standard deviation derived from triplicate wells. **c.** GFP-LC3 confocal images at 63x after knock-down with indicated siRNA duplex and induction of autophagy by incubation in EBSS plus 0.25mg/mL leupeptin. **d.** Anti-Actin and -LC3 blot after indicated siRNA treatment in HeLa cells and incubation in full medium (FM), EBSS (ES) or EBSS plus 0.25mg/mL leupeptin (EL). **e.** Quantification of LC3II/LC3I after indicated siRNA and incubation conditions. LC3II/LC3I values for siRASIP1-03 and siRASIP1-04 are the averages of duplicates. The experiment was done twice; a representative blot is shown.

TLK2 or tousled-like kinase 2 is a serine/threonine kinase that was first cloned together with TLK1 by Yamakawa *et al* who called them PKU-α and PKU-β respectively. Both genes contain a kinase domain and a nuclear localisation signal and

overexpressed TLK2 is shown to localise in the nucleus of cells (Yamakawa et al., 1997). TLK2 shares 86% sequence homology to TLK1 and 94% in their catalytic regions. TLK2 has three coiled-coil domains and has been shown to interact with TLK1 by a yeast-two-hybrid assay and interestingly, knock-down of TLK1 was seen to also increase GFP-LC3 spots in the primary screen though it did not pass the deconvolution screen in that only one individual duplex increased GFP-LC3 spots (Appendix Table 9.5). It was reported that both TLK1 and TLK2 are involved in the cell cycle and that their highest kinase activity is displayed in S phase and their function is linked to periods of DNA replication; both also regulate chromatin assembly (Sillje et al., 1999). More recently, TLK1 and TLK2 were shown to be targets of the DNA damage checkpoint and were rapidly inactivated (dephosphorylated) by ionizing radiation (Groth et al., 2003).

I first identified TLK2 as a potential negative regulator of autophagy during the pilot screen of plate 10 of the kinase; knock-down of TLK2 with its siRNA Smartpool increased GFP-LC3 spots. In the deconvolution screen, duplexes -03 and -04 increased SCPO and STAPO but duplex-04 confusingly decreased STIPO. Both duplexes reduce TLK2 mRNA levels but at least one third of the message remains after knock-down (Figure 5.15, panel b). Duplex-03 was not tested in the induction screen but TLK2 knock-down with duplex-04 in fact decreased GFP-LC3 STIPO like in the deconvolution screen but also decreased SCPO and STAPO in all conditions (Figure 5.15, panel a). The two duplexes have varying effects on GFP-LC3 spots as analysed by confocal microscopy. Knock-down with duplex-03 appears to lead to a slight increase in both GFP-LC3 intensity and spots as compared to RISCfree and though duplex-04 causes a decrease in GFP-LC3 intensity, the accumulation of large aggregates of GFP-LC3 is observed (Figure 5.15, panel c). The duplexes again have a differential effect on endogenous LC3 levels in that duplex-04 causes a strong reduction of LC3 protein levels (Figure 5.15, panel d). Duplex-03 does not increase LC3 lipidation but knock-down with duplex-04 causes a large increase in LC3 lipidation in full medium and EBSS with and without leupeptin. These differential abilities to induce LC3 lipidation are perhaps due to the ability of duplex-04 to better reduce TLK2 mRNA levels but this difference in efficiency is only slight and does not explain the varied GFP-LC3 spot phenotypes and LC3 protein levels.

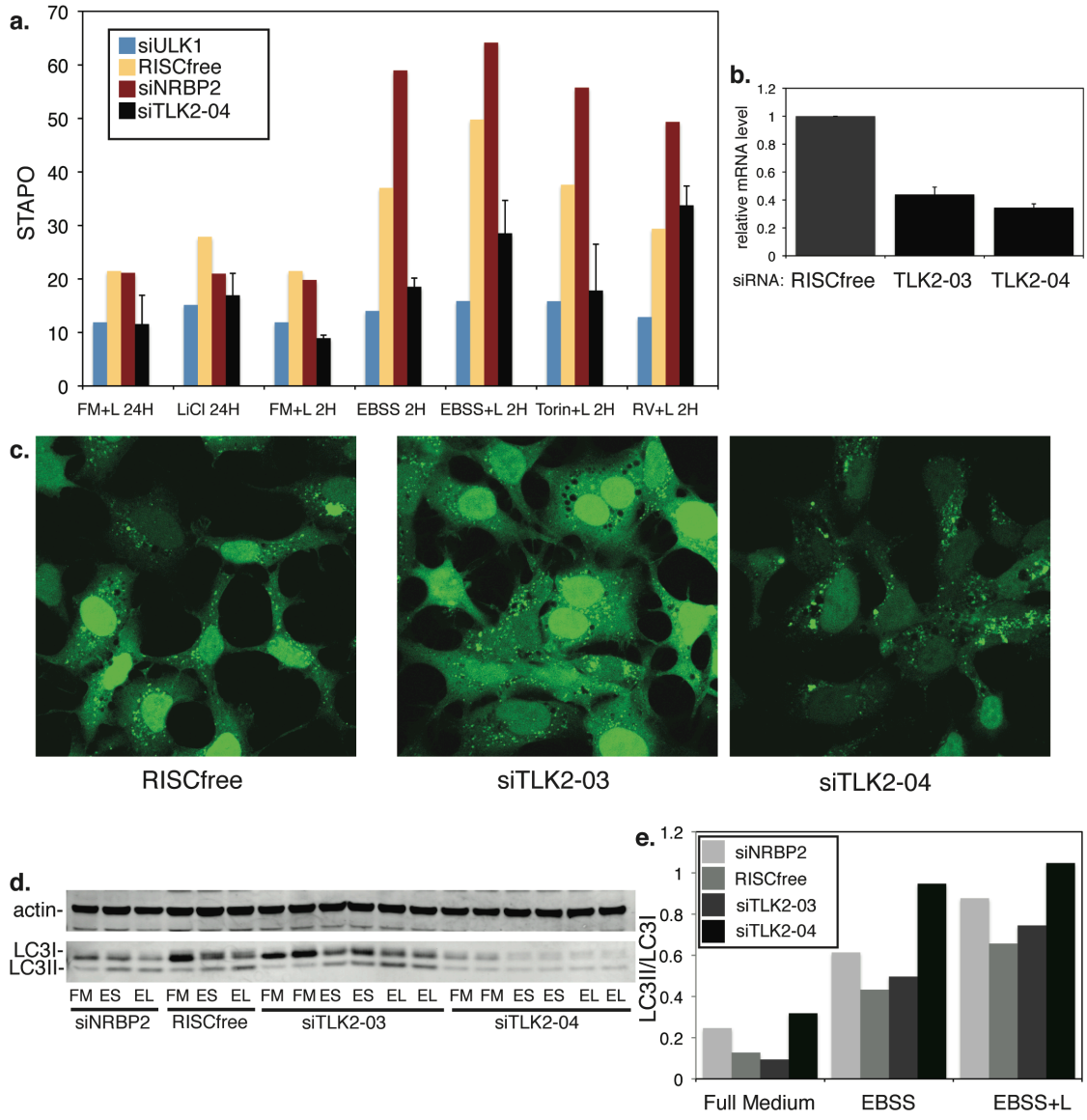

Figure 5.15 Knock-down of TLK2 increases autophagy
a. Quantification of STAPO after indicated siRNA knock-down and inductions in GFP-LC3-HEK cells. 24H is 24 hours treatment, 2H is 2 hours treatment, FM is full medium, LiCl is 10mM lithium chloride, EBSS+L is EBSS plus 0.25mg/mL leupeptin, Torin is 250nM Torin, and RV is 128μM resveratrol. Error bars represent the standard deviation of triplicate well values (from three plates). **b.** Quantification of TLK2 mRNA levels in GFP-LC3-HEK cells as determined by qRTPCR. Error bars represent the standard deviation derived from triplicate wells. **c.** GFP-LC3 confocal images at 63x after knock-down with indicated siRNA duplex and induction of autophagy by incubation in EBSS plus 0.25mg/mL leupeptin. **d.** Anti-Actin and -LC3 blot after indicated siRNA treatment in HeLa cells and incubation in full medium (FM), EBSS (ES) or EBSS plus 0.25mg/mL leupeptin (EL). **e.** Quantification of LC3II/LC3I after indicated siRNA and incubation conditions. LC3II/LC3I values for siTLK2-03 and siTLK2-04 are the averages of duplicates. The experiment was done twice; a representative blot is shown.

WD repeat domain 6, WDR6, contains eleven WD protein binding domains and a predicted transmembrane domain. As a result of its ability to complex with other proteins it has many interacting partners. WDR6 was found to interact with

serine/threonine kinase 11 (aka LKB1) by a yeast-two-hybrid assay and confirmed by co-immunoprecipitation and they were shown to localise together in the cytoplasm though both experiments were done with tagged, overexpressed WDR6 (Xie et al., 2007). LKB1 is a tumour suppressor and its inhibition of cell proliferation is thought to occur mostly through its modulation of p21/Cip1, which controls cell cycle arrest. WDR6 activity was shown to synergise with that of LKB1 as co-over-expression of both proteins caused an increased inhibition of HeLa cell proliferation (Xie et al., 2007). Xie *et al* suggest that WDR6 may also acts as a tumour suppressor by regulating the cyclin dependent kinase inhibitor p27/Kip1. In a different study, WDR6 was found to be among genes that are enriched in the rat brain hypothalamus, the functional site for coordination of metabolism, feeding behaviours and stress response and thus controller of energy balance (Chiba et al., 2009). The authors show that WDR6 gene expression was reduced by caloric restriction that has been shown to increase life span. They also show that WDR6 interacts *in vivo* with IRS-4, an important insulin receptor substrate in the brain, by co-immunoprecipitation of rat brain slices and WDR6 gene expression was increased by insulin signalling. WDR6 is also a potential drug target as it is contained in Dharmacon's 'Druggable library.'

The two best GFP-LC3 spot-increasing siRNA duplexes for WDR6, duplex-02 and duplex-03 increased GFP-LC3 STAPO after induction of autophagy with lithium chloride, Torin, resveratrol and incubation in starvation medium (Figure 5.15, panel a). Both duplexes greatly reduce WDR6 mRNA levels and lead to the formation of more GFP-LC3 spots (Figure 5.16, panel b,c). Both duplexes increase LC3 lipidation in HeLa cells and knock-down with duplex-03 causes an increase in LC3 protein levels (Figure 5.16, panel d,e). Of note, knock-down with duplex-02 greatly increased LC3 lipidation in full medium in HeLa cells.

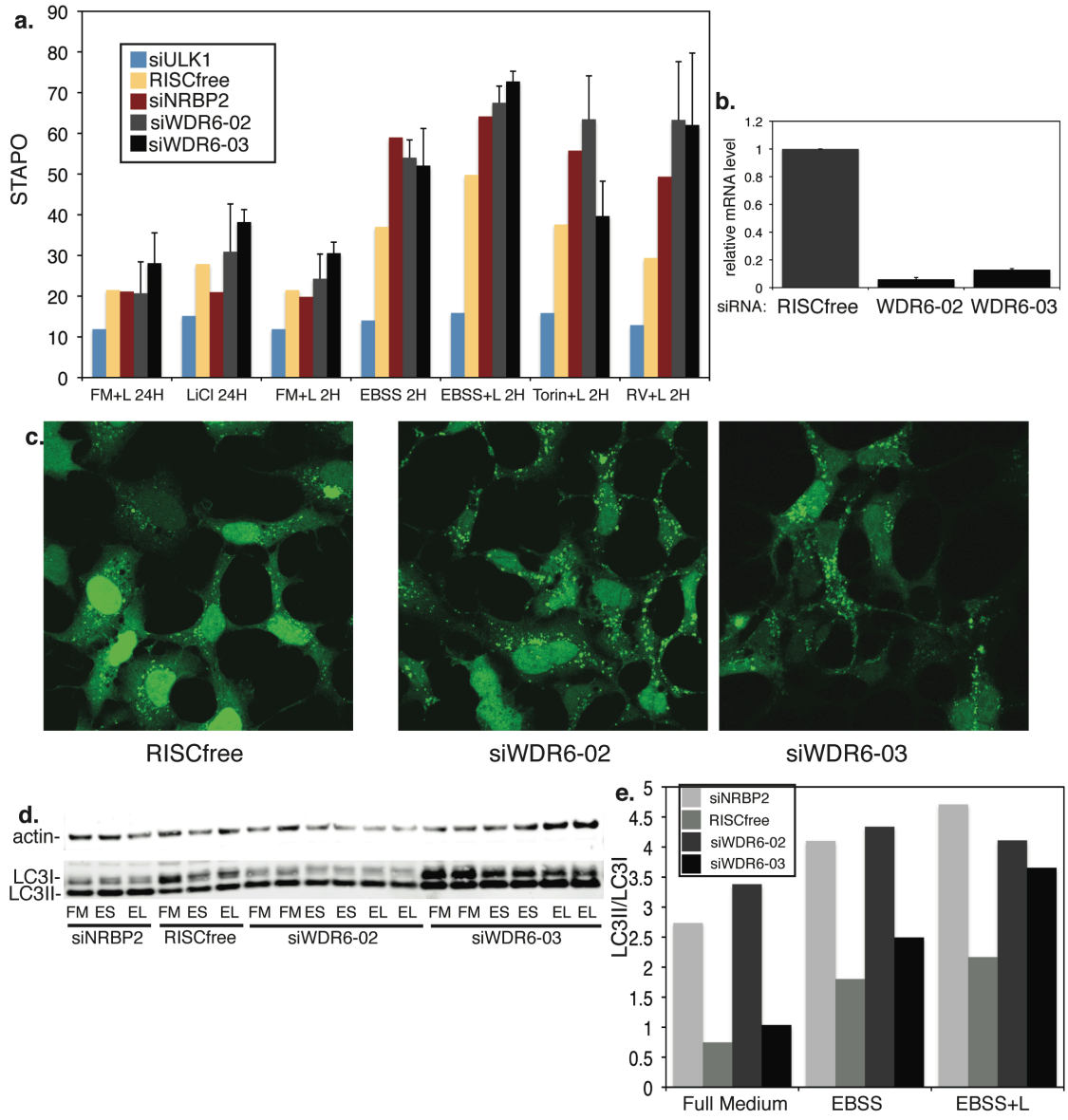

Figure 5.16 Knock-down of WDR6 increases autophagy

a. Quantification of STAPO after indicated siRNA knock-down and inductions in GFP-LC3-HEK cells. 24H is 24 hours treatment, 2H is 2 hours treatment, FM is full medium, LiCl is 10mM lithium chloride, EBSS+L is EBSS plus 0.25mg/mL leupeptin, Torin is 250nM Torin, and RV is 128μM resveratrol. Error bars represent the standard deviation of triplicate well values (from three plates). **b.** Quantification of WDR6 mRNA levels in GFP-LC3-HEK cells as determined by qRTPCR. Error bars represent the standard deviation derived from triplicate wells. **c.** GFP-LC3 confocal images at 63x after knock-down with indicated siRNA duplex and induction of autophagy by incubation in EBSS plus 0.25mg/mL leupeptin. **d.** Anti-Actin and -LC3 blot after indicated siRNA treatment in HeLa cells and incubation in full medium (FM), EBSS (ES) or EBSS plus 0.25mg/mL leupeptin (EL). **e.** Quantification of LC3II/LC3I after indicated siRNA and incubation conditions. LC3II/LC3I values for siWDR6-02 and siWDR6-03 are the averages of duplicates. The experiment was done three times; a representative blot is shown.

5.5 Discussion

5.5.1 Considerations for the further validation measuring mRNA levels and LC3 lipidation

The group of nine further-validated hits contain multiple proteins with protein binding domains (SCOC (CC), WAC (WW and CC), RASIP1 (RA), TLK2 (CC), WDR6 (WD40)). They are a diverse group of genes but their proteins seem to share some common functions. Two hits, PAFAH1B2 and WDR6 have been linked to metabolic pathways. Two bind nucleic acid (LARP1 and SUPT5H) and a large fraction of the nine are reported to be involved in cell-cycle control: LARP1, SUPT5H, TLK2, and WDR6. Last, SCOC, SUPT5H and RASIP1 have been implicated in development, a process that has been shown to require autophagy. Two proteins have been shown to reside in the Golgi: SCOC and RASIP1. Four are potential therapeutic targets: decreaser SUPT5H, and increasers KIF25, WDR6, and the kinase TLK2.

The five genes whose siRNA-mediated reduction leads to a decrease in autophagy are presumably positive regulators autophagy. More specifically, results from the induction screen suggest that they are involved in the initiation or formation of the autophagosome because they all appear to act down-stream of mTOR inactivation. The four hits whose gene knock-downs cause an increase of autophagy may be negative regulators of autophagy and when their inhibitory actions are reduced, autophagy proceeds at a higher rate. But also, inhibition of these genes may cause a stress response that the cells respond to by increasing the rate of autophagy. These genes could alternatively be required for the trafficking of endosomes required for proper maturation or transport of the autophagosomes themselves to the lysosome or even the degradative conditions of the lysosome itself. Perturbation of any of these processes may lead to the accumulation of undegraded autophagosomes and further upregulation of autophagy to compensate because the system is not working properly to recycle cytoplasmic contents in times of nutrient deprivation. Because I perceived it to be more straight-forward to work on hits that are required for autophagy, I chose to further characterise two ‘supervalidated’ positive regulators, SCOC and WAC. These two proteins were also of interest because of their protein-protein interacting domains and reported interacting partners (discussed in Chapter 6 and 7).

The endogenous LC3 lipidation data could be improved for seven of the nine hits; only the SCOC and WAC knock-downs have been done enough times to generated statistically significant data. In addition, though I chose the two best duplexes from the deconvolution screen, there are instances where one of these duplexes does not decrease mRNA levels (SCOC and RASIP1). In these cases, the third GFP-LC3 spot-affecting duplex could be ordered and tested (this was done with SCOC, see Chapter 6). Also, the knock-down of TLK2 is not complete which perhaps limits the autophagic response. It should also be noted that the mRNA levels were measured in GFP-LC3-HEK cells and corresponded to the coverslips that were examined by confocal microscopy. mRNA levels of the 20 genes were not tested in HeLa cells, in which I performed the LC3 lipidation assays.

Perhaps HeLa cells were not the best system to use for the endogenous lipidation assay. Although other labs do use HeLa cells in autophagy assays, in my hands, the levels of LC3I and II are not constant across experiments and the cells appear to have a higher amount of basal autophagy compared to HEK cells. HeLa cells are a commonly-used immortal epithelial cell line derived from cervical cancer cells and it has been shown that the tumour suppressor LKB1 is missing in HeLa cells (Shaw et al., 2004). Shaw *et al* show that in low ATP conditions, LKB1 is required for the repression of TOR thereby inhibiting cell growth. In turn, TOR signalling may be altered in HeLa cells lacking LKB1 and the loss of mTOR inhibition may lead to higher levels of autophagy. In contrast, it has been shown that LKB1 is a positive regulator of autophagy (Liang et al., 2007). LKB1 may be a toggle between cell growth and autophagy and may sense nutrient levels in order to switch between the two and regulate homeostasis; this system may be altered in HeLa cells.

5.5.2 LARP1

Knock-down of LARP1 decreases autophagy (Figure 5.8) and as LARP1 is a positive regulator of protein synthesis, it is conceivable that its effect on autophagy is due to a decreased expression of autophagy genes. There are a large number of reported phosphorylation sites on LARP1 and recently it was included in a screen of 375 phosphopeptides that include AKT, PDK1 or mitogen-activated protein kinase substrate recognition motifs (Andersen et al., 2010). The authors of the screen profiled the phosphorylation of LARP1, and suggest that LARP1 may be used as a phospho-specific

biomarker in order to personalise patients' oncology therapies with P13K pathway inhibitors. Interestingly, Merck, the director of the phospho-profiling screen also claims to have phospho-specific antibodies of LARP1 and it could be tested to see if the phosphorylation state of LARP1 is altered when autophagy is activated. Also, Merck possesses an inhibitor against LARP1 and this could potentially be a specific inhibitor of autophagy.

5.5.3 PAFAH1B2

Knock-down of PAFAH1B2 caused reduced autophagy (Figure 5.9). This protein was shown to be involved in brain development through its interactions with reelin (RELN) (Zhang et al., 2007a). Reelin shapes brain organisation during development by activating two receptors VLDLR and ApoER2 and phosphorylating Dab1 thereby controlling cell-cell interactions critical for cell positioning and neuronal migration. Zhang *et al* show that PAFAH1B2 binds to phosphorylated Dab1 downstream of reelin and also to VLDLR and through its interaction with VLDR, controls forebrain development.

PAFAH1B2 was shown in a large-scale two hybrid experiment to interact with parkin (Stelzl et al., 2005) the E3 ubiquitin ligase, mutations of which are known to cause Parkinson's disease. As discussed previously, parkin has been shown to interact with PINK1, and together they congregate mitochondria in a perinuclear region so that they can be eliminated by autophagy (Kawajiri et al., 2010). Also, parkin was found to recognise these damaged mitochondria (Narendra et al., 2010) though it is not known how and it would be interesting to find out whether PAFAH1B2 plays a role in this process.

5.5.4 SUPT5H

Knock-down of SUPT5H with both siRNA duplexes decreased the target mRNA levels and LC3 lipidation (Figure 5.11). During the deconvolution screen all four of its siGenome duplexes reduced STIPO below 80% or control. The siRNA Smartpool for SUPT5H resides in Dharmacon's 'Druggable Library' suggesting that SUPT5H is a known drug target and in turn, this drug could be a specific inhibitor of starvation-induced autophagy. It is suggested that this protein suppresses senescence and apoptosis (Komori et al., 2009) and it may suppress these pathways in order to

favour autophagy. Overexpression of ULK3 has been shown to induce autophagy and oncogene-induced senescence (Young et al., 2009) and it would be interesting to ask whether SUPT5H and ULK3 coordinate to function in the cell.

5.5.5 KIF25

Loss of the microtubule motor protein KIF25 was shown to increase autophagy (Figure 5.13). It has been shown that microtubules play a critical role in autophagy as disruption of their network inhibits autophagosome formation and fusion with the lysosome (Kochl et al., 2006). In addition, it is thought that specific cargo such as aggregated huntingtin is recruited to the autophagy pathway via microtubule transport (Iwata et al., 2005). KIF25 is an uncharacterised member of the kinesin molecular motor protein family and very little is known about this protein compared to the proteins in the kinesin 1 complex. KIF5B transcribes the kinesin heavy chain for the kinesin 1 complex and KIF5B knock-out mice are embryonic lethal and as a result of loss of KIF5B, lysosomes do not disperse and mitochondria cluster around the nucleus (Tanaka et al., 1998). KIF5B knock-down increased GFP-LC3 spot parameters in the primary and repeat screen but it did not pass deconvolution (Appendix Table 9.5). KIF25 differs from KIF5B and other KIFs in the C-terminal part of the protein, a region though to confer specificity of cargo (Verhey and Hammond, 2009). Perhaps KIF25 is a kinesin motor protein whose specific role is to transport needed components for the autophagy pathway. Or KIF25 may transport autophagosomes themselves to the lysosome in a similar way to dynein (Kimura et al., 2008) and its knock-down may impair autophagosome degradation leading to the vesicles' accumulation. Interestingly, the *C. elegans* homologue of ULK1, UNC-51 interacts with the kinesin heavy chain adaptor UNC-76 and these two proteins coordinate to control axon development (Toda et al., 2008); it would be interesting to ask whether KIF25 interacts with ULK1 or the human homologue of UNC-76, FEZ1. In addition, KIF25 is in Dharmacon's 'druggable' library.

5.5.6 RASIP1

RASIP1 is one of two Ras-interacting proteins found to increase GFP-LC3 spots. RASGRF2 was discussed above and I found that though knock-down of RASGRF2 was targeted to that gene and led to an increase in GFP-LC3 spots, LC3

lipidation was not increased. Perhaps RASGRF2 is required for the maturation of autophagosomes. RASIP1 knock-down, however, did increase GFP-LC3 spots and endogenous LC3 lipidation (Figure 5.14). RASIP1 has been found to be required for apoptosis and proper cell motility (Xu et al., 2009) and RASIP1 has been shown to localise on juxta-nuclear Golgi vesicles (Mitin et al., 2004). It would be interesting to find out if these vesicles are positive for autophagy markers. RASIP1 and RASGRF2 provide a link between autophagy and the important signalling molecule Ras, which itself has been implicated in autophagy induction on the ER (Wu and Terada, 2010) and has even been shown to down-regulate Beclin 1 (Yoo et al., 2010).

5.5.7 TLK2

TLK2 is a relatively uncharacterised kinase that is thought to act in the nucleus (Sillje et al., 1999). As mentioned above, both TLK1 and TLK2 were increasers in the primary screen but TLK1 did not pass deconvolution. TLK2 was a three-out-of-four hit for GFP-LC3 spots and knock-down also increased LC3 lipidation (Figure 5.15). I asked whether TLK2 could be regulating autophagy from the nucleus by affecting the transcription of autophagy genes. TLK2 was knocked down in HEK cells using Dharmacon siRNA duplex-03 and -04 and I found that the mRNA levels of ULK1, GABARAP, and LC3 were increased compared to treatment with RISCfree control (data not shown). This perhaps suggests that TLK2 is a negative regulator of autophagy by suppressing autophagy gene transcription. As a kinase, TLK2 is an especially interesting hit because drugs can be found to inhibit TLK2 kinase activity. Interestingly, a polymorphism in the TLK2 gene has been linked to breast cancer (Kelemen et al., 2009) and it would be important to ask whether this mutation alters TLK2's regulation of autophagy.

5.5.8 WDR6

WDR6 is also an interesting increaser that has potential links to cancer as it has been shown to interact with the tumour suppressor LKB1 (Xie et al., 2007). In Figure 5.16, I show that knock-down of WDR6 increases autophagy. WDR6 contains WD40 repeats that provide platforms for protein interactions and WDR6 may regulate autophagy by binding to autophagy proteins. WDR6 has also been shown to interact with insulin receptor substrate 4 and through this interaction, may sense growth factors

and negatively regulate autophagy (Sano et al., 2002). Like KIF25, WDR6 is also a potentially druggable increaser and these drugs may in the future be used to stimulate autophagy and provide therapy for neurodegenerative diseases by clearing protein aggregates in the cells via autophagy.

Chapter 6. SCOC

6.1 Introduction to SCOC

I chose to further characterise short coiled-coil protein (SCOC) as a positive regulator of autophagy for several reasons. First, it had been shown to localise to the Golgi apparatus, where Atg9, an essential autophagy protein resides. The Golgi, as discussed above, is also a proposed source of membrane for the autophagosome. Second, SCOC contains a coiled-coil domain presumably through which it interacts with other proteins, two of which, ADP-ribosylation factor-like 1 (ARL1) and fasciculation and elongation protein zeta 1 (zygin1) (FEZ1) have been previously studied and are involved in post-Golgi transport and axonal trafficking respectively. Last, SCOC homologues have been shown to play a role in important processes such as development and axonal transport.

6.1.1 SCOC is an ARL1 interactor

SCOC was first characterised as an interacting partner of ARL1, an ARF-like protein that at the time was not thought to share the ADP-ribosylation factor activities of ARFs but has since been shown to have GTP-ase activity and regulate endosomal trafficking in distinct ways from ARFs (Burd et al., 2004). ARL1 has more recently been shown to regulate the retrograde transport of Shiga toxin to the TGN through its interaction with SNARE proteins (Nishimoto-Morita et al., 2009). In an attempt to characterise the relatively unknown protein family of human ARLs, Van Valkenburgh *et al* performed a yeast two-hybrid screen with dominant active mutants of ARL1, ARL2 and ARL3 and discovered a set of proteins that interacted with one specific ARL or two or all three of the family members (Van Valkenburgh et al., 2001). SCOC, which they refer to as SCOCO, was found to only bind to ARL1 and more specifically, binds only to the dominant active form of ARL1, not the wild-type form. SCOC is widely expressed in human tissues including heart, brain, and skeletal muscle. SCOC was tested and found not to contain ARL1 GAP activity though after overexpression of ARL1, the two proteins were shown to colocalise with β-COP in the Golgi of NRK cells. The binding of SCOC to ARL1 was shown to be sensitive to the ARF GEF inhibitor brefeldin A suggesting that the SCOC-ARL1 interaction depends on the activity of one or more ARF GEFs and the activation state of ARL1 itself.

6.1.2 SCOC interacts with FEZ1 in *C. elegans* and mammals

6.1.2.1 SCOC is UNC-69 in *C. elegans* and interacts with the FEZ1 homologue UNC-76

The *C. elegans*' homologue of SCOC, UNC-69, has been shown to be required for normal development of neurons through its ability to complex with the FEZ1 homologue UNC-76 in order to properly regulate vesicle trafficking to the growing axons and dendrites of the cell (Su et al., 2006). UNC-69 and UNC-76 colocalise in puncta in the *C. elegans* nervous system and together promote axonal growth by directing these vesicles to sites of growth, extending the growth-cone and helping the synapse to form in the developing neurons. Interestingly and unlike in mammalian cells, these neuronal functions of SCOC do not depend on its interaction with the *C. elegans* ARL-1 as these two proteins do not interact. Instead, normal synaptic development requires the direct interaction of UNC-69 and UNC-76 on cytoplasmic vesicular structures for which they regulate the size and position. The authors note the conservation of both UNC-69 and UNC-76 and suggest that their mammalian homologues SCOC and FEZ1 may function in a similar way and be required for normal presynaptic organisation in those organisms.

In *Drosophila*, UNC-76 is a proposed kinesin heavy chain adaptor and is also required for functional axonal transport but not through its interaction with SCOC but through its interaction with the ULK1 homologue UNC-51 (Toda et al., 2008). Here, UNC-51 is shown to interact with phosphorylated UNC-76, which, when activated binds to synaptic vesicles through Synaptotagmin-1 and in turn, directs vesicles from the soma to the synapse. Though Toda *et al* suggest that the role of UNC-51/ATG1 in axonal transport in normal growth conditions is distinct from its role as the autophagy kinase, whose autophagy-specific activity is initiated by starvation, it is conceivable that the homologues of SCOC, FEZ1, and ULK1 cooperate to regulate both axonal outgrowth and autophagy in higher organisms.

6.1.2.2 Mammalian SCOC and FEZ1 interact

SCOC has in fact been shown to bind FEZ1 in human cells by yeast two-hybrid; SCOC was pulled out of a screen of a human foetal brain cDNA library using FEZ1 as bait (Assmann et al., 2006). The authors attempted to express soluble SCOC protein but did not succeed in doing so and did not confirm the SCOC-FEZ1 binding.

Nonetheless, the yeast two-hybrid interaction was repeated and the binding of SCOC was shown to not occur with a FEZ1 mutant missing its coiled-coil region (Figure 6.1). Also, SCOC was shown to interact with FEZ2, whose conserved coiled-coil region is highly similar to that of FEZ1.

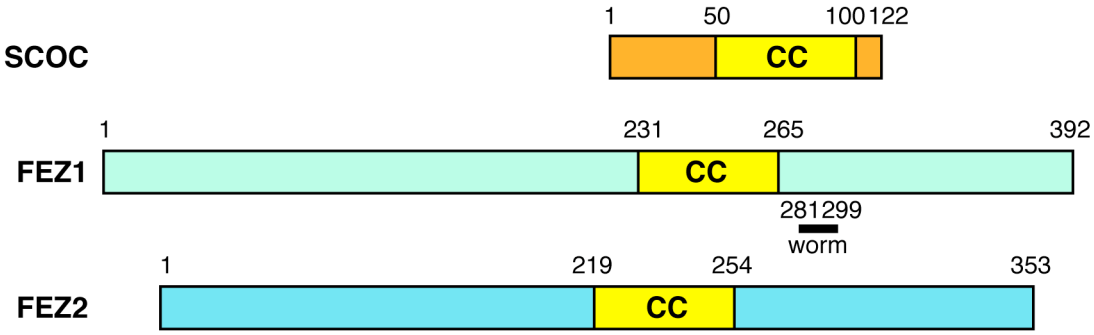

Figure 6.1 Human SCOC, FEZ1 and FEZ2 domain structures
Human SCOC, FEZ1 and FEZ2 are shown. Numbers represent amino acid residues. CC is coiled-coil domain. Worm 281 to 299 is the reported region in *C. elegans* FEZ homologue UNC-76 that is critical for SCOC binding (Su et al., 2006).

6.1.3 The yeast homologue of SCOC is most likely Slo1

A BLAST search of the *S. cerevisiae* genome against the human SCOC protein unveiled a novel protein that Panic *et al* named SCOCO-like ORF (SLO1) (Panic et al., 2003). These authors showed that SLO1 does not interact with the yeast ARL1 homologue Arl1p but in fact interacts *in vitro* with the ARF-like protein Arl3p. They identified a conserved tyrosine residue towards the C-terminal of SLO1 that is critical for this binding and suggest that the surrounding region is similar to that of a Golgi-targeting GRIP domain (golgin-97, RanBP2alpha, Imh1p and p230/golgin-245 domain). Yeast Arl3p is a Golgi-associated GTP-binding ARF and acts as a vesicle-tethering factor for endosomes at the Golgi.

Indeed, SLO1 is the best hit using a BLAST search of the *S. cerevisiae* genome against the mammalian SCOC protein, having the highest conservation, but performing my own BLAST search, I found two other yeast proteins that also show some similarity with SCOC. A 33% sequence identity similarity is seen between the human SCOC protein and Vps30, the yeast Beclin 1 homologue. Vps30, also known as Atg6, is a critical component of the yeast PI3-kinase complex and is required for autophagy. It contains a coiled-coil domain and it is in this domain that the similarity between the proteins is seen. Another protein that shows partial identity (27%) to SCOC around its coiled-coil is the golgin GOLGA2, also known as GM130. It should be noted that

coiled-coil domains are infamous for sharing homology and these findings may be nonspecific to SCOC.

6.1.4 BERT is the chicken homologue of SCOC and is required for early development

The SCOC *Gallus gallus* homologue, known as BERT, is critical for normal chick embryo development (Papanayotou et al., 2008). The chicken and human proteins have an identical sequence in the conserved C-terminal region containing the coiled-coil. In the chicken, the expression of BERT is low throughout the life span but is sharply upregulated in an early embryonic stage 4-4^{+} when the neural plate will emerge. Discovered by yeast two-hybrid as an ERNI-binding protein, BERT coordinates with ERNI to regulate the onset of expression of Sox2, a critical factor of neural plate development. BERT is an antagonist of ERNI and both bind to each other and the cell cycle control protein Geminin through their coiled-coil domains. The authors propose that BERT disrupts the inhibitory Geminin-ERNI interaction thereby removing a transcriptional repressor, inducing Sox2 expression and the onset of neural plate development. Also, RNAi-mediated knock-down of BERT results in guidance and fasciculation defects in the epaxial nerves (Su et al., 2006) further supporting the idea that SCOC promotes development in higher organisms.

6.2 Characterisation of SCOC as a positive regulator of autophagy

6.2.1 Multiple isoforms of SCOC

SCOC is a small protein whose tertiary structure is mostly comprised of a coiled-coil domain (Figure 6.1). There are four suggested isoforms arising from multiple transcript variants that are the result of alternative splicing; the C-terminal region containing the coiled-coil is highly similar between the isoforms (Figure 6.2). The Entrez Gene ID for SCOC is 60592 and the accession number listed for Dharmacon's SCOC Smartpool is NM_032547; this encodes a protein of with a molecular weight of approximately 14 kDa. When first characterising the human protein SCOC, the group of Richard Kahn cloned an EST of SCOC into pCDNA3.1 Myc-His (Van Valkenburgh et al., 2001) and we obtained this construct, from now on referred to as SCOC-myc, from this group. The clone used to do so has the Nucleotide Accession of AF330205 and corresponding Protein Accession AAK01707. This is a

shorter version of the protein whose translation begins at a conserved methionine within the coiled-coil and the predicted molecular weight of this protein is 9.4 kDa.

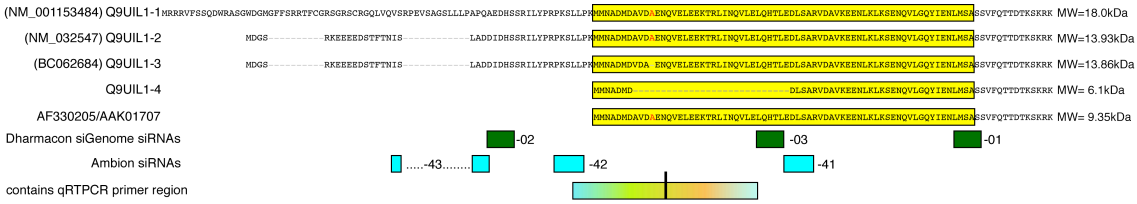

Figure 6.2 SCOC isoforms and siRNA targeting regions
Schematic depicting different isoforms of SCOC (Uniprot ID Q9UIL1). The amino acid sequence and predicted molecular weights of the protein is shown. Yellow box is the coiled-coil domain. Green boxes show Dharmacon siGenome duplex targeting areas; blue boxes show Ambion siRNA targeting areas. Rainbow box shows the region that is suggested to contain the Qiagen QuantiTect SCOC primer. (A larger version of this schematic can be found in the Appendix, Figure 9.1).

I asked which isoform or isoforms exist in HEK cells using an affinity purified rabbit antibody also received from Rick Kahn that was generated against recombinant SCOC-myc protein (Van Valkenburgh et al., 2001). I used this antibody to probe HEK cell lysates and like Van Valkenburgh *et al*, was not able to detect endogenous SCOC protein in these lysates. In order to enrich for the SCOC protein, I performed an immunoprecipitation, binding the SCOC antibody to Protein A beads, incubating with HEK cell lysate and probing the bead eluate with the SCOC antibody (Figure 6.3). After a very long exposure, a band of approximately 8 kDa is visible in the IP and not the control lane. This band is smaller than three of the Uniprot isoforms (Q9UIL1-1-3) and appears to be bigger than isoform 4 (Q9UIL1-4), which lacks just less than half of the conserved coiled-coil domain. It is likely is that this band corresponds to the AAK01707 isoform whose corresponding open reading frame was used to generate the SCOC-myc construct. Perhaps this form, which is not annotated as a Uniprot isoform, is the main isoform in HEK cells.

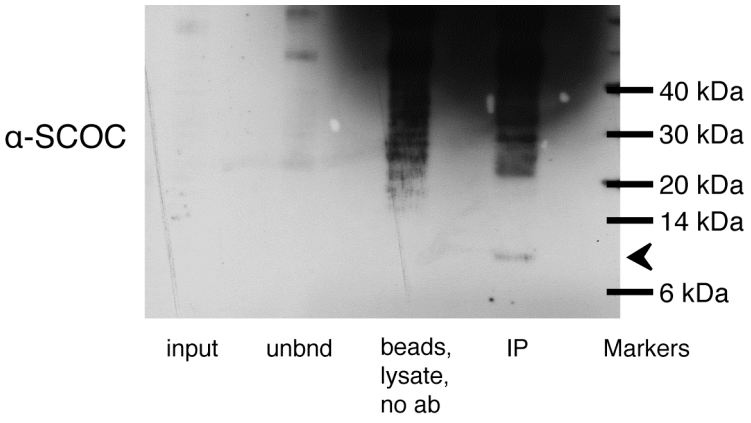

Figure 6.3 One isoform of SCOC is detected in HEK cells
Anti-SCOC blot of HEK lysates (input, unbnd) and supernatant eluted from beads after immunoprecipitation with SCOC antibody (IP). Unbnd is unbound HEK lysate after immunoprecipitation. IP is eluate after incubation of beads, lysate and SCOC antibody. Arrowhead indicates immunoprecipitated band.

6.2.2 Differential effects of SCOC siRNA duplexes on GFP-LC3 spots, SCOC mRNA levels and LC3 lipidation

I have previously shown that treating cells with SCOC Dharmacon siRNA duplexes-02 and -03 inhibits GFP-LC3 spot formation and endogenous LC3 lipidation in HeLa cells but while duplex-03 decreases SCOC mRNA levels, duplex-02 does not (Figure 5.10). I obtained the third duplex that decreased SCPO, STIPO and STAPO in the deconvolution screen, SCOC siRNA duplex-01, and tested that duplex in the same assays alongside duplex-02 and -03 (Figure 6.4, panel a). Observing the effect of duplex-01 on GFP-LC3 spots in GFP-LC3-HEK cells, one sees a reduction of spot number and intensity compared to RISCfree-treated cells, recapitulating the deconvolution screen data. Duplex-01 also reduced SCOC mRNA levels and does so to a greater extent than duplex-03 (Figure 6.4, panel b). However, while duplex-02 and -03 again decrease LC3 lipidation, knock-down with duplex-01 leads to an increase in LC3 lipidation (Figure 6.4, panel c,d). I postulate that duplex-02 is having an off-target effect in that I suspect it is knocking down an unknown gene that is required for autophagy. I cannot however explain at this point why knock-down of SCOC with duplex-01 decreases GFP-LC3 spots but increases endogenous LC3 lipidation in HeLa cells.

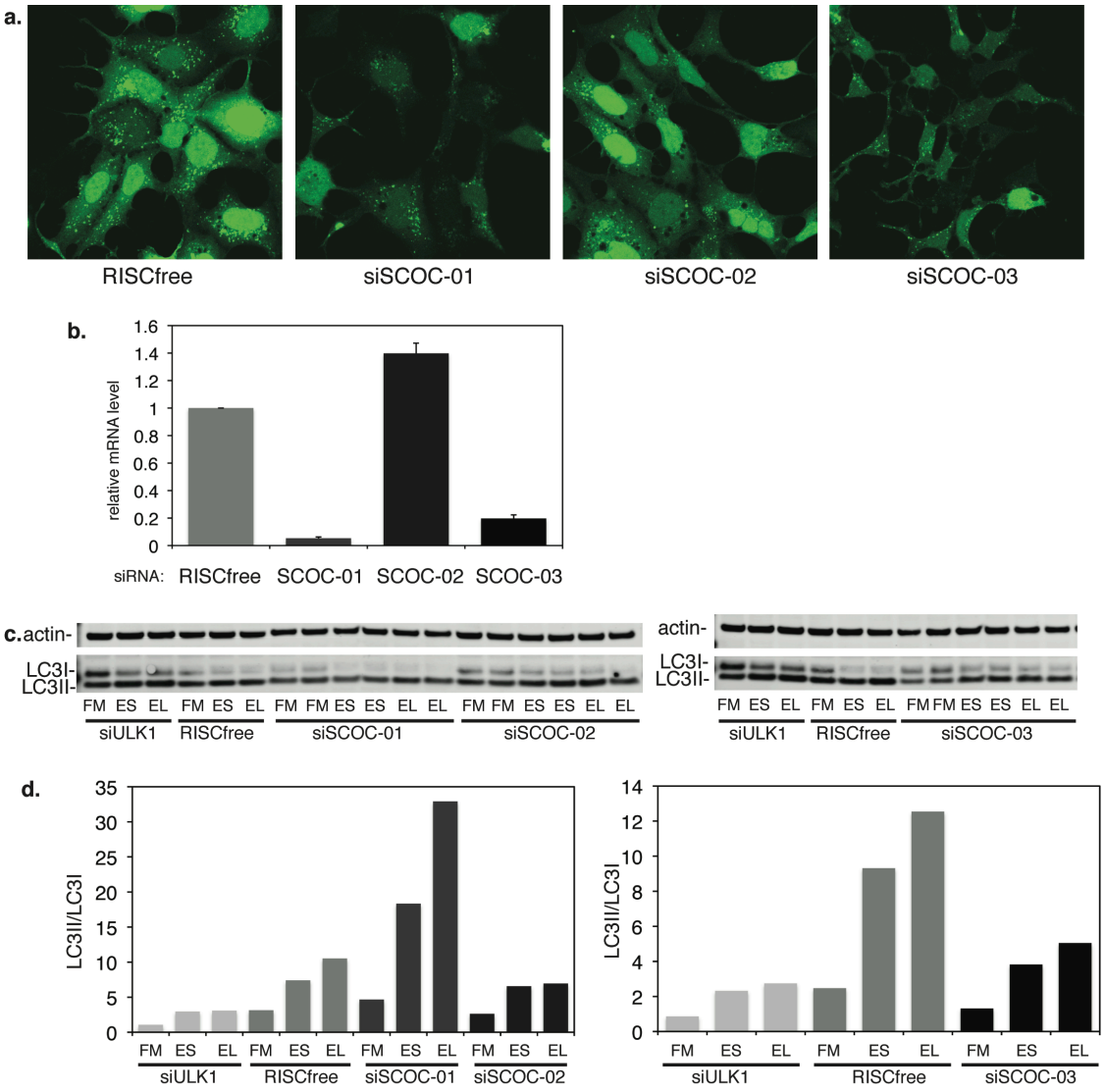

Figure 6.4 Dharmacon siRNA duplexes against SCOC decrease GFP-LC3 spots but have differential effects on SCOC mRNA levels and LC3 lipidation
a. GFP-LC3 confocal images at 63X after knock-down with indicated siRNA duplex and induction of autophagy by incubation in EBSS plus 0.25mg/mL leupeptin. **b.** Quantification of SCOC mRNA levels in GFP-LC3-HEK cells as determined by qRTPCR. Error bars represent the standard deviation derived from triplicate wells. **c.** Anti-Actin and -LC3 blot after indicated siRNA treatment in HeLa cells and incubation in full medium (FM), EBSS (ES) or EBSS plus 0.25mg/mL leupeptin (EL). **d.** Quantification of LC3II/LC3I after indicated siRNA and incubation conditions. LC3II/LC3I values for siSCOC-01, siSCOC-02 and siSCOC-03 are the averages of duplicates. The experiment was done twice with duplex -01 and four times with duplexes -02 and -03; representative blots are shown.

In order to further characterise the effects of SCOC knock-down with the three Dharmacon siRNA duplexes, I employed an alternate autophagy assay, p62 degradation. p62/SQSTM1 is an LC3- and ubiquitin-binding protein that is selectively degraded by autophagosomes (Pankiv et al., 2007) and p62 protein levels are used as a read-out for autophagy. As expected, after starvation of GFP-LC3-HEK cells treated with RISCfree control siRNA, a marked reduction in p62 levels is seen (Figure 6.5).

Knock-down of ULK1 inhibits the autophagic degradation of p62 and the protein accumulates; similarly and as expected, knock-down with SCOC duplexes-02 and -03 leads to an accumulation of p62 to similar levels as those seen after ULK1 knock-down. Surprisingly, knock-down with duplex-01 leads to a greater accumulation of p62 than that seen after ULK1 knock-down. One possible explanation is that duplex-01 induces cell death, as the protein levels are lower after treatment with that duplex, possibly skewing the quantification of p62 normalised to actin. Cell stress-induced autophagy could also explain the increase in LC3 lipidation in HeLa cells treated with duplex-01 but does not explain the inhibition of GFP-LC3 spots seen (Figure 6.4).

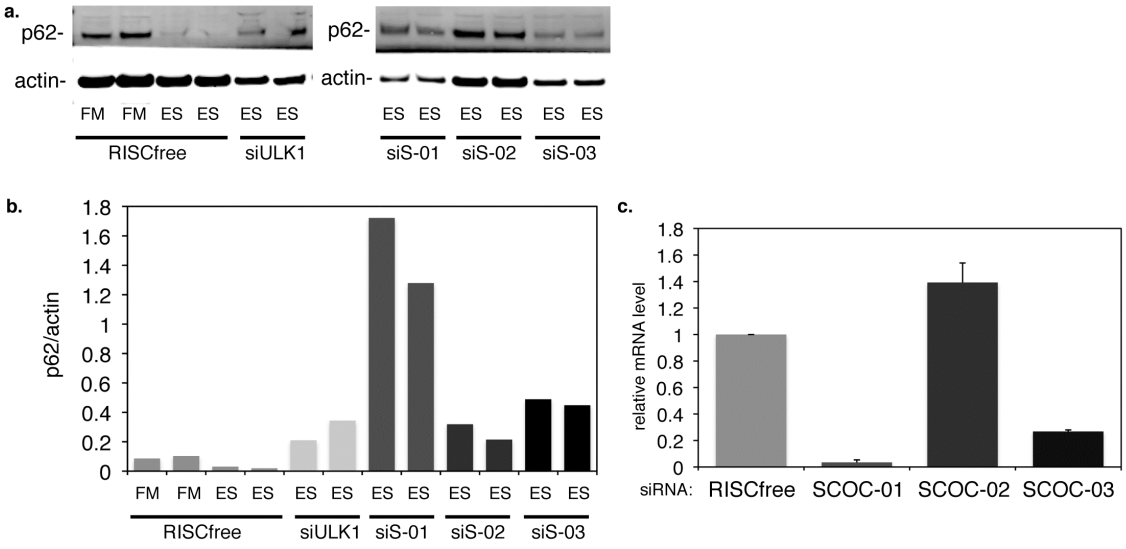

Figure 6.5 Knock-down of SCOC with Dharmacon siRNA duplexes against SCOC leads to an accumulation of p62

a. Anti-p62 and -actin blot after indicated siRNA treatment in GFP-LC3-HEK cells and incubation in full medium (FM) or EBSS (ES) for 4 hours. siS represents siSCOC. **b.** Quantification of p62/actin after indicated siRNA and incubation conditions. The experiment was done twice; representative blots are shown. **c.** Corresponding quantification of SCOC mRNA levels in GFP-LC3-HEK cells as determined by qRTPCR.

In order to assess the effect of different individual siRNA duplexes against SCOC, I ordered three duplexes from Ambion, siSCOC-41, -42, and -43. I tested their effects on GFP-LC3 spots and endogenous LC3 lipidation as well as their ability to knock-down SCOC (Figure 6.6). All three duplexes reduced GFP-LC3 spots in starvation conditions compared to an Ambion siRNA control pool, though duplex -43 was least effective in doing so. Duplex-43 was also least able to reduce SCOC mRNA levels and also least inhibitory to LC3 lipidation in HeLa cells suggesting that enough SCOC protein remains in these cells for autophagy to function almost normally. Duplex-43, like duplex-02, targets the N-terminal region of SCOC and does not target

isoforms Q9UIL1-1 and Q9UIL1-4 (Figure 4.2) reinforcing the theory that the main isoform in HEK cells is one of the shorter forms (Q9UIL1-4 or that corresponding to the est AAK01707) (Figure 4.3) and suggests that one or both of these isoforms is required for the function of SCOC as a positive regulator of autophagy.

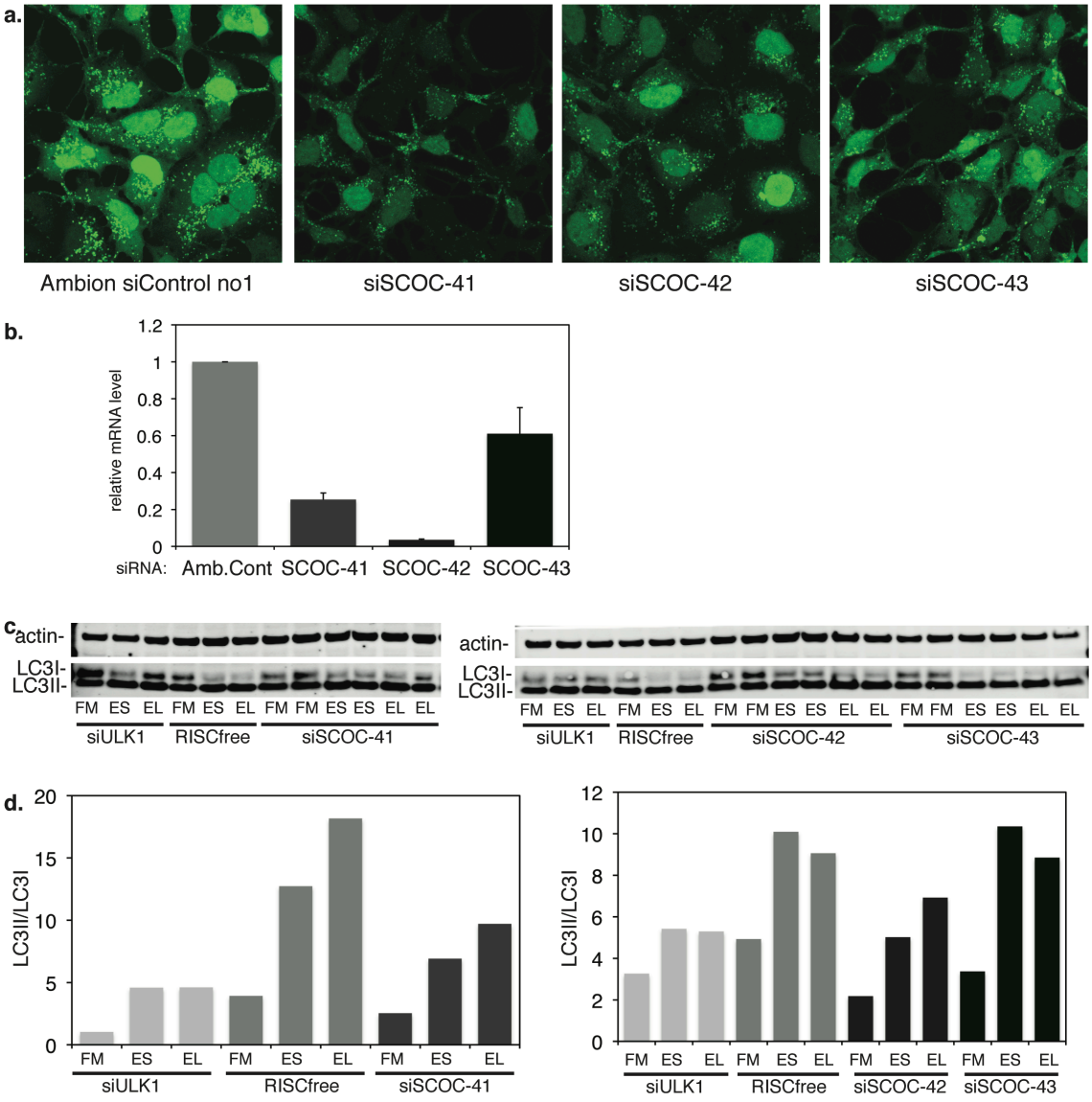

Figure 6.6 Ambion siRNA duplexes against SCOC decrease GFP-LC3 spots, SCOC mRNA levels and LC3 lipidation to various extents

a. GFP-LC3 confocal images at 63x after knock-down with indicated siRNA duplex and induction of autophagy by incubation in EBSS plus 0.25mg/mL leupeptin. **b**. Quantification of SCOC mRNA levels in GFP-LC3-HEK cells as determined by qRTPCR. Error bars represent the standard deviation derived from triplicate wells. **c.** Anti-Actin and -LC3 blot after indicated siRNA treatment in HeLa cells and incubation in full medium (FM), EBSS (ES) or EBSS plus 0.25mg/mL leupeptin (EL). **d.** Quantification of LC3II/LC3I after indicated siRNA and incubation conditions. LC3II/LC3I values for siSCOC-41, siSCOC-42 and siSCOC-43 are the averages of duplicates. The experiment was done twice; representative blots are shown.

Of the six individual SCOC siRNA duplexes that decrease GFP-LC3 spot parameters only three duplexes, -03,-41, and -42 reduce its mRNA levels and inhibit LC3 lipidation in HeLa cells. I confirmed that Dharmacon duplex-02, which also leads to a reduction of LC3 lipidation, is unable to target SCOC by testing the ability of duplex-02 to reduce the levels of overexpressed SCOC protein. However, the DNA sequence that is targeted by duplex-02 lies outside of the region expressed in the SCOC-myc construct (Figure 6.2), so I cloned the open reading frame of SCOC isoform Q9UIL1-3 into the GFP-containing vector pEGFP N1, placing SCOC on the N-terminal of eGFP, creating the construct hereafter referred to as SCOC-GFP. The SCOC sequence in the SCOC-GFP construct has an extended N-terminus compared to the SCOC-myc construct and siRNA duplex -02, if effective, should decrease SCOC-GFP expression levels. After knock-down with siSCOC-02 followed by overexpression of SCOC-GFP, a large amount of SCOC-GFP fusion protein is seen suggesting that duplex-02 is not targeting SCOC, corroborating the qRTPCR data for duplex-02 (Figure 6.7).

Using the same technique I confirmed that all five remaining SCOC siRNA duplexes reduce the levels of overexpressed SCOC-GFP protein (Figure 6.7). Duplex -01 is better than duplex-03 at reducing SCOC-GFP, corresponding to the mRNA data generated by qRTPCR. Duplex-43 was shown by qRTPCR to only reduce SCOC mRNA levels to 60% but in this overexpression system, it completely inhibits the overexpression of SCOC-GFP and does so to the same extent as duplex -41 and -42.

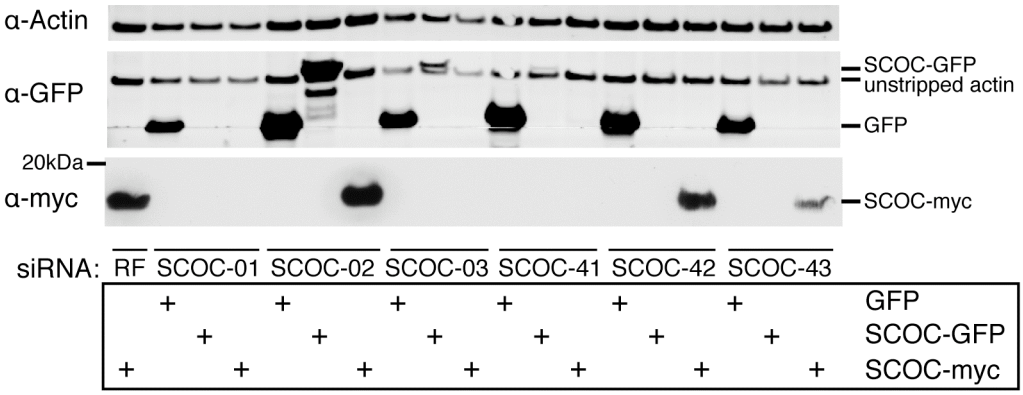

Figure 6.7 SCOC siRNA duplexes target SCOC expression vectors to various extents

Anti-Actin, -GFP, and -myc blots of HEK cells after knock-down with indicated SCOC siRNA duplexes and overexpression of indicated constructs.

SCOC siRNA	Isoforms that it targets (Uniprot Q9UIL1 or AAK01707)	Effect on SCOC mRNA in GFP-LC3-HEK cells	SCOC overexpression constructs it knocks down	Effect on GFP-LC3 spots	Effect on LC3 lipidation in HeLa cells	Effect on p62 degradation
Dharm. -01	-1, -2, -3, -4, AAK01707	Knocks down to 5%	SCOC-myc, SCOC-GFP	Decreases	Increases LC3II/I	Strongly inhibits
Dharm. -02	-2, -3	Does not knock down	Does not knock down	Decreases	Decreases LC3II/I	Inhibits
Dharm. -03	-1, -2, -3, AAK01707	Knocks down to 20%	SCOC-myc, SCOC-GFP	Decreases	Decreases LC3II/I	Inhibits
Dharm. -04		Does not knock down	Not tested	No effect	Not tested	Not tested
Ambion -41	-1, -2, -3, AAK01707	Knocks down to 25%	SCOC-myc, SCOC-GFP	Decreases	Decreases LC3II/I	Not tested
Ambion -42	-1, -2, -3	Knocks down to 4%	SCOC-GFP	Decreases	Decreases LC3II/I	Not tested
Ambion -43	-2, -3	Knocks down to 61%	SCOC-GFP	Decreases somewhat	No effect	Not tested

Table 6.1 Summary of SCOC siRNA duplexes
Summary of seven SCOC siRNA duplexes. Shown are: the isoforms it is expected to target (see Figure 4.2); effect of SCOC mRNA in GFP-LC3-HEK cells as measured by qRTPCR; effect on overexpressed SCOC constructs (see Figure 4.7); effect on GFP-LC3 spots; effect on LC3 lipidation in HeLa cells; effect in the p62 degradation assay in GFP-LC3-HEK cells (see Figure 6.5).

Three of the six siSCOC duplexes target a region outside, or upstream, of the region expressed by the SCOC-myc construct. These duplexes are duplex-02, as mentioned before, and Ambion duplexes -42 and -43 and when SCOC-myc is overexpressed after knock-down with these duplexes, the SCOC-myc fusion protein is detected in these lysates (Figure 6.7). Of note, the SCOC-myc fusion protein migrates by SDS-PAGE in both HEK and HeLa cells as a protein of approximately 14 kDa, which is larger than the expected 9 kDa size reported by Van Valkenburgh *et al*. Duplexes -01, -03, and -41 target a region downstream of the SCOC-myc start site and are all effective at decreasing SCOC-myc and SCOC-GFP overexpression (Figure 6.7). I utilised duplex-42 whose binding sequence lies upstream of the SCOC-myc start codon and duplexes -03 and -41 whose binding sequences lie downstream of the SCOC-myc start codon to perform a rescue experiment. Knock-down of SCOC with downstream duplexes -03 and -41 targets SCOC-myc, inhibits SCOC-myc expression and decreases LC3 lipidation after both pcDNA 3.1 empty vector and SCOC-myc

overexpression (Figure 6.8). Knock-down of SCOC with upstream duplex-42 however allows for the overexpression of SCOC-myc (Figure 6.6, Figure 6.7 panel c). After siSCOC-42 knockdown, LC3 lipidation is inhibited in starvation conditions but this is rescued by the presence of SCOC protein after expression of SCOC-myc. Overexpression of SCOC-myc after RISCfree control siRNA knock-down increased LC3 lipidation beyond the control and this response is repressed by ULK1 knock-down, suggesting that overexpression of SCOC increases autophagy.

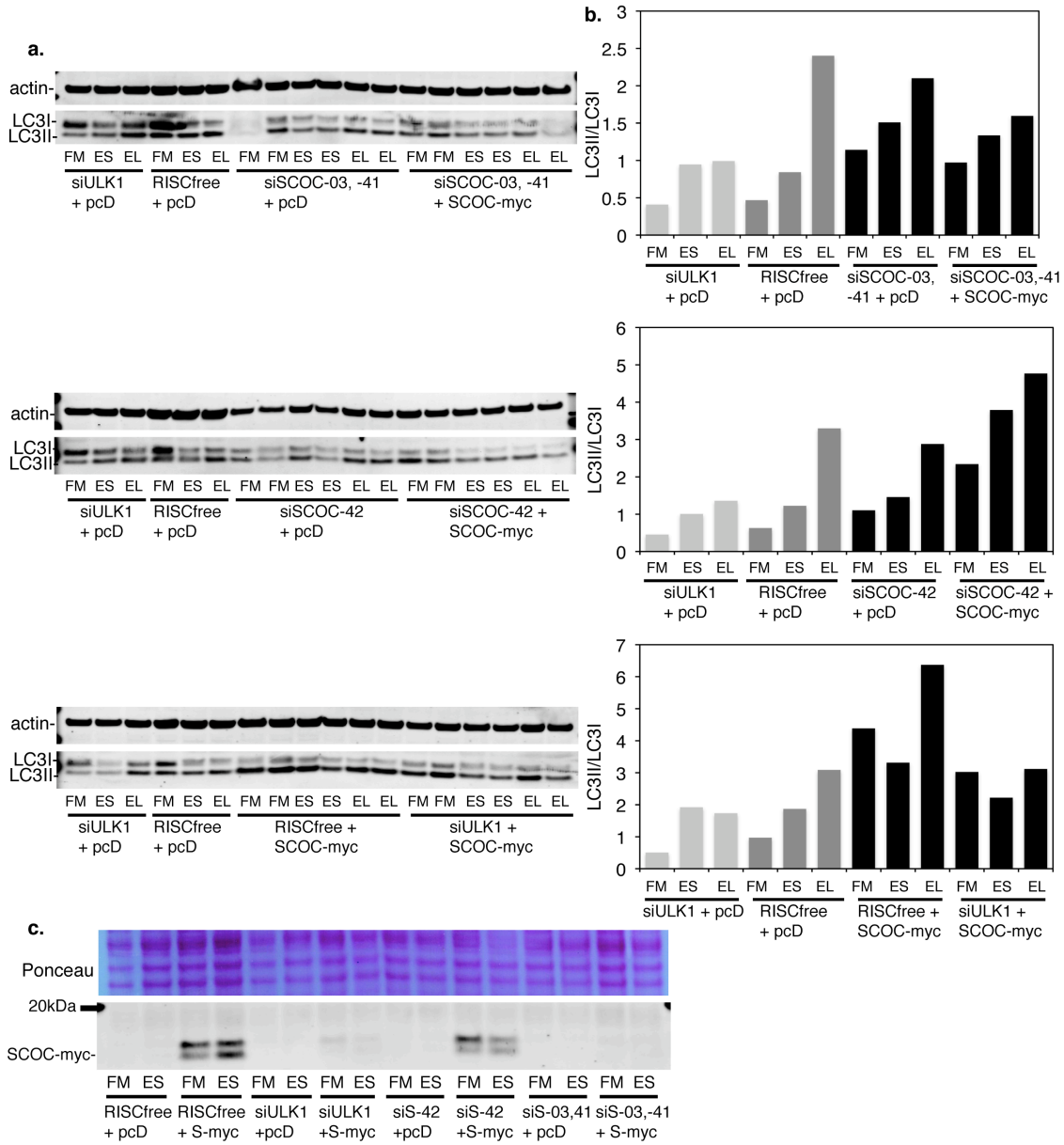

Figure 6.8 Inhibition of LC3 lipidation after SCOC knock-down is rescued by SCOC overexpression

a. Anti-Actin and -LC3 blots after indicated siRNA treatment and overexpression construct in HeLa cells and incubation in full medium (FM), EBSS (ES) or EBSS plus 0.25mg/mL leupeptin (EL). pcD is pcDNA3.1(-). **b.** Quantification of LC3II/LC3I after indicated siRNA, overexpression and incubation

conditions. LC3II/LC3I values for siSCOC-42, siSCOC-03,-41, RISCfree+SCOC-myc, and siULK1+SCOC-myc are the averages of duplicates. The experiment was done three times; representative blots are shown. **c.** PonseauS staining and anti-myc blot of HeLa lysates after corresponding siRNA treatments and construct expression. S-myc is SCOC-myc.

In HeLa cells, overexpressed SCOC-myc migrates as a distinct doublet of approximately 14 kDa (Figure 6.8, panel c); the doublet may result from two transcriptional start sites from two methionines at the N-terminal of the SCOC-myc construct (Figure 6.2). Its protein levels do not seem to be altered during starvation conditions but knock-down of ULK1 consistently led to a drastic reduction of SCOC-myc levels.

6.2.3 Overexpression of SCOC drives autophagy

I observed in HeLa cells that knock-down of SCOC inhibited LC3 lipidation and overexpression of SCOC-myc increased LC3 lipidation and I replicated the experiment in HEK cells. As in HeLa cells, when SCOC is reduced by knock-down with Dharmacon siRNA duplex-03, endogenous LC3 lipidation is inhibited (Figure 6.9, panel a,b,c). Overexpression of SCOC-myc increased LC3 lipidation when compared to overexpression of empty vector (Figure 6.9, panel d,e,f). In HEK cells, SCOC-myc also appears as a doublet though the bands are less distinct than in HeLa cells. Also, overexpression of SCOC-GFP increases LC3 lipidation compared to overexpression of GFP alone (Figure 6.9, panel g,h). Taken together, these results suggest that SCOC is a positive regulator of autophagy in GFP-LC3-HEK cells, HeLa cells and HEK cells.

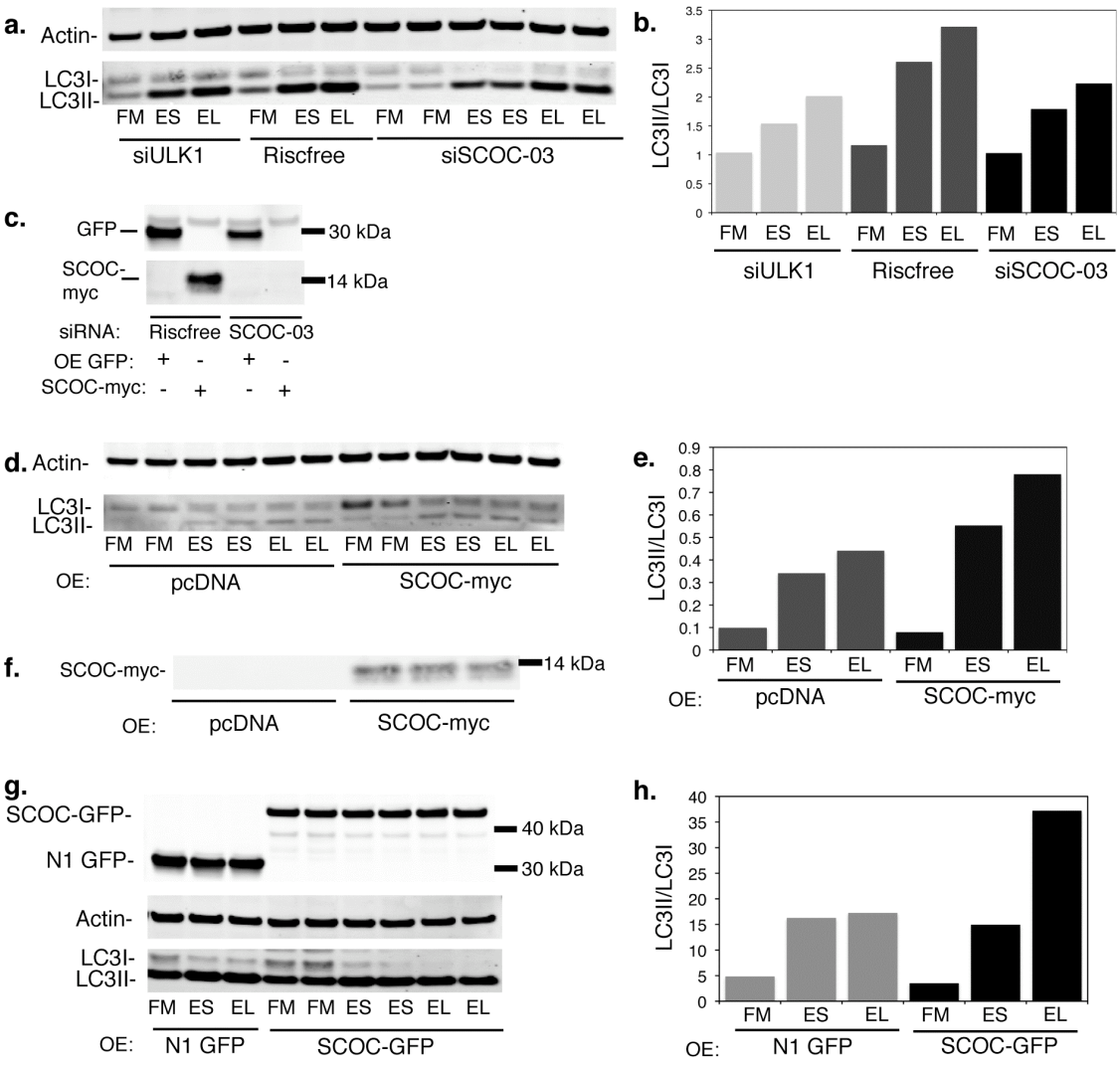

Figure 6.9 SCOC knock-down inhibits autophagy and overexpression augments autophagy in HEK cells

a. Anti-Actin and -LC3 blots after indicated siRNA treatment in HEK cells and incubation in full medium (FM), EBSS (ES) or EBSS plus 0.25mg/mL leupeptin (EL). **b.** Quantification of LC3II/LC3I after indicated siRNA and incubation conditions. LC3II/LC3I values for siSCOC-03 are the averages of duplicates. The experiment was done twice; representative blots are shown. **c.** Anti-GFP and -myc blots of HEK cells after treatment with RISCfree or SCOC siRNA and overexpression of GFP or SCOC-myc. **d**. Anti-Actin and -LC3 blots after indicated construct overexpression and incubation conditions in HEK cells. **e.** Quantification of LC3II/LC3I after indicated construct overexpression and incubation conditions. LC3II/LC3I values for siSCOC-myc are the averages of duplicates. The experiment was done three times; representative blots are shown. f. Anti-myc blot of HEK cells after treatment with control vector or SCOC-myc. **g.** Anti-GFP, -Actin and -LC3 blots after indicated construct overexpression and incubation conditions in HEK cells. **h**. Quantification of LC3II/LC3I after indicated construct overexpression and incubation conditions. LC3II/LC3I values for SCOC-GFP are the averages of duplicates. The experiment was done twice; representative blots are shown.

6.2.4 Characterisation of SCOC by immunofluorescence

Endogenous SCOC has been previously described in NRK cells using an affinity purified rabbit antibody raised against human SCOC (Van Valkenburgh et al., 2001); these authors observed a punctate cytoplasmic staining plus a perinuclear staining

pattern similar to that of Golgi markers, and some plasma membrane staining. Using the same antibody, I observe very similar staining patterns in HEK cells with the presence of juxta nuclear patches of SCOC and a punctate cytoplasmic population, though I do not see SCOC at the plasma membrane (Figure 6.10, panel a). SCOC is not reported to reside in the nucleus but its small size would allow it to diffuse into the nucleus and I sometimes note SCOC labelling in the nucleus. After co-labelling with SCOC and the Golgi markers GM130 and TGN46, I observe extensive overlap in clusters around the nucleus. Unlike Atg9, which has been shown to disperse from a juxta-nuclear Golgi pool to an endosomal cytoplasmic pool upon starvation (Young et al., 2006), SCOC labelling appears similar in full medium and EBSS (Figure 6.10, panel a). After siRNA-mediated knock-down of SCOC, less signal is seen and the vast majority of the pool that remains colocalises with the trans-Golgi network protein TGN46 (Figure 6.10, panel b).

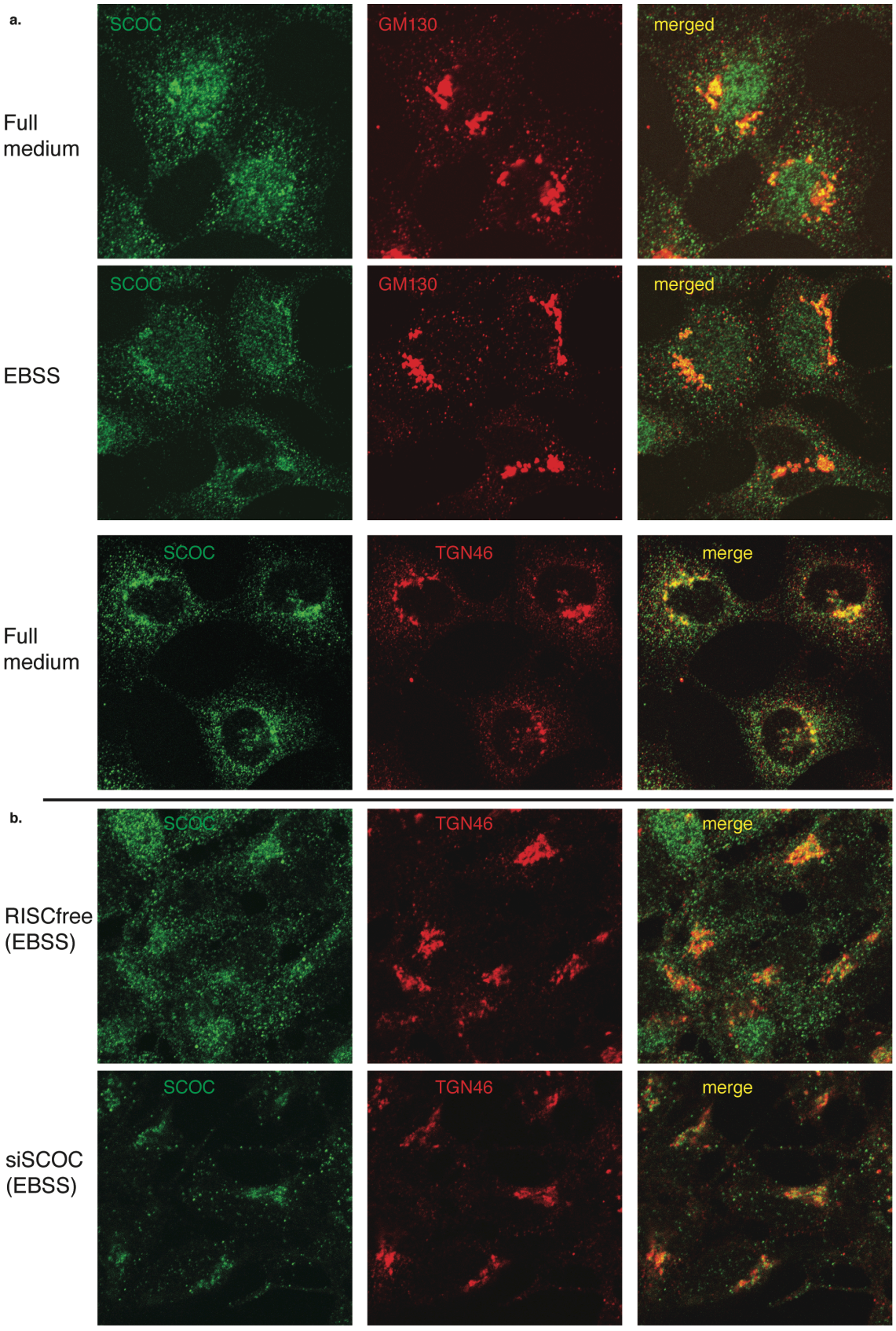

Figure 6.10 SCOC colocalises with Golgi markers and its signal is depleted by siRNA knock-down

a. HEK cells show SCOC and GM130 co-labelling or SCOC and TGN46 co-labelling after indicated incubation conditions for two hours, fixation and immunostaining with anti-SCOC and anti-GM130 or

anti-TGN46 antibodies. b. HEK cells show SCOC and TGN46 co-labelling after indicated siRNA treatment (siSCOC is siSCOC duplex-03) and incubation in EBSS for two hours, fixation and immunostaining with anti-SCOC and anti-TGN46 antibodies.

I next asked whether SCOC colocalises with known autophagy markers, the most obvious of which being the Golgi-resident protein Atg9. SCOC and endogenous Atg9 show extensive overlap in the juxta-nuclear Golgi region in both full medium and EBSS and while Atg9 disperses after starvation, SCOC does not (Figure 6.11, panel a,b). There is also occasional colocalisation on cytoplasmic vesicular structures in EBSS. More colocalisation on these cytoplasmic vesicular structures is seen between SCOC and Atg12 whose staining is wholly punctate and presumably marks the sites of autophagosomal assembly (Figure 6.11, panel c). SCOC also colocalises with GFP-LC3 spots and endogenous LC3 structures that appear to emerge from the juxta-nuclear region (Figure 6.11, panel d,e). SCOC also displays overlap with GFP-DFCP1, a protein that has been shown to localise to the Golgi in full medium (Axe et al., 2008) (Figure 6.11, panel f). In EBSS, a large amount of overlap is seen in a juxta-nuclear region and SCOC is occasional seen to decorate GFP-DFCP1-positive punctate structures. Of note, SCOC does not colocalise with LAMP2, a marker of lysosomes (data not shown). Taken together, these results suggest that SCOC is a bone fide autophagy protein that appears to be acting at the site of autophagosome formation. As the majority of the structure of SCOC is comprised of a coiled-coil protein-binding domain, it is possible that SCOC acts at this site as a scaffold, recruiting and binding critical autophagic machinery proteins such as Atg12.

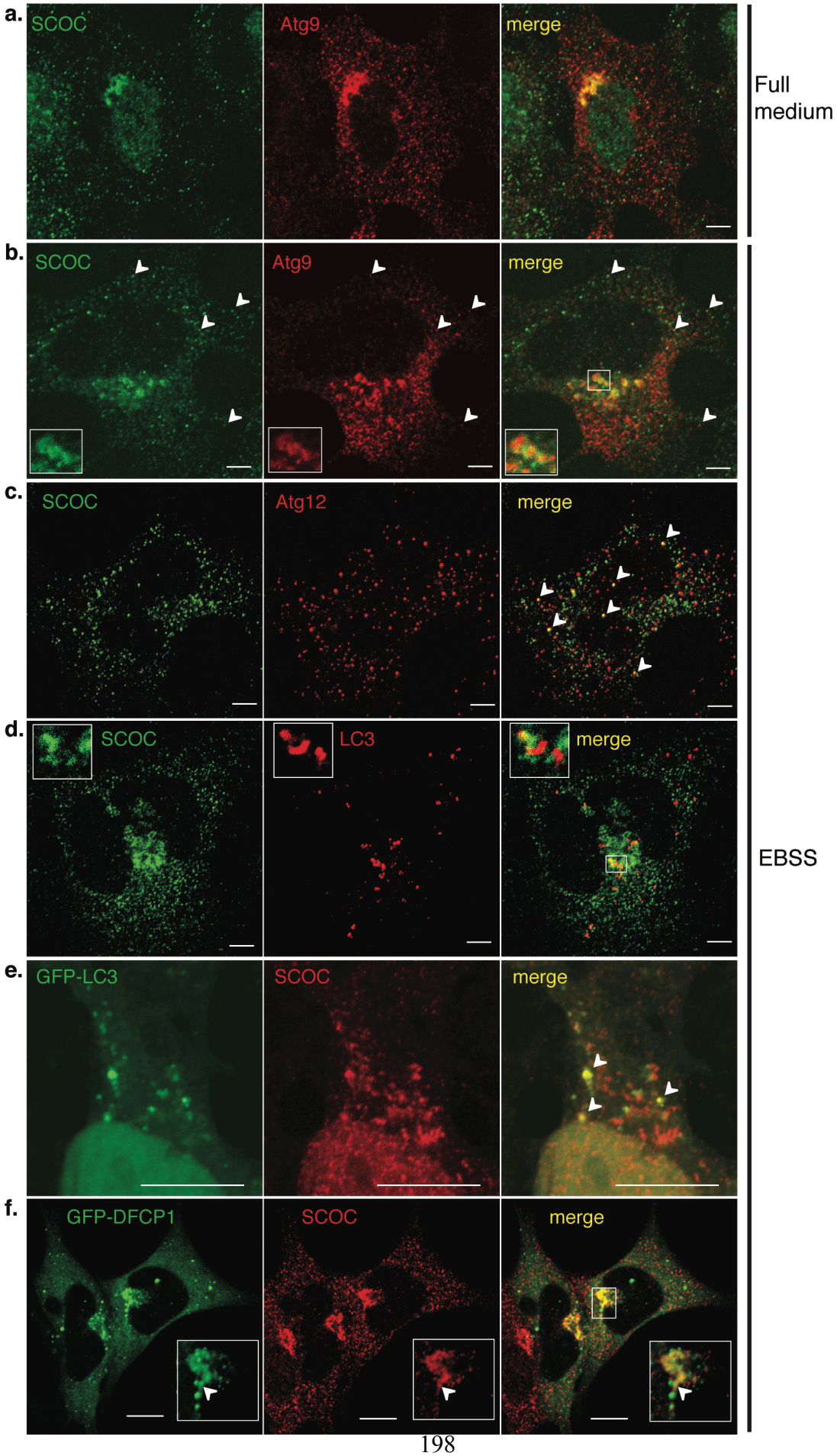
a.
SCOC
Atg9
merge
Full medium
b.
SCOC
Atg9
merge
c.
SCOC
Atg12
merge
d.
SCOC
LC3
merge
EBSS
e.
GFP-LC3
SCOC
merge
f.
GFP-DFCP1
SCOC
merge

Figure 6.11 Endogenous SCOC colocalises with known autophagy proteins
a. SCOC and mAtg9 in HEK cells after incubation for two hours in full medium. **b.** SCOC and mAtg9 in HEK cells after incubation for two hours in EBSS (arrowheads show co-localisation). **c.** SCOC and Atg12 in HEK cells after incubation for two hours in EBSS (arrowheads show co-localisation). **d.** SCOC and LC3 staining as indicated in HEK cells after incubation for two hours in EBSS. **a.-d.** Scale bars equal 5μm. **e.** SCOC staining in GFP-LC3-HEK cells after incubation for two hours in EBSS (arrowheads show co-localisation). Scale bar equals 10μm. **f.** SCOC staining in GFP-DFCP1 cells (arrowhead shows co-localisation). Scale bar equals 10μm. **b,f.** Enlarged inset shown in merge panels.

I next asked what cellular distribution was displayed by overexpressed SCOC and whether overexpressed SCOC colocalise with other autophagy markers for which we have only rabbit polyclonal antibodies and therefore cannot be used with the anti-SCOC polyclonal antibody. SCOC-myc and SCOC-GFP do not appear as endogenous SCOC in HEK cells (Figure 6.12). There are very few small cytoplasmic punctate structures and instead, more diffuse cytoplasmic staining. There are larger, rounded SCOC-myc structures and even larger patches of both overexpressed SCOC-myc and SCOC-GFP that are usually found somewhat close to the nucleus. It should be said however that these staining patterns could be artefacts of the overexpression of the SCOC constructs. Nonetheless, these areas of more-intense SCOC-myc staining are seen to colocalise with endogenous ULK1 and endogenous Atg16. Interestingly, when examining endogenous Atg16 in SCOC-GFP-overexpressing cells, Atg16-positive puncta are seen to congregate close to juxta-nuclear concentrations of SCOC-GFP. The Atg16 structures here are reminiscent of the endogenous LC3 and GFP-DFCP1 structures seen above that also appear to emerge from a Golgi-like pool of SCOC. I have shown that overexpression of both SCOC-myc and SCOC-GFP increases autophagy as measured by LC3 lipidation and it would be interesting to test whether overexpression of SCOC increases Atg12 or Atg16 puncta. Again, these immunofluorescence experiments place SCOC in the cell with early autophagy proteins.

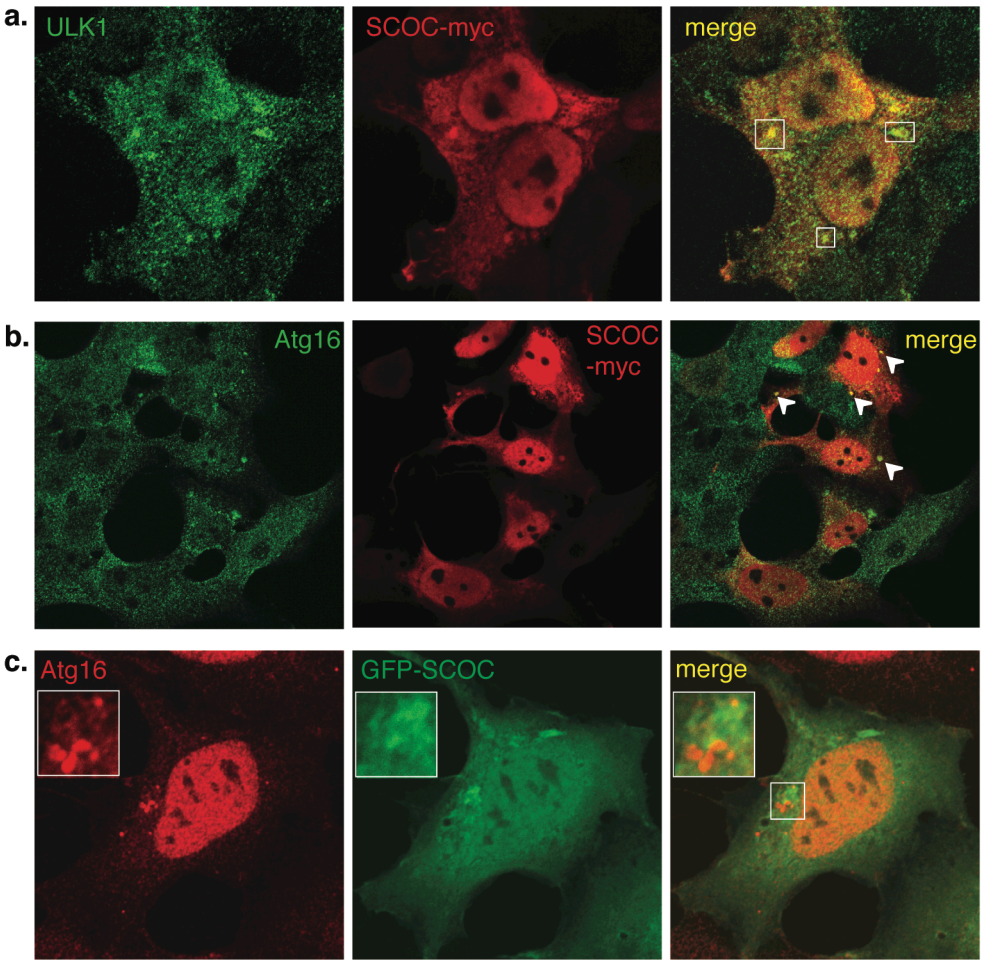

Figure 6.12 Overexpressed SCOC displays different staining than endogenous but also colocalises with autophagy markers
a. HEK cells are transfected with SCOC-myc, incubated for 2 hours in EBSS and fixed. Endogenous ULK1 staining (boxes show co-localisation). **b.** HEK cells are transfected with SCOC-myc, incubated for 2 hours in EBSS and fixed. Endogenous Atg16 staining (with polyclonal antibody) (arrowheads show co-localisation). **c.** HEK cells are transfected with GFP-SCOC, incubated for 2 hours in EBSS and fixed. Endogenous Atg16 staining (with monoclonal antibody). Enlarged inset shown in merge panels.

6.3 Regulation of SCOC by ULK1 and the effect of SCOC-interacting proteins on autophagy

6.3.1 Regulation of SCOC by ULK1

I have shown above that knock-down of ULK1 leads to a decrease in the amount of overexpressed SCOC protein in HeLa cells (Figure 6.8). I repeated this experiment and in addition, also overexpressed ULK1 and ULK1 kinase-dead mutant ULK1KI together with SCOC-myc. As before, a significant reduction of the SCOC-myc doublet is seen after siRNA depletion of ULK1 (Figure 6.13, panel a). This reduction, however, cannot be rescued by the overexpression of ULK1 as a marked loss of SCOC-myc is also seen after co-overexpression with both ULK1 wild-type and ULK1 kinase-dead

proteins. The ULK1KI mutant however does not appear to repress the SCOC expression as much as the wild-type in this experiment (performed only once), suggesting that the kinase activity of ULK1 is partially required for the reduction of SCOC (Figure 6.13, panel b). Co-overexpression of SCOC-myc with wild-type ULK1 does slightly increases the lipidation of endogenous LC3 but overexpression of the kinase-dead ULK1 inhibited LC3 lipidation as expected (Chan et al., 2009) (Figure 6.13, panel c).

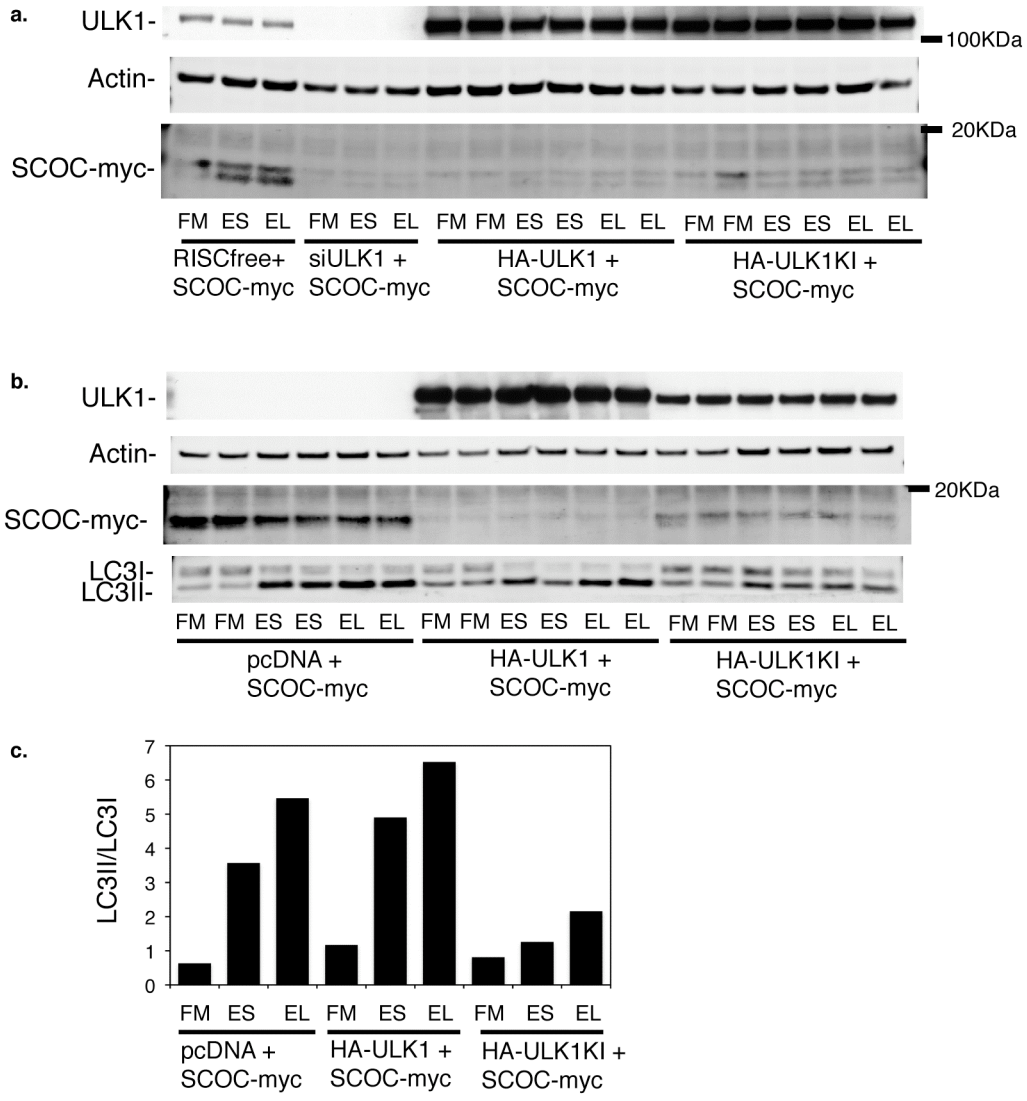

Figure 6.13 SCOC protein levels are regulated by ULK1

a. Anti-ULK1, -Actin, and -myc blots after indicated siRNA treatment, transfection with indicated DNA constructs, and incubation in full medium (FM), EBSS (ES), and EBSS plus 0.25mg/mL leupeptin (ES) in HeLa cells. **b.** Anti-ULK1, -Actin, -myc, and -LC3 blots after transfection with indicated DNA constructs and incubation in full medium (FM), EBSS (ES), and EBSS plus 0.25mg/mL leupeptin (ES) in HEK cells. **c.** Quantification of LC3II/LC3I after indicated construct overexpression and incubation conditions. LC3II/LC3I values for all bars are the averages of duplicates.

6.3.2 SCOC and FEZ1 interact and FEZ1 regulates autophagy

The *C. elegans* homologues of FEZ1 and SCOC have been shown to physically interact and co-ordinately control axonal development (Su et al., 2006) and this has also been shown for the *C. elegans* homologues of FEZ1 and ULK1 (Toda et al., 2008). Though mammalian ULK1 and FEZ1 have not been reported to interact, SCOC and FEZ1 have been shown to interact by yeast-two-hybrid in human cells (Assmann et al., 2006). I tested the SCOC-FEZ1 interaction in HEK cells and could demonstrate co-immunoprecipitation of SCOC-myc with GFP-FEZ1 (Figure 6.14, panel a). A large amount of SCOC-myc is pulled down by beads loaded with GFP antibody and an almost complete reduction of SCOC-myc is seen after the IP. There is a marked depletion of GFP-FEZ1 in the unbound lysate after IP and a band of approximately the right size, though slightly bigger, for endogenous FEZ1 that is also pulled down after co-IP. There is an unspecific band in the lysate lanes that is not decreased after co-IP and also not depleted after FEZ1 siRNA knock-down (Figure 2.2). Of interest, the amount of SCOC-myc pulled down by the GFP IP is not changed in HEK cells after incubation in EBSS starvation medium for two hours. By immunofluorescence examination, overexpressed GFP-FEZ1 appears cytoplasmic with some accumulation around the nucleus with some punctate and ring-like structures that partially colocalise with endogenous SCOC (Figure 1.14, panel b). From these experiments, I can confirm that SCOC and FEZ1 are binding partners in human cells.

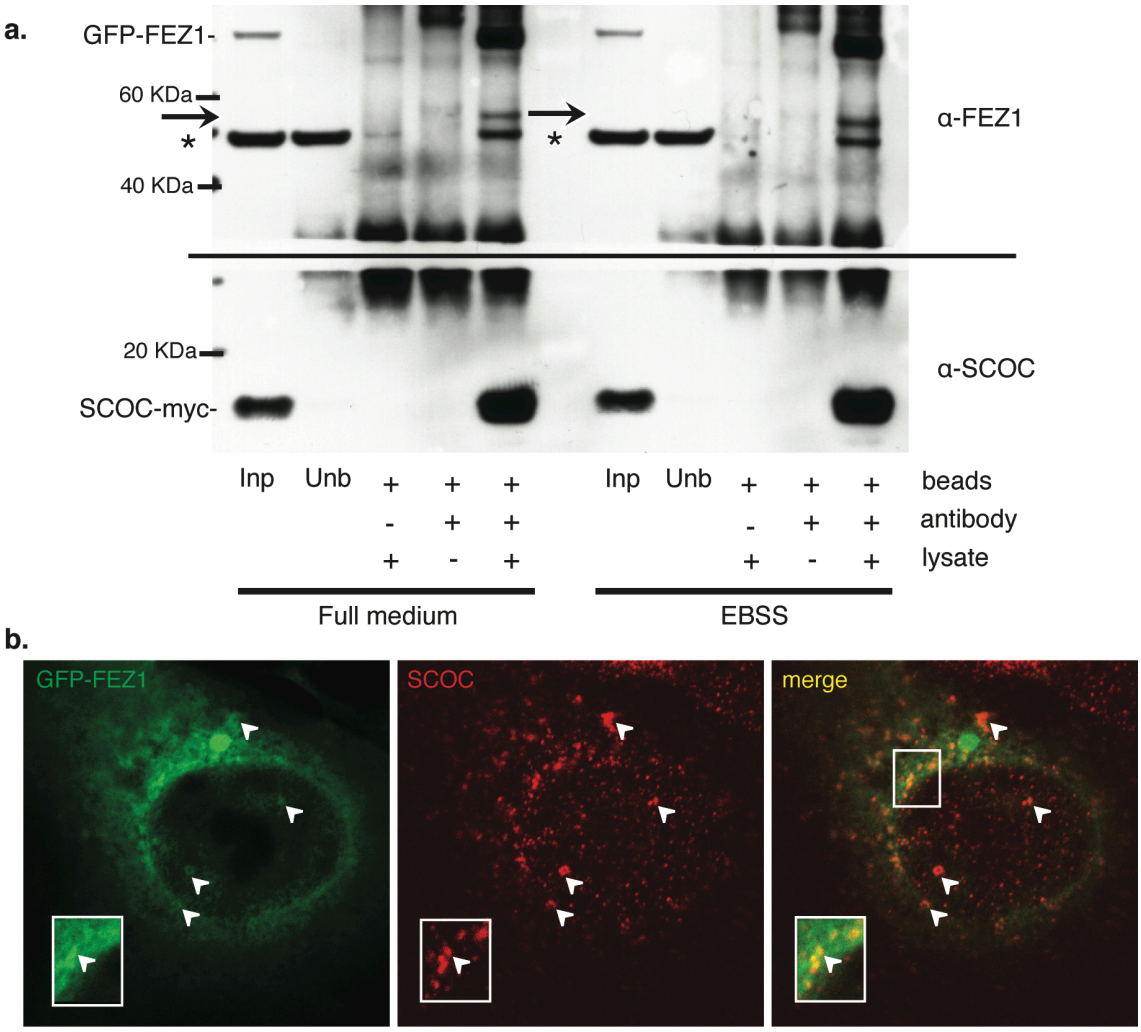

Figure 6.14 Overexpressed SCOC and FEZ1 co-immunoprecipitate and GFP-FEZ1 and SCOC colocalise to structures

a. Anti-SCOC and -FEZ1 blot after co-expression in HEK cells, incubation in full medium or EBSS for two hours, and co-immunoprecipitation of SCOC-myc and FEZ1-GFP with anti-GFP antibody. Input lysate (Inp), unbound supernatant (Unb). Asterix indicates non-specific band, arrow denotes co-precipitating band of similar size to endogenous FEZ1. **b.** HEK cells are transfected with GFP-FEZ1, incubated for two hours in EBSS and fixed. Endogenous SCOC staining as indicated (arrowheads show co-localisation). Enlarged inset shown in merge panels.

During the primary screen, GFP-LC3-HEK cells treated with an siRNA Smartpool against FEZ1 exhibited increased SCPO, STIPO and STAPO. FEZ1 ranked 2790th as an increaser, placing it in the 13th percentile of all hits. In order to further characterise the effect of FEZ1 knock-down on autophagy, I treated HEK cells with a specialised pool of FEZ1 siRNA duplexes previously deconvoluted to confirm that the individual duplexes reduced FEZ1 mRNA levels (Figure 6.15). After incubation in starvation medium and starvation medium with leupeptin, LC3 lipidation was increased compared to RISCfree control in cells treated with FEZ1 siRNA, comparable to the increase seen with the positive control NRBP2. FEZ1 appears to play a role in

autophagy, acting as a negative regulator of GFP-LC3 spot formation and LC3 lipidation.

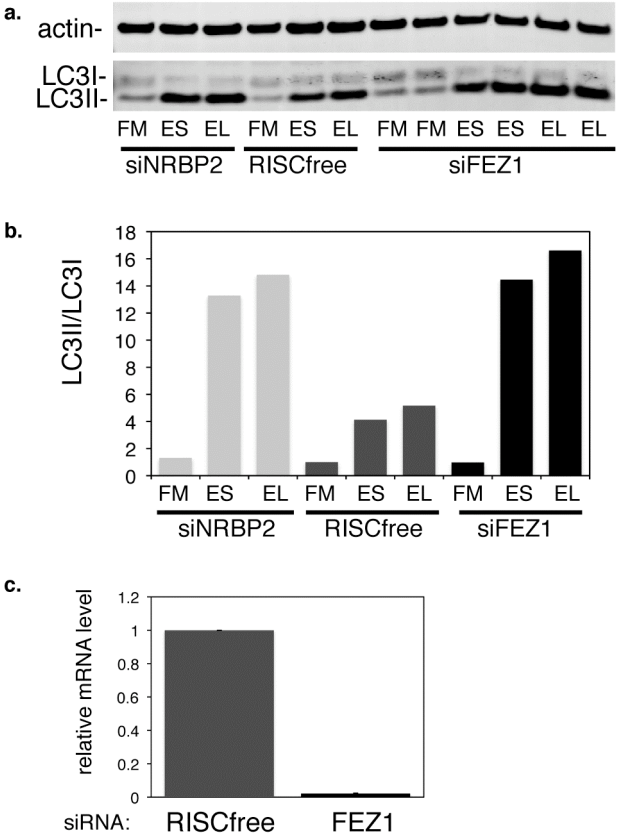

Figure 6.15 FEZ1 is a negative regulator of autophagy
a. Anti-Actin and -LC3 blot after indicated siRNA treatment in HEK cells and incubation in full medium (FM), EBSS (ES) or EBSS plus 0.25mg/mL leupeptin (EL). **b.** Quantification of LC3II/LC3I after indicated siRNA and incubation conditions. LC3II/LC3I values for siFEZ1 are the averages of duplicates. The experiment was done three times; representative blots are shown. **c.** Quantification of FEZ1 mRNA levels in HEK cells as determined by qRTPCR. Error bars represent the standard deviation derived from triplicate wells.

Besides SCOC, three other hits from the starvation-induced autophagy screen in GFP-LC3-HEK cells are reported as binding FEZ1 by yeast-two-hybrid: TLK2, TBC1D25 and TOMM20 (Assmann et al., 2006), (Stelzl et al., 2005). TLK2 has been discussed above and its knock-down was confirmed to increase autophagy by deconvolution and validation by an alternate autophagy assay, LC3 lipidation in HeLa cells. The binding of TLK2 to FEZ1 was shown to require the coiled-coil region of FEZ1, also a requirement of FEZ1 binding to another increaser hit from the screen, TBC1D25, or OATL1. Treatment with an siRNA Smartpool against TBC1D25 increased GFP-LC3 spot parameters in the primary and repeat screen but only one of the individual siRNA duplexes repeated this phenotype and thus was not validated by deconvolution (Appendix Table 8.5). TBC1D25 contains a TBC domain and thus could

act as a Rab GTPase activating protein though its Rab GTPase partner and function is unknown. A large-scale yeast-two hybrid screen showed that the translocase TOMM20, thought to be a member of the complex that controls cytoplasmic precursor proteins' import across the mitochondrial outer membrane, also binds FEZ1 (Stelzl et al., 2005). After knock-down of TOMM20, GFP-LC3 spot parameters were decreased and one of the individual siRNA duplexes led to a very large decrease of GFP-LC3 spots in the deconvolution screen while a second siRNA duplex narrowly missed the cut-off for decreasing SCPO and STAPO (Appendix Table 8.5).

6.3.3 SCOC and TLK2 interact

TLK2 was shown above to be a validated negative regulator of autophagy and has been shown to bind the SCOC-binding partner FEZ1 (Assmann et al., 2006) so I asked whether TLK2 and SCOC could interact in HEK cells. After co-transfection with HA-tagged TLK2 and SCOC-myc, HEK cells were incubated with beads and anti-HA antibody, and then probed for SCOC after immunoprecipitation. SCOC-myc was detected in the IP-specific lane suggesting that the two proteins do indeed interact (Figure 6.16, panel a). Of interest, overexpression of TLK2 appeared to increase the amount of SCOC-myc in HEK cells as demonstrated by the presence of more SCOC-myc in the input and unbound supernatant lanes compared to those after overexpression of GFP-FEZ1. I examined the cellular distribution of HA-TLK2 in HEK cells and found it on cytoplasmic punctate structures, a small number of which were also stained with endogenous SCOC (Figure 6.16, panel b). Mirroring the effect of TLK2 overexpression on SCOC protein levels by western blot, it appears by immunofluorescence that there is more endogenous SCOC in HEK cells overexpressing TLK2, especially in the peripheral non-Golgi pool, though this has not been quantified.

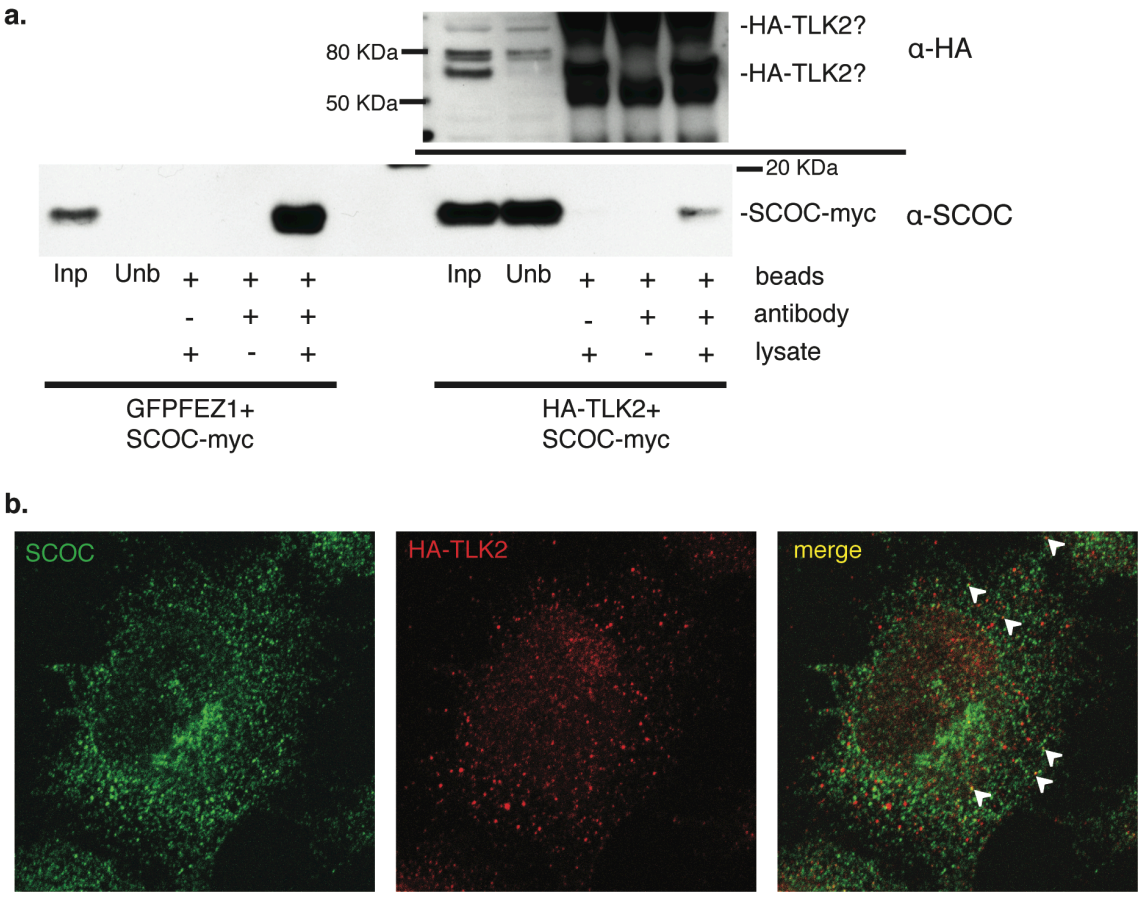

Figure 6.16 Overexpressed TLK2 and SCOC co-IP and partially colocalise
a. Anti-SCOC and -HA blot after indicated co-expression in HEK cells, incubation in full medium or EBSS for two hours, and co-immunoprecipitation of SCOC-myc and HA-TLK2 with anti-HA antibody and co-immunoprecipitation of SCOC-myc and GFP-FEZ1 with anti-GFP antibody. Input lysate (Inp), unbound supernatant (Unb). **b.** HEK cells are transfected with HA-TLK2, incubated for two hours in EBSS and fixed. Endogenous SCOC staining as indicated (arrowheads show co-localisation)

6.3.4 ARL1 regulates autophagy

Like FEZ1, the reported SCOC-binding protein ARL1 increased GFP-LC3 spots in the primary screen. As an increaser, it was ranked 2923rd also placing it in the 13th percentile of all genes tested in the primary screen. In order to confirm this finding I knocked down ARL1 with a customised pool of siRNA duplexes derived from the Smartpool used in the primary screen that I had determined decreased ARL1 mRNA levels. An increase of LC3 lipidation was seen in full medium and starvation conditions after ARL1 knock-down compared to the negative control. Thus, ARL1 acts as a negative regulator of autophagy.

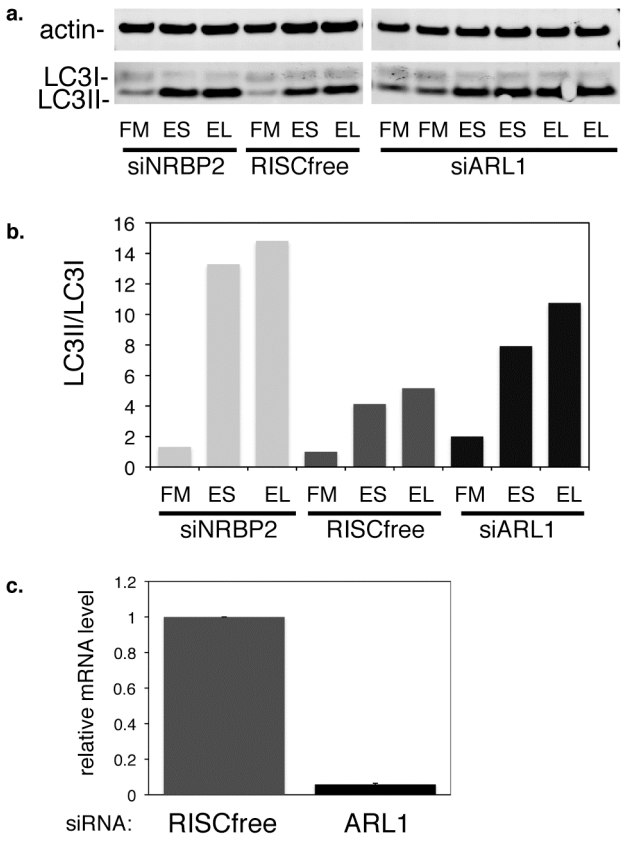

Figure 6.17 ARL1 is a negative regulator of autophagy
a. Anti-Actin and -LC3 blot after indicated siRNA treatment in HEK cells and incubation in full medium (FM), EBSS (ES) or EBSS plus 0.25mg/mL leupeptin (EL). (Note: this is the same blot but has been cut). **b.** Quantification of LC3II/LC3I after indicated siRNA and incubation conditions. LC3II/LC3I values for siARL1 are the averages of duplicates. The experiment was done three times; representative blots are shown. **c.** Quantification of ARL1 mRNA levels in HEK cells as determined by qRTPCR. Error bars represent the standard deviation derived from triplicate wells.

6.4 Discussion of SCOC

SCOC is a bone fide positive regulator of autophagy. Knock-down of the gene with a targeting siRNA decreases GFP-LC3 spot formation, p62 degradation and LC3 lipidation and overexpression of SCOC increases LC3 lipidation. SCOC also colocalises with multiple autophagy markers including Atg12. SCOC is found in a juxta-nuclear pool that is positive for Golgi markers and is also seen on peripheral punctate structures. These pools do not seem to change upon starvation like the Golgi-resident transmembrane autophagy protein Atg9, which disperses. The cytoplasmic SCOC structures can be Atg9-, Atg12- or GFP-LC3-positive. In addition, endogenous LC3 and GFP-DFCP1 structures were seen possibly budding off of SCOC-positive juxta-nuclear regions. SCOC does not colocalise with LAMP2; taken together, these results suggest that SCOC acts during autophagosome formation possibly by binding

autophagy proteins via its coiled-coil domain, thus serving as a platform or scaffold for autophagosome assembly.

As mentioned, SCOC does not seem to alter its cellular localisation during starvation and similarly, we have previously illustrated that ULK1 appears to be constitutively associated with membrane fractions (Chan et al., 2009). I have shown that overexpressed SCOC colocalises with endogenous ULK1 on cytoplasmic structures (Figure 6.12) and have attempted to co-immunoprecipitate the two proteins. Overexpressing the short SCOC-myc construct together with HA-tagged ULK1 and IP-ing with anti-HA antibody, I can occasionally see a very faint band of SCOC-myc pulled down and a depletion of HA-ULK1 and SCOC-myc after co-immunoprecipitation. I have also seen overexpressed HA-ULK1 pulled down with anti-SCOC antibody. In general, SCOC and ULK1 do not readily co-IP and their interaction may be transient. I would however like to test whether a longer form of SCOC such as the SCOC-GFP fusion protein could co-immunoprecipitate ULK1; perhaps the N-terminal of SCOC is required for SCOC binding to ULK1. It would also be of interested to ask whether SCOC interacts with Atg13 or FIP200. Nonetheless, I have shown that overexpressed SCOC protein levels are regulated by ULK1 (Figure 6.13) and perhaps SCOC receives signals from the ULK1 kinase complex upon initiation of autophagy and assembles the autophagy machinery downstream of that signal.

I show above that overexpressed SCOC and FEZ1 physically interact (Figure 6.14) and it has been reported that the *C. elegans* homologues of these proteins also interact and together, they control axonal trafficking (Su et al., 2006). The *C. elegans* homologues of FEZ1 and ULK1 have also been reported to bind and it would be of interest to know if mammalian FEZ1 and ULK1 are binding partners. Perhaps SCOC, FEZ1 and ULK1 form some sort of autophagy regulatory complex, for I have shown that FEZ1 is a negative regulator of autophagy. One way that FEZ1 might negatively regulate autophagy is by physically keeping SCOC, a positive regulator, away from its potential function as a scaffold for autophagosome formation. Conversely, I have seen that overexpression of FEZ1 inhibits LC3 lipidation (data not shown) reiterating that FEZ1 is a negative regulator of autophagy and I would like to ask whether FEZ1, like SCOC, colocalises with autophagy markers such as LC3 or DFCP-1. Although the binding of SCOC and FEZ1 did not appear to change in cells that had been incubated in EBSS for two hours, one theory could be that FEZ1 binding to SCOC may alter slightly

during starvation so that ULK1 may phosphorylate SCOC. It would be interesting to know if SCOC or FEZ1 are kinase substrates of ULK1.

Another potential regulator of SCOC is the kinase TLK2. I have shown that TLK2 is a potential negative regulator of autophagy as its knock-down increases autophagy (Figure 5.15) and I have also shown that overexpressed SCOC and TLK2 co-immunoprecipitate and partially colocalise on cytoplasmic puncta (Figure 6.16). Interestingly, overexpression of TLK2 seemed increase SCOC-myc expression levels and though the experiment has only been performed once, overexpression of a myc-tagged TLK2 construct seemed to increase LC3 lipidation possibly by stabilising SCOC and I have shown that increasing SCOC protein levels increases autophagy. TLK2 could also regulate SCOC and/or autophagy itself through its interaction with FEZ1, which has been shown by yeast-two-hybrid (Assmann et al., 2006). Perhaps TLK2, FEZ1 and SCOC form a complex together and it would be important to test whether knock-down of TLK2 disrupts SCOC-FEZ1 binding and vice versa. Last, TLK2 could potentially regulate SCOC on a transcriptional level. I have discussed that knock-down of TLK2 may increase the mRNA levels of autophagy proteins, potentially explaining how it is a negative regulator of autophagy. I would like to see if knock-down of TLK2 increases SCOC mRNA levels.

Taken together, the experiments discussed above, though preliminary, point to SCOC as a scaffold for autophagosome formation. Through its coiled-coil domain, SCOC has the potential to bind many proteins. Beclin 1 and Atg16 both possess coiled-coil domains as well and SCOC may recruit the PI(3)-kinase complex and members of the critical conjugation reactions. SCOC interacts with a coiled-coil protein that has not until now been implicated in autophagy, FEZ1. FEZ1 itself has many interactors, three of which, TLK2, TBC1D25 and TOMM20 were found to be regulators of starvation-induced autophagy in my screen. Perhaps SCOC sits between an initiation signal from the ULK1 kinase complex or other signalling molecules and the proteins of the autophagic machinery. In this way, SCOC could mark a pre-isolation membrane structure that acts as a hub between initiation and autophagosome formation in mammalian cells.

Another possible way that SCOC could influence autophagy is through its interacting partner ARL1. This GTPase has important functions in Golgi for regulating the membrane trafficking of endosomes (Burd et al., 2004), (Nishimoto-Morita et al.,

2009). I have shown that ARL1 is a potential negative regulator of autophagy in that knockdown of ARL1 increased LC3 lipidation. As ARL1 and SCOC have been shown to directly bind (Van Valkenburgh et al., 2001), it is possible that ARL1 holds SCOC on the Golgi when autophagy is inactivated and releases SCOC when autophagy is induced. It would be important to test whether the binding of SCOC to ARL1 is modulated by amino acid levels in the cell and if so, what signals mediate the response.

Of interest, alterations of SCOC have been linked to disease. SCOC is significantly down-regulated in Huntington's disease (Hodges et al., 2006) suggesting that SCOC is required for the autophagic clearance of aggregated proteins. An SNP mutation (C to T) in SCOC has also been associated to hypertension in humans (Wellcome Trust Case Control Consortium, 2007). These links to disease highlight the importance of SCOC in mammalian cells and it will be important in the future to dissect its role as a positive regulator of autophagy.

Chapter 7. WAC

7.1 Introduction to WAC

WAC, WW domain containing adaptor with coiled-coil, was a strong candidate to investigate further because both siRNA duplexes were consistently successful in decreasing GFP-LC3 spots and WAC mRNA levels as well as in inhibiting endogenous LC3 lipidation. The presence of a WW and a coiled-coil domain suggests that it has the potential, like SCOC, for autophagy binding partners. Two already known and interesting binding partners, ubiquilin 4 and huntingtin potentially link WAC to the ubiquitin-proteasome system (UPS) and aggrephagy respectively. Last, WAC has been implicated in two diseases that affect a large percentage of the human population, Huntington's disease and diabetes.

7.1.1 WAC is described as a splicing factor interactor

WAC is largely uncharacterised and to this date, only one publication describes it (Xu and Arnaout, 2002). It was discovered as a protein that interacted by yeast-two-hybrid with polycystin 1, or PKD1, a membrane protein that is mutated in Polycystic kidney disease. A WW domain is defined by two tryptophans and an asparagine residue separated by 20-23 amino acids and characteristically binds proline-rich regions that often contain phosphoserine and phosphotyrosine; proteins that contain WWs have a wide variety of functions. Using computational sequence analysis Xu *et al* establish *Drosophila* WAC as a Rosetta stone protein that is the result of fusion of two proteins or domains. They found that the N-terminal of WAC is similar to the pre-mRNA splicing factor SNRP70 and therefore suggest WAC is involved in mRNA processing. They went on to show that, like the pre-mRNA splicing complex marker SC35, over-expressed WAC appears in punctate speckles within subdomain boundaries in the nucleus. WAC was also found to interact with keratin 15 by yeast-two-hybrid (Rual et al., 2005).

7.1.2 WAC interacts with UBQLN4

Ubiquilin 4, also known as ataxin-1 ubiquitin-like interacting protein, was used as a bait in a large-scale yeast-two-hybrid screen searching for interactors of proteins

associated with proteins known to cause ataxias, such as ataxin 1 (Lim et al., 2006). This study identified WAC as an ubiquilin 4 or UBQLN4 interactor. UBQLN4 contains a UBQ or ubiquitin homologue domain and a UBA or ubiquitin association domain. Through these shared domains one of which binds proteasomal compartments and the other of which binds polyubiquitin, ubiquilins regulate protein degradation via the UPS most likely by targeting ubiquitinated proteins to the proteasome. Ubiquilins were first linked to autophagy when it was shown that UBQLN1 is a negative regulator of starvation-induced cell death in that its overexpression suppresses and knock-down enhances this process (Wang et al., 2006). More recently ubiquilin 1, also known as PLIC-1, has been shown to colocalise with LC3 and positively regulate autophagosome degradation (N'Diaye et al., 2009). Following on, Rothenberg *et al* found that ubiquilin 1 is enriched in purified autophagosomes and co-immunoprecipitates with LC3 (Rothenberg et al., 2010). They show that ubiquilin 1 regulates autophagy in a slightly unusual way in that knock-down of UBQLN1 increases LC3I and decreases LC3II but also reduces autophagosome number, suggesting it is required for the maturation of LC3I to LC3II. Ubiquilin 1, like p62, is taken up and degraded by autophagy but it is also an active substrate of CMA. As it regulates autophagy but is also a substrate of CMA, the authors speculate that ubiquilin 1 may act as a switch between CMA and its levels may control which degradative pathway a protein follows (Rothenberg and Monteiro, 2010).

Ataxin-1 ubiquitin-like interacting protein (A1Up) localises to the cytoplasm and nucleus and was discovered to interact with both wild-type and mutant ataxin-1 (Davidson et al., 2000). A mutation in ataxin-1 causes an expanded trinucleotide repeat in the protein, which is linked to spinocerebellar ataxia 1, and it was recently shown that the mutation leads to a gain-of-function and also a partial loss-of-function that both contribute to the disease (Zoghbi and Orr, 2009). The function of wild-type ataxin-1 is not known. In their recent publication describing the nucleo-cytoplasmic shuttling of p62, Pankiv *et al* show that p62 can facilitate the recruitment of proteosomes to polyglutamine-expanded ataxin-1 and is specifically recruited to nuclear aggregates of expanded ataxin-1 (Pankiv et al., 2010). Though autophagy has not been shown to degrade mutant ataxin-1 aggregates, p62 is a regulator of both the autophagy and

proteasome pathways. It is therefore a possibility that ataxin-1 may be connected to autophagy through both ubiquilins and p62.

7.1.3 The role of WAC in disease

As discussed above, Huntington's disease (HD) is a genetic disease in which defects in autophagy have been implicated. Interestingly, WAC was found to be upregulated in the symptomatic stages of HD as determined with mRNA from human blood samples collected from HD patients that were analysed by microarray (Borovecki et al., 2005). WAC was also found to be slightly upregulated in three brain regions of HD patients compared with control individuals, as also assessed by microarray (Hodges et al., 2006). In addition, WAC was identified as binding to huntingtin protein in a high-throughput yeast-two-hybrid screen (Kaltenbach et al., 2007). WAC was a strong hit in this screen in that 95 out of 97 htt-fragment baits bound to WAC expressed in human brain or mouse brain or muscle tissue, though the interaction was not confirmed.

WAC is also associated with diabetes; a SNP in the human WAC sequence was one of 78 found to be associated with was Non-insulin-dependent diabetes mellitus, otherwise known as type 2 diabetes (Florez et al., 2007). This A to T change had a p-value of 0.00164.

7.2 Characterisation of WAC's role in autophagy

WAC is highly conserved through vertebrates to the *Danio rerio* or zebrafish and the human protein sequence is 94% similar to the mouse (Xu and Arnaout, 2002). There are two invertebrate homologues known, one in *Brugia malayi* (nematode) and one in *Ciona intestinalis*, an urochordata or sea squirt.

There are multiple isoforms of WAC that are predicted to exist either as the result of alternative splicing (isoform Q9BTA9.2) or polymorphism (Q9BTA9.3 and Q9BTA9.4, Q9BTA9.5) or both (Q9BTA9.3) (Figure 7.1). The canonical sequence represented by isoform 1, NM_016628, is 647 amino acids long with a predicted molecular weight of 71 kDa. It contains an N-terminal WW domain and less-well conserved C-terminal coiled-coil domain.

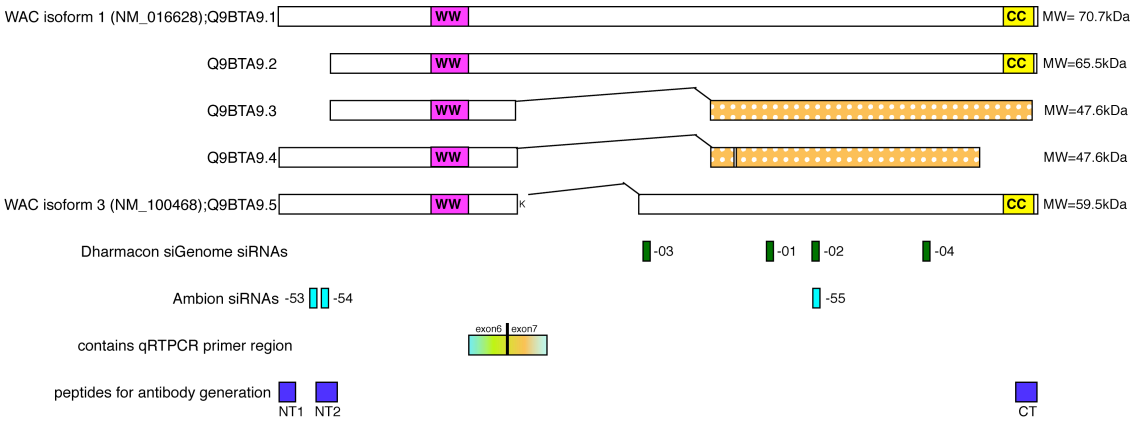

Figure 7.1 WAC isoforms and siRNA- and peptide antibody-targeting regions
Schematic depicting different isoforms of WAC. The amino acid sequence and predicted molecular weights of the protein is shown. The magenta box is the WW domain; the yellow box is the coiled-coil domain. The orange polka-dotted boxes and contained grey box show areas of alternate sequences. Green boxes show Dharmacon siGenome duplex targeting areas; blue boxes show Ambion siRNA targeting areas (note: the region targeted by duplex-54 is upstream of the start of isoforms 2 and 3). Duplexes -01, -02, -04 and -55 target the sequence of isoform 1, 2, and 5 not 3 and 4. Rainbow box shows the region that is suggested to contain the Qiagen QuantiTect WAC primer. The purple boxes show the peptide against which the various polyclonal antibodies were raised. For a larger version of this diagram, see Appendix Figure 9.2)

During the deconvolution screen, three of the four siRNA duplexes against WAC decreased SCPO below 80% of RISCfree control (Figure 7.2, panel a). This response in GFP-LC3-HEK cells corresponds to the degree of knock-down as measured by WAC mRNA levels in that duplex-01 is least efficient as reducing WAC mRNA and also least efficient as decreasing GFP-LC3 spot number (Figure 7.2, panel b). In the second, more directed deconvolution screen all four siRNA duplexes against WAC caused a significant decrease in SCPO. After the deconvolution screen, WAC was a three-out-of-four to four-out-of-four validated-by-deconvolution hit and I confirmed that the reduction of WAC mRNA levels corresponded to these effects.

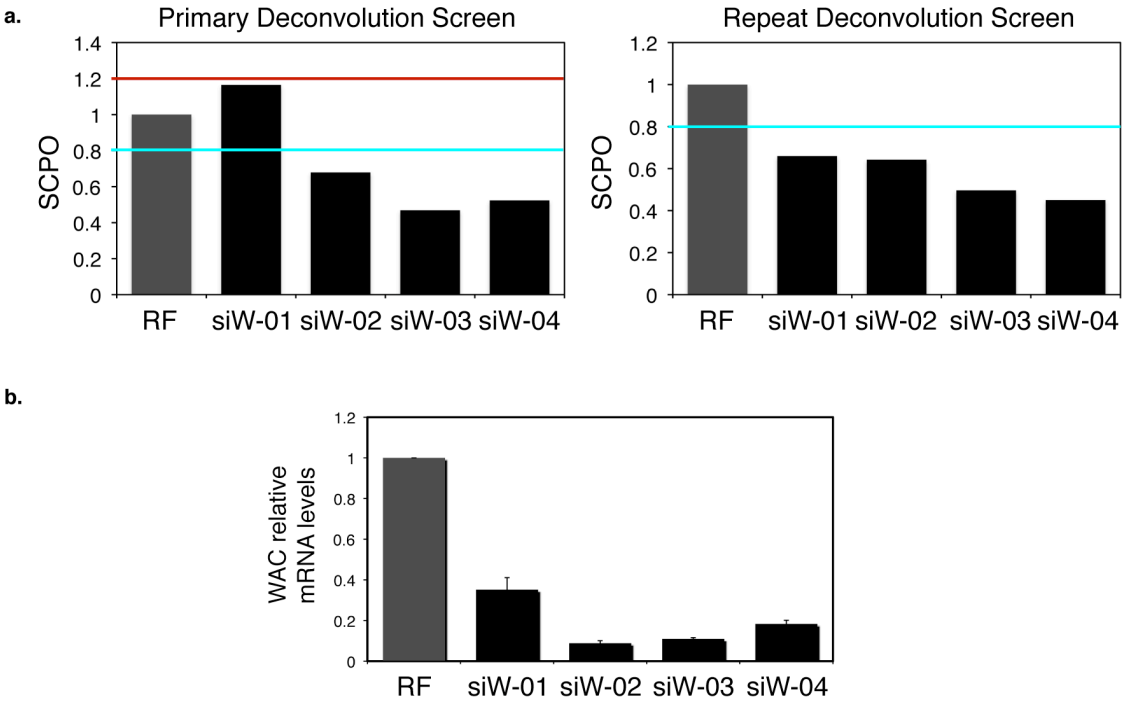

Figure 7.2 All four Dharmacon duplexes against WAC decrease WAC mRNA levels and decrease GFP-LC3 spot count

a. SCPO after knock-down of WAC with four individual siRNA duplexes during the primary deconvolution screen and secondary deconvolution screen of GFP-LC3-HEK in starvation conditions. The blue line marks the 80% of control cut-off for decreasers of GFP-LC3 spots; the red line marks the 120% of control, the cut-off for increasers of spots. RF is RISCfree control, siW is siWAC. **b.** Quantification of WAC relative mRNA levels after indicated siRNA treatment in GFP-LC3-HEK cells as measured by qRTPCR.

As shown in Chapter 5, Figure 5.12, knock-down of WAC with duplex-03 and -04 led to an inhibition of LC3 lipidation in HeLa cells and I show again here that these two duplexes also decrease GFP-LC3 spots and WAC message levels in GFP-LC3-HEK cells (Figure 7.3, part a,b,e,f). As duplex-01 and duplex-02 also reduced GFP-LC3 spots and WAC mRNA levels (Figure 7.2), I ordered these two duplexes and tested them along side duplex-03 and -04. Duplex-02 was as efficient at decreasing GFP-LC3 spots, WAC mRNA and LC3 lipidation in HeLa cells but again duplex-01 was least able to inhibit GFP-LC3 spots and LC3 lipidation (Figure 7.3, part a,b,c,d), most likely as a result of its inability to reduce WAC mRNA levels to the extent of the other three Dharmacon siRNA duplexes.

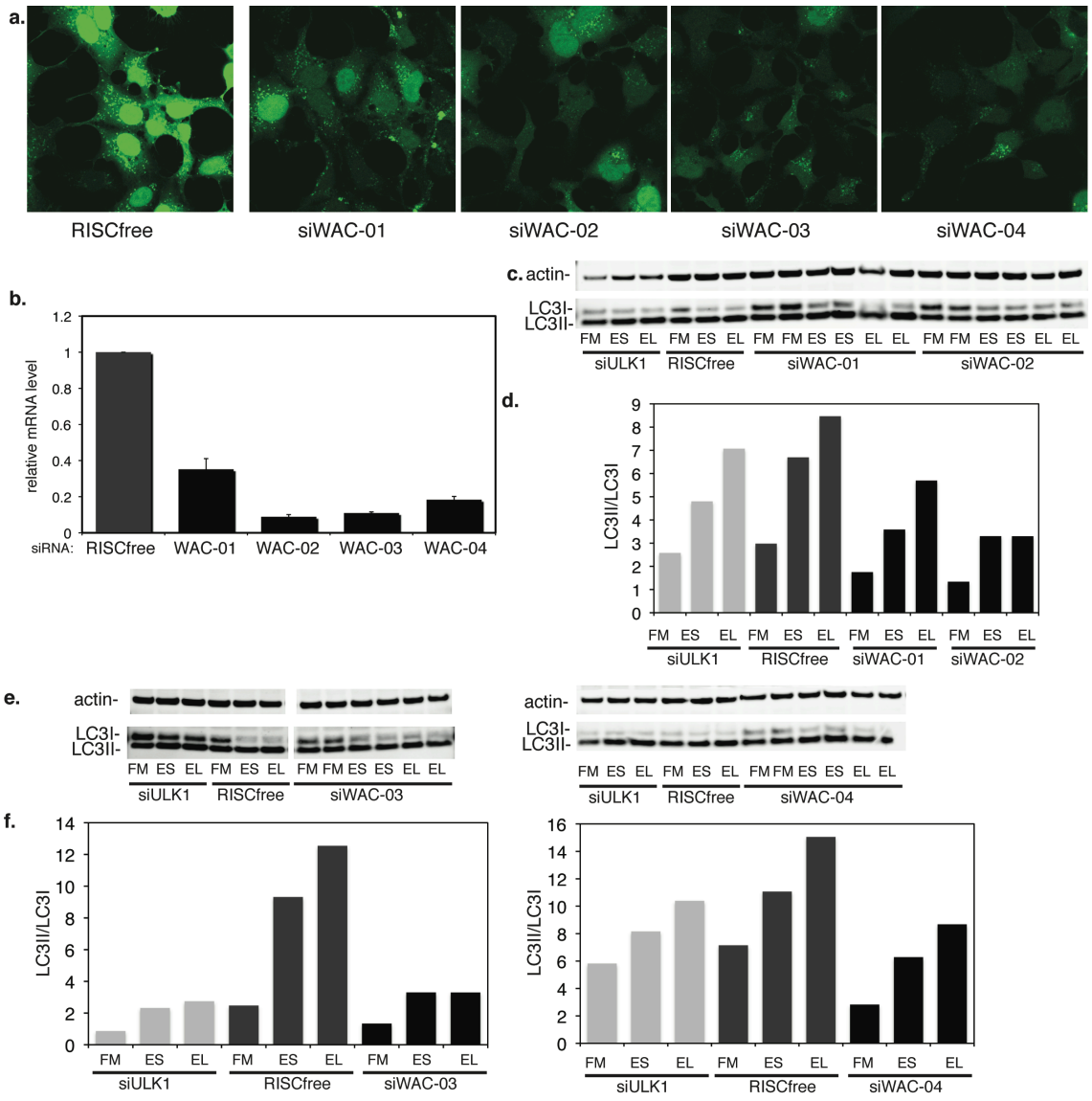

Figure 7.3 All four Dharmacon WAC siRNA duplexes reduce autophagy and do so in an mRNA dose-dependent manner

a. GFP-LC3 confocal images at 63x after knock-down with indicated siRNA duplex and induction of autophagy by incubation in EBSS plus 0.25mg/mL leupeptin. Images were captured with the same laser settings and levels were changed in Photoshop using the same adjustments. **b.** Quantification of WAC mRNA levels in GFP-LC3-HEK cells as determined by qRTPCR. Error bars represent the standard deviation derived from triplicate wells. **c.** Anti-Actin and -LC3 blot after indicated siRNA treatment in HeLa cells and incubation in full medium (FM), EBSS (ES) or EBSS plus 0.25mg/mL leupeptin (EL). **d.** Quantification of LC3II/LC3I after indicated siRNA and incubation conditions. LC3II/LC3I values for siWAC-01 and siWAC-02 are the averages of duplicates. The experiment was done twice; representative blots are shown. **e.** Anti-Actin and -LC3 blot after indicated siRNA treatment in HeLa cells and incubation in FM ES or EL. **f.** Quantification of LC3II/LC3I after indicated siRNA and incubation conditions. LC3II/LC3I values for siWAC-03 and siWAC-04 are the averages of duplicates. The experiment was done four times; representative blots are shown.

Next I asked whether WAC could be shown to be a positive regulator of autophagy using an alternate assay, p62 degradation. As discussed previously, p62 is specifically degraded by autophagosomes and its lack of degradation during starvation indicates a defect of autophagy. After starvation the levels of p62 decrease in RISCfree control siRNA-treated cells (Figure 7.4, panel a). Knock-down of ULK1 or WAC inhibits p62 degradation and the protein accumulates. Interestingly, the levels of p62, when normalised to actin loading, are higher in siWAC-treated cells as opposed to siULK1 treated cells perhaps suggesting that WAC is also required for the non-autophagic degradation of p62 by ubiquitin-proteasome system (Figure 7.4, panel b). I confirmed that WAC mRNA levels were depleted in this experiment (data not shown) but also wished to confirm that the increase in p62 levels after WAC knock-down was not due to an transcriptional upregulation of the p62 gene. To these ends, I plated GFP-LC3-HEK cells at the same density as those used in the p62 degradation assay described here and measured p62 mRNA levels by qRTPCR. Unexpectedly, knock-down of WAC decreased p62 mRNA levels (Figure 7.4, panel c) confirming that the accumulation of p62 after knock-down is due to a post-translational event.

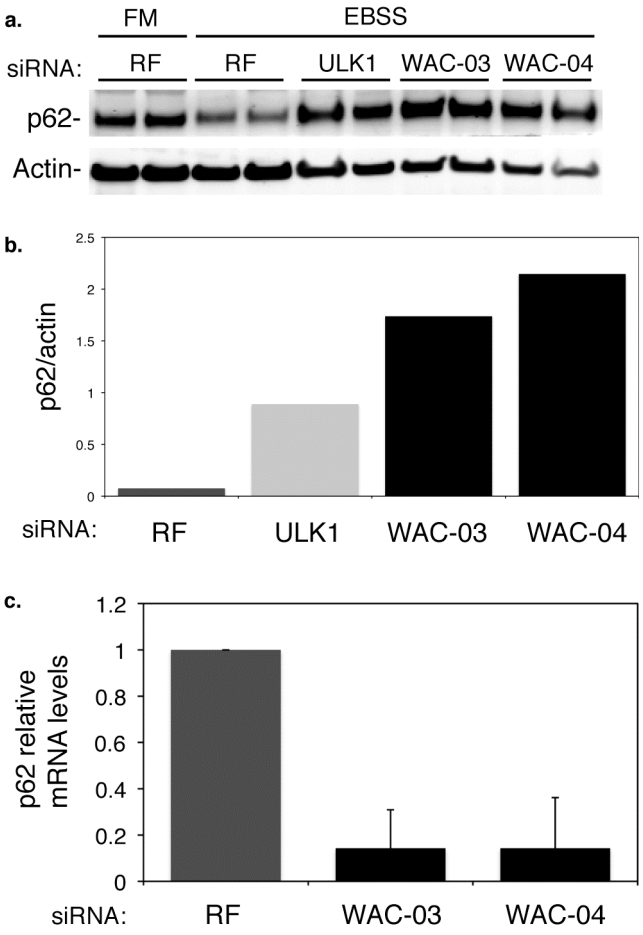

Figure 7.4 Knock-down of WAC leads to an accumulation of p62
a. Anti-p62 and -actin blot after indicated siRNA treatment in GFP-LC3-HEK cells and incubation in full medium (FM) or EBSS (ES) for 4 hours. **b.** Quantification of p62/actin after indicated siRNA in starvation conditions (EBSS for 4 hours). The experiment was done twice; representative blots are shown. **c.** Quantification of p62 mRNA levels in GFP-LC3-HEK cells after RISCfree or WAC knock-down as determined by qRTPCR. This experiment was done once.

Three siRNA duplexes against WAC manufactured by Ambion were also tested for their ability to knock-down WAC and modulate autophagy. All three siRNA duplexes reduced GFP-LC3 spots and WAC mRNA levels (Figure 7.5, panel a,b). Duplex-55 was best at decreasing GFP-LC3 spots and endogenous LC3 lipidation in HeLa cells. Duplex-53 did not inhibit LC3 lipidation perhaps because Duplex-53 does not target WAC isoforms Q9BTA9.2 and Q9BTA9.3 (Figure 7.1). It should, however be noted that the effectiveness of knock-down is questionable in this experiment because ULK1 knock-down is not having a strong effect on LC3 lipidation. Of the seven WAC siRNA duplexes tested, five greatly reduce WAC mRNA levels and inhibit autophagy as measured by LC3 lipidation.

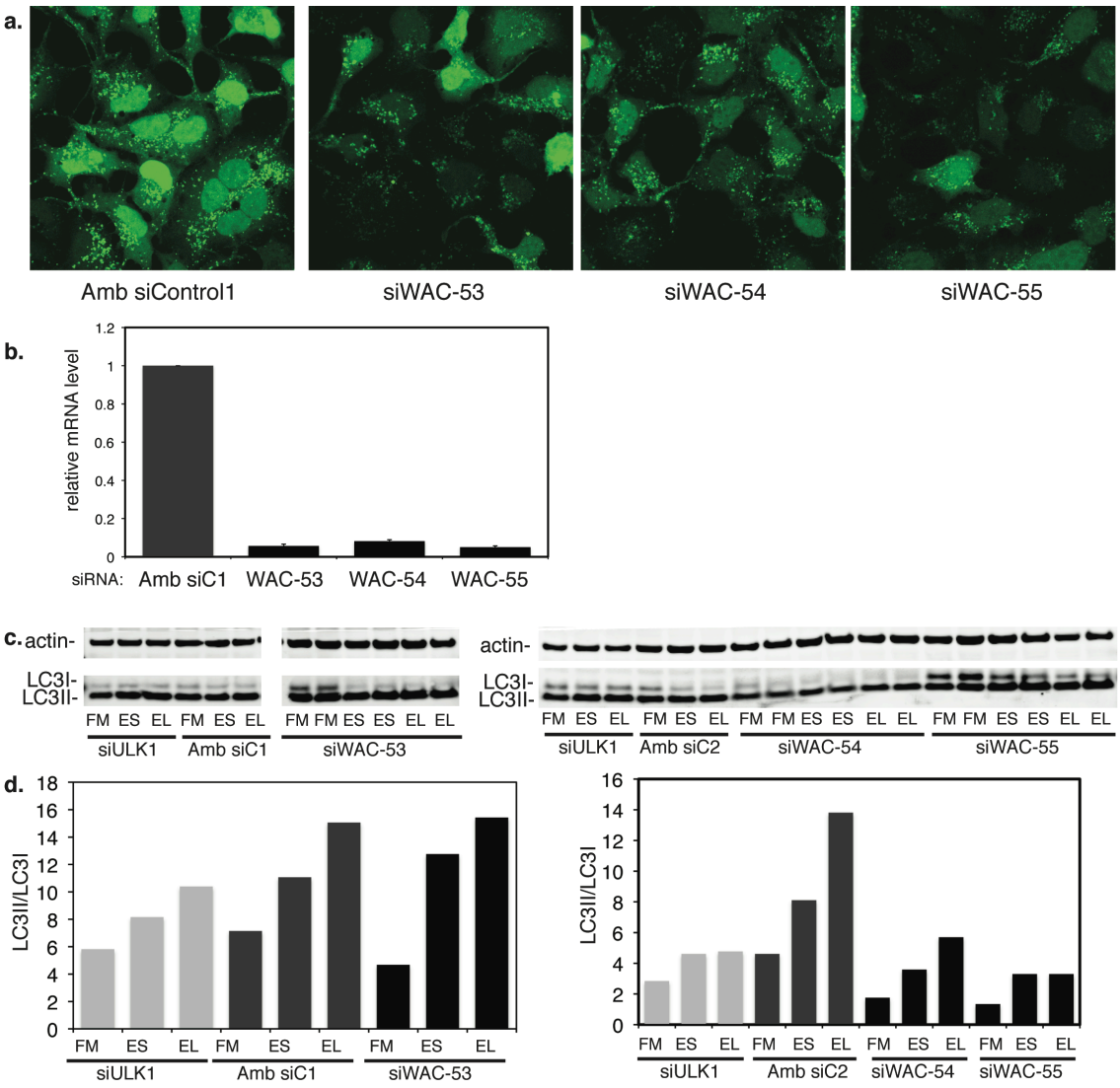

Figure 7.5 Ambion siRNA duplexes against WAC decrease GFP-LC3 spots, WAC mRNA levels and LC3 lipidation to various extents

a. GFP-LC3 confocal images at 63x after knock-down with indicated siRNA duplex and induction of autophagy by incubation in EBSS plus 0.25mg/mL leupeptin. Images were captured with the same laser settings. **b.** Quantification of WAC mRNA levels in GFP-LC3-HEK cells as determined by qRTPCR. Amb siC1 is Ambion siControl pool 1. Error bars represent the standard deviation derived from triplicate wells. **c.** Anti-Actin and -LC3 blot after indicated siRNA treatment in HeLa cells and incubation in full medium (FM), EBSS (ES) or EBSS plus 0.25mg/mL leupeptin (EL). **d.** Quantification of LC3II/LC3I after indicated siRNA and incubation conditions. Amb siC2 is Ambion siControl pool 2. LC3II/LC3I values for siWAC-53, siWAC-54, and siWAC-55 are the averages of duplicates. The experiment was done twice; representative blots are shown.

I next attempted to clone WAC into a mammalian expression vector in order to measure the effect on autophagy after WAC overexpression. I obtained the open reading frame corresponding to the canonical isoform, NM_016628, and cloned WAC into pcDNA3.1(-) adding a myc tag to either the N- and C-terminals or a FLAG tag to the C-terminal of the WAC ORF. None of these three constructs expressed in HEK cells after transfection, as measured by anti-myc or anti-FLAG blotting. Xu and Arnaout also attempted to overexpress a FLAG-tagged WAC construct but could not detect the fusion protein in three cell-lines tested including HEK and HeLa cells (Xu and Arnaout, 2002). After overexpression followed by immuno-concentration and western blotting, the authors did detect a band of 93 kDa that they conclude is a tyrosine-phosphorylated form of the protein.

We generated rabbit polyclonal antibodies against two N-terminal peptides and a C-terminal peptide of WAC. We affinity purified the serum of a rabbit immunised against NT2 (Figure 7.1) and I probed HEK cell lysates treated with either RISCfree control siRNA or WAC Dharmacon siRNA duplexes -01 through -04 with this anti-WAC antibody. In RISCfree knock-down cell lysates, WAC appears as a doublet band with the upper band migrating at approximately 81 kDa and the lower band at 72 kDa (Figure 7.6, panel a). These two bands could represent WAC isoforms 1 and 2 though they are migrating slower by SDS-PAGE than their predicted molecular weights of 71.5 and 65.5 kDa respectively. One possibility is that both isoforms are post-translationally modified. Another possibility is that the major, upper band is a post-translationally modified version of isoform 1. For instance, the addition of ubiquitin would add 8.5 kDa to the molecular weight of WAC, though it is unusual that this modified form would make up such a large percentage of the overall protein pool. Both protein bands are however specific to WAC, as their levels are reduced after knock-down with the four WAC siRNA duplexes. The extent of reduction correlates with the decrease of WAC mRNA levels of corresponding lysates (Figure 7.6, panel b). The amount of WAC protein does not appear to change after cells were incubated in starvation medium.

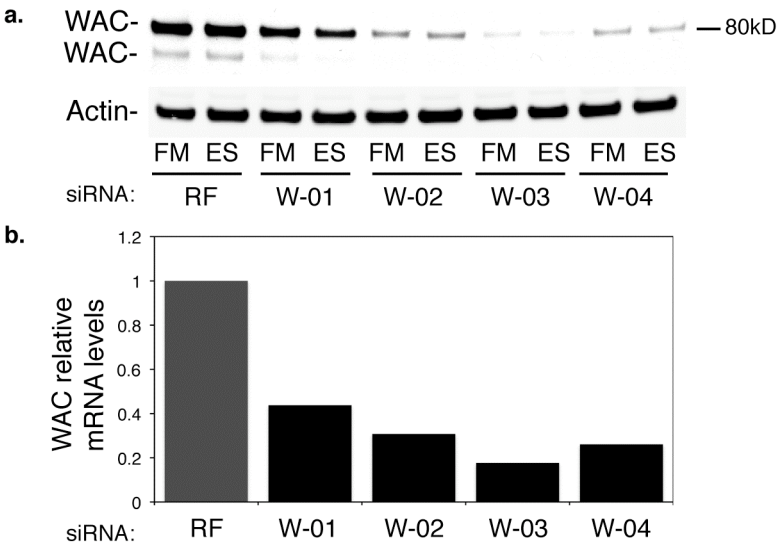

Figure 7.6 WAC antibody by western blot
a. Anti-WAC and -Actin blots after HEK cells are treated with the indicated siRNA and incubated in full medium (FM) or EBSS (ES) for 2 hours. siW is siWAC. **b.** Relative WAC mRNA levels after indicated siRNA treatment in HEK cells corresponding to a.

When examined by immunofluorescence, endogenous WAC displays both a nuclear and cytoplasmic staining pattern though the majority of the protein appears to be nuclear and reside in subdomains, similar to the FLAG-tagged WAC expression pattern seen previously (Xu and Arnaout, 2002) (Figure 7.7, panel a,b). Indeed, WAC has a predicted nuclear localisation signal (NLS) in the middle of its protein sequence. I do not observe WAC on the plasma membrane suggesting that it does not interact with polycystin 1 as it did by yeast-two-hybrid (Xu and Arnaout, 2002). But I do observe cytoplasmic WAC found on punctate structures that, when present, occur throughout the non-nuclear cell area. Strangely, not every cell displays this punctate WAC staining. The levels of WAC protein, the percentage of cells that display the punctate WAC staining, and the number of WAC puncta do not change after the cells are incubated in EBSS (Figure 7.7, panel a). After knock-down of WAC, the nuclear pool of the protein is drastically reduced, and some reduction in the number of cytoplasmic vesicular structures is observed.

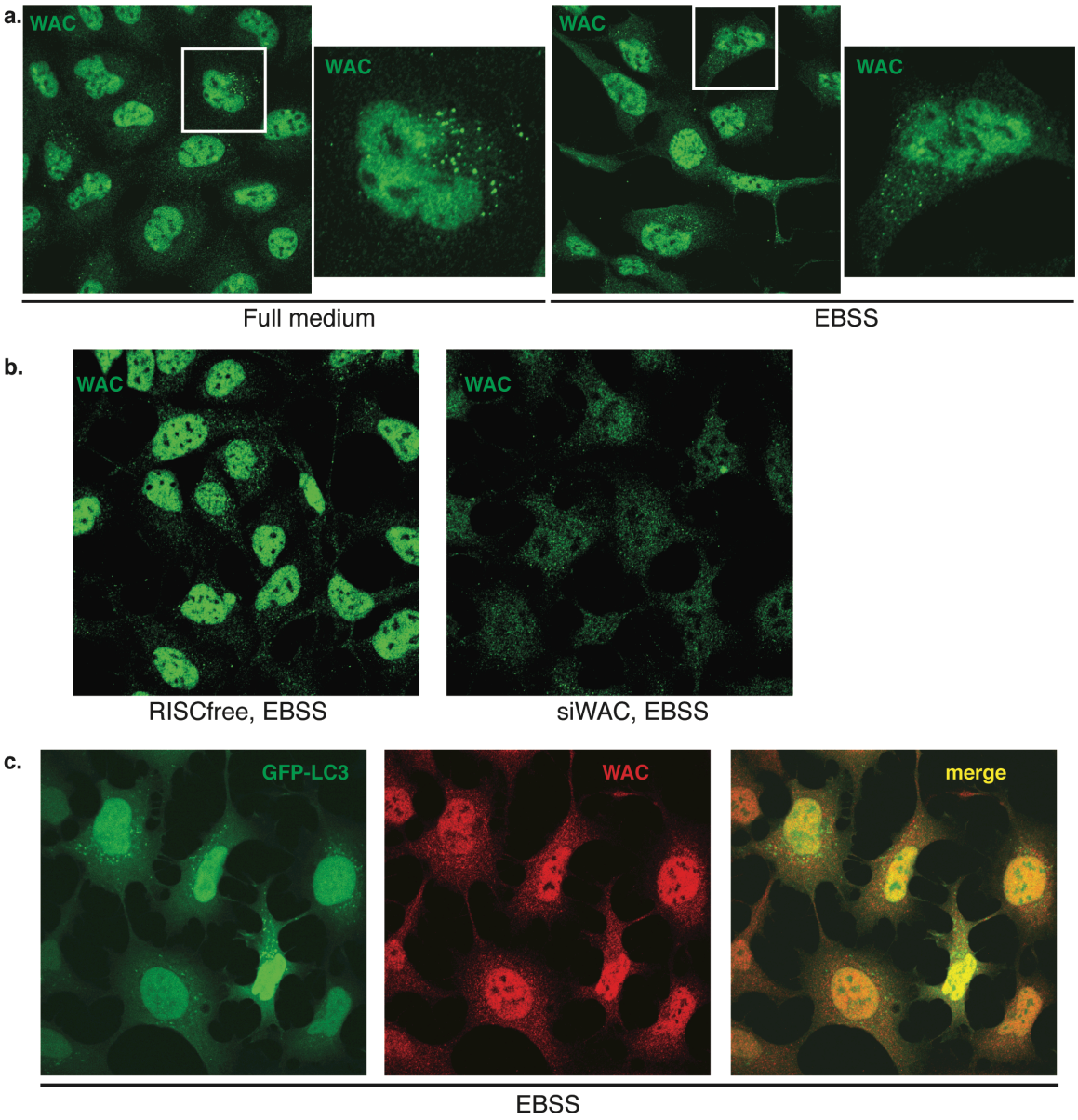

Figure 7.7 WAC is seen in the nucleus and cytoplasm of HEK cells, in the nucleus of GFP-LC3-HEK cells and is depleted by siRNA knock-down
a. HEK cells are incubated in full medium or EBSS, fixed, and labelled with anti-WAC antibody. Images were captured at 63X magnification or a zoomed area, indicated by boxes. **b.** HEK cells are treated with RISCfree siRNA or a pool of siWAC duplexes -02,-03, and -04, incubated in EBSS for 2 hours, fixed, and labelled with anti-WAC antibody. **c.** GFP-LC3-HEK cells are incubated EBSS, fixed, and labelled with anti-WAC antibody.

I next asked whether the punctate cytoplasmic WAC structures colocalise with GFP-LC3 spots in GFP-LC3-HEK cells. Such colocalisation was not seen (Figure 1.7, panel c) and surprisingly, the occurrence of cytoplasmic WAC structures seemed to be decreased in the GFP-LC3-HEK cell line compared to HEK293s, though this has not

been quantified. Of note, WAC does not contain a LIR domain, or LC3 interacting region, thought to comprise of the amino acids sequence DWxxL (Kirkin et al., 2009).

I determined that cytoplasmic WAC did not colocalise with GFP-LC3 but asked with what other autophagy markers it could be found together in HEK cells. As I showed that WAC is required for the degradation of p62, I double-labelled cells with WAC and p62 and saw that WAC could be found on a small number of p62-positive puncta though a vast amount of colocalisation was not seen (Figure 1.8, panel a, b). I triple-labelled HEK cells with p62 and GABARAP in order to determine whether WAC punctate structures are positive for an alternate mammalian Atg8 family member, GABARAP. Again, one or two WAC and p62 double positive vesicular structures were seen and also, GABARAP is seen to colocalise with WAC on small and large cytoplasmic structures (Figure 7.8, panel b). I next asked whether WAC was found together with the early autophagosome marker Atg12 and saw that though GABARAP does colocalise with Atg12 and WAC again is seen together with GABARAP on vesicular structures these puncta are mutually exclusive for WAC and Atg12 and no triple-staining of WAC, GABARAP and Atg12 is seen (Figure 7.8, panel c).

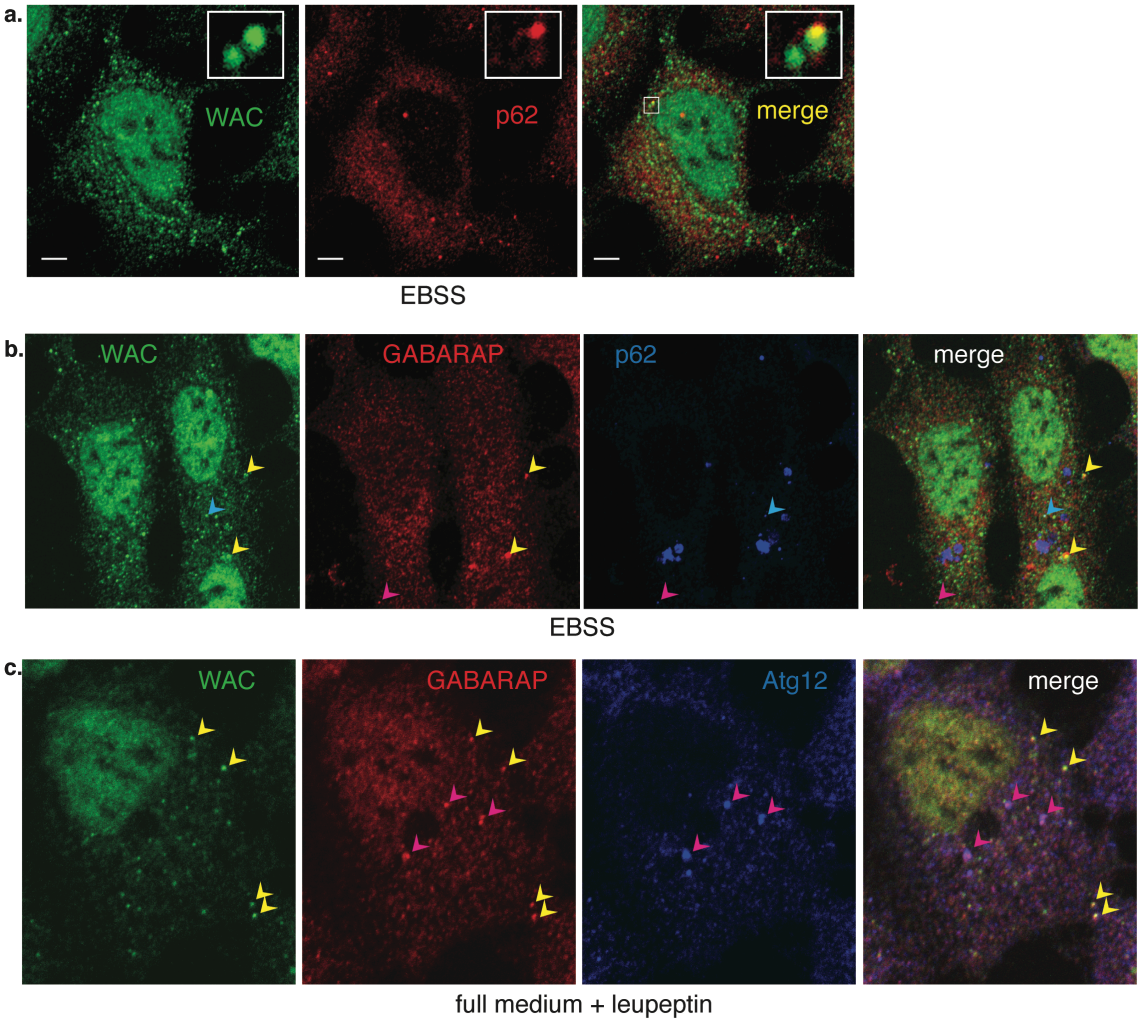

Figure 7.8 WAC can be found on p62-positive puncta and colocalises with GABARAP, but not with Atg12

a. HEK cells were incubated in EBSS for two hours, fixed, and labelled with anti-WAC and anti-p62 antibodies. Enlarged inset shown in merge panel. Scale bar equals 5µm. **b.** HEK cells were treated with RISCfree control siRNA, incubated in EBSS for two hours, fixed, and labelled with anti-WAC, anti-GABARAP and anti-p62 antibodies. Yellow arrows represent WAC and GABARAP colocalisation. Cyan arrows show WAC- and p62-positive structures. Purple arrows show GABARAP- and p62-positive structures. **c.** HEK cells were treated with RISCfree control siRNA, incubated in full medium plus 0.25mg/mL leupeptin for 24 hours, fixed, and labelled with anti-WAC, anti-GABARAP and anti-Atg12 antibodies. Yellow arrows represent WAC and GABARAP colocalisation. Purple arrows represent GABARAP- and Atg12-positive structures.

Unlike SCOC, WAC does not overlap with the markers of early autophagosome formation events, Atg12 and LC3. Instead, WAC is occasionally found on p62-positive structures and shows more extensive overlap with GABARAP. Though both LC3-like and GABARAP-like Atg8 family members have been shown to be present in cells and are required for mammalian autophagy to properly occur, recent research suggests that the two proteins perform functions at different stages (Weidberg et al., 2010).

Specifically, Weidberg *et al* propose that LC3s act at the earlier stages of autophagosome membrane elongation while GABARAPs act slightly later and are perhaps required for the closing or sealing the autophagosome. One possibility therefore is that WAC is also required for the sealing of the autophagosome and cooperates with GABARAP to do so. Of note, WAC does not colocalise with the lysosomal marker LAMP2 suggesting that WAC is not acting on autophagosomes at the stage where they fuse with lysosomes.

Because I know that WAC is required for LC3 lipidation and have seen that WAC and GABARAP colocalise, I assessed GABARAP lipidation by western blotting after knock-down of WAC. Knock-down of WAC decreased the amount of GABARAPII seen in starvation conditions (EBSS and EBSS plus leupeptin) as knock-down of ULK1 did. However, knock-down of WAC did not appear to decrease GABARAP lipidation in full medium as ULK1 knock-down did (this experiment was done once, data not shown).

In order to show that WAC can be found together in the cell with proteins suggested to be WAC binders by yeast-two-hybrid I performed immunofluorescence experiments with UBQLN4 and an overexpressed huntingtin fusion protein. Endogenous UBQLN4 appears in the nucleus and cytoplasm of HEK cells and extensive overlap of the two proteins is seen in the nucleus of the cell and occasional overlap in seen in cytoplasmic structures (Figure 7.9, panel a). I have not, however, determined if the UBQLN4 staining is specific, for instance by knocking down UBQLN4 and comparing the endogenous UBQLN4 staining to a control. In order to visualise the degree to which WAC overlaps with huntingtin protein, I overexpressed a mutant form of Htt in which exon 1 contained an abnormally expanded stretch of 80 glutamine repeats which was fused to GFP which has been shown to provide a cellular model for Huntington's disease (Tower et al., 2010). After transfection of HEK cells with this GFP-HttQ80 construct, I observed cells with various degrees of overexpression of the fusion protein and also various degrees of its aggregation. In a cell with some GFP-HttQ80 aggregation I saw some WAC staining on these cytoplasmic structures (Figure 7.9, panel b). Although, as discussed above, WAC expression has been shown to be altered in Huntington's disease and its upregulation perhaps suggests that WAC and mutant Htt do interact. It would also be interesting to

ask whether WAC colocalises with wild-type huntingtin fragments, replicating the yeast-two-hybrid data (Kaltenbach et al., 2007).

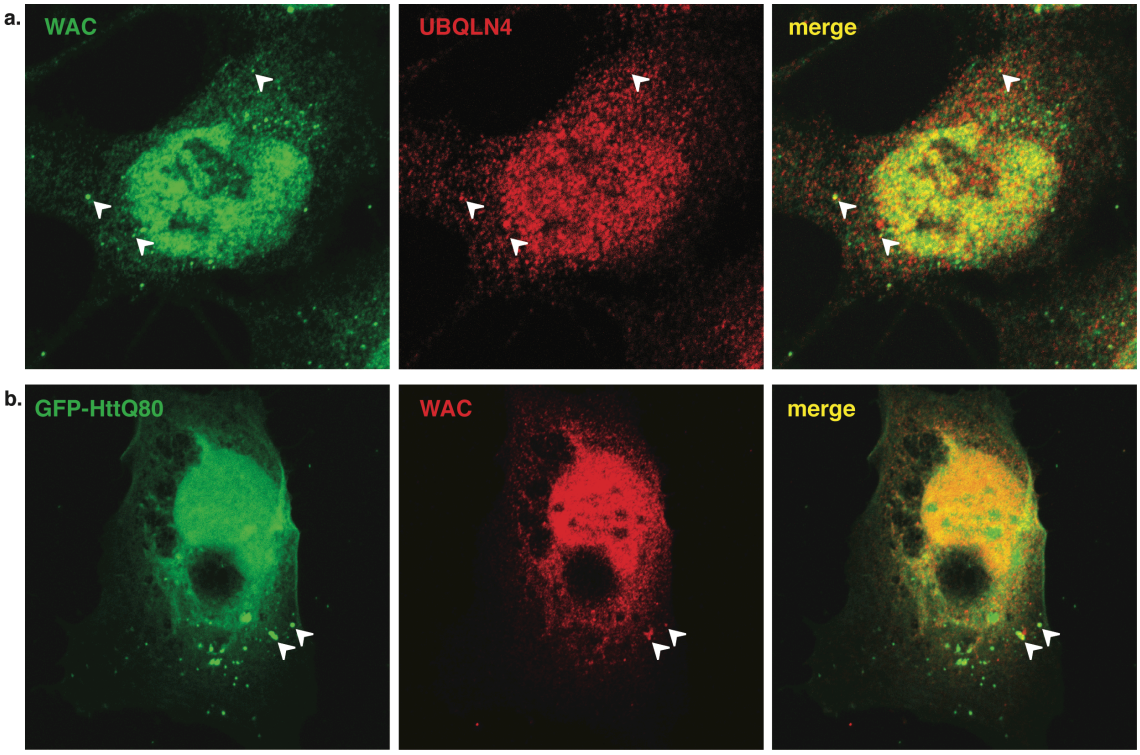

Figure 7.9 WAC shows partial co-occurrence with endogenous UBQLN4 and overexpressed, mutant Htt
a. HEK cells were fixed and labelled with anti-WAC and anti-p62 antibodies. Arrows show instances of co-occurrence **b.** HEK cells were transfected with GFP-HttQ80, fixed and labelled with anti-WAC antibodies. Arrows show instances of co-occurrence.

7.3 Regulation of WAC by ULK1

While analysing multiple experiments involving WAC knock-down and knock-down of ULK1 as a control, I noticed that WAC protein levels were decreased when ULK1 was knocked down. After HEK cells are treated with an siRNA duplex targeting ULK1, both the upper a lower molecular weight bands of WAC are less (Figure 7.10, panel a). Additionally, knock-down of WAC also appears to decrease the amount of ULK1 protein seen by western blot (Figure 7.10, panel b). Taken together, these results suggest that ULK1 is regulating WAC protein levels and reciprocally, WAC is regulating ULK1 protein levels though I have not investigated whether this is occurring by destabilisation or some other mechanism. In order to visualise this decrease in HEK cells and ascertain whether this ULK1-mediated decrease was affecting the nuclear or

cytoplasmic pool of WAC, I examined endogenous WAC staining by immunofluorescence after ULK1 knock-down. Though the overall amount of WAC protein seemed to be slightly diminished after ULK1 siRNA treatment, what was more striking was the reduction of cytoplasmic WAC vesicular structures (Figure 7.10, panel c). This was quantified using large panels of cells and IMARIS software.

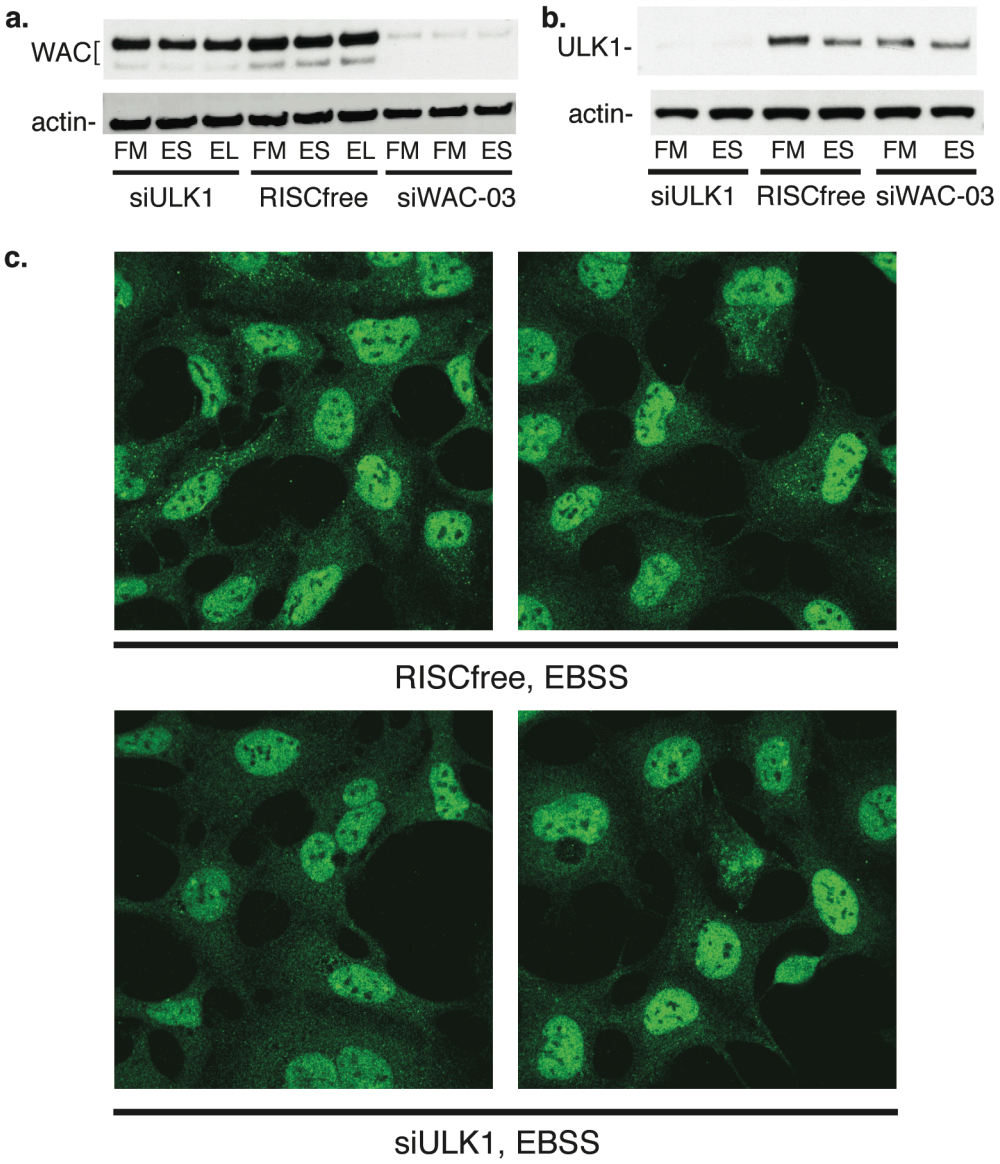

Figure 7.10 Knock-down of ULK1 decreases WAC protein levels and the occurrence of WAC-positive cytoplasmic puncta

a. Anti-WAC and -Actin blots after knock-down with an ULK1 or WAC siRNA duplex or RISCfree control. This experiment was done four times, a representative blot is shown. **b.** Anti-ULK1 and -Actin blots after knock-down with an ULK1 or WAC siRNA duplex or RISCfree control. This experiment was done twice. **c.** Two confocal images at 63x per condition of HEK cells treated with RISCfree control or ULK1 siRNA, starved for two hours, fixed and labelled with anti-WAC antibody. This experiment was done once.

As ULK1 is a kinase, one way that ULK1 could potentially regulate WAC is through phosphorylation. Xu and Arnaout propose that WAC has a great potential for regulation by other proteins because it is enriched for proline, serine and threonine residues (Xu and Arnaout, 2002). 9.4% of its amino acid sequence consists of proline residues, which are possible binding sites for other proteins. But also, WAC is rich in serines and threonines (15.8% and 7.1% respectively) and these amino acids are potential phosphorylation sites. In fact, WAC has 25 listed phosphorylation sites and one potential acetylation site at site 302 (Figure 7.11). WAC could be signalled to move in or out of the nucleus by phosphorylation, possibly by ULK1, and WAC's cellular distribution and translocation to or exclusion from the nucleus could control autophagy initiation.

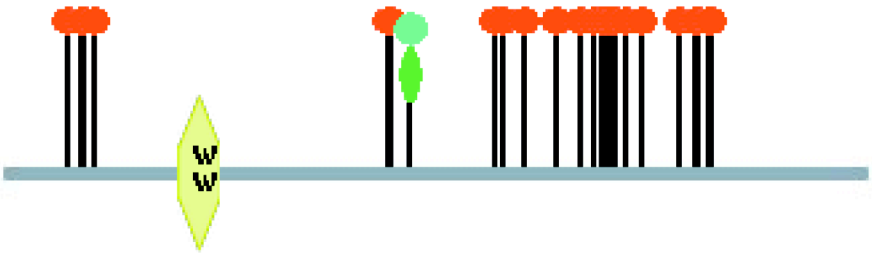

Figure 7.11 Putative post-translation modifications of WAC
Schematic obtained from HPRD of WAC protein sequence with potential sites of post-translational modifications. WW is the WW domain. Red-tipped lines represent phosphorylation sites; the green-tipped line represents a potential acetylation site.

7.4 WAC and the Ubiquitin-Proteasome system

WAC is reported to bind ubiquilin 4, the UBQ- and UBA-domain containing ubiquitin-specific protease and I have shown that WAC can be found together with UBQLN4 and p62, the ubiquitin-binding autophagy and proteasome substrate (Figure 7.9a, Figure 7.8a, respectively). I have also shown that WAC is required for the degradation of p62 perhaps beyond that of a protein that is merely required for autophagy. In turn, I wished to examine the role of WAC in the ubiquitin-proteasome system (UPS) and determine whether WAC is required for this degradation system. To these ends, I measured the effect of WAC knock-down on two UPS reporter cell lines stably over-expressing the ubiquitin mutant Ub^{G76V} fused to GFP or YFP. This fusion

protein is properly folded and soluble but the mutation prevents cleavage of the Ub from the GFP, targeting the fluorescent protein to the proteasome and thus serves a read-out for the efficiency of the UPS (Dantuma et al., 2000), (Menendez-Benito et al., 2005). When the UPS is compromised, for example after treatment with the proteasome inhibitor MG132, the Ub^{G76V}-GFP or Ub^{G76V}-YFP accumulates in the cell and can be quantified by western blotting or immunofluorescence. First I tested the effect of WAC and ULK1 knock-down HeLa Ub^{G76V}-GFP cell line. In RISCfree-treated cells, the fusion protein, which runs at approximately 39 kDa, is detected in full medium, its amounts decrease during starvation and starvation in the presence of leupeptin and drastically increases when the proteasome is inhibited with MG132 (Figure 7.12, panel a). Treatment with WAC and ULK1 siRNA did not alter the amount of Ub^{G76V}-GFP detected in full medium. This contrasts recent work by Korolchuk *et al* who show that inhibition of autophagy with siRNA against ATG7 and ATG12 impaired proteasomal degradation, which they determine is due to the autophagy deficiency-specific accumulation of p62 (Korolchuk et al., 2009). As before, I observed that ULK1 knock-down slightly decreased cellular WAC levels and vice versa. Surprisingly, I noticed a significant decrease in p62 levels after WAC knockdown as detected by western blot, even in starvation conditions when I had previously seen an accumulation of p62, though in a different cell line, GFP-LC3-HEK cells and after a longer starvation period. As before, I performed qRTPCR to determine the effect of WAC knock-down on p62 mRNA levels and again observed a decrease in p62 transcription (Figure 7.12, panel b).

I again employed the UPS reporter system but in a different cell line, the MelJuSo melanoma, that the authors claim are easy to transfect, accumulate reporter very well upon inhibition of the UPS and are excellent for imaging purposes (Menendez-Benito et al., 2005). This time I observed a decrease in the amount of Ub^{G76V}-YFP after WAC knock-down suggesting that degradation via the proteasome was proceeding at a greater rate. I observed that the cell line contained vastly more amounts of LC3II compared to LC3I suggesting a very high rate of basal autophagy (data not shown). I also examined endogenous WAC staining in these cells and did not see colocalisation of WAC and Ub^{G76V}-YFP in full medium or starvation conditions (data not shown).

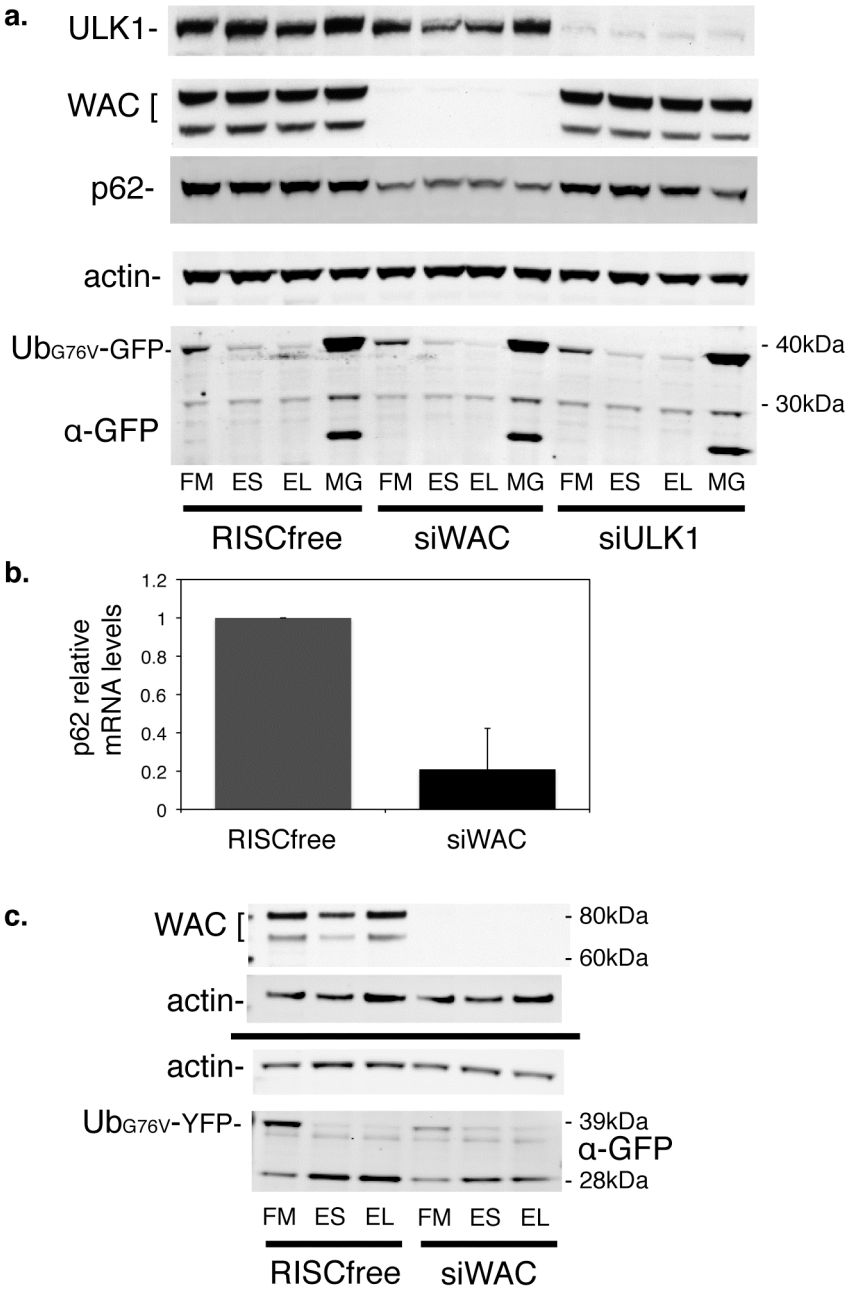

Figure 7.12 The effect of WAC knock-down on UPS reporter cell lines
a. Anti-ULK1, -WAC, -p62, -Actin, and -GFP blots after HeLa Ub^{G76V}-GFP cells were knocked down with ULK1 or WAC siRNA or RISCfree control. Cells were incubated in full medium (FM), EBSS (ES), EBSS plus 0.25mg/mL leupeptin (EL) or 10μM MG132 (MG) for two hours. This experiment was done once. **b.** Relative p62 mRNA levels after HeLa Ub^{G76V}-GFP cells were knocked down with WAC siRNA or RISCfree control as measured by qRTPCR with p62 primers. **c.** Anti-WAC, -Actin and -GFP blots after MelJuSo Ub^{G76V}-YFP cells were knocked down with WAC siRNA or RISCfree control. Cells were incubated in full medium (FM), EBSS (ES), EBSS plus 0.25mg/mL leupeptin (EL) for two hours. This experiment was done once.

To summarise, WAC is very thoroughly validated in that the siRNAs have a reliable effect on autophagy assays consistent with WAC being a positive regulator of

autophagy. Though I was unable to overexpress tagged versions of the protein, we have made an affinity purified antibody that detects endogenous WAC by western blot and in the cell by indirect immunofluorescence. WAC colocalises with autophagy markers, GABARAP and p62 but not Atg12 and LAMP2. Its protein levels may influence ULK1 and conversely, in the absence of ULK1, WAC may be destabilised. WAC is also required for p62 degradation and its knock-down possibly affects the ubiquitin-proteasome system.

7.5 WAC discussion

In HEK cells, endogenous WAC is seen mostly in the nucleus of the cell but also in the cytoplasm. Often, cytoplasmic puncta are seen and when a cell does have these puncta there seem to be quite a lot of them, but their occurrence does not seem to increase upon starvation (Figure 7.7). Occasionally, these puncta overlap with GABARAP and p62 but WAC is not found with a marker for the isolation membrane, Atg12 (Figure 7.8). It has been suggested that GABARAP is required for the sealing of the autophagosome (Weidberg et al., 2010) and it would be interesting to ask whether WAC is also required for sealing autophagosomes. It would also be interesting to ask whether WAC directly interacts with GABARAP. Though WAC does not possess a canonical LIR (DWxxL), there is an amino acid stretch towards the C-terminal of WAC with the sequence FSENL. Recently, it has been suggested that the sequence FxxL, when the first x is acidic, can also serve as an LC3 interacting region (Terje Johansen, Autophagy GRC, 2010) and the sequence FSENL, with Glutamate (E) being an acidic residue, could fit that model. If it were determined that WAC and GABARAP interact it could be asked whether this interaction requires the FSENL region and if the interaction is in turn required for WAC's positive regulation of autophagy. Interestingly, GABARAP has been crystallised (Bavro et al., 2002), so perhaps the potential binding region could be visualised and drug targets that disrupt this binding could be found.

Only a subset of WAC puncta colocalise with GABARAP and it would be interesting to ask whether WAC colocalises with other vesicular markers such as those of endosomes (APPL1, EEA1, and Rab5 for early endosomes, Rab11 for recycling endosomes or VAC14 and LBPA for MVBs). ULK1 is also found on vesicular

structures and as I have shown that ULK1 seems to regulate WAC levels, I would like to know if WAC and ULK1 interact in the cell. Though I cannot test this endogenously (both antibodies are polyclonal) I could overexpress ULK1 and see if it colocalises with endogenous WAC. One way that ULK1 could regulate WAC is by phosphorylation. Xu and Arnaout state that when they immunoprecipitate tagged WAC they visualise a band of approximately 93 kDa that is phospho-tyrosine positive (Xu and Arnaout, 2002). I performed a fractionation experiment in which cytosolic, membrane-bound and nuclear portions of HEK cells were separated and probed for WAC. Surprisingly, a band of higher molecular weight (about 93 kDa) was seen in the nuclear fraction. Usually a post-nuclear supernatant (after a five minute spin at 12,000 rpm) is run when probing for WAC as in Figure 7.6. But when the nuclear fraction is run, this higher band appears and interestingly, there appears to be less of this higher band when the cells are starved. Like FOXO3 whose retention in the cytoplasm is the result of its phosphorylation by AKT1 (Brunet et al., 1999), WAC's cellular distribution and translocation to or exclusion from the nucleus could similarly be controlled by ULK1 and possibly as the result of autophagy initiation.

As discussed above, there are many potential sites of phosphorylation on WAC (Figure 7.11) and another kinase that has the potential to regulate WAC is dystrophia myotonica-protein kinase (DMPK). DMPK has been shown to interact with GABARAP (Stelzl et al., 2005) and both ubiquilin 4 and ataxin 1 (Lim et al., 2006). A mutation in DMPK that leads to a repeat expansion of a region of the protein is linked to myotonic dystrophy (Boucher et al., 1995), and recently it was shown that overexpression of an isoform of DMPK with a long tail anchor led to fragmentation and clustering of mitochondria in a perinuclear region as well as increased autophagy (Oude Ophuis et al., 2009). In my screen, knock-down of DMPK led to an increase in GFP-LC3 spot parameters though only one of the four siRNA duplexes increased spots in the deconvolution screen (Appendix Table 9.5). I observed an interesting cellular phenotype when examining DMPK knock-down cells after the repeat screen; the cells were large and multinuclear, suggesting a defect in cytokinesis. Perhaps DMPK regulates autophagy by phosphorylating WAC or through interactions with WAC-interacting proteins.

The data that I have presented regarding WAC and p62 is puzzling. I have shown that knock-down of WAC inhibits p62 degradation and the increased amount of p62 is not due to an increased amount of p62 transcription because WAC knock-down actually decreases p62 mRNA levels (Figure 7.4). I have shown that WAC is present in the nucleus and it was originally characterised as potentially involved in pre-mRNA splicing machinery and colocalises with a marker of the splicing complex (Xu and Arnaout, 2002). Thus, WAC has the potential to regulate p62 mRNA levels but also its post-translational degradation. Recently it was shown that p62 shuttles to the nucleus and upon treatment of cells with the nuclear export inhibitor leptomycin B (LMB), p62 stays in the nucleus where it colocalises with PML bodies (Pankiv et al., 2010). I asked whether WAC is also retained in the nucleus like p62 but found that it was not; after LMB treatment I did see p62 congregate in the nucleus and form aggregates similar to the PML bodies shown by Pankiv *et al* but nuclear WAC, did not visibly increase (though most WAC is in the nucleus of the cell normally) and did not colocalise with the p62 aggregates. WAC is however seen to occasionally colocalise with p62 in the cytoplasm of the cell (Figure 7.8).

WAC is also potentially linked to the UPS through another ubiquitin-interacting protein, ubiquilin 4. WAC is reported to bind to ubiquilin 4 (Lim et al., 2006) and I see some colocalisation between the endogenous ubiquilin 4 and cytoplasmic WAC puncta (Figure 7.9). I would like to perform a co-immunoprecipitation in HEK cells to determine if I can find the proteins together. Recently, Rothenberg *et al* showed that LC3 and ubiquilin 1 co-immunoprecipitate; they could not, however, detect an interaction between their purified proteins, suggesting that there may be a common interacting partner that stabilises the interaction (Rothenberg and Monteiro, 2010). Perhaps WAC could bridge the interaction between ubiquilin 4 and GABARAP, for instance, thus aiding in the regulation of both the UPS and autophagy pathway by ubiquilins and helping ubiquilin to switch between the two. Consequently, WAC may also serve as a switch between the two pathways. Because WAC has a WW and a coiled-coil domain it may perform these functions by acting as an adaptor, bringing together components of the autophagy an UPS systems, such as ubiquilin 4. Another WW-domain-containing protein, salvador homolog 1 which contains two WWs,

provides a scaffold for the kinases and other proteins that direct the Hippo pathway of growth regulation (Tapon et al., 2002).

Preliminary experiments show that WAC may not be required for the UPS as its knock-down did not hinder the pathway (Figure 7.12). Instead, knock-down of WAC seemed to increase the degradation of the Ub^{G76V}-YFP reporter in MelJuSo cells. Perhaps WAC inhibits the UPS, favouring autophagic degradation and when WAC is removed from the cell autophagy is inhibited but ubiquitin-mediated degradation is increased. In this way, WAC may serve as an emergency brake for the UPS and this is how WAC toggles between the two pathways.

WAC may also regulate aggrephagy; WAC and huntingtin were shown to interact through a yeast-two-hybrid experiment (Kaltenbach et al., 2007) and I have shown that WAC colocalises with aggregated HttQ80 (Figure 7.9). I would like to confirm this interaction by co-IP and also ask whether WAC interacts with wild-type huntingtin as well as other aggregate-prone proteins. WAC may be required for aggrephagy and this may explain why WAC is upregulated in the symptomatic stages of Huntington's disease. A recently study showed that a failure in cargo-recognition is responsible for the inability for autophagy to degrade huntingtin aggregates, causing them to accumulate and become more toxic (Martinez-Vicente et al., 2010). The authors propose that there is an unknown factor, x, that recognises the cargo and allows it to be degraded by autophagy and perhaps WAC is this 'x factor.'

WAC is an interesting new regulator of autophagy with additional ties to the ubiquitin-proteasome system and aggrephagy. It is potentially highly regulated through multiple phosphorylation sites and may move in and out of the nucleus where it may affect transcription of autophagy proteins. I have shown that cytoplasmic WAC structures colocalise with autophagy markers and also with ubiquilin 4, a protein with links to both autophagy and the UPS. Perhaps through these functions and interactions, WAC is switch between autophagy, the UPS and a modulator of the degradation of aggregated proteins.

Chapter 8. Discussion

In the preceding pages I have described a genome-wide screen for mammalian autophagy. HEK cells stably expressing GFP-LC3 were knocked down with siRNA pools from the Dharmacon siGenome library and their ability to form GFP-LC3 tagged autophagosomes following amino acid starvation was assessed. The strongest candidates from the primary screen (both 'increasers' and 'decreasers' of spots) were re-assayed in a secondary screen and 190 robust hits were taken forward to a deconvolution screen. Of these, 20 genes had three out of four duplexes that repeated the primary spot phenotype and these were passed on for further validation. During this more-labour-intensive screen I quantified mRNA levels of the target protein after knock-down, visualised the effect of knock-down on GFP-LC3-HEK cells by confocal microscopy and analysed LC3 lipidation in full medium, starvation medium and starvation medium plus a lysosomal inhibitor in a different cell line.

siRNA for five genes targeted efficiently and decreased both GFP-LC3 spots and LC3 lipidation: LARP1, PAFAH1B2, SCOC, SUPT5H, and WAC. Experiments with two of these genes, SCOC and WAC, prove that they are true positive regulators of autophagy and through directed experiments, possible mechanisms for their positive regulation of autophagy were uncovered. These results confirm that the screen was successful in discovering bone fide autophagy proteins. siRNA for four genes targeted efficiently and increased both GFP-LC3 spots and LC3 lipidation: KIF25, TLK2, RASIP1, and WDR6. Though some of the results from the LC3 lipidation experiments should be repeated in order to confirm these findings, the seven genes that passed this further validation but not investigated further transcribe proteins with interesting binding partners and biological activities including a motor protein (KIF25) and a kinase (TLK2). Of the seven proteins not investigated further, SUPT5H, KIF25, WDR6 and TLK2 are potential drug targets and these drugs could become useful tools in the lab or even possible therapeutic agents in the clinic.

I discussed in Chapter 4 how the screens could have been improved, but overall the data generated from the primary, secondary and deconvolution screens were robust. All the data could be revisited or reanalysed and the information from the deconvolution

screen is especially valuable because individual siRNA duplexes were used. When combined with data regarding the ability of that individual siRNA to decrease its target's mRNA the GFP-LC3 spot data for all 190 genes is a valuable resource.

In summary, with a genome-wide screen, I have identified a number of known and novel components of autophagy including SCOC, a Golgi protein, and WAC, an uncharacterised protein. The proteins discovered may fill gaps in our knowledge of vesicle formation, regulation and even the source of the autophagosome membrane. Manipulation of autophagy in order to prevent and treat disease is a realistic goal and this work contributes towards that end.

Chapter 9. Appendix

9.1 Further explanation of screen data normalisation

9.1.1 B-score normalisation

Since the distribution of the raw values of each plate differed, the GFP-LC3 spot parameters SCPO, STAPO and STIPO were normalised to a reference point on each plate (Fig. 4.2 A). A B-score normalisation was performed in order to not only consider effects between plates, but also to account for any possible row or column effects. B-score normalisation is calculated for each well (W) in row *i* and column *j* on plate *p* by subtracting the estimated average of that plate (μ_p), the estimated offset of the well row (R_{ip}) and the estimated offset of the well column (C_{jp}):

$$W_{ijp} = \text{raw data value} - (\mu_p + R_{ip} + C_{jp})$$

The estimated row and column offsets are calculated by a two-way median polish (Tukey, 1960). By applying the B-score normalization, edge and row effects were reduced and as a consequence comparison of values amongst the plates was now more accurate.

9.1.2 Z-score normalisation

In order to produce a ranked list of all screened genes, Z-scores for each well (Z_{ijp}) were calculated. Z-scores represent the number of standard deviations away from a population mean and were calculated by dividing the well B-score (W_{ijp}) by the median absolute deviation of the plate (MAD_p):

$$Z_{ijp} = W_{ijp} / MAD_p$$

9.2 Screen data tables

inc.	GeneID	Gene Name	Cat No	SCPO r1	SCPO r2	SCPO r3	SCPO rank	STAPO r1	STAPO r2	STAPO r3	STAPO rank	STIPO r1	STIPO r2	STIPO r3	STIPO rank	OC r1	OC r2	OC r3	rank product
1	NM_003410	ZFX	M-006572-02	4.035	ND	4.995	3	3.299	ND	4.527	3	4.52	ND	6.382	1	164	0	155	2.1
2	NM_024829	FLJ22662	M-014472-00	3.974	5.599	4.671	2	3.628	5.149	5.033	1	3.707	5.826	4.869	5	187	247	222	2.2
3	NM_152636	FLJ33979	M-016943-00	3.569	ND	4.513	6	4.003	ND	4.862	2	4.147	ND	6.259	3	72	12	80	3.3
4	NM_000792	DIO1	M-011170-00	1.727	4.827	4.677	1	1.68	3.636	3.769	9	1.825	4.423	3.967	15	145	156	144	5.1
5	NM_000850	GSTM4	M-017188-00	2.677	4.38	4.495	4	1.567	3.815	3.86	4	2.454	5.718	4.178	10	77	53	94	5.4
6	NM_024913	FLJ21986	M-018816-00	2.847	3.987	4.101	7	2.356	3.297	3.997	13	4.349	5.269	5.419	2	206	159	150	5.7
7	NM_152611	C20ORF75	M-017183-00	2.293	ND	5.16	9	2.421	ND	3.887	21	3.106	ND	7.006	4	142	12	89	9.1
8	NM_012272	HYPC	M-012810-00	3.747	3.895	ND	8	3.384	2.79	ND	24	4.452	4.576	ND	6	156	142	15	10.5
9	NM_016284	KIAA1007	M-015369-00	3.095	3.531	3.865	13	2.653	3.074	3.12	25	4.343	4.398	6.178	8	143	163	124	13.8
10	NM_005112	WDR1	M-011984-00	2.844	ND	3.336	22	3.183	ND	3.234	17	3.033	ND	5.557	9	140	49	139	15.0
11	NM_004857	AKAP5	M-011954-00	4.502	1.851	3.144	20	5.28	2.695	3.538	10	3.874	2.419	3.404	31	167	246	149	18.4
12	XM_379260	LOC152742	M-028346-00	0.719	4.404	4.14	5	-0.129	2.772	3.111	50	1.004	3.536	3.866	25	224	167	128	18.4
13	NM_006145	DNDJB1	M-012735-00	4.716	1.534	3.167	18	4.796	1.621	2.76	52	4.881	3.447	4.466	7	166	70	222	18.7
14	NM_182971	COX8C	M-019415-00	1.041	4.146	3.562	11	0.567	3.641	3.656	8	0.548	4.254	2.712	90	154	137	110	19.9
15	NM_032122	DTNBP1	M-017455-00	3.627	4.341	2.462	10	2.586	4.985	2.766	51	3.635	4.335	2.784	22	82	88	114	22.4
16	NM_006551	SCGB1D2	M-012291-00	3.566	3.099	2.892	21	3.716	3.282	2.634	14	3.315	2.962	3.196	40	220	192	210	22.7
17	NM_002812	PSMD8	M-017583-00	3.515	3.137	4.026	14	1.66	2.668	2.898	67	2.79	3.971	5.219	14	130	84	145	23.6
18	NM_000075	CDK4	M-003238-02	-0.133	3.006	3.215	24	-0.045	3.173	3.725	19	0.191	3.388	4.384	32	223	145	95	24.4
19	NM_001633	AMBP	M-009696-00	2.292	3.324	1.332	116	3.758	3.668	1.957	7	3.781	4.908	1.724	18	72	134	126	24.4
20	NM_194289	LOC152195	M-019317-00	2.362	-0.113	3.539	98	3.872	-0.047	3.67	6	3.887	0.496	3.456	28	105	148	92	25.4
21	NM_023935	C20ORF116	M-014256-00	3.187	1.18	3.219	17	2.625	0.997	2.682	76	3.934	1.48	4.049	16	232	223	170	27.4
22	NM_014830	ZBTB39	M-021232-00	4.46	3.552	2.511	12	3.632	2.998	1.248	28	3.497	2.703	1.766	92	152	193	123	31.4
23	NM_021071	DO	M-009769-01	1.407	3.026	3.189	23	0.829	3.213	2.812	43	1.288	3.567	3.318	33	263	158	101	32.0
24	NM_004599	SREBF2	M-009549-00	2.649	3.279	3.491	16	2.519	3.136	3.763	22	2.51	2.839	2.679	96	105	121	110	32.3
25	NM_172005	WFDC13	M-017589-00	2.719	3.153	ND	29	2.24	2.568	ND	107	2.91	5.431	ND	11	221	93	31	32.4
26	NM_020437	LOC57168	M-017864-00	1.27	3.236	2.878	32	1.137	2.75	2.945	57	2.922	4.53	3.669	21	141	211	245	33.7
27	NM_002146	HOXB3	M-017537-00	2.816	2.837	2.235	36	3.4	3.279	2.787	15	3.275	2.737	2.781	78	225	245	143	34.8
28	NM_018323	PI4K2B	M-006769-01	-0.275	3.168	3.15	19	-0.355	2.912	2.845	39	-0.142	3.154	2.867	59	251	257	153	35.2
29	NM_006870	DSTN	M-012303-00	4.343	2.312	2.873	33	3.49	3.098	3.492	11	4.907	2.026	2.537	130	215	229	168	36.1
30	NM_001495	GFRA2	M-007914-00	2.722	0.248	4.572	44	2.943	-0.114	4.044	32	3.282	0.131	3.645	36	100	238	122	37.0
31	NM_001265	CDX2	M-015636-01	2.973	3.827	-0.427	27	3.466	5.099	-0.314	12	2.364	3.972	-0.255	174	224	195	255	38.3
32	XM_373886	LOC388738	M-027377-00	2.926	2.953	1.502	30	2.807	3.259	0.81	45	3.501	3.016	1.44	48	162	54	96	40.2
33	NM_152492	FLJ32825	M-016738-00	2.108	ND	3.502	38	2.259	ND	3.314	49	2.434	ND	4.074	37	219	7	100	41.0
34	NM_003456	ZNF205	M-019556-00	2.766	ND	2.127	77	3.171	ND	2.337	55	4.264	ND	3.088	20	64	0	87	43.9
35	NM_016604	JMJD1B	M-020378-00	ND	2.389	2.928	53	ND	2.138	2.743	100	ND	3.114	4.572	17	6	212	147	44.8
36	NM_001466	FZD2	M-005501-01	2.64	3.132	0	54	2.971	3.572	-0.522	30	3.01	2.904	0.33	57	191	149	256	45.2
37	NM_012307	EPB41L3	M-015330-00	3.912	2.6	2.614	58	3.48	2.837	2.895	35	3.28	2.932	3.035	47	232	232	235	45.7
38	NM_006404	PROCR	M-017326-00	3.254	2.155	2.785	39	3.219	2.025	2.415	105	3.414	2.538	3.448	29	224	233	234	49.2
39	NM_175892	FLJ37266	M-018066-00	2.198	2.729	2.883	43	1.213	1.932	2.021	282	3.361	4.04	4.543	12	226	195	95	52.6
40	NM_182631	LOC348840	M-018717-00	2.403	1.074	2.88	87	3.767	1.587	4.435	5	2.146	0.903	2.006	371	175	236	105	54.4
41	NM_207449	FLJ44674	M-032133-00	0.442	2.675	3.247	51	0.228	2.788	3.433	48	-0.058	2.835	3.128	66	222	136	110	54.5
42	NM_005810	KLRG1	M-016300-00	2.598	2.195	2.772	59	2.634	2.446	2.698	74	3.222	2.236	3.053	46	231	228	103	58.6
43	NM_000196	HSD11B2	M-008983-01	2.704	0.676	4.76	47	2.924	0.665	4.652	33	2.517	-0.245	3.127	135	171	255	197	59.4
44	XM_379306	LOC401169	M-028377-00	2.338	ND	2.94	55	2.184	ND	2.394	136	3.428	ND	3.399	30	51	39	84	60.8
45	XM_375608	LOC400692	M-031099-00	2.4	2.014	2.508	88	3.095	2.575	2.987	29	2.818	2.725	2.463	88	226	226	243	60.8
46	NM_152441	FBXL14	M-015718-00	3.579	2.865	1.341	34	2.646	2.88	1.09	69	2.707	2.667	1.238	97	232	181	203	61.1
47	NM_033051	TSCOT	M-018639-00	1.658	3.418	3.925	15	0.703	3.164	3.788	20	0.282	1.6	2.224	843	88	164	212	63.2
48	XM_372810	PLXND2	M-021532-00	2.87	1.731	2.7	48	2.47	1.536	2.306	131	3.124	2.693	3.437	42	138	61	150	64.2
49	XM_378706	LOC400621	M-030808-00	ND	3.21	2.217	45	ND	3.292	1.986	72	ND	3.767	1.77	82	9	89	168	64.3
50	NM_023074	FLJ12644	M-007057-00	1.833	3.218	2.687	49	1.503	2.531	2.415	106	2.765	2.913	2.942	56	250	123	221	66.3
51	NM_015008	KIAA0779	M-023594-00	2.182	2.97	2.993	28	1.652	2.209	2.541	150	1.711	2.814	3.429	70	169	190	97	66.5
52	NM_004409	DMPK	M-004637-00	1.972	2.683	3.289	50	1.305	2.244	2.854	144	2.437	3.182	3.122	43	222	116	156	67.6
53	NM_005845	ABCC4	M-007313-00	0.43	2.457	2.553	75	0.635	3.604	3.053	26	0.765	2.324	2.807	186	183	147	184	71.3
54	NM_023080	FLJ20989	M-014247-00	3.174	1.815	2.986	26	2.632	1.911	3.093	75	2.226	1.634	2.794	228	243	273	211	76.3
55	NM_213655	HSN2	M-032553-00	2.523	2.13	-2.099	170	2.52	2.235	-2.3	145	4	4	-2.176	19	177	177	237	77.7
56	NM_000689	ALDH1A1	M-008722-01	ND	2.335	2.609	73	ND	2.387	1.981	161	ND	3.047	3.231	41	2	95	161	78.4
57	NM_291105	MGC21874	M-024154-00	1.916	ND	3.199	61	1.949	ND	2.835	111	2.582	ND	2.985	77	98	0	90	80.5
58	XM_019597	HNRPH2	M-013245-00	2.997	1.554	3.212	25	2.948	1.415	3.885	31	1.692	0.976	2.933	701	61	174	92	81.6
59	NM_024048	MGC3020	M-016475-00	1.951	2.24	3.375	133	2.876	3.241	4.479	16	1.757	2.137	3.082	279	99	173	155	84.0
60																			

inc.	GeneID	Gene Name	Cat No	SCPO r1	SCPO r2	SCPO r3	SCPO rank	STAPO r1	STAPO r2	STAPO r3	STAPO rank	STIPO r1	STIPO r2	STIPO r3	STIPO rank	OC r1	OC r2	OC r3	rank product
61	XM_372812	LOC391162	M-027383-00	2.436	2.134	2.744	80	2.708	2.975	2.757	54	2.49	2.25	2.634	144	136	95	112	85.4
62	NM_001104	ACTN3	M-011197-01	2.351	2.404	ND	96	1.913	1.92	ND	292	3.949	3.208	ND	23	86	101	0	86.4
63	NM_000536	RAG2	M-012548-00	2.656	0.918	2.483	72	2.486	0.263	2.208	151	3.57	1.334	2.848	61	236	226	191	87.2
64	XM_375495	AATK	M-005301-01	1.36	2.255	2.762	129	1.508	2.898	3.777	34	1.333	3.072	2.398	163	151	150	236	89.4
65	NM_006668	CYP46A1	M-009292-00	1.238	2.837	2.187	145	0.839	2.895	2.216	149	1.232	3.699	3.288	35	145	120	209	91.1
66	NM_005355	KIF25	M-010082-00	0.372	2.392	2.067	205	0.646	2.595	2.449	95	1.269	3.529	3.245	39	269	135	245	91.2
67	NM_203423	LOC389199	M-031897-00	2.198	2.771	1.614	144	3.01	2.73	1.881	59	2.701	3.018	1.231	93	156	180	220	92.4
68	NM_012176	FBXO4	M-012433-00	1.694	2.097	2.08	196	1.451	2.176	2.424	163	3.511	3.703	3.069	26	68	113	223	94.0
69	NM_033050	GPR91	M-004541-00	2.632	1.054	2.85	56	2.29	0.864	2.494	135	2.604	0.996	2.827	111	231	204	178	94.3
70	NM_018366	CNO	M-021194-00	1.633	2.353	2.396	100	1.659	2.757	2.935	53	1.831	2.405	2.709	161	239	230	236	94.8
71	NM_030891	LRRC3	M-014654-00	1.379	2.031	2.356	224	1.703	2.882	3.022	36	1.884	2.604	3.103	112	227	76	155	96.7
72	NM_015537	NELF	M-016760-00	2.549	2.411	1.259	85	2.303	2.408	1.018	132	2.771	3.083	1.083	81	260	240	225	96.9
73	NM_018939	PCDHB6	M-013525-00	3.576	1.927	2.564	60	3.276	2.531	2.183	86	2.351	1.615	2.373	180	68	203	229	97.6
74	NM_001445	FABP6	M-008851-00	2.463	ND	2.236	103	2.521	ND	2.724	77	3.007	ND	2.152	118	202	11	188	97.8
75	NM_032875	FBXL20	M-015029-00	2.301	3.097	0.458	114	2.635	2.775	0.422	73	2.572	3.56	0.855	122	233	204	254	100.5
76	NM_001105	ACVR1	M-004924-01	2.498	0.83	2.766	71	2.812	0.706	3.124	42	2.049	0.505	2.024	356	249	179	252	102.0
77	NM_015859	GTF2A1	M-010910-00	2.733	2.537	2.223	67	2.714	2.784	1.707	61	2.202	2.102	1.043	307	235	221	224	107.9
78	NM_005550	KIFC3	M-008338-01	-1.502	2.537	2.671	66	-1.844	2.662	2.556	82	-1.131	2.196	3.296	243	115	133	174	109.6
79	NM_005147	DNDJA3	M-017792-00	2.403	1.596	2.002	235	2.74	1.975	2.078	209	3.46	1.574	3.479	27	172	209	51	109.9
80	NM_139245	PPM1L	M-008679-00	3.616	0.428	2.622	57	3.324	0.229	2.496	92	2.485	0	2.179	254	245	256	262	110.0
81	NM_031456	FBXW10	M-014733-00	2.283	2.288	0.796	119	2.542	2.812	1.08	85	2.654	2.525	2.006	133	196	211	230	110.4
82	XM_113678	NUP160	M-029990-00	2.1	2.688	2.349	102	2.097	2.905	1.702	200	2.549	3.73	2.83	68	171	96	190	111.5
83	NM_007003	GAGEC1	M-012344-00	2.908	2.261	1.981	126	3.454	2.798	2.256	47	2.405	1.797	2.165	263	147	153	97	115.9
84	NM_153031	FLJ32063	M-016518-00	2.204	-0.924	3.319	143	2.449	-0.942	3.326	96	2.583	-0.769	2.627	117	130	276	91	117.1
85	XM_292724	LOC342934	M-023877-00	2.436	2.392	1.11	92	2.812	2.642	1.649	71	3.01	2.182	1.269	251	134	186	245	117.9
86	NM_006047	RBM12	M-010094-00	1.72	2.092	1.958	255	2.267	2.832	2.51	87	2.027	4.061	2.79	74	255	230	191	118.0
87	NM_080753	WFDC10A	M-013266-00	1.967	2.798	ND	93	1.09	2.64	ND	337	2.029	3.846	ND	53	78	111	0	118.4
88	NM_004475	FLOT2	M-003666-00	2.544	1.464	ND	232	3.376	1.764	ND	80	3.522	1.87	ND	94	128	161	5	120.4
89	NM_014383	TZFP	M-020551-00	0.922	3.484	2.539	65	0.685	2.508	2.701	90	0.477	2.525	2.071	326	255	77	235	124.0
90	NM_005321	HIST1H1E	M-012048-00	1.898	2.88	3.549	31	0.759	2.197	2.83	156	1.291	1.973	2.436	398	101	164	176	124.4
91	NM_004521	KIF5B	M-008867-00	ND	1.642	2.554	191	ND	2.088	2.787	101	ND	2.07	3.23	100	3	221	207	124.5
92	NM_194292	DKFZP761A07	M-019156-00	2.481	2.165	ND	109	2.241	1.967	ND	193	2.475	2.894	ND	95	205	97	4	126.0
93	NM_005361	MAGEA2	M-006350-00	2.507	1.844	2.687	70	2.12	0.81	1.719	456	3.477	2.609	2.845	63	89	211	149	126.2
94	NM_016305	SS18L2	M-021092-00	1.067	ND	3.055	208	1.521	ND	4.729	23	0.427	ND	3.43	429	143	32	78	127.1
95	NM_175906	MGC33608	M-018170-00	3.156	2.814	2.176	37	2.54	2.054	1.581	218	2.176	2.261	1.266	255	72	105	84	127.2
96	NM_002734	PRKAR1A	M-007670-01	2.458	2.517	3.354	69	2.174	1.99	3.184	165	2.179	2.349	3.667	181	253	191	195	127.3
97	NM_005018	PDCD1	M-004435-00	2.988	2.426	-0.6	81	2.926	2.563	-0.656	81	2.555	2.057	-0.619	336	225	200	245	130.1
98	NM_016510	SCLY	M-017175-00	2.782	2.978	1.468	40	3.048	2.672	1.275	65	1.596	2.115	0.91	849	104	159	220	130.2
101	NM_002662	PLD1	M-009413-00	1.678	2.817	2.324	108	1.419	3.069	2.37	117	1.595	2.356	2.856	177	222	243	187	130.8
102	NM_030808	NDEL1	M-018571-00	3.878	2.306	2.346	104	2.981	2.117	2.126	179	4.143	2.574	2.391	121	105	183	135	131.1
103	NM_004443	EPHB3	M-003123-02	3.03	2.307	2.248	113	2.321	2.576	2.02	127	3.265	2.381	2.257	167	223	221	220	133.8
104	XM_373596	LOC387994	M-030305-00	-1.155	3.441	2.393	91	-1.386	2.967	2.165	167	-0.288	2.404	2.805	162	247	69	112	135.0
105	NM_000065	C6	M-011003-00	2.051	2.462	0.882	212	2.437	2.907	1.021	103	2.551	2.825	1.903	124	223	232	142	139.4
106	XM_371678	LOC389174	M-028196-00	2.39	2.108	0.968	185	2.681	3.163	1.337	64	2.927	2.225	1.724	229	71	129	133	139.4
107	NM_007183	PKP3	M-019664-00	2.398	ND	1.893	159	1.71	ND	1.894	389	4.034	ND	2.093	45	83	5	98	140.7
108	NM_019002	ETAA16	M-021193-00	2.554	1.177	2.263	124	1.813	0.781	1.719	455	3.016	2.981	2.485	50	241	115	129	141.3
109	NM_000095	COMP	M-011018-00	2.603	2.338	0.856	105	2.756	2.174	0.699	164	2.392	2.431	0.759	164	156	224	217	141.3
110	NM_020120	UGCGL1	M-006632-00	2.641	2.076	1.424	198	2.195	2.372	1.279	158	2.705	2.787	1.267	91	239	231	232	141.7
111	NM_004311	ARL3	M-011813-00	2.301	-0.048	2.229	134	2.752	0.014	2.709	63	2.047	-0.102	2.549	342	243	183	131	142.4
112	NM_182587	C2ORF21	M-018852-00	2.822	2.14	-0.302	163	2.703	2.498	-0.62	91	2.3	2.847	0.085	198	163	112	177	143.2
113	XM_371484	KIAA1724	M-027817-00	1.96	-0.485	2.428	252	2.142	-0.903	2.386	177	3.428	-0.509	2.833	67	122	180	191	144.0
114	NM_006030	CACND2D2	M-012719-00	4.137	ND	0.223	148	5.005	ND	0.496	56	3.489	ND	0.529	366	107	46	136	144.8
115	NM_000358	TGFBI	M-019370-00	2.677	2.068	0.457	204	2.445	2.442	0.646	99	2.873	2.406	1.169	160	231	246	261	147.8
116	NM_018349	FLJ11175	M-020810-00	2.178	1.753	2.321	149	1.318	1.608	2.129	599	2.456	3.277	3.245	38	118	71	152	150.2
117	XM_373092	LOC391807	M-028558-00	0.958	3.449	2.217	141	1.227	4.331	3.029	27	0.968	2.62	1.564	895	223	218	247	150.5
118	NM_002997	SDC1	M-010621-00	2.136	2.52	1.246	167	2.033	2.096	0.678	232	2.924	2.721	1.622	89	214	241	132	151.1
119	NM_000197	HSD17B3	M-008138-01	4.489	0.609	2.846	35	4.451	0.764	2.218	147	3.285	0.461	1.705	684	157	284	154	152.1
120	NM_018069	FLJ10352	M-032250-00	2.045	2.28	1.527	213	2.381	2.783	1.7	116	2.214	2.574	2.446	150	216	179	137	154.8

inc.	GeneID	Gene Name	Cat No	SCPO r1	SCPO r2	SCPO r3	SCPO rank	STAPO r1	STAPO r2	STAPO r3	STAPO rank	STIPO r1	STIPO r2	STIPO r3	STIPO rank	OC r1	OC r2	OC r3	rank product
121	XM_373489	LOC387746	M-029956-00	2.264	1.131	ND	493	2.559	1.213	ND	320	4.143	2.989	ND	24	70	55	5	155.9
122	NM_002142	HOXA9	M-006337-00	2.134	1.6	2.984	168	2.389	1.797	2.937	113	2.309	0.919	2.27	207	235	227	211	157.8
123	NM_006730	DNDSE1L1	M-019918-00	2.069	2.466	2.622	74	1.598	1.854	2.512	346	2.427	1.804	3.026	154	106	125	126	158.0
124	NM_174928	LOC221143	M-017843-00	3.044	2.137	2.131	166	2.178	1.148	1.93	284	3.353	2.734	2.682	85	137	183	132	158.8
125	NM_022068	FAM38B	M-013925-00	4.667	2.107	2.106	187	4.337	2.105	2.382	115	3.737	1.812	2.314	188	205	243	252	159.3
126	NM_003541	HIST1H4K	M-011459-00	2.036	2.998	2.315	112	1.351	2.396	1.665	510	2.426	3.46	2.81	71	166	221	110	159.5
127	XM_097622	LOC149297	M-022079-00	2.229	1.978	2.149	157	2.342	1.619	2.484	122	1.429	2.288	2.253	218	93	61	192	161.0
128	XM_058857	LOC124871	M-023210-00	3.228	1.89	1.872	295	3.145	2.227	2.862	37	4.293	1.968	1.991	383	97	100	131	161.1
129	NM_020851	KIAA1465	M-022273-00	2.553	2.835	-0.115	64	2.684	2.147	-0.43	173	1.979	2.958	0.237	389	75	111	122	162.7
130	XM_377919	LOC402237	M-028425-00	1.735	2.378	2.84	95	1.529	1.86	2.842	342	2.869	2.295	2.524	134	102	185	129	163.3
131	NM_000404	GLB1	M-012539-00	2.367	0.042	2.492	97	2.849	0.079	2.36	119	1.978	0.41	2.213	390	172	157	200	165.1
132	NM_138338	POLR3H	M-015503-00	1.307	ND	2.682	240	1.741	ND	3.095	104	1.521	ND	3.135	185	81	9	206	166.5
133	NM_000508	FGA	M-007901-01	1.757	2.141	4.896	161	1.865	2.346	4.554	121	1.368	2.19	4.94	246	195	255	112	168.6
134	XM_380040	LOC402693	M-029183-00	2.948	0.939	2.675	52	2.384	0.614	2.169	166	1.79	0.618	2.058	556	125	183	146	168.7
135	NM_005584	MAB21L1	M-012125-00	2.472	2.118	0.882	178	3.346	2.642	1.254	70	2.886	1.976	1.026	393	139	152	172	169.8
136	NM_003460	ZP2	M-011403-00	2.52	2.683	0.95	68	1.846	2.161	0.51	355	2.265	2.397	0.196	210	183	104	220	171.8
137	NM_016009	SH3GLB1	M-017086-00	2.182	1.044	1.839	343	2.806	1.58	2.978	46	2.685	1.62	2.067	328	226	139	175	173.0
138	NM_153225	RPESP	M-016495-00	3.123	0.671	1.919	279	4.087	0.982	2.328	125	3.52	0.559	2.456	149	55	225	55	173.2
139	NM_024902	FLJ13236	M-014507-00	2.821	2.318	1.711	111	2.837	2.433	2.816	41	1.436	1.578	0.486	1149	224	235	175	173.6
140	XM_291142	LOC115548	M-024508-00	2.104	2.101	4.125	188	2.013	1.48	2.518	237	2.576	1.977	3.705	120	140	205	122	174.9
141	NM_006438	COLEC10	M-012216-00	2.416	1.56	2.21	142	2.442	1.462	1.74	439	3.65	1.7	2.732	86	235	243	194	175.0
143	XM_379215	LOC132241	M-028163-00	2.259	2.06	2.458	127	2.849	1.851	3.124	38	1.691	0.931	1.442	1134	108	261	198	176.2
144	NM_002719	PPP2R5C	M-009433-00	ND	2.953	1.012	244	ND	3.042	1.153	199	ND	3.594	1.602	114	20	144	229	176.9
145	XM_029084	FLJ21438	M-031241-00	2.38	1.039	2.398	94	2.611	0.81	2.382	114	1.828	1.308	2.207	521	150	153	159	177.4
146	NM_005805	PSMD14	M-006024-00	2.074	2.868	0.394	200	1.014	2.242	-0.833	2211	4.275	3.998	0.677	13	83	89	146	179.1
147	NM_198502	FLJ43826	M-027247-00	0.926	ND	3.005	251	1.004	ND	3.063	231	1.908	ND	3.378	101	92	30	67	180.2
148	XM_373540	LOC387872	M-030045-00	2.477	2.052	-0.868	211	2.632	2.29	-0.358	134	2.266	3.164	0.507	209	57	74	60	180.8
149	NM_000256	MYBPC3	M-011085-00	2.109	1.076	3.394	182	1.505	0.808	3.805	764	3.085	1.244	3.421	44	77	168	228	182.9
150	NM_015894	STMN3	M-013600-00	0.048	2.222	2.074	201	0.054	2.898	2.447	97	0.055	2.253	2.088	314	150	100	112	182.9
151	NM_024994	FLJ12595	M-014541-00	2.309	2.155	1.574	156	2.121	2.258	1.883	183	2.565	1.891	2.259	215	141	221	165	183.1
152	NM_001299	CNN1	M-015851-00	2.22	2.111	0.952	180	1.866	2.489	1.37	336	3.441	2.636	1.97	102	66	70	78	183.4
153	XM_380114	LOC402523	M-029075-00	1.445	ND	3.368	86	1.535	ND	2.822	162	1.555	ND	2.273	446	199	7	170	183.8
154	NM_015071	ARHGAP26	M-008426-00	3.035	2.455	1.653	76	2.114	1.939	0.984	273	2.107	2.362	1.019	302	158	92	156	184.4
155	NM_004388	CTBS	M-019796-00	1.842	4.148	1.888	297	1.783	3.661	1.926	286	2.789	3.448	1.67	75	130	126	175	185.4
156	XM_371832	KIAA1411	M-028640-00	2.109	2.23	0.801	183	2.555	1.685	0.659	488	2.804	3.05	1.547	72	75	72	217	186.0
157	NM_002807	PSMD1	M-011363-00	ND	3.322	0.454	298	ND	4.482	-0.103	159	ND	4.054	0.957	138	17	53	73	187.0
158	NM_152427	CFLP1	M-015476-00	ND	1.483	3.357	82	ND	1.609	3.088	120	ND	1.364	2.065	666	0	112	87	187.1
159	NM_005217	DEFA3	M-012027-00	2.088	2.166	4.233	154	1.542	1.145	3.712	706	2.846	1.538	4.115	62	126	134	170	188.9
160	NM_138781	LOC113386	M-016568-00	2.328	0.633	1.774	408	2.384	0.265	2.076	210	3.02	1.35	2.773	79	110	214	59	189.2
161	NM_016563	RASL12	M-009634-00	2.296	2.075	1.128	199	2.64	1.896	1.02	313	2.616	3.157	1.342	109	225	211	181	189.4
162	XM_378546	LOC145820	M-030497-00	2.192	ND	2.058	173	2.127	ND	2.433	138	1.891	ND	2.362	285	223	ND	116	189.5
163	NM_022575	VPS16	M-013003-00	ND	2.318	1.506	284	ND	2.597	1.439	236	ND	3.391	1.87	103	15	203	212	190.4
164	XM_046570	KIAA1679	M-022909-00	1.954	2.508	0.73	259	2.274	2.467	0.553	139	2.478	2.301	1.346	197	210	88	222	192.1
165	XM_167072	BZRP1	M-028712-00	0.182	2.542	2.127	171	0.117	2.489	3.008	93	-0.27	2.357	1.913	447	161	180	184	192.3
166	NM_007368	RASA3	M-009117-00	1.07	2.808	2.441	78	0.39	2.113	2.119	187	0.436	2.436	1.864	492	195	215	210	192.9
167	NM_033182	FBXO44	M-019201-00	3.097	1.265	ND	146	3.844	1.589	ND	60	1.989	1.231	ND	824	163	105	5	193.3
168	NM_152707	SLC25A16	M-007475-00	1.949	2.297	ND	174	2.064	2.144	ND	194	1.846	2.622	ND	223	119	213	4	196.0
169	NM_005419	STAT2	M-012064-00	2.286	2.229	2.881	118	2.807	2.672	2.899	44	1.267	1.816	1.298	1513	108	209	228	198.8
170	XM_373685	LOC388276	M-030621-00	ND	1.702	1.814	427	ND	2.052	2.214	178	ND	2.064	3.177	108	ND	221	74	201.7
171	NM_016105	FKBP7	M-009436-00	0.926	2.3	2.649	115	1.175	2.55	2.593	84	0.889	1.578	1.919	872	216	238	255	203.5
172	NM_001236	CBR3	M-008597-00	ND	0.797	3.31	210	ND	0.374	3.627	244	ND	1.229	3.539	166	45	99	131	204.1
173	XM_166571	KIAA0363	M-025327-00	2.607	2.229	1.28	135	3.181	3.184	2.175	18	0.809	1.089	0.034	3547	188	52	124	205.0
174	NM_004593	SFRS10	M-007278-00	2.122	3.187	1.549	175	1.745	3.293	1.768	415	2.157	3.812	2.542	127	135	131	156	209.7
175	XM_373864	LOC388684	M-027688-00	1.307	1.774	ND	697	2.066	1.851	ND	264	2.537	3.402	ND	51	53	75	10	210.9
176	XM_352847	LOC340529	M-024839-00	ND	1.884	2.3	193	ND	1.371	1.588	814	ND	2.23	3.492	60	25	86	51	211.2
177	NM_001963	EGF	M-011650-00	1.145	2.621	2.017	228	1.416	2.984	2.332	124	1.621	2.772	2.056	337	118	164	230	212.0
178	XM_373555	LOC387897	M-030151-00	0.578	2.061	2.782	207	0.135	2.056	2.549	217	0.637	2.233	4.586	224	85	178	194	215.9
179	NM_019598	KLK12	M-005909-00	1.077	1.968	3.451	250	1.056	2.509	3.605	89	0.483	1.908	2.949	456	235	243	203	216.5
180	NM_004610	TCP10	M-019823-00	2.114	0.967	2.289	179	3.369	1.313	2.73	58	1.508	0.835	2.467	997	59	155	82	217.9

inc.	GeneID	Gene Name	Cat No	SCPO r1	SCPO r2	SCPO r3	SCPO rank	STAPO r1	STAPO r2	STAPO r3	STAPO rank	STIPO r1	STIPO r2	STIPO r3	STIPO rank	OC r1	OC r2	OC r3	rank product
181	NM_022828	YTHDC2	M-014220-00	2.27	1.874	1.466	305	2.47	1.705	1.475	469	2.8	2.328	3.28	73	166	96	62	218.6
182	NM_000573	CR1	M-007859-00	0.984	2.336	1.873	306	0.866	2.325	2.121	182	0.307	2.956	2.313	189	123	200	223	219.2
183	NM_014482	BMP10	M-013731-00	1.27	2.319	1.978	247	0.036	1.582	1.453	871	0.296	3.46	3.015	49	205	116	107	219.3
184	NM_018924	PCDHGB3	M-013290-00	2.639	1.863	1.937	269	2.511	1.931	1.678	283	3.049	2.458	2.498	139	222	229	242	219.5
185	XM_373746	LOC388416	M-030799-00	2.366	1.822	ND	192	3.056	2.366	ND	62	2.258	0.86	ND	902	108	125	4	220.6
186	NM_000770	CYP2C8	M-008286-00	2.169	2.786	0.967	153	1.849	2.573	1.007	353	2.274	3.498	1.048	205	149	132	215	222.9
187	NM_006298	ZNF192	M-020154-00	2.107	1.249	2.709	186	1.623	0.915	2.552	577	2.622	1.173	2.918	106	144	221	239	224.9
188	NM_005388	PDCL	M-013394-00	1.345	2.22	2.236	140	1.169	2.753	2.059	215	1.626	2.636	1.982	388	164	221	243	226.9
189	NM_004792	PPIG	M-008293-01	ND	0.6	3.721	155	ND	0.305	2.895	614	ND	0.939	4.16	125	26	170	85	228.3
190	NM_005049	PWP2H	M-019927-00	1.017	ND	2.694	324	0.602	ND	2.906	427	1.477	ND	3.977	87	114	1	89	229.2
191	NM_007278	GABARAP	M-012368-00	2.017	ND	1.033	722	2.881	ND	1.508	157	3.704	ND	1.539	107	155	23	80	229.8
192	XM_371726	LOC389267	M-028381-00	2.191	2.043	0.546	216	2.962	2.841	0.674	40	1.329	1.742	-0.188	1433	156	140	185	231.3
193	NM_005486	TOM1L1	M-003911-01	1.577	1.457	3.034	643	1.605	1.576	3.785	602	3.316	0.97	4.058	34	83	115	89	236.1
194	NM_012207	HNRPH3	M-012440-00	2.598	2.557	1.896	62	1.799	1.663	1.342	512	1.941	2.041	1.15	420	118	110	121	237.1
195	NM_018254	RCOR3	M-017112-00	1.063	2.506	2.354	99	0.938	2.622	2.23	146	1.34	2.433	1.542	938	149	177	229	238.4
196	NM_145170	TTC18	M-016390-00	2.756	-0.452	2.884	42	2.523	-1.128	1.957	265	1.407	-0.938	2.064	1223	97	182	178	238.8
197	XM_041964	KIAA0523	M-023005-00	2.287	2.372	0.744	117	2.049	2.238	0.354	221	1.822	1.854	0.481	527	140	132	245	238.9
198	XM_113776	LOC196913	M-021957-00	2.301	ND	1.314	381	3.169	ND	1.706	102	2.199	ND	1.857	352	98	5	131	239.2
199	NM_032030	FKSG83	M-014769-00	1.65	2.101	3.835	189	1.631	2.118	4.275	185	1.974	1.847	4.239	395	122	104	145	239.9
200	NM_001045	SLC6A4	M-007604-00	2.162	2.726	2.35	101	1.694	2.177	1.908	304	2.126	1.678	1.892	467	223	153	218	242.9
201	NM_006706	TCERG1	M-012278-00	2.16	1.981	1.513	246	1.864	1.927	1.269	338	2.398	2.362	2	175	232	196	242	244.1
202	XM_375150	LOC400301	M-030530-00	ND	2.353	0.738	685	ND	2.472	1.317	314	ND	3.73	1.899	69	ND	108	94	245.7
203	NM_207496	C6ORF214	M-032203-00	2.276	2.29	0.697	121	1.971	1.985	0.27	256	2.263	1.872	0.542	486	127	123	226	246.9
204	XM_373252	LOC392221	M-029392-00	2.186	2.109	1.785	181	1.813	2.026	1.613	384	1.99	2.967	2.246	220	96	74	75	248.2
205	NM_198995	C18ORF34	M-032008-00	2.273	1.772	ND	227	2.435	2.717	ND	79	1.692	1.495	ND	855	112	70	7	248.4
206	NM_012202	GNG3	M-012804-00	2.872	1.29	2.109	184	3.153	1.398	2.393	110	1.884	0.415	1.645	759	100	137	141	248.6
207	NM_006909	RASGRF2	M-024516-01	2.035	2.386	-0.589	220	1.908	2.894	-0.568	303	2.218	2.677	-0.532	231	154	113	239	248.8
208	NM_004537	NDP1L1	M-017274-00	3.361	0.582	2.396	90	2.721	0.192	1.742	437	2.955	0.55	1.977	392	165	182	161	248.9
209	NM_016542	MST4	M-003753-01	0.594	1.937	1.988	268	0.571	2.461	2.493	94	0.969	1.756	1.876	616	128	221	241	249.4
210	NM_172347	KCNG4	M-006231-01	2.221	2.322	0.192	139	1.845	2.072	0.093	356	2.281	2.086	0.994	316	223	95	164	250.1
211	NM_003882	WISP1	M-010555-00	2.75	0.441	2.323	110	3.661	0.561	2.094	201	4.127	0.519	1.688	709	99	104	112	250.3
212	NM_021932	RIC-8	M-016121-00	1.985	1.782	2.06	243	2.046	1.485	2.63	225	2.124	1.706	2.262	287	201	194	191	250.4
213	NM_00100053	OR6K3	M-032451-00	1.445	2.102	1.713	470	1.605	2.305	2.218	148	2.285	2.229	1.666	226	101	221	127	250.5
214	NM_003571	BFSP2	M-011471-00	3.659	2.278	1.785	120	3.837	1.738	1.254	442	5.147	1.659	2.101	308	113	221	113	253.7
215	NM_016224	SNX9	M-017335-00	1.561	2.705	2.171	152	1.339	2.863	2.106	192	1.781	3.173	1.519	568	158	225	249	255.0
216	NM_017874	C20ORF27	M-020857-00	2.681	2.264	1.388	123	3.171	1.653	1.433	528	2.659	2.174	2.034	258	245	245	231	255.9
217	NM_032347	ZNF397	M-014870-00	1.807	1.776	ND	395	2.165	2.001	ND	206	2.456	2.091	ND	206	243	178	14	255.9
218	NM_020311	CMKOR1	M-013212-00	2.14	1.329	2.574	162	1.394	1.052	1.971	1000	2.624	1.634	2.7	105	109	71	119	257.2
219	XM_376148	LOC401015	M-027987-00	2.147	1.401	2.005	231	2.386	1.398	1.934	279	2.413	0.984	2.162	266	208	217	225	257.8
220	NM_001276	CHI3L1	M-012568-00	1.31	2.232	0.772	1166	1.937	3.189	1.47	274	2.932	3.081	1.701	54	173	70	172	258.4
221	NM_006225	PLCD1	M-009149-00	2.243	1.691	1.709	478	2.586	1.716	2.145	175	2.663	1.666	2.27	208	220	115	125	259.1
222	NM_023940	RASL11B	M-014259-00	0.568	2.173	2.188	151	0.802	2.099	2.06	214	0.476	1.798	2.1	547	222	183	187	260.5
223	XM_379987	LOC402634	M-029049-00	1.343	3.099	2.224	137	0.609	2.801	1.412	952	1.625	3.844	2.514	136	87	99	111	260.8
224	NM_021135	RPS6KA2	M-004663-01	1.153	1.996	1.783	398	0.555	1.471	1.676	833	1.607	2.923	3.491	55	240	75	162	263.2
225	XM_035299	ZSWIM6	M-024465-00	1.741	1.138	3.698	442	2.34	0.918	4.487	123	2.048	1.975	3.386	341	59	71	212	264.7
226	NM_015037	KIAA0913	M-026438-00	1.623	2.914	2.44	79	1.651	2.893	1.983	251	0.844	1.536	1.84	947	212	169	244	265.8
227	NM_152698	FLJ38377	M-017019-00	ND	2.11	1.684	290	ND	2.203	2.314	142	ND	2.273	1.531	460	1	211	102	266.6
228	NM_017805	RASIP1	M-020794-00	2.12	2.329	1.476	177	2.506	2.076	1.699	211	1.841	2.097	1.011	510	88	237	227	267.1
229	NM_013255	MKLN1	M-019104-00	0.752	3.096	2.411	84	0.992	2.852	2.123	181	0.928	3.16	1.394	1257	117	103	124	267.4
230	NM_017590	ROXAN	M-017425-00	3.093	1.549	2.706	46	2.265	1.107	1.591	627	1.836	0.803	1.714	668	76	166	93	268.1
231	NM_015986	CRLF3	M-017786-00	1.924	1.614	1.879	302	1.972	1.867	1.784	334	2.309	1.849	3.044	192	113	179	66	268.5
232	NM_080723	VMP	M-018655-00	0.751	1.848	2.491	329	0.22	2.399	2.492	109	0.283	2.019	1.805	541	215	90	171	268.7
233	NM_002151	HPN	M-004332-00	3.222	1.567	2.256	128	2.701	1.079	1.909	301	1.939	0.904	1.815	533	178	116	84	273.8
234	NM_015432	PLEKHG4	M-022573-00	1.939	1.024	2.046	267	2.452	1.145	2	245	2.344	1.653	2.087	315	211	127	82	274.2
235	NM_003137	SRPK1	M-003982-02	2.132	3.45	1.572	169	1.855	2.864	1.543	345	2.015	3.244	1.858	363	203	95	97	276.6
236	NM_145650	MUC15	M-015614-00	ND	2.292	1.246	417	ND	2.345	1.247	392	ND	2.86	2.201	131	0	91	149	277.7
237	NM_0010055(	OR4K2	M-032482-00	2.411	1.438	2.001	236	2.31	1.748	2.156	170	1.88	0.804	1.808	537	114	226	134	278.3
238	NM_000853	GSTT1	M-011180-00	1.688	2.678	1.959	253	1.569	2.454	1.735	444	1.565	3.208	2.305	196	213	156	117	280.3
239	XM_043492	KIAA1728	M-023088-00	1.981	1.8	2.006	245	1.647	1.316	1.995	534	2.609	1.406	2.369	170	224	237	200	281.2
240	NM_199047	TBPL2	M-031738-00	2.138	1.733	-0.175	452	2.112	1.618	-0.21	586	2.772	2.747	-0.179	84	135	97	76	281.3

inc.	GeneID	Gene Name	Cat No	SCPO r1	SCPO r2	SCPO r3	SCPO rank	STAPO r1	STAPO r2	STAPO r3	STAPO rank	STIPO r1	STIPO r2	STIPO r3	STIPO rank	OC r1	OC r2	OC r3	rank product
241	NM_024850	BTNL8	M-014483-00	-0.48	2.305	1.915	281	-0.75	1.952	2.139	268	-0.036	2.112	2.441	296	237	238	127	281.4
242	NM_004064	CDKN1B	M-003472-00	0.57	2.082	3.172	195	0.973	2.392	3.611	112	0.715	1.491	2.564	1031	92	192	218	282.4
243	NM_016946	F11R	M-005053-00	2.626	1.944	-0.316	263	1.603	1.993	-0.519	604	3.368	2.493	0.025	142	76	202	208	282.5
244	NM_000983	RPL22	M-011143-00	1.689	2.553	1.868	317	1.753	2.525	1.834	365	2.159	3.393	2.298	199	198	166	135	284.5
245	NM_014876	KIAA0063	M-017674-00	2.161	ND	1.177	519	2.231	ND	1.057	539	3.752	ND	1.784	83	62	4	142	285.3
246	XM_371352	FMN2	M-022134-00	2.271	1.949	1.397	261	1.778	2.126	1.461	412	2.49	2.249	2.105	219	228	265	152	286.6
247	NM_022767	FLJ12484	M-016332-00	1.27	1.878	3.248	303	0.691	1.629	3.531	562	1.722	2.495	3.08	141	240	224	196	288.5
248	NM_004176	SREBF1	M-006891-00	1.815	0.842	2.069	371	1.627	0.78	1.76	567	2.59	1.578	2.996	116	221	247	233	290.0
249	NM_152390	MGC33926	M-016560-00	2.195	1.63	ND	283	2.295	1.571	ND	281	2.137	2.06	ND	309	243	263	1	290.7
250	NM_000942	PPIB	M-004606-00	1.818	-0.391	1.573	647	2.286	-0.017	2.392	137	2.254	-0.32	2.139	278	206	227	192	291.0
251	NM_181334	ARHGAP8	M-009427-00	2.103	0.217	1.624	572	3.215	0.511	2.606	78	3.514	0.15	1.793	553	115	269	175	291.1
252	NM_019009	TOLLIP	M-016930-00	2.329	0.458	2.483	107	1.596	-0.01	2.602	619	2.004	0.42	2.796	373	222	225	94	291.2
253	NM_006829	C10ORF116	M-012306-00	0.824	2.76	3.933	41	0.613	1.803	4.286	388	1.003	1.274	3.782	1568	127	145	123	292.2
254	XM_171489	LOC256144	M-026879-00	1.675	2.443	1.759	426	2.403	3.502	2.359	108	1.804	2.603	1.349	543	66	60	136	292.3
255	NM_00100054(	KRTAP5-11	M-032455-00	2.576	1.011	ND	393	2.071	0.863	ND	841	3.472	2.095	ND	76	124	234	13	292.9
256	NM_003829	MPDZ	M-019523-00	0.601	1.77	2.462	416	0.765	2.187	2.635	160	0.691	1.991	2.626	382	234	261	233	294.1
257	NM_00100038(	FLJ35429	M-032368-00	2.17	1.987	ND	197	2.247	1.949	ND	197	1.821	1.615	ND	662	70	114	7	295.1
258	NM_000629	IFNDR1	M-020209-00	1.752	0.967	2.468	430	1.916	1.207	2.567	293	2.276	1.022	2.433	204	236	248	253	295.1
259	NM_00100020	C4B	M-032347-00	2.038	2.66	-0.605	217	1.793	2.716	-0.517	395	2.106	3.585	-0.339	304	150	58	226	296.5
260	NM_194439	LOC285498	M-008019-00	2.025	2.219	ND	176	1.481	1.355	ND	940	1.927	2.89	ND	158	77	118	28	296.8
261	XM_370930	LOC388205	M-030677-00	ND	2.055	1.562	378	ND	2.347	1.873	189	ND	1.954	2.034	378	ND	197	163	300.0
262	NM_000412	HRG	M-013420-00	2.263	1.861	1.77	321	2.662	1.896	2.67	68	1.767	1.4	1.159	1239	244	231	240	300.2
263	NM_002534	OAS1	M-011344-00	2.207	1.796	1.324	389	1.763	1.813	0.876	419	2.774	2.375	1.52	168	160	209	168	301.4
264	XM_293293	LOC347359	M-024843-00	2.227	2.367	-0.848	136	1.621	2.155	-1.109	582	2.18	2.03	-0.738	349	151	140	51	302.3
265	NM_004556	NFKBIE	M-004766-00	3.894	1.554	1.975	248	3.894	1.863	1.866	335	3.048	1.207	2.052	338	231	140	217	304.0
266	NM_207329	MYADML	M-027825-00	2.397	2.617	0.38	89	2.587	1.89	-0.348	316	1.496	1.497	-0.803	1020	141	105	221	306.1
267	NM_152770	MGC35043	M-015942-00	ND	1.622	2.061	340	ND	1.658	2.144	312	ND	2.134	2.167	274	34	83	125	307.5
268	XM_371666	LOC389152	M-028170-00	2.538	1.445	1.885	300	3.071	1.401	2.022	235	3.031	0.308	1.942	418	91	131	211	308.9
269	NM_018410	DKFZP762E13	M-015443-00	ND	3.189	0.802	239	ND	2.83	-0.014	962	ND	4.041	1.016	132	43	236	129	311.9
270	NM_002319	LRCH4	M-011321-00	1.821	2.1	1.087	363	2.124	2.726	0.804	180	1.888	3.054	1.22	468	197	220	195	312.7
271	NM_006223	PIN4	M-020128-00	1.45	1.869	3.034	315	0.841	1.601	2.566	611	1.944	2.408	3.735	159	101	110	59	312.8
272	NM_144580	MGC31963	M-016364-00	2.166	-0.014	2.03	225	3.179	0.26	2.447	98	1.345	-0.276	2.121	1395	158	257	118	313.3
273	NM_000118	ENG	M-011026-00	1.911	1.771	1.868	318	2.202	2.036	2.221	155	1.621	1.743	1.789	633	221	189	249	314.8
274	NM_144605	FLJ25410	M-016227-00	2.044	2.211	1.678	215	1.925	1.887	1.233	318	1.532	1.906	1.964	458	228	245	222	315.2
275	NM_021065	HIST1H2AD	M-013147-00	1.823	2.689	0.549	361	1.902	2.432	0.582	309	2.132	3.34	0.965	282	91	79	134	315.7
276	XM_371691	LOC389203	M-027163-00	ND	1.062	2.758	286	ND	0.947	2.904	288	ND	1.199	2.757	391	7	146	82	318.2
277	NM_005050	ABCD4	M-009940-00	2.476	1.754	-1.046	429	2.668	2.032	-1.012	233	2.094	2.08	-1.264	323	205	129	180	318.4
278	NM_005593	MYF5	M-009759-00	0.976	1.699	2.049	489	1.121	1.723	2.35	453	2.46	2.119	3.434	148	163	222	138	320.1
279	NM_173512	FLJ39822	M-007336-00	1.982	0.885	1.901	288	2.479	0.92	1.644	538	2.061	2.259	2.423	214	74	65	90	321.3
280	NM_006696	BRD8	M-006377-00	1.394	2.703	1.407	928	1.212	2.604	2.265	141	1.579	2.176	2.421	256	224	225	128	322.4
281	NM_018974	UNC93A	M-018039-00	2.648	0.626	1.842	337	2.341	0.674	1.858	343	2.362	0.188	2.114	295	209	217	73	324.3
282	XM_378705	LOC400620	M-030805-00	1.521	2.034	2.082	222	1.329	2.126	1.832	370	2.171	1.158	1.936	425	238	164	151	326.8
283	NM_024816	RABEP2	M-009001-00	1.746	2.079	1.229	436	2.006	2.112	1.462	241	2.046	2.892	1.546	343	233	233	228	330.3
284	NM_182598	FLJ36980	M-018867-00	1.733	ND	1.785	425	2.003	ND	1.973	248	2.186	ND	1.889	346	127	8	134	331.6
285	XM_379642	LOC401528	M-029492-00	1.321	1.923	1.788	397	1.406	2.091	2.052	219	1.94	2.253	1.371	422	139	114	193	332.3
286	NM_005843	STAM2	M-017361-01	1.668	2.25	2.492	130	1.436	2.086	2.235	203	1.182	1.341	1.604	1404	207	193	157	333.4
287	NM_018992	KCTD5	M-021199-00	-3.195	1.625	2.605	570	-3.269	1.955	3.88	266	-2.544	2.189	3.24	247	64	215	286	334.6
288	NM_005380	NBL1	M-006540-00	2.143	2.003	0.353	233	1.635	2.077	0.13	554	2.119	2.684	0.633	291	248	236	129	334.9
289	NM_153838	GPR115	M-005536-01	2.201	2.072	1.463	202	2.265	1.945	1.442	270	2.213	1.4	1.702	691	98	153	124	335.3
290	NM_032558	FLJ14753	M-014918-00	2.179	1.559	1.114	666	2.245	1.89	1.367	317	2.735	2.352	1.029	179	101	109	103	335.6
291	NM_000893	KNG1	M-020202-00	2.261	2.59	-0.041	125	2.082	1.985	0.121	250	2.008	1.41	-0.122	1211	134	267	241	335.7
292	XM_373742	MGC40489	M-030925-00	2.943	1.632	1.76	424	3.265	1.642	1.873	330	2.178	1.693	2.152	272	273	245	95	336.4
293	NM_002094	GSPT1	M-019644-00	ND	2.159	1.78	249	ND	1.981	1.513	435	ND	2.113	1.94	353	0	184	194	336.9
294	NM_015984	UCHL5	M-006060-01	0.216	2.786	1.817	369	-0.05	2.671	1.759	424	0.436	2.182	2.197	252	220	156	265	340.4
295	XM_291253	KIAA0146	M-025937-00	1.834	1.925	0.361	349	1.753	1.812	0.339	428	2.163	2.355	0.728	265	81	65	186	340.8
296	XM_291107	NEK1	M-004864-00	1.89	1.627	1.659	529	1.927	1.892	1.784	315	2.28	2.204	2.05	238	223	106	101	341.0
297	NM_014863	GALNDC4S-6S	M-003960-00	1.546	2.269	0.902	684	2.001	2.446	1.148	243	2.199	2.985	1.307	240	118	205	229	341.7
298	NM_144650	ADHFE1	M-008453-00	1.872	-0.915	2.765	310	1.382	-1.061	2.458	1027	2.629	-0.919	2.547	126	93	96	89	342.3
299	NM_144707	PROM2	M-008551-00	0.596	2.817	2.242	132	0.405	1.987	1.993	249	0.86	2.297	1.402	1236	177	118	203	343.8
300	NM_152597	FSIP1	M-018333-00	1.837	-0.362	2.67	345	1.594	-0.533	1.737	622	2.312	-0.553	3.642	190	82	225	157	344.2

inc.	GeneID	Gene Name	Cat No	SCPO r1	SCPO r2	SCPO r3	SCPO rank	STAPO r1	STAPO r2	STAPO r3	STAPO rank	STIPO r1	STIPO r2	STIPO r3	STIPO rank	OC r1	OC r2	OC r3	rank product
301	NM_014026	DCPS	M-021338-00	1.236	2.314	1.87	313	1.463	2.948	2.67	66	1.149	2.23	1.149	1981	206	226	223	344.6
302	XM_085967	LOC147942	M-023632-00	2.293	2.138	1.643	165	1.891	1.436	1.425	902	2.15	1.349	2.421	275	97	230	165	344.6
303	XM_373520	LOC387824	M-029830-00	1.722	1.991	1.609	461	1.658	1.572	1.653	526	2.543	2.371	1.631	169	52	158	204	344.8
304	NM_000442	PECAM1	M-017029-01	1.833	2.57	1.935	273	1.444	2.761	1.279	891	2.368	2.731	2.159	172	157	206	210	347.2
305	NM_004239	TRIP11	M-012684-00	2.069	1.822	2.84	203	1.786	0.396	2.807	403	1.839	0.262	2.442	512	233	81	226	347.3
306	NM_018991	DKFZP434A01	M-021204-00	2.182	1.108	1.814	372	2.738	1.071	2.364	118	1.621	1.516	1.06	976	121	205	190	349.9
307	XM_291075	LOC339926	M-023672-00	2.968	ND	0.949	254	2.709	ND	1.222	259	2.673	ND	0.774	656	81	0	104	350.8
308	XM_033173	PCDH19	M-024773-00	ND	1.736	1.422	638	ND	2.055	1.344	475	ND	3.124	1.82	146	35	74	79	353.7
309	NM_173801	FLJ36198	M-018461-00	2.554	2.614	1.273	63	1.59	1.395	0.79	998	2.002	1.69	0.875	705	221	181	233	353.9
310	NM_005953	MT2A	M-018338-00	2.414	0.394	1.602	604	2.628	0.451	1.689	485	3.092	0.664	2.433	153	228	248	252	355.2
311	NM_002679	PMS2L2	M-012592-00	1.997	2.748	0.718	238	2.117	3.023	1	186	1.496	2.671	0.886	1017	188	126	202	355.7
312	XM_209140	LOC284323	M-023702-00	2.271	2.686	1.609	122	1.821	2.066	1.241	378	1.509	3.259	1.076	990	223	81	175	357.4
313	NM_002931	RING1	M-006554-02	2.126	1.454	1.773	410	2.332	1.754	2.098	198	1.857	1.565	1.78	572	224	222	249	359.4
314	NM_007203	AKAP2	M-017351-00	2.231	1.644	1.868	316	1.997	1.237	1.589	630	2.863	1.716	2.208	235	202	229	233	360.3
315	XM_290835	ZNF181	M-023641-00	1.894	3.655	1.297	292	2.149	3.339	1.104	172	1.544	4.667	0.432	936	183	169	158	360.9
316	NM_003391	WNT2	M-003938-01	1.274	2.132	ND	482	1.168	2.198	ND	492	1.862	2.717	ND	202	164	106	33	363.2
317	NM_003900	SQSTM1	M-010230-00	1.524	2.451	1.843	335	1.686	2.498	1.993	246	1.245	1.773	1.901	587	230	189	167	364.4
318	NM_024059	MGC5356	M-014284-00	1.858	3.02	1.614	322	2.099	2.619	1.689	195	1.504	2.046	1.635	772	223	72	227	364.6
319	NM_013433	TNPO2	M-020491-01	1.363	2.133	1.634	558	1.18	1.974	1.984	255	2.035	2.19	1.667	347	117	103	174	366.9
320	NM_020820	PREX1	M-010063-00	0.696	2.854	1.771	414	0.577	2.117	1.49	792	1.24	2.772	2.438	152	238	226	255	368.0
321	NM_033468	ZNF257	M-015111-00	0.215	2.122	1.592	620	-0.018	2.011	1.785	404	0.36	2.264	2.302	211	262	125	203	375.3
322	NM_052932	PORIMIN	M-015166-00	1.092	1.809	2.083	377	0.953	1.525	2.225	734	1.755	2.308	2.616	193	220	190	245	376.6
323	NM_022042	SLC26A1	M-007488-00	1.746	1.39	2.173	435	2.162	1.675	2.358	168	1.666	1.587	2.38	737	143	110	144	377.6
324	NM_003004	SECTM1	M-011387-00	-2.032	2.4	1.925	278	-1.721	2.589	1.852	352	-2.318	2.129	1.792	554	195	169	151	378.5
325	NM_002810	PSMD4	M-011365-00	2.336	1.726	2.223	138	1.672	1.579	1.48	642	2.109	1.758	1.472	613	157	196	227	378.7
326	XM_048675	KIAA1238	M-027036-00	2.035	2.109	1.238	218	1.663	1.748	1.084	514	1.871	1.932	0.716	487	159	220	240	379.3
327	NM_016300	ARPP-21	M-016091-00	0.766	2.139	3.284	164	0.415	1.573	3.139	658	0.881	1.843	3.728	508	117	69	116	379.9
328	NM_007244	PRR4	M-012367-00	0.799	ND	2.896	331	0.666	ND	3.263	260	0.239	ND	3.21	653	189	ND	163	383.0
329	NM_006564	CXCR6	M-005474-00	2.086	2.145	-0.128	194	2.51	2.611	0.1	88	1.038	0.855	-0.209	3299	241	246	231	383.3
330	NM_002127	HLA-G	M-017490-00	1.328	1.839	-0.409	1121	1.489	2.02	-0.554	794	2.84	3.459	0.318	64	110	69	79	384.8
331	NM_003608	GPR65	M-005589-00	2.306	1.864	0.865	320	2.66	1.926	0.709	287	1.749	2.019	0.037	622	249	152	253	385.1
332	NM_002982	CCL2	M-007831-00	1.915	2.229	2.177	150	1.882	1.877	2.052	323	1.414	1.235	1.767	1202	168	218	102	387.6
333	XM_373700	LOC388305	M-030687-00	1.924	1.819	-0.788	366	2.049	2.395	-1.021	222	2.069	1.677	-0.859	720	115	120	240	388.2
334	XM_047025	OATL1	M-024659-00	0.429	2.032	2.092	223	-0.25	1.344	1.761	1125	0.399	2.21	2.685	234	227	133	192	388.6
335	NM_032714	C14orf151	M-014972-00	1.521	1.181	1.542	734	1.773	1.63	1.518	561	2.622	2.492	2.145	143	235	227	220	389.0
336	NM_130776	GAGED4	M-017500-00	1.842	ND	1.834	344	1.583	ND	1.554	667	2.096	ND	2.253	257	95	20	103	389.2
337	XM_376049	LOC400950	M-027830-00	1.513	-1.195	1.959	747	2.139	-1.395	2.007	240	2.067	-0.333	3.212	330	156	103	138	389.7
338	NM_012101	TRIM29	M-012409-00	1.197	2.173	1.816	370	0.966	1.873	1.733	446	1.378	2.083	2.017	362	200	108	94	390.9
339	NM_000127	EXT1	M-011030-00	2.221	1.73	1.736	447	1.83	1.696	1.718	457	2.025	2.112	2.323	297	220	108	132	392.9
340	XM_374060	LOC389166	M-028181-00	3.355	2.012	1.475	230	2.899	1.743	0.952	436	3.76	1.762	1.565	610	87	125	121	394.0
341	NM_199280	LOC165186	M-027280-00	2.095	1.666	ND	301	1.534	1.501	ND	744	2.838	1.446	ND	277	80	187	0	395.9
342	XM_378201	LOC282980	M-029700-00	1.68	-0.371	1.85	505	1.363	-0.687	1.832	1074	2.884	0.287	2.578	119	129	77	52	401.1
343	NM_030754	SAA2	M-016279-00	1.347	2.775	1.844	332	1.495	2.556	1.718	459	1.167	2.535	1.925	430	136	118	125	403.2
344	NM_001142	AMELX	M-012489-00	2.788	1.45	-0.011	844	2.467	1.312	-0.379	1202	3.584	2.839	0.476	65	157	109	236	404.0
345	NM_003851	CREG	M-011534-00	1.426	1.869	2.814	314	0.897	1.508	2.808	758	1.192	2.134	2.451	281	225	208	173	405.9
346	NM_024835	ZNF403	M-014475-00	2.957	1.94	1.186	266	2.12	1.274	0.478	1303	3.125	2.307	1.603	194	236	258	235	406.6
347	NM_178450	MARCH3	M-007116-00	1.613	2.152	0.829	585	1.857	2.059	0.811	344	2.057	2.253	0.911	335	108	242	202	407.0
348	NM_052861	MGC21675	M-015145-00	2.091	1.65	1.935	272	1.696	1.481	1.593	625	2.321	1.614	1.973	397	228	195	129	407.1
349	NM_001066	TNFRSF1B	M-003934-00	1.247	0.749	2.347	1346	1.839	1.41	3.046	362	2.589	1.204	2.497	140	113	193	156	408.6
350	NM_004390	CTSH	M-005839-00	1.468	0.015	2.377	817	1.209	-0.289	2.306	1473	2.873	0.269	3.256	58	225	243	119	411.7
351	NM_016185	HN1	M-021065-00	1.573	0.87	1.562	663	1.902	0.752	2.476	311	2.049	1.48	2.583	340	91	121	75	412.3
352	NM_020156	C1GALT1	M-020490-00	1.438	3.53	1.826	358	1.085	3.381	1.739	441	1.883	3.312	1.912	450	149	101	190	414.2
353	NM_005124	NUP153	M-005283-00	1.728	1.025	1.738	455	2.202	1.714	2.551	154	1.497	0.907	2.175	1015	251	65	159	414.3
354	XM_378453	LOC400208	M-030286-00	-0.91	2.447	1.718	466	-1.043	3.017	2.312	129	-1.103	1.417	1.795	1196	246	244	232	415.8
355	NM_007231	SLC6A14	M-007601-00	0.978	ND	2.46	464	1.134	ND	2.936	229	0.654	ND	2.755	687	241	ND	232	417.9
356	NM_207502	C6ORF122	M-032204-00	2.164	ND	1.312	445	2.438	ND	1.232	363	2.231	ND	1.587	455	97	20	103	418.9
357	XM_379409	LOC401256	M-028701-00	1.944	1.359	2.843	262	2.312	1.654	3.654	130	1.085	0.638	2.537	2224	198	152	131	423.1
358	NM_012206	HAVCR1	M-019856-01	1.971	1.935	0.044	271	1.689	1.659	-0.287	520	1.806	1.881	0.127	540	94	174	237	423.8
359	NM_000537	REN	M-006026-00	1.793	1.518	1.206	740	1.734	1.539	1.335	711	2.511	2.49	1.734	145	229	145	213	424.1
360	NM_000965	RARB	M-003438-01	1.97	-0.979	1.826	356	1.906	-0.835	1.944	305	2.016	-1.352	1.688	707	254	233	185	425.0

inc.	GeneID	Gene Name	Cat No	SCPO r1	SCPO r2	SCPO r3	SCPO rank	STAPO r1	STAPO r2	STAPO r3	STAPO rank	STIPO r1	STIPO r2	STIPO r3	STIPO rank	OC r1	OC r2	OC r3	rank product
361	NM_012394	PFDN2	M-013011-00	1.79	1.568	ND	507	1.572	1.788	ND	495	1.956	2.252	ND	306	114	137	5	425.1
362	J05158	CPN2	M-023553-00	0.444	2.278	1.594	617	0.181	2.366	1.482	810	1.054	3.077	2.414	155	152	84	146	426.3
363	NM_004856	KIF23	M-004956-01	-0.096	2.03	4.105	226	-0.148	2.294	4.146	133	0.194	1.002	3.183	2578	52	67	105	426.3
364	NM_173043	IL18BP	M-017446-00	1.159	1.942	2.104	265	1.018	2.222	1.818	380	0.815	1.869	1.63	778	174	262	231	427.9
365	NM_024791	PDZK2	M-017027-00	1.802	1.989	1.986	242	2.062	1.925	2.894	213	1.293	1.027	1.861	1521	203	262	195	428.0
366	XM_172917	LOC256453	M-021998-00	1.937	1.871	1.089	312	1.924	1.884	1.547	322	1.627	1.906	1.231	784	137	105	89	428.7
367	NM_014168	HSPC133	M-020695-00	1.696	1.988	0.487	494	1.846	2.085	0.678	354	1.908	2.54	0.296	457	219	218	241	430.7
368	NM_033035	TSLP	M-013671-00	1.828	0.234	2.163	354	1.731	-0.279	1.54	710	2.546	0.331	2.079	324	153	237	228	433.4
369	NM_030974	DKFZP434N19	M-018575-00	2.061	-1.024	1.62	577	1.949	-0.948	1.606	600	2.207	-0.186	3.144	236	229	134	129	433.9
370	NM_005243	EWSR1	M-005119-02	1.988	2.047	1.766	241	1.783	1.772	1.727	414	1.532	1.611	1.972	820	116	160	158	434.1
371	NM_152384	BBS5	M-016478-00	1.886	1.793	1.176	394	2.099	1.468	2.165	196	1.478	1.771	1.086	1063	225	67	152	434.6
372	NM_005086	SSPN	M-011901-00	1.427	ND	2.573	237	0.891	ND	2.09	789	1.174	ND	2.656	444	163	43	118	436.3
373	NM_032681	TRIM51	M-010079-00	2.258	2.181	0.616	147	2.799	1.272	0.422	1306	2.987	1.924	0.323	433	175	84	225	436.4
374	NM_153371	LNX2	M-007164-00	1.749	0.676	2.391	432	1.122	0.313	2.848	1758	2.61	0.863	3.418	110	108	119	56	437.2
375	XM_048104	FLG	M-021718-00	2.865	0.456	ND	528	2.326	0.155	ND	1381	3.919	1.269	ND	115	59	160	0	437.7
376	XM_371933	PPP1R9A	M-025402-00	0.194	1.679	2.938	506	0.292	1.676	2.945	499	0.884	2.06	3.658	334	224	133	196	438.5
377	NM_006366	CAP2	M-012211-00	1.486	2.481	0.705	781	2.208	3.372	1.062	152	1.683	2.371	0.099	716	218	172	227	439.7
378	NM_006049	SNDPC5	M-020094-00	1.408	2.183	1.827	355	1.051	1.711	1.641	544	1.83	2.36	1.919	441	175	198	192	440.0
379	NM_004815	PARG1	M-008277-00	1.432	1.702	2.435	486	1.404	1.64	2.693	548	0.631	2.184	2.082	321	163	52	220	440.5
380	NM_006154	NEDD4	M-007178-01	1.702	1.379	1.213	995	1.769	1.311	1.588	631	2.721	1.983	2.51	137	96	218	105	441.4
381	NM_001043	SLC6A2	M-007602-00	2.176	ND	1.148	527	2.488	ND	1.434	262	2.607	ND	0.888	624	76	47	132	441.7
382	NM_016067	MRPS18C	M-013131-00	1.606	1.37	1.922	597	1.901	2.08	2.446	208	1.812	1.624	1.697	695	204	222	201	441.9
383	NM_018226	RNPEPL1	M-006032-00	ND	1.245	1.528	974	ND	1.128	1.94	722	ND	2.201	2.934	123	0	118	116	442.2
384	XM_371214	PLCL4	M-027529-00	1.611	1.35	1.614	589	1.994	1.251	1.4	988	2.682	2.442	2.407	151	109	91	53	444.6
385	XM_373845	LOC388638	M-027482-00	1.877	1.595	1.984	304	1.635	0.979	1.639	555	1.825	1.025	2.185	524	228	194	166	445.5
386	NM_015725	RDH8	M-009451-01	1.567	1.733	1.108	655	1.596	1.611	1.074	618	2.229	2.664	1.094	225	252	223	268	449.9
387	XM_371152	ZNF486	M-031256-00	-1.536	1.642	2.442	549	-2.01	1.572	1.271	1307	-2.022	2.627	2.538	128	236	120	152	451.2
388	XM_377974	LOC402300	M-028965-00	0.983	3.052	2.245	131	0.736	2.803	1.562	679	1.486	1.779	0.933	1044	71	99	245	452.8
389	NM_173685	FLJ32440	M-018070-00	1.849	ND	1.549	490	1.307	ND	1.579	894	2.484	ND	2.037	212	82	0	53	452.9
390	NM_007072	HHLA2	M-017669-00	1.622	ND	1.943	399	1.424	ND	1.925	500	1.723	ND	2.053	469	92	ND	235	454.0
391	NM_007071	HHLA3	M-019762-00	2.836	ND	0.71	409	3.273	ND	0.798	227	2.41	ND	0.588	1010	228	ND	223	454.3
392	NM_152529	GPR155	M-005494-00	1.726	0.185	1.696	495	1.737	0.022	1.753	443	1.934	0.32	1.935	428	229	182	249	454.4
393	XM_373771	LOC388456	M-031007-00	ND	1.843	1.501	512	ND	1.826	1.811	379	ND	1.792	1.953	485	0	77	207	454.9
394	NM_000076	CDKN1C	M-003244-03	1.535	1.84	2.386	342	1.91	1.908	2.776	300	1.544	1.075	2.095	935	236	223	220	457.8
395	NM_020470	YIF1	M-020155-00	1.072	3.011	1.757	428	1.009	2.49	1.534	721	1.772	2.868	2.094	312	226	158	174	458.3
396	NM_007046	EMILIN1	M-019765-00	1.603	2.496	1.415	601	1.333	1.683	1.562	678	1.69	3.261	2.202	239	123	70	184	460.1
397	XM_379437	LOC153910	M-028608-00	1.45	0.417	2.098	842	1.701	0.469	2.218	473	2.193	0.988	3.688	245	68	115	136	460.4
398	NM_021801	MMP26	M-005965-01	1.557	2.473	2.333	106	1.673	2.537	1.742	438	0.646	1.115	1.519	2105	255	247	252	460.6
399	NM_018126	TMEM33	M-020386-00	1.809	1.837	-0.436	379	1.936	2.088	-0.307	277	2.107	1.546	-0.666	931	160	150	259	460.6
400	XM_372160	LOC389814	M-029445-00	-0.419	2.127	3.401	172	-0.37	1.762	3.482	420	-0.047	1.355	3.192	1359	95	112	82	461.3
401	NM_016291	IHPK2	M-006738-00	-0.389	1.584	3.175	627	-0.824	1.584	2.579	632	-0.607	2.184	2.927	250	255	236	271	462.7
402	NM_014962	BTBD3	M-012943-00	1.799	1.29	ND	689	2.041	1.59	ND	383	2.215	1.774	ND	377	112	92	0	463.4
403	NM_013301	HSU79303	M-020402-00	1.919	1.271	1.835	348	1.459	1.225	1.065	1421	2.481	1.793	2.279	203	227	235	226	464.8
404	NM_005502	ABCA1	M-004128-02	1.38	1.645	2.312	544	1.734	2.084	2.917	205	1.558	1.307	2.326	906	260	241	228	465.8
405	NM_000376	VDR	M-003448-00	2.194	0.95	1.836	346	2.035	0.775	1.762	421	2.187	1.503	1.699	694	234	220	71	465.8
406	NM_021632	ZNF350	M-017814-00	2.244	0.674	1.725	459	1.939	0.453	1.42	936	2.205	0.863	2.644	237	200	223	188	467.0
407	NM_178496	LOC151963	M-018391-00	0.098	2.412	2.846	83	-0.002	1.626	2.487	570	-0.393	1.104	1.463	2157	153	184	101	467.3
408	NM_033209/	TTHY1	M-015090-00	1.047	2.987	1.771	413	1.267	2.885	1.684	491	0.78	2.245	1.842	509	261	196	246	469.1
409	NM_004771	MMP20	M-005960-00	1.418	0.431	1.642	906	1.329	0.148	1.44	1159	2.657	0.793	2.677	99	185	222	258	470.2
410	NM_173549	FLJ39553	M-018487-00	1.108	1.879	1.709	479	1.174	2.046	1.98	253	1.326	1.881	1.584	867	160	112	222	471.9
411	NM_021007	SCN2A2	M-006298-00	1.603	2.222	1.098	603	1.679	2.222	1.087	496	2.043	2.019	1.028	360	198	161	247	475.7
412	NM_025134	CHD9	M-031153-00	0.267	1.807	1.808	382	0.317	1.334	1.362	1146	1.099	1.103	2.186	248	114	139	75	477.1
413	NM_016153	LW-1	M-031953-00	2.099	1.739	1.957	256	1.961	1.505	1.598	616	1.099	1.703	1.826	689	217	223	106	477.2
414	NM_021005	NR2F2	M-003422-00	2.091	1.607	ND	327	2.119	1.7	0.452	474	2.352	1.637	1.69	703	222	236	220	477.6
415	XM_380129	LOC402564	M-031809-00	1.164	2.238	1.667	520	1.598	2.57	1.887	319	1.721	1.284	1.866	659	144	147	239	478.1
416	NM_002429	MMP19	M-004048-00	1.761	1.861	1.013	423	1.847	1.663	0.678	513	2.145	1.846	1.121	504	226	249	243	478.2
417	NM_024309	TNIP2	M-014328-00	1.636	2.188	-0.115	556	1.514	1.866	-0.009	751	2.387	2.169	0.168	262	190	93	228	478.3
418	NM_031429	RTBDN	M-014723-00	2.89	1.138	ND	229	1.722	0.927	ND	1174	2.369	1.543	ND	409	101	214	20	479.1
419	NM_145039	MGC16385	M-016551-00	2.478	0.926	ND	485	2.78	0.562	ND	504	2.581	1.239	ND	453	235	130	35	480.2
420	NM_145036	MGC33887	M-016483-00	0.668	1.85	2.442	326	0.513	1.832	2.176	371	1.115	1.55	2.029	921	52	134	151	481.2

inc.	GeneID	Gene Name	Cat No	SCPO r1	SCPO r2	SCPO r3	SCPO rank	STAPO r1	STAPO r2	STAPO r3	STAPO rank	STIPO r1	STIPO r2	STIPO r3	STIPO rank	OC r1	OC r2	OC r3	rank product
421	XM_293903	LOC345630	M-024320-00	ND	1.178	1.748	824	ND	1.45	1.46	868	ND	2.181	2.646	156	5	88	85	481.4
422	NM_018031	WDR6	M-013085-00	1.1	0.871	0.951	2489	2.003	1.822	1.975	254	1.637	3.108	2.353	178	263	130	119	482.8
423	NM_001336	CTSZ	M-005846-01	2.508	1.596	0.294	616	2.659	1.904	0.421	307	2.851	1.766	0.516	602	241	220	229	484.7
424	NM_004384	CSNK1G3	M-004679-02	1.132	ND	2.211	514	0.858	ND	2.308	634	1.5	ND	2.56	350	182	0	156	485.0
425	NM_006396	SSSCA1	M-020119-00	1.974	0.054	1.811	376	1.688	-0.013	1.788	486	1.745	0.358	2.528	629	192	87	154	486.2
426	NM_001206	BTEB1	M-011223-00	0.516	2.508	ND	749	0.684	2.521	ND	607	1.365	2.996	ND	253	202	194	14	486.3
427	NM_178168	OR10A5	M-008750-00	0.616	1.777	2.019	405	0.729	1.881	1.912	324	0.706	1.568	2.801	888	221	193	130	488.4
428	XM_374787	LOC399747	M-029675-00	0.6	1.363	2.734	1025	0.711	1.902	2.657	310	0.463	2.156	2.008	368	190	152	164	489.0
429	NM_144999	MGC20806	M-016887-00	0.266	1.447	1.955	850	0.344	1.937	2.165	275	0.227	1.851	2.26	503	178	146	194	489.9
430	NM_052850	GADD45GIP1	M-003752-00	1.412	1.65	1.876	537	1.231	1.681	1.728	494	1.089	1.914	2.586	445	128	88	85	490.6
431	NM_032889	MGC11308	M-018634-00	0.787	1.57	1.327	1124	1.19	1.956	1.868	332	1.479	2.734	2.083	318	200	180	230	491.4
432	NM_015884	MBTPS2	M-005940-01	1.676	1.892	1.941	293	1.79	1.764	1.655	416	1.216	1.511	1.828	985	210	121	239	493.3
433	NM_005122	NR1I3	M-003416-01	2.081	1.445	1.529	716	2.095	1.669	1.519	506	2.51	1.086	2.064	332	221	261	248	493.6
434	NM_052858	MRVLDC3	M-015143-00	-1.164	1.856	1.856	323	-1.379	1.712	1.57	665	-0.202	1.786	2.272	560	235	188	193	493.6
435	NM_000576	IL1B	M-007953-01	1.662	1.825	3.182	359	1.713	2.156	3.015	169	1.031	1.13	2.631	2048	104	227	244	499.0
436	NM_004789	LHX2	M-019197-00	1.601	1.719	2.045	463	1.991	1.331	1.879	326	1.607	1.564	1.748	831	238	203	169	500.6
437	NM_004004	GJB2	M-019285-00	1.842	-1.267	2.13	336	1.954	-1.48	2.57	267	1.34	-1.39	2.004	1409	147	214	186	501.9
438	XM_042066	MAP3K1	M-003575-01	0.861	1.744	2.734	438	0.653	1.909	2.575	302	0.988	1.524	2.226	966	121	224	193	503.7
439	NM_003480	MFAP5	M-011425-00	-0.169	1.74	2.11	443	-0.297	1.394	2.232	1001	-0.007	2.121	2.812	289	194	207	189	504.2
440	NM_018064	C6ORF166	M-031863-00	0.086	1.446	2.078	852	-0.112	1.087	1.68	1885	1.265	2.772	3.027	80	80	179	99	504.6
441	NM_001176	ARHGDIG	M-012566-00	ND	2.506	1.055	402	ND	2.462	1.265	339	ND	2.545	0.525	950	27	152	172	505.9
442	NM_016480	PAIP2	M-015376-00	1.385	2.188	0.813	979	1.911	2.33	1.442	297	1.912	3.539	1.839	449	241	192	97	507.3
443	NM_138960	TGIF2LX	M-019164-00	1.781	0.793	2.197	401	1.832	0.973	2.505	369	1.569	1.213	2.664	884	269	230	243	507.6
444	NM_021938	BRUNOL5	M-016648-00	1.288	1.919	1.446	851	1.407	2.011	2.125	239	1.619	1.732	1.931	647	172	174	127	508.6
445	NM_012288	TRAM2	M-032514-00	0.881	2.626	2.147	158	0.719	3.08	2.146	174	0.008	2.3	0.622	4835	247	206	104	510.3
446	NM_178124	LOC91966	M-018483-00	2.429	1.824	0.789	360	2.641	2.035	0.807	228	2.825	1.26	1.144	1621	204	225	221	510.5
447	NM_003061	SLIT1	M-012599-00	1.689	2.6	ND	160	0.886	1.981	ND	907	0.951	2.134	ND	937	146	104	9	514.2
448	XM_372124	ZCCHC6	M-026009-00	1.745	1.579	1.083	639	2.107	2.271	1.126	190	1.81	1.446	0.255	1124	185	241	221	514.8
449	NM_031446	C18ORF21	M-016886-00	-0.072	1.729	1.398	951	0.037	2.024	1.692	480	0.754	2.11	2.141	299	226	237	166	514.9
450	NM_173605	KCNRG	M-018264-00	1.914	4.684	1.229	282	1.577	4.748	1.296	648	1.372	5.268	1.656	749	139	151	204	515.3
451	NM_031430	RILP	M-008787-00	0.277	2.347	1.679	508	0.174	2.559	1.801	390	0.737	2.336	1.693	699	187	250	185	517.4
452	NM_004970	IGFALS	M-010929-00	1.926	2.044	1.741	277	1.903	2.183	1.724	308	1.212	2.05	1.259	1627	230	211	164	517.8
453	XM_290734	LOC339162	M-022959-00	3.232	1.565	1.342	657	3.481	1.462	1.326	853	3.251	2.184	1.762	249	168	90	144	518.7
454	NM_014172	PHPT1	M-016904-00	1.873	2.278	0.762	307	1.624	2.224	0.617	575	1.621	2.096	0.765	796	247	175	226	519.9
455	NM_006421	BIG1	M-012207-00	ND	0.843	1.793	1146	ND	0.499	1.456	2370	ND	2.841	3.092	52	28	121	99	520.8
456	NM_016546	C1RL	M-007816-00	1.735	2.248	0.27	450	1.845	1.496	0.014	780	1.967	2.636	0.994	403	138	226	209	521.0
457	NM_198075	DKFZP761L15	M-026730-00	1.772	-0.54	1.922	412	2.108	-0.876	1.79	398	1.586	-1.055	1.969	864	242	259	234	521.3
458	NM_001232	CASQ2	M-011228-00	1.844	2.255	0.562	333	1.982	2.31	0.388	252	1.237	1.997	0.276	1689	248	227	254	521.4
459	NM_018456	EAF2	M-006313-00	2.458	1.495	0.399	768	2.08	1.96	0.46	263	2.319	1.682	0.529	717	246	230	266	525.1
460	NM_020119	ZC3HAV1	M-017449-00	3.068	1.526	1.456	720	2.296	1.327	0.664	1166	3.258	2.278	2.366	173	226	185	147	525.6
461	NM_144770	RBM11	M-015436-00	1.953	0.04	1.843	334	1.613	-0.143	1.57	663	2.226	0.141	1.723	657	181	161	92	525.9
462	NM_130772	S100Z	M-015295-00	2.395	0.826	1.54	698	2.306	0.742	1.518	743	2.371	2.125	1.765	286	232	237	226	529.3
463	NM_182760	SUMF1	M-019387-00	1.794	1.857	0.945	392	1.622	1.58	0.822	640	1.94	1.768	0.686	597	128	115	91	531.1
464	NM_024735	FBXO31	M-016541-00	1.578	2.256	1.395	641	1.781	2.339	1.707	406	1.776	2.234	0.963	578	230	260	185	531.8
465	NM_153337	SLIC1	M-016514-00	2.657	0.829	ND	440	3.056	1.057	ND	216	1.946	0.592	ND	1587	237	222	29	532.3
466	NR_001435	HLA-DPB2	M-010949-00	1.598	1.899	ND	433	1.685	1.995	ND	361	1.275	1.766	ND	971	74	107	33	533.4
467	NM_145203	CSNK1A1L	M-004681-01	1.627	1.764	0.65	565	1.967	2.457	0.703	258	1.486	1.606	0.842	1042	139	173	193	533.6
468	NM_022486	SUSD1	M-014096-00	-0.326	1.955	2.029	258	-0.503	2.045	1.705	470	-0.714	1.394	1.722	1256	236	235	231	534.0
469	NM_020547	AMHR2	M-005307-01	1.193	1.552	2.439	673	1.318	2.088	2.465	202	0.931	1.446	2.204	1126	283	232	226	534.9
470	NM_003601	SMARCA5	M-011478-00	1.239	1.687	1.574	646	1.138	1.545	1.447	885	1.937	2.335	2.161	268	243	223	247	535.1
471	NM_017860	FLJ20519	M-016312-00	1.698	2.221	0.696	491	1.928	1.877	0.606	327	1.529	2.243	1.069	959	240	224	221	536.0
472	NM_002124	HLA-DRB1	M-011688-00	1.345	1.115	1.719	1069	1.684	2.249	2.084	204	1.894	1.688	1.372	708	244	163	191	536.5
473	NM_015462	DKFZP586L07	M-016695-00	1.934	1.359	1.593	619	1.835	1.445	1.546	700	2.342	2.023	1.461	357	281	189	225	536.8
474	NM_014623	MEA	M-020344-00	1.712	1.522	1.08	731	2.417	2.266	1.27	140	1.297	1.509	1.064	1515	211	155	140	537.2
475	NM_016641	MIR16	M-009233-00	1.783	1.484	1.732	454	2.04	1.376	2.025	234	3.23	1.314	1.225	1468	236	235	226	538.3
476	XM_371108	LOC388462	M-031016-00	3.617	1.955	1.682	257	3.724	1.843	1.478	359	3.667	0.689	1.236	1694	119	106	225	538.7
477	NM_017684	VPS13C	M-020641-00	1.234	1.952	2.208	260	1.007	1.468	2.473	839	0.439	1.677	2.53	719	216	134	167	539.3
478	NM_000667	ADH1A	M-006520-01	1.471	1.699	1.791	487	1.434	1.635	2.018	556	1.504	2.399	1.772	589	131	174	192	542.3
479	NM_014509	DJ222E13.1	M-004907-00	1.609	1.881	-1.3	591	2.144	2.933	-1.771	176	1.282	2.015	-1.303	1545	243	202	256	543.7
480	NM_005106	DLEC1	M-011983-00	3.186	1.765	1.445	422	2.244	1.639	1.436	550	3.028	1.033	1.697	696	139	116	164	544.6

inc.	GeneID	Gene Name	Cat No	SCPO r1	SCPO r2	SCPO r3	SCPO rank	STAPO r1	STAPO r2	STAPO r3	STAPO rank	STIPO r1	STIPO r2	STIPO r3	STIPO rank	OC r1	OC r2	OC r3	rank product
481	XM_378861	LOC400752	M-027469-00	1.82	-0.066	2.101	365	1.911	-0.441	2.632	299	1.434	-0.968	1.305	1493	116	148	131	546.2
482	NM_024585	FLJ22160	M-016231-00	0.806	1.833	2.182	353	0.75	1.424	1.881	926	1.06	2.292	1.854	499	148	123	220	546.4
483	XM_373395	LOC392582	M-031677-00	1.896	2.531	-1.489	291	2.048	2.203	-1.65	223	1.015	2.758	-0.981	2521	132	164	169	546.9
484	NM_006242	PPP1R3D	M-021439-01	-0.867	1.564	1.542	693	-0.952	1.66	1.96	518	-0.458	1.903	2.169	459	192	127	173	548.2
485	NM_000323	RET	M-003170-01	1.627	1.922	1.56	566	1.854	2.092	1.087	350	1.604	1.631	1.362	838	159	162	112	549.6
486	XM_379484	LOC401324	M-028834-00	1.74	1.672	0.769	513	1.948	1.668	0.703	508	1.876	1.739	1.679	639	119	82	181	550.2
487	XM_377630	LOC401983	M-027580-00	ND	1.935	1.554	437	ND	1.557	1.098	1165	ND	2.274	1.86	331	0	147	228	552.3
488	NM_018389	SLC35C1	M-010693-00	1.966	1.818	-0.01	367	1.832	1.399	-0.176	991	2.792	1.896	0.651	464	224	198	242	552.6
489	NM_006186	NR4A2	M-003427-02	1.906	1.272	ND	622	1.805	1.49	-0.329	791	3.134	2.046	0.924	344	239	155	142	553.1
490	NM_001983	ERCC1	M-006311-00	-0.442	1.497	1.869	766	-0.262	1.875	2.367	328	-0.152	2.237	1.711	676	235	141	128	553.8
491	NM_080878	ITLN2	M-008590-00	ND	1.545	1.719	561	ND	2.03	1.676	351	ND	1.952	1.204	871	45	124	237	555.6
492	NM_013356	SLC16A8	M-007410-00	0.63	2.17	2.045	214	0.43	2.349	1.672	503	0.632	1.266	1.549	1597	227	86	107	556.0
493	XM_371146	KIAA1683	M-031251-00	1.41	1.552	1.328	921	2.317	2.434	1.989	128	1.137	1.546	1.317	1460	99	172	225	556.3
494	NM_005601	NKG7	M-016047-00	2.255	1.523	1.801	387	1.589	1.625	1.656	571	1.629	1.228	2.417	779	200	222	173	556.3
495	NM_145025	C6ORF199	M-007254-01	1.158	1.665	2.117	524	1.045	1.458	2.009	859	1.658	1.99	2.126	385	225	222	241	557.5
496	NM_139241	FGD4	M-007123-00	1.71	0	1.885	475	1.595	-0.155	1.655	621	1.786	0.228	1.773	588	249	230	229	557.7
497	NM_004918	TCL1B	M-019892-00	0.75	2.759	0.968	2405	0.578	2.758	1.58	639	0.346	3.922	2.602	113	201	189	235	557.9
498	NM_005520	HNRPH1	M-012107-00	2.341	1.886	1.646	299	2.046	1.57	1.284	664	2.002	1.569	1.476	885	142	143	83	560.1
499	NM_001318	CSHL1	M-010962-00	1.928	1.973	0.36	276	1.868	2.127	0.693	333	2.005	1.162	0.203	1932	65	212	241	562.1
500	NM_015556	SIPA1L1	M-013936-00	1.796	1.823	1.077	390	1.826	1.827	1.171	375	1.766	1.408	0.765	1219	192	134	269	562.8
501	NM_058172	ANTXR2	M-015215-00	1.748	2.035	2.918	219	1.526	1.759	2.303	423	0.827	1.165	1.808	1926	162	221	173	563.0
502	NM_004914	RAB36	M-009553-00	1.055	2.002	2.417	234	1.208	1.553	2.842	691	1.236	1.461	2.758	1105	249	187	264	563.2
503	NM_006345	SLC30A9	M-007530-00	1.808	1.871	1.382	380	1.845	1.648	1.575	531	1.564	1.617	1.562	894	252	255	233	565.0
504	NM_018950	HLA-F	M-013397-00	1.608	1.872	2.517	308	1.425	1.779	2.256	410	1.186	1.331	2.851	1430	98	115	88	565.2
505	NM_016404	HSPC152	M-020786-00	1.074	2.258	ND	522	1.277	2.3	ND	401	1.149	2.021	ND	866	109	116	11	565.9
506	NM_021168	RAB40C	M-010368-00	1.937	2.376	-2.036	270	1.666	2.206	-2.058	509	1.367	2.583	-2.168	1327	226	145	165	567.1
507	NM_014451	B1	M-010940-00	-0.461	1.779	2.374	403	-0.633	1.31	2.303	1204	-0.289	1.996	2.141	376	155	111	80	567.2
508	NM_152715	MGC10233	M-015590-00	2.1	2.319	0.181	190	1.559	1.453	-0.003	874	1.532	1.45	-0.107	1115	156	79	158	570.0
509	NM_003157	NEK4	M-003519-01	1.86	1.43	1.155	881	1.863	1.798	1.164	391	2.387	1.784	1.802	545	174	172	161	572.6
510	NM_021098	CACND1H	M-006128-00	1.164	ND	1.965	658	1.432	ND	1.808	583	1.339	ND	2.387	493	224	3	167	574.0
511	NM_019891	ERO1LB	M-018108-00	2.076	1.629	0.01	562	1.625	1.64	-0.145	572	2.013	1.77	0.58	591	203	234	242	574.9
512	NM_015250	BICD2	M-014060-00	1.327	0.524	1.484	1129	2.072	0.757	2.301	212	1.616	0.394	1.708	806	235	262	220	577.8
513	XM_372917	LOC391353	M-027767-00	1.656	2.646	1.332	532	1.564	2.564	0.896	676	0.675	3.099	1.806	539	163	96	107	578.7
514	NM_023942	MGC3036	M-014261-00	2.067	1.834	-0.058	350	1.477	1.513	-0.282	821	1.708	1.737	-0.127	678	233	61	82	579.7
515	NM_032497	ZNF559	M-014904-00	1.576	1.522	0.604	728	1.593	1.671	0.414	624	2.015	1.924	0.923	432	220	225	233	581.1
516	NM_001662	ARF5	M-011584-00	0.711	1.54	2.519	699	0.308	1.569	2.667	668	1.938	1.506	2.211	423	102	159	104	582.4
517	NM_031280	MRPS15	M-013609-00	2.461	1.638	0.535	554	2.133	1.645	0.582	536	1.86	1.713	0.558	671	226	248	277	584.1
518	NM_023933	MGC2494	M-014255-00	1.899	1.413	1.181	917	2.26	1.816	1.384	381	2.219	1.679	1.78	574	240	116	120	585.3
519	NM_206895	UNQ830	M-031967-00	1.599	0.818	3.096	608	2.253	1.067	4.31	143	1.065	0.928	2.893	2317	215	181	117	586.2
520	NM_000895	LTA4H	M-005935-02	1.968	ND	0.783	1002	2.123	ND	0.591	1093	3.118	ND	1.553	184	92	10	119	586.3
521	NM_00100017	LOC401565	M-032325-00	0.775	2.134	1.71	474	0.602	1.785	1.922	405	0.975	2.139	1.482	1053	141	114	161	586.9
522	XM_374646	LOC392979	M-029178-00	0.587	2.229	1.69	501	0.479	2.681	1.824	376	0.674	1.973	1.466	1090	123	109	141	590.0
523	XM_371070	LOC388403	M-030916-00	1.774	ND	1.001	972	1.731	ND	1.135	909	2.616	ND	1.812	233	230	12	234	590.5
524	NM_015409	EP400	M-021272-00	1.161	0.656	1.309	1620	1.79	1.029	1.852	399	1.899	2.083	2.632	319	187	224	177	590.8
525	NM_203288	RP9	M-031918-00	2.566	ND	1.178	309	1.847	ND	1.257	693	1.848	ND	1.191	974	78	27	51	593.0
526	NM_004750	CRLF1	M-007863-01	1.924	1.028	1.31	1169	1.883	1.178	1.442	895	2.563	2.17	2.291	201	201	153	88	594.7
527	NM_004487	GOLGB1	M-019809-00	0.861	1.702	1.578	642	0.889	2.059	1.934	280	0.825	1.425	1.52	1175	149	238	175	595.5
38	NM_012290	TLK1	M-004174-00	3.172	2.601	2.49	60	2.87	2.824	2.389	42	3.231	3.616	2.468	40	677	166	392	46.5393354
99	NM_006852	TLK2	M-005389-02	4.009	1.054	2.275	125	4.099	1.076	2.352	124	4.358	1.888	2.494	143	864	565	714	130.383483
100	NM_006285	TESK1	M-005043-00	4.023	0.992	2.705	47	4.857	1.545	3.292	14	2.008	0.124	0.842	3388	687	606	661	130.634062
142	NM_013254	TBK1	M-003788-02	4.171	1.342	2.195	150	4.524	1.692	2.479	97	3.518	1.892	2.009	373	305	181	509	175.734599

Table 9.1 500plus genes whose siRNA knock-down increased GFP-LC3 spots in the primary screen

Table of approximately 500 best 'increasers'. Rank based on rank product (RP); GeneID; Gene name; Dharmacon Smartpool catalogue number; SCPO for 3 replicates; STAPO for 3 replicates; STIPO for 3 replicates; Object count (OC) for three replicates; and rank product are shown. ND is not determined, as less than 50 valid objects were counted. Genes highlighted in blue are of interest and spoken of in the text. Genes highlighted in yellow were contained on plate 10 and not processed with screen plates.

dec.	GeneID	Gene Name	Smartpool Cat	SCPO r1	SCPO r2	SCPO r3	SCPO rank	STAPO r1	STAPO r2	STAPO r3	STAPO rank	STIPO r1	STIPO r2	STIPO r3	STIPO rank	OC r1	OC r2	OC r3	rank product
1	NM_003973	RPL14	M-012948-00	-3.87	ND	-3.231	1	-3.456	ND	-2.848	2	-3.234	ND	-2.483	2	74	12	68	1.6
2	NM_130467	PAGE-5	M-017468-00	-0.082	-3.109	-4.702	4	-0.199	-3.299	-3.768	1	-0.336	-2.618	-3.353	6	201	155	125	2.9
3	NM_002039	GAB1	M-003553-00	-4.472	-1.495	-3.176	2	-3.971	-1.319	-2.663	10	-3.646	-1.112	-2.61	7	239	255	236	5.2
4	NM_031287	SF3B5	M-014706-00	-2.182	ND	-3.921	5	-1.718	ND	-3.598	12	-1.747	ND	-3.723	3	125	26	122	5.6
5	NM_001060	TBXA2R	M-005740-01	-1.31	-2.966	-3.007	7	-0.785	-2.322	-2.367	50	-1.661	-3.066	-2.894	1	194	220	240	7.0
6	NM_015127	MCLC	M-010024-00	-2.86	0.898	-2.979	14	-2.972	0.826	-3.292	3	-2.458	0.926	-3.19	15	247	223	82	8.6
7	NM_024507	KREMEN2	M-003847-02	-3.123	-3.349	-2.437	3	-2.296	-2.877	-2.213	54	-2.733	-2.843	-2.184	4	172	248	235	8.7
8	NM_024650	FLJ22531	M-018410-00	-2.73	-1.696	-3.32	20	-2.662	-1.599	-3.273	11	-2.657	-1.356	-2.392	19	241	240	129	16.1
9	NM_003586	DOC2A	M-011476-00	-3.111	ND	-2.427	16	-2.782	ND	-2.276	21	-2.699	ND	-2.265	13	179	0	223	16.3
10	XM_034086	KIAA1107	M-021628-00	-3.6	-1.588	ND	30	-3.399	-1.836	ND	15	-3.273	-1.723	ND	11	227	143	0	17.0
11	NM_080928	ASB15	M-031158-00	-2.399	-3.004	-2.878	12	-1.9	-2.894	-2.501	25	-2.432	-2.674	-1.904	17	205	117	156	17.2
12	NM_019886	CHST7	M-008443-00	-3.234	-2.562	0.141	33	-2.867	-2.862	0.057	6	-2.7	-2.281	-0.113	28	282	228	130	17.7
13	NM_022467	CHST8	M-010067-00	-3.124	-2.054	-2.772	15	-3.694	-1.778	-2.88	5	-2.826	-1.771	-2.02	91	227	223	241	19.0
14	NM_015971	MRPS7	M-013580-00	-3.095	-2.87	-1.78	13	-2.888	-2.478	-1.897	27	-2.785	-2.32	-1.798	23	123	222	229	20.1
15	NM_005277	GPM6A	M-010598-00	-2.648	-2.61	-0.011	28	-2.996	-2.688	0.03	8	-2.254	-2.182	0.333	45	119	151	78	21.6
16	NM_003820	TNFRSF14	M-008096-00	-2.89	-2.956	-1.614	11	-2.098	-3.069	-1.002	106	-2.525	-2.705	-1.263	9	228	236	224	21.9
17	NM_173557	RNF152	M-007160-00	-2.622	-3.429	ND	6	-1.979	-2.362	ND	80	-2.18	-2.48	ND	22	72	99	26	21.9
18	NM_021818	SAV1	M-013070-00	-2.135	-3.489	-2.893	10	-1.913	-2.166	-2.607	82	-1.736	-2.437	-2.359	21	220	239	222	25.8
19	NM_032790	FLJ14466	M-014998-00	-2.714	-3.203	-0.948	23	-1.948	-2.791	-0.718	171	-2.725	-2.801	-1.323	5	232	228	185	27.0
20	NM_181775	DKFZP434G06	M-018881-00	-2.185	-3.245	-2.937	8	-2.274	-2.86	-2.436	37	-1.711	-2.689	-2.068	71	222	247	211	27.6
21	NM_003820	TNFRSF14	M-008096-00	-2.89	-2.956	-1.614	11	-2.098	-3.069	-1.002	106	-2.525	-2.705	-1.263	9	228	236	224	21.9
22	XM_377566	LOC401940	M-027646-00	-2.157	-2.84	ND	43	-2.545	-2.63	ND	18	-1.885	-2.506	ND	43	230	164	49	32.2
23	NM_021210	TRAPPC1	M-013781-00	-2.876	-2.557	-2.519	35	-2.887	-2.426	-2.166	39	-2.851	-2.285	-2.059	27	143	111	189	33.3
24	NM_013379	DPP7	M-005854-00	-0.681	-2.465	-3.992	46	-0.661	-2.547	-4.171	20	-0.719	-2.179	-3.142	46	229	249	270	34.8
25	NM_018250	FLJ10871	M-020275-00	-4.198	-2.147	0.085	127	-3.803	-2.693	0.241	7	-3.284	-2.154	-0.063	51	248	151	226	35.7
26	NM_021948	BCAN	M-016130-00	-2.818	-1.619	-2.731	19	-2.335	-1.101	-2.106	105	-2.277	-1.747	-2.348	29	230	87	240	38.7
27	XM_370618	FLJ20294	M-029987-00	-2.233	1.255	-2.043	174	-2.492	0.555	-2.402	41	-2.542	0.949	-2.505	10	261	122	199	41.5
28	XM_372046	LOC389667	M-029395-00	-2.252	-3.569	-2.893	9	-1.859	-3.31	-2.314	52	-1.859	-2.906	-1.842	162	237	262	245	42.3
29	NM_003123	SPN	M-027326-00	-3.337	-2.417	0.043	52	-2.667	-2.737	0.031	9	-2.861	-1.852	0.49	167	192	216	240	42.8
30	NM_015163	TRIM9	M-012974-00	-0.495	-2.969	-2.471	45	-0.146	-2.869	-2.646	14	0.032	-1.913	-1.946	133	95	207	166	43.8
31	NM_021267	LASS1	M-010275-00	-0.826	-2.395	-3.259	59	-0.523	-2.648	-2.781	13	-0.773	-1.953	-2.946	111	166	214	72	44.0
32	NM_032836	FLJ14768	M-015014-00	-2.963	-2.169	-1.422	120	-2.917	-3.077	-1.596	4	-2.545	-1.816	-1.314	196	201	213	177	45.5
33	XM_376307	DKFZP667E05	M-028343-00	-1.183	-2.585	-2.833	32	-0.912	-2.46	-2.578	29	-1.027	-3.468	-1.95	114	234	106	118	47.3
34	NM_031448	C19ORF12	M-014731-00	-2.647	-0.278	-2.283	89	-2.506	-0.189	-2.54	24	-2.147	-0.226	-2.265	52	176	235	246	48.1
35	XM_372213	USP27X	M-031532-00	0	-4.377	-2.758	17	-0.074	-3.508	-1.945	172	-0.387	-2.897	-2.198	42	128	122	233	49.7
36	NM_004934	CDH18	M-011992-00	-2.277	ND	-2.629	48	-1.81	ND	-2.187	149	-1.995	ND	-2.743	20	246	39	171	52.3
37	NM_018487	HCA112	M-019157-00	-1.59	-2.577	-2.45	49	-1.405	-2.498	-2.437	35	-1.591	-2.035	-2.072	86	250	264	233	52.8
38	NM_003877	SOCS2	M-017604-00	-3.533	-2.054	-1.303	170	-2.792	-2.515	-1.39	22	-3.043	-2.213	-0.627	40	266	186	248	53.1
39	NM_032850	ZFYVE19	M-017961-00	-2.4	-2.524	0.765	56	-2.393	-3.503	0.686	42	-2.078	-2.142	0.675	65	261	235	231	53.5
40	NM_014147	HSPC047	M-020654-00	-2.541	-2.242	ND	60	-2.521	-2.019	ND	60	-2.415	-1.977	ND	44	219	125	15	54.1
41	NM_182505	C9ORF85	M-019397-00	-2.426	ND	-2.768	29	-2.196	ND	-2.041	98	-2.156	ND	-2.094	57	159	10	254	54.5
42	NM_152360	ZNF573	M-016620-00	-2.209	-2.59	-1.336	110	-2.017	-2.22	-1.314	139	-2.487	-2.767	-1.193	12	251	224	258	56.8
43	XM_374501	LOC392762	M-031823-00	-1.261	-2.642	-2.968	26	-1.113	-2.447	-2.708	32	-0.795	-1.736	-2.475	256	160	155	192	59.7
44	NM_173351	OR6B3	M-032532-00	-2.124	-2.709	ND	53	-1.832	-2.338	ND	110	-1.997	-2.453	ND	37	248	121	35	60.0
45	NM_020828	ZFP28	M-014089-00	-3.106	-2.136	-2.735	18	-3.028	-1.743	-2.421	40	-2.683	-1.466	-1.663	322	111	111	138	61.4
46	NM_032852	APG4C	M-005788-00	-2.847	-2.199	-0.653	115	-2.451	-2.686	-0.725	31	-3.059	-2.073	-0.954	68	254	161	235	62.4
47	NM_017969	FLJ10006	M-010671-00	-2.42	-2.867	-0.236	51	-2.238	-3.248	-0.024	67	-2.067	-2.188	-0.415	72	265	232	229	62.7
48	XM_372884	CECR2	M-024450-00	-1.715	-3.023	-2.637	27	-1.387	-2.15	-2.57	86	-1.791	-3.204	-1.957	109	190	188	236	63.3
49	NM_002336	LRP6	M-003845-01	-1.548	-2.724	-2.818	22	-1.56	-2.053	-2.594	121	-1.808	-1.985	-2.331	102	280	256	236	64.8
50	NM_001375	DNDSE2	M-009667-00	-2.322	-2.237	-2.943	77	-1.935	-2.114	-2.595	100	-2.527	-1.81	-2.229	36	194	230	245	65.2
51	NM_014548	TMOD2	M-020360-00	-2.296	-2.503	-1.614	84	-2.261	-2.485	-1.816	62	-2.137	-2.484	-1.713	54	245	252	216	65.5
52	XM_209076	LOC284232	M-023380-00	-1.972	-2.701	-2.514	39	-1.613	-2.288	-3.374	58	-1.483	-1.92	-2.378	128	211	222	142	66.2
53	NM_015320	ARHGEF4	M-008235-00	-3.043	-2.249	-0.032	99	-2.143	-2.03	0.556	129	-2.364	-2.317	-0.362	24	224	235	200	67.4
54	NM_031461	LOC83690	M-016681-00	-3.217	-2.461	-0.71	47	-2.155	-2.12	-0.425	95	-2.247	-2.07	-1.336	69	230	232	220	67.5
55	NM_006362	NXF1	M-013680-00	-2.481	ND	-1.941	108	-2.428	ND	-1.811	96	-2.484	ND	-2.008	31	80	48	59	68.5
56	NM_130830	LRRC15	M-015301-00	-3.847	-2.292	-1.093	86	-4.05	-2.177	-1.28	79	-3.062	-2.169	-1.082	48	151	242	195	68.8
57	XM_374026	LOC389081	M-028024-00	-3.127	-2.518	-0.359	38	-2.422	-2.384	-0.623	45	-2.493	-1.822	-0.789	191	271	243	239	68.9
58	NM_006793	PRDX3	M-010355-00	-1.218	-2.403	-2.429	54	-0.967	-2.086	-2.385	108	-1.087	-2.104	-2.511	60	249	265	265	70.5
59	NM_005548	KARS	M-012114-00	-3.272	-2.558	-2.286	34	-3.05	-2.205	-1.622	72	-2.726	-1.879	-1.875	152	155	72	163	71.9
60	XM_374185	LOC389437	M-028618-00	-1.844	-2.547	-2.386	64	-1.704	-2.725	-2.512	23	-1.7	-2.513	-1.522	286	232	141	175	74.9

dec.	GeneID	Gene Name	Smartpool Cat	SCPO r1	SCPO r2	SCPO r3	SCPO rank	STAPO r1	STAPO r2	STAPO r3	STAPO rank	STIPO r1	STIPO r2	STIPO r3	STIPO rank	OC r1	OC r2	OC r3	rank product
61	NM_025026	FLJ14107	M-014554-00	-2.451	-2.301	-0.985	81	-2.631	-2.589	-1.227	17	-2.658	-1.669	-0.568	318	219	235	132	75.9
62	NM_138333	C9ORF42	M-015499-00	-3.453	-1.504	-2.556	36	-4.507	-1.304	-2.169	81	-2.78	-0.988	-1.878	153	237	239	257	76.4
63	XM_371092	LOC388440	M-030992-00	-2.135	ND	-2.419	92	-2.137	ND	-2.135	90	-2.317	ND	-1.944	56	185	7	222	77.4
64	NM_004676	PRY	M-019833-00	-2.054	-1.903	-2.519	169	-1.796	-2.383	-2.319	51	-2.136	-1.94	-2.279	55	248	218	150	78.0
65	NM_004189	SOX14	M-019055-00	-0.401	-2.274	-2.222	106	-0.703	-2.28	-2.109	103	-0.309	-2.651	-2.176	47	197	137	137	80.1
66	NM_006360	GA17	M-016219-00	-1.646	-2.21	-2.693	109	-1.611	-2.611	-2.556	19	-1.181	-1.74	-2.169	249	223	164	225	80.2
67	NM_032324	MGC13186	M-006805-00	-0.822	-2.22	-3.526	107	-0.582	-2.39	-3.041	44	-0.835	-1.945	-2.731	116	255	238	231	81.7
68	NM_016930	STX18	M-020624-00	-2.631	-1.99	-2.056	167	-2.439	-1.652	-2.482	34	-2.074	-1.985	-1.976	101	229	198	275	83.1
69	NM_207433	FLJ44874	M-032108-00	-2.373	-1.878	-2.677	67	-2.027	-1.866	-2.688	131	-1.917	-2.175	-2.077	67	126	165	138	83.8
70	NM_080924	LOC91219	M-013362-00	-2.579	-2.398	-2.43	50	-3.012	-2.08	-2.295	55	-2.075	-1.78	-1.545	222	160	209	58	84.8
71	NM_020789	IGSF9	M-014056-00	-2.466	-1.657	-2.041	176	-1.996	-0.657	-1.652	439	-2.557	-2.228	-2.657	8	235	268	260	85.2
72	XM_375500	MGC16597	M-030964-00	-2.269	-0.121	-2.386	94	-2.478	0.068	-2.287	59	-2.067	0.044	-1.937	123	193	165	126	88.0
73	NM_003169	SUPT5H	M-016234-00	-2.513	-2.004	-2.395	58	-2.114	-2.122	-2.191	93	-1.92	-1.656	-2.016	127	256	213	122	88.2
74	NM_001709	BDNF	M-017626-00	-2.292	-2.761	-0.723	85	-1.792	-2.799	-0.47	273	-2.241	-3.19	-0.737	32	237	240	238	90.6
75	NM_005000	NDUFA5	M-012000-00	-2.353	-1.075	-3.62	70	-2.06	-0.92	-3.079	119	-2.024	-1.024	-3.067	90	237	197	199	90.8
76	NM_024019	NEUROG2	M-009009-00	-3.82	-0.91	-2.319	78	-3.589	-0.456	-1.83	241	-3.178	-1.349	-2.21	41	245	166	235	91.7
77	NM_003598	TEAD2	M-012611-00	-1.885	-2.569	-2.267	95	-1.684	-2.227	-2.11	102	-1.87	-2.684	-2.025	89	233	176	226	95.2
78	NM_024331	C20ORF121	M-014340-00	-1.633	-2.129	-2.448	132	-1.239	-1.785	-2.112	281	-1.497	-2.287	-2.305	26	225	241	249	98.8
79	NM_198851	LOC348645	M-024639-00	-1.929	-2.651	-2.773	25	-1.632	-2.02	-2.361	137	-1.106	-1.687	-1.937	299	127	146	88	100.8
80	NM_020389	TRPC7	M-006512-01	-2.291	-0.863	-2.379	87	-2.229	-0.954	-2.486	68	-1.838	-0.646	-2.023	179	227	152	225	101.9
81	XM_059923	LOC137829	M-021527-00	-2.25	-2.549	ND	57	-1.844	-2.35	ND	107	-1.658	-1.989	ND	190	222	87	30	105.0
82	NM_003420	ZNF35	M-006577-00	-0.442	-3.03	-2.497	44	-0.31	-1.963	-2.325	166	-0.341	-2.245	-1.854	164	244	153	223	106.2
84	NM_001561	TNFRSF9	M-008105-01	-1.88	-2.455	1.311	297	-2.429	-2.526	1.009	38	-1.939	-2.357	1.073	120	211	228	180	110.6
85	NM_004638	BAT2	M-013299-00	-2.044	-2.831	-0.959	173	-1.86	-2.593	-1.269	221	-2.22	-2.469	-0.485	38	179	185	62	113.3
86	NM_021969	NR0B2	M-003410-00	-2.078	-1.259	-2.445	158	-1.967	-0.985	-1.782	285	-2.238	-1.123	-2.338	33	207	258	187	114.1
87	NM_021196	SLC4A5	M-007585-00	-2.777	0.837	-2.233	103	-2.823	1.372	-2.056	120	-2.385	0.202	-1.936	124	229	89	265	115.3
88	NM_032644	MGC2452	M-014948-00	ND	-1.964	-2.762	68	ND	-1.484	-2.305	205	ND	-1.669	-2.242	110	11	101	240	115.3
89	NM_031310	PLVAP	M-014714-00	-2.867	-0.469	-2.253	97	-2.071	-0.131	-2.024	134	-1.943	-0.418	-2.138	118	197	227	245	115.3
90	NM_198989	DLEU7	M-032243-00	-1.017	-2.5	-2.567	42	-0.729	-1.795	-2.589	269	-1.029	-1.901	-2.487	141	194	205	54	116.8
91	NM_052931	SLAMF6	M-013423-01	-3.223	-2.038	-0.17	180	-3.305	-2.081	0.154	112	-3.276	-2.048	0.242	81	241	228	229	117.8
92	XM_085236	LOC145788	M-022246-00	-0.873	-2.207	-2.733	112	-0.489	-2.211	-2.494	70	-0.869	-1.796	-2.014	211	159	220	125	118.3
93	NM_152355	ZNF441	M-016909-00	-2.525	-1.98	-1.711	215	-2.578	-1.786	-1.898	201	-2.425	-2.216	-1.472	39	257	235	243	119.0
94	NM_021153	CDH19	M-013105-00	-2.482	-2.229	-2.033	104	-1.861	-1.685	-1.739	326	-2.156	-1.861	-2.173	50	161	234	147	119.2
95	NM_032825	ZNF382	M-018627-00	-3.522	-0.505	-2.066	164	-3.29	-1.128	-2.162	83	-2.76	0.121	-1.933	125	133	99	262	119.4
96	NM_018953	HOXC5	M-013381-00	-2.151	ND	-2.496	76	-1.786	ND	-1.916	227	-1.973	ND	-1.989	104	76	18	220	121.5
97	NM_016932	SIX2	M-017024-00	-2.269	-1.687	-2.193	117	-2.385	-1.776	-2.197	75	-2.064	-1.767	-1.788	217	245	231	253	123.9
98	NM_173597	FLJ37587	M-018271-00	-2.209	-2.313	-0.687	111	-2.004	-2.183	-0.455	146	-1.941	-2.146	-0.977	119	243	241	160	124.5
99	NM_174980	VN1R3	M-017659-00	-2.35	-2.201	-1.059	113	-2.114	-1.77	-0.562	302	-2.457	-2.104	-1.424	59	237	260	222	126.3
100	NM_024953	FLJ13089	M-014530-00	ND	-2.487	-1.518	201	ND	-2.628	-1.544	109	ND	-2.335	-1.667	97	7	142	203	128.6
101	NM_005496	SMC4L1	M-006837-00	-2.309	-2.414	-0.561	79	-2.24	-2.108	-0.559	104	-1.83	-1.722	-0.6	267	251	241	224	129.9
102	NM_138457	FOXP4	M-008255-00	-1.742	-0.024	-2.691	419	-1.929	0.138	-1.877	210	-2.304	-0.484	-2.324	25	125	230	197	130.1
103	NM_017566	DKFZP434G05	M-017013-00	-2.095	-0.08	-2.179	151	-2.145	-0.145	-3.05	88	-1.857	0.14	-1.844	173	65	109	242	132.0
104	NM_020653	ZNF287	M-007035-00	-2.096	-2.265	-1.898	149	-1.945	-1.519	-1.773	296	-2.308	-2.147	-2.06	53	225	189	238	132.7
105	XM_371844	TSPYL1	M-028592-00	-2.168	-2.357	-0.918	121	-2.436	-2.67	-0.984	36	-1.994	-1.48	-0.343	569	106	90	54	135.3
106	NM_017751	FLJ20297	M-020681-00	-2.321	-0.064	-1.98	216	-2.346	0	-2.027	132	-2.127	-0.282	-2.027	88	229	222	239	135.9
107	NM_004267	CHST2	M-008963-00	-0.21	-1.914	-2.307	262	-0.512	-1.983	-2.42	152	-0.607	-2.078	-2.259	64	208	193	239	136.6
108	NM_205851	FLJ35700	M-017921-00	ND	-1.997	-2.163	156	ND	-2.027	-1.566	267	ND	-2.148	-2.022	63	7	244	137	137.9
109	XM_378798	LOC400690	M-031095-00	-1.185	-2.285	-2.724	88	-1.006	-2.607	-2.204	73	-1.101	-2.038	-1.584	413	224	262	228	138.4
110	NM_017714	C20ORF13	M-004745-00	-2.569	-0.9	-2.079	157	-2.123	-0.653	-1.604	502	-2.235	-1.111	-2.357	34	285	246	229	138.9
111	NM_020307	CCNL1	M-008682-00	-1.151	ND	-2.501	340	-1.603	ND	-2.975	57	-1.289	ND	-2.516	139	73	4	67	139.1
112	NM_152505	C21ORF13	M-016527-00	-1.88	-0.682	-2.775	296	-2.07	-0.474	-2.241	116	-2.052	-0.494	-2.331	80	263	281	246	140.0
113	XM_373731	KRTAP4-9	M-030880-00	-0.7	-2.193	-2.517	116	-0.578	-1.968	-2.889	164	-0.575	-1.889	-2.44	146	233	240	222	140.6
114	NM_015896	ZMYND10	M-021401-00	-2.201	-2.94	-1.378	114	-1.678	-2.507	-1.225	405	-2.091	-2.601	-1.449	62	249	258	242	142.0
115	NM_001147	ANGPT2	M-006315-00	-2.673	-1.918	-2.102	147	-2.707	-1.929	-2.068	117	-2.458	-1.852	-1.769	168	242	233	228	142.4
116	XM_376179	LOC401034	M-028023-00	-2.607	-2.338	-0.158	74	-2.104	-2.078	-0.025	114	-2.086	-1.639	-0.393	348	208	108	189	143.2
117	NM_152235	SFRS8	M-011893-00	-2.125	-2.402	-0.289	134	-2.116	-2.112	-0.095	101	-1.775	-1.883	-0.634	223	237	232	108	144.5
118	XM_210826	LOC286404	M-024668-00	-2.41	-1.016	-1.91	267	-2.146	-1.145	-2.182	87	-1.918	-0.848	-2.025	130	233	129	240	144.5
119	XM_378684	LOC400604	M-030908-00	-1.242	-2.907	-2.117	138	-1.318	-3.037	-2.035	128	-1.025	-2.345	-1.849	171	192	241	231	144.6
120	NM_024512	LRRC2	M-014349-00	0.046	-1.976	-2.843	221	0.092	-2.015	-2.488	140	0.151	-2.087	-2.001	98	236	158	225	144.7

dec.	GeneID	Gene Name	Smartpool Cat	SCPO r1	SCPO r2	SCPO r3	SCPO rank	STAPO r1	STAPO r2	STAPO r3	STAPO rank	STIPO r1	STIPO r2	STIPO r3	STIPO rank	OC r1	OC r2	OC r3	rank product
121	NM_001884	HAPLN1	M-019514-00	-2.148	-2.497	-2.097	126	-1.939	-2.611	-1.855	176	-1.938	-1.658	-1.904	138	178	139	135	145.2
122	NM_017867	FLJ20534	M-020849-00	-2.374	-2.373	-1.773	66	-2.04	-1.574	-1.817	252	-2.399	-1.83	-1.649	185	225	228	225	145.4
123	NM_002965	S100A9	M-011384-00	-1.397	-1.946	-2.566	239	-1.06	-2.578	-2.391	43	-0.781	-1.673	-1.73	315	209	129	229	147.9
124	NM_032814	FLJ14627	M-007097-00	-2.386	-2.021	0.087	188	-2.468	-2.64	0.077	28	-2.232	-1.432	0.333	658	128	122	246	151.3
125	NM_015184	PLCL2	M-008544-00	ND	-1.317	-1.922	585	ND	-1.518	-2.281	200	ND	-1.762	-2.784	30	21	160	116	152.0
126	NM_024814	CBLL1	M-007069-00	-1.284	-3.26	-2.548	37	-0.827	-2.456	-1.966	165	-0.843	-1.993	-1.473	581	243	108	109	152.5
127	NM_006817	C12ORF8	M-012312-00	-1.233	-2.214	-2.094	152	-1.487	-1.983	-2.778	151	-1.441	-1.867	-2.388	160	217	260	178	154.3
128	NM_152742	GPC2	M-016251-00	-2.401	-2.372	ND	63	-1.732	-1.836	ND	282	-2.007	-1.589	ND	210	111	120	11	155.1
129	NM_012467	TPSG1	M-006058-01	0.628	-2.251	-2.016	191	0.492	-2.343	-2.323	48	0.834	-2.018	-1.588	407	231	233	221	155.1
130	NM_001896	CSNK2A2	M-004752-00	-1.916	ND	-2.327	135	-1.363	ND	-2.064	351	-1.688	ND	-2.405	82	186	0	116	157.2
131	NM_153032	FLJ32065	M-016502-00	ND	-2.235	-2.093	122	ND	-1.873	-1.516	381	ND	-2.397	-1.69	84	7	129	124	157.5
132	NM_020631	KIAA0720	M-013873-00	-1.885	-2.129	-1.505	287	-2.153	-2.462	-1.713	84	-1.858	-2.467	-1.036	163	231	239	244	157.8
133	XM_372763	LOC391003	M-027640-00	-2.142	-1.234	-2.489	130	-2.138	-0.847	-2.013	142	-1.791	-1.091	-2.142	216	164	112	201	158.6
134	NM_002139	RBMX	M-011691-00	ND	-2.491	-1.867	118	ND	-2.067	-1.81	177	ND	-2.319	-1.32	192	9	143	114	158.9
135	NM_024015	HOXB4	M-012892-00	-2.142	-1.939	ND	178	-2.318	-1.921	ND	97	-1.9	-1.613	ND	236	70	95	0	159.7
136	NM_004620	TRAF6	M-004712-00	-1.845	-2.049	-2.044	172	-1.808	-2.092	-1.972	158	-1.882	-2.389	-1.663	150	245	223	254	159.7
137	NM_002854	PVALB	M-019703-00	-2.717	-2.401	0.1	55	-2.141	-2.726	0.236	89	-1.355	-2.229	0.056	834	111	73	78	159.8
138	NM_033427	CTTNBP2	M-015103-00	ND	-2.849	-1.655	98	ND	-3.06	-1.423	64	ND	-2.076	-0.785	660	3	82	134	160.6
139	NM_022834	WARP	M-016331-00	-2.467	-2.298	-2.139	82	-2.503	-1.889	-2.444	33	-1.106	-1.255	-0.948	1564	209	154	194	161.8
140	NM_022356	LEPRE1	M-004271-00	-1.978	-1.769	-2.809	220	-2.052	-1.58	-3.123	123	-2.122	-1.545	-1.869	158	265	225	239	162.3
141	NM_153345	FLJ90586	M-016794-00	-2.481	-1.376	-2.125	133	-1.895	-1.191	-2.399	203	-1.865	-1.529	-2.217	161	194	225	102	163.2
142	NM_054021	GPR101	M-005526-01	ND	-2.096	-1.913	199	ND	-1.804	-1.172	680	ND	-2.116	-2.353	35	24	111	82	167.9
143	NM_003248	THBS4	M-017834-00	-2.839	-2.179	-1.156	119	-2.19	-1.585	-0.826	529	-2.745	-2.055	-1.306	76	190	161	231	168.5
144	NM_198402	PTPLB	M-027184-02	-2.651	-1.902	-0.735	271	-2.81	-2.239	-0.741	66	-2.254	-1.716	-0.545	270	274	253	230	169.0
145	NM_207437	FLJ43486	M-032115-00	-2.606	-1.245	ND	250	-2.721	-1.129	ND	186	-2.336	-1.613	ND	105	149	96	0	169.6
146	NM_016178	OAZ3	M-013344-00	-0.614	-2.482	-2.152	125	-0.343	-2.401	-1.907	196	-1.074	-2.371	-1.807	200	212	236	224	169.8
147	NM_152425	FLJ40249	M-017003-00	0.06	-2.696	-2.513	40	0.174	-2.318	-1.519	619	-1.084	-1.807	-2.038	201	238	239	135	170.7
148	NM_138571	HINT3	M-015800-00	-1.309	ND	-2.643	222	-1.487	ND	-3.007	63	-0.666	ND	-2.595	360	223	9	241	171.4
149	XM_059730	C6ORF159	M-028645-00	-2.12	-2.529	ND	75	-2.028	-2.353	ND	77	-0.787	-1.88	ND	878	108	259	0	171.8
150	NM_153700	STRC	M-015712-00	-2.822	-1.503	ND	123	-2.283	-1.507	ND	204	-2.063	-1.529	ND	212	137	126	19	174.6
151	NM_014023	WDR37	M-020390-00	-1.728	-2.449	-2.347	73	-1.532	-2.64	-2.178	78	-1.107	-1.762	-1.303	955	141	87	77	175.8
152	NM_004299	ABCB7	M-007305-00	-2.085	-2.35	-2.442	71	-1.89	-1.923	-2.579	188	-1.587	-1.571	-1.958	411	180	230	247	176.4
153	NM_005938	MLLT7	M-003016-01	-2.042	-2.087	-1.867	175	-1.972	-1.97	-1.456	160	-1.804	-1.76	-1.961	204	258	243	232	178.8
154	XM_293656	LOC339951	M-023970-00	-2.097	-2.232	-0.242	148	-2.062	-2.476	-0.324	118	-1.906	-1.653	-0.04	332	234	120	190	179.7
155	NM_031917	ANGPTL6	M-007809-00	-2.919	-1.335	-2.377	65	-2.706	-1.223	-1.634	469	-2.034	-1.268	-1.817	195	187	145	140	181.2
156	NM_020535	KIR2DL5	M-020310-00	-1.743	-1.88	-0.42	416	-1.855	-1.921	-0.366	223	-2.798	-2.077	-0.216	66	234	229	222	182.9
157	NM_006775	QKI	M-024905-00	-1.91	-1.976	-1.29	266	-2.684	-1.968	-1.457	163	-1.894	-1.982	-1.197	144	224	184	228	184.1
158	NM_178122	LOC90529	M-018310-00	-2.278	0.074	-2.294	90	-2.541	0.105	-1.757	309	-2.849	0.067	-1.764	229	225	258	234	185.4
159	NM_014363	SACS	M-020571-00	-1.709	-0.781	-1.681	499	-2.3	-1.108	-2.121	94	-2.209	-0.802	-1.903	140	237	253	220	187.3
160	NM_004465	FGF10	M-011857-00	-0.213	-2.296	-2.27	93	-0.086	-1.59	-1.88	514	-0.295	-1.902	-1.9	142	232	193	227	189.3
161	NM_080607	C20ORF102	M-015237-00	-2.007	-2.774	ND	61	-1.68	-1.715	ND	377	-1.116	-2.255	ND	301	219	121	44	190.6
162	NM_000938	POLR2B	M-011187-00	-1.922	-1.885	-3.773	254	-1.563	-1.175	-2.945	565	-2.164	-1.846	-3.219	49	174	240	218	191.6
163	NM_020299	AKR1B10	M-009691-00	-0.226	-2.265	-1.997	204	-0.415	-2.084	-2.284	111	-0.348	-1.853	-1.677	311	222	202	207	191.7
164	NM_207430	FLJ46266	M-032202-00	-1.758	-1.985	ND	301	-1.511	-2.087	ND	265	-1.824	-2.208	ND	92	162	75	18	194.3
165	NM_002717	PPP2R2A	M-004824-01	-2.211	-2.015	-1.741	192	-2.112	-1.863	-1.723	219	-1.815	-1.849	-1.84	176	229	239	267	194.9
166	XM_378183	MGC5457	M-014945-00	-2.342	-0.993	-2.223	105	-2.516	-0.698	-1.852	225	-2.507	-0.824	-1.67	316	226	127	273	195.4
167	XM_380012	LOC402670	M-031824-00	-0.085	-2.116	-2.404	139	0.201	-2.007	-2.437	144	-0.141	-1.617	-2.037	373	129	180	210	195.4
168	NM_144618	MGC29891	M-016074-00	-2.704	-2.093	-1.085	153	-2.566	-1.813	-1.252	254	-2.249	-1.818	-1.385	194	123	108	187	196.1
169	NM_014632	MICAL2	M-010189-00	-1.854	-2.67	-0.378	322	-1.935	-3.707	-0.479	181	-1.915	-2.937	-0.237	131	58	102	151	196.9
170	NM_181785	LOC283537	M-018594-00	-1.09	-2.319	-1.827	339	-0.695	-2.36	-1.755	311	-0.752	-2.143	-2.064	73	169	245	238	197.4
171	NM_197954	CLECSF12	M-021476-00	-1.743	0.286	-2.112	417	-2.322	0.691	-2.473	49	-1.636	-0.049	-1.606	389	87	127	112	199.6
172	NM_003401	XRCC4	M-004494-02	-1.335	-2.012	-2.054	193	-0.581	-1.796	-1.644	453	-1.337	-2.004	-2.074	94	108	269	222	201.8
173	XM_372563	LOC390566	M-030458-00	-7.248	-2.589	-1.21	31	-5.828	-2.041	-1.058	125	-4.414	-0.943	-0.779	2258	54	95	68	206.1
174	NM_004801	NRXN1	M-011941-00	-2.91	-0.252	-1.84	330	-3.481	-0.506	-1.979	153	-2.443	-0.381	-1.844	174	232	180	237	206.3
175	NM_005715	UST	M-020052-00	-1.89	-0.82	-1.984	284	-1.834	-0.656	-1.886	237	-2.347	-1.116	-1.915	132	207	138	145	207.1
176	NM_000751	CHRND	M-006146-00	-2.655	-1.693	-1.711	455	-2.982	-2.003	-1.779	147	-2.616	-1.909	-1.462	135	235	243	258	208.2
177	NM_001878	CRABP2	M-008385-00	-1.16	-2.385	-2.007	196	-1.186	-3.242	-1.936	180	-0.543	-1.735	-1.837	257	224	116	151	208.5
178	NM_152262	ZNF439	M-015506-00	-0.571	-2.602	-2.155	124	-0.627	-2.706	-1.673	410	-1.293	-3.335	-1.837	181	246	227	165	209.6
179	NM_022894	PAPOLG	M-009854-00	-1.46	-2.037	-1.982	213	-1.098	-1.542	-2.106	589	-1.228	-2.063	-2.119	74	235	213	256	210.2
180	NM_018908	PCDHA5	M-013257-00	-1.996	-1.144	-1.897	276	-2.1	-1.448	-1.662	427	-2.11	-1.331	-2.053	79	223	226	224	210.4

dec.	GeneID	Gene Name	Smartpool Cat	SCPO r1	SCPO r2	SCPO r3	SCPO rank	STAPO r1	STAPO r2	STAPO r3	STAPO rank	STIPO r1	STIPO r2	STIPO r3	STIPO rank	OC r1	OC r2	OC r3	rank product
181	NM_006690	MMP24	M-005963-01	-2.218	-1.856	-1.878	298	-1.966	-1.391	-1.7	370	-2.035	-1.717	-2.156	85	151	154	221	210.8
182	NM_006040	HS3ST4	M-022514-00	-2.026	-2.072	-0.395	185	-1.679	-1.598	0.069	508	-2.032	-1.986	-0.652	100	260	234	151	211.0
183	NM_015149	RGL1	M-008387-00	-0.531	-2.225	-2.054	168	-0.142	-2.194	-2.006	145	-0.773	-1.771	-1.593	402	228	232	239	213.9
184	NM_006380	APPBP2	M-013316-00	-2.385	0.204	-2.112	142	-2.454	0.174	-1.805	261	-2.272	0	-1.724	265	231	241	254	214.2
185	NM_001702	BAI1	M-005433-00	-1.973	-0.682	-1.627	572	-1.865	-0.662	-1.858	222	-2.053	-0.851	-2.089	78	257	192	228	214.8
186	NM_025109	MYOHD1	M-017137-00	-2.21	ND	-1.159	491	-2.203	ND	-1.355	289	-2.688	ND	-1.448	70	238	8	257	215.0
187	XM_291763	LOC340947	M-026480-00	-1.922	ND	-1.858	282	-1.859	ND	-2.085	157	-1.673	ND	-1.856	227	143	20	96	215.8
188	NM_015442	CNOT10	M-013968-00	-1.89	-1.425	-1.939	283	-2.207	-1.323	-2.153	85	-1.578	-1.303	-1.632	421	143	126	59	216.4
189	NM_014455	ZNF364	M-006974-00	-1.229	-3.001	ND	140	-1.175	-2.629	ND	198	-0.516	-2.731	ND	369	150	188	36	217.1
190	NM_014977	ACIN1	M-014157-00	-2.788	-2.083	-0.613	155	-2.32	-1.678	-0.571	403	-1.854	-2.122	-0.77	166	258	274	261	218.1
191	XM_059051	LOC126520	M-023896-00	-0.117	-3.304	-1.869	303	-0.018	-2.977	-2.203	74	-0.419	-3.158	-1.527	495	184	223	221	223.1
192	NM_019020	TBC1D16	M-019420-00	ND	-1.382	-2.381	293	ND	-1.316	-2.52	191	ND	-1.377	-2.234	203	35	258	245	224.8
193	XM_372747	FLJ00060	M-031877-00	-1.704	-0.874	-1.917	464	-1.842	-0.891	-2.44	229	-2.118	-0.988	-1.965	107	239	255	237	224.9
194	NM_052884	SIGLEC11	M-015154-00	-2.106	-2.21	-0.012	145	-1.972	-2.096	0.092	155	-1.516	-1.796	-0.443	506	235	258	141	224.9
195	NM_016494	LOC51255	M-006985-00	-2.067	-2.478	-2.064	161	-1.728	-1.808	-1.949	259	-1.714	-2.16	-1.675	276	227	217	155	225.8
196	NM_015315	LARP	M-027187-00	-1.947	-2.084	-2.004	200	-1.575	-1.924	-1.482	543	-2.022	-1.973	-1.603	106	226	225	220	225.8
197	NM_174908	C3ORF6	M-017781-00	ND	-3.211	-1.486	72	ND	-2.227	-1.128	406	ND	-2.185	-1.018	394	0	243	72	225.8
198	NM_005347	HSPA5	M-008198-01	-1.937	-2.064	-0.463	244	-1.852	-1.907	0.106	226	-1.786	-2.4	-0.415	218	222	249	199	229.1
199	NM_053043	MGC20460	M-015189-00	-2.966	-2.063	-1.27	165	-2.647	-1.757	-0.925	308	-2.463	-1.756	-1.409	237	231	252	256	229.2
200	XM_210062	RAC4	M-031617-00	-2.463	-2.263	-0.904	96	-3.169	-1.938	-1.105	178	-2.163	-1.412	-0.591	706	147	93	212	229.3
201	NM_018361	LPAAT-E	M-008554-00	-1.926	0.119	-2.407	249	-1.903	0.327	-2.423	197	-1.811	0.563	-1.743	246	231	199	235	229.4
202	NM_024805	C18ORF22	M-014455-00	-2.503	-2.304	-0.722	80	-2.575	-1.817	-0.862	251	-1.811	-1.457	-0.36	607	122	305	196	230.1
203	NM_173507	FLJ37118	M-018529-00	-2.147	-2.18	-1.797	128	-2.213	-1.644	-0.844	452	-2.469	-1.796	-1.574	213	188	204	131	231.0
204	NM_00100016	FLJ46257	M-032320-00	-2.4	-1.859	-1.898	275	-1.759	-1.294	-1.706	361	-1.963	-1.924	-1.435	126	220	191	229	232.1
205	NM_145719	TIGD3	M-017439-00	ND	-2.108	-2.126	137	ND	-1.201	-2.067	467	ND	-1.55	-2.068	198	18	91	167	233.1
206	NM_018256	WDR12	M-012972-00	-2.56	-0.548	-2.358	69	-1.655	-0.075	-1.943	435	-1.574	-0.35	-2.314	425	196	160	108	233.7
207	NM_001816	CEACAM8	M-017056-00	-1.903	-1.858	-1.187	315	-2.329	-1.997	-1.269	150	-2.593	-1.716	-1.484	273	236	185	189	234.5
208	NM_006509	RELB	M-004767-01	-1.978	-1.83	-2.732	219	-1.878	-1.585	-2.344	209	-1.627	-1.7	-2.002	289	265	221	254	236.5
209	NM_058222	TECTB	M-015223-00	-1.95	-3.647	-1.744	238	-1.456	-2.889	-1.318	745	-2.055	-3.361	-1.682	75	144	130	120	236.9
210	XM_379322	LOC340109	M-028502-00	-1.667	ND	-2.559	141	-1.809	ND	-2.231	136	-1.414	ND	-1.422	694	73	15	94	237.0
211	XM_208563	LOC283202	M-026686-00	-2.122	-0.968	-1.804	359	-2.004	-0.51	-1.68	400	-2.23	-1.289	-2.014	93	138	262	110	237.3
212	NM_000749	CHRNB3	M-006144-01	-2.181	-1.747	-0.965	411	-2.786	-2.028	-1.345	130	-2.515	-1.737	-1.004	252	245	248	254	237.9
213	NM_014982	PCNX	M-014158-00	-1.888	-2.332	-1.942	242	-1.773	-2.269	-1.461	298	-1.438	-2.02	-1.825	189	237	234	227	238.9
214	NM_030934	C1ORF25	M-019040-00	-1.195	-3.21	-1.592	623	-0.787	-2.198	-1.193	1371	-1.541	-2.592	-2.454	16	168	273	257	239.1
215	NM_173803	FLJ39599	M-018370-00	ND	-1.653	-2.274	231	ND	-1.615	-1.992	263	ND	-1.551	-1.98	226	13	138	97	239.5
216	NM_012146	DUX1	M-019955-00	-1.988	-2.285	-0.255	210	-1.861	-2.194	0.039	220	-1.678	-2.779	-1.205	310	234	237	238	242.8
217	NM_00100061	RBMY1B	M-032502-00	-2.422	-2.147	1.242	129	-2.392	-1.811	1.036	257	-2.095	-1.569	1.022	434	293	271	90	243.2
218	NM_002492	NDUFB5	M-019209-00	-1.981	-1.601	-2.773	214	-1.462	-1.653	-2.239	437	-1.876	-1.873	-2.453	154	142	143	173	243.3
219	NM_021081	GHRH	M-019005-00	-2.754	-0.919	-1.971	227	-2.193	-0.553	-1.678	404	-2.543	-0.915	-1.868	159	254	230	265	244.3
220	NM_004660	DDX3Y	M-011904-00	-1.897	-2.123	-0.447	277	-2.117	-2.412	-0.423	99	-1.499	-2.187	-0.155	536	268	236	251	245.0
221	NM_194249	DND1	M-019345-00	-2.069	-1.5	-1.938	243	-2.214	-1.312	-1.971	159	-2.281	-1.278	-1.613	384	238	287	235	245.7
222	XM_042698	USP22	M-006072-00	-0.866	-2.285	-1.849	327	-0.81	-2.21	-1.812	255	-1.015	-1.838	-2.08	178	231	161	247	245.8
223	NM_012382	OSRF	M-009819-00	-1.292	-1.964	-2.35	230	-1.597	-1.791	-2.326	276	-1.385	-1.758	-1.987	234	229	250	252	245.8
224	NM_017921	NPL4	M-020796-00	-1.016	-2.185	-1.923	253	-1	-2.753	-1.961	167	-0.769	-1.637	-1.778	354	239	256	221	246.4
225	NM_003822	NR5A2	M-003430-01	-2.634	0.748	-2.11	143	-2.247	0.899	-1.961	168	-3.144	0.413	-1.441	646	227	223	234	249.4
226	NM_182590	FLJ33651	M-018857-00	-1.394	ND	-3.198	83	-1.337	ND	-2.168	313	-0.896	ND	-2.017	608	133	18	245	250.9
227	NM_001442	FABP4	M-008853-00	-2.052	-1.608	-2.179	171	-1.424	-1.499	-1.879	660	-1.897	-1.763	-2.057	143	137	118	239	252.7
228	NM_004694	SLC16A6	M-007408-00	0.677	-1.651	-2.912	540	0.719	-2.309	-2.673	53	0.863	-1.477	-2.599	575	227	185	148	254.4
229	XM_374123	LOC389295	M-029332-00	-2.077	-1.571	ND	345	-1.666	-1.373	ND	620	-2.06	-2.049	ND	77	197	237	11	254.4
230	NM_031485	GRWD1	M-027146-00	-2.239	-0.996	-2.329	102	-1.465	-0.824	-2.13	729	-1.76	-0.799	-2.351	232	230	244	242	258.4
231	XM_374517	LOC392779	M-029128-00	-2.389	-1.215	-2.387	62	-1.5	-0.441	-2.025	656	-1.566	-1.094	-2.671	437	241	230	220	261.0
232	NM_001487	BLOC1S1	M-012580-00	-1.582	-1.785	ND	493	-1.95	-1.911	ND	184	-1.989	-1.632	ND	197	100	112	24	261.4
233	NM_032706	MGC12966	M-014968-00	-1.484	-2.563	0.393	796	-1.699	-1.817	0.541	374	-2.302	-2.096	0.086	61	215	300	235	262.8
234	NM_004190	LIPF	M-009060-00	-2.065	-1.81	-0.774	354	-2.352	-2.015	-0.914	141	-1.966	-1.628	-0.901	365	224	236	265	263.1
235	NM_004265	FADS2	M-008211-00	-1.792	-0.752	-2.509	372	-2.454	-0.929	-2.546	30	-1.082	-0.651	-2.563	1650	86	141	217	264.1
236	NM_002281	KRTHB1	M-011313-00	-2.182	-1.812	ND	205	-1.832	-1.758	ND	270	-1.956	-1.323	ND	347	216	220	0	267.8
237	XM_371359	LOC388763	M-027732-00	ND	-1.889	-1.862	299	ND	-1.98	-1.655	250	ND	-1.872	-1.593	258	9	94	149	268.2
238	NM_153212	GJB4	M-016916-00	-2.61	-1.585	-1.817	349	-2.795	-1.284	-1.854	224	-2.075	-1.743	-1.684	247	143	241	186	268.3
239	NM_058229	FBXO32	M-013005-00	-1.432	-0.849	-1.902	895	-1.818	-0.841	-1.881	249	-2.029	-0.421	-2.117	87	240	203	251	268.6
240	NM_020402	CHRND10	M-006135-00	-1.769	-1.161	-2.053	395	-2.024	-1.58	-2.11	135	-1.885	-1.285	-1.617	374	277	229	315	271.2

dec.	GeneID	Gene Name	Smartpool Cat	SCPO r1	SCPO r2	SCPO r3	SCPO rank	STAPO r1	STAPO r2	STAPO r3	STAPO rank	STIPO r1	STIPO r2	STIPO r3	STIPO rank	OC r1	OC r2	OC r3	rank product
241	NM_021223	MYL7	M-021478-00	-1.121	ND	-2.945	181	-1.123	ND	-2.38	314	-1.259	ND	-2.018	351	170	7	229	271.2
242	NM_018170	P15RS	M-007734-01	-1.806	-0.237	-2.375	357	-1.785	-0.44	-2.695	280	-2.026	-0.739	-1.807	202	216	231	236	272.3
243	XM_055636	KIAA1912	M-022684-00	-2.955	-1.242	-1.884	290	-2.679	-1.181	-2.123	92	-1.993	-0.753	-1.383	761	243	254	244	272.8
244	NM_021038	MBNL1	M-014136-00	-1.456	-1.929	-1.852	326	-1.315	-2.265	-2.383	61	-1.261	-1.962	-1.273	1038	243	196	171	274.3
245	NM_006637	OR5I1	M-008791-00	-1.963	-1.543	-2.006	233	-1.251	-1.721	-1.833	342	-2.076	-1.675	-1.727	261	81	181	234	275.0
246	NM_152422	PTPDC1	M-008584-00	-0.674	-1.761	-2.085	400	-0.728	-2.042	-2.191	124	-0.762	-1.574	-1.759	424	238	144	239	276.0
247	NM_015350	TA-LRRP	M-014003-00	-1.744	-3.245	-0.328	414	-1.841	-3.413	-0.177	230	-1.767	-2.893	-0.642	224	268	231	230	277.3
248	NM_017723	FLJ20245	M-020707-00	-2.61	-1.62	-1.671	507	-2.67	-1.064	-2.229	69	-2.33	-1.221	-1.455	612	250	226	242	277.7
249	NM_007175	C8ORF2	M-017943-00	-1.065	ND	-2.246	534	-1.347	ND	-2.597	156	-1.326	ND	-2.132	259	204	ND	199	278.4
250	NM_018148	WINS1	M-019129-00	-0.155	-2.01	-1.791	375	-0.173	-2.329	-1.918	190	-0.144	-1.683	-1.942	303	225	221	194	278.4
251	NM_019103	LOC55954	M-020592-00	-1.218	-2.166	-1.708	457	-1.303	-2	-1.628	478	-1.349	-1.995	-2.113	99	238	245	256	278.6
252	XM_113871	LOC197350	M-022614-00	-1.755	-2.593	-1.184	404	-2.012	-2.274	-0.601	143	-1.617	-2.507	-0.861	375	163	74	84	278.8
253	NM_004463	FGD1	M-009612-01	-0.584	-1.853	-2.719	324	-0.424	-1.943	-1.948	174	-0.428	-1.605	-2.775	390	226	266	212	280.1
254	NM_000754	COMT	M-009520-00	-2.021	0.157	-2.153	187	-1.799	0.054	-1.689	387	-2.289	0	-1.679	309	234	226	83	281.7
255	NM_014063	HIP-55	M-016867-00	0.631	-1.7	-2.588	472	0.612	-1.934	-2.353	182	0.44	-1.723	-1.824	266	236	241	157	283.8
256	NM_004597	SNRPD2	M-013617-00	-1.914	-2.615	-1.391	261	-1.762	-2.737	-1.375	306	-1.7	-2.385	-1.362	287	118	87	103	284.1
257	NM_020892	DTX2	M-007114-01	-1.513	-2.27	-1.853	323	-1.562	-2.063	-1.775	295	-1.03	-1.75	-1.802	241	232	253	250	284.2
258	NM_021259	TMEM8	M-013841-00	-1.753	-0.43	-1.885	407	-1.985	-0.067	-1.937	179	-1.697	-0.183	-1.667	319	230	110	215	285.4
259	XM_371302	LOC388686	M-027710-00	-0.269	-2.089	-1.73	435	-0.286	-2.398	-1.838	235	-0.802	-2.001	-1.764	228	216	158	244	285.6
260	NM_022574	PERQ1	M-014174-00	-1.788	-1.445	-1.831	377	-2.389	-1.518	-2.324	47	-1.579	-0.854	-1.175	1318	223	154	252	285.8
261	NM_004722	AP4M1	M-011918-00	-1.86	-2.09	-0.409	311	-1.49	-2.386	0.015	672	-1.952	-2.102	-0.705	112	231	230	223	286.1
262	NM_004074	COX8A	M-011819-00	ND	-2.014	-1.371	481	ND	-2.764	-1.34	122	ND	-1.873	-1.319	400	46	114	170	286.3
263	XM_378360	LOC400043	M-030078-00	-1.658	-1.959	-2.158	235	-1.991	-2.017	-2.068	138	-1.168	-1.591	-1.393	745	220	240	221	289.1
264	NM_030573	THAP7	M-003821-00	-1.792	-2.337	-1.551	373	-1.617	-2.064	-1.225	491	-1.909	-2.477	-1.696	134	91	78	97	290.6
265	NM_138962	MSI2	M-017248-00	-2.309	-2.091	-1.192	154	-1.826	-1.379	-0.695	880	-1.947	-1.836	-1.036	182	252	264	252	291.1
266	NM_032607	CREB3L3	M-014937-00	-3.211	-2.04	-0.789	179	-3.747	-1.737	-0.881	329	-3.086	-1.578	-0.409	420	244	199	238	291.4
267	NM_016628	WAC	M-013325-00	-2.05	-1.919	-1.246	256	-1.861	-1.564	-1.121	562	-1.849	-1.928	-1.36	172	240	242	190	291.4
268	NM_138450	ARL11	M-018083-00	-0.654	-1.966	-3.722	229	-0.977	-1.779	-3.135	288	-0.602	-1.616	-2.624	376	219	253	223	291.6
269	NM_002040	GABPA	M-011662-00	0.868	-1.939	-1.912	264	0.789	-2.07	-1.872	213	0.614	-1.562	-1.768	443	238	239	226	292.1
270	XM_046808	NFASC	M-021839-00	-4.504	-1.042	-1.544	685	-3.788	-0.912	-1.648	444	-3.646	-1.115	-2.046	83	222	231	231	293.3
271	NM_020673	RAB22A	M-019214-00	-2.859	-1.196	-1.772	391	-2.687	-1.444	-1.912	194	-2.287	-1.264	-1.649	335	229	229	225	294.0
272	NM_004538	NDP1L3	M-011879-00	-1.019	-1.624	-2.837	577	-0.892	-1.866	-2.754	216	-1.081	-1.803	-2.529	207	229	175	214	295.5
273	NM_020536	CSRP2BP	M-008481-00	-0.865	-2.185	-1.866	305	-0.641	-1.46	-1.742	739	-0.947	-2.072	-1.95	115	272	275	242	295.9
274	NM_000891	KCNJ2	M-006247-00	-3.135	ND	-0.59	307	-3.433	ND	-0.218	243	-2.545	ND	-0.713	362	145	11	246	300.0
275	NM_019617	GKN1	M-019077-00	-0.859	ND	-2.547	466	-0.819	ND	-3.184	148	-0.627	ND	-2.574	396	229	12	124	301.1
276	NM_006097	MYL9	M-019044-00	-1.799	-0.99	-2.148	363	-1.733	-1.161	-2.342	332	-1.761	-0.924	-2.374	230	242	158	253	302.6
277	NM_002572	PAFAH1B2	M-008797-00	-2.076	-1.959	-0.44	234	-1.796	-1.982	-0.334	268	-1.846	-1.557	-0.617	447	240	225	222	303.8
278	NM_005241	EVI1	M-006530-01	-1.839	-1.739	-1.645	425	-1.971	-1.663	-1.275	424	-2.158	-1.869	-1.435	157	249	222	226	304.7
279	XM_370878	KIAA2002	M-005339-00	-1.775	0.407	-1.916	387	-2.072	0.077	-2.512	115	-1.445	0.297	-1.559	639	205	168	224	305.2
280	NM_144712	SLC23A3	M-007463-00	-2.178	ND	-2.307	100	-1.524	ND	-1.664	510	-1.261	ND	-1.695	572	80	0	139	307.8
281	NM_005655	TIEG	M-006566-00	-2.012	-2.063	-1.803	194	-1.662	-1.71	-1.301	426	-1.603	-2.001	-1.634	357	62	215	87	309.0
282	XM_379643	LOC401530	M-029413-00	-2.006	-0.527	-2.773	197	-1.703	-0.215	-2.562	369	-1.587	-0.67	-2.112	409	228	250	245	309.8
283	NM_031420	MRPL9	M-013498-00	-1.995	-2.66	-0.982	206	-1.716	-2.014	-0.847	348	-1.569	-1.851	-1.079	433	241	245	208	314.3
284	XM_379391	LOC401230	M-028627-00	-0.674	-1.921	-2.012	255	-0.613	-1.894	-1.928	206	-0.937	-1.465	-1.477	594	211	222	257	314.8
285	NM_022091	DJ467N11.1	M-013914-00	-2.068	-1.426	-3.035	160	-1.435	-0.743	-2.343	780	-1.74	-1.201	-2.491	251	185	199	224	315.2
286	NM_054105	OR6C2	M-032525-00	-0.979	-2.791	ND	288	-0.87	-2.506	ND	389	-1.076	-2.344	ND	280	155	98	48	315.4
287	XM_044178	KIAA1211	M-024133-00	-2.255	-1.854	-0.916	321	-2.432	-1.729	-0.93	338	-1.863	-1.699	-0.856	290	239	277	235	315.7
288	NM_133467	CITED4	M-015355-00	-1.394	-2.37	ND	292	-1.282	-2.069	ND	408	-1.514	-1.915	ND	275	222	256	22	320.0
289	NM_032409	PINK1	M-004030-01	-1.032	-1.925	-1.882	291	-0.812	-1.874	-1.84	233	-1.293	-1.975	-1.533	484	224	192	124	320.2
290	NM_182610	SAMD7	M-009146-00	-1.608	-2.057	-2.324	166	-1.393	-1.507	-1.564	641	-1.363	-1.674	-1.85	313	138	93	114	321.7
291	NM_025029	FLJ14346	M-014555-00	-1.514	-2.223	-1.226	734	-1.819	-2.523	-1.784	247	-1.942	-1.83	-1.125	184	113	123	198	321.9
292	XM_375849	LOC400809	M-027575-00	ND	-1.767	-1.951	314	ND	-1.477	-2.171	244	ND	-1.572	-1.557	438	18	57	87	322.6
293	NM_001642	APLP2	M-004179-01	-1.871	-0.911	-2.507	302	-1.988	-0.674	-1.69	386	-1.691	-0.913	-2.499	296	260	231	221	325.6
294	NM_003536	HIST1H3H	M-013723-00	-1.704	-2.822	0.564	463	-1.916	-2.744	0.776	192	-1.605	-2.636	0.518	391	162	225	117	326.4
295	NM_022354	SPATA1	M-014045-00	-2.473	-0.841	-1.924	251	-3.391	-0.522	-2.132	91	-2.551	-0.526	-1.115	1526	51	230	227	326.7
296	NM_006947	SRP72	M-019716-00	-1.7	ND	-2.333	190	-1.43	ND	-1.709	554	-1.19	ND	-2.104	337	176	4	79	328.6
297	NM_024960	PANK2	M-003797-01	-0.764	-1.601	-2.22	609	-0.742	-1.698	-2.225	376	-0.075	-1.873	-2.019	156	197	173	225	329.3
298	NM_138963	RPS4Y2	M-016659-00	-1.978	-0.235	-2.005	218	-1.569	-0.31	-1.373	897	-2.488	-0.64	-1.833	183	63	134	157	329.5
299	NM_032632	PAPOLA	M-018882-00	-2.028	-1.722	-1.12	443	-2.109	-2.026	-1.357	133	-1.456	-1.508	-1.001	610	228	236	204	330.0
300	NM_003850	SUCLA2	M-008237-00	-1.952	-3.102	-0.722	237	-1.778	-2.963	-0.389	293	-1.507	-2.796	-0.5	521	198	225	239	330.7

dec.	GeneID	Gene Name	Smartpool Cat	SCPO r1	SCPO r2	SCPO r3	SCPO rank	STAPO r1	STAPO r2	STAPO r3	STAPO rank	STIPO r1	STIPO r2	STIPO r3	STIPO rank	OC r1	OC r2	OC r3	rank product
301	NM_145167	PIGM	M-017388-00	-2.867	-1.282	ND	159	-2.588	-0.923	ND	310	-1.624	-1.174	ND	734	216	171	23	330.7
302	NM_004122	GHSR	M-005513-00	-1.851	-1.826	-1.499	342	-1.651	-1.682	-1.265	442	-2.222	-1.748	-1.398	242	226	243	227	332.0
303	XM_058743	LOC123876	M-022500-00	-0.792	-1.855	-2.349	318	-0.513	-1.4	-1.865	846	-0.961	-1.907	-2.127	136	253	268	256	332.0
304	NM_002634	PHB	M-010530-00	-1.72	-2.182	-1.831	337	-1.442	-1.881	-1.646	447	-1.529	-1.947	-1.745	244	193	256	231	332.5
305	NM_130773	CNTNDP5	M-010914-00	-2.687	-2.067	-1.687	163	-2.145	-1.276	-1.6	505	-1.554	-1.611	-1.409	450	144	234	177	333.3
306	NM_002855	PVRL1	M-004300-00	-0.498	-2.413	-2.032	183	-0.402	-2.757	-1.949	170	-0.032	-1.767	-1.22	1191	244	230	175	333.4
307	NM_003494	DYSF	M-003652-01	-2.18	-1.7	-1.689	473	-1.611	-1.497	-1.457	663	-1.938	-2.089	-1.442	121	226	238	255	336.0
308	NM_173050	SCUBE1	M-017693-00	ND	-2.174	-1.262	446	ND	-2.701	-1.197	169	ND	-1.7	-1.331	507	14	151	259	336.8
309	NM_176817	TAS2R38	M-018451-00	-2.074	-1.943	-1	241	-2.024	-1.772	-0.923	299	-1.774	-1.5	-0.874	533	238	258	220	337.4
310	NM_004214	FIBP	M-011916-00	-1.972	-1.4	-1.864	306	-1.829	-1.185	-1.849	242	-1.507	-1.086	-1.808	520	265	277	244	337.7
311	NM_003001	SDHC	M-011385-00	-2.847	-1.524	-1.88	294	-2.261	-1.163	-1.888	207	-2.491	-1.446	-1.356	634	275	236	231	337.9
312	NM_015720	PODLX2	M-020755-00	-1.66	-1.134	-2.788	526	-1.553	-0.905	-2.512	577	-1.918	-1.037	-2.183	129	237	219	246	339.6
313	NM_005704	PTPRU	M-009328-01	-0.483	-1.915	-2.253	260	-0.422	-1.633	-1.59	517	-0.852	-1.693	-2.441	295	65	183	225	341.0
314	NM_007346	OGFR	M-019185-00	-1.862	-0.247	-2.367	308	-1.303	-0.771	-1.943	1057	-1.98	-0.348	-1.938	122	242	132	237	341.2
315	NM_001943	DSG2	M-011645-00	-1.924	-0.536	-1.987	252	-1.672	-0.026	-1.637	461	-1.641	-1.079	-1.816	343	245	238	240	341.6
316	NM_022917	NOL6	M-017285-00	-2.629	-2.277	-1.769	91	-2.015	-1.528	-1.199	604	-2.076	-1.374	-1.393	742	238	170	202	344.2
317	NM_016270	KLF2	M-006928-01	-1.07	-1.988	-2.611	209	-0.837	-1.7	-1.551	581	-1.088	-1.648	-1.985	336	246	224	241	344.3
318	NM_198483	FLJ46536	M-027237-00	-1.955	-1.916	-1.097	258	-2.029	-1.944	-0.86	173	-1.799	-1.307	-0.917	945	268	127	217	348.1
319	XM_370946	LOC388226	M-027173-00	-1.741	-0.431	-1.765	421	-1.596	-0.549	-1.578	539	-1.829	-0.674	-1.852	186	203	85	52	348.2
320	NM_003154	STATH	M-012654-00	-1.463	-2.124	-1.835	335	-1.228	-1.937	-1.866	218	-1.473	-1.779	-1.475	579	222	140	173	348.4
321	NM_145111	DKFZP727G13	M-017383-00	-2.084	-2.067	-0.733	162	-1.571	-1.676	-0.585	550	-1.893	-1.536	-1.209	479	107	225	116	349.5
322	NM_012445	SPON2	M-020027-00	-1.859	-2.391	-0.784	313	-1.599	-1.892	-0.449	507	-2.464	-1.716	-0.718	272	223	230	242	350.8
323	XM_378028	LOC402336	M-029391-00	-1.992	-2.149	-0.231	208	-1.823	-2.124	-0.228	246	-1.644	-1.35	-0.236	844	221	235	231	350.8
324	NM_015601	HERC4	M-021426-00	-2.259	-0.638	-1.685	492	-2.118	-0.688	-1.738	327	-2.219	-0.432	-1.718	269	272	234	100	351.1
325	AF113887	IGKC	M-032259-00	-2.356	-1.838	0.119	332	-1.726	-1.508	0.236	638	-2.163	-1.804	0	205	259	222	210	351.5
326	NM_152349	MGC45562	M-016589-00	-2.009	-1.797	-2.164	195	-1.76	-1.211	-1.404	833	-1.687	-1.748	-1.719	268	245	250	248	351.8
327	NM_020992	PDLIM1	M-016116-00	-1.679	-0.684	-1.669	511	-1.571	-0.533	-1.161	1479	-2.118	-0.803	-2.16	58	187	187	141	352.6
328	NM_014384	ACAD8	M-008501-00	ND	-1.363	-2.45	269	ND	-1.55	-2.272	195	ND	-0.811	-1.877	858	45	54	100	355.7
329	NM_001225	CASP4	M-004404-00	-1.582	0.163	-2.489	634	-1.72	-0.034	-2.88	343	-1.801	-0.342	-2.73	209	271	237	225	356.9
330	NM_019599	TAS2R1	M-013246-00	-2.263	-1.282	ND	390	-1.936	-1.013	ND	709	-2.047	-1.662	ND	165	256	229	0	357.3
331	NM_014772	KIAA0427	M-021020-00	-0.819	-1.974	-2.325	224	-0.049	-1.206	-2.165	1323	-0.835	-1.874	-2.542	155	186	186	149	358.1
332	NM_025065	RPF1	M-031267-00	-1.91	-0.939	-1.647	544	-2.342	-1.121	-2.294	56	-2.045	-0.78	-1.115	1527	133	119	221	359.6
333	XM_377720	LOC150356	M-031490-00	-2.5	-0.605	-1.905	270	-2.515	-0.439	-1.833	238	-1.614	-0.811	-1.402	725	254	155	141	359.8
334	NM_031295	WBSCR21	M-009682-00	-1.398	-1.916	-2.235	259	-0.671	-1.385	-1.827	872	-0.955	-2.107	-1.802	208	230	233	223	360.8
335	NM_012287	CENTB2	M-012811-00	-1.969	-0.1	-1.884	289	-2.104	-0.267	-1.873	212	-1.627	0.329	-1.382	769	260	174	192	361.2
336	NM_005065	SEL1L	M-004885-01	-2.107	-1.791	-1.497	374	-2.213	-1.684	-1.495	393	-2.487	-1.606	-1.664	321	250	224	220	361.3
337	NM_181522	WFDC3	M-013334-00	ND	-1.695	-2.541	136	ND	-1.072	-1.861	726	ND	-1.3	-1.773	478	39	131	150	361.4
338	XM_379432	LOC285733	M-028602-00	-1.697	-1.621	ND	528	-1.477	-1.565	ND	617	-1.791	-1.992	ND	145	92	103	6	361.5
339	NM_000401	EXT2	M-011031-00	-1.278	-1.927	-1.857	316	-1.066	-1.675	-1.584	530	-1.055	-1.805	-1.703	284	169	234	72	362.3
340	NM_001898	CST1	M-017398-00	-0.71	-2.093	-1.818	348	-0.695	-2.363	-1.742	321	-1.151	-1.573	-1.715	427	125	216	157	362.7
341	NM_024604	FLJ21908	M-014385-00	-0.309	-1.999	-1.811	353	-0.235	-1.748	-1.828	316	-0.674	-1.62	-1.571	428	229	222	247	362.8
342	NM_012433	SF3B1	M-020061-00	-1.642	-1.925	ND	381	-1.661	-2.188	ND	187	-1.187	-1.653	ND	685	75	75	5	365.4
343	NM_020903	USP29	M-006077-00	-2.08	0.042	-1.56	665	-2.307	0.116	-1.652	441	-2.046	0.06	-1.851	169	233	231	250	367.3
344	NM_019887	DIABLO	M-004447-00	-1.091	-1.77	-1.723	442	-0.995	-1.791	-1.819	275	-1.107	-1.582	-1.887	414	236	133	211	369.2
345	NM_018013	FLJ10159	M-021094-00	-1.969	-0.013	-2.277	228	-2.081	0.517	-1.638	458	-2.591	0	-1.535	482	225	218	242	369.2
346	NM_032026	TATDN1	M-014767-00	-1.872	-1.751	ND	352	-1.626	-1.678	ND	440	-1.421	-1.898	ND	325	127	219	7	369.2
347	NM_020676	ABHD6	M-008683-00	0.207	-2.175	-1.932	246	0.504	-1.645	-1.653	449	0.619	-1.547	-1.583	460	227	227	226	370.4
348	XM_370870	MGC4809	M-031986-00	-3.903	-1.887	-1.182	285	-3.725	-1.703	-0.949	368	-2.833	-1.53	-0.923	488	222	248	224	371.3
349	NM_022164	LCN7	M-008373-00	-0.99	-3.693	-1.88	295	-1.065	-3.379	-1.671	411	-1.133	-2.653	-1.575	423	244	182	247	371.5
350	NM_198580	SLC27A1	M-010759-00	-2.724	-1.985	-1.56	212	-2.355	-1.628	-1.164	479	-2.045	-1.514	-1.343	509	97	145	200	372.5
351	NM_024082	TMG3	M-010369-00	-1.077	-3.749	-1.911	265	-1.183	-2.715	-1.683	398	-1.294	-2.395	-1.518	502	64	220	237	375.5
352	NM_017880	FLJ20558	M-020863-00	-1.108	ND	-2.177	550	-1.3	ND	-2.169	331	-1.619	ND	-1.777	291	267	1	226	375.6
353	NM_000426	LAMA2	M-011070-00	-2.065	-1.668	-0.775	514	-2.396	-1.714	-0.779	352	-2.125	-1.693	-0.609	294	205	228	231	376.1
354	NM_194309	C21ORF125	M-019297-00	-1.868	-2.084	-1.715	304	-1.59	-1.817	-1.665	422	-1.319	-1.581	-1.712	416	157	132	99	376.5
355	NM_152424	FLJ39827	M-016075-00	0	-1.987	-2.47	211	0.232	-1.77	-2.095	301	0.338	-1.351	-1.684	842	106	132	160	376.8
356	NM_021988	UBE2V1	M-010064-01	-1.67	-1.101	-3.018	510	-1.793	-1.027	-2.886	271	-1.604	-0.785	-2.5	392	269	225	234	378.4
357	NM_138795	ARL10B	M-016577-00	-1.902	-2.426	-1.811	272	-1.653	-1.681	-1.868	399	-1.16	-2.382	-1.52	501	254	238	247	378.8
358	NM_016011	CGI-63	M-009881-00	-0.855	-3.074	-1.606	603	-0.984	-3.247	-1.915	193	-0.533	-2.657	-1.542	473	230	246	246	380.4
359	NM_001146	ANGPT1	M-007802-01	-2.116	-1.688	-0.035	486	-2.627	-1.837	-0.104	236	-1.956	-1.533	-0.03	485	241	226	239	381.7
360	XM_373907	LOC388787	M-031332-00	0.016	-2.005	-2.058	198	0.082	-1.903	-1.623	486	-0.474	-1.465	-1.603	593	226	243	194	385.0

dec.	GeneID	Gene Name	Smartpool Cat	SCPO r1	SCPO r2	SCPO r3	SCPO rank	STAPO r1	STAPO r2	STAPO r3	STAPO rank	STIPO r1	STIPO r2	STIPO r3	STIPO rank	OC r1	OC r2	OC r3	rank product
361	XM_379179	LOC152274	M-028076-00	ND	-2.697	-1.521	144	ND	-1.812	-1.211	630	ND	-1.688	-1.211	630	0	143	247	385.2
362	NM_144636	CHCHD4	M-016042-00	-1.817	ND	-1.693	405	-2.375	ND	-2.041	71	-0.978	ND	-1.015	1996	53	43	78	385.7
363	NM_022098	LOC63929	M-005930-01	-2.072	-1.465	ND	396	-1.945	-1.551	ND	317	-1.946	-1.148	ND	462	137	255	39	387.1
364	NM_017837	FLJ20477	M-015531-00	-1.817	-1.403	-2.79	350	-1.744	-1.513	-2.557	319	-1.505	-1.323	-2.688	523	228	138	247	388.0
365	XM_378436	LOC400163	M-030254-00	-1.641	-3.824	-1.607	552	-1.54	-3.313	-1.399	594	-1.252	-2.921	-1.838	180	225	240	268	389.3
366	NM_022096	ANKRD5	M-016466-00	-1.574	-1.637	-0.243	644	-1.896	-1.897	-0.265	202	-1.598	-1.549	-0.013	458	220	236	149	390.6
367	XM_371423	LOC388846	M-031422-00	-1.794	0.596	-1.944	368	-1.482	0.877	-1.489	693	-1.752	0.297	-1.825	240	220	242	248	394.1
368	NM_017703	FBXL12	M-005204-01	-1.666	-2.068	-0.314	516	-1.415	-1.839	-0.062	817	-2.071	-1.88	-0.355	151	236	143	224	399.3
369	NM_004249	RAB28	M-008582-00	-1.677	-1.682	-1.993	494	-1.48	-1.724	-1.781	340	-1.615	-1.656	-1.44	380	257	257	211	399.6
370	NM_003064	SLPI	M-011391-00	0.554	-1.557	-2.071	672	0.527	-1.507	-1.814	640	-0.077	-2.224	-1.883	149	218	232	224	400.2
371	NM_138342	LOC89944	M-018681-00	-1.83	-1.541	-3.238	338	-1.181	-0.905	-3.037	1405	-1.906	-1.687	-2.725	137	240	229	220	402.2
372	XM_374179	LOC389422	M-028585-00	-1.266	-1.93	-1.961	248	-1.015	-1.588	-1.737	522	-1.312	-1.606	-1.513	511	202	212	139	404.4
373	NM_000145	FSHR	M-005497-01	-1.872	-0.212	-1.728	438	-1.752	-0.152	-1.846	315	-1.758	-0.519	-1.528	492	193	202	241	407.9
374	NM_018263	ASXL2	M-022638-00	-2.179	-1.999	-1.188	203	-1.712	-1.645	-0.935	450	-1.39	-1.483	-1.25	748	220	220	236	408.8
375	XM_294743	LOC338918	M-021979-00	-1.918	0.186	-1.873	300	-1.759	0.136	-1.559	567	-1.589	-0.139	-1.651	405	167	129	191	409.9
376	XM_370844	LOC388094	M-030572-00	ND	-1.562	-1.756	529	ND	-2.01	-1.671	232	ND	-1.626	-1.341	563	ND	206	190	410.3
377	NM_145175	NSE1	M-015929-00	-0.11	-1.693	-1.83	480	0.147	-1.612	-1.496	664	-0.506	-2.153	-1.785	219	132	226	239	411.7
378	NM_138390	LOC92691	M-018989-00	-0.507	-1.795	-1.932	367	-0.266	-1.719	-1.85	344	-0.463	-1.492	-2.137	554	207	154	85	412.0
379	NM_007345	ZNF236	M-012794-00	-1.622	-0.602	-2.773	582	-1.874	-0.792	-3.077	211	-1.48	-0.425	-2.12	570	98	104	222	412.1
380	NM_003459	SLC30A3	M-007524-00	-1.793	-1.678	-2.201	370	-1.59	-1.254	-2.489	516	-1.622	-1.41	-2.004	370	227	236	231	413.4
381	NM_020319	ANKMY2	M-013766-00	-2.47	-1.835	-0.873	334	-2.228	-1.506	-0.491	643	-2.293	-1.654	-1.072	329	188	224	153	413.4
382	XM_376007	DEPDC5	M-020708-00	-1.8	-1.815	-0.895	361	-1.594	-1.523	-0.746	613	-1.785	-1.661	-0.947	324	122	167	91	415.4
383	NM_032726	PLCD4	M-005065-01	0.222	-1.623	-2.129	580	0.445	-1.213	-1.801	1302	-0.855	-2.437	-2.002	96	232	241	232	417.0
384	XM_294894	LOC339281	M-023297-00	-1.58	-2.192	-1.931	247	-0.698	-1.51	-1.817	633	-1.546	-1.539	-1.848	464	250	226	153	417.1
385	XM_373979	LOC388938	M-027821-00	-0.763	-2.465	-2.041	177	-0.007	-2.199	-1.43	786	-0.309	-1.774	-1.499	535	93	142	216	420.6
386	NM_004816	C9ORF61	M-021464-00	0.26	-1.844	-1.706	460	0.065	-1.782	-1.915	284	0.231	-1.738	-1.479	571	148	143	91	421.0
387	NM_020695	TCEB3BP1	M-021445-00	-1.869	-1.092	-1.856	317	-1.699	-0.973	-1.735	373	-1.912	-1.393	-1.446	636	239	220	242	422.1
388	NM_002187	IL12B	M-007930-00	-1.563	-1.77	-2.293	393	-1.472	-1.739	-1.875	324	-1.379	-1.463	-1.998	597	258	285	315	423.6
389	XM_379184	LOC401059	M-028085-00	-2.042	-1.936	-1.064	245	-1.7	-1.824	-1.181	371	-1.349	-1.348	-0.905	850	256	223	148	425.9
390	NM_153248	MGC14276	M-018374-00	-1.707	-1.45	ND	641	-1.403	-1.038	ND	1279	-1.778	-2.23	ND	95	118	89	5	427.1
391	NM_017743	DPP8	M-005855-01	-1.576	-1.847	-1.674	503	-1.763	-1.719	-2.069	305	-1.393	-1.515	-1.512	512	164	245	227	428.3
392	NM_001974	EMR1	M-005487-01	-1.77	-1.428	-2.087	394	-1.339	-1.244	-1.893	973	-1.803	-1.535	-1.904	206	238	223	232	429.0
393	XM_373962	LOC388903	M-031472-00	-3.58	-2.136	0.479	131	-3.063	-1.901	0.485	199	-2.913	-0.799	1.414	3069	157	131	67	430.9
394	NM_001399	ED1	M-003654-00	-1.653	-1.871	-0.58	537	-2.068	-1.97	-0.731	162	-1.593	-1.315	-0.084	927	225	195	236	432.0
395	NM_024669	FLJ11795	M-014406-00	-2.622	-1.203	ND	263	-2.566	-0.77	ND	414	-2.402	-0.384	ND	743	72	208	44	432.5
396	NM_207324	LOC147650	M-023802-00	-2.207	ND	-1.751	217	-2.084	ND	-1.36	341	-1.286	ND	-1.216	1094	106	4	60	432.6
397	NM_020755	TDE2	M-010725-00	-1.391	-2.281	ND	333	-1.337	-2.028	ND	397	-0.937	-1.971	ND	617	67	239	15	433.7
398	NM_014765	TOMM20	M-006487-00	-3.041	-1.526	-1.478	721	-2.729	-1.028	-1.341	968	-2.204	-1.533	-1.944	117	248	227	221	433.8
399	XM_056434	TTC6	M-021944-00	-2.193	-1.112	-1.944	240	-2.341	-0.941	-1.467	725	-1.822	-0.962	-1.543	471	269	260	257	434.4
400	NM_024840	ZNF613	M-016574-00	-0.561	-2.068	-1.758	403	-0.328	-1.869	-1.921	215	-0.451	-1.334	-1.307	946	230	233	248	434.4
401	XM_371690	LOC389202	M-028347-00	-0.603	-1.973	-2.605	226	-0.808	-1.807	-2.241	260	-0.59	-1.15	-1.436	1395	223	249	223	434.4
402	NM_013257	SGKL	M-004162-00	-0.155	-2.054	-1.569	656	-0.428	-1.85	-1.695	380	-0.367	-1.896	-1.654	331	221	184	231	435.3
403	NM_022831	FLJ12806	M-014222-00	-1.941	-1.522	-1.761	401	-1.715	-1.171	-1.867	349	-1.458	-1.383	-1.677	605	249	245	230	439.1
404	NM_032547	SCOC	M-014916-00	-0.026	-3.366	-1.788	378	0.057	-2.381	-1.707	358	0.037	-2.447	-1.449	626	234	227	249	439.2
405	NM_024657	ZCWCC2	M-016180-00	-1.008	-1.997	-1.544	689	-1.192	-2.407	-1.838	234	-1.502	-1.942	-1.089	526	231	238	220	439.3
406	NM_003860	BANF1	M-011536-00	-1.654	-2.401	-1.444	536	-1.655	-2.538	-1.37	434	-1.452	-2.607	-1.626	368	226	221	260	440.7
407	NM_006969	ZNF28	M-023811-00	-1.631	-2.613	-0.916	567	-1.611	-2.534	-0.565	496	-1.673	-2.224	-1.008	314	79	166	212	445.3
408	NM_012070	ATRN	M-012403-00	-2.066	-1.108	-1.747	412	-1.945	-1.002	-1.626	483	-1.948	-1.145	-1.56	444	199	191	132	445.4
409	NM_001284	AP3S1	M-012569-00	-1.908	-2.032	-2.134	184	-1.387	-2.228	-1.634	470	-1.734	-1.277	-0.936	1024	78	155	145	445.7
410	XM_373885	LOC388735	M-027375-00	-0.81	-1.774	-2.013	388	-0.598	-1.844	-1.704	367	-0.875	-1.54	-1.449	631	227	232	189	447.9
411	NM_152396	MGC24132	M-016329-00	-0.809	-1.994	-2.049	207	-0.654	-1.534	-2.007	600	-0.927	-1.4	-2.194	728	148	197	136	448.8
412	NM_153611	MGC20446	M-016374-00	ND	-1.494	-1.733	592	ND	-1.331	-1.944	459	ND	-1.464	-1.837	333	10	52	65	448.9
413	NM_014351	SULT4A1	M-010393-00	-0.724	-1.982	-1.66	525	-0.846	-2.087	-1.692	383	-0.557	-1.554	-1.578	451	106	90	105	449.3
414	NM_005027	PIK3R2	M-003021-01	-1.451	-1.544	-1.958	688	-1.287	-1.57	-1.809	553	-1.632	-1.744	-1.874	245	252	218	221	453.4
415	NM_005441	CHAF1B	M-019937-00	-1.308	-1.715	-2.022	449	-1.144	-1.521	-2.102	616	-0.966	-1.644	-1.937	338	160	281	196	453.9
416	XM_031561	FLJ14502	M-022219-00	-1.402	-2.454	-0.313	953	-1.74	-2.645	-2.186	323	-1.682	-2.7	-0.105	305	195	222	222	454.5
417	NM_006660	CLPX	M-008763-00	-1.527	-2.361	0.058	715	-1.372	-2.186	0.314	901	-1.889	-2.461	0.212	147	241	246	221	455.8
418	XM_291099	LOC339977	M-024136-00	-2.012	-1.443	ND	437	-2.004	-1.395	ND	372	-1.661	-1.276	ND	585	196	59	18	456.5
419	NM_006122	MAN2A2	M-009110-01	-1.822	-2.605	-1.73	347	-1.439	-2.477	-1.778	290	-1.204	-2.295	-1.304	954	245	187	183	457.9
420	NM_001437	ESR2	M-003402-02	-1.613	-2.019	-1.523	593	-1.701	-2.182	-1.74	322	-1.481	-1.517	-1.646	505	221	275	185	458.6

dec.	GeneID	Gene Name	Smartpool Cat	SCPO r1	SCPO r2	SCPO r3	SCPO rank	STAPO r1	STAPO r2	STAPO r3	STAPO rank	STIPO r1	STIPO r2	STIPO r3	STIPO rank	OC r1	OC r2	OC r3	rank product
421	NM_005831	NDP52	M-010637-00	-0.674	-1.862	-1.699	475	-0.763	-2.266	-1.633	472	-1.023	-2.092	-1.569	431	239	89	230	458.9
422	NM_181501	ITGA1	M-008516-00	-1.773	-1	-2.139	389	-1.54	-0.822	-1.728	593	-1.579	-0.767	-1.878	419	158	144	229	458.9
423	NM_018906	PCDHA3	M-013259-00	-1.821	-1.494	-0.868	769	-1.922	-1.663	-0.708	425	-1.827	-1.688	-1.104	297	97	241	210	459.6
424	NM_017908	FLJ20626	M-020365-00	-1.241	-1.458	-2.845	842	-0.833	-1.747	-2.598	318	-0.519	-1.626	-2.862	367	160	91	107	461.5
425	NM_025201	PP9099	M-015750-00	ND	-2.361	-1.333	328	ND	-2.222	-1.038	474	ND	-1.614	-1.279	633	8	214	130	461.7
426	NM_004518	KCNQ2	M-006272-01	-2.122	-1.201	ND	523	-2.47	-0.993	ND	334	-1.609	-1.358	ND	564	60	63	12	461.9
427	XM_379154	LOC151300	M-028016-00	-2.071	-1.974	-1.576	223	-1.859	-1.651	-1.333	443	-1.225	-2.231	-1.284	1004	100	54	221	462.9
428	NM_005303	GPR40	M-005571-01	-1.409	-2.221	ND	351	-0.993	-1.646	ND	1020	-1.314	-2.109	ND	278	101	161	0	463.4
429	NM_006449	CDC42EP3	M-017358-00	-1.227	-1.963	-1.988	232	-1.134	-1.684	-1.859	394	-0.54	-1.251	-1.87	1096	193	221	168	464.4
430	NM_015693	PDZK6	M-031873-00	-2.125	-1.682	-1.203	497	-1.878	-1.503	-1.429	651	-2.016	-1.676	-0.474	312	222	249	139	465.6
431	NM_032809	C9ORF54	M-017149-00	-2.343	1.092	-1.614	591	-2.455	0.56	-1.833	239	-2.09	0.765	-1.402	721	224	171	97	467.0
432	NM_207390	FLJ45910	M-032064-00	-0.774	-1.697	-1.862	477	-0.8	-1.623	-1.415	814	-0.88	-1.726	-1.835	263	240	161	183	467.4
433	XM_290714	RAB43	M-028161-00	-1.676	-1.156	-1.961	501	-1.589	-0.79	-1.608	518	-1.986	-1.023	-1.601	395	221	227	105	468.0
434	NM_004338	C18ORF1	M-019789-00	-1.678	-1.812	-1.736	428	-1.455	-1.666	-1.695	418	-1.387	-1.834	-1.477	574	194	105	219	468.3
435	XM_048235	HYPM	M-025036-00	-1.583	-1.697	ND	554	-1.826	-1.346	ND	527	-1.637	-1.638	ND	352	204	186	15	468.4
436	NM_014734	KIAA0247	M-020259-00	-2.131	-1.745	-1.58	413	-1.981	-1.33	-1.247	991	-2.053	-1.737	-1.684	254	246	237	220	470.2
437	NM_005837	POP7	M-020033-00	-1.426	-2.143	-1.861	309	-1.279	-1.843	-1.735	330	-0.959	-1.787	-1.278	1021	225	238	235	470.4
438	XM_372689	LOC390828	M-031028-00	-1.415	-1.629	-0.011	923	-1.687	-1.888	-0.213	390	-2.21	-1.695	-0.837	293	195	228	252	472.5
439	XM_378309	LOC399951	M-029804-00	-1.475	ND	-2.471	225	-0.912	ND	-2.078	668	-1.067	ND	-1.752	709	71	13	152	474.1
440	NM_014713	LAPTM4A	M-013439-00	ND	-1.146	-2.201	504	ND	-1.201	-2.685	175	ND	-0.471	-1.951	1216	5	219	178	475.1
441	NM_003614	GALR3	M-004141-01	-2.693	-1.633	-1.519	564	-2.54	-1.345	-1.503	653	-2.663	-1.696	-1.546	292	242	253	254	475.5
442	NM_002694	POLR2C	M-009620-00	-2.979	-1.955	-1.725	236	-2.25	-1.335	-1.33	980	-1.923	-1.545	-1.154	466	104	207	135	475.9
443	NM_138567	SYT8	M-019166-00	-0.716	-1.825	-1.594	616	-0.691	-1.689	-1.973	388	-0.035	-1.623	-1.553	452	90	174	128	476.3
444	NM_004942	DEFB4	M-012997-00	-1.928	-0.425	-1.446	866	-1.87	-0.428	-1.898	214	-1.624	-0.579	-1.471	583	191	223	233	476.3
445	NM_012131	CLDN17	M-019991-00	-1.427	-1.708	-1.965	458	-1.127	-1.941	-1.639	456	-0.625	-1.588	-1.508	518	113	100	222	476.5
446	NM_015426	DKFZP434C24	M-017717-00	-1.565	-2.336	-1.004	661	-1.886	-2.369	-0.988	208	-1.373	-2.151	-1.04	788	232	232	225	476.7
447	NM_016255	FAM8A1	M-021014-00	-1.991	-1.644	-0.153	547	-2.024	-1.431	-0.1	785	-1.815	-1.737	-0.475	255	219	268	233	478.4
448	NM_014352	POU2F3	M-020587-00	-1.754	-1.149	-2.165	406	-1.675	-0.846	-1.712	409	-1.426	-0.888	-1.444	664	245	242	254	479.5
449	NM_015919	ZNF226	M-019147-00	-0.798	ND	-2.645	444	-0.765	ND	-2.966	217	-0.407	ND	-2.05	1160	86	0	58	481.7
450	NM_005835	SLC17A2	M-007412-00	-1.58	-0.242	-2.068	638	-1.636	-0.101	-2.19	463	-1.986	-0.417	-1.615	379	191	100	228	482.0
451	NM_015630	EPC2	M-016776-00	-0.228	-1.516	-2.415	732	-0.168	-1.776	-1.952	294	-0.395	-1.504	-1.714	524	228	172	218	483.1
452	NM_032705	MGC14801	M-014967-00	-2.055	0.018	-1.896	278	-2.377	0.43	-1.471	717	-2.405	-0.864	-1.473	582	191	81	267	487.7
453	NM_002059	GH2	M-011668-00	-1.839	-0.458	-2.283	331	-1.558	-0.302	-1.953	569	-1.453	-0.244	-1.729	620	232	252	298	488.8
454	NM_012429	SEC14L2	M-012478-00	0.627	-2.207	-1.692	482	0.545	-2.106	-1.792	272	0.76	-1.922	-1.328	892	82	91	64	489.0
455	NM_015558	SS18L1	M-013929-00	ND	-1.507	-1.864	489	ND	-1.389	-1.786	523	ND	-1.483	-1.593	475	46	89	117	495.3
456	NM_004572	PKP2	M-012692-00	-1.896	-0.919	-1.854	319	-1.625	-0.779	-1.939	485	-1.729	-1.104	-1.374	786	135	183	106	495.4
457	NM_000207	INS	M-011058-00	-1.748	-1.663	-3.255	409	-1.506	-1.573	-3.806	545	-1.17	-1.493	-2.634	548	282	247	260	496.2
458	NM_002614	PDZK1	M-010615-01	-1.599	ND	-1.454	718	-1.463	ND	-1.567	626	-1.786	ND	-1.645	274	268	10	64	497.5
459	XM_374655	LOC392997	M-029186-00	-1.07	ND	-2.072	650	-0.953	ND	-2.619	279	-0.832	ND	-2.011	681	133	26	174	498.0
460	XM_293398	RAB41	M-031575-00	-0.842	-2.482	-1.783	380	-0.643	-2.05	-1.638	460	-0.634	-1.598	-1.405	715	117	181	147	500.0
461	NM_152413	MGC33309	M-016864-00	-1.898	-2.119	-0.65	274	-1.648	-1.796	-0.92	445	-1.277	-2.048	-0.322	1026	222	229	115	500.1
462	XM_060278	LOC126987	M-021647-00	-1.28	-2.056	ND	513	-1.286	-2.122	ND	364	-1.089	-1.758	ND	671	89	187	1	500.4
463	XM_291989	LOC338756	M-026922-00	-1.578	-0.477	-1.754	640	-1.771	-0.305	-1.694	382	-1.509	-0.505	-1.516	515	122	166	228	501.2
464	XM_374273	LOC389669	M-029383-00	-0.293	-1.612	-1.866	595	-0.223	-1.415	-1.833	815	-0.837	-1.97	-1.724	264	251	239	251	504.0
465	NM_152409	FLJ37562	M-015517-00	-1.58	-2.688	-1.239	636	-1.137	-2.315	-1.195	1366	-1.266	-2.178	-1.886	148	226	227	236	504.7
466	NM_030903	OR2W1	M-014666-00	-1.73	-1.766	-0.879	434	-1.302	-1.801	-0.449	1062	-1.705	-2.696	-1.093	282	226	243	134	506.5
467	NM_181648	LOC286161	M-018733-00	-1.874	-0.373	-1.639	557	-2.394	-0.21	-1.636	464	-1.9	-0.928	-1.517	503	199	173	115	506.6
468	NM_020201	NT5M	M-013214-00	-1.698	-1.669	-1.335	512	-1.251	-1.336	-1.265	1150	-1.952	-1.78	-1.52	221	227	259	231	506.7
469	NM_004292	RIN1	M-019891-00	-2.065	-1.593	-1.701	470	-1.61	-1.1	-1.16	1486	-1.936	-1.379	-1.827	187	234	235	227	507.4
470	XM_372371	LOC390084	M-030025-00	2.042	-2.239	-1.586	629	1.605	-1.846	-1.938	228	1.366	-1.948	-1.318	921	137	118	259	509.3
471	XM_040265	KIAA0217	M-026388-00	0.728	-1.894	-2.335	280	0.761	-1.4	-1.935	847	0.167	-1.489	-2.074	557	124	210	309	509.3
472	NM_177998	OTOP1	M-017748-00	-1.118	-2.07	-1.652	539	-0.941	-1.78	-1.477	705	-0.896	-2.028	-1.639	349	242	101	129	510.0
473	NM_181435	C1QTNF3	M-014681-00	-2.033	-2.664	-0.823	182	-1.448	-2.385	-0.521	758	-1.3	-1.972	-0.914	967	109	223	238	511.0
474	XM_375593	ZNF536	M-020506-00	-0.662	-1.63	-1.534	706	-0.64	-1.729	-1.799	337	-0.588	-1.642	-1.482	567	150	210	228	512.9
475	NM_006084	ISGF3G	M-020858-01	0.518	-1.824	-3.004	346	0.715	-1.468	-1.97	721	0.197	-1.494	-2.155	546	103	170	255	514.5
476	NM_152334	FLJ25005	M-015734-00	-2	-1.528	-0.496	713	-1.788	-1.717	-0.772	347	-1.489	-1.662	-0.744	559	249	241	222	517.1
477	NM_000100	CSTB	M-017240-00	-1.393	ND	-2.169	382	-0.939	ND	-1.782	928	-1.519	ND	-1.68	398	55	0	231	520.6
478	NM_003225	TFF1	M-003715-00	-0.15	-1.47	-2.329	821	0.041	-1.365	-2.032	915	0.037	-1.826	-2.054	188	189	96	227	520.8
479	XM_037759	KIAA0376	M-024592-00	-1.555	-1.514	-1.966	674	-1.392	-1.447	-1.593	759	-1.761	-1.711	-1.686	279	229	235	251	522.6
480	NM_178424	SOX30	M-012355-00	-1.073	-1.94	-1.576	642	-0.977	-1.361	-1.659	924	-1.628	-1.747	-1.886	243	223	223	223	524.3

dec.	GeneID	Gene Name	Smartpool Cat	SCPO r1	SCPO r2	SCPO r3	SCPO rank	STAPO r1	STAPO r2	STAPO r3	STAPO rank	STIPO r1	STIPO r2	STIPO r3	STIPO rank	OC r1	OC r2	OC r3	rank product
481	NM_015570	AUTS2	M-013932-00	-1.518	-2.171	-0.374	729	-1.328	-1.947	-0.175	996	-1.808	-1.808	-0.364	199	227	187	217	524.7
482	NM_024804	FLJ12606	M-014454-00	-1.852	-2.009	-0.678	325	-1.8	-1.79	-0.874	277	-1.093	-1.237	-0.13	1615	266	62	224	525.8
483	NM_012145	DTYMK	M-006720-00	-2.464	-0.468	-1.435	890	-1.935	-0.471	-1.626	482	-2.097	-0.469	-1.641	341	253	253	245	526.9
484	NM_024751	FLJ13273	M-014433-00	-1.707	-1.475	-2.678	459	-1.768	-1.367	-3.16	303	-1.266	-0.902	-2.208	1055	228	215	250	527.4
485	NM_138417	MGC20419	M-015576-00	-1.51	-1.66	0.52	739	-1.978	-2.309	0.781	154	-1.475	-1.184	0.886	1294	77	60	124	528.1
486	NM_138371	MGC16044	M-015532-00	-2.462	-1.809	0.079	355	-3.137	-1.781	-0.174	286	-1.97	-1.131	0.047	1478	232	235	158	531.4
487	NM_006744	RBP4	M-008289-00	-1.682	-0.988	-1.466	830	-1.841	-0.634	-1.587	525	-1.93	-0.696	-1.64	345	254	228	221	531.7
488	NM_152631	FLJ35782	M-016939-00	-1.709	-0.094	-1.477	807	-1.737	-0.504	-1.967	328	-1.481	-0.293	-1.637	568	231	78	165	531.7
489	NM_198486	RPL7L1	M-027238-00	-1.748	-2.73	-1.176	410	-1.615	-1.574	-0.808	544	-1.422	-1.841	-0.976	677	245	202	113	532.5
490	NM_144595	FLJ30046	M-018736-00	-1.775	0.151	-1.814	386	-1.641	0.14	-1.815	455	-1.433	-0.009	-1.343	860	280	220	246	532.6
491	NM_005538	INHBC	M-012113-01	-1.731	1.008	-1.542	690	-1.73	0.674	-1.762	336	-1.523	0.474	-1.436	653	222	226	258	533.0
492	XM_291020	LOC339809	M-023119-00	-2.184	ND	-0.961	647	-2.355	ND	-0.698	609	-2.368	ND	-0.845	388	227	13	187	534.7
493	NM_003942	RPS6KA4	M-004664-00	-1.472	-1.78	-1.796	383	-1.488	-1.29	-1.606	683	-1.099	-1.489	-1.468	588	238	148	200	535.8
494	NM_198999	PRES	M-031941-00	-1.605	-1.919	-2.045	257	-1.167	-1.579	-1.542	591	-0.853	-1.398	-1.279	1020	114	73	119	537.1
495	NM_021951	DMRT1	M-012668-00	-1.331	ND	-2.094	453	-1.079	ND	-2.084	536	-1.087	ND	-1.802	641	101	40	267	537.9
496	XM_373082	LOC391784	M-028498-00	ND	-1.885	-1.456	508	ND	-1.629	-1.753	385	ND	-1.511	-1.232	796	30	119	116	538.0
497	NM_015374	UNC84B	M-009959-00	-1.814	-1.564	-1.096	662	-2.164	-1.704	-1.367	362	-1.496	-1.438	-0.903	650	153	162	184	538.1
498	NM_020967	NCOA5	M-013157-00	-2.109	-1.011	-1.705	461	-1.952	-1.276	-1.739	325	-1.871	-1.241	-1.272	1043	155	150	151	538.6
499	XM_373574	LOC387943	M-030186-00	-2.129	0.398	-1.702	468	-2.48	0.28	-1.668	413	-1.554	0.551	-1.366	813	235	159	92	539.6
500	XM_293745	LOC345222	M-024158-00	-1.503	-0.144	-2.888	751	-1.804	-0.268	-2.454	262	-1.371	-0.543	-2.516	799	184	185	206	539.7
501	XM_372210	PPP1R3F	M-024661-00	-1.271	-2.589	-1.587	627	-1.074	-2.316	-1.459	740	-1.643	-2.337	-1.473	340	236	261	252	540.3
502	NM_001807	CEL	M-008871-00	-2.242	ND	-0.76	756	-2.178	ND	-0.965	549	-2.103	ND	-1.126	381	67	12	141	540.8
503	NM_005181	CA3	M-008714-00	-1.593	-1.769	-1.009	620	-1.659	-1.721	-1.065	431	-1.463	-1.674	-1.164	599	122	242	88	543.0
504	NM_022911	SLC26A6	M-007494-00	-1.818	-0.534	-1.475	815	-1.934	-0.334	-1.819	248	-1.611	-0.269	-1.371	803	249	202	181	545.5
505	NM_004270	CRSP9	M-017313-00	-1.713	-1.324	-3.757	451	-1.416	-1.148	-3.145	813	-1.551	-1.022	-2.865	455	224	223	100	550.5
506	NM_144694	ZNF570	M-015736-00	1.049	-1.86	-2.182	312	1.018	-1.885	-1.778	291	0.613	-1.034	-1.041	1845	156	77	61	551.2
507	NM_014292	CBX6	M-009555-00	-1.354	-1.793	-1.92	371	-1.234	-1.64	-1.512	628	-1.127	-1.742	-1.4	729	211	164	137	553.8
508	NM_032849	FLJ14834	M-016348-00	-1.843	-2.174	0.819	329	-2.078	-3.277	0.612	113	-0.602	-1.41	1.488	4577	155	201	222	554.1
509	XM_376519	ANKRD6	M-020396-00	-1.177	-1.691	-2.676	483	-0.891	-1.798	-2.074	266	-0.882	-1.171	-2.513	1333	226	220	253	555.3
510	NM_021018	HIST1H3F	M-013127-00	-1.942	-0.386	-1.762	399	-1.538	-0.252	-1.363	918	-1.621	-0.636	-1.543	469	217	75	118	555.9
511	NM_000903	NQO1	M-005133-01	-0.582	-2.846	-1.893	281	-0.366	-2.552	-1.528	606	-0.214	-2.269	-1.283	1009	174	92	142	555.9
512	XM_373984	LOC388947	M-027837-00	-2.15	0.504	-1.666	517	-2.228	0.356	-1.605	501	-1.897	-0.039	-1.426	665	244	245	263	556.4
513	NM_018168	C14ORF105	M-020507-00	-1.338	-2.491	-1.667	515	-0.948	-2.311	-1.47	720	-1.755	-1.544	-1.529	467	54	57	104	557.4
514	NM_145017	FLJ32771	M-016619-00	-0.907	-1.854	-2.155	320	-0.52	-1.198	-2.179	1360	-0.882	-1.598	-2.023	399	203	194	238	557.9
515	NM_138569	C6ORF142	M-015915-00	-1.359	0.347	-2.897	1048	-1.507	0.773	-1.876	642	-1.729	0.304	-2.322	260	232	232	108	559.3
516	XM_378449	LOC400201	M-030279-00	-2.017	-3.633	-1.065	189	-1.427	-2.934	-0.805	789	-1.225	-1.664	-0.195	1176	69	98	84	559.7
517	NM_024621	FLJ12604	M-014390-00	-1.686	-1.158	-1.729	487	-1.371	-0.59	-1.26	1174	-1.817	-1.193	-1.68	307	234	240	243	559.9
518	NM_020777	SORCS2	M-013162-00	-0.376	-1.273	-1.954	1269	-0.509	-1.801	-1.898	264	-0.23	-1.616	-1.503	525	135	224	95	560.3
83	NM_003565	ULK1	M-005049-00	-2.786	-1.913	-2.012	192	-2.556	-1.95	-1.969	164	-2.557	-2.207	-1.85	40	1270	526	947	107.994513

Table 9.2 500plus genes whose siRNA knock-down decreased GFP-LC3 spots in the primary screen

Table of approximately 500 best 'increasers'. Rank based on rank product (RP); GeneID; Gene name; Dharmacon Smartpool catalogue number; SCPO for 3 replicates; STAPO for 3 replicates; STIPO for 3 replicates; Object count (OC) for three replicates; and rank product are shown. ND is not determined, as less than 50 valid objects were counted. Genes highlighted in blue are of interest and spoken of in the text. Genes highlighted in yellow were contained on plate 10 and not processed with screen plates.

inc.	"No" if I did not look at the images	In deconvolution screen?	hit/repeat without toxicity	toxic?	discontinued/ withdrawn or not available from Dharmacon	pseudogene	gene ID	gene symbol	full name	Primary and repeat screen combined rank product	Primary screen rank product as increaser	Repeat screen rank product as increaser	Repeat screen SCPO rank	Repeat screen STAPO rank	Repeat screen STIPO rank	Repeat screen median SCPO score	Repeat screen rank with new images	Repeat screen OC rep1	Repeat screen OC rep2	Repeat screen OC rep3
1			toxic	x			NM_152636	METT5D1	methyltransferase 5 domain containing 1	6.20	3.3	11.7	22	18	4	2.873	5	133	312	135
2			yes		not avail. Dharm.		XM_375608	DKFZp761D15	hypothetical protein DKFZp761D1918	8.75	60.8	1.3	1	1	2	4.296	119	837	1531	402
3		yes	yes				NM_024829	FLJ22662	hypothetical protein FLJ22662	11.29	2.2	57.9	97	80	25	1.699	41	1182	854	942
4		yes	yes				NM_024913	C7orf58	chromosome 7 open reading frame 58	17.21	5.7	52.0	45	48	65	1.837	21	718	460	456
5		yes	yes				XM_378706	PRCD	progressive rod-cone degeneration	20.13	64.3	6.3	5	10	5	3.074	154	779	1018	423
6			yes*		discontinued		XM_375150	LOC400301	similar to protein kinase CHK2 isoform b	21.13	245.7	1.8	3	2	1	3.751	189	950	1103	553
7		yes	yes				NM_001265	CDX2	caudal type homeobox 2	27.16	38.3	19.3	17	15	28	2.323	31	1108	659	885
8		yes	yes				XM_373685	hCG2045437	LOC388276	27.61	201.7	3.8	6	3	3	3.709	493	1022	978	780
9		yes	yes				NM_006047	RBM12	RNA binding motif protein 12	28.74	118	7.0	7	7	7	3.111	14	359	817	518
10		yes	yes				NM_016284	CNOT1	CCR4-NOT transcription complex, subunit	32.49	13.8	76.5	94	119	40	1.8	39	207	226	779
11			toxic	x			NM_003456	ZNF205	zinc finger protein 205	32.86	43.9	24.6	60	31	8	2.247	4	123	232	239
12		yes	yes				NM_006870	DSTN	destrin (actin depolymerizing factor)	34.54	36.1	33.0	20	22	82	2.144	8	510	596	1021
13		yes	yes				NM_000412	HRG	histidine-rich glycoprotein	37.57	300.2	4.7	2	4	13	2.834	3	1272	559	921
14			no				NM_003410	ZFX	zinc finger protein, X-linked	41.05	2.1	802.5	812	904	704	-0.66	279	789	547	717
15		yes	yes				NM_000629	IFNAR1	interferon (alpha, beta and omega) recept	42.82	295.1	6.2	4	5	12	3.034	6	889	821	946
16		yes	yes				NM_012290	TLK1	tousled-like kinase 1		46.54		60	42	40			677	166	392
17			toxic	x			NM_015894	STMN3	stathmin-like 3	47.48	182.9	12.3	9	8	26	2.345	106	402	165	263
18			no				NM_021071	ART4	ADP-ribosyltransferase 4 (Dombrock blood	48.07	32	72.2	56	84	80	1.559	50	950	584	401
19		yes	yes				NM_000983	RPL22	ribosomal protein L22	48.13	284.5	8.1	10	9	6	3.11	25	658	1059	1358
20		yes	yes				XM_372810	PLXNA2	plexin A2	50.61	64.2	39.9	39	44	37	1.92	62	699	688	737
21			yes*		not avail. Dharm.	pseudo	XM_373092	LOC391807	hypothetical LOC391807	51.87	150.5	17.9	14	17	24	2.401	10	777	489	960
22			no				NM_000792	DIO1	deiodinase, iodothyronine, type I	53.58	5.1	562.9	546	593	551	-0.156		747	867	621
23		yes	yes				NM_006145	DNAJB1	DnaJ (Hsp40) homolog, subfamily B, mem	54.57	18.7	159.3	225	187	96	1.177	121	1051	1163	589
24		yes	yes				NM_006551	SCGB1D2	secretoglobin, family 1D, member 2	54.94	22.7	132.9	138	132	129	1.193	358	1010	1066	1427
25		yes	yes				NM_152611	LRRN4	leucine rich repeat neuronal 4	55.91	9.1	343.5	369	384	286	0.586	314	819	1090	797
26		yes	yes				NM_152492	CCDC27	coiled-coil domain containing 27	56.10	41	76.8	63	133	54	1.63	103	1570	1118	4
27		yes	yes				NM_001633	AMBP	alpha-1-microglobulin/bikunin precursor	57.30	24.4	134.6				1.265	180	1073	611	940
28			yes		not avail. Dharm.	pseudo	NM_194289	NUDT16P	nudix (nucleoside diphosphate linked moie	57.54	25.4	130.3	148	136	110	1.189	24	536	996	421
29		yes	yes				NM_012272	PRPF40B	PRP40 pre-mRNA processing factor 40 hor	57.60	10.5	316.0	344	354	259	0.674	63	447	822	1254
30		yes	yes				NM_012307	EPB41L3	erythrocyte membrane protein band 4.1-li	58.08	45.7	73.8	54	49	152	1.661	22	1201	873	1282
31		yes	yes				NM_002142	HOXA9	homeobox A9	58.10	157.8	21.4	12	16	51	2.487	19	1138	540	783
32			toxic	x	discontinued		XM_379306	LOC401169	hypothetical gene supported by BC034612	58.56	60.8	56.4	40	118	38	1.875	418	460	83	262
33			toxic	x			XM_058857	FLJ40194	hypothetical FLJ40194	58.80	161.1	21.5	31	29	11	2.276	450	510	304	785
34		yes	yes				NM_004521	KIF5B	kinesin family member 5B	59.63	124.5	28.6	52	28	16	2.15	2	383	549	449
35		yes	yes				NM_001105	ACVR1	activin A receptor, type I	59.98	102	35.3	38	33	35	1.924	108	1158	1137	1475
36		yes	yes				NM_152441	FBXL14	F-box and leucine-rich repeat protein 14	60.34	61.1	59.6	72	70	42	1.614	63	1323	1148	899
37			no/toxic	x			NM_000850	GSTM4	glutathione S-transferase M4	61.33	5.4	696.6	742	753	605	-0.464	391	455	178	387
38		yes	yes				NM_001466	FZD2	frizzled homolog 2 (Drosophila)	64.70	45.2	92.6	87	110	83	1.419	36	1313	480	950
39			yes/no				NM_182971	COX8C	cytochrome c oxidase subunit 8C	64.77	19.9	210.8	244	230	167	0.885	380	837	643	585
40			yes/no				XM_379260	LOC152742	hypothetical protein LOC152742	65.11	18.4	230.4	243	258	195	0.721	294	1042	1259	1139
41			yes*		discontinued		XM_373746	LOC388416	hypothetical LOC388416	65.77	220.6	19.6	29	13	20	2.309	16	1093	1092	746
42		yes	yes				XM_047025	TBC1D25	TBC1 domain family, member 25	67.19	388.6	11.6	8	14	14	2.684	12	549	564	306
43		yes	yes				NM_000196	HSD11B2	hydroxysteroid (11-beta) dehydrogenase :	67.73	59.4	77.2	55	46	182	1.685	76	1315	862	907
44		yes	yes				NM_006829	C10ORF116	chromosome 10 open reading frame 116	68.08	292.2	15.9	19	21	10	2.323	27	483	961	490
45		yes	yes				XM_375495	AATK	apoptosis-associated tyrosine kinase	69.26	89.4	53.7	34	64	71	1.727	78	953	809	1315
46		yes	yes				NM_002146	HOXB3	homeobox B3	69.52	34.8	138.9	159	106	159	1.178	107	513	443	934
47		yes	yes				NM_000075	CDK4	cyclin-dependent kinase 4	72.92	24.4	217.9	269	239	161	0.748	327	1232	1064	1057
48			yes*		discontinued		XM_370930	LOC388205	similar to RIKEN cDNA 1520401A03 gene	73.94	300	18.2	11	11	50	2.411	75	568	1307	200
49		yes	yes				NM_012288	TRAM2	translocation associated membrane protei	76.28	510.3	11.4	13	6	19	2.266	11	1048	1174	580
50			toxic	x			XM_291105	TADA2B	transcriptional adaptor 2 (ADA2 homolog,	76.29	80.5	72.3	112	125	27	1.307	28	309	253	330
51		yes	yes				NM_182587	C2ORF21	chromosome 2 open reading frame 21	76.69	143.2	41.1	37	36	52	1.936	18	596	911	519
52		yes	yes				NM_032714	INF2	inverted formin, FH2 and WH2 domain cor	78.21	389	15.7	18	12	18	2.312	123	838	45	648
53			no				NM_018069	CEP192	centrosomal protein 192kDa	78.46	154.8	39.8	43	43	34	1.933	288	1044	573	525
54			yes/no				NM_032122	DTNBP1	dystrobrevin binding protein 1	81.46	22.4	296.2	275	289	327	0.617	613	628	440	1009
55			yes/no	x			NM_015008	TMCC1	transmembrane and coiled-coil domain far	82.19	66.5	101.6	82	94	136	1.175	225	371	1016	1106
56			yes*		not avail. Dharm.		XM_372812	LOC391162	similar to mCG118656	83.54	85.4	81.7	76	63	114	1.272	375	636	530	992
57			toxic	x			NM_152427	CFLP1	coflin pseudogene 1	85.99	187.1	39.5	35	41	43	1.988	82	341	232	106
58		yes	yes				NM_004857	AKAP5	A kinase (PRKA) anchor protein 5	86.06	18.4	402.5	378	460	375	0.271	295	1581	1297	1425
59		yes	yes				XM_371484	SELI	selenoprotein I	86.57	144	52.0	50	47	60	1.779	72	1054	577	1063
60			yes*		not avail. Dharm.		NM_182631	LOC348840	hypothetical LOC348840	88.78	54.4	144.9	175	164	106	1.106	395	1078	1186	1364

inc.	"No" if I did not look at the images	In deconvolution screen?	hit/repeat without toxicity	toxic?	discontintued/ withdrawn or not available from Dharmacon	pseudogene	gene ID	gene symbol	full name	Primary and repeat screen combined rank product	Primary screen rank product as increaser	Repeat screen rank product as increaser	Repeat screen SCPO rank	Repeat screen STAPO rank	Repeat screen STIPO rank	Repeat screen median SCPO score	Repeat screen rank with new images	Repeat screen OC rep1	Repeat screen OC rep2	Repeat screen OC rep3
61			yes/no				XM_378453	LOC400208	chromosome 14 open reading frame 26	90.19	415.8	19.6	32	26	9	2.385	378	1259	1576	775
62		yes	yes				NM_005810	KLRG1	killer cell lectin-like receptor subfamily G,	90.37	58.6	139.3	160	151	112	1.105	30	547	1101	1433
63		yes	yes				NM_005355	KIF25	kinesin family member 25	91.46	91.2	91.7	111	79	88	1.403	98	1009	465	891
64			no/toxic	x			NM_005112	WDR1	WD repeat domain 1	92.19	15	566.6	680	555	482	-1.001		714	349	883
65			yes/no				NM_023074	ZNF649	zinc finger protein 649	92.38	66.3	128.7	124	117	147	1.249	368	678	712	790
66		yes	yes				NM_172347	KCNG4	potassium voltage-gated channel, subfami	92.44	250.1	34.2	49	37	22	1.854	88	774	1232	489
67		yes	yes				NM_032875	FBXL20	F-box and leucine-rich repeat protein 20	93.18	100.5	86.4	119	86	63	1.551	20	663	598	1168
68		yes	yes	x			XM_035299	ZSWIM6	zinc finger, SWIM-type containing 6	93.91	264.7	33.3	24	23	67	2.213	15	634	317	106
69		yes	yes				XM_371832	FAM135A	family with sequence similarity 135, meml	94.36	186	47.9	46	45	53	1.791	83	1297	753	1128
70		yes	yes				NM_005147	DNAJA3	DnaJ (Hsp40) homolog, subfamily A, mem	97.37	109.9	86.3	91	98	72	1.455	38	1213	1474	1809
71		yes	yes				NM_004599	SREBF2	sterol regulatory element binding transcrip	98.95	32.3	303.1	299	319	292	0.562	95	1275	1062	657
72			yes*		not avail. Dharm.		XM_373771	LOC388456	hypothetical gene supported by BC039671	99.98	454.9	22.0	26	24	17	2.422	74	880	885	864
73		yes	yes				NM_007003	PAGE4	P antigen family, member 4 (prostate assc	104.63	115.9	94.5	103	101	81	1.426	130	702	770	741
74		yes	yes				NM_023080	C8orf33	chromosome 8 open reading frame 33	104.70	76.3	143.7	122	130	187	1.255	176	956	963	1189
75			toxic	x			XM_373252	LOC392221	similar to 16.7Kd protein	104.83	248.2	44.3	51	74	23	1.776	252	182	94	229
76			off-target	x			NM_002812	PSMD8	proteasome (prosome, macropain) 26S su	104.90	23.6	466.2	457	480	462	0.157	325	466	577	337
77			no				NM_023935	DDRGK1	DDRGK domain containing 1	105.28	27.4	404.5	456	476	305	0.172	536	1299	748	1145
78		yes	yes				XM_113678	NUP160	nucleoporin 160kDa	105.87	111.5	100.5	83	68	180	1.167	228	789	773	503
79		yes	yes				NM_005419	STAT2	signal transducer and activator of transcrip	106.55	198.8	57.1	23	32	253	2.063	51	612	852	818
80			yes				NM_014026	DCPS	decapping enzyme, scavenger	107.21	344.6	33.4	21	19	93	1.875	100	310	517	523
81			no	x			NM_172005	WFDC13	WAP four-disulfide core domain 13	107.61	32.4	357.4	353	408	317	0.415	263	875	862	428
82		yes	yes				NM_139241	FGD4	FYVE, RhoGEF and PH domain containing 4	109.84	557.7	21.6	25	27	15	2.324	66	665	1090	1016
83			no	x			NM_213655	HSN2	hereditary sensory neuropathy, type II	110.72	77.7	157.8	140	75	374	0.445	242	333	246	139
84		yes	yes				NM_000256	MYBPC3	myosin binding protein C, cardiac	110.96	182.9	67.3	68	65	69	1.602	46	772	1312	1451
85			toxic	x	discontinued		XM_373540	LOC387872	hypothetical gene supported by BC044741	111.62	180.8	68.9	58	91	62	1.614	254	189	113	150
86		yes	yes				NM_144650	ADHFE1	alcohol dehydrogenase, iron containing, 1	112.58	342.3	37.0	27	40	47	1.977	398	1218	785	761
87		yes	yes				NM_018349	MCTP2	multiple C2 domains, transmembrane 2	116.54	150.2	90.4	85	87	100	1.491	205	1079	1040	1028
88		yes	yes				XM_167072	BZRPL1	benzodiazapine receptor (peripheral)-like	117.48	192.3	71.8	92	82	49	1.573	125	705	860	387
89		yes	yes	x			NM_020437	ASPHD2	aspartate beta-hydroxylase domain contai	119.79	33.7	425.8	465	477	348	0.225		1090	559	522
90			no/toxic	x			NM_024994	FLJ12595	guanine nucleotide binding protein-like 3 (	120.99	183.1	79.9	79	77	84	1.477	246	892	387	415
91		yes	yes				NM_005845	ABCC4	ATP-binding cassette, sub-family C (CFTR/	121.66	71.3	207.6	153	174	336	0.734	291	1351	713	1095
92			yes*		not avail. Dharm.		XM_373742	MGC40489	hypothetical protein MGC40489	121.73	336.4	44.0	74	55	21	1.788	239	1090	962	455
93			toxic	x			NM_030891	LRRC3	leucine rich repeat containing 3	122.70	96.7	155.7	169	137	163	1.026	156	1156	563	1123
94			no				NM_033051	SLC46A2	solute carrier family 46, member 2	123.19	63.2	240.1	201	240	287	0.587	287	540	277	450
95		yes	yes				NM_033050	SUCNR1	succinate receptor 1	124.73	94.3	165.0	149	157	192	1.108	73	728	577	690
96		yes	yes				NM_004388	CTBS	chitobiase, di-N-acetyl-	126.15	185.4	85.8	95	52	128	1.393	318	1032	832	854
97		yes	yes				NM_024902	DNAJC22	DnaJ (Hsp40) homolog, subfamily C, mem	126.70	173.6	92.5	71	85	131	1.154	60	1401	925	1469
98			no/toxic	x			XM_373886	LOC388738	hypothetical LOC388738	129.31	40.2	416.0	425	501	338	0.232	630	711	292	544
99			yes/no				NM_00100202	C4B	complement component 4B (Childo blood	130.27	296.5	57.2	84	72	31	1.66	473	1054	1506	758
100		yes	yes				NM_006852	TLK2	tousled-like kinase 2		130.383483		125	124	143			864	565	714
101		yes	yes				NM_006285	TESK1	testis-specific kinase 1		130.634062		47	14	3388			687	606	661
102			yes				NM_002124	HLA-DRB1	major histocompatibility complex, class II,	133.65	536.5	33.3	41	25	36	2.247	99	1157	870	963
103		yes	yes	x			NM_144999	LRRC45	leucine rich repeat containing 45	133.76	489.9	36.5	28	30	58	2.151	13	324	961	185
104		yes	yes				NM_032347	ZNF397	zinc finger protein 397	134.59	255.9	70.8	57	61	102	1.619	248	1425	647	1027
105			toxic	x			NM_000576	IL1B	interleukin 1, beta	135.19	499	36.6	30	42	39	1.936	56	105	389	365
106			no				XM_097622	FAM78B	family with sequence similarity 78, membe	135.81	161	114.6	135	131	85	1.262	362	545	489	1284
107		yes	yes	x			NM_004443	EPHB3	EPH receptor B3	136.18	133.8	138.6	170	145	108	1.263	463	530	457	718
108			no				NM_00100532	OR6K3	olfactory receptor, family 6, subfamily K, r	136.52	250.5	74.4	130	96	33	1.466	457	1031	1026	344
109			no				NM_020120	UGCGL1	UDP-glucose ceramide glucosyltransferase	136.75	141.7	132.0	126	152	120	1.179	158	1652	479	367
110	no						NM_175892	DLG2	discs, large homolog 2, chapsyn-110 (Dros	137.06	52.6	357.1				0.266				
111		yes	yes				NM_017805	RASIP1	Ras interacting protein 1	137.19	267.1	70.5	62	62	91	1.403	128	676	538	440
112			toxic	x			NM_005018	PDCD1	programmed cell death 1	137.25	130.1	144.8				1.215	67			
113		yes	yes				NM_178124	CXorf40A	chromosome X open reading frame 40A	137.97	510.5	37.3	16	20	162	2.338	91	997	998	991
114		yes	yes				NM_018992	KCTD5	potassium channel tetramerisation domair	138.70	334.6	57.5	64	54	55	1.693	94	879	812	748
115	no						NM_024048	MGC3020	chromosome 16 open reading frame 67	139.74	84	232.5				0.715				
116			no				XM_291142	FCHO2	FCH domain only 2	140.28	174.9	112.5	142	170	59	1.387	186	1016	1307	1117
117	no						NM_006404	PROCR	protein C receptor, endothelial (EPCR)	140.56	49.2	401.6				0.22				
118			no				NM_052858	MRVLDC3	MARVEL domain containing 3	140.90	493.6	40.2	44	51	29	1.895	129	1305	1261	922
119			yes/no	x			NM_005593	MYF5	myogenic factor 5	140.94	320.1	62.1	90	59	45	1.537	272	689	527	328
120			yes/no				NM_018064	AKIRIN2	akirin 2	141.32	504.6	39.6	53	39	30	1.987	132	1138	762	629

inc.	"No" if I did not look at the images	In deconvolution screen?	hit/repeat without toxicity	toxic?	discontintued/ withdrawn or not available from Dharmacon	pseud ogene	gene ID	gene symbol	full name	Primary and repeat screen combined rank product	Primary screen rank product as increaser	Repeat screen rank product as increaser	Repeat screen SCPO rank	Repeat screen STAPO rank	Repeat screen STIPO rank	Repeat screen median SCPO score	Repeat screen rank with new images	Repeat screen OC rep1	Repeat screen OC rep2	Repeat screen OC rep3
121			yes/no				XM_379215	RPL32P3	ribosomal protein L32 pseudogene 3	144.36	176.2	118.3	88	100	188	1.435	113	672	731	641
122		yes	yes				NM_018031	WDR6	WD repeat domain 6	145.45	482.8	43.8	33	34	75	2.037	193	1091	705	924
123	no						NM_014830	ZBTB39	zinc finger and BTB domain containing 39	149.57	31.4	712.5				-0.983				
124		yes	yes	x			NM_022575	VPS16	vacuolar protein sorting 16 homolog (S. cc	149.67	190.4	117.7	152	141	76	1.22	85	460	552	239
125	no						NM_203423	LOC389199	hypothetical gene supported by BC031673	150.17	92.4	244.1				0.804				
126	no						NM_001495	GFRA2	GDNF family receptor alpha 2	151.33	37	618.9				-0.343				
127	no						NM_005550	KIFC3	kinesin family member C3	151.89	109.6	210.5				0.754				
128	no						NM_000404	GLB1	galactosidase, beta 1	153.79	165.1	143.3				1.162				
129	no						NM_005321	HIST1H1E	histone cluster 1, H1e	153.82	124.4	190.2				0.73				
130	no						NM_006668	CYP46A1	cytochrome P450, family 46, subfamily A,	154.40	91.1	261.7				0.671				
131		yes	yes				NM_012202	GNG3	guanine nucleotide binding protein (G prot	154.50	248.6	96.0	65	60	227	1.438	70	1077	518	922
132	no						XM_380114	LOC402523		157.23	183.8	134.5				1.063				
133			yes/no		discontinued		XM_373864	LOC388684	hypothetical LOC388684	157.70	210.9	117.9	128	105	122	1.239	501	610	391	920
134			toxic	x			NM_016604	JMJD1B	jumonji domain containing 1B	158.48	44.8	560.6	607	631	460	-0.73	419	366	269	160
135		yes	yes				NM_018389	SLC35C1	solute carrier family 35, member C1	158.80	552.6	45.6	61	38	41	1.829	301	1719	1349	1516
136	no						NM_019002	ETAA16	Ewing tumor-associated antigen 1	159.75	141.3	180.6				0.87				
137	no						NM_015859	GTF2A1	general transcription factor IIA, 1, 19/37k	160.03	107.9	237.3				0.749				
138	no						NM_031456	FBXW10	F-box and WD repeat domain containing 1	160.28	110.4	232.7				0.877				
139		yes	yes				NM_016224	SNX9	sorting nexin 9	160.60	255	101.2	93	107	104	1.404	416	387	371	1174
140			yes/no				NM_006223	PIN4	protein (peptidylprolyl cis/trans isomerase	162.48	312.8	84.4	99	66	92	1.372	589	626	333	484
141		yes	yes				NM_007071	HHLA3	HERV-H LTR-associating 3	163.45	454.3	58.8	36	50	113	1.519	92	737	1062	803
142		yes	yes				NM_022068	FAM38B	family with sequence similarity 38, membe	164.22	159.3	169.3				1.078	80			
143	no						NM_207449	FLJ44674	FLJ44674 protein	165.64	54.5	503.4				-1.142				
144		yes	yes				NM_005486	TOM1L1	target of myb1 (chicken)-like 1	166.64	236.1	117.6	117	88	158	1.274	460	1330	1359	1274
145	no						XM_029084	FLJ21438		167.47	177.4	158.1				0.94				
146		yes	yes				NM_033209	THY1	Thy-1 cell surface antigen	169.62	469.1	61.3	89	81	32	1.608	77	1294	1444	1225
147		yes	yes				NM_032681	SPRYD5	SPRY domain containing 5	169.98	436.4	66.2	67	76	57	1.631	169	1232	592	945
148		yes	yes				NM_006909	RASGRF2	Ras protein-specific guanine nucleotide-rel	170.23	248.8	116.5	70	99	228	0.899	410	929	701	1115
149	no						NM_194292	SAS56	spindle assembly 6 homolog (C. elegans)	170.59	126	231.0				0.674	37			
150	no						NM_001104	ACTN3	actinin, alpha 3	170.64	86.4	337.0				0.445	84			
151		yes	yes				NM_022767	AEN	apoptosis enhancing nuclease	172.99	288.5	103.7	110	139	73	1.254	177	1171	1169	823
152	no						NM_000065	C6	complement component 6	173.27	139.4	215.4				0.911	26			
153		yes	yes				NM_014876	JOSD1	Josephin domain containing 1	174.66	285.3	106.9	147	126	66	1.293	273	914	988	1293
154			toxic	x			NM_173605	KCNRG	potassium channel regulator	174.94	515.3	59.4	69	44	66	1.639	53	236	484	724
155			toxic	x			NM_007183	PKP3	plakophilin 3	175.37	140.7	218.6	248	242	174	0.744	52	292	511	1032
156		yes	yes				NM_002662	PLD1	phospholipase D1, phosphatidylcholine-spe	175.44	130.8	235.3				0.784	71			
157			toxic	x			NM_001445	FABP6	fatty acid binding protein 6, ileal	175.72	97.8	315.7	347	341	266	0.472	345	392	578	695
158		yes	yes				NM_015432	PLEKHG4	pleckstrin homology domain containing, fa	178.87	274.2	116.7	132	102	118	1.212	23	580	820	1075
159	no						NM_198502	FLJ43826	FLJ43826 protein	179.34	180.2	178.5				0.91				
160		yes	yes				NM_000893	KNG1	kininogen 1	180.35	335.7	96.9	78	53	220	1.494	64	766	596	1316
161			toxic	x			NM_019009	TOLLIP	toll interacting protein	181.76	291.2	113.4	136	176	61	1.2	79	87	198	242
162		yes	yes				NM_004409	DMPK	dystrophia myotonica-protein kinase	182.34	67.6	491.8	484	523	470	0.115	526	1003	364	737
163		yes	yes				NM_144605	SEPT12	septin 12	183.20	315.2	106.5	127	97	98	1.344	179	953	1057	538
164		yes	yes				NM_002931	RING1	ring finger protein 1	183.45	359.4	93.6	75	92	119	1.496	33	473	658	1408
165			yes	x			XM_172917	LOC256453	hypothetical LOC256453	184.51	428.7	79.4	86	104	56	1.438	663	329	284	1063
166			toxic	x			NM_032558	HJATL1	hippocampus abundant transcript-like 1	184.72	335.6	101.7	77	78	175	0.974	42	685	189	441
167		yes	yes				NM_153337	SNX20	sorting nexin 20	187.03	532.3	65.7	81	73	48	1.586	235	894	1046	890
168	no						NM_012176	FBXO4	F-box protein 4	188.60	94	378.4				0.618				
169		yes	yes	x			NM_015986	CRLF3	cytokine receptor-like factor 3	189.52	268.5	133.8	120	150	133	1.173	122	812	475	848
170		yes	yes				NM_018323	PI4K2B	phosphatidylinositol 4-kinase type 2 beta	189.82	35.2	1023.7	1025	1027	1019	-1.626	983	895	902	720
171	no				discontinued		XM_373555	LOC387897	hypothetical LOC387897	196.37	215.9	178.6				1.006				
172			yes/no	x			XM_033173	PCDH19	protocadherin 19	197.02	353.7	109.7	96	90	153	1.39	210	777	134	413
173			toxic	x			XM_291075	LOC339926	hypothetical LOC339926	197.57	350.8	111.3	100	112	123	1.362	421	158	77	514
174		yes	yes				NM_016300	ARPP-21	cyclic AMP-regulated phosphoprotein, 21 k	197.57	379.9	102.7	104	149	70	1.341	29	646	1190	944
175		yes	yes				NM_022042	SLC26A1	solute carrier family 26 (sulfate transporte	200.60	377.6	106.6	80	89	170	1.036	144	1068	789	1011
176	no						NM_030808	NDEL1	nudE nuclear distribution gene E homolog	201.04	131.1	308.3				0.742	57			
177			yes/no	x		pseudo	NR_001435	HLA-DPB2	major histocompatibility complex, class II,	202.22	533.4	76.7	59	57	134	1.63	not in excel lis	1049	414	470
178	no						XM_371678	LOC389174	similar to 6130401L20Rik protein	202.77	139.4	294.9				0.583	87			
179	no						NM_033182	FBXO44	F-box protein 44	203.33	193.3	213.9				0.855				
180	no						NM_145170	TTC18	tetratricopeptide repeat domain 18	203.98	238.8	174.2				0.919				

inc.	"No" if I did not look at the images	In deconvolution screen?	hit/repeat without toxicity	toxic?	discontintued/ withdrawn or not available from Dharmacon	pseudogene	gene ID	gene symbol	full name	Primary and repeat screen combined rank product	Primary screen rank product as increaser	Repeat screen rank product as increaser	Repeat screen SCPO rank	Repeat screen STAPO rank	Repeat screen STIPO rank	Repeat screen median SCPO score	Repeat screen rank with new images	Repeat screen OC rep1	Repeat screen OC rep2	Repeat screen OC rep3
181		yes	yes				NM_014623	MEA	male-enhanced antigen 1	208.55	537.2	81.0	48	67	165	1.514	102	1147	333	667
182	no						NM_002719	PPP2R5C	protein phosphatase 2, regulatory subunit	210.66	176.9	250.9				0.679	86			
183		yes	yes				NM_003480	MFAP5	microfibrillar associated protein 5	211.95	504.2	89.1	66	114	94	1.366	34	1217	1212	1172
184		yes	yes	x			NM_016153	HSFX1	heat shock transcription factor family, X lir	215.65	477.2	97.5	105	113	78	1.366	55	549	674	526
185			toxic	x			NM_012394	PFDN2	prefoldin subunit 2	219.36	425.1	113.2				1.347	9			
186	no						XM_378705	LOC400620	hypothetical LOC400620	219.93	326.8	148.0				1.113	96			
187		yes	yes				NM_004918	TCL1B	T-cell leukemia/lymphoma 1B	224.05	557.9	90.0	108	71	95	1.36	7	1373	760	1260
188			no				XM_371108	ARHGAP28	Rho GTPase activating protein 28	224.58	538.7	93.6	73	146	77	1.47	316	538	1247	304
189	no						NM_0010038(	FLJ35429	hypothetical protein FLJ35429	234.70	295.1	186.7				1.228				
190			no				NM_031429	RTBDN	retbindin	236.92	479.1	117.2	137	121	97	1.314	196	860	179	1396
191	no						XM_378546	LOC145820	hypothetical protein LOC145820	240.59	189.5	305.5				0.738	48			
192			toxic	x			NM_004475	FLOT2	flotillin 2	243.08	120.4	490.8	505	519	451	0.058	297	394	392	291
193			toxic	x			NM_080723	NRSN1	neurensin 1	243.43	268.7	220.5	286	266	141	0.68	201	578	355	278
194		yes	yes				NM_138960	TGIF2LX	TGFB-induced factor homeobox 2-like, X-li	244.22	507.6	117.5	116	111	126	1.276	167	933	759	971
195			yes/no				NM_198075	LRRC56	leucine rich repeat containing 56	246.24	521.3	116.3	101	95	164	1.357	271	825	826	861
196	no						NM_181334	ARHGAP8	PRR5-ARHGAP8 fusion	251.14	291.1	216.7				0.758	54			
197		yes	yes				NM_019598	KLK12	kallikrein-related peptidase 12	251.20	216.5	291.5				0.472	90			
198	no						NM_018226	RNPEPL1	arginyl aminopeptidase (aminopeptidase B	251.23	442.2	142.7				1.159	61			
199			toxic	x			NM_052932	TMEM123	transmembrane protein 123	254.35	376.6	171.8				1.053	81			
200	no						NM_018974	UNC93A	unc-93 homolog A (C. elegans)	263.74	324.3	214.5					97			
201	no						XM_371214	PLCH2	phospholipase C, eta 2	266.10	444.6	159.3					32			
202	no						NM_080878	ITLN2	intelectin 2	268.91	555.6	130.2					59			
203			toxic	x			NM_000770	CYP2C8	cytochrome P450, family 2, subfamily C, p	275.43	222.9	340.3					49			
204	no						NM_016009	SH3GLB1	SH3 DOMAIN, GRB2-LIKE, ENDOPHILIN B	277.11	173	443.9								
205	no						NM_013301	CCDC106	coiled-coil domain containing 106	283.53	464.8	173.0					69			
206	no						NM_022828	YTHDC2	YTH domain containing 2	295.61	218.6	399.7								
207	no						NM_002734	PRKAR1A	protein kinase, cAMP-dependent, regulator	295.88	127.3	687.7								
208	no					discontinued	XM_352847	LOC340529	similar to hypothetical protein LOC340529	296.54	211.2	416.4								
209		yes	yes				NM_020820	PREX1	phosphatidylinositol-3,4,5-trisphosphate-d	297.53	368	240.6					126			
210	no						NM_005502	ABCA1	ATP-binding cassette, sub-family A (ABC1)	302.00	465.8	195.8					44			
211	no						NM_152597	FSIP1	fibrous sheath interacting protein 1	304.47	344.2	269.3					68			
212	no						NM_007244	PRR4	proline rich 4 (lacrimal)	305.42	383	243.5					40			
213	no						NM_000127	EXT1	exostoses (multiple) 1	308.05	392.9	241.5					17			
214			toxic	x			NM_015071	ARHGAP26	Rho GTPase activating protein 26	309.60	184.4	519.8								
215			toxic	x			NM_004856	KIF23	kinesin family member 23	314.42	426.3	231.9					1			
216	no						NM_007278	GABARAP	GABA(A) receptor-associated protein	319.38	229.8	443.9								
217	no						NM_005217	DEFA3	defensin, alpha 3, neutrophil-specific	345.82	188.9	633.1								
218	no						NM_152770	C4orf22	chromosome 4 open reading frame 22	353.50	307.5	406.4					58			
219	no						NM_017860	C1orf56	chromosome 1 open reading frame 56	357.19	536	238.0					47			
220	no						NM_130776	GAGED4	X antigen family, member 3	385.73	389.2	382.3								
221	no						NM_004176	SREBF1	sterol regulatory element binding transcrip	428.71	290	633.8								
222			toxic	x			NM_182760	SUMF1	sulfatase modifying factor 1	444.72	531.1	372.4								
223	no						NM_003900	SQSTM1	sequestosome 1	448.97	364.4	553.2								
224	no						NM_001206	KLF9	Kruppel-like factor 9	452.57	486.3	421.2					35			
225	no						NM_001142	AMELX	amelogenin (amelogenesis imperfecta 1, X	466.77	404	539.3					93			
226	no						XM_374787	CCNYL2	cyclin Y-like 2	473.01	489	457.5								
227	no						NM_031430	RILP	Rab interacting lysosomal protein	530.46	517.4	543.9								

Table 9.3 Results of the repeat screen for a subset of Smartpools that cause an increase in GFP-LC3 spots

227 Smartpools are listed in order of primary and repeat screen combined rank product (not all 500 increasers are shown). Whether their images were examined, whether they were included in the subsequent deconvolution screen and whether I scored it as a non-toxic, non-off-target repeat hit as a result of visual analysis are indicated. Toxicity and availability of a deconvoluted set of siGenome siRNA duplexes for that given Smartpool are indicated. It is noted whether the gene is annotated as a psudogene. Gene ID, current gene symbol and full name are given. The rank product that combines the primary and repeat screen rank products, and the primary screen rank product and repeat screen rank product as increasers is shown. The repeat screen SCPO, STAPO, and STIPO ranks (as increasers) and the repeat screen median SCPO score are shown. The repeat screen rank generated with the second set of 14 images as well as the valid object count (OC) for three replicates in the repeat screen are shown. Genes highlighted in blue are of interest and are referred to in the text.

dec.	"No" if I did not look at the images	In deconvolution screen?	hit/repeat without toxicity	toxic?	discontintued/ withdrawn or not available from Dharmacon	pseudogene	gene ID	gene symbol	full name	Primary and repeat screen combined rank product	Primary screen rank product as increaser	Repeat screen rank product as increaser	Repeat screen SCPO rank	Repeat screen STAPO rank	Repeat screen STIPO rank	Repeat screen median SCPO score	Repeat screen rank with new images	Repeat screen OC rep1	Repeat screen OC rep2	Repeat screen OC rep3
1		yes	yes				NM_002039	GAB1	GRB2-associated binding protein 1	17.03	5.2	55.8	53	42	78	-1.276	10	1148	1428	1844
2		yes	yes				NM_024507	KREMEN2	kringle containing transmembrane protein	17.18	8.7	33.9	44	37	24	-1.396	57	1292	1404	1216
3			yes	x			NM_003973	RPL14	ribosomal protein L14	19.30	1.6	232.9	213	244	243	-0.677	242	451	485	1180
4			yes*		discontinued		XM_374185	LOC389437		20.08	74.9	5.4	3	4	13	-1.801	5	590	418	1276
5		yes	yes				NM_001896	CSNK2A2	casein kinase 2, alpha prime polypeptide	20.66	157.2	2.7	1	2	10	-2.103	36	515	516	351
6		yes	yes				NM_080928	ASB15	ankyrin repeat and SOCS box-containing 1	21.47	17.2	26.8	22	19	46	-1.567	61	1124	1337	708
7			no				NM_00100169	FLJ46257		23.93	232.1	2.5	5	3	1	-1.952	706	939	1840	655
8		yes	yes				NM_015971	MRPS7	mitochondrial ribosomal protein S7	24.23	20.1	29.2	33	36	21	-1.466	58	561	704	607
9			yes*		discontinued		XM_378436	LOC400163		24.86	389.3	1.6	2	1	2	-2.281	143	1515	1024	1322
10		yes	yes				XM_372213	USP27X	ubiquitin specific peptidase 27, X-linked	27.82	49.7	15.6	42	30	3	-1.402	809	839	2158	2159
11			yes	x			NM_031287	SF3B5	splicing factor 3b, subunit 5, 10kDa	33.40	5.6	199.2	161	203	242	-0.702	179	458	271	302
12		yes	yes				NM_021153	CDH19	cadherin 19, type 2	33.81	119.2	9.6	7	9	14	-1.724	11	1010	767	814
13		yes	yes				XM_371092	CCL4L1	chemokine (C-C motif) ligand 4-like 1	34.28	77.4	15.2	35	25	4	-1.736	888	1460	1264	693
14		yes	yes				NM_003820	TNFRSF14	tumor necrosis factor receptor superfamily	35.39	21.9	57.2	66	81	35	-1.14	76	1061	1532	1524
15		yes	yes				NM_181775	PLXNA4	plexin A4	37.05	27.6	49.7	49	27	93	-1.18	68	1037	1260	1413
16		yes	yes				NM_006690	MMP24	matrix metallopeptidase 24 (membrane-in	37.14	210.8	6.5	8	5	7	-1.839	29	497	380	1224
17			no				NM_130467	PAGE-5	P antigen family, member 5 (prostate assc	37.27	2.9	479.1	431	443	576	0.019	524	1294	621	581
18			yes*				NM_207433	FLJ44874	FLJ44874 protein	38.40	83.8	17.6	11	15	33	-1.464	3	913	732	630
19		yes	yes				XM_377566	PRAMEF3	PRAME family member 3	39.13	32.2	47.5	52	53	39	-1.33	54	788	767	114
20			yes		not avail. Dharm.		XM_376307	DKFZP667E05	hypothetical protein DKFZp667E0512	41.74	47.3	36.8	31	26	62	-1.43	52	676	899	539
21			no/toxic	x			NM_001060	TBXA2R	thromboxane A2 receptor	41.89	7	250.7	222	269	265	-0.601	192	373	250	296
22		yes	yes				NM_021818	SAV1	salvador homolog 1 (Drosophila)	44.58	25.8	77.0	59	79	98	-1.069	22	2123	1051	1296
23			yes*		discontinued		XM_372046	LOC389667	similar to tropomyosin 4	47.17	42.3	52.6	38	58	66	-1.187	105	1147	915	1776
24		yes	yes				NM_022467	CHST8	carbohydrate (N-acetylgalactosamine 4-0)	48.19	19	122.2	126	109	133	-0.944	94	1086	872	807
25		yes	yes				NM_138962	MSI2	musashi homolog 2 (Drosophila)	51.50	291.1	9.1	4	7	27	-1.71	13	1252	1362	874
26		yes	yes				NM_004299	ABCB7	ATP-binding cassette, sub-family B (MDR/T	51.67	176.4	15.1	17	17	12	-1.611	2	997	1099	1425
27		yes	yes				NM_004934	CDH18	cadherin 18, type 2	53.37	52.3	54.5	39	46	90	-1.223	71	636	796	734
28			off-target				NM_000938	POLR2B	polymerase (RNA) II (DNA directed) polyp	55.29	191.6	16.0	14	10	29	-1.664	24	554	457	634
29		yes	yes				NM_003248	THBS4	thrombospondin 4	56.40	168.5	18.9	29	29	8	-1.658	12	766	1217	1197
30			toxic	x			NM_173557	RNF152	ring finger protein 152	58.10	21.9	154.1	197	169	110	-0.82	223	154	200	137
31		yes	yes				NM_182505	C9ORF85	chromosome 9 open reading frame 85	59.96	54.5	66.0	82	50	70	-1.177	38	1046	1166	642
32			yes*		discontinued		XM_059923	LOC137829	similar to Nuclear receptor binding factor 2	60.95	105	35.4	19	44	53	-1.48	80	757	549	2573
33			toxic	x			NM_024015	HOXB4	homeobox B4	60.96	159.7	23.3	18	28	25	-1.431	44	305	422	466
34		yes	yes				NM_003169	SUPT5H	suppressor of Ty 5 homolog (S. cerevisiae)	62.37	88.2	44.1	43	35	57	-1.328	7	900	728	880
35			no				NM_003586	DOC2A	double C2-like domains, alpha	64.75	16.3	257.2	222	269	285	-0.591		1558	1525	1717
36		yes	yes				NM_018170	RPRD1A	regulation of nuclear pre-mRNA domain co	66.00	272.3	16.0	12	11	31	-1.653	9	2056	1469	1582
37		yes	yes				NM_021210	TRAPPC1	trafficking protein particle complex 1	67.11	33.3	135.3	145	101	169	-0.896	134	670	530	368
38			yes*		not avail. Dharm.		XM_085236	LOC145788	hypothetical LOC145788	67.36	118.3	38.4	32	43	41	-1.412	81	766	765	847
39		yes	yes				NM_003942	RPS6KA4	ribosomal protein S6 kinase, 90kDa, polyp	68.09	535.8	8.7	6	6	18	-1.802	1	1082	519	1582
40		yes	yes				NM_024650	C11orf80	chromosome 11 open reading frame 80	68.96	16.1	295.4	287	258	348	-0.515	444	1419	788	1313
41			yes/no	x			NM_005277	GPM6A	glycoprotein M6A	69.13	21.6	221.2	246	253	174	-0.629	437	706	217	428
42		yes	yes				NM_005938	FOXO4	forkhead box O4	69.34	178.8	26.9	30	18	36	-1.381	27	1737	1364	1501
43		yes	yes				XM_372884	CECR2	cat eye syndrome chromosome region, car	69.46	63.3	76.2	74	73	82	-1.134	20	814	713	1305
44			yes*		not avail. Dharm.		XM_034086	KIAA1107	KIAA1107	69.85	17	287.0	270	322	272	-0.554	263	661	450	716
45		yes	yes				NM_032800	C1orf198	chromosome 1 open reading frame 198	73.42	29.8	180.9	192	188	164	-0.797	274	1454	445	595
46		yes	yes				NM_001442	FABP4	fatty acid binding protein 4, adipocyte	73.91	252.7	21.6	27	34	11	-1.509	8	757	873	915
47			yes				NM_032790	ORAI1	ORAI calcium release-activated calcium m	74.59	27	206.1	240	206	177	-0.696	508	816	337	368
48			no				NM_015127	CLCC1	chloride channel CLIC-like 1	76.06	8.6	672.7	670	697	652	0.39	656	822	507	1163
49			yes*	x	discontinued		NM_014147	HSPC047		77.76	54.1	111.8	112	121	103	-1.022	221	389	482	555
50		yes	yes				NM_005303	FFAR1	free fatty acid receptor 1	79.28	463.4	13.6	13	12	16	-1.628	35	788	535	662
51			toxic	x			NM_006362	NXF1	nuclear RNA export factor 1	79.83	68.5	93.0	132	100	61	-1.167	137	73	104	108
52		yes	yes				NM_021948	BCAN	brevican	79.97	38.7	165.3	146	184	168	-0.824	154	1089	488	636
53		yes	yes				XM_040265	LARP5	La ribonucleoprotein domain family, memb	80.63	509.3	12.8	10	8	26	-1.66	6	1741	1151	1491
54		yes	yes				NM_005441	CHAF1B	chromatin assembly factor 1, subunit B (p	83.95	453.9	15.5	9	13	32	-1.628	42	829	682	1146
55		yes	yes				NM_001702	BAI1	brain-specific angiogenesis inhibitor 1	84.89	214.8	33.5	26	33	44	-1.365	79	921	584	1192
56		yes	yes				NM_017867	C4orf27	chromosome 4 open reading frame 27	85.54	145.4	50.3	51	51	49	-1.278	108	604	926	954
57		yes	yes				NM_015601	HERC4	hect domain and RLD 4	86.38	351.1	21.3	24	20	20	-1.522	4	1099	749	834
58		yes	yes				NM_019886	CHST7	carbohydrate (N-acetylglucosamine 6-O) s	86.96	17.7	427.3	437	425	420	-0.196	333	1644	1614	1323
59			yes*		discontinued		XM_374026	LOC389081	hypothetical LOC389081	91.34	68.9	121.1	118	114	132	-0.963	228	962	739	1039
60			toxic	x			NM_000754	COMT	catechol-O-methyltransferase	91.40	281.7	29.7	23	21	54	-1.506	132	220	319	280

dec.	"No" if I did not look at the images	In deconvolution screen?	hit/repeat without toxicity	toxic?	discontintued/ withdrawn or not available from Dharmacon	pseudogene	gene ID	gene symbol	full name	Primary and repeat screen combined rank product	Primary screen rank product as increaser	Repeat screen rank product as increaser	Repeat screen SCPO rank	Repeat screen STAPO rank	Repeat screen STIPO rank	Repeat screen median SCPO score	Repeat screen rank with new images	Repeat screen OC rep1	Repeat screen OC rep2	Repeat screen OC rep3
61			no				XM_370844	GOLGA8G	golgi autoantigen, golgin subfamily a, 8G	91.76	410.3	20.5	45	32	6	-1.393	737	1091	1143	681
62		yes	yes				NM_006793	PRDX3	peroxiredoxin 3	92.43	70.5	121.2	123	134	108	-0.954	122	1152	854	1985
63			no				NM_003123	SPN	sialophorin	93.10	42.8	202.5	186	183	244	-0.777	262	1136	1538	1706
64		yes	yes				NM_004122	GHSR	growth hormone secretagogue receptor	94.57	332	26.9	25	23	34	-1.466	50	1186	789	1451
65		yes	yes				NM_014548	TMOD2	tropomodulin 2 (neuronal)	96.02	65.5	140.8	124	119	189	-0.951	163	529	524	899
66		yes	yes				NM_003420	ZNF35	zinc finger protein 35	96.13	106.2	87.0	87	75	101	-1.11	135	1982	1607	1343
67		yes	yes				NM_003877	SOCS2	suppressor of cytokine signaling 2	97.28	53.1	178.2	205	232	119	-0.75	209	677	954	1304
68		yes	yes				NM_153248	ZMYM6	zinc finger, MYM-type 6	98.32	427.1	22.6	21	24	23	-1.541	75	517	463	0
69			yes*		not avail. Dharm.		NM_198851	C22orf34	chromosome 22 open reading frame 34	100.00	100.8	99.2	90	96	113	-1.007	202	929	606	620
70		yes	yes				NM_153212	GJB4	gap junction protein, beta 4, 30.3kDa	100.48	268.3	37.6	55	57	17	-1.411	67	435	686	738
71			no				NM_018250	INTS9	integrator complex subunit 9	101.33	35.7	287.6	284	266	315	-0.526	205	1700	1410	1592
72		yes	yes				NM_005715	UST	uronyl-2-sulfotransferase	103.49	207.1	51.7	67	48	43	-1.255	69	825	815	704
73			off-target	x			NM_002694	POLR2C	polymerase (RNA) II (DNA directed) polyp	104.68	475.9	23.0	15	22	37	-1.533	25	389	176	253
74			toxic	x			NM_153032	FLJ32065	hypothetical protein FLJ32065	109.92	157.5	76.7	57	80	99	-1.062	64	432	275	219
75			no				XM_291763	LOC340947	similar to eukaryotic translation initiation f	110.03	215.8	56.1	34	59	88	-1.156	308	2174	1724	1591
76		yes	yes				NM_152235	SFRS8	splicing factor, arginine/serine-rich 8 (supp	110.16	144.5	84.0	75	56	141	-1.022	102	511	1024	1237
77		yes	yes				NM_000100	CSTB	cystatin B (stefin B)	111.25	520.6	23.8	20	16	42	-1.58	46	450	826	715
78		yes	yes				NM_138333	FAM122A	family with sequence similarity 122A	112.09	76.4	164.5	152	124	236	-0.74	248	1309	1249	1567
79		yes	yes				NM_002965	S100A9	S100 calcium binding protein A9	112.41	147.9	85.4	98	95	67	-1.066	23	1614	1270	1372
80		yes	yes				NM_031461	CRISPLD1	cysteine-rich secretory protein LCCL doma	114.33	67.5	193.6	169	217	198	-0.755	187	1240	608	807
81		yes	yes				NM_017969	IWS1	IWS1 homolog (S. cerevisiae)	115.60	62.7	213.1	202	214	224	-0.693	125	1945	1823	1532
82		not novel	yes				NM_032852	APG4C	ATG4 autophagy related 4 homolog C (S. c	116.24	62.4	216.5	181	228	246	-0.66		1560	700	992
83		yes	yes				NM_006040	HS3ST4	heparan sulfate (glucosamine) 3-O-sulfotr	118.74	211	66.8	79	64	59	-1.145	84	1313	1358	1290
84		yes	yes	x			NM_032644	PPARA	peroxisome proliferator-activated receptor	119.64	115.3	124.1	97	136	145	-1.018	124	281	510	670
85			yes*	x	not avail. Dharm.	pseudo	XM_209076	LOC284232	LOC284232 similar to ankyrin repeat dom	119.69	66.2	216.4	237	243	176	-0.665	211	514	368	479
86			toxic	x			NM_021223	MYL7	myosin, light chain 7, regulatory	120.40	271.2	53.5	46	40	83	-1.289	34	251	79	456
87			yes/no	x			NM_002336	LRP6	low density lipoprotein receptor-related pr	122.77	64.8	232.6	265	223	213	-0.663	153	483	534	1034
88		yes	yes				NM_005065	SEL1L	sel-1 suppressor of lin-12-like (C. elegans	122.95	361.3	41.8	47	41	38	-1.341	16	1769	1477	1088
89		yes	yes				NM_002634	PHB	prohibitin	125.91	332.5	47.7	85	85	15	-1.13	63	699	1071	1238
90		yes	yes				NM_015315	LARP	La ribonucleoprotein domain family, memb	125.97	225.8	70.3	58	88	68	-1.195	53	307	355	340
91		yes	yes				NM_014982	PCNX	pecanex homolog (Drosophila)	126.48	238.9	67.0	68	69	64	-1.196	21	496	710	1089
92		yes	yes				NM_031310	PLVAP	plasmalemma vesicle associated protein	127.23	115.3	140.4	113	155	158	-0.843	215	1221	428	1009
93		yes	yes				NM_014765	TOMM20	translocase of outer mitochondrial membra	127.32	433.8	37.4	37	47	30	-1.413	65	1399	1475	1157
94		yes	yes				NM_030934	C1ORF25	chromosome 1 open reading frame 25	130.42	239.1	71.1	60	60	100	-1.175	130	1501	1141	1605
95			no				NM_013379	DPP7	dipeptidyl-peptidase 7	130.58	34.8	489.9	450	495	528	-0.366	401	646	836	816
96			yes/no				NM_006947	SRP72	signal recognition particle 72kDa	131.80	328.6	52.9	36	54	76	-1.233	26	1182	576	1085
97		yes	yes				NM_194249	DND1	dead end homolog 1 (zebrafish)	131.90	245.7	70.8	91	83	47	-1.101	119	992	1208	980
98			no				NM_031448	C19ORF12	chromosome 19 open reading frame 12	131.93	48.1	361.8	338	365	384	-0.409	519	1342	648	1064
99			toxic	x			NM_005548	KARS	lysyl-tRNA synthetase	132.57	71.9	244.4	254	286	201	-0.608	373	683	298	205
100			no/toxic	x			NM_004572	PKP2	plakophilin 2	132.63	495.4	35.5	41	39	38	-1.372	14	397	653	498
101		yes	yes				XM_037759	SPECC1L	SPECC1-like	133.16	522.6	33.9	28	31	45	-1.392	93	548	767	733
102			yes	x			NM_024814	CBLL1	Cas-Br-M (murine) ecotropic retroviral tra	133.24	152.5	116.4	71	138	161	-0.901	255	542	157	311
103		yes	yes				NM_021081	GHRH	growth hormone releasing hormone	134.03	244.3	73.5	142	70	40	-1.08	123	592	868	1349
104		yes	yes				NM_058222	TECTB	tectorin beta	134.20	236.9	76.0	81	113	48	-1.14	97	1404	1624	1604
105		yes	yes				NM_021969	NR0B2	nuclear receptor subfamily 0, group B, me	134.94	114.1	159.6	225	215	84	-0.901	167	973	1327	1435
106		yes	yes				NM_020789	IGSF9	immunoglobulin superfamily, member 9	135.39	85.2	215.1	242	211	195	-0.686	126	1240	1184	1084
107		yes	yes				NM_001878	CRABP2	cellular retinoic acid binding protein 2	135.87	208.5	88.5	94	71	104	-1.078	37	1365	993	1649
108			no/toxic	x			NM_031917	ANGPTL6	angiopoietin-like 6	137.82	181.2	104.8	95	94	129	-1.042	177	765	667	539
109			no				NM_207437	DNAH10	dynein, axonemal, heavy chain 10	138.69	169.6	113.4	99	106	139	-0.907	106	1179	1274	796
110			no/toxic	x			NM_020828	ZFP28	zinc finger protein 28 homolog (mouse)	139.69	61.4	317.8	336	325	294	-0.403	293	398	273	326
111			no				NM_018487	HCA112		141.55	52.8	379.5	380	404	356	-0.317	234	1722	1771	1007
112			no				NM_001884	HAPLN1	hyaluronan and proteoglycan link protein 1	142.05	145.2	139.0	129	219	95	-0.843	115	1127	924	1058
113		yes	yes				NM_014363	SACS	spastic ataxia of Charlevoix-Saguenay (sac	142.08	187.3	107.8	56	108	207	-0.979	51	1514	1350	1910
114		yes	yes				NM_024953	C12orf30	chromosome 12 open reading frame 30	142.58	128.6	158.1	140	170	166	-0.828	286	535	472	381
115		yes	yes				NM_004189	SOX14	SRY (sex determining region Y)-box 14	142.95	80.1	255.1	271	247	248	-0.588	145	596	1300	1309
116		yes	yes				NM_024331	TTPAL	tocopherol (alpha) transfer protein-like	144.48	98.8	211.3	212	196	227	-0.729	160	654	440	554
117			no/toxic	x			XM_372763	PRAMEF18	PRAME family member 18	147.24	158.6	136.7	201	179	71	-0.978	73	744	589	578
118			no				NM_138457	FOXP4	forkhead box P4	147.40	130.1	167.0	189	176	140	-0.886	266	811	1360	1149
119			no				NM_006509	RELB	v-rel reticuloendotheliosis viral oncogene h	149.85	236.5	95.0	102	77	109	-1.051	89	2038	1247	1730
120		yes	yes				NM_017714	TASP1	taspase, threonine aspartase, 1	151.15	138.9	164.5	149	181	165	-0.829	111	1555	400	765

dec.	"No" if I did not look at the images	In deconvolution screen?	hit/repeat without toxicity	toxic?	discontintued/ withdrawn or not available from Dharmacon	pseudogene	gene ID	gene symbol	full name	Primary and repeat screen combined rank product	Primary screen rank product as increaser	Repeat screen rank product as increaser	Repeat screen SCPO rank	Repeat screen STAPO rank	Repeat screen STIPO rank	Repeat screen median SCPO score	Repeat screen rank with new images	Repeat screen OC rep1	Repeat screen OC rep2	Repeat screen OC rep3
121		yes	yes				NM_002281	KRT81	keratin 81	151.46	267.8	85.7	86	84	87	-1.12	30	781	829	1130
122			tox	x			NM_020307	CCNL1	cyclin L1	153.18	139.1	168.7	200	189	127	-0.773	28	246	237	426
123		yes	yes				NM_138342	GLB1L2	galactosidase, beta 1-like 2	153.97	402.2	58.9	50	45	91	-1.224	144	774	517	530
124			no				NM_015320	ARHGEF4	Rho guanine nucleotide exchange factor ((	154.36	67.4	353.5	493	435	206	-0.584	361	719	772	1085
125		not novel	yes				XM_370618	AMBRA1	autophagy/beclin-1 regulator 1	155.01	41.5	579.0	579	539	622	0.147	431	1709	1266	1094
126			toxic	x			NM_014023	WDR37	WD repeat domain 37	155.72	175.8	137.9	131	126	159	-0.926	103	145	183	196
127			no				XM_375500	CCDC137	coiled-coil domain containing 137	156.12	88	277.0	274	296	262	-0.543	142	937	861	618
128			no/toxic	x			NM_018953	HOXC5	homeobox C5	156.21	121.5	200.8	226	224	160	-0.835	389	236	209	290
129	no						NM_003598	TEAD2	TEA domain family member 2	156.21	95.2	256.3				-0.634				
130	no						NM_025026	FLJ14107	hypothetical protein FLJ14107	156.74	75.9	323.7				-0.43				
131			no		discontinued		XM_372689	LOC390828	LOC390828 similar to mitochondrial carrie	156.99	472.5	52.2	220	129	5	-1.905	605	1235	1520	990
132		yes	yes				NM_012382	TTC33	tetratricopeptide repeat domain 33	157.06	245.8	100.4	72	65	216	-0.861	86	816	1134	1404
133			no				NM_006360	EIF3M	eukaryotic translation initiation factor 3, su	158.50	80.2	313.2	310	324	206	-0.446	284	1024	1097	1139
134		yes	yes				NM_001642	APLP2	amyloid beta (A4) precursor-like protein 2	159.52	325.6	78.2	78	72	85	-1.123	117	1107	545	610
135	no						NM_005000	NDUFA5	NADH dehydrogenase (ubiquinone) 1 alpha	161.27	90.8	286.4				-0.598				
136		yes	yes				NM_003154	STATH	statherin	161.99	348.4	75.3	80	89	60	-1.148	17	696	937	1284
137		yes	yes				NM_198402	PTPLB	protein tyrosine phosphatase-like (proline	162.13	169	155.5				-0.873	60			
138	no						NM_021267	LASS1	LAG1 homolog, ceramide synthase 1	162.62	44	601.0				0.244				
139			toxic	x	discontinued		XM_378309	LOC399951	hypothetical LOC399951	163.00	474.1	56.0	40	55	80	-1.193	139	630	353	1690
140			toxic	x			NM_015163	TRIM9	tripartite motif-containing 9	163.60	43.8	611.1	588	629	1080	0.246	517	1080	509	429
141	no						NM_080924	LOC91219	hypothetical protein similar to CGI-67 prot	163.80	84.8	316.4				-0.44				
142			yes*		not avail. Dharm.		XM_379179	LOC152274	hypothetical protein LOC152274	166.32	385.2	71.8	61	66	92	-1.098	19	1190	1595	971
143	no						NM_152360	ZNF573	zinc finger protein 573	168.56	56.8	500.2				-0.135				
144			tox	x			NM_002492	NDUFB5	NADH dehydrogenase (ubiquinone) 1 beta	168.68	243.3	116.9	121	112	118	-0.974	32	561	313	286
145	no						NM_052931	SLAMF6		168.78	117.8	241.8				-0.629				
146	no						NM_032324	C1orf57	chromosome 1 open reading frame 57	170.49	81.7	355.8				-0.378				
147			no/toxic	x			NM_145719	TIGD3	tigger transposable element derived 3	171.11	233.1	125.6	167	172	69	-0.909	164	540	593	215
148			no				NM_031420	MRPL9	mitochondrial ribosomal protein L9	172.47	314.3	94.6	77	91	121	-1.02	98	1352	1054	1251
149		yes	yes				NM_024082	PRRG3	proline rich Gla (G-carboxyglutamic acid) 3	172.88	375.5	79.6	62	76	107	-1.026	33	538	703	819
150		yes	yes				NM_006969	ZNF28	zinc finger protein 28	173.64	445.3	67.7	64	97	50	-1.222	206	772	725	766
151		yes	yes				XM_370946	ERN2	endoplasmic reticulum to nucleus signaling	173.80	348.2	86.8	84	67	116	-1.095	59	540	307	973
152	no						XM_374501	MUC3B	mucin 3B, cell surface associated	174.38	59.7	509.3				0.133				
153			no/toxic	x			NM_018013	SOBP	sine oculis binding protein homolog (Drosc	175.25	369.2	83.2	69	103	81	-1.141	66	461	694	890
154	no						NM_054021	GPR101	G protein-coupled receptor 101	176.57	167.9	185.7				-0.789				
155	no						NM_032836	FIZ1	FLT3-interacting zinc finger 1	176.62	45.5	685.6				0.411				
156			no				NM_001375	DNASE2	deoxyribonuclease II, lysosomal	178.23	65.2	487.2	551	575	365	0.102	407	1204	884	1032
157			toxic	x			NM_000749	CHRNB3	cholinergic receptor, nicotinic, beta 3	178.35	237.9	133.7				-0.933	100			
158							NM_152355	ZNF441		178.78	119	268.6				-0.576				
159		yes	yes	x			NM_002572	PAFAH1B2	platelet-activating factor acetylhydrolase,	178.84	303.8	105.3	116	107	94	-1.004	49	855	661	662
160	no						NM_020653	ZNF287		179.03	132.7	241.5				-0.65				
161	no						NM_173351	OR6B3	olfactory receptor, family 6, subfamily B, m	179.13	60	534.8				0.017				
162			no				NM_016270	KLF2	Kruppel-like factor 2 (lung)	180.18	344.3	94.3	96	118	74	-1.069	83	1606	844	1864
163			no				NM_004465	FGF10	fibroblast growth factor 10	180.18	189.3	171.5				-0.853	27			
164			no/toxic	x			NM_007346	OGFR	opioid growth factor receptor	181.07	341.2	96.1	130	105	65	-1.051	175	471	905	1232
165			no				NM_014977	ACIN1	apoptotic chromatin condensation inducer	181.07	218.1	150.3	153	182	122	-0.901	146	1148	1115	1190
166			no				NM_032850	ZFYVE19	zinc finger, FYVE domain containing 19	181.23	53.5	613.9	607	605	630	0.235	796	1560	686	1160
167			no/toxic	x			NM_002614	PDZK1	PDZ domain containing 1	184.56	497.5	68.5	127	133	19	-1.328	101	545	383	497
168	no				discontinued		XM_372563	LOC390566	similar to amyloid beta A4 precursor prote	186.46	206.1	168.7				-0.924				
169			no/toxic	x			NM_016930	STX18	syntaxin 18	186.79	83.1	419.9	403	401	458	-0.525	415	384	470	268
170		yes	yes				NM_022091	ASCC3	activating signal cointegrator 1 complex su	187.26	315.2	111.3	83	122	136	-0.939	43	1283	857	800
171		yes	yes				NM_015426	WDR51A	WD repeat domain 51A	187.81	476.7	74.0	73	74	75	-1.115	116	1050	1036	1073
172			no				NM_182610	SAMD7	sterile alpha motif domain containing 7	188.96	321.7	111.0	109	123	102	-1.028	107	1086	1115	713
173	no						NM_205851	FLJ35700		188.97	137.9	259.0				-0.571				
174			toxic	x			NM_015630	EPC2	enhancer of polycomb homolog 2 (Drosopl	189.93	483.1	74.7	65	61	105	-1.14	114	496	642	591
175			toxic	x			XM_379432	LOC285733	hypothetical LOC285733	191.99	361.5	102.0	122	110	79	-1.125	48	359	259	375
176	no						NM_006637	OR5I1	olfactory receptor, family 5, subfamily I, m	192.02	275	134.1				-0.839				
177		yes	yes				NM_173597	MYO1H	myosin IH	192.74	124.5	298.4				-0.608	74			
178	no						NM_130830	LRRC15	leucine rich repeat containing 15	194.13	68.8	547.8				0.144				
179	no						NM_031485	GRWD1	glutamate-rich WD repeat containing 1	194.20	258.4	146.0				-0.928				
180	no						NM_020389	TRPC7	transient receptor potential cation channel	194.61	101.9	371.7				-0.889				

dec.	"No" if I did not look at the images	In deconvolution screen?	hit/repeat without toxicity	toxic?	discontintued/ withdrawn or not available from Dharmacon	pseudogene	gene ID	gene symbol	full name	Primary and repeat screen combined rank product	Primary screen rank product as increaser	Repeat screen rank product as increaser	Repeat screen SCPO rank	Repeat screen STAPO rank	Repeat screen STIPO rank	Repeat screen median SCPO score	Repeat screen rank with new images	Repeat screen OC rep1	Repeat screen OC rep2	Repeat screen OC rep3
181			yes	x			NM_005837	POP7	processing of precursor 7, ribonuclease P/	194.79	470.4	80.7	70	49	153	-1.095	95	915	615	1066
182	no						NM_144618	GABPB2	GA binding protein transcription factor, bet	194.80	196.1	193.5				-0.777				
183		yes	yes				NM_004249	RAB28	RAB28, member RAS oncogene family	194.93	399.6	95.1	105	92	89	-1.041	78	1257	943	1870
184			yes/no				NM_053043	MGC20460	RNA binding motif protein 33	195.53	229.2	166.8				-0.857	45			
185	no						NM_030573	THAP7	THAP domain containing 7	195.60	290.6	131.7				-0.939				
186			no				XM_373907	LOC388787	hypothetical LOC728329	197.06	385	100.9	323	353	9	-0.715	914	1297	1125	780
187			no				NM_012445	SPON2	spondin 2, extracellular matrix protein	198.29	350.8	112.1	150	149	63	-1.13	138	1488	1503	1185
188		yes	yes				NM_003494	DYSF	dysferlin, limb girdle muscular dystrophy 2	198.35	336	117.1	187	148	58	-0.879	170	824	693	1230
189			no			pseudo	NM_152349	KRT222P	keratin 222 pseudogene	199.04	351.8	112.6	76	116	162	-0.891	294	1681	1391	1393
190			yes*	x	discontinued		XM_373082	LOC391784	similar to CG12279-PA	200.93	538	75.0	63	78	26	-1.144	178	764	460	664
191			no				NM_174908	CCDC50	coiled-coil domain containing 50	202.15	225.8	181.0	182	177	184	-1.611	195	1183	1119	220
192		yes	yes				NM_005347	HSPA5	heat shock 70kDa protein 5 (glucose-regu	203.64	229.1	181.0	234	198	128	-0.747	72	1346	1078	1109
193	no						NM_015442	CNOT10	CCR4-NOT transcription complex, subunit	204.51	216.4	193.3				-0.751				
194		yes	yes				NM_198580	SLC27A1	solute carrier family 27 (fatty acid transpo	205.02	372.5	112.8	103	90	155	-0.992	147	651	970	687
195			no/toxic	x			XM_291020	LOC339809	KIAA2012 protein	205.21	534.7	78.8	101	93	52	-1.055	193	490	523	398
196			no				NM_006084	ISGF3G	interferon regulatory factor 9	205.40	514.5	82.0	106	102	51	-1.066	182	1147	908	907
197	no						NM_153700	STRC		206.48	174.6	244.2				-0.685				
198			toxic	x			NM_014772	KIAA0427	KIAA0427	207.74	358.1	120.5	148	162	73	-1.039	112	375	560	391
199			toxic	x			XM_291099	LRRC66	leucine rich repeat containing 66	214.15	456.5	100.5	134	157	123	-1.085	419	241	68	238
200		yes	yes				NM_019103	ZMAT5	zinc finger, matrin type 5	217.37	278.6	169.6				-0.831	91			
201			no				NM_002854	PVALB	parvalbumin	217.38	159.8	295.7				-0.45	56			
202			no				XM_294743	LOC730011	hypothetical LOC730011	220.40	409.9	118.5	108	115	134	-0.96	220	521	663	1245
203		yes	yes				NM_005241	EVI1	ecotropic viral integration site 1	221.23	304.7	160.6				-0.848	39			
204		yes	yes				NM_020673	RAB22A	RAB22A, member RAS oncogene family	222.26	294	168.0	117	218	186	-0.783	55	1676	1327	1335
205			no				NM_003850	SUCLA2	succinate-CoA ligase, ADP-forming, beta s	223.74	330.7	151.4				-0.798	92			
206			yes/no				NM_004942	DEFB4	defensin, beta 4	226.64	476.3	107.8	201	210	77	-0.968	364	1164	703	764
207		yes	yes				NM_032547	SCOC	short coiled-coil protein	226.89	439.2	117.2	107	99	152	-0.999	109	1740	525	1357
208	no						AF113887	IGKC	immunoglobulin kappa constant	227.95	351.5	147.8				-0.947				
209		yes	yes				NM_001709	BDNF	brain-derived neurotrophic factor	228.21	90.6	574.8	719	712	371	0.499	613	745	1136	1318
210			toxic	x			NM_198999	SLC26A5	solute carrier family 26, member 5 (presti	237.34	537.1	104.9	89	87	149	-1.033	99	342	384	271
211			toxic	x			NM_012070	ATRN	attractin	247.27	445.4	137.3	115	163	138	-0.903	184	909	647	817
212		yes	yes				NM_016628	WAC	WW domain containing adaptor with coilec	247.40	291.4	210.0				-0.735	77			
213			toxic	x			NM_021259	TMEM8	transmembrane protein 8 (five membrane-spanning dom		285.4	256.5					85			
214			no				NM_001974	EMR1	egf-like module containing, mucin-like, hormone receptor		429	174.6					88			
215		yes	yes				NM_001816	CEACAM8	carcinoembryonic antigen-related cell adhesion molecule		234.5	342.9					90			
216		yes	yes				NM_006122	MAN2A2	mannosidase, alpha, class 2A, member 2		457.9	193.8					18			
217			no				NM_031295	ABHD11	abhydrolase domain containing 11		360.8	258.6					70			
218			no				NM_022164	TINAGL1	tubulointerstitial nephritis antigen-like 1		371.5	308.8					96			
219			toxic	x			NM_001898	CST1	cystatin SN		362.7	359.6					82			
220			no				NM_194309	C21ORF125	chromosome 21 open reading frame 125		376.5	375.1					87			
221			toxic	x			NM_006449	CDC42EP3	CDC42 effector protein (Rho GTPase binding) 3		464.4	309.1					47			
222	no				discontinued		XM_371302	LOC388686	similar to peptidylprolyl isomerase A (cyclophilin A)-like 4		285.6	510.8								
223	no						NM_005027	PIK3R2	phosphoinositide-3-kinase, regulatory subunit 2 (beta)		453.4	323.1								
224	no						XM_376007	DEPDC5	DEP domain containing 5		415.4	448.8								
225	no						NM_138567	SYT8	synaptotagmin VIII		476.3	451.8								
226	no						NM_032409	PINK1	PTEN induced putative kinase 1		320.2	904.9								

Table 9.4 Results of the repeat screen for a subset of Smartpools that cause a decrease in GFP-LC3 spots

226 Smartpools are listed in order of primary and repeat screen combined rank product (not all 500 decreasers are shown). Whether their images were examined, whether they were included in the subsequent deconvolution screen and whether I scored it as a non-toxic, non-off-target repeat hit as a result of visual analysis are indicated. Toxicity and availability of a deconvoluted set of siGenome siRNA duplexes for that given Smartpool are indicated. It is noted whether the gene is annotated as a psudogene. Gene ID, current gene symbol and full name are given. The rank product that combines the primary and repeat screen rank products, and the primary screen rank product and repeat screen rank product as decreasers is shown. The repeat screen SCPO, STAPO, and STIPO ranks (as decreasers) and the repeat screen median SCPO score are shown. The repeat screen rank generated with the second set of 14 images as well as the valid object count (OC) for three replicates in the repeat screen are shown. Genes highlighted in blue are of interest and are referred to in the text.

	GeneID	SirnaID	Gene Symbol	STIPO median score	STIPO positive	STIPO negative	SCPO median score	SCPO positive	SCPO negative	STAPO median score	STAPO positive	STAPO negative	Median OC	Primary Screen class	succesful deconvolution same as primary po	3 or 4 out of 4 duplexes	2 out of 4 duplexes	Official Symbol (if different)
1	NM_005938	D-003016-05	MLLT7	1.346	1	0	1.224	1	0	1.211	1	0	1972	decreaser	yes		yes	FOXO4
2	NM_005938	D-003016-06	MLLT7	1.16	0	0	1.051	0	0	1.056	0	0	1690					
3	NM_005938	D-003016-07	MLLT7	0.527	0	1	0.636	0	1	0.634	0	1	3037					
4	NM_005938	D-003016-08	MLLT7	0.706	0	1	1.012	0	0	0.985	0	0	4547					
5	NM_004443	D-003123-09	EPHB3	1.166	0	0	0.984	0	0	1.002	0	0	2426	increaser	no			
6	NM_004443	D-003123-10	EPHB3	1.954	1	0	1.745	1	0	1.926	1	0	3022					
7	NM_004443	D-003123-11	EPHB3	0.946	0	0	0.855	0	0	0.842	0	0	2457					
8	NM_004443	D-003123-12	EPHB3	0.735	0	1	0.659	0	1	0.625	0	1	2725					
9	NM_000075	D-003238-05	CDK4	1.029	0	0	1.007	0	0	1.008	0	0	4414	increaser	no			
10	NM_000075	D-003238-06	CDK4	1.489	1	0	1.105	0	0	1.189	0	0	1281					
11	NM_000075	D-003238-07	CDK4	0.99	0	0	0.92	0	0	0.93	0	0	4218					
12	NM_000075	D-003238-08	CDK4	1.005	0	0	0.926	0	0	0.914	0	0	4257					
13	NM_021969	D-003410-02	NR0B2	1.144	0	0	1	0	0	1.015	0	0	2910	decreaser	no			
14	NM_021969	D-003410-03	NR0B2	0.793	0	1	1.061	0	0	1.051	0	0	4266					
15	NM_021969	D-003410-04	NR0B2	1.293	1	0	1.116	0	0	1.162	0	0	2520					
16	NM_021969	D-003410-17	NR0B2	2.25	1	0	1.754	1	0	1.993	1	0	3129					
17	NM_005036/NM	D-003434-01	PPARA	1.459	1	0	1.122	0	0	1.188	0	0	3273	decreaser	no			
18	NM_005036/NM	D-003434-02	PPARA	2.735	1	0	1.931	1	0	2.088	1	0	2739					
19	NM_005036/NM	D-003434-03	PPARA	1.429	1	0	1.013	0	0	1.07	0	0	1066					
20	NM_005036/NM	D-003434-04	PPARA	1.153	0	0	1.033	0	0	1.058	0	0	3846					
21	NM_002039	D-003553-01	GAB1	1.391	1	0	1.673	1	0	1.787	1	0	3731	decreaser	no			
22	NM_002039	D-003553-02	GAB1	0.407	0	1	0.524	0	1	0.512	0	1	4686					
23	NM_002039	D-003553-03	GAB1	0.596	0	1	0.599	0	1	0.582	0	1	4895					
24	NM_002039	D-003553-04	GAB1	1.41	1	0	1.53	1	0	1.578	1	0	5311					
25	NM_003494	D-003652-04	DYSF	0.779	0	1	0.858	0	0	0.858	0	0	4335	decreaser	no			
26	NM_003494	D-003652-04	DYSF	1.058	0	0	1.091	0	0	1.111	0	0	3131					
27	NM_003494	D-003652-05	DYSF	0.996	0	0	0.931	0	0	0.94	0	0	3562					
28	NM_003494	D-003652-05	DYSF	1.328	1	0	1.237	1	0	1.297	1	0	2793					
29	NM_024507	D-003847-01	KREMEN2	0.982	0	0	1.176	0	0	1.187	0	0	4967	decreaser	no			
30	NM_024507	D-003847-03	KREMEN2	1.12	0	0	1.177	0	0	1.235	1	0	4569					
31	NM_024507	D-003847-04	KREMEN2	1.108	0	0	1.217	1	0	1.245	1	0	3602					
32	NM_024507	D-003847-05	KREMEN2	0.569	0	1	0.811	0	0	0.786	0	1	4393					
33	NM_005486	D-003911-02	TOM1L1	0.782	0	1	0.818	0	0	0.79	0	1	5836	increaser	no			
34	NM_005486	D-003911-03	TOM1L1	1.85	1	0	1.811	1	0	2.023	1	0	4926					
35	NM_005486	D-003911-05	TOM1L1	0.425	0	1	0.524	0	1	0.498	0	1	5427					
36	NM_005486	D-003911-06	TOM1L1	0.604	0	1	0.792	0	1	0.77	0	1	6878					
37	NM_012290	D-004174-01	TLK1	1.397	1	0	1.108	0	0	1.112	0	0	4764	increaser	no			
38	NM_012290	D-004174-02	TLK1	0.922	0	0	0.967	0	0	0.95	0	0	2566					
39	NM_012290	D-004174-03	TLK1	0.762	0	1	0.771	0	1	0.76	0	1	4862					
40	NM_012290	D-004174-04	TLK1	0.54	0	1	0.548	0	1	0.528	0	1	3337					
41	NM_001642	D-004179-01	APLP2	0.842	0	0	1.074	0	0	1.093	0	0	5924	decreaser	no			
42	NM_001642	D-004179-03	APLP2	0.996	0	0	0.982	0	0	1.026	0	0	4613					
43	NM_001642	D-004179-04	APLP2	1.501	1	0	1.257	1	0	1.295	1	0	5175					
44	NM_001642	D-004179-05	APLP2	1.125	0	0	1.106	0	0	1.118	0	0	4632					
45	NM_033050	D-004541-01	GPR91	1.136	0	0	1.181	0	0	1.16	0	0	5108	increaser	no			
46	NM_033050	D-004541-02	GPR91	0.733	0	1	0.784	0	1	0.761	0	1	3124					
47	NM_033050	D-004541-03	GPR91	1.38	1	0	1.275	1	0	1.368	1	0	3396					
48	NM_033050	D-004541-04	GPR91	0.627	0	1	0.778	0	1	0.761	0	1	3362					
49	NM_004409/NM	D-004637-02	DMPK	0.896	0	0	0.863	0	0	0.834	0	0	6855	increaser	no			
50	NM_004409/NM	D-004637-03	DMPK	0.641	0	1	0.81	0	0	0.761	0	1	5826					
51	NM_004409/NM	D-004637-04	DMPK	0.909	0	0	0.692	0	1	0.685	0	1	3758					
52	NM_001081562	D-004637-17	DMPK	1.603	1	0	1.438	1	0	1.494	1	0	5529					
53	NM_003942/NM	D-004664-01	RPS6KA4	0.978	0	0	1.061	0	0	1.066	0	0	4271	decreaser	no			
54	NM_003942/NM	D-004664-02	RPS6KA4	1.059	0	0	0.949	0	0	1.001	0	0	5998					
55	NM_003942/NM	D-004664-03	RPS6KA4	0.926	0	0	0.995	0	0	0.939	0	0	4706					
56	NM_003942/NM	D-004664-04	RPS6KA4	0.854	0	0	0.961	0	0	1.005	0	0	4025					
57	NM_017714	D-004745-01	C20ORF13	0.754	0	1	0.761	0	1	0.761	0	1	3923	decreaser	no			
58	NM_017714	D-004745-02	C20ORF13	1.298	1	0	1.236	1	0	1.328	1	0	4725					
59	NM_017714	D-004745-03	C20ORF13	0.791	0	1	0.803	0	0	0.756	0	1	2992					
60	NM_017714	D-004745-04	C20ORF13	1.226	1	0	0.927	0	0	0.911	0	0	4033					

	GeneID	SirnaID	Gene Symbol	STIPO median score	STIPO positive	STIPO negative	SCPO median score	SCPO positive	SCPO negative	STAPO median score	STAPO positive	STAPO negative	Median OC	Primary Screen class	succesful deconvolution same as primary po	3 or 4 out of 4 duplexes	2 out of 4 duplexes	Official Symbol (if different)
61	NM_001896	D-004752-01	CSNK2A2	1.106	0	0	1.001	0	0	0.963	0	0	1854	decreaser	no			
62	NM_001896	D-004752-02	CSNK2A2	0.234	0	1	0.428	0	1	0.386	0	1	4225					
63	NM_001896	D-004752-03	CSNK2A2	1.009	0	0	1.081	0	0	1.032	0	0	3862					
64	NM_001896	D-004752-04	CSNK2A2	1.193	0	0	1.228	1	0	1.291	1	0	5473					
65	XM_370947/NM	D-004878-10	ERN2	0.819	0	0	0.901	0	0	0.896	0	0	4867	decreaser	no			
66	XM_370947/NM	D-004878-12	ERN2	0.899	0	0	1.003	0	0	0.977	0	0	3645					
67	XM_370947/NM	D-004878-13	ERN2	1.194	0	0	1.169	0	0	1.219	1	0	5858					
68	XM_370947/NM	D-004878-26	ERN2	1.303	1	0	1.314	1	0	1.487	1	0	2362					
69	NM_005065	D-004885-02	SEL1L	2.046	1	0	1.814	1	0	1.968	1	0	6677	decreaser	yes		yes	
70	NM_005065	D-004885-03	SEL1L	0.98	0	0	0.845	0	0	0.842	0	0	4809					
71	NM_005065	D-004885-04	SEL1L	0.691	0	1	0.809	0	0	0.787	0	1	6930					
72	NM_005065	D-004885-05	SEL1L	0.567	0	1	0.698	0	1	0.633	0	1	5352					
73	NM_001105	D-004924-01	ACVR1	1.189	0	0	1.042	0	0	1.05	0	0	3718	increaser	no			
74	NM_001105	D-004924-02	ACVR1	0.887	0	0	0.902	0	0	0.912	0	0	3784					
75	NM_001105	D-004924-03	ACVR1	1.015	0	0	1.003	0	0	1.015	0	0	4612					
76	NM_001105	D-004924-18	ACVR1	1.346	1	0	1.217	1	0	1.251	1	0	2661					
77	NM_006285	D-005043-01	TESK1	0.341	0	1	0.619	0	1	0.59	0	1	5330	increaser	no			
78	NM_006285	D-005043-02	TESK1	0.664	0	1	0.747	0	1	0.747	0	1	3493					
79	NM_006285	D-005043-03	TESK1	1.014	0	0	1.053	0	0	1.154	0	0	2324					
80	NM_006285	D-005043-04	TESK1	1.353	1	0	1.323	1	0	1.46	1	0	4435					
81	XM_375495/NM	D-005301-02	AATK	0.686	0	1	0.807	0	0	0.738	0	1	3006	increaser	yes		yes	
82	XM_375495/NM	D-005301-03	AATK	1.988	1	0	1.586	1	0	1.694	1	0	4488					
83	XM_375495/NM	D-005301-04	AATK	0.765	0	1	0.958	0	0	0.94	0	0	3016					
84	XM_375495/NM	D-005301-05	AATK	1.566	1	0	1.327	1	0	1.333	1	0	5624					
85	NM_006852	D-005389-01	TLK2	1.84	1	0	1.575	1	0	1.826	1	0	4555	increaser	yes	yes		
86	NM_006852	D-005389-03	TLK2	1.557	1	0	1.228	1	0	1.26	1	0	7182					
87	NM_006852	D-005389-04	TLK2	0.791	0	1	1.139	0	0	1.15	0	0	6809					
88	NM_006852	D-005389-05	TLK2	1.243	1	0	1.037	0	0	0.999	0	0	5225					
89	NM_001702	D-005433-01	BAI1	0.645	0	1	0.635	0	1	0.634	0	1	5672	decreaser	no			
90	NM_001702	D-005433-02	BAI1	1.126	0	0	0.955	0	0	0.955	0	0	4347					
91	NM_001702	D-005433-03	BAI1	1.144	0	0	1.147	0	0	1.203	1	0	2851					
92	NM_001702	D-005433-04	BAI1	1.934	1	0	1.498	1	0	1.549	1	0	6158					
93	NM_001466	D-005501-02	FZD2	0.887	0	0	0.959	0	0	0.946	0	0	7878	increaser	no			
94	NM_001466	D-005501-03	FZD2	1.941	1	0	1.231	1	0	1.31	1	0	4693					
95	NM_001466	D-005501-04	FZD2	1.007	0	0	0.897	0	0	0.88	0	0	4300					
96	NM_001466	D-005501-05	FZD2	0.736	0	1	0.701	0	1	0.69	0	1	9253					
97	NM_004122	D-005513-01	GHSR	0.711	0	1	0.797	0	1	0.829	0	0	5439	decreaser	yes	yes		
98	NM_004122	D-005513-02	GHSR	0.758	0	1	0.737	0	1	0.686	0	1	4507					
99	NM_004122	D-005513-03	GHSR	0.64	0	1	0.62	0	1	0.597	0	1	4385					
100	NM_004122	D-005513-04	GHSR	1.14	0	0	1.454	1	0	1.427	1	0	6653					
101	NM_005303	D-005571-03	GPR40	0.693	0	1	0.944	0	0	0.95	0	0	6030	decreaser	no			
102	NM_005303	D-005571-05	GPR40	0.966	0	0	1.129	0	0	1.102	0	0	4096					
103	NM_005303	D-005571-06	GPR40	1.75	1	0	1.567	1	0	1.736	1	0	5137					
104	NM_005303	D-005571-07	GPR40	1.053	0	0	1.435	1	0	1.482	1	0	4267					
105	NM_145895	D-005909-01	KLK12	1.034	0	0	0.858	0	0	0.84	0	0	1993	increaser	yes		yes	
106	NM_145895	D-005909-02	KLK12	1.304	1	0	1.272	1	0	1.355	1	0	5378					
107	NM_145895	D-005909-04	KLK12	1.757	1	0	1.451	1	0	1.715	1	0	5573					
108	NM_145895	D-005909-18	KLK12	0.947	0	0	0.851	0	0	0.856	0	0	3793					
109	NM_006690	D-005963-01	MMP24	1.029	0	0	0.957	0	0	0.95	0	0	4498	decreaser	no			
110	NM_006690	D-005963-02	MMP24	0.997	0	0	1.195	0	0	1.269	1	0	4062					
111	NM_006690	D-005963-04	MMP24	0.309	0	1	0.554	0	1	0.499	0	1	4498					
112	NM_006690	D-005963-05	MMP24	1.01	0	0	0.984	0	0	0.954	0	0	3708					
113	NM_172347	D-006231-05	KCNG4	0.781	0	1	0.737	0	1	0.71	0	1	7413	increaser	no			
114	NM_172347	D-006231-21	KCNG4	0.806	0	0	0.813	0	0	0.799	0	1	5932					
115	NM_172347	D-006231-22	KCNG4	0.799	0	1	0.799	0	1	0.785	0	1	5875					
116	NM_172347	D-006231-23	KCNG4	0.978	0	0	0.824	0	0	0.838	0	0	4656					
117	NM_002142/NM	D-006337-01	HOXA9	1.07	0	0	1.129	0	0	1.196	0	0	4185	increaser	no			
118	NM_002142/NM	D-006337-02	HOXA9	1.328	1	0	1.584	1	0	1.631	1	0	9403					
119	NM_002142/NM	D-006337-03	HOXA9	0.789	0	1	0.698	0	1	0.638	0	1	4818					
120	NM_002142/NM	D-006337-04	HOXA9	0.815	0	0	0.879	0	0	0.857	0	0	7744					

	GeneID	SirnaID	Gene Symbol	STIPO median score	STIPO positive	STIPO negative	SCPO median score	SCPO positive	SCPO negative	STAPO median score	STAPO positive	STAPO negative	Median OC	Primary Screen class	succesful deconvolution same as primary po	3 or 4 out of 4 duplexes	2 out of 4 duplexes	Official Symbol (if different)
121	NM_014765	D-006487-01	TOMM20	1.169	0	0	1.162	0	0	1.192	0	0	4277	decreaser	no			
122	NM_014765	D-006487-02	TOMM20	0.865	0	0	0.818	0	0	0.804	0	0	4326					
123	NM_014765	D-006487-03	TOMM20	0.938	0	0	0.854	0	0	0.876	0	0	4959					
124	NM_014765	D-006487-04	TOMM20	0.383	0	1	0.576	0	1	0.54	0	1	3997					
125	NM_005241	D-006530-03	EVI1	1.194	0	0	1.047	0	0	1.064	0	0	7151	decreaser	no			
126	NM_005241	D-006530-04	EVI1	0.922	0	0	0.905	0	0	0.891	0	0	6927					
127	NM_005241	D-006530-06	EVI1	1.154	0	0	0.94	0	0	0.962	0	0	6582					
128	NM_005241	D-006530-19	EVI1	0.886	0	0	0.943	0	0	0.965	0	0	4844					
129	NM_002931	D-006554-03	RING1	1.143	0	0	1.177	0	0	1.179	0	0	4947	increaser	no			
130	NM_002931	D-006554-04	RING1	0.902	0	0	0.857	0	0	0.81	0	0	4476					
131	NM_002931	D-006554-05	RING1	0.963	0	0	0.872	0	0	0.852	0	0	4202					
132	NM_002931	D-006554-06	RING1	1.033	0	0	1.077	0	0	1.093	0	0	2911					
133	NM_003420	D-006577-01	ZNF35	0.818	0	0	0.829	0	0	0.81	0	0	6292	decreaser	no			
134	NM_003420	D-006577-02	ZNF35	1.107	0	0	0.896	0	0	0.882	0	0	5643					
135	NM_003420	D-006577-03	ZNF35	0.965	0	0	1.178	0	0	1.245	1	0	7074					
136	NM_003420	D-006577-04	ZNF35	0.876	0	0	0.971	0	0	0.952	0	0	6031					
137	NM_018323	D-006769-01	PI4K2B	0.81	0	0	0.833	0	0	0.816	0	0	5750	increaser	no			
138	NM_018323	D-006769-03	PI4K2B	0.562	0	1	0.796	0	1	0.758	0	1	6899					
139	NM_018323	D-006769-04	PI4K2B	0.957	0	0	0.972	0	0	0.942	0	0	7431					
140	NM_018323	D-006769-05	PI4K2B	1.004	0	0	0.971	0	0	0.965	0	0	7101					
141	NM_139241	D-007123-01	FGD4	0.808	0	0	0.898	0	0	0.882	0	0	5493	increaser	no			
142	NM_139241	D-007123-02	FGD4	1.014	0	0	0.992	0	0	0.966	0	0	2625					
143	NM_139241	D-007123-03	FGD4	0.882	0	0	0.99	0	0	0.978	0	0	4782					
144	NM_139241	D-007123-04	FGD4	1.017	0	0	1.073	0	0	1.094	0	0	4915					
145	NM_004299	D-007305-01	ABCB7	1.329	1	0	0.996	0	0	0.907	0	0	3845	decreaser	no			
146	NM_004299	D-007305-02	ABCB7	0.555	0	1	0.598	0	1	0.566	0	1	5201					
147	NM_004299	D-007305-03	ABCB7	1.294	1	0	1.256	1	0	1.282	1	0	3933					
148	NM_004299	D-007305-04	ABCB7	0.7	0	1	0.787	0	1	0.786	0	1	4287					
149	NM_005845/NM	D-007313-02	ABCC4/ABCC4	0.522	0	1	0.628	0	1	0.607	0	1	4136	increaser	no			
150	NM_005845/NM	D-007313-03	ABCC4/ABCC4	1.671	1	0	1.338	1	0	1.434	1	0	4704					
151	NM_005845/NM	D-007313-04	ABCC4/ABCC4	1.236	1	0	1.148	0	0	1.139	0	0	3970					
152	NM_001105515	D-007313-17	ABCC4/ABCC4	0.851	0	0	0.827	0	0	0.793	0	1	4724					
153	NM_022042	D-007488-02	SLC26A1	0.603	0	1	0.622	0	1	0.608	0	1	3715	increaser	no			
154	NM_022042	D-007488-13	SLC26A1	1.027	0	0	1.006	0	0	1.013	0	0	3886					
155	NM_022042	D-007488-14	SLC26A1	1.569	1	0	1.331	1	0	1.35	1	0	4647					
156	NM_022042	D-007488-15	SLC26A1	0.645	0	1	0.701	0	1	0.684	0	1	3996					
157	NM_018170	D-007734-01	P15RS	1.275	1	0	1.242	1	0	1.279	1	0	4797	decreaser	no			
158	NM_018170	D-007734-02	P15RS	1.295	1	0	1.245	1	0	1.273	1	0	6740					
159	NM_018170	D-007734-04	P15RS	0.791	0	1	0.893	0	0	0.892	0	0	7618					
160	NM_018170	D-007734-18	P15RS	1.117	0	0	1.013	0	0	0.995	0	0	8856					
161	NM_003820	D-008096-01	TNFRSF14	0.78	0	1	0.796	0	1	0.765	0	1	5552	decreaser	no			
162	NM_003820	D-008096-02	TNFRSF14	1.2925	1	0	1.3005	1	0	1.372	1	0	6565					
163	NM_003820	D-008096-03	TNFRSF14	0.872	0	0	0.962	0	0	0.983	0	0	8491					
164	NM_003820	D-008096-04	TNFRSF14	1.296	1	0	1.373	1	0	1.435	1	0	6180					
165	NM_005347	D-008198-03	HSPA5	1.058	0	0	1.202	1	0	1.239	1	0	6854	decreaser	no			
166	NM_005347	D-008198-04	HSPA5	0.938	0	0	0.998	0	0	0.989	0	0	5417					
167	NM_005347	D-008198-05	HSPA5	1.035	0	0	1.113	0	0	1.138	0	0	6534					
168	NM_005347	D-008198-18	HSPA5	1.134	0	0	0.982	0	0	0.999	0	0	6283					
169	NM_001878	D-008385-01	CRABP2	1.005	0	0	0.949	0	0	0.95	0	0	5584	decreaser	no			
170	NM_001878	D-008385-02	CRABP2	1.089	0	0	1.009	0	0	1	0	0	4774					
171	NM_001878	D-008385-03	CRABP2	0.843	0	0	0.928	0	0	0.876	0	0	4699					
172	NM_001878	D-008385-04	CRABP2	1.367	1	0	1.26	1	0	1.287	1	0	6221					
173	NM_019886	D-008443-01	CHST7	1.165	0	0	0.994	0	0	0.957	0	0	4551	decreaser	no			
174	NM_019886	D-008443-02	CHST7	1.178	0	0	1.175	0	0	1.308	1	0	4485					
175	NM_019886	D-008443-03	CHST7	1.335	1	0	1.486	1	0	1.618	1	0	4976					
176	NM_019886	D-008443-04	CHST7	1.208	1	0	0.996	0	0	0.999	0	0	4805					
177	NM_144650	D-008453-01	ADHFE1	1.062	0	0	1.215	1	0	1.244	1	0	2713	increaser	yes	yes		
178	NM_144650	D-008453-02	ADHFE1	1.291	1	0	1.15	0	0	1.172	0	0	1904					
179	NM_144650	D-008453-03	ADHFE1	1.489	1	0	1.17	0	0	1.3515	1	0	1987					
180	NM_144650	D-008453-04	ADHFE1	2.196	1	0	1.536	1	0	1.64	1	0	6449					

	GeneID	SirnaID	Gene Symbol	STIPO median score	STIPO positive	STIPO negative	SCPO median score	SCPO positive	SCPO negative	STAPO median score	STAPO positive	STAPO negative	Median OC	Primary Screen class	succesful deconvolution same as primary po	3 or 4 out of 4 duplexes	2 out of 4 duplexes	Official Symbol (if different)
181	NM_004249	D-008582-01	RAB28	0.839	0	0	0.813	0	0	0.709	0	1	6133	decreaser	no			
182	NM_004249	D-008582-02	RAB28	0.824	0	0	0.815	0	0	0.807	0	0	3813					
183	NM_004249	D-008582-03	RAB28	1.511	1	0	1.407	1	0	1.466	1	0	5488					
184	NM_004249	D-008582-18	RAB28	1.045	0	0	1.019	0	0	1.026	0	0	3410					
185	NM_002572	D-008797-01	PAFAH1B2	0.81	0	0	0.831	0	0	0.85	0	0	3540	decreaser	yes		yes*	
186	NM_002572	D-008797-02	PAFAH1B2	1.09	0	0	0.972	0	0	0.968	0	0	2506					
187	NM_002572	D-008797-03	PAFAH1B2	0.755	0	1	0.85	0	0	0.841	0	0	4895					
188	NM_002572	D-008797-04	PAFAH1B2	0.745	0	1	0.824	0	0	0.786	0	1	5820					
189	NM_001442	D-008853-01	FABP4	2.129	1	0	1.951	1	0	2.136	1	0	4757	decreaser	yes		yes	
190	NM_001442	D-008853-02	FABP4	0.781	0	1	0.833	0	0	0.753	0	1	4099					
191	NM_001442	D-008853-03	FABP4	0.746	0	1	0.678	0	1	0.642	0	1	5834					
192	NM_001442	D-008853-04	FABP4	0.955	0	0	0.955	0	0	0.996	0	0	4160					
193	NM_004521	D-008867-01	KIF5B	0.674	0	1	0.782	0	1	0.764	0	1	9725	increaser	no			
194	NM_004521	D-008867-02	KIF5B	0.431	0	1	0.552	0	1	0.541	0	1	2141					
195	NM_004521	D-008867-03	KIF5B	1.72	1	0	1.068	0	0	1.159	0	0	2676					
196	NM_004521	D-008867-04	KIF5B	0.785	0	1	1.164	0	0	1.202	1	0	3126					
197	NM_000196	D-008983-01	HSD11B2	0.818	0	0	0.776	0	1	0.795	0	1	7585	increaser	no			
198	NM_000196	D-008983-03	HSD11B2	0.693	0	1	0.849	0	0	0.786	0	1	5749					
199	NM_000196	D-008983-04	HSD11B2	1.204	1	0	1.056	0	0	1.042	0	0	4644					
200	NM_000196	D-008983-05	HSD11B2	0.674	0	1	0.902	0	0	0.873	0	0	1859					
201	NM_006122	D-009110-01	MAN2A2	1.52	1	0	1.387	1	0	1.453	1	0	7508	decreaser	no			
202	NM_006122	D-009110-04	MAN2A2	1.11	0	0	1.026	0	0	1.062	0	0	5208					
203	NM_006122	D-009110-06	MAN2A2	1.452	1	0	1.371	1	0	1.523	1	0	10625					
204	NM_006122	D-009110-19	MAN2A2	1.458	1	0	1.529	1	0	1.559	1	0	14945					
205	NM_002662	D-009413-01	PLD1	1.015	0	0	1.019	0	0	1.022	0	0	915	increaser	no			
206	NM_002662	D-009413-02	PLD1	1.758	1	0	1.665	1	0	1.889	1	0	4125					
207	NM_002662	D-009413-03	PLD1	0.851	0	0	0.843	0	0	0.846	0	0	7024					
208	NM_002662	D-009413-04	PLD1	1.087	0	0	1.096	0	0	1.11	0	0	3809					
209	NM_004599	D-009549-01	SREBF2	0.714	0	1	0.729	0	1	0.715	0	1	1998	increaser	no			
210	NM_004599	D-009549-02	SREBF2	0.883	0	0	0.844	0	0	0.808	0	0	1063					
211	NM_004599	D-009549-03	SREBF2	0.832	0	0	0.919	0	0	0.887	0	0	4658					
212	NM_004599	D-009549-04	SREBF2	1.028	0	0	0.899	0	0	0.854	0	0	6659					
213	NM_001633	D-009696-01	AMBP	0.815	0	0	0.752	0	1	0.774	0	1	8956	increaser	no			
214	NM_001633	D-009696-02	AMBP	1.696	1	0	1.292	1	0	1.5	1	0	4361					
215	NM_001633	D-009696-17	AMBP	1.008	0	0	0.896	0	0	0.893	0	0	5553					
216	NM_001633	D-009696-18	AMBP	0.521	0	1	0.696	0	1	0.695	0	1	4727					
217	NM_012382	D-009819-01	OSRF	0.949	0	0	0.8235	0	0	0.884	0	0	5326	decreaser	no			
218	NM_012382	D-009819-02	OSRF	1.781	1	0	1.334	1	0	1.323	1	0	11078					
219	NM_012382	D-009819-04	OSRF	0.675	0	1	0.75	0	1	0.722	0	1	2547					
220	NM_012382	D-009819-17	OSRF	1.217	1	0	1.049	0	0	1.07	0	0	3316					
221	NM_020820	D-010063-01	PREX1	1.325	1	0	1.079	0	0	1.085	0	0	1711	increaser	no			
222	NM_020820	D-010063-03	PREX1	1.06	0	0	1.05	0	0	1.054	0	0	11775					
223	NM_020820	D-010063-17	PREX1	0.9	0	0	0.697	0	1	0.661	0	1	4634					
224	NM_020820	D-010063-18	PREX1	1.024	0	0	1.06	0	0	1.089	0	0	9389					
225	NM_022467	D-010067-01	CHST8	1.247	1	0	1.104	0	0	1.069	0	0	5934	decreaser	no			
226	NM_022467	D-010067-02	CHST8	0.741	0	1	0.854	0	0	0.857	0	0	4340					
227	NM_022467	D-010067-03	CHST8	0.696	0	1	0.707	0	1	0.679	0	1	6897					
228	NM_022467	D-010067-17	CHST8	2.876	1	0	1.956	1	0	2.167	1	0	4952					
229	NM_032681	D-010079-01	TRIM51	1.034	0	0	1.089	0	0	1.133	0	0	4323	increaser	no			
230	NM_032681	D-010079-03	TRIM51	0.912	0	0	0.947	0	0	0.947	0	0	8048					
231	NM_032681	D-010079-04	TRIM51	1.304	1	0	1.064	0	0	1.082	0	0	9065					
232	NM_032681	D-010079-17	TRIM51	0.746	0	1	0.93	0	0	0.992	0	0	986					
233	NM_005355	D-010082-01	KIF25	1.348	1	0	0.951	0	0	1.001	0	0	6893	increaser	yes	yes		
234	NM_005355	D-010082-02	KIF25	0.892	0	0	1.211	1	0	1.211	1	0	3390					
235	NM_005355	D-010082-03	KIF25	2.2545	1	0	1.818	1	0	2.071	1	0	3782					
236	NM_005355	D-010082-04	KIF25	1.208	1	0	1.261	1	0	1.297	1	0	2984					
237	NM_006047	D-010094-01	RBM12	1.083	0	0	0.928	0	0	0.975	0	0	2943	increaser	yes		yes*	
238	NM_006047	D-010094-02	RBM12	0.966	0	0	1.041	0	0	1.033	0	0	4514					
239	NM_006047	D-010094-03	RBM12	1.312	1	0	1.304	1	0	1.364	1	0	4835					
240	NM_006047	D-010094-04	RBM12	2.184	1	0	1.756	1	0	2.228	1	0	9189					

	GeneID	SirnaID	Gene Symbol	STIPO median score	STIPO positive	STIPO negative	SCPO median score	SCPO positive	SCPO negative	STAPO median score	STAPO positive	STAPO negative	Median OC	Primary Screen class	succesful deconvolution same as primary po	3 or 4 out of 4 duplexes	2 out of 4 duplexes	Official Symbol (if different)
241	NM_006793	D-010355-01	PRDX3	0.974	0	0	0.917	0	0	0.921	0	0	3724	decreaser	no			
242	NM_006793	D-010355-02	PRDX3	0.61	0	1	0.659	0	1	0.648	0	1	4739					
243	NM_006793	D-010355-03	PRDX3	1.401	1	0	1.242	1	0	1.322	1	0	6423					
244	NM_006793	D-010355-04	PRDX3	0.987	0	0	0.932	0	0	0.987	0	0	5716					
245	NM_024082	D-010369-01	TMG3	0.576	0	1	0.584	0	1	0.533	0	1	10062	decreaser	no			
246	NM_024082	D-010369-02	TMG3	1.126	0	0	1.124	0	0	1.151	0	0	6822					
247	NM_024082	D-010369-03	TMG3	0.806	0	0	0.817	0	0	0.814	0	0	5151					
248	NM_024082	D-010369-04	TMG3	0.984	0	0	1.109	0	0	1.167	0	0	4864					
249	NM_002634	D-010530-01	PHB	1.702	1	0	1.416	1	0	1.418	1	0	4295	decreaser	no			
250	NM_002634	D-010530-02	PHB	0.878	0	0	1.067	0	0	1.081	0	0	5726					
251	NM_002634	D-010530-03	PHB	0.827	0	0	1.182	0	0	1.225	1	0	2678					
252	NM_002634	D-010530-04	PHB	0.728	0	1	0.774	0	1	0.786	0	1	4276					
253	NM_017969	D-010671-01	FLJ10006	1.147	0	0	1.015	0	0	1.01	0	0	4641	decreaser	no			
254	NM_017969	D-010671-02	FLJ10006	0.896	0	0	1	0	0	0.993	0	0	4460					
255	NM_017969	D-010671-03	FLJ10006	1.497	1	0	1.341	1	0	1.431	1	0	5850					
256	NM_017969	D-010671-04	FLJ10006	0.86	0	0	0.812	0	0	0.772	0	1	8696					
257	NM_018389	D-010693-01	SLC35C1	1.737	1	0	1.502	1	0	1.665	1	0	2019	increaser	yes		yes	
258	NM_018389	D-010693-02	SLC35C1	1.16	0	0	0.98	0	0	0.934	0	0	7189					
259	NM_018389	D-010693-03	SLC35C1	1.003	0	0	0.889	0	0	0.918	0	0	4852					
260	NM_018389	D-010693-04	SLC35C1	1.567	1	0	1.199	0	0	1.233	1	0	4075					
261	NM_198580	D-010759-01	SLC27A1	1.671	1	0	1.684	1	0	1.747	1	0	8543	decreaser	no			
262	NM_198580	D-010759-02	SLC27A1	0.709	0	1	0.557	0	1	0.554	0	1	7593					
263	NM_198580	D-010759-03	SLC27A1	0.588	0	1	0.729	0	1	0.671	0	1	5245					
264	NM_198580	D-010759-04	SLC27A1	1.364	1	0	1.501	1	0	1.563	1	0	5702					
265	NM_000256	D-011085-01	MYBPC3	0.997	0	0	0.827	0	0	0.848	0	0	1967	increaser	yes	yes§		
266	NM_000256	D-011085-02	MYBPC3	1.652	1	0	1.272	1	0	1.373	1	0	6091					
267	NM_000256	D-011085-03	MYBPC3	1.509	1	0	1.328	1	0	1.418	1	0	4686					
268	NM_000256	D-011085-04	MYBPC3	1.26	1	0	1.206	1	0	1.256	1	0	4657					
269	NM_000983	D-011143-01	RPL22	0.885	0	0	0.93	0	0	0.861	0	0	6167	increaser	no			
270	NM_000983	D-011143-02	RPL22	2.902	1	0	1.853	1	0	2.178	1	0	4014					
271	NM_000983	D-011143-03	RPL22	0.907	0	0	0.949	0	0	0.968	0	0	8979					
272	NM_000983	D-011143-04	RPL22	0.844	0	0	0.812	0	0	0.811	0	0	7666					
273	NM_002281	D-011313-01	KRTHB1	0.824	0	0	0.907	0	0	0.867	0	0	4030	decreaser	no			
274	NM_002281	D-011313-02	KRTHB1	1.067	0	0	0.823	0	0	0.815	0	0	5171					
275	NM_002281	D-011313-03	KRTHB1	1.619	1	0	1.48	1	0	1.544	1	0	7590					
276	NM_002281	D-011313-04	KRTHB1	0.97	0	0	0.986	0	0	0.96	0	0	5548					
277	NM_002965	D-011384-01	S100A9	2.51	1	0	2.193	1	0	2.338	1	0	5978	decreaser	no			
278	NM_002965	D-011384-02	S100A9	1.004	0	0	0.971	0	0	0.924	0	0	3378					
279	NM_002965	D-011384-04	S100A9	1.093	0	0	0.887	0	0	0.875	0	0	3244					
280	NM_002965	D-011384-18	S100A9	0.753	0	1	0.975	0	0	0.931	0	0	6134					
281	NM_003480	D-011425-01	MFAP5	1.386	1	0	1.229	1	0	1.285	1	0	3669	increaser	yes		yes	
282	NM_003480	D-011425-02	MFAP5	1.555	1	0	1.299	1	0	1.271	1	0	8851					
283	NM_003480	D-011425-03	MFAP5	1.011	0	0	0.98	0	0	1.004	0	0	4973					
284	NM_003480	D-011425-04	MFAP5	1.049	0	0	0.956	0	0	0.929	0	0	7022					
285	NM_152235/NM	D-011893-01	SFRS8	0.963	0	0	1.091	0	0	1.081	0	0	4315	decreaser	no			
286	NM_152235/NM	D-011893-02	SFRS8	0.865	0	0	0.8	0	1	0.794	0	1	9548					
287	NM_152235/NM	D-011893-03	SFRS8	1.532	1	0	1.123	0	0	1.118	0	0	6695					
288	NM_152235/NM	D-011893-04	SFRS8	1.088	0	0	1.152	0	0	1.117	0	0	4112					
289	NM_004857	D-011954-01	AKAP5	0.769	0	1	0.824	0	0	0.822	0	0	9121	increaser	no			
290	NM_004857	D-011954-02	AKAP5	0.718	0	1	0.813	0	0	0.811	0	0	3934					
291	NM_004857	D-011954-03	AKAP5	1.07	0	0	0.948	0	0	0.95	0	0	2063					
292	NM_004857	D-011954-04	AKAP5	1.541	1	0	1.162	0	0	1.133	0	0	4125					
293	NM_004934	D-011992-01	CDH18	0.868	0	0	0.987	0	0	0.955	0	0	3287	decreaser	no			
294	NM_004934	D-011992-02	CDH18	1.275	1	0	1.41	1	0	1.515	1	0	5449					
295	NM_004934	D-011992-03	CDH18	1.088	0	0	1.15	0	0	1.076	0	0	5594					
296	NM_004934	D-011992-04	CDH18	0.482	0	1	0.619	0	1	0.591	0	1	4817					
297	NM_005419	D-012064-01	STAT2	1.264	1	0	1.314	1	0	1.374	1	0	4473	increaser	yes	yes		
298	NM_005419	D-012064-02	STAT2	0.793	0	1	1.192	0	0	1.186	0	0	5070					
299	NM_005419	D-012064-03	STAT2	1.01	0	0	1.288	1	0	1.359	1	0	4463					
300	NM_005419	D-012064-04	STAT2	1.398	1	0	1.658	1	0	1.851	1	0	3685					

	GeneID	SirnaID	Gene Symbol	STIPO median score	STIPO positive	STIPO negative	SCPO median score	SCPO positive	SCPO negative	STAPO median score	STAPO positive	STAPO negative	Median OC	Primary Screen class	succesful deconvolution same as primary po	3 or 4 out of 4 duplexes	2 out of 4 duplexes	Official Symbol (if different)
301	NM_006551	D-012291-01	SCGB1D2	1.153	0	0	1.189	0	0	1.199	0	0	5708	increaser	no			
302	NM_006551	D-012291-02	SCGB1D2	0.988	0	0	0.928	0	0	0.955	0	0	3827					
303	NM_006551	D-012291-03	SCGB1D2	0.944	0	0	1.028	0	0	1.016	0	0	6053					
304	NM_006551	D-012291-04	SCGB1D2	1.221	1	0	1.412	1	0	1.506	1	0	3514					
305	NM_006870	D-012303-01	DSTN	1.086	0	0	1.006	0	0	0.967	0	0	4749	increaser	no			
306	NM_006870	D-012303-04	DSTN	1.135	0	0	1.199	0	0	1.244	1	0	4165					
307	NM_006870	D-012303-17	DSTN	0.8	0	1	0.83	0	0	0.815	0	0	4411					
308	NM_006870	D-012303-18	DSTN	0.899	0	0	0.982	0	0	0.983	0	0	4359					
309	NM_006829	D-012306-01	C10orf116	1.257	1	0	1.154	0	0	1.237	1	0	3127	increaser	yes	yes§		
310	NM_006829	D-012306-02	C10orf116	1.256	1	0	1.235	1	0	1.218	1	0	3016					
311	NM_006829	D-012306-03	C10orf116	1.34	1	0	1.105	0	0	1.29	1	0	5754					
312	NM_006829	D-012306-04	C10orf116	0.86	0	0	0.81	0	0	0.725	0	1	5749					
313	NM_007003	D-012344-01	GAGEC1	0.642	0	1	0.588	0	1	0.572	0	1	7047	increaser	no			
314	NM_007003	D-012344-02	GAGEC1	0.745	0	1	0.727	0	1	0.707	0	1	5860					
315	NM_007003	D-012344-03	GAGEC1	0.849	0	0	0.754	0	1	0.723	0	1	6033					
316	NM_007003	D-012344-04	GAGEC1	2.531	1	0	1.828	1	0	1.865	1	0	7407					
317	NM_003154/NM	D-012654-01	STATH	0.921	0	0	0.816	0	0	0.821	0	0	7087	decreaser	no			
318	NM_003154/NM	D-012654-03	STATH	0.879	0	0	0.998	0	0	1.023	0	0	4948					
319	NM_003154/NM	D-012654-17	STATH	1.338	1	0	0.996	0	0	0.996	0	0	4390					
320	NM_003154/NM	D-012654-18	STATH	1.195	0	0	1.358	1	0	1.395	1	0	3011					
321	NM_006145	D-012735-01	DNAJB1	1.297	1	0	1.142	0	0	1.235	1	0	4976	increaser	no			
322	NM_006145	D-012735-04	DNAJB1	1.007	0	0	0.868	0	0	0.875	0	0	9481					
323	NM_006145	D-012735-18	DNAJB1	0.778	0	1	0.811	0	0	0.807	0	0	10669					
324	NM_006145	D-012735-19	DNAJB1	1.143	0	0	1.041	0	0	1.065	0	0	3671					
325	NM_022091	D-012757-21	DJ467N11.1	1.156	0	0	0.979	0	0	1.004	0	0	6945	decreaser	no			
326	NM_022091	D-012757-22	DJ467N11.1	0.972	0	0	0.846	0	0	0.772	0	1	4568					
327	NM_022091	D-012757-23	DJ467N11.1	1.081	0	0	1.287	1	0	1.334	1	0	3698					
328	NM_022091	D-012757-24	DJ467N11.1	1.012	0	0	1.116	0	0	1.189	0	0	7594					
329	NM_012202	D-012804-21	GNG3	0.865	0	0	0.784	0	1	0.742	0	1	10377	increaser	no			
330	NM_012202	D-012804-22	GNG3	0.773	0	1	1.06	0	0	1.005	0	0	6693					
331	NM_012202	D-012804-23	GNG3	0.632	0	1	0.605	0	1	0.549	0	1	7307					
332	NM_012202	D-012804-24	GNG3	0.679	0	1	0.698	0	1	0.652	0	1	1972					
333	NM_012272	D-012810-01	HYPC	1.018	0	0	1.111	0	0	1.11	0	0	8815	increaser	no			
334	NM_012272	D-012810-02	HYPC	0.943	0	0	0.895	0	0	0.881	0	0	4170					
335	NM_012272	D-012810-03	HYPC	0.998	0	0	1.017	0	0	1.025	0	0	4401					
336	NM_012272	D-012810-04	HYPC	2.706	1	0	1.768	1	0	1.892	1	0	8099					
337	NM_022575	D-013003-01	VPS16	1.023	0	0	0.968	0	0	0.987	0	0	4037	increaser	no			
338	NM_022575	D-013003-02	VPS16	1.663	1	0	1.225	1	0	1.443	1	0	4418					
339	NM_022575	D-013003-03	VPS16	1.144	0	0	1.12	0	0	1.158	0	0	1415					
340	NM_022575	D-013003-04	VPS16	1.102	0	0	1.025	0	0	1.071	0	0	7854					
341	NM_021818	D-013070-01	SAV1	0.58	0	1	0.755	0	1	0.716	0	1	10721	decreaser	no			
342	NM_021818	D-013070-03	SAV1	1.055	0	0	1.096	0	0	1.093	0	0	5740					
343	NM_021818	D-013070-04	SAV1	0.866	0	0	1.004	0	0	1.049	0	0	3898					
344	NM_021818	D-013070-18	SAV1	0.851	0	0	0.916	0	0	0.883	0	0	5994					
345	NM_018031	D-013085-01	WDR6	0.741	0	1	0.867	0	0	0.83	0	0	5270	increaser	yes	yes		
346	NM_018031	D-013085-02	WDR6	1.354	1	0	1.403	1	0	1.499	1	0	5441					
347	NM_018031	D-013085-03	WDR6	1.327	1	0	1.235	1	0	1.26	1	0	5062					
348	NM_018031	D-013085-04	WDR6	1.321	1	0	1.165	0	0	1.221	1	0	7065					
349	NM_021153	D-013105-01	CDH19	0.88	0	0	1.145	0	0	1.219	1	0	5563	decreaser	yes	yes		
350	NM_021153	D-013105-02	CDH19	0.21	0	1	0.363	0	1	0.328	0	1	7858					
351	NM_021153	D-013105-03	CDH19	0.662	0	1	0.859	0	0	0.872	0	0	4285					
352	NM_021153	D-013105-04	CDH19	0.749	0	1	0.868	0	0	0.841	0	0	3947					
353	NM_016628	D-013325-01	WAC	0.913	0	0	1.144	0	0	1.19	0	0	5535	decreaser	yes	yes		
354	NM_016628	D-013325-02	WAC	0.607	0	1	0.676	0	1	0.671	0	1	3881					
355	NM_016628	D-013325-03	WAC	0.41	0	1	0.475	0	1	0.468	0	1	7755					
356	NM_016628	D-013325-04	WAC	0.368	0	1	0.565	0	1	0.521	0	1	7213					
357	NM_000412	D-013420-01	HRG	0.953	0	0	0.779	0	1	0.783	0	1	6778	increaser	no			
358	NM_000412	D-013420-02	HRG	0.515	0	1	0.729	0	1	0.693	0	1	6392					
359	NM_000412	D-013420-03	HRG	0.839	0	0	0.898	0	0	0.867	0	0	4814					
360	NM_000412	D-013420-17	HRG	0.806	0	0	0.849	0	0	0.83	0	0	4384					

	GeneID	SirnaID	Gene Symbol	STIPO median score	STIPO positive	STIPO negative	SCPO median score	SCPO positive	SCPO negative	STAPO median score	STAPO positive	STAPO negative	Median OC	Primary Screen class	succesful deconvolution same as primary po	3 or 4 out of 4 duplexes	2 out of 4 duplexes	Official Symbol (if different)
361	NM_015971	D-013580-01	MRPS7	1.609	1	0	1.277	1	0	1.326	1	0	5842	decreaser	yes		yes	
362	NM_015971	D-013580-02	MRPS7	1.066	0	0	0.979	0	0	0.975	0	0	7221					
363	NM_015971	D-013580-03	MRPS7	0.238	0	1	0.475	0	1	0.396	0	1	7114					
364	NM_015971	D-013580-04	MRPS7	0.453	0	1	0.528	0	1	0.519	0	1	6445					
365	NM_021210	D-013781-01	TRAPPC1	1.139	0	0	1.148	0	0	1.097	0	0	3962	decreaser	no			
366	NM_021210	D-013781-02	TRAPPC1	0.497	0	1	0.592	0	1	0.549	0	1	4926					
367	NM_021210	D-013781-04	TRAPPC1	2.074	1	0	1.425	1	0	1.412	1	0	4796					
368	NM_021210	D-013781-17	TRAPPC1	0.992	0	0	0.94	0	0	0.927	0	0	6123					
369	NM_022068	D-013925-01	FAM38B	1.189	0	0	1.273	1	0	1.293	1	0	4142	increaser	no			
370	NM_022068	D-013925-02	FAM38B	0.643	0	1	0.857	0	0	0.797	0	1	7381					
371	NM_022068	D-013925-03	FAM38B	0.796	0	1	0.775	0	1	0.755	0	1	4200					
372	NM_022068	D-013925-04	FAM38B	0.655	0	1	1.083	0	0	1.123	0	0	4074					
373	NM_020789	D-014056-01	IGSF9	1.121	0	0	0.991	0	0	0.978	0	0	7253	decreaser	no			
374	NM_020789	D-014056-02	IGSF9	1.445	1	0	1.19	0	0	1.224	1	0	7644					
375	NM_020789	D-014056-03	IGSF9	0.147	0	1	0.289	0	1	0.269	0	1	4898					
376	NM_020789	D-014056-04	IGSF9	1.484	1	0	1.226	1	0	1.271	1	0	8118					
377	NM_022489/NM	D-014097-01	FLJ22056	0.652	0	1	0.596	0	1	0.544	0	1	6103	increaser	no			
378	NM_022489/NM	D-014097-03	FLJ22056	1.872	1	0	1.476	1	0	1.602	1	0	3921					
379	NM_022489/NM	D-014097-04	FLJ22056	0.913	0	0	0.934	0	0	0.876	0	0	5070					
380	NM_022489/NM	D-014097-17	FLJ22056	0.892	0	0	0.859	0	0	0.834	0	0	4679					
381	NM_014982	D-014158-01	PCNX	0.619	0	1	0.682	0	1	0.665	0	1	8284	decreaser	no			
382	NM_014982	D-014158-02	PCNX	1.485	1	0	1.312	1	0	1.339	1	0	7454					
383	NM_014982	D-014158-03	PCNX	1.874	1	0	1.614	1	0	1.717	1	0	11009					
384	NM_014982	D-014158-04	PCNX	0.992	0	0	0.898	0	0	0.869	0	0	5286					
385	NM_023080	D-014247-01	FLJ20989	0.351	0	1	0.531	0	1	0.474	0	1	3291	increaser	yes		yes	C8orf33
386	NM_023080	D-014247-02	FLJ20989	1.093	0	0	1.134	0	0	1.204	1	0	2976					
387	NM_023080	D-014247-03	FLJ20989	0.9	0	0	0.856	0	0	0.845	0	0	12940					
388	NM_023080	D-014247-04	FLJ20989	1.605	1	0	1.457	1	0	1.48	1	0	4263					
389	NM_024331/NM	D-014340-01	C20orf121	1.11	0	0	1.006	0	0	0.953	0	0	3547	decreaser	no			
390	NM_024331/NM	D-014340-02	C20orf121	1.427	1	0	0.982	0	0	0.96	0	0	3602					
391	NM_024331/NM	D-014340-03	C20orf121	0.615	0	1	0.724	0	1	0.727	0	1	9573					
392	NM_024331/NM	D-014340-04	C20orf121	2.002	1	0	1.681	1	0	1.793	1	0	5390					
393	NM_024829	D-014472-01	FLJ22662	0.816	0	0	0.836	0	0	0.818	0	0	3821	increaser	no			
394	NM_024829	D-014472-02	FLJ22662	0.888	0	0	1.08	0	0	1.088	0	0	3926					
395	NM_024829	D-014472-03	FLJ22662	1.097	0	0	0.959	0	0	1.001	0	0	4930					
396	NM_024829	D-014472-04	FLJ22662	2.132	1	0	1.446	1	0	1.695	1	0	4215					
397	NM_024902	D-014507-01	FLJ13236	0.854	0	0	0.919	0	0	0.85	0	0	7609	increaser	no			
398	NM_024902	D-014507-02	FLJ13236	0.302	0	1	0.518	0	1	0.484	0	1	5136					
399	NM_024902	D-014507-03	FLJ13236	0.718	0	1	0.925	0	0	0.953	0	0	5410					
400	NM_024902	D-014507-04	FLJ13236	1.302	1	0	1.288	1	0	1.33	1	0	11222					
401	NM_024953	D-014530-01	FLJ13089	0.561	0	1	0.705	0	1	0.671	0	1	4953	decreaser	yes	yes		
402	NM_024953	D-014530-02	FLJ13089	0.316	0	1	0.546	0	1	0.486	0	1	10701					
403	NM_024953	D-014530-03	FLJ13089	0.793	0	1	0.849	0	0	0.815	0	0	6310					
404	NM_024953	D-014530-04	FLJ13089	1.47	1	0	1.294	1	0	1.272	1	0	4927					
405	NM_031310	D-014714-01	PLVAP	0.625	0	1	0.701	0	1	0.677	0	1	4342	decreaser	no			
406	NM_031310	D-014714-02	PLVAP	0.941	0	0	0.93	0	0	0.904	0	0	7151					
407	NM_031310	D-014714-03	PLVAP	0.961	0	0	1.001	0	0	1.01	0	0	3949					
408	NM_031310	D-014714-04	PLVAP	1.108	0	0	1.045	0	0	1.011	0	0	2833					
409	NM_032347	D-014870-01	ZNF397	1.154	0	0	0.993	0	0	0.939	0	0	5207	increaser	no			
410	NM_032347	D-014870-02	ZNF397	0.993	0	0	1.076	0	0	1.124	0	0	6655					
411	NM_032347	D-014870-03	ZNF397	0.906	0	0	1.023	0	0	1.053	0	0	3714					
412	NM_032347	D-014870-04	ZNF397	0.829	0	0	1.002	0	0	0.979	0	0	5087					
413	NM_032547	D-014916-01	SCOC	0.601	0	1	0.782	0	1	0.772	0	1	4694	decreaser	yes	yes		
414	NM_032547	D-014916-02	SCOC	0.621	0	1	0.645	0	1	0.636	0	1	3231					
415	NM_032547	D-014916-03	SCOC	0.412	0	1	0.61	0	1	0.552	0	1	5685					
416	NM_032547	D-014916-04	SCOC	1.817	1	0	1.514	1	0	1.667	1	0	5517					
417	NM_032800	D-015001-01	FLJ14525	1.482	1	0	1.351	1	0	1.385	1	0	5879	decreaser	yes	yes		
418	NM_032800	D-015001-02	FLJ14525	0.47	0	1	0.562	0	1	0.562	0	1	6345					
419	NM_032800	D-015001-03	FLJ14525	0.437	0	1	0.692	0	1	0.627	0	1	9595					
420	NM_032800	D-015001-04	FLJ14525	0.664	0	1	0.839	0	0	0.853	0	0	6526					

	GeneID	SirnaID	Gene Symbol	STIPO median score	STIPO positive	STIPO negative	SCPO median score	SCPO positive	SCPO negative	STAPO median score	STAPO positive	STAPO negative	Median OC	Primary Screen class	succesful deconvolution same as primary po	3 or 4 out of 4 duplexes	2 out of 4 duplexes	Official Symbol (if different)
421	NM_032875	D-015029-01	FBXL20	0.728	0	1	0.704	0	1	0.67	0	1	8805	increaser	no			
422	NM_032875	D-015029-02	FBXL20	0.772	0	1	0.735	0	1	0.705	0	1	6156					
423	NM_032875	D-015029-03	FBXL20	0.635	0	1	0.586	0	1	0.555	0	1	7065					
424	NM_032875	D-015029-04	FBXL20	1.379	1	0	1.366	1	0	1.48	1	0	5019					
425	NM_058222	D-015223-01	TECTB	0.857	0	0	1.119	0	0	1.144	0	0	2723	decreaser	no			
426	NM_058222	D-015223-02	TECTB	0.642	0	1	0.737	0	1	0.744	0	1	3268					
427	NM_058222	D-015223-03	TECTB	1.014	0	0	0.941	0	0	0.936	0	0	4786					
428	NM_058222	D-015223-04	TECTB	0.879	0	0	0.88	0	0	0.845	0	0	9677					
429	NM_012307	D-015330-01	EPB41L3	0.805	0	0	1.221	1	0	1.276	1	0	4354	increaser	no			
430	NM_012307	D-015330-02	EPB41L3	0.699	0	1	0.715	0	1	0.659	0	1	5117					
431	NM_012307	D-015330-03	EPB41L3	0.879	0	0	0.891	0	0	0.866	0	0	11578					
432	NM_012307	D-015330-04	EPB41L3	0.736	0	1	0.732	0	1	0.711	0	1	6448					
433	NM_006288	D-015337-01	THY1	1.211	1	0	1.036	0	0	1.025	0	0	4192	increaser	no			
434	NM_006288	D-015337-02	THY1	0.723	0	1	0.692	0	1	0.663	0	1	3246					
435	NM_006288	D-015337-03	THY1	0.685	0	1	0.874	0	0	0.824	0	0	3397					
436	NM_006288	D-015337-04	THY1	1.448	1	0	1.318	1	0	1.372	1	0	9265					
437	NM_016284	D-015369-01	KIAA1007	1.317	1	0	1.146	0	0	1.173	0	0	6072	increaser	yes	yes		
438	NM_016284	D-015369-02	KIAA1007	1.877	1	0	1.697	1	0	1.812	1	0	5382					
439	NM_016284	D-015369-03	KIAA1007	1.071	0	0	0.995	0	0	0.968	0	0	4625					
440	NM_016284	D-015369-04	KIAA1007	2.972	1	0	1.926	1	0	2.111	1	0	4290					
441	NM_138333	D-015499-01	C9ORF42	0.618	0	1	0.601	0	1	0.572	0	1	6617	decreaser	no			
442	NM_138333	D-015499-02	C9ORF42	0.899	0	0	0.998	0	0	1.006	0	0	5806					
443	NM_138333	D-015499-03	C9ORF42	1.013	0	0	0.862	0	0	0.813	0	0	10701					
444	NM_138333	D-015499-04	C9ORF42	1.582	1	0	1.472	1	0	1.523	1	0	6565					
445	NM_001265	D-015636-01	CDX2	0.783	0	1	1.162	0	0	1.185	0	0	6053	increaser	no			
446	NM_001265	D-015636-03	CDX2	0.807	0	0	0.939	0	0	0.922	0	0	4840					
447	NM_001265	D-015636-04	CDX2	0.873	0	0	0.864	0	0	0.903	0	0	11866					
448	NM_001265	D-015636-05	CDX2	1.195	0	0	1.155	0	0	1.254	1	0	4425					
449	NM_152441	D-015718-01	FBXL14	1.595	1	0	1.207	1	0	1.326	1	0	7724	increaser	yes		yes*	
450	NM_152441	D-015718-02	FBXL14	1.004	0	0	1.133	0	0	1.146	0	0	5612					
451	NM_152441	D-015718-03	FBXL14	0.69	0	1	0.713	0	1	0.669	0	1	6722					
452	NM_152441	D-015718-04	FBXL14	1.425	1	0	1.265	1	0	1.336	1	0	8174					
453	NM_016300/NM	D-016091-01	ARPP-21	1.23	1	0	1.266	1	0	1.28	1	0	6217	increaser	yes	yes		ARPP21
454	NM_016300/NM	D-016091-02	ARPP-21	0.5	0	1	0.594	0	1	0.55	0	1	7164					
455	NM_016300/NM	D-016091-03	ARPP-21	0.85	0	0	0.996	0	0	0.983	0	0	4703					
456	NM_016300/NM	D-016091-04	ARPP-21	1.783	1	0	1.399	1	0	1.511	1	0	4508					
457	NM_021948/NM	D-016130-01	BCAN	1.963	1	0	1.991	1	0	2.272	1	0	3263	decreaser	no			
458	NM_021948/NM	D-016130-02	BCAN	1.224	1	0	1.274	1	0	1.405	1	0	3909					
459	NM_021948/NM	D-016130-03	BCAN	0.479	0	1	0.636	0	1	0.652	0	1	3933					
460	NM_021948/NM	D-016130-17	BCAN	2.037	1	0	1.577	1	0	1.758	1	0	7754					
461	NM_144605	D-016227-01	FLJ25410	1.211	1	0	1.122	0	0	1.185	0	0	6239	increaser	no			
462	NM_144605	D-016227-02	FLJ25410	0.805	0	0	0.827	0	0	0.799	0	1	5541					
463	NM_144605	D-016227-04	FLJ25410	1.12	0	0	1.047	0	0	1.077	0	0	7236					
464	NM_144605	D-016227-17	FLJ25410	1.084	0	0	0.976	0	0	0.96	0	0	8861					
465	NM_003169/NM	D-016234-01	SUPT5H/SUPT5	0.621	0	1	0.694	0	1	0.693	0	1	4068	decreaser	yes	yes		
466	NM_003169/NM	D-016234-02	SUPT5H/SUPT5	0.601	0	1	0.795	0	1	0.769	0	1	7081					
467	NM_003169/NM	D-016234-03	SUPT5H/SUPT5	0.694	0	1	0.931	0	0	0.895	0	0	4014					
468	NM_003169/NM	D-016234-04	SUPT5H/SUPT5	0.58	0	1	0.765	0	1	0.778	0	1	5422					
469	NM_005810	D-016300-01	KLRG1	1.031	0	0	1.195	0	0	1.228	1	0	4352	increaser	yes	yes§		
470	NM_005810	D-016300-02	KLRG1	1.331	1	0	1.253	1	0	1.289	1	0	9100					
471	NM_005810	D-016300-03	KLRG1	1.399	1	0	1.139	0	0	1.274	1	0	2164					
472	NM_005810	D-016300-17	KLRG1	0.947	0	0	0.951	0	0	0.961	0	0	4825					
473	NM_022767	D-016332-01	FLJ12484	0.989	0	0	0.934	0	0	0.897	0	0	5172	increaser	no			
474	NM_022767	D-016332-02	FLJ12484	1.867	1	0	1.625	1	0	1.845	1	0	3393					
475	NM_022767	D-016332-03	FLJ12484	0.754	0	1	0.927	0	0	0.886	0	0	3817					
476	NM_022767	D-016332-04	FLJ12484	0.953	0	0	0.901	0	0	0.896	0	0	8924					
477	NM_153337/NM	D-016514-01	SLIC1	1.567	1	0	1.118	0	0	1.14	0	0	5239	increaser	yes	yes		
478	NM_153337/NM	D-016514-02	SLIC1	1.347	1	0	1.229	1	0	1.268	1	0	7262					
479	NM_153337/NM	D-016514-03	SLIC1	1.45	1	0	1.475	1	0	1.613	1	0	4550					
480	NM_153337/NM	D-016514-04	SLIC1	0.653	0	1	0.631	0	1	0.603	0	1	4075					

	GeneID	SirnaID	Gene Symbol	STIPO median score	STIPO positive	STIPO negative	SCPO median score	SCPO positive	SCPO negative	STAPO median score	STAPO positive	STAPO negative	Median OC	Primary Screen class	succesful deconvolution same as primary po	3 or 4 out of 4 duplexes	2 out of 4 duplexes	Official Symbol (if different)
481	NM_031461	D-016681-01	LOC83690	1.042	0	0	0.923	0	0	0.94	0	0	5145	decreaser	no			
482	NM_031461	D-016681-02	LOC83690	0.785	0	1	0.944	0	0	0.945	0	0	7246					
483	NM_031461	D-016681-03	LOC83690	1.407	1	0	1.372	1	0	1.439	1	0	4226					
484	NM_031461	D-016681-04	LOC83690	1.162	0	0	1.169	0	0	1.221	1	0	4701					
485	NM_152492	D-016738-01	FLJ32825	1.12	0	0	1.107	0	0	1.13	0	0	11615	increaser	no			
486	NM_152492	D-016738-02	FLJ32825	1.095	0	0	1.128	0	0	1.158	0	0	6733					
487	NM_152492	D-016738-03	FLJ32825	1.088	0	0	0.842	0	0	0.844	0	0	4839					
488	NM_152492	D-016738-04	FLJ32825	0.847	0	0	0.899	0	0	0.899	0	0	4590					
489	NM_144999	D-016887-01	MGC20806	1.045	0	0	1.069	0	0	1.135	0	0	4693	increaser	no			
490	NM_144999	D-016887-02	MGC20806	1.061	0	0	0.968	0	0	0.998	0	0	7594					
491	NM_144999	D-016887-03	MGC20806	1.739	1	0	1.392	1	0	1.422	1	0	4968					
492	NM_144999	D-016887-04	MGC20806	0.832	0	0	0.984	0	0	1.011	0	0	3986					
493	NM_153212	D-016916-04	GJB4	1.289	1	0	1.164	0	0	1.203	1	0	4995	decreaser	no			
494	NM_153212	D-016916-17	GJB4	0.664	0	1	0.799	0	1	0.776	0	1	6329					
495	NM_153212	D-016916-18	GJB4	0.692	0	1	0.92	0	0	0.884	0	0	13176					
496	NM_153212	D-016916-19	GJB4	1.264	1	0	1.187	0	0	1.19	0	0	5416					
497	NM_001816	D-017056-01	CEACAM8	1.162	0	0	1.102	0	0	1.088	0	0	16431	decreaser	no			
498	NM_001816	D-017056-02	CEACAM8	1.153	0	0	1.163	0	0	1.183	0	0	6054					
499	NM_001816	D-017056-03	CEACAM8	0.918	0	0	0.936	0	0	0.934	0	0	4838					
500	NM_001816	D-017056-17	CEACAM8	1.149	0	0	1.009	0	0	1.011	0	0	4169					
501	NM_152611	D-017183-01	C20ORF75	0.987	0	0	0.97	0	0	1.012	0	0	6297	increaser	yes		yes	LRRN4
502	NM_152611	D-017183-02	C20ORF75	1.264	1	0	1.123	0	0	1.156	0	0	5041					
503	NM_152611	D-017183-03	C20ORF75	1.161	0	0	1.224	1	0	1.26	1	0	11812					
504	NM_152611	D-017183-04	C20ORF75	1.575	1	0	1.194	0	0	1.295	1	0	6019					
505	NM_000100	D-017240-01	CSTB	1.152	0	0	1.037	0	0	1.024	0	0	6198	decreaser	yes		yes	
506	NM_000100	D-017240-02	CSTB	0.673	0	1	0.668	0	1	0.626	0	1	12342					
507	NM_000100	D-017240-03	CSTB	1.002	0	0	1.018	0	0	0.981	0	0	6507					
508	NM_000100	D-017240-04	CSTB	0.619	0	1	0.831	0	0	0.813	0	0	8017					
509	NM_138962	D-017248-02	MSI2	1.13	0	0	1.207	1	0	1.216	1	0	10190	decreaser	no			
510	NM_138962	D-017248-03	MSI2	0.7985	0	1	0.8625	0	0	0.836	0	0	8417					
511	NM_138962	D-017248-04	MSI2	1.277	1	0	1.174	0	0	1.218	1	0	6414					
512	NM_138962	D-017248-18	MSI2	1.373	1	0	1.316	1	0	1.349	1	0	8112					
513	NM_016224	D-017335-01	SNX9	0.775	0	1	0.755	0	1	0.744	0	1	8415	increaser	no			
514	NM_016224	D-017335-02	SNX9	0.999	0	0	1.069	0	0	1.027	0	0	4977					
515	NM_016224	D-017335-03	SNX9	0.936	0	0	1.186	0	0	1.188	0	0	4898					
516	NM_016224	D-017335-18	SNX9	0.676	0	1	0.848	0	0	0.777	0	1	2636					
517	NM_002146	D-017537-01	HOXB3	1.095	0	0	1.053	0	0	1.048	0	0	6765	increaser	yes		yes	
518	NM_002146	D-017537-02	HOXB3	0.97	0	0	1.017	0	0	1.124	0	0	6858					
519	NM_002146	D-017537-03	HOXB3	1.333	1	0	1.252	1	0	1.289	1	0	6566					
520	NM_002146	D-017537-04	HOXB3	2.258	1	0	1.691	1	0	1.912	1	0	12808					
521	NM_003877	D-017604-01	SOCS2	1.956	1	0	1.629	1	0	1.819	1	0	5012	decreaser	no			
522	NM_003877	D-017604-02	SOCS2	0.852	0	0	0.826	0	0	0.808	0	0	6450					
523	NM_003877	D-017604-03	SOCS2	0.728	0	1	0.801	0	0	0.824	0	0	13349					
524	NM_003877	D-017604-04	SOCS2	1.094	0	0	0.865	0	0	0.85	0	0	7787					
525	NM_001709	D-017626-01	BDNF	1.09	0	0	1.101	0	0	1.047	0	0	6375	decreaser	no			
526	NM_001709	D-017626-02	BDNF	0.44	0	1	0.531	0	1	0.498	0	1	8413					
527	NM_001709	D-017626-03	BDNF	1.959	1	0	1.853	1	0	1.992	1	0	10829					
528	NM_001709	D-017626-04	BDNF	1.227	1	0	1.324	1	0	1.367	1	0	7846					
529	NM_014876	D-017674-01	KIAA0063	0.865	0	0	0.785	0	1	0.782	0	1	4373	increaser	no			
530	NM_014876	D-017674-02	KIAA0063	0.804	0	0	0.785	0	1	0.768	0	1	5970					
531	NM_014876	D-017674-03	KIAA0063	1.248	1	0	1.295	1	0	1.421	1	0	6439					
532	NM_014876	D-017674-04	KIAA0063	1.404	1	0	1.241	1	0	1.268	1	0	5005					
533	NM_015426	D-017717-01	DKFZP434C24	1.31	1	0	1.171	0	0	1.189	0	0	17528	decreaser	no			
534	NM_015426	D-017717-02	DKFZP434C24	0.738	0	1	0.79	0	1	0.809	0	0	3774					
535	NM_015426	D-017717-03	DKFZP434C24	0.993	0	0	1.077	0	0	1.017	0	0	4896					
536	NM_015426	D-017717-17	DKFZP434C24	1.019	0	0	0.882	0	0	0.897	0	0	12257					
537	NM_015986	D-017786-01	CRLF3	1.339	1	0	1.306	1	0	1.379	1	0	5798	increaser	no			
538	NM_015986	D-017786-04	CRLF3	0.975	0	0	0.853	0	0	0.861	0	0	1654					
539	NM_015986	D-017786-17	CRLF3	0.795	0	1	0.798	0	1	0.767	0	1	4197					
540	NM_015986	D-017786-18	CRLF3	0.777	0	1	0.926	0	0	0.952	0	0	5372					

	GeneID	SirnaID	Gene Symbol	STIPO median score	STIPO positive	STIPO negative	SCPO median score	SCPO positive	SCPO negative	STAPO median score	STAPO positive	STAPO negative	Median OC	Primary Screen class	succesful deconvolution same as primary po	3 or 4 out of 4 duplexes	2 out of 4 duplexes	Official Symbol (if different)
541	NM_005147	D-017792-01	DNAJA3	1.959	1	0	1.559	1	0	1.717	1	0	6108	increaser	yes		yes	
542	NM_005147	D-017792-02	DNAJA3	1.011	0	0	1.101	0	0	1.144	0	0	3414					
543	NM_005147	D-017792-03	DNAJA3	0.881	0	0	0.839	0	0	0.835	0	0	1354					
544	NM_005147	D-017792-04	DNAJA3	1.042	0	0	1.249	1	0	1.31	1	0	6400					
545	NM_003248	D-017834-01	THBS4	1.577	1	0	1.22	1	0	1.247	1	0	7974	decreaser	no			
546	NM_003248	D-017834-02	THBS4	0.222	0	1	0.498	0	1	0.451	0	1	13562					
547	NM_003248	D-017834-03	THBS4	1.032	0	0	1.215	1	0	1.199	0	0	5297					
548	NM_003248	D-017834-04	THBS4	1.852	1	0	1.725	1	0	1.686	1	0	10135					
549	NM_020437	D-017864-01	LOC57168	1.418	1	0	1.209	1	0	1.252	1	0	5433	increaser	yes		yes	ASPHD2
550	NM_020437	D-017864-03	LOC57168	1.564	1	0	1.381	1	0	1.511	1	0	3089					
551	NM_020437	D-017864-04	LOC57168	1.175	0	0	1.185	0	0	1.136	0	0	8240					
552	NM_020437	D-017864-17	LOC57168	0.773	0	1	0.893	0	0	0.916	0	0	4379					
553	NM_173597	D-018271-02	FLJ37587	1.041	0	0	1.011	0	0	1.003	0	0	3091	decreaser	no			
554	NM_173597	D-018271-03	FLJ37587	1.845	1	0	1.552	1	0	1.652	1	0	5798					
555	NM_173597	D-018271-04	FLJ37587	1.104	0	0	1.051	0	0	1.064	0	0	2803					
556	NM_173597	D-018271-09	FLJ37587	2.068	1	0	1.739	1	0	1.956	1	0	6460					
557	NM_024650	D-018410-01	FLJ22531	1.176	0	0	1.004	0	0	0.931	0	0	6361	decreaser	no			
558	NM_024650	D-018410-02	FLJ22531	1.144	0	0	1.092	0	0	1.04	0	0	4980					
559	NM_024650	D-018410-03	FLJ22531	1.022	0	0	1.216	1	0	1.243	1	0	968					
560	NM_024650	D-018410-04	FLJ22531	1.037	0	0	0.963	0	0	0.93	0	0	4836					
561	NM_178124	D-018483-01	LOC91966	0.946	0	0	0.931	0	0	0.933	0	0	2884	increaser	no			
562	NM_178124	D-018483-02	LOC91966	1.229	1	0	1.398	1	0	1.434	1	0	2314					
563	NM_178124	D-018483-04	LOC91966	0.941	0	0	0.851	0	0	0.8	0	1	5048					
564	NM_178124	D-018483-17	LOC91966	1.005	0	0	1.061	0	0	1.045	0	0	5498					
565	NM_138342	D-018681-01	LOC89944	0.787	0	1	0.946	0	0	0.874	0	0	4217	decreaser	yes		yes	GLB1L2
566	NM_138342	D-018681-02	LOC89944	1.573	1	0	1.089	0	0	1.1	0	0	8018					
567	NM_138342	D-018681-03	LOC89944	0.924	0	0	1	0	0	1.027	0	0	4750					
568	NM_138342	D-018681-04	LOC89944	0.189	0	1	0.397	0	1	0.348	0	1	7504					
569	NM_001105533	D-018816-02	FLJ21986	1.964	1	0	1.903	1	0	2.097	1	0	2493	increaser	yes		yes	C7orf58
570	NM_001105533	D-018816-17	FLJ21986	0.921	0	0	0.886	0	0	0.922	0	0	4586					
571	NM_001105533	D-018816-18	FLJ21986	0.774	0	1	0.705	0	1	0.733	0	1	4635					
572	NM_001105533	D-018816-19	FLJ21986	1.342	1	0	1.374	1	0	1.424	1	0	4065					
573	NM_182587	D-018852-01	C2orf21	0.718	0	1	0.851	0	0	0.85	0	0	5894	increaser	yes		yes	UNC80
574	NM_182587	D-018852-02	C2orf21	1.134	0	0	1.112	0	0	1.144	0	0	6811					
575	NM_182587	D-018852-03	C2orf21	1.375	1	0	1.315	1	0	1.357	1	0	3419					
576	NM_182587	D-018852-04	C2orf21	1.52	1	0	1.204	1	0	1.261	1	0	4787					
577	NM_181775	D-018881-01	DKFZP434G06	0.721	0	1	0.905	0	0	0.877	0	0	7298	decreaser	yes		yes	PLXNA4
578	NM_181775	D-018881-03	DKFZP434G06	0.914	0	0	1.002	0	0	1.001	0	0	2607					
579	NM_181775	D-018881-04	DKFZP434G06	0.747	0	1	0.718	0	1	0.698	0	1	1871					
580	NM_181775	D-018881-18	DKFZP434G06	1.45	1	0	1.311	1	0	1.311	1	0	6081					
581	NM_021081	D-019005-01	GHRH	1.055	0	0	1.242	1	0	1.268	1	0	7614	decreaser	no			
582	NM_021081	D-019005-02	GHRH	1.027	0	0	1.015	0	0	0.986	0	0	1887					
583	NM_021081	D-019005-04	GHRH	0.564	0	1	0.698	0	1	0.654	0	1	7139					
584	NM_021081	D-019005-17	GHRH	1.23	1	0	1.127	0	0	1.105	0	0	2179					
585	NM_030934	D-019040-01	C1orf25	1.323	1	0	1.139	0	0	1.118	0	0	7178	decreaser	yes		yes	
586	NM_030934	D-019040-02	C1orf25	0.291	0	1	0.502	0	1	0.477	0	1	683					
587	NM_030934	D-019040-03	C1orf25	0.719	0	1	0.849	0	0	0.796	0	1	6992					
588	NM_030934	D-019040-04	C1orf25	1.312	1	0	1.185	0	0	1.19	0	0	5421					
589	NM_004189	D-019055-01	SOX14	1.199	0	0	0.979	0	0	1.001	0	0	6712	decreaser	yes		yes	
590	NM_004189	D-019055-02	SOX14	0.9225	0	0	0.644	0	1	0.6055	0	1	3832					
591	NM_004189	D-019055-03	SOX14	0.342	0	1	0.569	0	1	0.51	0	1	7150					
592	NM_004189	D-019055-04	SOX14	1.245	1	0	1.246	1	0	1.357	1	0	2882					
593	NM_138960	D-019164-01	TGIF2LX	0.62	0	1	0.594	0	1	0.553	0	1	10851	increaser	no			
594	NM_138960	D-019164-02	TGIF2LX	0.744	0	1	0.79	0	1	0.801	0	0	5684					
595	NM_138960	D-019164-03	TGIF2LX	2.573	1	0	1.62	1	0	1.963	1	0	3341					
596	NM_138960	D-019164-04	TGIF2LX	1.146	0	0	1.286	1	0	1.301	1	0	8224					
597	NM_020673	D-019214-01	RAB22A	2.007	1	0	1.581	1	0	1.6885	1	0	7252	decreaser	no			
598	NM_020673	D-019214-02	RAB22A	0.963	0	0	0.975	0	0	0.972	0	0	2791					
599	NM_020673	D-019214-03	RAB22A	2.264	1	0	1.579	1	0	1.724	1	0	3289					
600	NM_020673	D-019214-04	RAB22A	0.391	0	1	0.509	0	1	0.485	0	1	8371					

	GeneID	SirnaID	Gene Symbol	STIPO median score	STIPO positive	STIPO negative	SCPO median score	SCPO positive	SCPO negative	STAPO median score	STAPO positive	STAPO negative	Median OC	Primary Screen class	succesful deconvolution same as primary po	3 or 4 out of 4 duplexes	2 out of 4 duplexes	Official Symbol (if different)
601	NM_194249	D-019345-01	DND1	0.874	0	0	1.247	1	0	1.356	1	0	9031	decreaser	no			
602	NM_194249	D-019345-02	DND1	0.94	0	0	1.005	0	0	1	0	0	6556					
603	NM_194249	D-019345-03	DND1	1.653	1	0	1.418	1	0	1.581	1	0	5424					
604	NM_194249	D-019345-04	DND1	0.889	0	0	1.038	0	0	1.031	0	0	9601					
605	NM_182505	D-019397-01	C9orf85	0.685	0	1	0.749	0	1	0.661	0	1	5267	decreaser	yes		yes	
606	NM_182505	D-019397-02	C9orf85	0.911	0	0	0.87	0	0	0.847	0	0	7052					
607	NM_182505	D-019397-04	C9orf85	0.555	0	1	0.586	0	1	0.577	0	1	9049					
608	NM_182505	D-019397-17	C9orf85	1.151	0	0	1.121	0	0	1.099	0	0	8205					
609	NM_007071/NM	D-019762-01	HHLA3	1.206	1	0	1.105	0	0	1.08	0	0	13670	increaser	no			
610	NM_007071/NM	D-019762-02	HHLA3	0.56	0	1	0.794	0	1	0.765	0	1	8379					
611	NM_007071/NM	D-019762-03	HHLA3	0.689	0	1	0.803	0	0	0.838	0	0	536					
612	NM_007071/NM	D-019762-04	HHLA3	1.156	0	0	0.963	0	0	0.922	0	0	4701					
613	NM_004388	D-019796-01	CTBS	0.709	0	1	0.721	0	1	0.682	0	1	7973	increaser	no			
614	NM_004388	D-019796-02	CTBS	1.037	0	0	1.038	0	0	1.072	0	0	6436					
615	NM_004388	D-019796-03	CTBS	0.976	0	0	0.884	0	0	0.851	0	0	5464					
616	NM_004388	D-019796-04	CTBS	1.522	1	0	1.339	1	0	1.415	1	0	8073					
617	NM_004918	D-019892-01	TCL1B	1.269	1	0	1.082	0	0	1.066	0	0	10274	increaser	yes	yes§		
618	NM_004918	D-019892-02	TCL1B	0.94	0	0	0.874	0	0	0.906	0	0	9335					
619	NM_004918	D-019892-03	TCL1B	1.267	1	0	1.253	1	0	1.254	1	0	7190					
620	NM_004918	D-019892-04	TCL1B	1.524	1	0	1.422	1	0	1.542	1	0	4875					
621	NM_005441	D-019937-01	CHAF1B	1.914	1	0	1.378	1	0	1.488	1	0	8131	decreaser	no			
622	NM_005441	D-019937-02	CHAF1B	0.325	0	1	0.417	0	1	0.383	0	1	4686					
623	NM_005441	D-019937-03	CHAF1B	1.007	0	0	1.176	0	0	1.27	1	0	6817					
624	NM_005441	D-019937-04	CHAF1B	0.94	0	0	1.051	0	0	1.063	0	0	10625					
625	NM_005715	D-020052-01	UST	1.021	0	0	0.872	0	0	0.821	0	0	5315	decreaser	no			
626	NM_005715	D-020052-02	UST	1.295	1	0	1.141	0	0	1.162	0	0	7849					
627	NM_005715	D-020052-03	UST	1.516	1	0	1.198	0	0	1.227	1	0	8643					
628	NM_005715	D-020052-04	UST	1.102	0	0	1.155	0	0	1.227	1	0	6693					
629	NM_000893	D-020202-01	KNG1	0.756	0	1	0.915	0	0	0.872	0	0	4618	increaser	no			
630	NM_000893	D-020202-17	KNG1	0.878	0	0	0.846	0	0	0.799	0	1	8368					
631	NM_000893	D-020202-18	KNG1	0.962	0	0	1.124	0	0	1.137	0	0	7157					
632	NM_000893	D-020202-19	KNG1	1.182	0	0	1.276	1	0	1.323	1	0	2881					
633	NM_000629	D-020209-01	IFNAR1	0.759	0	1	0.844	0	0	0.83	0	0	7668	increaser	no			
634	NM_000629	D-020209-02	IFNAR1	1.158	0	0	1.165	0	0	1.263	1	0	2474					
635	NM_000629	D-020209-03	IFNAR1	1.722	1	0	1.597	1	0	1.784	1	0	7529					
636	NM_000629	D-020209-04	IFNAR1	0.708	0	1	0.973	0	0	0.964	0	0	3852					
637	NM_014623	D-020344-01	MEA	0.977	0	0	0.907	0	0	0.899	0	0	7771	increaser	no			
638	NM_014623	D-020344-02	MEA	1.532	1	0	1.268	1	0	1.34	1	0	13617					
639	NM_014623	D-020344-03	MEA	0.632	0	1	0.613	0	1	0.588	0	1	6915					
640	NM_014623	D-020344-04	MEA	0.817	0	0	1.008	0	0	1	0	0	5575					
641	NM_014548	D-020360-01	TMOD2	0.809	0	0	0.855	0	0	0.831	0	0	5206	decreaser	no			
642	NM_014548	D-020360-02	TMOD2	1.68	1	0	1.189	0	0	1.313	1	0	7402					
643	NM_014548	D-020360-03	TMOD2	0.552	0	1	0.626	0	1	0.603	0	1	6326					
644	NM_014548	D-020360-04	TMOD2	1.622	1	0	1.361	1	0	1.416	1	0	4829					
645	NM_014363	D-020571-01	SACS	1.889	1	0	1.308	1	0	1.435	1	0	6568	decreaser	no			
646	NM_014363	D-020571-03	SACS	0.97	0	0	0.98	0	0	0.917	0	0	8648					
647	NM_014363	D-020571-04	SACS	1	0	0	0.853	0	0	0.821	0	0	2354					
648	NM_014363	D-020571-17	SACS	1.216	1	0	1.071	0	0	1.107	0	0	4419					
649	NM_019103/NM	D-020592-01	LOC55954	0.611	0	1	0.853	0	0	0.841	0	0	5766	decreaser	no			
650	NM_019103/NM	D-020592-02	LOC55954	1.596	1	0	1.25	1	0	1.37	1	0	11989					
651	NM_019103/NM	D-020592-03	LOC55954	0.81	0	0	0.851	0	0	0.784	0	1	7933					
652	NM_019103/NM	D-020592-04	LOC55954	1.419	1	0	1.137	0	0	1.115	0	0	6504					
653	NM_017805	D-020794-01	RASIP1	0.965	0	0	0.807	0	0	0.756	0	1	9811	increaser	yes	yes		
654	NM_017805	D-020794-02	RASIP1	1.232	1	0	1.339	1	0	1.411	1	0	6325					
655	NM_017805	D-020794-03	RASIP1	1.974	1	0	1.665	1	0	1.832	1	0	6888					
656	NM_017805	D-020794-04	RASIP1	1.284	1	0	1.173	0	0	1.164	0	0	5188					
657	NM_018349	D-020810-01	FLJ11175	0.724	0	1	0.772	0	1	0.681	0	1	9426	increaser	no			
658	NM_018349	D-020810-02	FLJ11175	1.136	0	0	1.121	0	0	1.143	0	0	4849					
659	NM_018349	D-020810-03	FLJ11175	0.872	0	0	0.933	0	0	0.976	0	0	10079					
660	NM_018349	D-020810-04	FLJ11175	1.993	1	0	1.497	1	0	1.714	1	0	4654					

	GeneID	SirnaID	Gene Symbol	STIPO median score	STIPO positive	STIPO negative	SCPO median score	SCPO positive	SCPO negative	STAPO median score	STAPO positive	STAPO negative	Median OC	Primary Screen class	succesful deconvolution same as primary po	3 or 4 out of 4 duplexes	2 out of 4 duplexes	Official Symbol (if different)
661	NM_017867	D-020849-01	FLJ20534	0.496	0	1	0.615	0	1	0.598	0	1	5303	decreaser	no			
662	NM_017867	D-020849-02	FLJ20534	1.627	1	0	1.396	1	0	1.454	1	0	5859					
663	NM_017867	D-020849-03	FLJ20534	0.462	0	1	0.493	0	1	0.507	0	1	5171					
664	NM_017867	D-020849-04	FLJ20534	1.863	1	0	1.667	1	0	1.754	1	0	5071					
665	NM_018992	D-021199-01	KCTD5	0.17	0	1	0.323	0	1	0.296	0	1	7310	increaser	no			
666	NM_018992	D-021199-02	KCTD5	1.567	1	0	1.574	1	0	1.683	1	0	3847					
667	NM_018992	D-021199-03	KCTD5	1.049	0	0	0.967	0	0	0.974	0	0	5017					
668	NM_018992	D-021199-04	KCTD5	0.689	0	1	0.702	0	1	0.694	0	1	11306					
669	NM_015601	D-021426-01	HERC4	0.872	0	0	0.991	0	0	1.015	0	0	4975	decreaser	yes		yes	
670	NM_015601	D-021426-02	HERC4	0.642	0	1	0.704	0	1	0.67	0	1	4615					
671	NM_015601	D-021426-03	HERC4	0.996	0	0	0.888	0	0	0.916	0	0	6250					
672	NM_015601	D-021426-04	HERC4	0.72	0	1	0.615	0	1	0.634	0	1	4294					
673	XM_372810/NM	D-021532-01	PLXNA2	0.954	0	0	0.937	0	0	0.957	0	0	13702	increaser	no			
674	XM_372810/NM	D-021532-02	PLXNA2	1.793	1	0	1.484	1	0	1.76	1	0	5832					
675	XM_372810/NM	D-021532-03	PLXNA2	0.939	0	0	0.996	0	0	0.995	0	0	7378					
676	XM_372810/NM	D-021532-04	PLXNA2	0.799	0	1	0.877	0	0	0.857	0	0	4703					
677	NM_006040	D-022514-01	HS3ST4	0.99	0	0	0.871	0	0	0.871	0	0	5662	decreaser	yes		yes	
678	NM_006040	D-022514-02	HS3ST4	0.492	0	1	0.72	0	1	0.683	0	1	4838					
679	NM_006040	D-022514-03	HS3ST4	0.715	0	1	0.947	0	0	0.996	0	0	4691					
680	NM_006040	D-022514-04	HS3ST4	1.189	0	0	0.975	0	0	0.947	0	0	8798					
681	NM_015432	D-022573-01	PLEKHG4	0.991	0	0	1.097	0	0	1.187	0	0	13515	increaser	no			
682	NM_015432	D-022573-02	PLEKHG4	1.057	0	0	1.115	0	0	1.104	0	0	3463					
683	NM_015432	D-022573-03	PLEKHG4	0.917	0	0	1.034	0	0	1.065	0	0	3065					
684	NM_015432	D-022573-04	PLEKHG4	0.941	0	0	0.904	0	0	0.862	0	0	5159					
685	NM_006969	D-023811-01	ZNF28	1.184	0	0	1.003	0	0	1.031	0	0	7018	decreaser	no			
686	NM_006969	D-023811-02	ZNF28	0.703	0	1	0.822	0	0	0.791	0	1	6495					
687	NM_006969	D-023811-03	ZNF28	0.836	0	0	1.09	0	0	1.109	0	0	9788					
688	NM_006969	D-023811-04	ZNF28	1.06	0	0	1.077	0	0	1.091	0	0	8935					
689	XM_372884	D-024450-01	CECR2	1.105	0	0	1.114	0	0	1.056	0	0	8941	decreaser	no			
690	XM_372884	D-024450-02	CECR2	1.071	0	0	0.89	0	0	0.887	0	0	2865					
691	XM_372884	D-024450-03	CECR2	2.19	1	0	1.565	1	0	1.726	1	0	6741					
692	XM_372884	D-024450-04	CECR2	0.123	0	1	0.283	0	1	0.236	0	1	4958					
693	XM_035299	D-024465-01	ZSWIM6	2.504	1	0	1.832	1	0	2.1895	1	0	8670	increaser	yes		yes	
694	XM_035299	D-024465-02	ZSWIM6	1.646	1	0	1.529	1	0	1.527	1	0	13876					
695	XM_035299	D-024465-03	ZSWIM6	0.796	0	1	0.733	0	1	0.729	0	1	7127					
696	XM_035299	D-024465-04	ZSWIM6	0.973	0	0	0.992	0	0	1	0	0	6918					
697	NM_006909	D-024516-01	RASGRF2	0.703	0	1	0.862	0	0	0.816	0	0	10676	increaser	yes	yes		
698	NM_006909	D-024516-04	RASGRF2	1.566	1	0	1.414	1	0	1.562	1	0	6673					
699	NM_006909	D-024516-05	RASGRF2	1.569	1	0	1.482	1	0	1.502	1	0	7892					
700	NM_006909	D-024516-06	RASGRF2	1.561	1	0	1.288	1	0	1.467	1	0	11835					
701	XM_037759/NM	D-024592-01	KIAA0376	1	0	0	1.201	1	0	1.198	0	0	14310	decreaser	no			
702	XM_037759/NM	D-024592-02	KIAA0376	1.006	0	0	0.874	0	0	0.887	0	0	8449					
703	XM_037759/NM	D-024592-03	KIAA0376	1.259	1	0	1.175	0	0	1.151	0	0	5850					
704	XM_037759/NM	D-024592-04	KIAA0376	0.422	0	1	0.637	0	1	0.616	0	1	6879					
705	XM_047025/NM	D-024659-03	TBC1D25	0.811	0	0	0.672	0	1	0.627	0	1	10479	increaser	no			
706	XM_047025/NM	D-024659-05	TBC1D25	1.364	1	0	1.352	1	0	1.491	1	0	6021					
707	XM_047025/NM	D-024659-06	TBC1D25	0.656	0	1	0.71	0	1	0.682	0	1	3693					
708	XM_047025/NM	D-024659-07	TBC1D25	0.936	0	0	1.076	0	0	1.028	0	0	5326					
709	XM_040265/NM	D-026388-01	LARP5	0.414	0	1	0.58	0	1	0.556	0	1	9995	decreaser	no			
710	XM_040265/NM	D-026388-04	LARP5	1.971	1	0	1.801	1	0	1.908	1	0	4971					
711	XM_040265/NM	D-026388-19	LARP5	1.262	1	0	1.138	0	0	1.114	0	0	8405					
712	XM_040265/NM	D-026388-20	LARP5	1.458	1	0	1.732	1	0	1.839	1	0	4669					
713	NM_198402	D-027184-01	PTPLB	0.961	0	0	0.878	0	0	0.879	0	0	7664	decreaser	no			
714	NM_198402	D-027184-03	PTPLB	0.385	0	1	0.499	0	1	0.511	0	1	4268					
715	NM_198402	D-027184-04	PTPLB	0.891	0	0	0.971	0	0	0.982	0	0	918					
716	NM_198402	D-027184-06	PTPLB	1.704	1	0	1.261	1	0	1.313	1	0	7441					
717	NM_015315	D-027187-01	LARP1	0.698	0	1	0.872	0	0	0.916	0	0	8878	decreaser	yes	yes		
718	NM_015315	D-027187-02	LARP1	0.516	0	1	0.689	0	1	0.672	0	1	8910					
719	NM_015315	D-027187-03	LARP1	0.902	0	0	1.051	0	0	1.053	0	0	9049					
720	NM_015315	D-027187-04	LARP1	0.602	0	1	0.643	0	1	0.645	0	1	4717					

	GeneID	SirnaID	Gene Symbol	STIPO median score	STIPO positive	STIPO negative	SCPO median score	SCPO positive	SCPO negative	STAPO median score	STAPO positive	STAPO negative	Median OC	Primary Screen class	succesful deconvolution same as primary po	3 or 4 out of 4 duplexes	2 out of 4 duplexes	Official Symbol (if different)
721	NM_001013692	D-027646-21	PRAMEF3	1.038	0	0	1.153	0	0	1.165	0	0	4255	decreaser	no			
722	NM_001013692	D-027646-22	PRAMEF3	1.511	1	0	1.337	1	0	1.409	1	0	7275					
723	NM_001013692	D-027646-23	PRAMEF3	1.056	0	0	1.037	0	0	1.01	0	0	5098					
724	NM_001013692	D-027646-24	PRAMEF3	1.202	1	0	1.263	1	0	1.289	1	0	5052					
725	XM_371484/NM	D-027817-01	KIAA1724	2	1	0	1.491	1	0	1.697	1	0	12998	increaser	no			
726	XM_371484/NM	D-027817-02	KIAA1724	0.847	0	0	1.024	0	0	1.04	0	0	8270					
727	XM_371484/NM	D-027817-03	KIAA1724	0.791	0	1	0.73	0	1	0.715	0	1	5265					
728	XM_371484/NM	D-027817-04	KIAA1724	1.172	0	0	1.078	0	0	1.076	0	0	5464					
729	XM_371832/NM	D-028640-01	KIAA1411	0.807	0	0	0.899	0	0	0.884	0	0	5958	increaser	no			
730	XM_371832/NM	D-028640-02	KIAA1411	0.937	0	0	0.899	0	0	0.938	0	0	5536					
731	XM_371832/NM	D-028640-03	KIAA1411	1.744	1	0	1.564	1	0	1.676	1	0	8053					
732	XM_371832/NM	D-028640-04	KIAA1411	1.134	0	0	1.098	0	0	1.101	0	0	1690					
733	XM_167072/NM	D-028712-01	BZRPL1	0.714	0	1	0.759	0	1	0.786	0	1	4370	increaser	no			
734	XM_167072/NM	D-028712-02	BZRPL1	0.756	0	1	0.742	0	1	0.717	0	1	9699					
735	XM_167072/NM	D-028712-03	BZRPL1	1.001	0	0	0.912	0	0	0.913	0	0	9194					
736	XM_167072/NM	D-028712-04	BZRPL1	1.476	1	0	1.132	0	0	1.2	1	0	10694					
737	XM_113678/NM	D-029990-01	NUP160	1.164	0	0	1.285	1	0	1.446	1	0	6716	increaser	yes		yes	
738	XM_113678/NM	D-029990-02	NUP160	1.165	0	0	1.174	0	0	1.224	1	0	7774					
739	XM_113678/NM	D-029990-03	NUP160	0.856	0	0	0.839	0	0	0.85	0	0	4803					
740	XM_113678/NM	D-029990-04	NUP160	1.235	1	0	1.098	0	0	1.14	0	0	6160					
741	XM_373685	D-030621-01	LOC388276	1.049	0	0	1.013	0	0	1.043	0	0	8861	increaser	no			
742	XM_373685	D-030621-03	LOC388276	1.193	0	0	1.005	0	0	1.047	0	0	1979					
743	XM_373685	D-030621-19	LOC388276	0.826	0	0	0.868	0	0	0.856	0	0	5118					
744	XM_373685	D-030621-20	LOC388276	0.611	0	1	0.571	0	1	0.557	0	1	8615					
745	NM_080928	D-031158-01	ASB15	0.9775	0	0	1.1535	0	0	1.1635	0	0	9578	decreaser	no			
746	NM_080928	D-031158-02	ASB15	1.335	1	0	1.312	1	0	1.323	1	0	10498					
747	NM_080928	D-031158-04	ASB15	0.959	0	0	1.185	0	0	1.215	1	0	10691					
748	NM_080928	D-031158-17	ASB15	1.088	0	0	1.197	0	0	1.218	1	0	4800					
749	XM_372213	D-031532-02	USP27X	0.879	0	0	0.885	0	0	0.867	0	0	8359	decreaser	no			
750	XM_372213	D-031532-03	USP27X	0.878	0	0	0.859	0	0	0.81	0	0	5332					
751	XM_372213	D-031532-04	USP27X	0.839	0	0	0.885	0	0	0.886	0	0	9402					
752	XM_372213	D-031532-05	USP27X	1.087	0	0	0.995	0	0	0.981	0	0	10025					
753	NM_016153	D-031953-01	LW-1	0.794	0	1	0.806	0	0	0.768	0	1	8164	increaser	no			HSFX1
754	NM_016153	D-031953-03	LW-1	0.717	0	1	0.749	0	1	0.69	0	1	9299					
755	NM_016153	D-031953-04	LW-1	0.701	0	1	0.737	0	1	0.732	0	1	12794					
756	NM_016153	D-031953-17	LW-1	0.574	0	1	0.67	0	1	0.633	0	1	7323					
757	NM_012288	D-032514-01	TRAM2	1.464	1	0	1.263	1	0	1.395	1	0	6475	increaser	yes		yes	
758	NM_012288	D-032514-02	TRAM2	0.749	0	1	0.903	0	0	0.923	0	0	5700					
759	NM_012288	D-032514-03	TRAM2	1.265	1	0	1.266	1	0	1.31	1	0	6122					
760	NM_012288	D-032514-17	TRAM2	0.667	0	1	0.734	0	1	0.738	0	1	8319					

Table 9.5 Results of the deconvolution screen

Gene ID and Gene symbol for the 190 genes tested in the deconvolution screen. Dharmacon siRNA catalogue number is shown for the 4 individual siRNA duplexes used. The median STIPO, SCPO, and STAPO scores, expressed as a percentage of RISCfree control are shown. If greater than 1.2 it is scored as a positive, if less than 0.8 then it is scored as a negative. The median valid object count (OC) for the three replicates is shown. The GFP-LC3 spot phenotype from the primary screen (increaser or decreaser) and whether the individual siRNA duplexes, taken together, repeat this phenotype is indicated. If classed as a 2 out of 4 hit a yes is added in that column and if classed as a 3 out of 4 hit a yes is added in that column. **(*)** indicates a hit that is seen to be a 2 out of 4 here but with an alternate method of normalisation, could be classified as a 3 out of 4. **(§)** indicates genes with non-universal expression patterns and were therefore not chosen

(NM_001153484) Q9UIL1-1
MRRRVFSSQDWRASGWDGMGFFSRRTFCGRSGRSCRGQLVQVSRPEVSAGSLLLPAPQAEDHSSRILYPRPKSLLPKMMNADMDAVDAENQVELEEKTRLINQVLELQHTLEDLSARVDAVKEENLKLKSENQVLGQYIENLMSASSVFQTTDTKSKRK MW=18.0kDa
(NM_032547) Q9UIL1-2
MDGS RKEEEEDSTFTNIS LADDIDHSSRILYPRPKSLLPKMMNADMDAVDAENQVELEEKTRLINQVLELQHTLEDLSARVDAVKEENLKLKSENQVLGQYIENLMSASSVFQTTDTKSKRK MW=13.93kDa
(BC062684) Q9UIL1-3
MDGS RKEEEEDSTFTNIS LADDIDHSSRILYPRPKSLLPKMMNADMDVDA ENQVELEEKTRLINQVLELQHTLEDLSARVDAVKEENLKLKSENQVLGQYIENLMSASSVFQTTDTKSKRK MW=13.86kDa
Q9UIL1-4
MMNADMD DLSARVDAVKEENLKLKSENQVLGQYIENLMSASSVFQTTDTKSKRK MW= 6.1kDa
AF330205/AAK01707
MMNADMDAVDAENQVELEEKTRLINQVLELQHTLEDLSARVDAVKEENLKLKSENQVLGQYIENLMSASSVFQTTDTKSKRK MW= 9.35kDa
Dharmacon siGenome siRNAs
-02
-03
-01
Ambion siRNAs
-43.....
-42
-41
contains qRTPCR primer region

Figure 9.1 SCOC isoforms
A larger version of the schematic of SCOC isoforms corresponding to Figure 6.2.

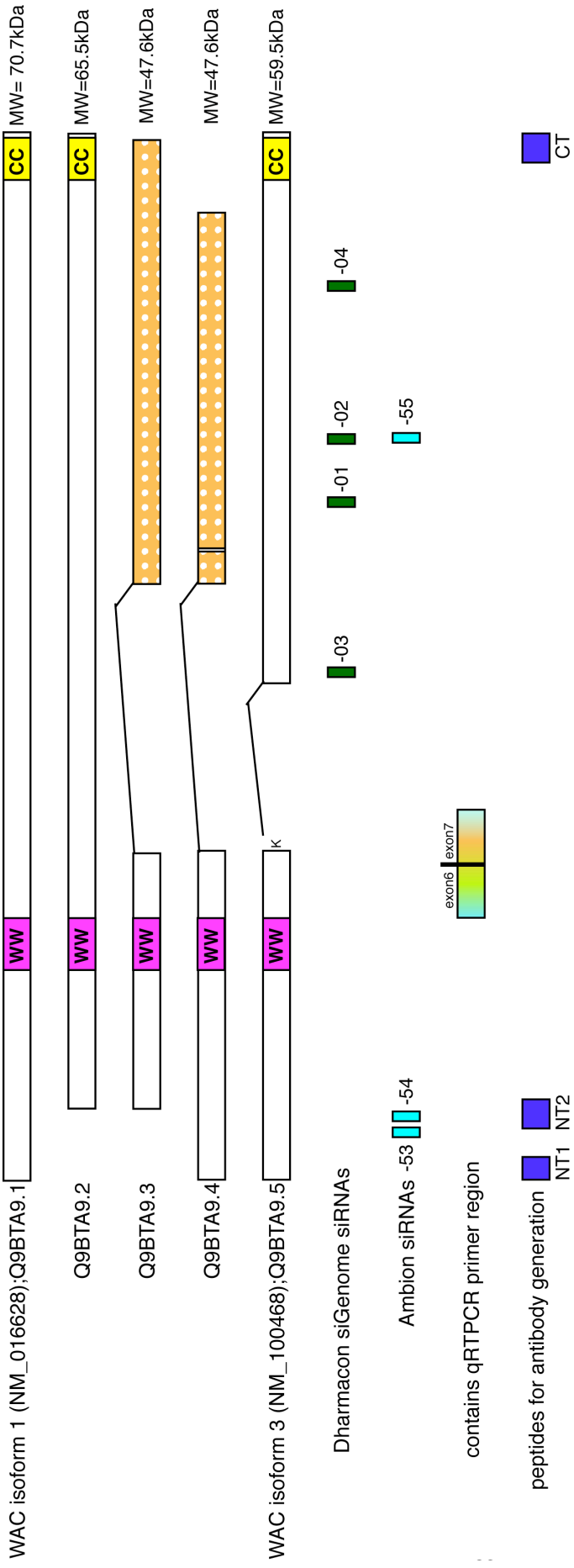
WAC isoform 1 (NM_016628);Q9BTA9.1
WW
CC
MW= 70.7kDa
Q9BTA9.2
MW=65.5kDa
Q9BTA9.3
MW=47.6kDa
Q9BTA9.4
MW=47.6kDa
WAC isoform 3 (NM_100468);Q9BTA9.5
K
MW=59.5kDa
Dharmacon siGenome siRNAs
-03
-01
-02
-04
Ambion siRNAs -53
-54
-55
contains qRTPCR primer region
exon6
exon7
peptides for antibody generation
NT1
NT2
CT

Figure 9.2 WAC isoforms
A larger version of the schematic of WAC isoforms corresponding to Figure 7.1.

Reference List

"Format your reference here"

Reference List

AITA, V. M., LIANG, X. H., MURTY, V. V., PINCUS, D. L., YU, W., CAYANIS, E., KALACHIKOV, S., GILLIAM, T. C. & LEVINE, B. (1999) Cloning and genomic organization of beclin 1, a candidate tumor suppressor gene on chromosome 17q21. *Genomics,* 59**,** 59-65.

ANDERSEN, J. N., SATHYANARAYANAN, S., DI BACCO, A., CHI, A., ZHANG, T., CHEN, A. H., DOLINSKI, B., KRAUS, M., ROBERTS, B., ARTHUR, W., KLINGHOFFER, R. A., GARGANO, D., LI, L., FELDMAN, I., LYNCH, B., RUSH, J., HENDRICKSON, R. C., BLUME-JENSEN, P. & PAWELETZ, C. P. (2010) Pathway-based identification of biomarkers for targeted therapeutics: personalized oncology with PI3K pathway inhibitors. *Sci Transl Med,* 2**,** 43ra55.

ARICO, S., PETIOT, A., BAUVY, C., DUBBELHUIS, P. F., MEIJER, A. J., CODOGNO, P. & OGIER-DENIS, E. (2001) The tumor suppressor PTEN positively regulates macroautophagy by inhibiting the phosphatidylinositol 3-kinase/protein kinase B pathway. *J Biol Chem,* 276**,** 35243-6.

ARSTILA, A. U., NUUJA, I. J. & TRUMP, B. F. (1974) Studies on cellular autophagocytosis. Vinblastine-induced autophagy in the rat liver. *Exp Cell Res,* 87**,** 249-52.

ASSMANN, E. M., ALBORGHETTI, M. R., CAMARGO, M. E. & KOBARG, J. (2006) FEZ1 dimerization and interaction with transcription regulatory proteins involves its coiled-coil region. *J Biol Chem,* 281**,** 9869-81.

AXE, E. L., WALKER, S. A., MANIFAVA, M., CHANDRA, P., RODERICK, H. L., HABERMANN, A., GRIFFITHS, G. & KTISTAKIS, N. T. (2008) Autophagosome formation from membrane compartments enriched in phosphatidylinositol 3-phosphate and dynamically connected to the endoplasmic reticulum. *J Cell Biol,* 182**,** 685-701.

BAINS, M., ZAEGEL, V., MIZE-BERGE, J. & HEIDENREICH, K. A. (2010) IGF-I stimulates Rab7-RILP interaction during neuronal autophagy. *Neurosci Lett*.

BANDYOPADHYAY, U., SRIDHAR, S., KAUSHIK, S., KIFFIN, R. & CUERVO, A. M. (2010) Identification of regulators of chaperone-mediated autophagy. *Mol Cell,* 39**,** 535-47.

BARD, F., CASANO, L., MALLABIABARRENA, A., WALLACE, E., SAITO, K., KITAYAMA, H., GUIZZUNTI, G., HU, Y., WENDLER, F., DASGUPTA, R., PERRIMON, N. & MALHOTRA, V. (2006) Functional genomics reveals genes involved in protein secretion and Golgi organization. *Nature,* 439**,** 604-7.

BARTH, H., MEILING-WESSE, K., EPPLE, U. D. & THUMM, M. (2001) Autophagy and the cytoplasm to vacuole targeting pathway both require Aut10p. *FEBS Lett,* 508**,** 23-8.

BAVRO, V. N., SOLA, M., BRACHER, A., KNEUSSEL, M., BETZ, H. & WEISSENHORN, W. (2002) Crystal structure of the GABA(A)-receptor-associated protein, GABARAP. *EMBO Rep,* 3**,** 183-9.

BEHRENDS, C., SOWA, M. E., GYGI, S. P. & HARPER, J. W. (2010) Network organization of the human autophagy system. *Nature,* 466**,** 68-76.

BJORKOY, G., LAMARK, T., BRECH, A., OUTZEN, H., PERANDER, M., OVERVATN, A., STENMARK, H. & JOHANSEN, T. (2005) p62/SQSTM1 forms protein aggregates degraded by autophagy and has a protective effect on huntingtin-induced cell death. *J Cell Biol,* 171**,** 603-14.

BLAGDEN, S. P., GATT, M. K., ARCHAMBAULT, V., LADA, K., ICHIHARA, K., LILLEY, K. S., INOUE, Y. H. & GLOVER, D. M. (2009) Drosophila Larp associates with poly(A)-binding protein and is required for male fertility and syncytial embryo development. *Dev Biol,* 334**,** 186-97.

BLOMMAART, E. F., LUIKEN, J. J., BLOMMAART, P. J., VAN WOERKOM, G. M. & MEIJER, A. J. (1995) Phosphorylation of ribosomal protein S6 is inhibitory for autophagy in isolated rat hepatocytes. *J Biol Chem,* 270**,** 2320-6.

BOLENDER, R. P. & WEIBEL, E. R. (1973) A morphometric study of the removal of phenobarbital-induced membranes from hepatocytes after cessation of threatment. *J Cell Biol,* 56**,** 746-61.

BOROVECKI, F., LOVRECIC, L., ZHOU, J., JEONG, H., THEN, F., ROSAS, H. D., HERSCH, S. M., HOGARTH, P., BOUZOU, B., JENSEN, R. V. & KRAINC, D. (2005) Genome-wide expression profiling of human blood reveals biomarkers for Huntington's disease. *Proc Natl Acad Sci U S A,* 102**,** 11023-8.

BOUCHER, C. A., KING, S. K., CAREY, N., KRAHE, R., WINCHESTER, C. L., RAHMAN, S., CREAVIN, T., MEGHJI, P., BAILEY, M. E., CHARTIER, F. L. & ET AL. (1995) A novel homeodomain-encoding gene is associated with a large CpG island interrupted by the myotonic dystrophy unstable (CTG)n repeat. *Hum Mol Genet,* 4**,** 1919-25.

BOUTROS, M., BRAS, L. P. & HUBER, W. (2006) Analysis of cell-based RNAi screens. *Genome Biol,* 7**,** R66.

BRUNET, A., BONNI, A., ZIGMOND, M. J., LIN, M. Z., JUO, P., HU, L. S., ANDERSON, M. J., ARDEN, K. C., BLENIS, J. & GREENBERG, M. E. (1999) Akt promotes cell survival by phosphorylating and inhibiting a Forkhead transcription factor. *Cell,* 96**,** 857-68.

BURD, C. G., STROCHLIC, T. I. & GANGI SETTY, S. R. (2004) Arf-like GTPases: not so Arf-like after all. *Trends Cell Biol,* 14**,** 687-94.

BURROWS, C., LATIP, N. A., LAM, S. J., CARPENTER, L., SAWICKA, K., TZOLOVSKY, G., GABRA, H., BUSHELL, M., GLOVER, D. M., WILLIS, A. E. & BLAGDEN, S. P. (2010) The RNA binding protein Larp1 regulates cell division, apoptosis and cell migration. *Nucleic Acids Res*.

CHAN, E. Y., KIR, S. & TOOZE, S. A. (2007) siRNA screening of the kinome identifies ULK1 as a multidomain modulator of autophagy. *J Biol Chem,* 282**,** 25464-74.

CHAN, E. Y., LONGATTI, A., MCKNIGHT, N. C. & TOOZE, S. A. (2009) Kinase-inactivated ULK proteins inhibit autophagy via their conserved C-terminal domains using an Atg13-independent mechanism. *Mol Cell Biol,* 29**,** 157-71.

CHAN, E. Y. & TOOZE, S. A. (2009) Evolution of Atg1 function and regulation. *Autophagy,* 5**,** 758-65.

CHANG, Y. Y. & NEUFELD, T. P. (2009) An Atg1/Atg13 complex with multiple roles in TOR-mediated autophagy regulation. *Mol Biol Cell,* 20**,** 2004-14.

CHIBA, T., INOUE, D., MIZUNO, A., KOMATSU, T., FUJITA, S., KUBOTA, H., LUISA TAGLIARO, M., PARK, S., TRINDADE, L. S., HAYASHIDA, T., HAYASHI, H., YAMAZA, H., HIGAMI, Y. & SHIMOKAWA, I. (2009) Identification and characterization of an insulin receptor substrate 4-interacting protein in rat brain: implications for longevity. *Neurobiol Aging,* 30**,** 474-82.

CHONG, S., SHAO, Y., PAULUS, H., BENNER, J., PERLER, F. B. & XU, M. Q. (1996) Protein splicing involving the Saccharomyces cerevisiae VMA intein. The steps in the splicing pathway, side reactions leading to protein cleavage, and establishment of an in vitro splicing system. *J Biol Chem,* 271**,** 22159-68.

CHUA, J. J., NG, M. M. & CHOW, V. T. (2004) The non-structural 3 (NS3) protein of dengue virus type 2 interacts with human nuclear receptor binding protein and is associated with alterations in membrane structure. *Virus Res,* 102**,** 151-63.

CRIGHTON, D., WILKINSON, S., O'PREY, J., SYED, N., SMITH, P., HARRISON, P. R., GASCO, M., GARRONE, O., CROOK, T. & RYAN, K. M. (2006) DRAM, a p53-induced modulator of autophagy, is critical for apoptosis. *Cell,* 126**,** 121-34.

CUERVO, A. M., STEFANIS, L., FREDENBURG, R., LANSBURY, P. T. & SULZER, D. (2004) Impaired degradation of mutant alpha-synuclein by chaperone-mediated autophagy. *Science,* 305**,** 1292-5.

DANTUMA, N. P., LINDSTEN, K., GLAS, R., JELLNE, M. & MASUCCI, M. G. (2000) Short-lived green fluorescent proteins for quantifying ubiquitin/proteasome-dependent proteolysis in living cells. *Nat Biotechnol,* 18**,** 538-43.

DAVIDSON, J. D., RILEY, B., BURRIGHT, E. N., DUVICK, L. A., ZOGHBI, H. Y. & ORR, H. T. (2000) Identification and characterization of an ataxin-1-interacting protein: A1Up, a ubiquitin-like nuclear protein. *Hum Mol Genet,* 9**,** 2305-12.

DE DUVE, C. & WATTIAUX, R. (1966) Functions of lysosomes. *Annu Rev Physiol,* 28**,** 435-92.

DE LANGHE, S., HAATAJA, L., SENADHEERA, D., GROFFEN, J. & HEISTERKAMP, N. (2002) Interaction of the small GTPase Rac3 with NRBP, a protein with a kinase-homology domain. *Int J Mol Med,* 9**,** 451-9.

DEGENHARDT, K., MATHEW, R., BEAUDOIN, B., BRAY, K., ANDERSON, D., CHEN, G., MUKHERJEE, C., SHI, Y., GELINAS, C., FAN, Y., NELSON, D. A., JIN, S. & WHITE, E. (2006) Autophagy promotes tumor cell survival and restricts necrosis, inflammation, and tumorigenesis. *Cancer Cell,* 10**,** 51-64.

DEHAY, B., BOVE, J., RODRIGUEZ-MUELA, N., PERIER, C., RECASENS, A., BOYA, P. & VILA, M. (2010) Pathogenic lysosomal depletion in Parkinson's disease. *J Neurosci,* 30**,** 12535-44.

DICE, J. F. (2007) Chaperone-mediated autophagy. *Autophagy,* 3**,** 295-9.

DUNWELL, T., HESSON, L., RAUCH, T. A., WANG, L., CLARK, R. E., DALLOL, A., GENTLE, D., CATCHPOOLE, D., MAHER, E. R., PFEIFER, G. P. & LATIF, F. (2010) A genome-wide screen identifies frequently methylated genes in haematological and epithelial cancers. *Mol Cancer,* 9**,** 44.

DUTTA, S. & BAEHRECKE, E. H. (2008) Warts is required for PI3K-regulated growth arrest, autophagy, and autophagic cell death in Drosophila. *Curr Biol,* 18**,** 1466-75.

FARKAS, T., HOYER-HANSEN, M. & JAATTELA, M. (2009) Identification of novel autophagy regulators by a luciferase-based assay for the kinetics of autophagic flux. *Autophagy,* 5**,** 1018-25.

FENGSRUD, M., ERICHSEN, E. S., BERG, T. O., RAIBORG, C. & SEGLEN, P. O. (2000) Ultrastructural characterization of the delimiting membranes of isolated autophagosomes and amphisomes by freeze-fracture electron microscopy. *Eur J Cell Biol,* 79**,** 871-82.

FIMIA, G. M., STOYKOVA, A., ROMAGNOLI, A., GIUNTA, L., DI BARTOLOMEO, S., NARDACCI, R., CORAZZARI, M., FUOCO, C., UCAR, A., SCHWARTZ, P., GRUSS, P., PIACENTINI, M., CHOWDHURY, K. & CECCONI, F. (2007) Ambra1 regulates autophagy and development of the nervous system. *Nature,* 447**,** 1121-5.

FLOREZ, J. C., MANNING, A. K., DUPUIS, J., MCATEER, J., IRENZE, K., GIANNINY, L., MIREL, D. B., FOX, C. S., CUPPLES, L. A. & MEIGS, J. B. (2007) A 100K genome-wide association scan for diabetes and related traits in the Framingham Heart Study: replication and integration with other genome-wide datasets. *Diabetes,* 56**,** 3063-74.

FUJITA, N., HAYASHI-NISHINO, M., FUKUMOTO, H., OMORI, H., YAMAMOTO, A., NODA, T. & YOSHIMORI, T. (2008) An Atg4B mutant hampers the lipidation of LC3 paralogues and causes defects in autophagosome closure. *Mol Biol Cell,* 19**,** 4651-9.

FUJITA, N., SAITOH, T., KAGEYAMA, S., AKIRA, S., NODA, T. & YOSHIMORI, T. (2009) Differential involvement of Atg16L1 in Crohn disease and canonical autophagy: analysis of the organization of the Atg16L1 complex in fibroblasts. *J Biol Chem,* 284**,** 32602-9.

FUNAKOSHI, T., MATSUURA, A., NODA, T. & OHSUMI, Y. (1997) Analyses of APG13 gene involved in autophagy in yeast, Saccharomyces cerevisiae. *Gene,* 192**,** 207-13.

GANLEY, I. G., LAM DU, H., WANG, J., DING, X., CHEN, S. & JIANG, X. (2009) ULK1.ATG13.FIP200 complex mediates mTOR signaling and is essential for autophagy. *J Biol Chem,* 284**,** 12297-305.

GENG, J., NAIR, U., YASUMURA-YORIMITSU, K. & KLIONSKY, D. J. (2010) Post-golgi sec proteins are required for autophagy in Saccharomyces cerevisiae. *Mol Biol Cell,* 21**,** 2257-69.

GROTH, A., LUKAS, J., NIGG, E. A., SILLJE, H. H., WERNSTEDT, C., BARTEK, J. & HANSEN, K. (2003) Human Tousled like kinases are targeted by an ATM- and Chk1-dependent DNA damage checkpoint. *EMBO J,* 22**,** 1676-87.

GUO, S., YAMAGUCHI, Y., SCHILBACH, S., WADA, T., LEE, J., GODDARD, A., FRENCH, D., HANDA, H. & ROSENTHAL, A. (2000) A regulator of transcriptional elongation controls vertebrate neuronal development. *Nature,* 408**,** 366-9.

GUTIERREZ, M. G., MUNAFO, D. B., BERON, W. & COLOMBO, M. I. (2004) Rab7 is required for the normal progression of the autophagic pathway in mammalian cells. *J Cell Sci,* 117**,** 2687-97.

HAILEY, D. W., RAMBOLD, A. S., SATPUTE-KRISHNAN, P., MITRA, K., SOUGRAT, R., KIM, P. K. & LIPPINCOTT-SCHWARTZ, J. (2010) Mitochondria supply membranes for autophagosome biogenesis during starvation. *Cell,* 141**,** 656-67.

HAMPE, J., FRANKE, A., ROSENSTIEL, P., TILL, A., TEUBER, M., HUSE, K., ALBRECHT, M., MAYR, G., DE LA VEGA, F. M., BRIGGS, J., GUNTHER, S., PRESCOTT, N. J., ONNIE, C. M., HASLER, R., SIPOS, B., FOLSCH, U. R., LENGAUER, T., PLATZER, M., MATHEW, C. G., KRAWCZAK, M. & SCHREIBER, S. (2007) A genome-wide association scan of nonsynonymous SNPs identifies a susceptibility variant for Crohn disease in ATG16L1. *Nat Genet,* 39**,** 207-11.

HANADA, T., NODA, N. N., SATOMI, Y., ICHIMURA, Y., FUJIOKA, Y., TAKAO, T., INAGAKI, F. & OHSUMI, Y. (2007) The Atg12-Atg5 conjugate has a novel E3-like activity for protein lipidation in autophagy. *J Biol Chem,* 282**,** 37298-302.

HANNON, G. J. (2002) RNA interference. *Nature,* 418**,** 244-51.

HARA, T., NAKAMURA, K., MATSUI, M., YAMAMOTO, A., NAKAHARA, Y., SUZUKI-MIGISHIMA, R., YOKOYAMA, M., MISHIMA, K., SAITO, I., OKANO, H. & MIZUSHIMA, N. (2006) Suppression of basal autophagy in neural cells causes neurodegenerative disease in mice. *Nature,* 441**,** 885-9.

HARA, T., TAKAMURA, A., KISHI, C., IEMURA, S., NATSUME, T., GUAN, J. L. & MIZUSHIMA, N. (2008) FIP200, a ULK-interacting protein, is required for autophagosome formation in mammalian cells. *J Cell Biol,* 181**,** 497-510.

HAYASHI-NISHINO, M., FUJITA, N., NODA, T., YAMAGUCHI, A., YOSHIMORI, T. & YAMAMOTO, A. (2009) A subdomain of the endoplasmic reticulum forms a cradle for autophagosome formation. *Nat Cell Biol,* 11**,** 1433-7.

HEMELAAR, J., LELYVELD, V. S., KESSLER, B. M. & PLOEGH, H. L. (2003) A single protease, Apg4B, is specific for the autophagy-related ubiquitin-like proteins GATE-16, MAP1-LC3, GABARAP, and Apg8L. *J Biol Chem,* 278**,** 51841-50.

HODGES, A., STRAND, A. D., ARAGAKI, A. K., KUHN, A., SENGSTAG, T., HUGHES, G., ELLISTON, L. A., HARTOG, C., GOLDSTEIN, D. R., THU, D., HOLLINGSWORTH, Z. R., COLLIN, F., SYNEK, B., HOLMANS, P. A., YOUNG, A. B., WEXLER, N. S., DELORENZI, M., KOOPERBERG, C., AUGOOD, S. J., FAULL, R. L., OLSON, J. M., JONES, L. & LUTHI-CARTER, R. (2006) Regional and cellular gene expression changes in human Huntington's disease brain. *Hum Mol Genet,* 15**,** 965-77.

HOSOKAWA, N., HARA, T., KAIZUKA, T., KISHI, C., TAKAMURA, A., MIURA, Y., IEMURA, S., NATSUME, T., TAKEHANA, K., YAMADA, N., GUAN, J. L., OSHIRO, N. & MIZUSHIMA, N. (2009) Nutrient-dependent mTORC1 association with the ULK1-Atg13-FIP200 complex required for autophagy. *Mol Biol Cell,* 20**,** 1981-91.

ICHIMURA, Y., KUMANOMIDOU, T., SOU, Y. S., MIZUSHIMA, T., EZAKI, J., UENO, T., KOMINAMI, E., YAMANE, T., TANAKA, K. & KOMATSU, M. (2008) Structural basis for sorting mechanism of p62 in selective autophagy. *J Biol Chem,* 283**,** 22847-57.

ITAKURA, E., KISHI, C., INOUE, K. & MIZUSHIMA, N. (2008) Beclin 1 forms two distinct phosphatidylinositol 3-kinase complexes with mammalian Atg14 and UVRAG. *Mol Biol Cell,* 19**,** 5360-72.

ITAKURA, E. & MIZUSHIMA, N. (2010) Characterization of autophagosome formation site by a hierarchical analysis of mammalian Atg proteins. *Autophagy,* 6**,** 764-76.

IWATA, A., RILEY, B. E., JOHNSTON, J. A. & KOPITO, R. R. (2005) HDAC6 and microtubules are required for autophagic degradation of aggregated huntingtin. *J Biol Chem,* 280**,** 40282-92.

JAGER, S., BUCCI, C., TANIDA, I., UENO, T., KOMINAMI, E., SAFTIG, P. & ESKELINEN, E. L. (2004) Role for Rab7 in maturation of late autophagic vacuoles. *J Cell Sci,* 117**,** 4837-48.

JUNG, C. H., JUN, C. B., RO, S. H., KIM, Y. M., OTTO, N. M., CAO, J., KUNDU, M. & KIM, D. H. (2009) ULK-Atg13-FIP200 complexes mediate mTOR signaling to the autophagy machinery. *Mol Biol Cell,* 20**,** 1992-2003.

KABEYA, Y., KAMADA, Y., BABA, M., TAKIKAWA, H., SASAKI, M. & OHSUMI, Y. (2005) Atg17 functions in cooperation with Atg1 and Atg13 in yeast autophagy. *Mol Biol Cell,* 16**,** 2544-53.

KABEYA, Y., MIZUSHIMA, N., UENO, T., YAMAMOTO, A., KIRISAKO, T., NODA, T., KOMINAMI, E., OHSUMI, Y. & YOSHIMORI, T. (2000) LC3, a mammalian homologue of yeast Apg8p, is localized in autophagosome membranes after processing. *EMBO J,* 19**,** 5720-8.

KABEYA, Y., MIZUSHIMA, N., YAMAMOTO, A., OSHITANI-OKAMOTO, S., OHSUMI, Y. & YOSHIMORI, T. (2004) LC3, GABARAP and GATE16 localize to autophagosomal membrane depending on form-II formation. *J Cell Sci,* 117**,** 2805-12.

KALTENBACH, L. S., ROMERO, E., BECKLIN, R. R., CHETTIER, R., BELL, R., PHANSALKAR, A., STRAND, A., TORCASSI, C., SAVAGE, J., HURLBURT, A., CHA, G. H., UKANI, L., CHEPANOSKE, C. L., ZHEN, Y., SAHASRABUDHE, S., OLSON, J., KURSCHNER, C., ELLERBY, L. M., PELTIER, J. M., BOTAS, J. & HUGHES, R. E. (2007) Huntingtin interacting proteins are genetic modifiers of neurodegeneration. *PLoS Genet,* 3**,** e82.

KAMADA, Y., FUNAKOSHI, T., SHINTANI, T., NAGANO, K., OHSUMI, M. & OHSUMI, Y. (2000) Tor-mediated induction of autophagy via an Apg1 protein kinase complex. *J Cell Biol,* 150**,** 1507-13.

KANNO, A., OZAWA, T. & UMEZAWA, Y. (2006) Intein-mediated reporter gene assay for detecting protein-protein interactions in living mammalian cells. *Anal Chem,* 78**,** 556-60.

KANNO, A., OZAWA, T. & UMEZAWA, Y. (2009) Bioluminescent imaging of MAPK function with intein-mediated reporter gene assay. *Methods Mol Biol,* 574**,** 185-92.

KAWAJIRI, S., SAIKI, S., SATO, S., SATO, F., HATANO, T., EGUCHI, H. & HATTORI, N. (2010) PINK1 is recruited to mitochondria with parkin and associates with LC3 in mitophagy. *FEBS Lett,* 584**,** 1073-9.

KELEMEN, L. E., WANG, X., FREDERICKSEN, Z. S., PANKRATZ, V. S., PHAROAH, P. D., AHMED, S., DUNNING, A. M., EASTON, D. F., VIERKANT, R. A., CERHAN, J. R., GOODE, E. L., OLSON, J. E. & COUCH, F. J. (2009) Genetic variation in the chromosome 17q23 amplicon and breast cancer risk. *Cancer Epidemiol Biomarkers Prev,* 18**,** 1864-8.

KIHARA, A., KABEYA, Y., OHSUMI, Y. & YOSHIMORI, T. (2001a) Beclin-phosphatidylinositol 3-kinase complex functions at the trans-Golgi network. *EMBO Rep,* 2**,** 330-5.

KIHARA, A., NODA, T., ISHIHARA, N. & OHSUMI, Y. (2001b) Two distinct Vps34 phosphatidylinositol 3-kinase complexes function in autophagy and

carboxypeptidase Y sorting in Saccharomyces cerevisiae. *J Cell Biol,* 152**,** 519-30.

KIM, S., WAIRKAR, Y. P., DANIELS, R. W. & DIANTONIO, A. (2010) The novel endosomal membrane protein Ema interacts with the class C Vps-HOPS complex to promote endosomal maturation. *J Cell Biol,* 188**,** 717-34.

KIMURA, S., NODA, T. & YOSHIMORI, T. (2008) Dynein-dependent movement of autophagosomes mediates efficient encounters with lysosomes. *Cell Struct Funct,* 33**,** 109-22.

KIRKIN, V., LAMARK, T., SOU, Y. S., BJORKOY, G., NUNN, J. L., BRUUN, J. A., SHVETS, E., MCEWAN, D. G., CLAUSEN, T. H., WILD, P., BILUSIC, I., THEURILLAT, J. P., OVERVATN, A., ISHII, T., ELAZAR, Z., KOMATSU, M., DIKIC, I. & JOHANSEN, T. (2009) A role for NBR1 in autophagosomal degradation of ubiquitinated substrates. *Mol Cell,* 33**,** 505-16.

KLIONSKY, D. J. (2005) The molecular machinery of autophagy: unanswered questions. *J Cell Sci,* 118**,** 7-18.

KLIONSKY, D. J., ABELIOVICH, H., AGOSTINIS, P., AGRAWAL, D. K., ALIEV, G., ASKEW, D. S., BABA, M., BAEHRECKE, E. H., BAHR, B. A., BALLABIO, A., BAMBER, B. A., BASSHAM, D. C., BERGAMINI, E., BI, X., BIARD-PIECHACZYK, M., BLUM, J. S., BREDESEN, D. E., BRODSKY, J. L., BRUMELL, J. H., BRUNK, U. T., BURSCH, W., CAMOUGRAND, N., CEBOLLERO, E., CECCONI, F., CHEN, Y., CHIN, L. S., CHOI, A., CHU, C. T., CHUNG, J., CLARKE, P. G., CLARK, R. S., CLARKE, S. G., CLAVE, C., CLEVELAND, J. L., CODOGNO, P., COLOMBO, M. I., COTO-MONTES, A., CREGG, J. M., CUERVO, A. M., DEBNATH, J., DEMARCHI, F., DENNIS, P. B., DENNIS, P. A., DERETIC, V., DEVENISH, R. J., DI SANO, F., DICE, J. F., DIFIGLIA, M., DINESH-KUMAR, S., DISTELHORST, C. W., DJAVAHERI-MERGNY, M., DORSEY, F. C., DROGE, W., DRON, M., DUNN, W. A., JR., DUSZENKO, M., EISSA, N. T., ELAZAR, Z., ESCLATINE, A., ESKELINEN, E. L., FESUS, L., FINLEY, K. D., FUENTES, J. M., FUEYO, J., FUJISAKI, K., GALLIOT, B., GAO, F. B., GEWIRTZ, D. A., GIBSON, S. B., GOHLA, A., GOLDBERG, A. L., GONZALEZ, R., GONZALEZ-ESTEVEZ, C., GORSKI, S., GOTTLIEB, R. A., HAUSSINGER, D., HE, Y. W., HEIDENREICH, K., HILL, J. A., HOYER-HANSEN, M., HU, X., HUANG, W. P., IWASAKI, A., JAATTELA, M., JACKSON, W. T., JIANG, X., JIN, S., JOHANSEN, T., JUNG, J. U., KADOWAKI, M., KANG, C., KELEKAR, A., KESSEL, D. H., KIEL, J. A., KIM, H. P., KIMCHI, A., KINSELLA, T. J., KISELYOV, K., KITAMOTO, K., KNECHT, E., et al. (2008) Guidelines for the use and interpretation of assays for monitoring autophagy in higher eukaryotes. *Autophagy,* 4**,** 151-75.

KLIONSKY, D. J., CREGG, J. M., DUNN, W. A., JR., EMR, S. D., SAKAI, Y., SANDOVAL, I. V., SIBIRNY, A., SUBRAMANI, S., THUMM, M., VEENHUIS, M. & OHSUMI, Y. (2003) A unified nomenclature for yeast autophagy-related genes. *Dev Cell,* 5**,** 539-45.

KOCHL, R., HU, X. W., CHAN, E. Y. & TOOZE, S. A. (2006) Microtubules facilitate autophagosome formation and fusion of autophagosomes with endosomes. *Traffic,* 7**,** 129-45.

KOMATSU, M., TANIDA, I., UENO, T., OHSUMI, M., OHSUMI, Y. & KOMINAMI, E. (2001) The C-terminal region of an Apg7p/Cvt2p is required

for homodimerization and is essential for its E1 activity and E1-E2 complex formation. *J Biol Chem,* 276**,** 9846-54.

KOMATSU, M., WAGURI, S., CHIBA, T., MURATA, S., IWATA, J., TANIDA, I., UENO, T., KOIKE, M., UCHIYAMA, Y., KOMINAMI, E. & TANAKA, K. (2006) Loss of autophagy in the central nervous system causes neurodegeneration in mice. *Nature,* 441**,** 880-4.

KOMATSU, M., WANG, Q. J., HOLSTEIN, G. R., FRIEDRICH, V. L., JR., IWATA, J., KOMINAMI, E., CHAIT, B. T., TANAKA, K. & YUE, Z. (2007) Essential role for autophagy protein Atg7 in the maintenance of axonal homeostasis and the prevention of axonal degeneration. *Proc Natl Acad Sci U S A,* 104**,** 14489-94.

KOMORI, T., INUKAI, N., YAMADA, T., YAMAGUCHI, Y. & HANDA, H. (2009) Role of human transcription elongation factor DSIF in the suppression of senescence and apoptosis. *Genes Cells,* 14**,** 343-54.

KORNMANN, B. (2010) [ERMES, a multifunctional complex connecting endoplasmic reticulum and mitochondria]. *Med Sci (Paris),* 26**,** 145-6.

KOROLCHUK, V. I., MANSILLA, A., MENZIES, F. M. & RUBINSZTEIN, D. C. (2009) Autophagy inhibition compromises degradation of ubiquitin-proteasome pathway substrates. *Mol Cell,* 33**,** 517-27.

KRAUSZ, E. (2007) High-content siRNA screening. *Mol Biosyst,* 3**,** 232-40.

KUMA, A., HATANO, M., MATSUI, M., YAMAMOTO, A., NAKAYA, H., YOSHIMORI, T., OHSUMI, Y., TOKUHISA, T. & MIZUSHIMA, N. (2004) The role of autophagy during the early neonatal starvation period. *Nature,* 432**,** 1032-6.

KUMAR, D., NATH, L., KAMAL, M. A., VARSHNEY, A., JAIN, A., SINGH, S. & RAO, K. V. (2010) Genome-wide analysis of the host intracellular network that regulates survival of Mycobacterium tuberculosis. *Cell,* 140**,** 731-43.

KUNDU, M., LINDSTEN, T., YANG, C. Y., WU, J., ZHAO, F., ZHANG, J., SELAK, M. A., NEY, P. A. & THOMPSON, C. B. (2008) Ulk1 plays a critical role in the autophagic clearance of mitochondria and ribosomes during reticulocyte maturation. *Blood,* 112**,** 1493-502.

LANG, T., SCHAEFFELER, E., BERNREUTHER, D., BREDSCHNEIDER, M., WOLF, D. H. & THUMM, M. (1998) Aut2p and Aut7p, two novel microtubule-associated proteins are essential for delivery of autophagic vesicles to the vacuole. *EMBO J,* 17**,** 3597-607.

LARSSON, J., FORSBERG, M., BRANNVALL, K., ZHANG, X. Q., ENARSSON, M., HEDBORG, F. & FORSBERG-NILSSON, K. (2008) Nuclear receptor binding protein 2 is induced during neural progenitor differentiation and affects cell survival. *Mol Cell Neurosci,* 39**,** 32-9.

LEE, J. H., YU, W. H., KUMAR, A., LEE, S., MOHAN, P. S., PETERHOFF, C. M., WOLFE, D. M., MARTINEZ-VICENTE, M., MASSEY, A. C., SOVAK, G., UCHIYAMA, Y., WESTAWAY, D., CUERVO, A. M. & NIXON, R. A. (2010) Lysosomal proteolysis and autophagy require presenilin 1 and are disrupted by Alzheimer-related PS1 mutations. *Cell,* 141**,** 1146-58.

LEE, S. B., KIM, S., LEE, J., PARK, J., LEE, G., KIM, Y., KIM, J. M. & CHUNG, J. (2007) ATG1, an autophagy regulator, inhibits cell growth by negatively regulating S6 kinase. *EMBO Rep,* 8**,** 360-5.

LEVINE, B. & DERETIC, V. (2007) Unveiling the roles of autophagy in innate and adaptive immunity. *Nat Rev Immunol,* 7**,** 767-77.
LIANG, C., FENG, P., KU, B., DOTAN, I., CANAANI, D., OH, B. H. & JUNG, J. U. (2006) Autophagic and tumour suppressor activity of a novel Beclin1-binding protein UVRAG. *Nat Cell Biol,* 8**,** 688-99.
LIANG, C., LEE, J. S., INN, K. S., GACK, M. U., LI, Q., ROBERTS, E. A., VERGNE, I., DERETIC, V., FENG, P., AKAZAWA, C. & JUNG, J. U. (2008) Beclin1-binding UVRAG targets the class C Vps complex to coordinate autophagosome maturation and endocytic trafficking. *Nat Cell Biol,* 10**,** 776-87.
LIANG, J., SHAO, S. H., XU, Z. X., HENNESSY, B., DING, Z., LARREA, M., KONDO, S., DUMONT, D. J., GUTTERMAN, J. U., WALKER, C. L., SLINGERLAND, J. M. & MILLS, G. B. (2007) The energy sensing LKB1-AMPK pathway regulates p27(kip1) phosphorylation mediating the decision to enter autophagy or apoptosis. *Nat Cell Biol,* 9**,** 218-24.
LIANG, X. H., JACKSON, S., SEAMAN, M., BROWN, K., KEMPKES, B., HIBSHOOSH, H. & LEVINE, B. (1999) Induction of autophagy and inhibition of tumorigenesis by beclin 1. *Nature,* 402**,** 672-6.
LIM, J., HAO, T., SHAW, C., PATEL, A. J., SZABO, G., RUAL, J. F., FISK, C. J., LI, N., SMOLYAR, A., HILL, D. E., BARABASI, A. L., VIDAL, M. & ZOGHBI, H. Y. (2006) A protein-protein interaction network for human inherited ataxias and disorders of Purkinje cell degeneration. *Cell,* 125**,** 801-14.
LIPINSKI, M. M., HOFFMAN, G., NG, A., ZHOU, W., PY, B. F., HSU, E., LIU, X., EISENBERG, J., LIU, J., BLENIS, J., XAVIER, R. J. & YUAN, J. (2010) A genome-wide siRNA screen reveals multiple mTORC1 independent signaling pathways regulating autophagy under normal nutritional conditions. *Dev Cell,* 18**,** 1041-52.
LONGATTI, A. & TOOZE, S. A. (2009) Vesicular trafficking and autophagosome formation. *Cell Death Differ,* 16**,** 956-65.
MALO, N., HANLEY, J. A., CERQUOZZI, S., PELLETIER, J. & NADON, R. (2006) Statistical practice in high-throughput screening data analysis. *Nat Biotechnol,* 24**,** 167-75.
MARI, M., GRIFFITH, J., RIETER, E., KRISHNAPPA, L., KLIONSKY, D. J. & REGGIORI, F. (2010) An Atg9-containing compartment that functions in the early steps of autophagosome biogenesis. *J Cell Biol,* 190**,** 1005-22.
MARINO, G., SALVADOR-MONTOLIU, N., FUEYO, A., KNECHT, E., MIZUSHIMA, N. & LOPEZ-OTIN, C. (2007) Tissue-specific autophagy alterations and increased tumorigenesis in mice deficient in Atg4C/autophagin-3. *J Biol Chem,* 282**,** 18573-83.
MARTINEZ-VICENTE, M., TALLOCZY, Z., WONG, E., TANG, G., KOGA, H., KAUSHIK, S., DE VRIES, R., ARIAS, E., HARRIS, S., SULZER, D. & CUERVO, A. M. (2010) Cargo recognition failure is responsible for inefficient autophagy in Huntington's disease. *Nat Neurosci,* 13**,** 567-76.
MATHEW, R., KARP, C. M., BEAUDOIN, B., VUONG, N., CHEN, G., CHEN, H. Y., BRAY, K., REDDY, A., BHANOT, G., GELINAS, C., DIPAOLA, R. S., KARANTZA-WADSWORTH, V. & WHITE, E. (2009) Autophagy suppresses tumorigenesis through elimination of p62. *Cell,* 137**,** 1062-75.
MATHEW, R., KONGARA, S., BEAUDOIN, B., KARP, C. M., BRAY, K., DEGENHARDT, K., CHEN, G., JIN, S. & WHITE, E. (2007) Autophagy

suppresses tumor progression by limiting chromosomal instability. *Genes Dev,* 21**,** 1367-81.

MATSUNAGA, K., MORITA, E., SAITOH, T., AKIRA, S., KTISTAKIS, N. T., IZUMI, T., NODA, T. & YOSHIMORI, T. (2010) Autophagy requires endoplasmic reticulum targeting of the PI3-kinase complex via Atg14L. *J Cell Biol,* 190**,** 511-21.

MATSUNAGA, K., SAITOH, T., TABATA, K., OMORI, H., SATOH, T., KUROTORI, N., MAEJIMA, I., SHIRAHAMA-NODA, K., ICHIMURA, T., ISOBE, T., AKIRA, S., NODA, T. & YOSHIMORI, T. (2009) Two Beclin 1-binding proteins, Atg14L and Rubicon, reciprocally regulate autophagy at different stages. *Nat Cell Biol,* 11**,** 385-96.

MATSUURA, A., TSUKADA, M., WADA, Y. & OHSUMI, Y. (1997) Apg1p, a novel protein kinase required for the autophagic process in Saccharomyces cerevisiae. *Gene,* 192**,** 245-50.

MAVRAKIS, M., LIPPINCOTT-SCHWARTZ, J., STRATAKIS, C. A. & BOSSIS, I. (2007) mTOR kinase and the regulatory subunit of protein kinase A (PRKAR1A) spatially and functionally interact during autophagosome maturation. *Autophagy,* 3**,** 151-3.

MENENDEZ-BENITO, V., VERHOEF, L. G., MASUCCI, M. G. & DANTUMA, N. P. (2005) Endoplasmic reticulum stress compromises the ubiquitin-proteasome system. *Hum Mol Genet,* 14**,** 2787-99.

MERCER, C. A., KALIAPPAN, A. & DENNIS, P. B. (2009) A novel, human Atg13 binding protein, Atg101, interacts with ULK1 and is essential for macroautophagy. *Autophagy,* 5**,** 649-62.

METZGER, S., SAUKKO, M., VAN CHE, H., TONG, L., PUDER, Y., RIESS, O. & NGUYEN, H. P. (2010) Age at onset in Huntington's disease is modified by the autophagy pathway: implication of the V471A polymorphism in Atg7. *Hum Genet,* 128**,** 453-9.

MITIN, N. Y., RAMOCKI, M. B., ZULLO, A. J., DER, C. J., KONIECZNY, S. F. & TAPAROWSKY, E. J. (2004) Identification and characterization of rain, a novel Ras-interacting protein with a unique subcellular localization. *J Biol Chem,* 279**,** 22353-61.

MIZUSHIMA, N., KUMA, A., KOBAYASHI, Y., YAMAMOTO, A., MATSUBAE, M., TAKAO, T., NATSUME, T., OHSUMI, Y. & YOSHIMORI, T. (2003) Mouse Apg16L, a novel WD-repeat protein, targets to the autophagic isolation membrane with the Apg12-Apg5 conjugate. *J Cell Sci,* 116**,** 1679-88.

MIZUSHIMA, N., LEVINE, B., CUERVO, A. M. & KLIONSKY, D. J. (2008) Autophagy fights disease through cellular self-digestion. *Nature,* 451**,** 1069-75.

MIZUSHIMA, N., NODA, T. & OHSUMI, Y. (1999) Apg16p is required for the function of the Apg12p-Apg5p conjugate in the yeast autophagy pathway. *EMBO J,* 18**,** 3888-96.

MIZUSHIMA, N., NODA, T., YOSHIMORI, T., TANAKA, Y., ISHII, T., GEORGE, M. D., KLIONSKY, D. J., OHSUMI, M. & OHSUMI, Y. (1998a) A protein conjugation system essential for autophagy. *Nature,* 395**,** 395-8.

MIZUSHIMA, N., SUGITA, H., YOSHIMORI, T. & OHSUMI, Y. (1998b) A new protein conjugation system in human. The counterpart of the yeast Apg12p conjugation system essential for autophagy. *J Biol Chem,* 273**,** 33889-92.

MIZUSHIMA, N., YAMAMOTO, A., HATANO, M., KOBAYASHI, Y., KABEYA, Y., SUZUKI, K., TOKUHISA, T., OHSUMI, Y. & YOSHIMORI, T. (2001) Dissection of autophagosome formation using Apg5-deficient mouse embryonic stem cells. *J Cell Biol,* 152**,** 657-68.

MORSELLI, E., MAIURI, M. C., MARKAKI, M., MEGALOU, E., PASPARAKI, A., PALIKARAS, K., CRIOLLO, A., GALLUZZI, L., MALIK, S. A., VITALE, I., MICHAUD, M., MADEO, F., TAVERNARAKIS, N. & KROEMER, G. (2010) The life span-prolonging effect of sirtuin-1 is mediated by autophagy. *Autophagy,* 6**,** 186-8.

MUNZ, C. (2010) Selective macroautophagy for immunity. *Immunity,* 32**,** 298-9.

N'DIAYE, E. N., KAJIHARA, K. K., HSIEH, I., MORISAKI, H., DEBNATH, J. & BROWN, E. J. (2009) PLIC proteins or ubiquilins regulate autophagy-dependent cell survival during nutrient starvation. *EMBO Rep,* 10**,** 173-9.

NARENDRA, D. P., JIN, S. M., TANAKA, A., SUEN, D. F., GAUTIER, C. A., SHEN, J., COOKSON, M. R. & YOULE, R. J. (2010) PINK1 is selectively stabilized on impaired mitochondria to activate Parkin. *PLoS Biol,* 8**,** e1000298.

NEUFELD, T. P. (2007) Contribution of Atg1-dependent autophagy to TOR-mediated cell growth and survival. *Autophagy,* 3**,** 477-9.

NISHIMOTO-MORITA, K., SHIN, H. W., MITSUHASHI, H., KITAMURA, M., ZHANG, Q., JOHANNES, L. & NAKAYAMA, K. (2009) Differential effects of depletion of ARL1 and ARFRP1 on membrane trafficking between the trans-Golgi network and endosomes. *J Biol Chem,* 284**,** 10583-92.

NODA, T., KIM, J., HUANG, W. P., BABA, M., TOKUNAGA, C., OHSUMI, Y. & KLIONSKY, D. J. (2000) Apg9p/Cvt7p is an integral membrane protein required for transport vesicle formation in the Cvt and autophagy pathways. *J Cell Biol,* 148**,** 465-80.

NODA, T. & OHSUMI, Y. (1998) Tor, a phosphatidylinositol kinase homologue, controls autophagy in yeast. *J Biol Chem,* 273**,** 3963-6.

OGIER-DENIS, E., PATTINGRE, S., EL BENNA, J. & CODOGNO, P. (2000) Erk1/2-dependent phosphorylation of Galpha-interacting protein stimulates its GTPase accelerating activity and autophagy in human colon cancer cells. *J Biol Chem,* 275**,** 39090-5.

OH-OKA, K., NAKATOGAWA, H. & OHSUMI, Y. (2008) Physiological pH and acidic phospholipids contribute to substrate specificity in lipidation of Atg8. *J Biol Chem,* 283**,** 21847-52.

OKAMOTO, S., MATSUSHIMA, M. & NAKAMURA, Y. (1998) Identification, genomic organization, and alternative splicing of KNSL3, a novel human gene encoding a kinesin-like protein. *Cytogenet Cell Genet,* 83**,** 25-9.

OUDE OPHUIS, R. J., WIJERS, M., BENNINK, M. B., VAN DE LOO, F. A., FRANSEN, J. A., WIERINGA, B. & WANSINK, D. G. (2009) A tail-anchored myotonic dystrophy protein kinase isoform induces perinuclear clustering of mitochondria, autophagy, and apoptosis. *PLoS One,* 4**,** e8024.

OVERBYE, A., FENGSRUD, M. & SEGLEN, P. O. (2007) Proteomic analysis of membrane-associated proteins from rat liver autophagosomes. *Autophagy,* 3**,** 300-22.

PANIC, B., WHYTE, J. R. & MUNRO, S. (2003) The ARF-like GTPases Arl1p and Arl3p act in a pathway that interacts with vesicle-tethering factors at the Golgi apparatus. *Curr Biol,* 13**,** 405-10.

PANKIV, S., CLAUSEN, T. H., LAMARK, T., BRECH, A., BRUUN, J. A., OUTZEN, H., OVERVATN, A., BJORKOY, G. & JOHANSEN, T. (2007) p62/SQSTM1 binds directly to Atg8/LC3 to facilitate degradation of ubiquitinated protein aggregates by autophagy. *J Biol Chem,* 282**,** 24131-45.

PANKIV, S., LAMARK, T., BRUUN, J. A., OVERVATN, A., BJORKOY, G. & JOHANSEN, T. (2010) Nucleocytoplasmic shuttling of p62/SQSTM1 and its role in recruitment of nuclear polyubiquitinated proteins to promyelocytic leukemia bodies. *J Biol Chem,* 285**,** 5941-53.

PAPANAYOTOU, C., MEY, A., BIROT, A. M., SAKA, Y., BOAST, S., SMITH, J. C., SAMARUT, J. & STERN, C. D. (2008) A mechanism regulating the onset of Sox2 expression in the embryonic neural plate. *PLoS Biol,* 6**,** e2.

PARKES, M., BARRETT, J. C., PRESCOTT, N. J., TREMELLING, M., ANDERSON, C. A., FISHER, S. A., ROBERTS, R. G., NIMMO, E. R., CUMMINGS, F. R., SOARS, D., DRUMMOND, H., LEES, C. W., KHAWAJA, S. A., BAGNALL, R., BURKE, D. A., TODHUNTER, C. E., AHMAD, T., ONNIE, C. M., MCARDLE, W., STRACHAN, D., BETHEL, G., BRYAN, C., LEWIS, C. M., DELOUKAS, P., FORBES, A., SANDERSON, J., JEWELL, D. P., SATSANGI, J., MANSFIELD, J. C., CARDON, L. & MATHEW, C. G. (2007) Sequence variants in the autophagy gene IRGM and multiple other replicating loci contribute to Crohn's disease susceptibility. *Nat Genet,* 39**,** 830-2.

PATTINGRE, S., TASSA, A., QU, X., GARUTI, R., LIANG, X. H., MIZUSHIMA, N., PACKER, M., SCHNEIDER, M. D. & LEVINE, B. (2005) Bcl-2 antiapoptotic proteins inhibit Beclin 1-dependent autophagy. *Cell,* 122**,** 927-39.

PELKMANS, L., FAVA, E., GRABNER, H., HANNUS, M., HABERMANN, B., KRAUSZ, E. & ZERIAL, M. (2005) Genome-wide analysis of human kinases in clathrin- and caveolae/raft-mediated endocytosis. *Nature,* 436**,** 78-86.

PETIOT, A., OGIER-DENIS, E., BLOMMAART, E. F., MEIJER, A. J. & CODOGNO, P. (2000) Distinct classes of phosphatidylinositol 3'-kinases are involved in signaling pathways that control macroautophagy in HT-29 cells. *J Biol Chem,* 275**,** 992-8.

POLISENO, L., SALMENA, L., ZHANG, J., CARVER, B., HAVEMAN, W. J. & PANDOLFI, P. P. (2010) A coding-independent function of gene and pseudogene mRNAs regulates tumour biology. *Nature,* 465**,** 1033-8.

POLSON, H. E., DE LARTIGUE, J., RIGDEN, D. J., REEDIJK, M., URBE, S., CLAGUE, M. J. & TOOZE, S. A. (2010) Mammalian Atg18 (WIPI2) localizes to omegasome-anchored phagophores and positively regulates LC3 lipidation. *Autophagy,* 6.

PROIKAS-CEZANNE, T., WADDELL, S., GAUGEL, A., FRICKEY, T., LUPAS, A. & NORDHEIM, A. (2004) WIPI-1alpha (WIPI49), a member of the novel 7-bladed WIPI protein family, is aberrantly expressed in human cancer and is linked to starvation-induced autophagy. *Oncogene,* 23**,** 9314-25.

RADOSHEVICH, L., MURROW, L., CHEN, N., FERNANDEZ, E., ROY, S., FUNG, C. & DEBNATH, J. (2010) ATG12 conjugation to ATG3 regulates mitochondrial homeostasis and cell death. *Cell,* 142**,** 590-600.

RAVIKUMAR, B., DUDEN, R. & RUBINSZTEIN, D. C. (2002) Aggregate-prone proteins with polyglutamine and polyalanine expansions are degraded by autophagy. *Hum Mol Genet,* 11**,** 1107-17.

RAVIKUMAR, B., MOREAU, K., JAHREISS, L., PURI, C. & RUBINSZTEIN, D. C. (2010) Plasma membrane contributes to the formation of pre-autophagosomal structures. *Nat Cell Biol,* 12**,** 747-57.

RAVIKUMAR, B., VACHER, C., BERGER, Z., DAVIES, J. E., LUO, S., OROZ, L. G., SCARAVILLI, F., EASTON, D. F., DUDEN, R., O'KANE, C. J. & RUBINSZTEIN, D. C. (2004) Inhibition of mTOR induces autophagy and reduces toxicity of polyglutamine expansions in fly and mouse models of Huntington disease. *Nat Genet,* 36**,** 585-95.

RAZI, M., CHAN, E. Y. & TOOZE, S. A. (2009) Early endosomes and endosomal coatomer are required for autophagy. *J Cell Biol,* 185**,** 305-21.

REGGIORI, F., TUCKER, K. A., STROMHAUG, P. E. & KLIONSKY, D. J. (2004) The Atg1-Atg13 complex regulates Atg9 and Atg23 retrieval transport from the pre-autophagosomal structure. *Dev Cell,* 6**,** 79-90.

RIOUX, J. D., XAVIER, R. J., TAYLOR, K. D., SILVERBERG, M. S., GOYETTE, P., HUETT, A., GREEN, T., KUBALLA, P., BARMADA, M. M., DATTA, L. W., SHUGART, Y. Y., GRIFFITHS, A. M., TARGAN, S. R., IPPOLITI, A. F., BERNARD, E. J., MEI, L., NICOLAE, D. L., REGUEIRO, M., SCHUMM, L. P., STEINHART, A. H., ROTTER, J. I., DUERR, R. H., CHO, J. H., DALY, M. J. & BRANT, S. R. (2007) Genome-wide association study identifies new susceptibility loci for Crohn disease and implicates autophagy in disease pathogenesis. *Nat Genet,* 39**,** 596-604.

ROTHENBERG, C. & MONTEIRO, M. J. (2010) Ubiquilin at a crossroads in protein degradation pathways. *Autophagy,* 6.

ROTHENBERG, C., SRINIVASAN, D., MAH, L., KAUSHIK, S., PETERHOFF, C. M., UGOLINO, J., FANG, S., CUERVO, A. M., NIXON, R. A. & MONTEIRO, M. J. (2010) Ubiquilin functions in autophagy and is degraded by chaperone-mediated autophagy. *Hum Mol Genet,* 19**,** 3219-32.

RUAL, J. F., VENKATESAN, K., HAO, T., HIROZANE-KISHIKAWA, T., DRICOT, A., LI, N., BERRIZ, G. F., GIBBONS, F. D., DREZE, M., AYIVI-GUEDEHOUSSOU, N., KLITGORD, N., SIMON, C., BOXEM, M., MILSTEIN, S., ROSENBERG, J., GOLDBERG, D. S., ZHANG, L. V., WONG, S. L., FRANKLIN, G., LI, S., ALBALA, J. S., LIM, J., FRAUGHTON, C., LLAMOSAS, E., CEVIK, S., BEX, C., LAMESCH, P., SIKORSKI, R. S., VANDENHAUTE, J., ZOGHBI, H. Y., SMOLYAR, A., BOSAK, S., SEQUERRA, R., DOUCETTE-STAMM, L., CUSICK, M. E., HILL, D. E., ROTH, F. P. & VIDAL, M. (2005) Towards a proteome-scale map of the human protein-protein interaction network. *Nature,* 437**,** 1173-8.

RUBINSZTEIN, D. C., CUERVO, A. M., RAVIKUMAR, B., SARKAR, S., KOROLCHUK, V., KAUSHIK, S. & KLIONSKY, D. J. (2009) In search of an "autophagomometer". *Autophagy,* 5**,** 585-9.

SAITOH, T., FUJITA, N., HAYASHI, T., TAKAHARA, K., SATOH, T., LEE, H., MATSUNAGA, K., KAGEYAMA, S., OMORI, H., NODA, T., YAMAMOTO, N., KAWAI, T., ISHII, K., TAKEUCHI, O., YOSHIMORI, T. & AKIRA, S. (2009) Atg9a controls dsDNA-driven dynamic translocation of STING and the innate immune response. *Proc Natl Acad Sci U S A,* 106**,** 20842-6.

SANCAK, Y., BAR-PELED, L., ZONCU, R., MARKHARD, A. L., NADA, S. & SABATINI, D. M. (2010) Ragulator-Rag complex targets mTORC1 to the

lysosomal surface and is necessary for its activation by amino acids. *Cell,* 141**,** 290-303.

SANJUAN, M. A., DILLON, C. P., TAIT, S. W., MOSHIACH, S., DORSEY, F., CONNELL, S., KOMATSU, M., TANAKA, K., CLEVELAND, J. L., WITHOFF, S. & GREEN, D. R. (2007) Toll-like receptor signalling in macrophages links the autophagy pathway to phagocytosis. *Nature,* 450**,** 1253-7.

SANO, H., LIU, S. C., LANE, W. S., PILETZ, J. E. & LIENHARD, G. E. (2002) Insulin receptor substrate 4 associates with the protein IRAS. *J Biol Chem,* 277**,** 19439-47.

SARKAR, S., FLOTO, R. A., BERGER, Z., IMARISIO, S., CORDENIER, A., PASCO, M., COOK, L. J. & RUBINSZTEIN, D. C. (2005) Lithium induces autophagy by inhibiting inositol monophosphatase. *J Cell Biol,* 170**,** 1101-11.

SARKAR, S., KRISHNA, G., IMARISIO, S., SAIKI, S., O'KANE, C. J. & RUBINSZTEIN, D. C. (2008) A rational mechanism for combination treatment of Huntington's disease using lithium and rapamycin. *Hum Mol Genet,* 17**,** 170-8.

SCARLATTI, F., MAFFEI, R., BEAU, I., CODOGNO, P. & GHIDONI, R. (2008) Role of non-canonical Beclin 1-independent autophagy in cell death induced by resveratrol in human breast cancer cells. *Cell Death Differ,* 15**,** 1318-29.

SCHERZ-SHOUVAL, R., SHVETS, E., FASS, E., SHORER, H., GIL, L. & ELAZAR, Z. (2007) Reactive oxygen species are essential for autophagy and specifically regulate the activity of Atg4. *EMBO J,* 26**,** 1749-60.

SCHLUMPBERGER, M., SCHAEFFELER, E., STRAUB, M., BREDSCHNEIDER, M., WOLF, D. H. & THUMM, M. (1997) AUT1, a gene essential for autophagocytosis in the yeast Saccharomyces cerevisiae. *J Bacteriol,* 179**,** 1068-76.

SCOTT, R. C., JUHASZ, G. & NEUFELD, T. P. (2007) Direct induction of autophagy by Atg1 inhibits cell growth and induces apoptotic cell death. *Curr Biol,* 17**,** 1-11.

SEGLEN, P. O. & GORDON, P. B. (1982) 3-Methyladenine: specific inhibitor of autophagic/lysosomal protein degradation in isolated rat hepatocytes. *Proc Natl Acad Sci U S A,* 79**,** 1889-92.

SHAW, R. J., BARDEESY, N., MANNING, B. D., LOPEZ, L., KOSMATKA, M., DEPINHO, R. A. & CANTLEY, L. C. (2004) The LKB1 tumor suppressor negatively regulates mTOR signaling. *Cancer Cell,* 6**,** 91-9.

SHVETS, E., FASS, E. & ELAZAR, Z. (2008a) Utilizing flow cytometry to monitor autophagy in living mammalian cells. *Autophagy,* 4**,** 621-8.

SHVETS, E., FASS, E., SCHERZ-SHOUVAL, R. & ELAZAR, Z. (2008b) The N-terminus and Phe52 residue of LC3 recruit p62/SQSTM1 into autophagosomes. *J Cell Sci,* 121**,** 2685-95.

SILLJE, H. H., TAKAHASHI, K., TANAKA, K., VAN HOUWE, G. & NIGG, E. A. (1999) Mammalian homologues of the plant Tousled gene code for cell-cycle-regulated kinases with maximal activities linked to ongoing DNA replication. *EMBO J,* 18**,** 5691-702.

SIMONSEN, A. & TOOZE, S. A. (2009) Coordination of membrane events during autophagy by multiple class III PI3-kinase complexes. *J Cell Biol,* 186**,** 773-82.

SINGH, S. B., DAVIS, A. S., TAYLOR, G. A. & DERETIC, V. (2006) Human IRGM induces autophagy to eliminate intracellular mycobacteria. *Science,* 313**,** 1438-41.

SOU, Y. S., TANIDA, I., KOMATSU, M., UENO, T. & KOMINAMI, E. (2006) Phosphatidylserine in addition to phosphatidylethanolamine is an in vitro target of the mammalian Atg8 modifiers, LC3, GABARAP, and GATE-16. *J Biol Chem,* 281**,** 3017-24.

SOU, Y. S., WAGURI, S., IWATA, J., UENO, T., FUJIMURA, T., HARA, T., SAWADA, N., YAMADA, A., MIZUSHIMA, N., UCHIYAMA, Y., KOMINAMI, E., TANAKA, K. & KOMATSU, M. (2008) The Atg8 conjugation system is indispensable for proper development of autophagic isolation membranes in mice. *Mol Biol Cell,* 19**,** 4762-75.

STARHEIM, K. K., ARNESEN, T., GROMYKO, D., RYNINGEN, A., VARHAUG, J. E. & LILLEHAUG, J. R. (2008) Identification of the human N(alpha)-acetyltransferase complex B (hNatB): a complex important for cell-cycle progression. *Biochem J,* 415**,** 325-31.

STELZL, U., WORM, U., LALOWSKI, M., HAENIG, C., BREMBECK, F. H., GOEHLER, H., STROEDICKE, M., ZENKNER, M., SCHOENHERR, A., KOEPPEN, S., TIMM, J., MINTZLAFF, S., ABRAHAM, C., BOCK, N., KIETZMANN, S., GOEDDE, A., TOKSOZ, E., DROEGE, A., KROBITSCH, S., KORN, B., BIRCHMEIER, W., LEHRACH, H. & WANKER, E. E. (2005) A human protein-protein interaction network: a resource for annotating the proteome. *Cell,* 122**,** 957-68.

STROMHAUG, P. E., BERG, T. O., FENGSRUD, M. & SEGLEN, P. O. (1998) Purification and characterization of autophagosomes from rat hepatocytes. *Biochem J,* 335 (Pt 2)**,** 217-24.

SU, C. W., THARIN, S., JIN, Y., WIGHTMAN, B., SPECTOR, M., MEILI, D., TSUNG, N., RHINER, C., BOURIKAS, D., STOECKLI, E., GARRIGA, G., HORVITZ, H. R. & HENGARTNER, M. O. (2006) The short coiled-coil domain-containing protein UNC-69 cooperates with UNC-76 to regulate axonal outgrowth and normal presynaptic organization in Caenorhabditis elegans. *J Biol,* 5**,** 9.

SUN, H., KING, A. J., DIAZ, H. B. & MARSHALL, M. S. (2000) Regulation of the protein kinase Raf-1 by oncogenic Ras through phosphatidylinositol 3-kinase, Cdc42/Rac and Pak. *Curr Biol,* 10**,** 281-4.

SUN, Q., FAN, W., CHEN, K., DING, X., CHEN, S. & ZHONG, Q. (2008) Identification of Barkor as a mammalian autophagy-specific factor for Beclin 1 and class III phosphatidylinositol 3-kinase. *Proc Natl Acad Sci U S A,* 105**,** 19211-6.

SUZUKI, K., KUBOTA, Y., SEKITO, T. & OHSUMI, Y. (2007) Hierarchy of Atg proteins in pre-autophagosomal structure organization. *Genes Cells,* 12**,** 209-18.

TAKAHASHI, Y., COPPOLA, D., MATSUSHITA, N., CUALING, H. D., SUN, M., SATO, Y., LIANG, C., JUNG, J. U., CHENG, J. Q., MULE, J. J., PLEDGER, W. J. & WANG, H. G. (2007) Bif-1 interacts with Beclin 1 through UVRAG and regulates autophagy and tumorigenesis. *Nat Cell Biol,* 9**,** 1142-51.

TAKESHIGE, K., BABA, M., TSUBOI, S., NODA, T. & OHSUMI, Y. (1992) Autophagy in yeast demonstrated with proteinase-deficient mutants and conditions for its induction. *J Cell Biol,* 119**,** 301-11.

TANAKA, Y., KANAI, Y., OKADA, Y., NONAKA, S., TAKEDA, S., HARADA, A. & HIROKAWA, N. (1998) Targeted disruption of mouse conventional kinesin heavy chain, kif5B, results in abnormal perinuclear clustering of mitochondria. *Cell,* 93**,** 1147-58.

TANIDA, I., MIZUSHIMA, N., KIYOOKA, M., OHSUMI, M., UENO, T., OHSUMI, Y. & KOMINAMI, E. (1999) Apg7p/Cvt2p: A novel protein-activating enzyme essential for autophagy. *Mol Biol Cell,* 10**,** 1367-79.

TANIDA, I., SOU, Y. S., EZAKI, J., MINEMATSU-IKEGUCHI, N., UENO, T. & KOMINAMI, E. (2004) HsAtg4B/HsApg4B/autophagin-1 cleaves the carboxyl termini of three human Atg8 homologues and delipidates microtubule-associated protein light chain 3- and GABAA receptor-associated protein-phospholipid conjugates. *J Biol Chem,* 279**,** 36268-76.

TANIDA, I., SOU, Y. S., MINEMATSU-IKEGUCHI, N., UENO, T. & KOMINAMI, E. (2006) Atg8L/Apg8L is the fourth mammalian modifier of mammalian Atg8 conjugation mediated by human Atg4B, Atg7 and Atg3. *FEBS J,* 273**,** 2553-62.

TANIDA, I., TANIDA-MIYAKE, E., KOMATSU, M., UENO, T. & KOMINAMI, E. (2002) Human Apg3p/Aut1p homologue is an authentic E2 enzyme for multiple substrates, GATE-16, GABARAP, and MAP-LC3, and facilitates the conjugation of hApg12p to hApg5p. *J Biol Chem,* 277**,** 13739-44.

TAPON, N., HARVEY, K. F., BELL, D. W., WAHRER, D. C., SCHIRIPO, T. A., HABER, D. A. & HARIHARAN, I. K. (2002) salvador Promotes both cell cycle exit and apoptosis in Drosophila and is mutated in human cancer cell lines. *Cell,* 110**,** 467-78.

TASDEMIR, E., CHIARA MAIURI, M., MORSELLI, E., CRIOLLO, A., D'AMELIO, M., DJAVAHERI-MERGNY, M., CECCONI, F., TAVERNARAKIS, N. & KROEMER, G. (2008a) A dual role of p53 in the control of autophagy. *Autophagy,* 4**,** 810-4.

TASDEMIR, E., MAIURI, M. C., GALLUZZI, L., VITALE, I., DJAVAHERI-MERGNY, M., D'AMELIO, M., CRIOLLO, A., MORSELLI, E., ZHU, C., HARPER, F., NANNMARK, U., SAMARA, C., PINTON, P., VICENCIO, J. M., CARNUCCIO, R., MOLL, U. M., MADEO, F., PATERLINI-BRECHOT, P., RIZZUTO, R., SZABADKAI, G., PIERRON, G., BLOMGREN, K., TAVERNARAKIS, N., CODOGNO, P., CECCONI, F. & KROEMER, G. (2008b) Regulation of autophagy by cytoplasmic p53. *Nat Cell Biol,* 10**,** 676-87.

TASDEMIR, E., MAIURI, M. C., ORHON, I., KEPP, O., MORSELLI, E., CRIOLLO, A. & KROEMER, G. (2008c) p53 represses autophagy in a cell cycle-dependent fashion. *Cell Cycle,* 7**,** 3006-11.

THOREEN, C. C., KANG, S. A., CHANG, J. W., LIU, Q., ZHANG, J., GAO, Y., REICHLING, L. J., SIM, T., SABATINI, D. M. & GRAY, N. S. (2009) An ATP-competitive mammalian target of rapamycin inhibitor reveals rapamycin-resistant functions of mTORC1. *J Biol Chem,* 284**,** 8023-32.

THORESEN, S. B., PEDERSEN, N. M., LIESTOL, K. & STENMARK, H. (2010) A phosphatidylinositol 3-kinase class III sub-complex containing VPS15, VPS34, Beclin 1, UVRAG and BIF-1 regulates cytokinesis and degradative endocytic traffic. *Exp Cell Res*.

TODA, H., MOCHIZUKI, H., FLORES, R., 3RD, JOSOWITZ, R., KRASIEVA, T. B., LAMORTE, V. J., SUZUKI, E., GINDHART, J. G., FURUKUBO-

TOKUNAGA, K. & TOMODA, T. (2008) UNC-51/ATG1 kinase regulates axonal transport by mediating motor-cargo assembly. *Genes Dev,* 22**,** 3292-307.
TOOZE, S. A. & SCHIAVO, G. (2008) Liaisons dangereuses: autophagy, neuronal survival and neurodegeneration. *Curr Opin Neurobiol,* 18**,** 504-15.
TOOZE, S. A. & YOSHIMORI, T. (2010) The origin of the autophagosomal membrane. *Nat Cell Biol,* 12**,** 831-5.
TOWER, C., FU, L., GILL, R., PRICHARD, M., LESORT, M. & SZTUL, E. (2010) Human cytomegalovirus UL97 kinase prevents the deposition of mutant protein aggregates in cellular models of Huntington's disease and Ataxia. *Neurobiol Dis*.
TRINCHERI, N. F., FOLLO, C., NICOTRA, G., PERACCHIO, C., CASTINO, R. & ISIDORO, C. (2008) Resveratrol-induced apoptosis depends on the lipid kinase activity of Vps34 and on the formation of autophagolysosomes. *Carcinogenesis,* 29**,** 381-9.
TSUKADA, M. & OHSUMI, Y. (1993) Isolation and characterization of autophagy-defective mutants of Saccharomyces cerevisiae. *FEBS Lett,* 333**,** 169-74.
TSVETKOV, A. S., MILLER, J., ARRASATE, M., WONG, J. S., PLEISS, M. A. & FINKBEINER, S. (2010) A small-molecule scaffold induces autophagy in primary neurons and protects against toxicity in a Huntington disease model. *Proc Natl Acad Sci U S A*.
VALENTE, E. M., ABOU-SLEIMAN, P. M., CAPUTO, V., MUQIT, M. M., HARVEY, K., GISPERT, S., ALI, Z., DEL TURCO, D., BENTIVOGLIO, A. R., HEALY, D. G., ALBANESE, A., NUSSBAUM, R., GONZALEZ-MALDONADO, R., DELLER, T., SALVI, S., CORTELLI, P., GILKS, W. P., LATCHMAN, D. S., HARVEY, R. J., DALLAPICCOLA, B., AUBURGER, G. & WOOD, N. W. (2004) Hereditary early-onset Parkinson's disease caused by mutations in PINK1. *Science,* 304**,** 1158-60.
VAN DER VAART, A., GRIFFITH, J. & REGGIORI, F. (2010) Exit from the golgi is required for the expansion of the autophagosomal phagophore in yeast Saccharomyces cerevisiae. *Mol Biol Cell,* 21**,** 2270-84.
VAN DER VAART, A. & REGGIORI, F. (2010) The Golgi complex as a source for yeast autophagosomal membranes. *Autophagy,* 6**,** 800-1.
VAN VALKENBURGH, H., SHERN, J. F., SHARER, J. D., ZHU, X. & KAHN, R. A. (2001) ADP-ribosylation factors (ARFs) and ARF-like 1 (ARL1) have both specific and shared effectors: characterizing ARL1-binding proteins. *J Biol Chem,* 276**,** 22826-37.
VERHEY, K. J. & HAMMOND, J. W. (2009) Traffic control: regulation of kinesin motors. *Nat Rev Mol Cell Biol,* 10**,** 765-77.
VOUSDEN, K. H. & RYAN, K. M. (2009) p53 and metabolism. *Nat Rev Cancer,* 9**,** 691-700.
WANG, H., LIM, P. J., YIN, C., RIECKHER, M., VOGEL, B. E. & MONTEIRO, M. J. (2006) Suppression of polyglutamine-induced toxicity in cell and animal models of Huntington's disease by ubiquilin. *Hum Mol Genet,* 15**,** 1025-41.
WEBBER, J. L. & TOOZE, S. A. (2010) Coordinated regulation of autophagy by p38alpha MAPK through mAtg9 and p38IP. *EMBO J,* 29**,** 27-40.
WEI, Y., PATTINGRE, S., SINHA, S., BASSIK, M. & LEVINE, B. (2008) JNK1-mediated phosphorylation of Bcl-2 regulates starvation-induced autophagy. *Mol Cell,* 30**,** 678-88.

WEIDBERG, H., SHVETS, E., SHPILKA, T., SHIMRON, F., SHINDER, V. & ELAZAR, Z. (2010) LC3 and GATE-16/GABARAP subfamilies are both essential yet act differently in autophagosome biogenesis. *EMBO J,* 29**,** 1792-802.

WHITE, E., KARP, C., STROHECKER, A. M., GUO, Y. & MATHEW, R. (2010) Role of autophagy in suppression of inflammation and cancer. *Curr Opin Cell Biol,* 22**,** 212-7.

WOOTEN, M. W., GEETHA, T., BABU, J. R., SEIBENHENER, M. L., PENG, J., COX, N., DIAZ-MECO, M. T. & MOSCAT, J. (2008) Essential role of sequestosome 1/p62 in regulating accumulation of Lys63-ubiquitinated proteins. *J Biol Chem,* 283**,** 6783-9.

WU, R. F. & TERADA, L. S. (2010) Focal oxidant and Ras signaling on the ER surface activates autophagy. *Autophagy,* 6**,** 828-9.

XIE, X., WANG, Z. & CHEN, Y. (2007) Association of LKB1 with a WD-repeat protein WDR6 is implicated in cell growth arrest and p27(Kip1) induction. *Mol Cell Biochem,* 301**,** 115-22.

XIE, Z. & KLIONSKY, D. J. (2007) Autophagosome formation: core machinery and adaptations. *Nat Cell Biol,* 9**,** 1102-9.

XU, G. M. & ARNAOUT, M. A. (2002) WAC, a novel WW domain-containing adapter with a coiled-coil region, is colocalized with splicing factor SC35. *Genomics,* 79**,** 87-94.

XU, K., CHONG, D. C., RANKIN, S. A., ZORN, A. M. & CLEAVER, O. (2009) Rasip1 is required for endothelial cell motility, angiogenesis and vessel formation. *Dev Biol,* 329**,** 269-79.

YAMADA, T., YAMAGUCHI, Y., INUKAI, N., OKAMOTO, S., MURA, T. & HANDA, H. (2006) P-TEFb-mediated phosphorylation of hSpt5 C-terminal repeats is critical for processive transcription elongation. *Mol Cell,* 21**,** 227-37.

YAMAKAWA, A., KAMEOKA, Y., HASHIMOTO, K., YOSHITAKE, Y., NISHIKAWA, K., TANIHARA, K. & DATE, T. (1997) cDNA cloning and chromosomal mapping of genes encoding novel protein kinases termed PKU-alpha and PKU-beta, which have nuclear localization signal. *Gene,* 202**,** 193-201.

YAMAMOTO, A., CREMONA, M. L. & ROTHMAN, J. E. (2006) Autophagy-mediated clearance of huntingtin aggregates triggered by the insulin-signaling pathway. *J Cell Biol,* 172**,** 719-31.

YANG, Z. & KLIONSKY, D. J. (2010) Eaten alive: a history of macroautophagy. *Nat Cell Biol,* 12**,** 814-22.

YEN, W. L., SHINTANI, T., NAIR, U., CAO, Y., RICHARDSON, B. C., LI, Z., HUGHSON, F. M., BABA, M. & KLIONSKY, D. J. (2010) The conserved oligomeric Golgi complex is involved in double-membrane vesicle formation during autophagy. *J Cell Biol,* 188**,** 101-14.

YLA-ANTTILA, P., VIHINEN, H., JOKITALO, E. & ESKELINEN, E. L. (2009) 3D tomography reveals connections between the phagophore and endoplasmic reticulum. *Autophagy,* 5**,** 1180-5.

YOO, B. H., WU, X., LI, Y., HANIFF, M., SASAZUKI, T., SHIRASAWA, S., ESKELINEN, E. L. & ROSEN, K. V. (2010) Oncogenic ras-induced down-regulation of autophagy mediator Beclin-1 is required for malignant transformation of intestinal epithelial cells. *J Biol Chem,* 285**,** 5438-49.

YOUNG, A. R., CHAN, E. Y., HU, X. W., KOCHL, R., CRAWSHAW, S. G., HIGH, S., HAILEY, D. W., LIPPINCOTT-SCHWARTZ, J. & TOOZE, S. A. (2006) Starvation and ULK1-dependent cycling of mammalian Atg9 between the TGN and endosomes. *J Cell Sci,* 119**,** 3888-900.

YOUNG, A. R., NARITA, M., FERREIRA, M., KIRSCHNER, K., SADAIE, M., DAROT, J. F., TAVARE, S., ARAKAWA, S., SHIMIZU, S. & WATT, F. M. (2009) Autophagy mediates the mitotic senescence transition. *Genes Dev,* 23**,** 798-803.

YU, W. H., CUERVO, A. M., KUMAR, A., PETERHOFF, C. M., SCHMIDT, S. D., LEE, J. H., MOHAN, P. S., MERCKEN, M., FARMERY, M. R., TJERNBERG, L. O., JIANG, Y., DUFF, K., UCHIYAMA, Y., NASLUND, J., MATHEWS, P. M., CATALDO, A. M. & NIXON, R. A. (2005) Macroautophagy--a novel Beta-amyloid peptide-generating pathway activated in Alzheimer's disease. *J Cell Biol,* 171**,** 87-98.

YUE, Z., JIN, S., YANG, C., LEVINE, A. J. & HEINTZ, N. (2003) Beclin 1, an autophagy gene essential for early embryonic development, is a haploinsufficient tumor suppressor. *Proc Natl Acad Sci U S A,* 100**,** 15077-82.

ZHANG, G., ASSADI, A. H., MCNEIL, R. S., BEFFERT, U., WYNSHAW-BORIS, A., HERZ, J., CLARK, G. D. & D'ARCANGELO, G. (2007a) The Pafah1b complex interacts with the reelin receptor VLDLR. *PLoS One,* 2**,** e252.

ZHANG, L., YU, J., PAN, H., HU, P., HAO, Y., CAI, W., ZHU, H., YU, A. D., XIE, X., MA, D. & YUAN, J. (2007b) Small molecule regulators of autophagy identified by an image-based high-throughput screen. *Proc Natl Acad Sci U S A,* 104**,** 19023-8.

ZHONG, Y., WANG, Q. J., LI, X., YAN, Y., BACKER, J. M., CHAIT, B. T., HEINTZ, N. & YUE, Z. (2009) Distinct regulation of autophagic activity by Atg14L and Rubicon associated with Beclin 1-phosphatidylinositol-3-kinase complex. *Nat Cell Biol,* 11**,** 468-76.

ZOGHBI, H. Y. & ORR, H. T. (2009) Pathogenic mechanisms of a polyglutamine-mediated neurodegenerative disease, spinocerebellar ataxia type 1. *J Biol Chem,* 284**,** 7425-9.